EVALUATING A FAST PYROLYSIS AND HYDRODEOXYGENATION PROCESS FOR THE PRODUCTION OF JET FUEL AND JET-FUEL RANGE AROMATICS
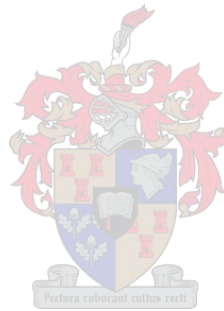
by

Suandrie Cornel McLaren

Thesis presented in partial fulfilment
of the requirements for the Degree

of

MASTER OF ENGINEERING (CHEMICAL ENGINEERING)

in the Faculty of Engineering
at Stellenbosch University

Supervisor
Professor JH Knoetze

Co-Supervisor/s
Professor JF Görgens

December 2015

DECLARATION

By submitting this thesis electronically, I declare that the entirety of the work contained therein is my own, original work, that I am the sole author thereof (save to the extent explicitly otherwise stated), that reproduction and publication thereof by Stellenbosch University will not infringe any third party rights and that I have not previously in its entirety or in part submitted it for obtaining any qualification.

Date: December 2015

ABSTRACT

The aviation industry is considering alternative fuels to reduce its dependency on fossil-derived jet fuel, and to mitigate environmental impacts of the latter. Governing bodies have set ambitious goals for the implementation of renewable fuels into the aviation industry and infrastructure. This study aims to investigate the possibility of utilizing fast pyrolysis followed by bio-oil upgrading, via hydrotreating, to produce an aromatic-rich renewable jet fuel. The study consists of two sections: an experimental fast pyrolysis section where the influence of pre-treatment and processing factors on product yields, bio-oil quality and bio-oil characteristics were investigated and a modelling section, where literature data was used to develop a simulation for a fast pyrolysis and hydrodeoxygenation process, using Aspen Plus®. The mass and energy balances from the simulation were used to estimate product yields, utility requirements and waste products.

Fast pyrolysis screening experiments utilized a 2^3 experimental factorial design with different levels of particle size, biomass moisture content and pyrolysis reactor temperature over ranges of 0.25 - 2mm, 3% - 10% (wet basis) and 450–500 $^{\circ}$C respectively. Chars were analysed with ultimate analysis and proximate analysis. Bio-oils were analysed using ultimate analysis, Karl Fischer, viscosity analysis, quantified GC-MS, ^{13}C NMR and ^{1}H NMR. Design Expert® was used to perform statistical analyses on the results to determine whether the process parameters had a significant effect on product yield and bio-oil quality. From the results, the optimal point of operation for transportation fuel production, that will require the least upgrading treatment, could be identified.

Optimal conditions were identified based on a high organic yield and a high quality bio-oil best suited for fuel, with the most important criteria as: the higher heating value (HHV), a low acid content, a low aldehyde content and a low pyrolytic water content. Particle size had a significant influence on the organic liquid yield, with a small particle size increasing the organic liquid yield. Temperature did not have a statistically significant influence on the organic liquid yield. However, operation at a high temperatures and low biomass moisture contents did improve the quality of the bio-oil. Maximum bio-oil yield and quality was achieved at small particle sizes, low moisture contents and high temperatures.

The screening experiment results were used in conjunction with literature ranges to guide to a selection of preferred operating conditions for the fast pyrolysis unit in the simulation. Literature reports on experimental studies producing hydrodeoxygenated bio-oils that are close to jet fuel specifications were limited, with details of processing conditions, especially temperature, pressure, yields and catalysts, often not reported fully within a particular study. Therefore, a combination of available literature was used to develop a simulation model to describe all the steps in the conversion process. The simulation consisted of a fast pyrolysis unit, followed by a hydrodeoxygenation and distillation unit. The simulation also included auxiliary units for hydrogen production, heat recovery, steam production and electricity generation. A pinch point analysis was performed for heat integration. The plant capacity was 92 dry tons/h of biomass feed.

Mass balances showed that the aromatic yield in the jet fuel boiling range was only 0.76wt% (dry biomass basis). Furthermore, a jet fuel yield of 3.7wt% (dry biomass basis) was obtained, indicating that the process was not selective towards jet fuel production. The other fuels produced included naphtha, diesel and gas oil, at yields of 4.9wt%, 3.5wt% and 2.3wt% (dry biomass basis) respectively.

A high thermal efficiency, 56.8%, compared to the liquid fuel efficiency, 34.1% considering liquid fuels as products, indicated that the energy content of the biomass was not concentrated into the fuel products, but was present in many other streams, including waste streams. The further decrease in liquid fuel efficiency to 11.7%, considering jet fuel as product, indicated that a significant amount of the biomass energy is transferred to the other liquid fuel products. The waste streams and by-products were exploited for thermal use to generate electricity and allowed the plant to produce three times more electricity than it consumes - i.e. 70.2 MW produced with a surplus of 46.4 MW.

The simulated bio-oil`s properties were comparable to bio-oil properties determined from the fast pyrolysis experiments in this study, showing a similar HHV, density and moisture content. The distillation gradient of the pyrolysis to jet synthesized paraffinic kerosene (PTJ-SPK) were lower than the minimum specification requirement for SPK in ASTM International D7566 (ASTM D7566), however this is partially due to the limited selection of modelling components, all within a similar boiling range. The lower heating value of the PTJ-SPK was lower than minimum requirement for a SSJF. Both of these deviations from the specification can be addressed by blending PTJ-SPK with a conventional jet fuel with a high boiling range, or with a heavy Hydroprocessed Esters and Fatty Acids jet fuel SPK (HEFA-SPK). The high density and a high aromatic content (20vol%) of PTJ-SPK differentiates it from other SPK fuels. These properties provide an opportunity for producing a fully synthetic jet fuel that contains aromatics by blending 40vol% of PTJ-SPK with 60% of HEFA-SPK or Fischer Tropsch (FT) SPK to obtain a minimum of 8vol% aromatics. However, excessive biomass requirements, due to low PTJ-SPK yields, makes such an option unfavourable. The fast pyrolysis plant capacity in this study will produce sufficient PTJ-SPK to produce a 10vol% PTJ-SPK blend for a FT-facility producing 304 000 tonnes of jet fuel per annum, yet such a blend will not be able to comply with the minimum specification requirement of 8vol% aromatics.

Increasing the bio-oil yield from fast pyrolysis and the hydrodeoxygenated oil from hydrotreating, will improve the viability of the process and might render this a feasible option in future. The process effectiveness can be improved by utilizing all the final fuel fractions as products and by exploiting the by-products for electricity generation. This will produce additional gasoline and diesel products, which will require upgrading to meet their final specification requirements. Speciality high value chemicals production from the remaining fuel fractions could also be considered.

OPSOMMING

Die lugvaart industrie oorweeg alternatiewe brandstowwe om hul afhanklikheid van fossielbrandstowwe te verminder. Regulatoriese instansies het ambisieuse doelwitte gestel vir die implimentering van die gebruik van hernubare brandstowwe in die lugvaart-industrie en infrastruktuur. Hierdie studie beoog om die moontlikheid van die gebruik van snel piroliese, gevolg deur hidrodeoksigenering, te ondersoek om `n aromatiese-ryk, hernubare vliegtuig-brandstof te produseer. Hierdie studie bestaan uit twee afdelings: `n ekspirimentele snel piroliese afdeling waar die effek van biomassa behandeling en proses-toestande op die produk opbrengste, bio-olie kwaliteit en bio-olie eienskappe ondersoek is, sowel as `n modellerings afdeling, waar literatuur data gebruik is om `n Aspen Plus® simulasie te ontwikkel. Massa-en energie-balanse is gebruik om die produk opbrengste, utiliteit behoeftes en afval-produkte te bepaal.

Snel piroliese siftings-ekspirimente is gedoen, deur gebruik te maak van `n $2^3$ faktoriaal ontwerp. Verskillende vlakke van partikelgrootte, biomassa vog-inhoud en piroliese reaktor temperatuur is ondersoek oor `n spektrum van 0.25 -2mm, 3% - 10% (nat basis) en 450–500 ^{o}C onderskeidelik. Die houtskool is geanaliseer deur elementele (C,H,N) analise en komposisie ("proximate") analise. Die bio-olie is geanaliseer deur elementele (C,H,N) analise, Karl Fischer analise, viskositeits-bepaling, gekwantifiseerde GC-MS analise, ^{13}C NMR analise en ^{1}H NMR analise. Design Expert® sagteware is gebruik om statistiese analises op die resultate te doen, om te bepaal of die proses toestande `n noemenswaardige invloed op die produk opbrengste en bio-olie kwaliteit het. Vanuit die resultate kan die optimum punt vir bedryf geïdentifiseer word om `n produk vir vervoerbrandstof te produseer wat minimale opgradering vereis. Optimale toestande is geïdentifiseer gebaseer op `n hoë organiese opbrengs en `n hoë kwaliteit bio-olie, met die belangrikste kwaliteit-kriteria as: die hoër warmte waarde (HHV), `n lae suur konsentrasie, `n lae aldehied inhoud en `n lae pirolitiese-water inhoud. Die partikelgrootte het `n noemenswaardige invloed op die organiese vloeistof opbrengs gehad, met klein partikelgroottes wat die organiese vloeistof opbrengs verhoog. Temperatuur het nie `n noemenswaardige effek op die organiese vloeistof obrengs getoon nie. Tog het hoë temperature en `n lae biomassa vog-inhoud die bio-olie kwaliteit verbeter. Die maksimum bio-olie opbrengs en kwaliteit is bereik by `n klein partikelgrootte, lae vog-inhoud en hoë temperature.

Die siftings-ekspiriment resultate en literatuur data is saam as riglyn gebruik om die beste bedryfspunt te identifiseer vir die snel piroliese eenheid in die simulasie. `n Beperkte hoeveelheid ekspirimentele studies is beskikbaar waar die proses-toetande, veral temperatuur, druk, opbreng en katalis, gerapporteer word vir hidrodeoksigeneerde bio-olie wat naby aan die vliegtuig-brandstof spesifikasies is. Daarom is `n kombinasie van beskikbare literatuur bronne gebruik om die simulasie model vir die proses te ontwikkel. Die simulasie het bestaan uit `n snel piroliese eenheid, gevolg deur `n hidrodeoksigenerings en distillasie eenheid. Die simulasie het ook addisionele eenhede vir waterstof-produksie, hitte-integrasie, stoom-produksie en elektrisiteits-generering gehad. `n Knyp-punt analise is gedoen vir hitte-integrasie. Die aanlegkapasiteit was 92 droë ton biomassa/h.

Massa balanse het aangedui dat die aromatiese opbrengs in die vliegtuig brandstof kook-reeks, slegs 0.76wt% (droë biomassa basis) was. Die opbrengs vir die lugvaart-brandstof kook-reeks, was slegs 3.7 wt% (droë biomassa basis), wat aandui dat die proses nie selektief is vir die produksie van lugvaart-brandstof nie. Ander brandstowwe wat ook geproduseer is, is nafta, diesel en gas-olie (brandstof-olie), met opbrengste van 4.9wt%, 3.5wt% en 2.3wt% (droë biomassa basis) onderskeidelik.

Die hoë termiese effektiwiteit van 56.8%, in vergelyking met die vloeibare brandstof effektiwiteit van 34.1%, vir vloeibare brandstowwe as produkte, toon dat die energie wat in die biomassa teenwoordig is nie gekonsentreer word in die brandstowwe nie, maar versprei word in ander strome insluitend afval strome. `n Verdere afname in vloeibare brandstof effektiwiteit tot 11.7% vir slegs vliegtuigbrandstof as produk, dui aan dat `n noemenswaardige hoeveelheid van die biomassa se energie voorkom in ander vloeibare brandstowwe. Die afval strome en by-produkte is vir termiese gebruik benut om elektrisiteit op te wek. Dit het die aanleg in staat gestel om drie keer meer elektrisiteit te produseer as wat die elektrisiteit gebruik is; met `n totale produksie van 70.2 MW en `n surplus van 46.4 MW.

Die bio-olie eienskappe in die simulasie en die bio-olie eienskappe wat ekspirimenteel bepaal is in die studie, vir die HHV, vog-inhoud en digtheid, was soortgelyk. Die distillasie gradiënt van die piroliese tot vliegtuigbrandstof gesintetiseerde paraffiniese keroseen (PTJ-SPK) was laer as die minimum spesifikasie wat vereis word vir SPK in ASTM Internasionaal D7566, alhoewel hierdie gedeeltelik veroorsaak is deur die beperkte keuse van model-komponente wat in die simulasie gebruik is, aangesien die komponente soortgelyke kookpunte het. Die laer warmte waarde van die gesimuleerde PTJ-SPK was laer as die minimm vereiste vir SSJF. Beide die afwykings vanaf die spesifikasie kan aangespreek word deur PTJ-SPK te meng met `n konvensionele vliegtuigbrandstof met `n hoë kook-reeks, of deur dit te meng met `n swaar gehidrogineerde esters en vetterige sure vliegtuig-brandstof SPK (HEFA-SPK). Die hoë digtheid en hoë aromatiese inhoud (20vol%) maak PTJ-SPK uniek relatief tot die ander SPK-brandstowwe. Hieride eienskappe skep `n geleentheid om `n volledige sintetiese vliegtuigbrandstof wat aromatiese komponente bevat, te vervaardig, deur 40vol% PTJ-SPK met 60vol% HEFA-SPK of Fischer Tropsch (FT) SPK te meng, sodat `n 8vol% aromatiese inhoud bereik word. Buitensporige hoë biomassa vereistes, wat veroorsaak word deur lae PTJ-SPK opbrengste, maak egter die proses ongunstig. Die snel piroliese aanleg in hierdie studie sal voldoene PTJ-SPK produseer om `n 10vol% PTJ-SPK mengsel vir `n 304 000 ton vliegtuigbrandstof per jaar FT-aanleg te produseer. Hierdie mengsel sal egter nie aan die minimum 8vol% vereiste in die spesifikasie voldoen nie.

Deur die bio-olie opbrengs en die hidrodeoksigeneerde olie vanaf hidrogenering te verhoog, sal die lewensvatbaarheid van die proses verhoog en kan hierdie proses `n haalbare opsie in die toekoms raak. Verder kan die effektiwiteit van die proses verhoog word deur al die finale brandstowwe as produkte te benut en die newe-produkte vir elektrisiteit-generering te gebruik. Dit sal addisionele vervoer-brandstowwe, soos petrol en diesel, produseer wat egter verdere opgradering sal moet ondergaan om te voldoen aan die finale brandstof-vereistes. Hoë-waarde spesialiteits-chemikalieë kan ook geproduseer word vanaf die finale brandstof fraksies wat nie vir vliegtuig-brandstof gebruik word nie.

AKNOWLEDGEMENTS

NOMENCLATURE

ASTM:	ASTM International, formerly known as American Society of Testing and Materials
ATJ:	Alcohol to jet
BO:	Bio-oil
BTL:	Biomass to liquid
CFB:	Circulating fluid bed
CV:	Coefficient of variance
DEF STAN:	Defence standard
DOD:	Degree of deoxygenation
DOE:	Design of experiments
FRJ:	Fermented renewable jet
FSJF:	Fully synthetic jet fuel
FT:	Fischer Tropsch
GC-MS:	Gas chromatography – mass spectroscopy
GHG:	Greenhouse gas
GTL:	Gas to liquid
HDO-BO:	Hydrodeoxygenated bio-oil
HDO:	Hydrodeoxygenation oil
HEFA:	Hydroprocessed esters and fatty acids
HEN:	Heat exchanger network
HHV:	Higher heating value
HPO:	Hydroprocessed pyrolysis oil
HRJ:	Hydrotreated Renewable jet fuel
HT:	High temperature
LHSV:	Liquid hourly space velocity
LHV:	Lower heating value
LPG:	Liquefied petroleum gas
MF:	Moisture free
NMR:	Nuclear magnetic resonance
PAH:	Polycyclic aromatic hydrocarbon
PFD:	Process flow diagram
PTJ:	Pyrolysis to jet
SAA:	South African Airways
SPK:	Synthesized paraffinic kerosene
SSJF:	Semi-synthetic jet fuel
TAN:	Total acid number
TOS:	Time on stream
SU:	Stellenbosch University

TABLE OF CONTENTS

List of Tables

List of Figures

1. INTRODUCTION

1.1 Background/ Project motivation and outline of thesis

The increase in greenhouse gas (GHG) emissions and their effect on global warming have contributed to environmental concerns. Many sectors, including the aviation sector, contribute to these greenhouse gas emissions. Commercial aviation growth has increased significantly over the past 20 years, with annual growth rates of 5.0% and 5.7% for Europe and North America respectively, which is small compared to the 13% increase the Middle East experienced from 2000-2007 [1]. The current contribution of the aviation sector to anthropogenic CO_2 emissions is estimated at 3% [1], which is expected to increase up to 15% by 2050, [2]. Current aviation fuel consumption is estimated at 200-250 million tons/yr. [3], [4].

The private and public sector, as well as trade associations like IATA, have set ambitious goals to decrease the contribution of the aviation industry to greenhouse gas emissions and global warming. These goals include a 10% use of renewable fuels by 2017, [5], carbon-neutral growth by 2020 and a 50% emissions decrease between 2005 and 2050 [6], [7]. South African Airways (SAA) collaborated with Boeing and SkyNRG in the Solaris Project, which aims for SAA to become a biofuel airliner by 2020 through the conversion of Solaris tobacco plants to jet fuels [8], [9]. The partners aim to have a biofuel production of 750 tons of jet fuel by 2016, 140 000 tons by 2020 and 700 000 tons by 2025 [9]. Other organizations include AIREG, a German organization, which has a strategy to use 10% alternative fuels by 2025 and BioFuels Flight Plan, a private-public partnership, which has a program to guarantee 2 million tonnes of aviation biofuel by 2020 [4].

Since aviation fuels are not limited to a specific country, specifications and regulations (DEF STAN 91-91 in the United Kingdom and ASTM D1655 in the United States of America) control the properties of aviation fuels. Since the entry of the alternative fuel components (such as Fischer Tropsch synthesized paraffinic kerosene, called FT-SPK, and Hydroprocessed Esters and Fatty Acids synthesized paraffinic kerosene, called HEFA-SPK) into the aviation industry, special allowance has been made for these fuel components after passing through the certification process and being found to be acceptable. This special allowance is provided in ASTM D7566 and DEF STAN 91-91. Unless a fuel complies with the specifications applicable to that fuel, it is not considered to be fit-for-purpose. It is therefore important that any potential alternative or renewable fuel, must adhere to the jet fuel specifications. Different options have been investigated in literature to produce renewable jet fuel, including Fischer Tropsch, Hydroprocessed Esters and Fatty Acids (HEFA) from vegetable or waste oil, Alcohol to Jet fuel, Pyrolysis oil to jet fuel and Fermented Renewable Jet.

Strict regulations regarding the aromatic content in synthetic jet fuels were introduced to prevent potential problems arising from seal swell differences [10], [11]. These regulations ensure the aromatic content in both SSJF and FSJF will not be less than a minimum of 8 volume%. It is challenging to produce sufficient quantities of aromatics with the FT process, in various distillation ranges including the jet fuel boiling range [12]. The option that was investigated in this study to produce a renewable fuel, is to perform pyrolysis on biomass to produce bio-oil, which is then upgraded, using hydrotreatment, to jet fuel and other fuels. This processing route was selected for two reasons: (1) it can utilize a renewable feedstock and (2) the bio-oil that is produced could contain a high quantity of aromatics and can possibly have a higher aromatic content present in the final jet fuel, than some of the other alternative jet fuel processing routes.

1

This study consists of two parts. Firstly the aim is to examine the effect of process parameters, specifically the feedstock particle size, moisture content and the reactor temperature, on the yields from pyrolysis and the quality and characteristics of the bio-oil product, using an experimental investigation. This will be accomplished using an experimental study for screening purposes with statistical analysis of the experimental results. Secondly, the aim is to quantify mass and energy-balances for the process where biomass is used to produce bio-oil, which is then upgraded to jet fuel, as indication of the effectiveness of upgrading bio-oil to a fuel within the jet-fuel boiling range. The results from the experimental study will be utilized, in conjunction with literature information, to determine the best pre-treatment and operating conditions for the Aspen Plus® simulation, taking into account the characteristics and quality of the final product.

1.2 Motivation, aims and objectives

1.2.1 Project motivation

Hydrodeoxygenated fast pyrolysis bio-oil has been promoted as a feasible option to serve as an additive or as a drop-in alternative to jet fuel, due to its favourable physical properties [5]. The lignin fraction in the biomass feedstock is a poly-aromatic compound that experiences structural depolymerisation during pyrolysis [13] to form phenolic compounds, char, gas and water [14]. Due to the high phenolic content of the raw bio-oil, the aromatic yield after upgrading is expected to be significant, opening the option for an aromatic rich fuel. This is especially relevant to the aviation industry as it will fulfil two important issues the aviation industry is currently confronted with, namely that conventional jet fuel is non-renewable and that the FT process for alternative fuels, produces minimal aromatics in the jet fuel boiling range. This aromatic rich fuel will have the advantage that:

1) it can be made from a renewable source
2) it is expected to contain a significant amount of aromatic components.

However, the upgrading process requires extreme hydrotreating and the aromatic content of the upgraded oil might still not be high enough to comply with the strict aviation requirements for synthetic fuels of 8-25 vol% of aromatics [10].

1.2.2 Aims and objectives

This study comprises of two main aims:

1. Firstly to obtain an understanding of fast pyrolysis process, the factors influencing it and the characteristics and properties of the bio-oil products in order to be able to develop a fast pyrolysis with upgrading simulation. This will be accomplished through the following objectives:

    a) Investigate the effect of changes in the preparation- and process-conditions, specifically the moisture content, particle size and reactor temperature, on the yield, quality and properties of the bio-oil.

    b) Determine whether these factors are statistically significant when considering the bio-oil yield and the aromatic content.

    c) Establish statistical correlations for predicting the effect of these factors on responses (e.g. the product distributions and the moisture content).

2. Secondly, to develop a fast pyrolysis upgrading simulation that can be used to quantify mass and energy balances for the biomass to bio-oil to jet fuel process to evaluate the effectiveness of the pyrolysis-to-jet processing route. This will be accomplished through the following objectives:

a) Determine how effective the process of upgrading fast pyrolysis bio-oil via hydrotreating to produce an additive or drop-in aromatic containing jet-fuel is, with regards to product mass yields, fuel properties and energy efficiency.
b) Determine the utilities and waste products associated with a pyrolysis-to-jet processing plant.
c) Establish a base-model for further use as a stand-alone fast-pyrolysis-upgrading refinery to fuels or chemical products.

1.3 Project Scope

This study is aimed at investigating the mass and energy balances associated with the production of aromatics in the jet fuel boiling range (160 ^{o}C-290 ^{o}C) from a renewable source [12]. Although many processes can be used for this purpose, the particular process that will be investigated is a fast pyrolysis process, followed by catalytic hydrotreating of the bio-oil.

The renewable feedstock investigated is limited to biomass, in particular, pine wood. The statistical significance of variability in typical operating conditions and process parameters will be investigated on a bench scale fast pyrolysis reactor available at Stellenbosch University (SU). The variable factors investigated include the fast pyrolysis reactor temperature (450°C – 500°C), the particle size (0.25mm – 2mm) and the moisture content (4% -10%). A full factorial experimental design will be used and the statistical analysis on the response results will be performed using Design Expert® software. The most significant responses that will be considered include: the liquid yield, the aromatic content, the moisture content and the HHV. The process will be simulated using Aspen Plus® v7.1 software to perform mass and energy balances to determine yields and energy requirements associated with the process. An existing fast pyrolysis model, initially developed by NREL, will be adapted for this purpose. Literature data [15], [16], [17] will serve as a basis for mass balances on the hydrodeoxygenation unit, while fast pyrolysis experimental results will be used as a guideline to identify acceptable operating and processing conditions within literature data.

2. LITERATURE REVIEW

2.1 Aviation literature and background

2.1.1 Aviation fuel background

Since commercial aviation is not limited to a country, the fuel used has to be of such a standard that it is compatible with all commercial aircrafts. This is achieved by strict standards and regulations that govern commercial aviation fuel Jet A/Jet A-1 [DEF STAN 91-91 in Europe, and ASTM D1655 in the United States of America [18]]. Historically the aviation industry relied on crude oil. Therefore, the standards and regulations were developed based on crude-derived jet fuel (conventional fuel). With the increased focus on environmental impact, alternative jet fuels have received more attention. These alternative jet fuels include synthesized paraffinic kerosene (SPK), which is a kerosene-range boiling fraction produced from non-conventional fuel (i.e. not crude oil). With the acceptance of synthetic fuels into the aviation fuel market, the regulations had to be adapted. Accepted final synthetic jet fuel blends are categorized either as semi-synthetic jet fuel (SSJF), where the synthesized paraffinic kerosene is blended up to a maximum of 50 vol% with conventional jet fuel, or as fully synthetic jet fuel (FSJF), where the entire fuel comprises of synthetic fuel. These synthetic fuels have to comply with the requirements in ASTM D7566 or DEF STAN 91-91 Annex D. The only synthesized paraffinic kerosene which are currently allowed for use in SSJF, according to ASTM D7566, are Fischer-Tropsch Synthesized Paraffinic Kerosene (FT-SPK) and Hydroprocessed Esters and Fatty Acid Synthesized Paraffinic Kerosene (HEFA-SPK), also known as Hydroprocessed Renewable Jet (HRJ). Certification of Alcohol-to-Jet Synthesized Paraffinic Kerosene (ATJ-SPK) is underway. Other options which are not yet certified but under investigation, are Pyrolysis-to-Jet Synthesized Paraffinic Kerosene (PTJ-SPK) and Fermented Renewable Jet Synthesized Paraffinic Kerosene (FRJ-SPK).

SPK fuels typically have a low aromatic content and consequently also a low density, often resulting in failure of the conventional jet fuel standards. SPK is consequently limited to a maximum of 50 vol% in SSJF, to ensure the density and aromatic content of the SSJF are still acceptable (aromatics between 8-25vol%, [10]). In a study where the material compatibility of synthetic jet fuel in fuel systems and aircraft was investigated, one item responded unfavourably – nitrile elastomer. It was concluded that the aromatics aid in the sealing characteristics of nitrile rubber [7]. Nitrile rubber represents the limiting case as it has the greatest response to the aromatic content of the fuel [19]. In the study by Corporan et al. [19], nitrile rubber absorbed significant amounts of SPK and was in good agreement with what was expected, based on the SPK fuel composition. However, when exposed to SPK after exposure to JP-8, the rubber O-rings shrank with between 7-9vol% [19]. Nitrile rubber is commonly used in commercial fleet, especially for sealing fuel tanks [7] and can therefore lead to fuel leakage problems if seals are exposed to a pure SPK after exposure to conventional jet fuel. The aromatic content is therefore an important consideration when examining alternative fuels and new synthetic jet fuels.

The main factor limiting the extent/quantity of synthetic fuel that can be used at present, is the aromatic content. If a way can be found wherein an aromatic component can be added to the processes that produce FT-SPK and HEFA-SPK, it can assist in achieving the required aromatic content of 8-25vol%, without limiting the quantity of synthetic fuel based on a too low aromatic content in the final blended fuel. This will produce a fully-synthetic jet fuel that can meet the stringent conventional fuel requirements [20].

One way to achieve this, is to consider the production of aromatics via pyrolysis, followed by upgrading. This can be motivated in three ways: (1) pyrolysis oils have relatively high aromatic

contents, with between 22.6-32.1wt% of the carbons being aromatic [21] and high densities (2) pyrolysis–to-jet has already been identified as a potential route for producing synthetic jet fuel and (3) renewable sources can be used, complying with the ambitious GHG emission reduction goals many aviation bodies and governments have set.

2.1.2 Renewable jet fuel technologies available and their commercial readiness

It is important to distinguish between renewable and alternative jet fuel. Renewable jet fuel, is jet fuel derived from a source that can be replenished in a sustainable manner. Alternative jet fuel on the other hand, is non-conventional jet fuel; jet fuel derived from a non-conventional source (i.e. not derived from crude oil). For example, FT-SPK using coal as feedstock produces an alternative jet fuel, as the feedstock (coal) is not crude oil, however it is not renewable as coal is considered a fossil fuel that can diminish. Alternatively, if the feedstock was biomass, then the jet fuel produced would still have been an alternative jet fuel, however it can now be considered a renewable fuel as the biomass feedstock is renewable with the potential to be sustainable. Renewable fuels are preferred as it has a lower contribution to the carbon cycle.

In a study on renewable jet fuel by Massachusetts Institute of Technology (MIT) and RAND Corporation, the three alternative fuels that were considered to be viable within the next decade were: (1) jet fuel from Venezuela`s heavy fuels or Canadian oil sands, (2) FT jet fuel with natural gas, coal, or coal and biomass as feedstock and (3) hydroprocessed renewable jet fuel (HRJ) [22]. Of these possibilities, only HRJ and FT with biomass feedstock, or coal and biomass combined with carbon capture and sequestration, will aid in reducing the aviation industries` contribution to climate change [22] and only HRJ and FT, with biomass as feedstock, can be considered as renewable.

For renewable-derived jet fuel production, FT-SPK, HEFA-SPK, also known as HRJ, and ATJ-SPK are the most promising technologies within the next decade [23]. Of these technologies, FT-SPK and HEFA-SPK are already approved and ATJ-SPK certification is underway [23]. Most commercial test flights have been performed on HEFA-SPK [23]. Other technologies which are still in the initial stages of commercialization, are Pyrolysis-to-Jet Synthesized Paraffinic Kerosene (PTJ-SPK) and Fermented-Renewable-Jet Synthesized Paraffinic Kerosene (FRJ-SPK) [23]. A detailed review on the advantages and disadvantages is provided by Guell et al. [23], with only a summary thereof discussed hereafter.

With FT-SPK, the feedstock is gasified to produce syngas which is passed over a Fisher Tropsch catalyst to produce a variety of commercially valuable products such as naphtha, gasoline, jet fuel, diesel, as well as heat (and potentially also electricity depending on the process configuration) [12]. The gasification products from renewable sources are similar to that of already established FT processes and the uncertainty therefore lies with the gasification of biomass [23]. No additional hydrogen is required. Major disadvantages include that a large scale is required for processing to be economical and catalyst deactivation can occur due to impurities [23].

HEFA-SPK, also referred to as HRJ, uses tallow or oil extracted from oil crops which is catalytically hydrotreated [20]. A diverse range of feedstocks needs to be considered to avoid sustainability concerns for it to replace petroleum derived fuels [23]. The main advantages include a high quality product and lower life cycle emissions compared to fossil fuels [23]. Disadvantages include that the oil yield is small, feedstocks have to compete with diesel production and the process has high hydrogen requirements [22], [23].

For the production of ATJ-SPK, feedstocks can include: sugars, starch and some lignocellulosic biomass [7]. Alcohols produced typically include ethanol, or iso-butanol [20]. Alcohols` production can either be by hydrolysis followed by microbial fermentation to alcohols; or by using thermochemical routes such as gasification to produce syngas, which can be catalytically hydrogenated or fermented, using microbial catalysts to produce alcohols [23]. The pathway from alcohols to jet fuel includes dehydration to produce olefins, followed by oligomerization, and hydrogenation to produce the correct components [23]. Main advantages include a limited hydrogen requirement and limited by-products are produced [23]. Many of the processes used are established in the petrochemical industry. Disadvantages include high production costs and low production rates, with micro-organisms having different sensitivities to impurities [23].

 In the production of PTJ-SPK, biomass is heated very fast in an inert atmosphere, to produce vapours which are then condensed to form an oil, known as bio-oil [24]. This product can be upgraded using various techniques such as hydrotreating, catalytic cracking, fluid catalytic cracking, zeolites or a combination [25]. An advantage is that a wide variety of biomass types can be used[23]. Disadvantages include that upgrading is still at the research stage and is limited by catalyst coking problems [23]. Large hydrogen requirements are necessary for upgrading [23]. In the production of FRJ-SPK, sugars are fermented by genetically designed micro-organisms to directly produce hydrocarbons, alternatively, the process can occur via catalytic chemical processing [23].

The results from Guell et al. [23] regarding the technological readiness of the different type of technologies, are summarised in Table 1. The results indicate that the FT-SPK is at the most advanced in terms of technological readiness, with a rating between 7-8 [23]. This rating represent the point where a model demonstration was completed to where an actual system was completed and had passed the tests, as can be seen from the explanations in Table 2 [26]. The fact that FT-SPK is certified also indicates greater commercial readiness. When considering the HEFA-SPK, the commercial readiness for producing diesel is much greater than is the case for jet fuel production, at 9 and 5-6 respectively [23]. According to the definitions in Table 2, the jet fuel production is at a stage where the validation in a certain environment was performed, with system demonstration in a planned environment [26]. Even though this technology is already certified, its commercial readiness is less than that of ATJ-SPK, even though ATJ-SPK has not yet been certified [23]. For sugar and starch feedstocks, the commercial readiness is at 6-7 and for lignocellulosic feedstocks it is at 4-5 [23]. For starch and sugars, the system was demonstrated in a relevant and planned environment [26]. For lignocellulose, the component validation has been performed in a laboratory environment and a relevant environment [26]. PTJ-SPK and FRJ-SPK have not yet been certified and their commercial readiness are not reported, however since PTJ-SPK is at pilot stage, it can be expected to be at level 3-4, according to the definitions in Table 2. For FRJ-SPK, which is at the research and development stage, the technological readiness can be expected at 1-2, according to the definition in Table 2.

Table 1 Technology readiness level for different technologies [a]

	FT-SPK	HEFA-SPK	ATJ-SPK	PTJ-SPK	FRJ-SPK
Certification and approval [a]	ASTM certified (50vol% blend)	ASTM certified (50vol% blend)	In certification process	Not certified	Not certified
Technology Readiness level [a]	Jet fuel: 7-8	Diesel : 9 Jet fuel : 5-6	• Jet fuel from starches and sugars: 6-7 • Jet fuel from lignocellulosic biomass: 4-5	*	*
Commerciali-zation [a]	Demonstration stage	Pilot/ Demonstration stage	Pilot/ Demonstration stage	Pilot stage	Research and development stage

* not reported , [a] all information obtained from Guell et al. [23]

Table 2 Technological Readiness Level and corresponding actions taken*

Technological readiness Level	Description of actions
9	Actual system proven by successful system and mission operations
8	Actual system completed and qualified through tests and demonstration
7	Prototype/ system model demonstration in planned environment
6	Prototype/ system model demonstration in relevant environment
5	Component validation in relevant environment
4	Component validation in laboratory environment
3	Characteristic proof-of-concept
2	Technology concept and formulated application
1	Basic principles observed and reported

*Data obtained from [26]

2.1.3 Pyrolysis to Jet route

As part of evaluating how effective the PTJ pathway is, the PTJ route can be compared to conventional jet fuel (obtained from crude oil). In particular, the properties of the raw fuels (crude oil and bio-oil) can be compared, to determine the bio-oil processing that is required to obtain a final product that is similar to conventional jet fuel. This section will also compare differences in product yields when using crude oil as feedstock, compared to using bio-oil as feedstock. Furthermore, the yields of chemical families in the final fuel, when using crude oil and bio-oil respectively, will also be considered.

Due to the significant differences between crude oil (feedstock for conventional jet fuel) and bio-oil (BO), BO has to be chemically treated to produce a fuel that will have similar characteristics and properties as that of conventional jet fuel. Bio-oil and conventional petroleum derived oils are not miscible [27]. A comparison between crude oil and bio-oil is given in Table 3. The oxygen content in bio-oil is extremely high at 37.8-40.5wt% compared to <1wt% oxygen in crude oil. The American Petroleum Institute estimated the average oxygen content in conventional petroleum derived feeds at 0.5wt% [28]. Other differences include the high moisture content of 20-30wt% in bio-oil compared to 0.1wt% in crude oil and a greater Total Acid Number (TAN) of 72-112 mg KOH/g bio-oil compared to 1 mg KOH/g crude oil.

Table 3 Comparison between crude oil and bio-oil properties

Properties	Crude oil	Raw Bio-oil
Density @15°C [kg/m³]	860 [d]	1180 [a]
Kinematic viscosity [mm²/s]	6 [e] (@50°C)	35-87 [b] (@50°C)
Moisture content [wt%]	0.1 [b]	20-30 [c]
Lower Heating Value [MJ/kg]	42-44 [b, c]	13 – 18 [c]
Carbon content [wt%] *[wt% moisture free basis]*	83-86 [d]	53.0-55.1 [a] *38.8-43.9 [a]*
Hydrogen content [wt%] *[wt% moisture free basis]*	11-14 [d]	6.4-6.7 [a] *7.6-7.7 [a]*
Oxygen content [wt%] *[wt% moisture free basis]*	<1 [b]	37.8-40.5 [a] *48.2-53.4 [a]*
H/C mole [%] **[moisture free]**	1.8-1.9 [d]	1.45 [a]
O/C mole [%] **[moisture free]**	0-0.01 [d]	0.574 [a]
TAN [mg KOH/g]	<1 [d]	72-117 [a]

[a][17], [b][25], [c][29], [d] [30], [e] data for light-medium fuel oil obtained from [31]

For the bio-oil to be compatible with current infrastructure, it is important to address these deviations from crude oil by means of upgrading the bio-oil. During the upgrading processes, waste products and by-products are also produced - reducing the mass yield of the desired product (jet fuel). The desired final product from the bio-oil feedstock determines the best-suited upgrading option. The main categories for upgrading are physical upgrading and catalytic upgrading, with the latter including catalytic cracking and hydrotreating [32]. During catalytic cracking, zeolites are often utilized. No additional hydrogen is required for the catalytic cracking process. The extent of deoxygenation in zeolite cracking is less than for hydrotreatment and the liquid mass yield also tend to be lower [25]. During hydrotreatment, hydrogen reacts with bio-oil components to remove impurities, or to hydrogenate components, resulting in the saturation of unsaturated bonds in the bio-oil components. Hydrodeoxygenation (HDO) is the hydrotreatment process where oxygen is the targeted impurity to be removed. Hydrotreatment significantly influences the components present in bio-oil and consequently also the elemental composition of the bio-oil. The aliphatic/aromatic ratio of the bio-oil is also improved through hydrotreatment, which leads to improved physical properties compared to raw bio-oil [33]. The different catalytic upgrading options are discussed in detail in Section 2.3 Upgrading literature background, to determine which upgrading option is better suited. A literature review on this indicated that HDO seems to have the best potential [25].

Table 4 summarizes the difference between product yields from treated crude oil and HDO-upgraded bio-oil from different studies. Even mild hydrotreatment products are distillable with virtually no coke formation [34]. The light fraction (gases) and the watery phase by-product streams after HDO-treatment, are expected to range between 60-75wt% (based on BO feed). This is much higher than the maximum expected from crude oils, which is only 7.9wt%. Only between 25-40 wt% of the initial BO will produce an oily phase that can be used for transportation fuel production, indicating low yields for this pathway compared to the 92.1wt% that is available from the crude oil as feed. For equal amounts of crude and BO fed, the BO will only deliver 27-43wt% of the products that crude oil produces. The main reason for this is the removal of oxygen as water, CO or CO_2. All of these products will contribute to the water phase and the gas phase, resulting in a high yield of these two by-product streams. The hydrogen consumption in HDO is estimated to be between 3-5 wt% of the BO fed for HDO of BO.

Table 4 Expected yields from BO as feed compared to crude oil as feed

Feed [wt% on BO]	Crude oil major cuts [f]	Crude oil major cuts [e]	Estimated product from HDO-BO [a]	HDO experiments [b]	HDO-BO (low O$_2$ content HDO-BO) [c,d]
Oil	100	100	100	100	100
H$_2$	*	*	3-4.5	3.2-5	3.1
Products [wt% on oil]					
Water phase	*	*	ca. 60	51-55.5	59.8
Lights (gases)	7.9	0.8		15.9-18.5	10.2
Coke	5.2	*	*	*	8.01
Naphtha range	44.0	8.9	ca. 21	[0-200°C] 7.2-13.4	8.8
Jet	9.2	7.7	*	*	6.4
Diesel range	27.5	14.8	ca. 21	[200-350°C] 10.2-12.6	6.0
Vacuum gas oil	1.0	41.8	*	6.8-9.3	3.9
Residue fuel oil	5.1	25.9	*	0.8-8.7	*

* Not reported, [a] [30], [b] [27], [c] [15], [d] BO yields obtained from mixed wood feed in [16], [e] [35], [f] [36], with lights=liquid refinery gases + still gas, Naphtha=finished aviation gasoline, jet=finished aviation gasoline, kerosene type fuel + kerosene, diesel=distillate fuel oil, VGO=lubricants + waxes, residue = residue fuel oil + asphalt road oil, coke = petroleum coke, normalized

Simulated distillation of HDO-BO shows a wide distillation range, which is also observed for petroleum products [33]. However when comparing the distillation fractions from HDO-BO to that of crude oil after distillation, there are still differences in the mass yield in the various fractions, even though the oxygen content in the low oxygen content BO (0.4wt% oxygen) is similar to the oxygen content in conventional fuel (estimated average of 0.5wt% according to the American Petroleum Institute [28]). A trade-off seems to exist between the naphtha and the jet fractions obtained from distillation, as demonstrated in Table 5. The naphtha range for crude oil is 44wt% compared to a lower 17.7-30.2wt% for HDO-BO. However the jet range for the crude oil is lower at approximately 9.2wt% compared to almost doubling to 18.7-23.1wt% from HDO-BO. It is important to take into account that the yield of the jet fraction can be manipulated (decreased) to accommodate the naphtha and diesel fractions more favourably (since the light end of the jet fuel fraction overlaps with the naphtha fraction and the heavy end of the jet fuel fraction overlaps with the diesel fraction), and this might be the case here. The diesel fraction from crude oil is higher at 27.5wt% compared to 17.2-20.6wt% from HDO-BO. However, this seems to be at the expense of the gas oil fractions, which are less than half (6.1wt%) of that of the HDO-BO (13.5-30.3wt%). The fractionation of the low oxygen content HDO-BO is also the most similar to that of crude oil, with the HDO-BO fraction of naphtha, diesel and gas oil yields being the closest to crude oil fractions` yields [33].

The process conditions for HDO-upgrading of BO to HDO BO, reported in Table 5, were selected to achieve a range of oxygen containing bio-oils [15]. The difference in fraction distribution can thus be the result of the differences in the processing conditions. Some chemical families would preferentially hydrodeoxygenate at certain processing conditions [34]. The gas oil fraction of the medium and high oxygen content BO is both significantly higher than that of the low oxygen content BO and the crude oil. This can be the result of heavy components such as the oligomers in the BO not being hydrodeoxygenated in the processing conditions that were used. During the stabilization stage, an increase in diols might be observed due to hydrogenation of sugars and aldehydes [33]. As the severity of upgrading increases, the diols disappear and at moderate hydrotreating levels of 10-

15wt% oxygen, partial demethoxylation of guaiacol to phenol occurs and furans and unsaturated ketones have been hydrogenated [33], [16].

Table 5 HDO-BO distillation fractions compared to crude oil distillation fractions

Products [wt% feed]	Crude oil feed [a]	HDO-BO feed (Low O$_2$ content of 0.4wt%) [c]	HDO-BO feed (Medium O$_2$ content of 4.9wt%) [c]	HDO-BO feed (High O$_2$ content of 8.2wt%) [c]
Oxygen in feed [wt%]	<1[b]	0.4	4.9	8.2
Lights (gases)	7.9	13.9	4.6	5.3
Naphtha range	44.0	30.2	17.7	19.7
Jet	9.2	22.0	23.1	18.7
Diesel range	27.5	20.6	18.3	17.2
Gas oil	6.1 (residue + gas oil)	13.5	32.6	30.3
Coke	5.2	*	*	*

[a] Obtained from [36], with lights= liquid refinery gases + still gas, Naphtha= finished aviation gasoline, jet=finished aviation gasoline, kerosene type fuel + kerosene, diesel= distillate fuel oil, Gas oil= lubricants + waxes + residue fuel oil + asphalt road oil, coke = petroleum coke, normalized, [b][25], [c][15]

Products from HDO-BO are expected to be different to that of crude oil refining due to differences in initial components followed by extensive hydrotreating. In Table 6 a drastic increase in naphthenes (cycloalkanes) from 7 wt% (gasoline from crude oil) to 39.6-55wt% (gasoline from HDO-BO) can be observed. This is the result of extensive hydrotreating resulting in the aromatics being saturated and forming cycloalkanes [33]. It has been found that the energy required to remove the oxygen from a phenol-ring is higher than the energy required to remove oxygen from a cyclohexane-ring [28], and consequently the deoxygenation route often occurs by first hydrogenating the aromatic-ring to a cycloalkane-ring, whereafter the oxygen is more easily removed by hydrogen to form water [28]. This is the result of the lower bond energy of R-OH than of Ar-OH, at 385 kJ/mole and 468 kJ/mole respectively [28].

In Table 6 the increase in cycloalkanes in HDO-BO is at the expense of the paraffins, which decreases from 44.2wt% to 5.2-9.5wt%. The same phenomenon observed in the gasoline is expected for the jet and diesel fractions due to similar chemical reactions occurring.

Different severities of HDO result in the removal of different oxygen-containing compounds. In a study by Oasmaa et al. [33], the oxygenated compounds found at 8.2wt% oxygen were restricted amounts of ethers, carboxyls and carbonyls in the naphtha and gasoline fraction, with noticeable amounts of phenolics in the jet, diesel and gas oil fractions. For oxygen contents of 4.9wt% just phenolic components were detected and at 0.4wt% oxygen, oxygen functional groups were not detectable in the distillate fractions [33].

Although the HDO-BO yield is only 25-44wt% (calculated from Table 4), compared to the upgraded crude oil yield of 86.8-99.1wt% (calculated from Table 4), the jet fraction in the HDO-BO will be higher than what is observed in upgraded crude oil, potentially double that from crude oil (Table 5). The high fraction of jet fuel components in HDO-BO is the main advantage of the PTJ process, to balance the disadvantage of low mass yields due to oxygen removal.

A more detailed comparison between the different options for bio-oil upgrading and the final jet fuel specifications is provided in Section 2.3.4 Upgraded bio-oil property requirements in order to select a suitable catalyst.

Table 6 Chemical compound family comparison between gasoline and HDO-BO

	Gasoline range product from HDO-BO (mixed wood) [a]		Naphtha fraction [b] [<180°C]	Hydrotreated & hydrocracked BO [c]	Typical Gasoline
Chemical compound family	Min [wt%]	Max [wt%]		[wt%]	[wt%]
Oxygenates		0.8	*	*	
Olefins	0.6	0.9	*	*	4.1
Paraffin	5.2	9.5	20.7	10.3-13.6	44.2
Iso-paraffin	16.7	24.9	12.5		35
Naphthene (cycloalkanes)	39.6	55.0	61.4 + 1.5 (poly-naphthenes)	67.9-71.6	7
Aromatic	9.9	34.6	4.03	12.0-14.1	38
Unknown	*	*	*	4.5-5.6	

*not reported, [a] [30], [b] [27] , [c] [16]

2.2 Fast Pyrolysis literature background

2.2.1 Fast Pyrolysis as thermochemical conversion overview

Thermochemical conversion is considered to be an efficient way of utilizing biomass for fuel production [37]. Pyrolysis is typically classified according to the vapour residence time and/or the medium in which it occurs: fast pyrolysis, intermediate pyrolysis, slow pyrolysis, vacuum pyrolysis. Processing conditions and product distribution differ depending on the type of pyrolysis, see Table 7. A decrease in the temperature results in an increase in char formation, from fast pyrolysis to torrefaction (500°C to 290°C), an increase of 12% to 80% char can be observed. An increase in the residence time, from fast pyrolysis to intermediate pyrolysis (2s to e.g.10s) results in an increase in the char yield, from 12%-25%. Generally, lengthy vapour residence times and low temperatures favour char production, whereas long vapour residence times and high temperatures increase gas yields, due to secondary reactions occurring [32]. Short residence times and intermediate temperatures favour the production of liquid [32].

Depending on the desired final product (liquid, char or gas), the best suited pyrolysis process can be selected. Fast pyrolysis has been selected for this study due to high liquid yields. During the fast pyrolysis process, a high heat transfer rate through the feedstock occurs, resulting in the breakage of the natural bonds found in biomass. Fast cooling of the vapours result in condensed light and heavier organic compounds to form bio-oil, the main product, while non-condensable gas and char are also formed in smaller quantities. Different constituents of biomass experience various breakdown mechanisms and consequently favour the occurrence of different phases [38]. The extent of decomposition of the biomass constituents depends on the process parameters, such as heating rate and pyrolysis reactor temperature [39]. The extent of secondary reactions, which impacts the products yield, depends on the time-temperature history to which the vapours are subjected [39]. The pyrolysis product characteristics are significantly influenced by the structural properties of the components [40].

Table 7 Process conditions and product distribution for different pyrolysis

Manner of classifi-cation	Pyrolysis process	Residence Time	Heating rate[a]	Final Tempera-ture [^{o}C]	Major Products	Char yield [wt%]	Liquid yield [wt%]	Gas yield [wt%]
Fast	Fast	<2s	Very high	approx. 500	Bio-oil	12%[a]	75%[a]	13%[a]
	Flash	<1s	High	<650	Bio-oil, chemicals, gas			
	Ultra-rapid	<0.5s	Very high	approx. 1000	Chemicals, gas			
Interme-diate[a]	Intermediate[a]	10-30 s[a]	High[a]	approx. 500[a]	Bio-oil[a]	25%[a]	50%[a] (2phase)	25%[a]
Slow	Conventional	5- 30 min	Low	600	Char, bio-oil, gas			
	Torrefaction[a]	10 - 60min[a]	Low[a]	~290[a]	Solid[a]	80%[a]	0%[a] (condensed: <5%)	20%[a]
	Carbonization	Days	Very low	400	Charcoal	35%[a]	30%[a]	35%[a]
Pyrolysis in a medium	Vacuum	2-30s	Medium	400	Bio-oil			
	Hydro-pyrolysis	<10s	High	<500	Bio-oil			
	Methano-pyrolysis	<10s	High	>700	Chemicals			

All data obtained and adapted from [24], except where [a] [32]

2.2.2 Biomass constituents, characteristics and pyrolysis-derived components

Lignocellulosic biomass mainly consists of three natural polymers; cellulose, hemicelluloses and lignin with small amounts of extractives and a variable content of inorganics [40], [39]. These components decompose at different temperatures. Cellulose decomposes at 275 – 350°C, hemicellulose at 150 – 350 ^{o}C and lignin over an extended temperature range of 250 – 500°C [41], [24]. It was found that biomass pyrolysis reactions generally consist of two stages [42]. In the first stage the cellulose is volatilized, in a very rapid reaction, resulting in a high pyrolysis rate [42]. Earlier stages of wood pyrolysis are mainly endothermic reactions that require high energy inputs to heat the biomass sufficiently for decomposition in an oxygen deficient environment (A V Bridgwater, 2012). When cellulose decomposes, vapours are formed and can be partially condensed to bio-oil. This bio-oil phase contains levoglucosan as the most significant component, as well as ketones, aldehydes, water, organic acids and char [42]. In the second stage, the lignin decomposes more slowly, resulting in a decrease of the pyrolysis reaction rate compared to the initial pyrolysis rate [42].

Cellulose is a linear polymer whereas hemicelluloses are derived from sugars like mannose, galactose, xylose and arabinose. Lignin is a branched polymer, containing phenylpropane units substituted with methoxyl and hydroxyl functional groups [43]. Lignin has an aromatic nature and contains a significant amount of aromatic rings [43], [40]. Of the three constituents, cellulose and hemicelluloses are considered to be the major contributors to the volatile matter, with cellulose being the main source of condensable vapours and light gases [24]. The hemicelluloses constituent is considered to be the main contributor to the non-condensable gases [44]. Piskorz et al. [45] reports that in a study by Evans and co-workers it was observed that light gases were derived primarily from cellulose. When cellulose is pyrolyzed in the absence of a catalyst, a monomer, levoglucosan is formed [46]. Levoglucosan is the main primary intermediate from cellulose decomposition [45]. At temperatures higher than 500°C, the monomer is vaporized and primarily contributes to the oil and

gas yields [44]. Lv et al. [42] observed that the gas yield increased as the cellulose content of the biomass increased, supporting their conclusion that the cellulose component is thought to be responsible for the volatile matter.

Different proposed mechanisms have been developed to explain the structural mechanisms occurring during pyrolysis of cellulose. In a study by Piskorz et al. [45], a simple scheme involving two parallel reactions from cellulose to char and the other reaction to volatiles/gases were described. In their study, this model was further adapted to include a pathway for decomposition of tar to gas. The scheme shows that the polymer chain, consisting of monomeric glucose units, is disrupted to form anhydrosugars, such as levoglucosan. The anhydrosugar can be further degraded in a number of ways; further dehydration followed by decomposition, or alternatively by direct cleavage and rearrangement of the levoglucosan. From the study by Piskorz et al. [45], it was concluded that the decomposition of cellulose to liquid, for high temperatures and short residence times, occurs via a preferred route and not randomly. The cellulose monomer is usually cleaved at the C-O bonds, resulting in a two-carbon (2C) and a four-carbon (4C) segment. The rearrangement of the 2C-segment allows the production of a fairly stable product, such as hydroxyacetaldehyde. The 4C-segment undergoes a series of reactions such as dehydration, decarbonylation, scission and condensation to a range of products. Stable products from the 4C-segment can include hydroxycarbonyl and carbonyl compounds [45]. Degradation products from fast pyrolysis of biomass for the cellulose fraction yields levoglucosan, hydroxyacetaldehyde, 5-hydroxymethylfurfural, acetol and formaldehyde.

Branca et al. [47] similarly observed two main routes for cellulose degradation during their studies on the conventional pyrolysis of beech wood; degradation to produce levoglucosan, and fragmentation and partial recombination to hydroxyacetaldehyde, acetic acid, hydroxypropanone and a few minor species [47]. From their investigation of the chemical products produced from conventional pyrolysis of beech wood, it was concluded that holocellulose (i.e., hemicelluloses and cellulose) decomposition leads to the formation of carbohydrates and furan derivatives.

Hemicelluloses comprise of a hetero-polysaccharide composition [14]. Hemicelluloses are considered to be the least stable of the three biomass constituents and produce more volatiles than cellulose [14]. It is thought that this instability can be a consequence of the structure of hemicelluloses [44]. The degradation of hemicelluloses produces furan and furfural [48], [49]. Acetic acid in bio-oil originates from the acetyl-groups released from hemicelluloses during degradation [14].

It is reported that although lignin decomposes over a large temperature range, the maximum decomposition occurs from 350-450°C [50]. Only about 10% of the lignin weight ends up in the gaseous products and contributes almost 35% to the liquid yield [24]. Lignin produces mainly oligomeric products and to a lesser extent phenols, cresols, syringols and guaiacols [48], [49]. Lignin is considered to be the main contributor of phenolics in pyrolysis liquids [51], [14]. During lignin decomposition, ether bonds as well as some carbon-carbon bonds are cleaved, which yield phenols [52]. Lignin is reported to produce more aromatics and char compared to cellulose decomposition [53], [42]. Lignin decomposition also yields bio-oil and water [42]. Branca et al. [47] observed that the primary degradation products from lignin were syringol and guaiacols, with phenols produced as secondary products at increasing temperatures [47], [14]. Syringol and guaiacol production is maximized between 477-527°C [47].

Woody biomass can be classified into softwood and hardwood. Softwoods mainly contain coniferyl alcohols (approximately 90%), whereas hardwoods contain approximately equal amounts of coniferyl alcohol and sinapyl alcohol. The presence of additional methoxy groups on the aromatic rings in hardwoods result in more linear structures compared to softwood [54]. The products derived from lignin, and the ratio of these products, produced during the fast pyrolysis of hardwood and softwood biomass, differ. Softwood lignin yields 98% guaiacyl derivatives, whereas hardwood lignin yields 37% guaiacyl and 63% syringyl derivatives [55]. The weight-average molecular weight of hardwood pyrolytic lignin is smaller than that of softwood pyrolytic lignin due to the unsubstituted ortho-position to the phenol hydroxyl which is present in softwood lignin, resulting in a greater tendency to polymerize [55].

Since the pyrolysis product characteristics are significantly influenced by the structural properties of the components, an appropriate biomass feedstock should be selected, to maximise the yields of particular products of interest in the pyrolysis oil [40]. Woody biomass produces higher liquid yields compared to straws, hay and grasses, therefore woody biomass was the biomass of choice for this study [56]. Since the abundance of lignin is greater in softwood than in hardwood [54], it is expected that a woody biomass with a high lignin content (like a softwood) will result in greater aromatics content present in the bio-oil, compared to a woody biomass with a low lignin fraction (like a hardwood), due to the aromatic nature of lignin [43], [40].

2.2.3 Pyrolysis products and possible uses

The bio-oil constituents are produced by different pyrolysis reactions from the various components of biomass, resulting in certain components favouring the formation of specific products [24]. The proportions of products (solid, gas and liquid) depend on several factors including the operating conditions [24] and ash content in the biomass [32]. Inorganics present in the biomass and char (formed during pyrolysis) act as catalyst for secondary cracking reaction of vapours [32].

Bio-oil consists primarily of phenolic compounds and can be considered as a micro-emulsion [24]**.** The continuous phase of the micro-emulsion is a solution of small lignin decomposition molecules and cellulose and hemicelluloses decomposition products [24]**.** The discontinuous phase consists of some of the molecular fragments of the cellulose, hemicelluloses and lignin polymers, which neglected to be pyrolyzed, but is largely composed of lignin macromolecules [46]. The liquid produced usually contains a significant amount of oxygenated compounds [57]. The bio-oil product is mostly from vapours and aerosols, which is cooled and condensed to form a dark brown liquid [32]. The bio-oil can be used as a feedstock for energy generation, to produce heat, electricity or transport fuels, or for chemicals production [32].

The non-condensable gaseous phase, which evolves from primary decomposition reactions, is reported as primary gas. Non-condensable gases are typically: H_2O, CO_2, CO, C_2H_2, C_2H_4, C_2H_6 and C_6H_6 [24]. Often when the vapour residence time is long enough, the condensable gases undergo secondary decomposition reactions [24]**.** This decomposition occurs through gas phase homogeneous reactions and/or through gas-solid heterogeneous reactions [24]**.** The gas-phase reactions that occur, are cracking reactions of the vapours, leading to non-condensable gases with low molecular weights that are non-condensable [24]**.** These gases are known as secondary gases [24]. The final gas mixture is therefore a combination of both primary and secondary gases [24]**.** The remaining gases after cooling and electrostatic precipitation are usually not condensable and are

vented to the atmosphere, or burned as an additional energy source for the pyrolyzer, depending on the design [32].

The char produced can be used as bio-material for the production of high added value solids such as bio-char and adsorbent after upgrading. Otherwise, it can also be burned to generate heat for the process to make the process more energy efficient [32]. The ratio in which the char, bio-oil and non-condensable is produced can be manipulated. This will be studied in Section 2.2.4 Factors influencing fast pyrolysis products.

2.2.4 Factors influencing fast pyrolysis products

The product yields and bio-oil composition depend on the process conditions and feedstock composition [32], [24]. Various literature studies have investigated the influence of pyrolysis process parameters and feedstock conditions on the product yields [27] , [58], [59], [38], [21], [56]. Some studies have also investigated the impact of the process conditions and feedstock on bio-oil composition [60], [42], [21]. According to literature, the factors that influence the product yields and bio-oil composition are: heat transfer rate, biomass particle size, reactor temperature, moisture content, biomass composition and the hot vapour residence times. Some of the influential factors cannot be changed directly, but needs to be manipulated using other physical changes.

a. Heat transfer

Heat transfer rate is a critical parameter for the pyrolysis process since high energy inputs are required for the process due to the endothermic nature of the pyrolysis process [32]. Heat transfer can be influenced by the particle size, depending on the type of pyrolysis reactor, and reactor temperature [39].

b. Biomass particle size

Particle size influences both the pathway of the product vapour to exit the particle and the heat transfer within the particle. The biomass particle size needs to be small enough to increase the heat transfer rate throughout the biomass particles [32], [38]. Large particles will have larger thermal gradients within the particle and thus require longer periods to heat the centre of the particle. Furthermore in large biomass particles the pathway before the vapour product is released is longer, resulting in an extended contact period between the gas and char [24]. Since the char has a catalytic effect, this can result in more secondary reactions occurring [27].

Meier and Faix (1999) reported that particle sizes should typically not exceed sizes of 2-6mm. This fits recommended particle sizes smaller than 3mm [32]. Kalgo (2011) states that particle sizes should be smaller than 2mm [38]. However too small particle sizes are not practically and economically feasible and can also result in entrainment if particles are smaller than 250 µm [61], [62]. Maximum bio-oil yield have been reported with particle sizes of 0.25-1mm (0.54mm average) compared to a 1-2mm particle size range [63].

c. Reactor temperature

Temperature has an effect on the yield and the composition of the products [24]. One of the reasons for the important role of temperature on the yields and quality of products, is that different constituents of the biomass decompose at different temperatures [24]. Elliott (1986) suggested a hypothetical pathway of tar chemical degradation, see below [64], [14].

$$\underset{(400\ ^oC)}{mixed\ oxygenates} \rightarrow \underset{(500\ ^oC)}{phenolic\ ethers} \rightarrow \underset{(600\ ^oC)}{alkyl\ phenolics} \rightarrow \underset{(700\ ^oC)}{heterocyclic\ ethers} \rightarrow \underset{(800\ ^oC)}{PAH} \rightarrow \underset{(900\ ^oC)}{larger\ PAH}$$

15
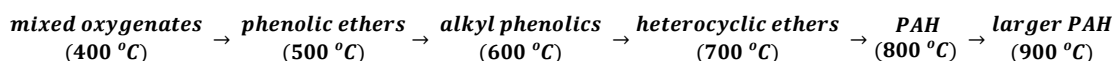
The type of components can be related to the reaction temperature the vapours were exposed to before cooling [14]. The pathway does not consider steps being bypassed, or the formation of gas or char products, although these mechanisms are also possible [64]. According to Elliott (1986) an increase in temperature from 600°C to 800°C results in a decrease in the phenolic nature of products, accompanied by an increase in the polycyclic aromatic hydrocarbon (PAH) components [64]. This fits with the explanation by Mohan et al. [14], which reports an increase in temperature results in the alkyl groups` splitting from aromatic compounds, where after the aromatic compounds condense to form PAH and larger PAH`s. According to the hypothetical chemical degradation pathway, an increase in alkyl phenolics should be observed from 500°C to 600°C. Results from a study by Heo et al. [65] supported this and showed an increase in the mono-aromatic and polycyclic hydrocarbon content of the bio-oil (derived from *Miscanthus sinensis*) at the maximum temperature investigated (550°C), even with biomass containing low lignin contents (10-20 % for *Miscanthus sinensis* vs 27-30% for softwoods). It was also observed that the oxygenates, such as levoglucosan, decrease rapidly at high temperatures of 550°C whereas the alkyl phenolic components, like phenol and 4-methyl phenol, increases [65]. This agrees with Elliott`s (2010) hypothetical chemical degradation pathway mentioned above. In a different study, an increase in reactor temperature (from 400°C to 600°C) also increased the aromatic fraction, however a decrease in the alkyl hydrocarbon fraction occurred [21].

Studies by Joubert et al. [63] and Kim et al. [66] have indicated that reactor temperature is the most significant factor for optimization of the bio-oil yield. Maximum bio-oil yield was reported to occur at 460°C for rice husk and rice straw [67]. For woody biomass materials, the maximum bio-oil yield is typically obtained at 500°C [52], [58]. In a study by Chen et al. [59], the maximum bio-oil yield produced from forest waste (camphor tree) was at 500°C. Other studies have also observed maximum liquid yields at 500°C, for both Indian Jatropha and African Moringa biomass [38] and for *Pinus strobus* [21]**.** However for *Eucalyptus grandis*, maximum bio-oil yields were obtained at 470°C [63]. For Indian Jatropha, it was determined that the maximum organic liquid is produced at 550°C, indicating that the optimal temperature for organic liquid yield can differ from the optimal point of maximum liquid yield [38]**.** The temperature also influences the char yield, with an increase in reactor temperature decreasing the char yield [59]. In the study by [21] an increase in temperature (from 500°C to 600°C) increased the gas yield.

d. Moisture content

The total moisture present in the bio-oil is the combined initial biomass moisture and the pyrolytic water by-product from pyrolysis. Reaction water can contribute as much as 12 wt% on dry wood basis [32]. Moisture present in biomass requires volatilization, which increases the energy demand for biomass heating to reach the pyrolysis temperature, and therefore lowers the temperature gradient and increases the residence time from entry into the reactor as a solid to vapour. It has also been suggested that free water will vaporize explosively, which can tatter the feed particles [14]. This process can possibly aid in heat transfer [37], [14]. It is recommended that the moisture content of biomass should be below 10 wt%, as this helps in minimizing the total water present in the bio-oil [32].

e. Biomass constituents

When identifying the factors which influence the pyrolysis product distribution, the biomass composition (cellulose, hemicelluloses, lignin and alkali-salts) also needs to be included [68]. It has previously been found that the agricultural residues with high lignin contents produced low organic yields; whereas woody biomass with high cellulose contents, produced high organic yields [69], [38]. This is further supported by the fact that cellulose is considered to be the main source of

16

condensable vapours, whereas hemicelluloses are considered to be the major contributors to volatile matter [24]. Lignin is reported to produce more char than cellulose [53], [42]. Nowakowski et al. [70] found that the fast pyrolysis of lignin resulted in a lower bio-oil and a higher char yield. Mohan et al. [14] agreed that high lignin contents result in lower liquid yields, in the range of 60-65 wt%, however a higher energy density is obtained compared to liquids high in cellulose-derived components. In a study by Lv et al. [42], it was observed that a higher cellulose content leads to a faster pyrolysis rate and a higher lignin content leads to a slower pyrolysis rate. Faster pyrolysis rates will produce higher liquid yields and slower fast pyrolysis rates will produce lower organic liquid yields. The study by Lv et al. [42] therefore fits with the other studies discussed.

Alkali-salts also influence the pyrolysis product yield and product composition. Huber et al. [13] stated that alkali-salts can have an even greater effect than temperature on the reaction mechanism. The metals/ash present in the biomass and the char formed during pyrolysis act as catalyst for secondary cracking reaction of the vapours [24], [32]. Alkali-metals catalyse secondary reactions, thereby decreasing the organic yield and increasing the gas and total water yields [56]. In a study by Fahmi et al. [60], the product yields and bio-oil composition were analysed using different types of biomass. The results showed that metal components had a more significant effect on the product yields than the lignin content had. In order to ensure that the liquid yield is high, the char needs to be removed rapidly to limit cracking, alternatively the hot vapour can be cooled swiftly to condense to bio-oil [32]. The alkali-metal content also influences the bio-oil quality, with metal constituents favouring ring opening and reducing acidic compound production [60].

f. Hot vapour residence time

The residence time of the hot vapours in the reactor influences the extent to which secondary cracking between the char, or ash in the char, and the volatile products occur. Secondary reactions will lead to the condensable gases being converted to lower molecular weight molecules, which are often not condensable, resulting in a reduced bio-oil yield and a larger gas yield [32]. Lower process temperatures and longer vapour residence times tend to favour char production [37]; high temperatures and longer vapour residence times favour gas production and moderate temperatures with short vapour residence times favour liquid production [32].

A summary of the ranges that has been investigated in literature, is provided in Table 89 in Appendix B.1.

2.2.5 Bio-oil properties and characteristics

In a review of fast pyrolysis and product upgrading, bio-oil is considered to be a micro-emulsion [32]. The continuous phase, a solution of holocellulose decomposition products, stabilizes the pyrolytic lignin macro-molecules which forms the discontinuous phase, by means of hydrogen bonding [32]. Bio-oil is typically a dark brown liquid, and is typically influenced by the presence of micro-carbons present in the liquid and the composition of the liquid.

The bio-oil heating value, density and viscosity can vary significantly, depending on the amount of water present. Bio-oil`s water content can range from 15wt% to almost 50wt%, with an oxygen content varying between 35-51wt% [32], [24]. At 25wt% water, the higher heating value is roughly 17MJ/kg. Bio-oil density is approximately 1200 kg/m^3 [24]. The bio-oil viscosity is further influenced by the thermal and storage degradation which have occurred and the feedstock used. Viscosities measured at 40°C, were observed to range from 25m^2/s up to 1000m^2/s. Bio-oil is thermally unstable and when heated above 100°C, a rapid reaction occurs and a solid starts to form. Viscosity can

change on account of thermal changes, as well as aging (time). Usually a slow increase in viscosity is observed with time, due to secondary chemical reactions occurring. The presence of char in bio-oil can increase the rate at which the secondary reactions occur [32]. Due to the acidity of the bio-oil (pH typically ranging between 2-3), normal materials of construction, like aluminium and carbon steel, have proven to be unsuitable [71], [72], [25], [24]. Materials found to be resistant to corrosion include: cobalt materials, stainless steel and some polymers like polyethylene and polypropylene [72].

2.2.6 Bio-oil composition analysis

Bio-oil can contain as many as 300 different compounds [73], which complicates the analysis. Bio-oil comprises of hundreds of components, of which approximately only 40-50 % of the oil`s character have been identified, excluding the moisture [74]. The complexity of bio-oil analysis is supported by the differences in analytical results obtained from analysis of the same oil by various laboratories. In a study by Branca et al. [47], bio-oil analysis is compared to that of round robin testing results. Round robin testing concluded that chemical characterization was not consistent [75]. This is supported by another study conducted in 1997 in which not a single compound (from over 100 identified) was identified by all 10 laboratories able to analyse for bio-oil at the time [76], [74].

Due to the complex compositional nature of bio-oil, detailed analysis cannot be performed using a single method, instead a combination of methods are utilized to characterize as many as possible components. Compositional analysis is typically performed using a combination of Gas Chromatography (GC) with Mass Spectroscopy (MS) and Nuclear Magnetic Resonance (NMR) methods. Due to the complexity of the composition analysis, a literature review on the different approaches follow.

2.2.6.1 Using GC-MS analysis to determine bio-oil composition

Components with high molecular masses (such as components which were less harshly cracked during pyrolysis, components with high polarity and re-polymerized and de-polymerized components), have a low volatility and make using GC analysis difficult [29], [74]. Components that do not evaporate in the injector systems cannot be identified by GC techniques [74], which limits the use of GC to lighter distillable components.

A large quantity of sugars are expected to be present in bio-oil, up to 30 wt% [74].   However many of the sugars cannot be detected by GC, therefore the focus has mainly been on quantification of levoglucosan [74].

Marsman et al. [77] reports that hyphenated methods are usually suitable for the analysis of complex mixtures, such as pyrolysis oils. In their study, the ability of Gas Chromatography-Mass Spectroscopy (GC-MS) and 2 dimensional GC with Flame Ionization Detection (GCxGC-FID), to analyse bio-oil and hydrodeoxygenated bio-oil is examined and compared. The columns used were a SolGel (polydimethylsilicone: PDMS) column and a phenyl cyanopropyl modified PDMS column, with Helium as carrier gas and split injection techniques. It was reported that GCxGC-FID analysis resulted in improved analysis compared to GC-MS [77].

 The relative area of the GC chromatograph for a specific component can be used for an approximation of the quantity of the components present in the bio-oil for relative comparison between two samples [78]. The main variation between GC-MS analyses, is in the type of column used. Different columns are more sensitive to detect different components. Kim et al. [66] used a HP-

5MS capillary column with helium acting as the carrier gas, to analyse the composition of palm kernel shell derived bio-oil, focusing specifically on the phenolic compounds. In the study by Heo et al. [65], the GC-MS analysis was used qualitative and quantitatively for the characterisation of *Miscanthus sinensis* derived bio-oil. The column used was also a HP-5MS capillary column, with helium gas as the carrier gas [65].

In another analysis, a GC-MS analysis performed on rice residue derived bio-oil, the column used was a Varian Cp-sil 8cb capillary column, with helium as carrier gas [67]. The MS was conducted at 70eV, similar to the analysis performed by Marsman et al. [77] on beech pyrolysis oil. The study by Li et al. [67] obtained two-phase bio-oil. The components identified in the GC-MS analysis of the upper phase can be classified into the family classes such as: carbonyls, acids, sugars, phenols, substituted phenols and furans. The lower phase of the study consisted only of four groups: phenols, phenolic substitutes, carbonyls and furans [67]. In one study the components identified in the GC-MS analysis were classified into the following classes: organic acids, aldehydes, furans, ketones, sugar based compounds and syringols and guaiacols [77]. In a different study where the bio-oil produced from *Eucalyptus grandis* was investigated, the component classes were characterized according to: aldehydes, ketones, phenols, sugars, furans and acids [79]. In this particular study, it was observed that the overall results of the chemical families were similar for the small and large biomass particle size [79].

From the GC-MS literature, it can be concluded that hyphenated methods such as GC-MS are acceptable for qualitative and quantitative analysis. However, even with GC-MS analysis available, identification and quantification of components can be difficult. Both the type of GC-detector and the type of GC-column affects the results and should be selected with care.

2.2.6.2 Using NMR analysis to determine bio-oil composition

Nuclear Magnetic Resonance (NMR) is a method which uses the magnetic property of different structural groups and bonds to determine which quantity of an element (in this study 13-C isotope and 1-H proton) is present in that specific structural group or bond type. The chemical shift values give an indication of which functional group is present. The integrated area for the specific chemical shift is used to determine the quantity of the element that contains the specific functional groups associated with that chemical shift range. Deviation from the true content and the analysis results can be experienced due to complete substitution of the Carbon atom [80]. This will result in no NMR signal and these carbons will accordingly not be accounted for using the C-NMR analysis. Proton NMR spectroscopy does not account for all aromatic carbons. When methyl groups are attached to a carbon in a ring structure (e.g. xylene), there are no remaining hydrogen and consequently no signal [80]. Furthermore the chemical shift ranges can measure more than a single type of bond, for example the proton NMR range from 8-10 ppm measures aldehyde protons, but also low field aromatic protons. Distinguishing between the types of proton/carbon in a shift range that experiences change can therefore be difficult and might skew results for the whole shift range due to a single type of bond changing.

To obtain a quantified value of the different chemical groups, a method which utilizes the ^{1}H NMR analysis results can be used. This method was used for the analysis of gasoline`s aromatics, olefins and paraffins from the ^{1}H NMR results [80]. This method relates the NMR analysis results of %C or %H atom quantities to vol%. The aromatic, paraffin and olefin content can be determined using this method from Equation 1-3, obtained from Myers et al. [80]. The ranges of A - F in Equations 1-3, as

obtained from [80], are indicated in Table 8. The chemical shift ranges using proton-NMR, available in literature, are also provided in Table 8.

$$Aromatics\ [vol\%] = \frac{\left(A + \frac{C}{3}\right) \times 10^2}{\left(A + \frac{C}{3}\right) + \left(D + \frac{E}{2} + \frac{F}{3}\right) + B} \qquad\qquad\text{Equation 1}$$

$$Paraffins\ [vol\%] = \frac{\left(D + \frac{E}{2} + \frac{F}{3}\right) \times 10^2}{\left(A + \frac{C}{3}\right) + \left(D + \frac{E}{2} + \frac{F}{3}\right) + B} \qquad\qquad\text{Equation 2}$$

$$Olefins\ [vol\%] = \frac{B \times 10^2}{\left(A + \frac{C}{3}\right) + \left(D + \frac{E}{2} + \frac{F}{3}\right) + B} \qquad\qquad\text{Equation 3}$$

Table 8 Chemical shift ranges as reported in literature for H-NMR

Chemical shift range [ppm]	[14]	[80], [81]	[82]	[37]
10				
9				-CHO, -COOH, downfield ArH
8	Aromatic protons			
6.8		Ring aromatic [A]	Aromatic ring [a]	ArH, HC=C (conjugated)
6.6				HC=C (unconjugated)
6.5				
6.4	Phenolic or olefinic protons			
6				=CHO, ArOH, HC=C (non-conjugated)
5		Olefins [B]	Olefins [b]	
4.5				
4.2	Ring-joined methylene			
4				CH3O-, -CH2O-,=CHO
3.3				
3				
2.5		Alpha methyl [C]		$CH3\ddot{C}-$, CH3-Ar, -CH2Ar
2.2			Methine (paraffins) [d]	
2				-CH2-, aliphatic OH
1.6	CH$_2$, CH beta to an aromatic ring (naphtenic)	Methine (paraffins) [D]		
1.5	beta-CH$_3$, CH$_2$, and CH gamma or further from an aromatic ring			-CH3, -CH2-
1		Methylene (paraffins) [E]	Methylene and methyl (paraffins) [e, f]	
0.9	CH$_3$ gamma or further from an aromatic ring	Methyl (paraffins) [F]		
0.6				
0.5				
0				

[c] obtained at approximately 2.5 ppm.

A similar method and correlations, based on the correlations described above, have been used in the analysis of bio-oils [81], [83]. The aromatic, olefinic and paraffin content of pyrolytic liquids can be determined using Equations 4-6, as described by [81]. The chemical shift ranges associated with a - f

20

in Equations 4-6, are provided in Table 8. The table should be interpreted as: the ring aromatic protons, according to Myers et al. [80], ranges from 6.6 to 8 ppm, whereas it ranges from 6.5 to 8 ppm, according to Sınağ et al. [82].

$$Aromatics\ [vol\%] = \frac{\left(a+\frac{c}{3}\right)0.97 \times 10^2}{\left(a+\frac{c}{3}\right)0.97 + \left(d-2b+\frac{e}{2}+\frac{f}{3}\right)1.02 + 3.33b} \qquad \text{Equation 4}$$

$$Aliphatics\ [vol\%] = \frac{\left(d-2b+\frac{e}{2}+\frac{f}{3}\right)1.02 \times 10^2}{\left(a+\frac{c}{3}\right)0.97 + \left(d-2b+\frac{e}{2}+\frac{f}{3}\right)1.02 + 3.33b} \qquad \text{Equation 5}$$

$$Olefins\ [vol\%] = \frac{3.33b \times 10^2}{\left(a+\frac{c}{3}\right)0.97 + \left(d-2b+\frac{e}{2}+\frac{f}{3}\right)1.02 + 3.33b} \qquad \text{Equation 6}$$

For a ^{13}C NMR analysis, the typical chemical shift ranges found in literature are provided below in Table 9. The table should be interpreted as: the carbonyl carbons, according to DeSisto et al. [21], ranges from 163 to 215 ppm, whereas the carbonyl carbons, according to Christensen et al. [15], ranges from 170 – 205 ppm and from 205 ppm to 225 ppm.

Table 9 Chemical shift ranges as reported in literature for 13C-NMR

Chemical Shift Range[ppm]	DeSisto et al. [21], Ingram et al. [37]	Christensen et al. [15]
225		
215		
205		Carbonyl carbons
180	Carbonyl carbons	
170		Carboxyl carbons
163		
158		
145	Aromatic (general)	Phenolic carbons
125		
120	Aromatic Carbons (guaiacyl compounds)	Aromatic H-C
112		
110	Aromatic compounds (syringyl compounds)	
84	Carbohydrate type carbons	
65		
55	Methoxy-, hydroxyl-bound compounds	Ether carbons
54		
34	Primary, secondary, tertiary & quaternary alkyl carbons	
24	Primary, secondary, tertiary & quaternary alkyl carbons (secondary & tertiary carbons)	
6	Primary, secondary, tertiary & quaternary alkyl carbons (most primary & some secondary carbons)	Aliphatic carbons
1	Primary, secondary, tertiary & quaternary alkyl carbons	
0		

2.3 Upgrading literature background

2.3.1 Bio-oil upgrading and upgrading options

Significant differences exist between raw bio-oil properties and jet fuel specifications. A comparison is provided in Table 10. In Table 10 column SSJF indicates the specifications for the overall blended jet fuel (conventional jet fuel blended with <50 vol% FT-SPK or HEFA-SPK) and column FT/HEFA-SPK indicates the specifications applicable only to the synthetic part of the fuel (the FT-SPK or HEFA-SPK before it is blended to less than 50 vol% with conventional fuel to produce a SSJF). Major differences include a considerably lower carbon content in bio-oil than the jet fuel specifications allow, with a bio-oil maximum of 55.1 wt%, compared to minimum requirement of 99.5 wt% according to the FT/HEFA-SPK   specification. The moisture content and TAN values in bio-oil exceed the jet fuel specification for FT/HEFA-SPK. The moisture content in bio-oil ranges between 20-30 wt%, compared to a maximum of 0.0075 wt% allowed in FT/HEFA-SPK. The TAN value of 72-117 mg KOH/g in bio-oil exceeds the maximum specifications of 0.015 mg KOH/g SPK and the 0.1 mg KOH/g SSFJ. These deviations between the bio-oil properties and the jet fuel specifications can be addressed by upgrading the bio-oil to produce a product similar to conventional jet fuel.

Table 10 Comparison between raw bio-oil properties and jet fuel specifications

Properties	Raw Bio-oil	SSJF (ASTM D7566) [d]	FT/ HEFA- SPK (ASTM D7566) [d]
Density @15°C [kg/m³]	1180 [a]	775-840	730-770
Kinematic viscosity [mm²/s]	35-87 [b] (@50°C)	≤ 8 (@-20°C)	*
Moisture content [wt%]	20-30 [c]	*	<0.0075
Lower Heating Value [MJ/kg]	13 – 18 [c]	42.8	*
Carbon content [wt%] *[wt% moisture free basis]*	53.0-55.1 [a] *38.8-43.9 [a]*	*	>99.5
Hydrogen content [wt%] *[wt% moisture free basis]*	6.4-6.7 [a] *7.6-7.7 [a]*	*	
Oxygen content [wt%] *[wt% moisture free basis]*	37.8-40.5 [a] *48.2-53.4 [a]*	-	-
H/C mole [%] *[moisture free]*	1.45 [a]	-	-
O/C mole [%] *[moisture free]*	0.574 [a]	-	-
Total Acid Number [mg KOH/g]	72-117 [a]	<0.1	<0.015
Aromatics [wt%]	-	8-25vol%	<0.5

[a][17], [b][25], [c][29],   [d] [11], * Not directly specified in ASTM D7566

Upgrading of bio-oil has been extensively reviewed with a variety of processes available [32], [34]. The major groups include: physical upgrading (emulsion forming, filtration and solvent addition) and catalytic upgrading (esterification, gasification, catalytic cracking and hydrotreating) [32]. The desired final product from the bio-oil feedstock determines the best suited upgrading option.

Experimental results from Venderbosch et al. [74] indicated that during upgrading of the bio-oil, polymerization of the bio-oil occurs to form char components if a catalyst or hydrogen is not present, however in the presence of hydrogen or a catalyst, stabilized components form. Catalytic upgrading processes are usually used in biofuel production due to the improved product stability when using a catalyst [32]. Options available for catalytic upgrading are primarily modified conventional hydrotreating, (typically via hydrodeoxygenation) yielding a naphtha-like product, or zeolite cracking yielding an aromatic product [84].

Fuel yields for pyrolysis with bio-oil upgrading have been estimated to range between 15-45wt%, depending on the type of upgrading process used [85]. Early estimations showed that the maximum stoichiometric yield that can be obtained by hydrotreating bio-oil is 56-58 wt% on bio-oil. This relates to an energetic yield of 69-73% (includes the hydrogen generation requirements) [84]. The maximum stoichiometric yield that can be achieved by zeolite cracking is 42% on bio-oil for a mono-functional catalyst and 55 wt% on bio-oil for a bi-functional or multi-functional catalyst [84]. Predicted yields for hydrotreating and zeolite processes can be viewed in Table 11. Crude oil products from hydrotreating are approximately 8.4 wt% higher than is the case for zeolite cracking and 2.6 wt% higher for refined hydrocarbons, for the more conservative 70% bio-oil yield as is estimated to be the case for commercial scale bio-oil production [86]. The maximum yield of aromatics that can be expected from wood is 42-55% [87].

From a study by Baldauf et al. [27], the final upgraded and distilled fuels did not meet the required gasoline and diesel specifications, therefore it was proposed that the pyrolysis oil should be a co-feedstock to a crude oil refinery where it can be fed to the crude oil distillation tower. Processes such as co-refining have recently received more attention as this process requires a smaller extent of hydrodeoxygenation and less catalyst deactivation occurs. In a study by De Miguel Mercader et al. [88], it was concluded that the molecular weight distribution for a co-refining process was similar to hydrotreating only fossil oil and that the origin of the HDO oil did not influence the molecular weight distribution. Such an approach will be useful for an integrated bio-oil and petrochemical refinery. Hydrotreated bio-oil with approximately 5 wt% oxygen were co-fed with an aromatic hydrocarbon feedstock in a minor FCC facility to produce a gasoline with a RON value of 96, that met the EU specifications [89]. However the extent to which deoxygenation needs to be performed prior to co-processing for successful operation is unclear [90].

Catalyst deactivation has been a reported in various studies and is regarded as a major hindrance in the development of bio-oil upgrading [84], [27], [25]. Concerns regarding the commercial feasibility have been expressed due to inadequate catalyst life-time and performance [84], [27], [25]. Limited catalyst lifetime has been identified as a concern for both hydrodeoxygenation and zeolite cracking upgrading options [25].

Table 11 HDO vs Zeolite cracking predicted product yields

	Hydrotreating		Zeolite cracking	
	Mass basis [wt% dry wood feed] [a]	Mass basis [wt% dry wood feed] [a,b]	Mass basis [wt% dry wood feed] [a]	Mass basis [wt% dry wood feed] [a,b]
Pyrolysis oil	83%	70%	83%	70%
Crude hydrocarbons	30.5%	25.7%	20.5%	17.3%
Refined hydrocarbons	27.5%	23.3%	24.5%	20.7%

Data obtained and adapted from, [a][84], [b] Bio-oil yield modified to a more conservative 70% as in [86] for commercial scale

In summary of the above discussion, jet fuel specifications and raw bio-oil show significant differences indicating that bio-oil upgrading is required. This can be achieved using various processes, however zeolite cracking and hydrotreating are considered to be the most advanced and are well researched in literature. A recent development includes co-refining, however data on co-refining is still too limited for simulations that will meet the objectives of this study. The catalytic upgrading options identified were reviewed more closely in Sections 2.3.2 Zeolite Cracking and Section 2.3.3

Hydrotreating. The review will assist to determine which catalytic upgrading option is best suited to meet the requirements, as discussed in Section 2.3.4 Upgraded bio-oil property requirements in order to select a suitable catalyst of this study.

2.3.2 Zeolite Cracking

When catalytic cracking occurs in the presence of zeolite catalysts, chemical reactions occur where impurities (present in the reactant molecule), are removed to produce by-products and smaller product molecules. In zeolite cracking processes, the oxygen impurity is removed from the system as H_2O and CO_2. However, as no additional hydrogen is added, the reaction is hydrogen limited for both the aromatics produced and the water formation [84].

Zeolite catalytic research initially investigated mono-functional ZSM-5 catalysts [84]. A wide range of zeolite cracking catalysts has been tested in continuous set-up systems. These include typical fluid catalytic catalysts (HZSM-5), as well as some modified catalysts such as GaHZSM-5, ZnHZSm-5, H-Y, H-mordenite, MgAPO-36, SAPO-11 and SAPO-5 [25]. Studies on bi-functional and multi-functional catalysts have also been performed. These catalysts are expected to operate in a carbon limited environment due to their capability to generate hydrogen in-situ, by means of shifting the CO in the product gas [84]. Processing conditions are typically at atmospheric pressure, while temperatures range between $330^{o}C – 600^{o}C$ with hourly space velocities of approximately 2 [84], [25]. In a review, the degree of deoxygenation [DOD= (1- wt% oxygen in product/ wt% oxygen in feed) x 100] ranged between 50-53% and oil yields ranged between 12-28 wt% for a variety of different catalysts [25]. The similarity in zeolite cracking processing conditions to that of bio-oil production, potentially makes it processing and economically advantageous [84].

2.3.3 Hydrotreating

Hydrotreating of bio-oil employs high pressures ranging between 70-200 bar to ensure a high hydrogen partial pressure [84]. High hydrogen requirements exist for this process, with the excess hydrogen varying between 100-200% to maintain the required high hydrogen partial pressure [84]. This increases the solubility of hydrogen in the bio-oil, resulting in a greater hydrogen availability in the area of the catalyst [25].

Hydrotreatment is often performed in two reactors, with the first reactor performing a milder hydrotreatment to   stabilize the oil at 250-275°C [84]. The first stage`s purpose is to prevent polymerization at the higher temperatures ($350 – 400^{o}C$) employed in the second reactor, where more extensive hydrotreatment occurs [84]. The first stage significantly reduces the TAN and the oxygen content [30]. During this stabilization stage, the sugars and aldehydes are hydrogenated to alcohols [33]. It has been suggested that the cellulose-derived fraction preferably be converted first, in a mild-hydrotreating step to alcohols [90]. It is believed that the carbonyls are mainly responsible for the instability of bio-oil [33]. As the hydrotreatment increases in severity, a decrease in the alcohols occur, together with the hydrogenation of furans and ketones and the demethoxylation of guaiacols to yield phenols [33].

Many studies have employed a two stage reactor set-up to prevent charring and help hydrogenation [91]. In a previous study, a two stage reactor set-up was found to reduce the hydrogen consumption by 13%. Furthermore using a hydrocracking catalyst in the second reactor was observed to lead to a 30% increase in the gasoline yield [34]. Recently a single non-isothermal reactor set-up with two

separate catalyst beds have been investigated [16],[17]. When the same bio-oil was tested on the two-stage set-up and the non-isothermal reactor, similar bio-oil compositions were obtained [16].

The different phases produced during hydrotreatment upgrading are organic liquid (oil), aqueous liquid (watery phase), gas and char. The severity of hydrotreatment and the degree of deoxygenation determine whether one or two organic liquid phases will form [90]. According to a study, the bio-oil remains in a single organic liquid phase at mild hydrotreatment conditions [33]. At moderate conditions, a heavy oxygenated organic phase forms at the bottom, with an aqueous phase in the middle and a low-density hydrocarbon phase at the top [33]. At the most severe hydrotreating conditions the aqueous phase forms at the bottom with only a single organic phase, consisting of low density hydrocarbons, forming at the top [33].

In addition to the severity of the hydrotreatment, the hydrotreating residence time also influences the product composition, with an increase in reaction time resulting in less reactive components, such as guaiacols, being converted to more stable products like catechols and finally to phenols [55]. The type of catalyst used in hydrotreatment will also influence the product composition. Typical product composition from hydrotreating usually include methyl-, ethyl-, and propyl-substituted phenols, catechols and guaiacols, although this is also affected by the catalyst selection [55].

Conventional hydrotreating catalysts, such as $NiMo/Al_2O_3$ and $CoMo/Al_2O_3$, were initially used, although alumina or alumina silicate supported catalysts were found to be unstable, which resulted in high degrees of coking and catalyst deactivation [91], [32]. More recent investigations have been into noble-metal and bi-metal catalysts. A wide range of conventional catalysts ($Ni-MoS_2/Al_2O_3$, $Co-MoS_2/Al_2O_3$) and more recently developed noble metal catalysts (Pd, Pt, Ru and Rh on supports of C, ZrO_2, TiO_2, Al_2O_3 and Al_2O_3/SiO_2) have been tested in batch and continuous set-ups for the HDO process [92], [25]. A summary of such experiments is provided elsewhere [25]. Temperature and pressure ranges over which hydrotreating experiments have been performed are 300 - 400°C and 80 – 300 Bar over 0.2-4 hrs. The degree of deoxygenation {DOD= (1- wt% oxygen in product/ wt% oxygen in feed) x 100} vary between 28-100% and oil yields between 26-81% [25].

2.3.3.1 Conventional Catalysts

Traditional catalysts for hydrotreating include CoMo or NiMo on alumina and were initially used in the petrochemical refinery industry. Between CoMo and NiMo, CoMo has higher selectivity for hydrodeoxygenation [34]. Furthermore, the NiMo catalyst produced a more saturated product and had a larger hydrogen consumption compared to CoMo [17].

Conventional catalysts experience instability in the presence of high water contents [93], [32]. This is problematic as much of the oxygen is removed from the bio-oil components in the form of water, producing large water quantities during upgrading. The catalyst instability at high water quantities leads to coking and catalyst deactivation [91]. In the study by Baldauf et al. [27], catalyst deactivation occurred and steady state could only be achieved for short periods. In a study by Elliott et al. [16], a conventional hydrocracking catalyst (expected to be $NiMo/AlSO_3$), was used to investigate the hydrocracking of already hydrotreated bio-oil. In their investigation catalyst deactivation did not occur. Conventional sulphurized catalysts also experience sulphur stripping, requiring constant re-sulphurization of the catalyst [32].

Due to the limitations of the conventional catalysts, research into more recent noble-metal catalysts and bi-functional catalysts has increased [32], [94]. In a study where conventional catalysts (NiMo

and CoMo on alumina) were compared to noble metal catalysts, it was observed that the conventional catalysts are less active than the noble metal catalysts [91].

2.3.3.2 Noble metal Catalysts

Noble metal catalysts which have been investigated in literature include palladium (Pd), platinum (Pt), ruthenium (Ru) and rhodium (Rh) on a variety of supports, including carbon (C), ZrO_2, TiO_2, Al_2O_3 and Al_2O_3/SiO_2 [25]. Both the noble metal and the catalyst support influence the oil yield and the extent of deoxygenation. The type of catalyst also influences the product composition, however other factors such as the catalyst online time and the reaction time can also have an impact on product composition.

The catalyst support can influence both the oil yield and the extent of deoxygenation. Carbon was the best catalyst support to maximize deoxygenation and TiO_2 was the best for maximizing the oil yield, with carbon being the second best for maximizing the oil yield [91]. It was concluded that carbon support seems to be the best option for maximizing both the oil yield and the extent of deoxygenation [91].

Catalysts containing different metals of Ru, Pt and Pd metals were investigated for mild hydrotreatment (250°C and 100 bar) and severe hydrotreatment (350°C and 200 bar) [91]. For mild hydrotreating Pt/C produced the largest oil yield of approximately 57wt% at a 27wt% oxygen content. Pd/C had the second largest oil yield at approximately 44wt%, but with a lower oxygen content of 18.5 wt%. A trade-off between the oil yield and the oxygen content seems to exist. The catalyst that best maximizes the oil yield and minimizes the oxygen content, is Pd/C for mild hydrotreating [91]. When considering severe hydrotreating, Pd/C had an oil yield of 65wt% and approximately 6.2wt% oxygen, Ru/C had a lower oil yield of 53wt% and a lower oxygen content of approximately 5.8 wt%, while Pt/C had the lowest oxygen content of approximately 10wt%, but a low oil yield of only 27wt% [91]. For severe hydrotreating Ru/C showed the best performance with regards to achieving a low oxygen content [91]. It can be concluded that the Pd/C is the best catalyst for mild hydrotreating and Ru/C is the best catalyst for severe hydrotreating [91].

The hydrotreating products are also influenced by the type of catalyst used [95]. Pd and Pt catalysts are known for their decarboxylation activities with regards to organic acids, resulting in high quantities of CO_2 produced, although Pd catalysts also produced significant amounts of CH_4 [91]. CO_2 is also produced during thermal cracking (22mole%), therefore the CO_2 production can be attributed to two different processes: catalytic cracking and thermal cracking [91]. In a study where different noble-metal catalysts (Ru, Pd and Pt) were investigated, it was confirmed that Pd and Pt catalysts have a higher hydrogen requirement. Both these catalysts enable the saturation of the double C-C bonds and this was especially the case for Pd/C [91]. The aliphatic/aromatic ratio was higher for Pd/C than for Ru/C [91], showing that Pd allows for the most saturation of double bonds between the metals Ru, Pd and Pt. Very little char was produced when using a carbon support, with the lowest char yields observed for Pd, nearly at zero [91]. Ru/C catalysts typically produce methane (process of methane production known as methanation), which results in a higher methane production for Ru/C than for Pd/C [95]. Methane production was found to be a strong function of the catalyst used, more specifically it was related to the level of Ru dispersion on the support, with a decrease in the dispersion of metals for a Ru/C catalyst resulting in methane reduction [95].

From empirical equations obtained from experiments, the difference between the stoichiometric amounts of methane produced for Ru/C and Pd/C can be seen: 0.026 mole/1mole BO and 0.06

mole/1mole BO for the Ru/C and Pd/C respectively, with the Pd/C catalyst producing more methane. However Pd/C produces more ethane and propane at 0.02 mole/mole BO and 0.005 mole/1mole BO (for ethane and propane respectively) compared to 0.01 mole/1mole BO and 0.0025 mole/1mole BO for Ru/C. Total gas yields for Pd/C is higher than for Ru/C at 0.085 mole/1mole BO and 0.0385 mole/1mole BO respectively [91].

In addition to the type of catalyst, the hydrotreating products are also influenced by the online time of the catalyst and the reaction time [95], [96]. The CO_2 fraction increases with use, and the CH_4 decreases with catalyst operation/ catalyst recycling; with the CO_2 increasing at the expense of CH_4 when using a Ru/C catalyst [95]. Reaction time also influences the gaseous products and carbon distribution, with a gradual increase in the amount of higher alkanes (C_2H_6, C_3H_8, C_3H_6) observed for an increase in reaction time from 1 to 6hr using a Ru/C catalyst [96].

Catalyst deactivation of noble metal catalysts have also been observed in some studies [16], [95]. Commercial application will require catalyst regeneration once the catalyst starts to become ineffective. Typical regeneration includes controlled oxidation to eliminate coke, although carbon-supported catalyst will not be regenerable with methods used for alumina support [97], [17]. It has been proposed that the noble metal present in the catalyst can be recovered by burning the carbon-support catalyst [17].

Comparison between noble metal catalysts and conventional catalysts indicated that noble metal catalysts are more reactive. Carbon support is best suited as it has a good trade-off between oil yield and deoxygenation, with Pd/C preferred for mild hydrotreatment at less severe conditions and Ru/C preferred for severe hydrotreatment at more severe conditions.

2.3.4 Upgraded bio-oil property requirements in order to select a suitable catalyst

For jet fuel (produced from bio-oil) to be compatible with current infrastructure and to comply with the jet fuel specifications (discussed in Section 2.3.1 Bio-oil upgrading and upgrading options), deviations between bio-oil and jet fuel specifications have to be addressed by upgrading of the bio-oil, either through hydrodeoxygenation or zeolite cracking.

When determining which of the bio-oil upgrading options are best suited, it is important to take the final product into account - making sure that the final product is fit-for-purpose, ideally with minimal processing and compatible with current infrastructure [25]. Since the final application is aimed at producing an aromatic-rich jet fuel or additive, it is important to identify the strict jet fuel standards where there will likely be deviation between jet fuel and upgraded bio-oil. Stricter specifications apply to SPK than to the conventional fuel (to which the SPK is added), or to the final blended product (SSJF). This can be seen in Table 12. The TAN requirements for SPK are a low 0.015mg KOH/g SPK compared to the allowed 0.1mg KOH/g crude derived Jet A fuel. The SPK fuels also have the additional requirement that the combined hydrogen and carbon should equal or exceed 99.5wt%. This implies that the oxygen content in these fuels must be lower than 0.5wt%. Another important requirement is that the moisture content of the SPK must be equal to, or less than 0.0075wt%. These specifications, the TAN, oxygen content and moisture content, are important considerations when determining which of the upgrading processes will produce a fuel fit-for-purpose.   The one exception where the specifications are less strict, is the density of the SPK, at 730-770 kg/m^3 compared to 775-840 kg/m^3. The SPK requirements therefore provide a limiting case as the

specifications it needs to comply with are harder to accomplish. Setting these specifications as the benchmark is therefore a conservative approach.

Table 12 Jet fuel property requirements which HDO-BO are most likely to fail

	Specifications for Aviation Turbine Fuels (conventional fuel) and Aviation Turbine Fuel Containing Synthesized Hydrocarbons (SSJF)		FT-SPK / HEFA-SPK (blending component)	
Specification	**Acceptable range**	**Standard**	**Acceptable range**	**Standard**
Density [@ 15 ^{C}C]	775-840 kg/m^3	ASTM D7566 & DEF STAN 91-91	730-770 kg/m^3	ASTM D7655
Total Acid Number	<0.10 mg KOH/g < 0.015 mg KOH/g	ASTM D7566 DEF STAN 91-91	0.015 mg KOH/g	ASTM D7655
Carbon + Hydrogen content	*	*	>99.5wt%	ASTM D7655
Moisture content	*	*	<75 mg/kg	ASTM D7566

* Not directly specified in [11], [98] or [10].

A comparison between the fuels produced from the different types of upgrading processes compared to the jet fuel specifications, is given in Table 13. Although both HDO and zeolite cracking result in significant changes in the bio-oil properties, the product from HDO is closer to the requirements for jet fuel. The oxygen content in the HDO is much lower than for zeolite treated oil, at 0.2-2.7wt% for HDO and 13.3-24.4wt% for zeolite treated bio-oil, see Table 13. This is much higher than the <1wt% oxygen in crude oil (reported in Table 3) and 27 times greater than the maximum contribution oxygen can have in SPK (assuming a maximum of 0.5wt% oxygen), see Table 13. The elemental carbon content in raw bio-oil ranges from 53-55%, while this increases to 61.4-79.0wt% for zeolite treated bio-oil and to 84–88% for hydrotreated bio-oil. The carbon content for HDO bio-oil overlaps with the 83-86 wt% carbon in crude oil (reported in Table 3), with the zeolite treated bio-oil not meeting this quantity even after upgrading. The elemental hydrogen content range also compares favourably with that of crude oil (11-14wt%, reported in Table 3) after upgrading, with an increase from 6.4-6.7wt% to 10.4-13.6wt% for HDO bio-oil. Zeolite treated bio-oil`s hydrogen content is much smaller than that of crude oil and HDO bio-oil at 1.5-7.8wt%.

Table 13 Comparison between raw bio-oil, upgraded bio-oil and jet fuel specifications

Properties	Raw Bio-oil	Upgraded Bio-oil (HDO)	Upgraded Bio-oil (Zeolite)	SSJF (ASTM D7566) [e]	FT/ HEFA- SPK (ASTM D7566) [e]
Density @15°C [kg/m³]	1180 [a]	760-920 [a]	-	775-840	730-770
Kinematic viscosity [mm²/s]	35-87 [b] (@50°C)	0.8-4.2 [b] (@50°C)	-	≤ 8 (@-20°C)	*
Moisture content [wt%]	20-30 [c]	0.01-0.33 [a]	-	*	<0.0075
Lower Heating Value [MJ/kg]	13 – 18 [c]	40-42 [b, c]	22-34 [b, c]	42.8	*
Carbon content [wt%] *[wt% moisture free basis]*	53.0-55.1 [a] *38.8-43.9 [a]*	83.5-87.5 [a]	61.4-79.0 [d]	*	>99.5
Hydrogen content [wt%] *[wt% moisture free basis]*	6.4-6.7 [a] *7.6-7.7 [a]*	10.4-13.6 [a]	1.5-7.8 [d]	*	
Oxygen content [wt%] *[wt% moisture free basis]*	37.8-40.5 [a] *48.2-53.4 [a]*	0.2-2.7 [a]	13.3-24.4 [d]	-	-
H/C mole% [moisture free]	1.45 [a]	1.53-1.94 [a]	-	-	-
O/C mole% [moisture free]	0.574 [a]	0.002-0.042 [a]	-	-	-
Total Acid Number [mg KOH/g]	72-117 [a]	<0.01-2.7 [a]	-	<0.1	<0.015
Aromatics [wt%]	-	-	-	8-25vol%	<0.5

Data obtained and adapted from a review by [25], [a][17], [b][25], [c][29], [d][99], [e][11], * Not directly specified in ASTM D7566

From a mass balance perspective, HDO produces more oil. The phase yields after upgrading using HDO can be up to 65wt% compared to a maximum of 28% for zeolite cracking, see Table 14. The carbon or char yield for zeolite cracking is larger than is the case for HDO, with the maximum carbon from HDO similar to the minimum of zeolite cracking at 26wt%. The yield of crude hydrocarbons and refined hydrocarbons is 25.7wt% and 23.3wt% on a dry wood basis for HDO, compared to 17.3wt% and 20.7wt% on a dry wood basis for zeolite cracking, as indicated in Table 11.The HDO yields are again higher compared to the zeolite cracking yields.

Table 14 Phase yield for HDO vs catalytic cracking

	HDO [a]	HDO [c]	Zeolite cracking [a]
Oil yield [wt%]	21-65	32.3 – 36.3	12-28
Water phase [wt%]	13-49	51.0 – 55.5	24-28
Gas yield [wt%]	3-15	15.9 – 18.5	6-13
Carbon yield [wt%]	4-26		26-39

Data obtained from [a][25], initially obtained from [99], [100], [b][99], [c][27]

Overall HDO upgrading has less concern regarding catalyst coking and also produces higher crude and refined hydrocarbon yields (see Table 11) [25]. Although zeolite cracking produces a higher

aromatic content, which is desired in this study, efforts to produce a fuel that has a high aromatic content, but poor grade qualities, will be in vain as the product will fail the strict jet fuel specifications [25]. High aromatic contents with low mass yields and high waste products are also not desirable. Fuels produced from zeolite cracking are not of an acceptable grade for current infrastructures [25]. Mortensen et al. [25] concluded that HDO is the most feasible option for hydrotreating of bio-oil for a commercial scale facility since it is the most promising route to produce similar grade and priced fuels to fossil fuels . However both of these routes still have a significant way to go to industrial application [25].

2.3.5 Reactor types for bio-oil hydrotreating

Due to rapid catalyst deactivation, fixed bed reactors are not recommended as these reactors require frequent regeneration of the catalyst [27]. It was suggested that the bio-oil be pre-filtered to remove any char carry over, specifically for fixed bed hydroprocessing [17]. Depending on the catalyst support, regeneration might not be possible. Catalysts on alumina support, such as NiMo and CoMo, are regenerable [17]. More recent catalysts for the hydrodeoxygenation of bio-oil are often on carbon support, which cannot be regenerated using typical oxidative methods employed on alumina supported catalyst [17]. However the metal can be recovered by burning of the carbon- supported catalyst as a cost effective method [17]. Limited experimental information is available for alternatives to fixed bed reactors, however ebullated bed or liquid phase reactors with a homogenous catalyst, could be more promising in the future [27].

2.3.6 Mass balances on hydrotreating

Each stage of the bio-oil hydrotreating process produces four different phases: an oily phase (the desired phase), an aqueous phase, a solid phase and a gaseous phase. The experimental literature often contains information regarding the final oily phase, although information regarding the elemental and molecular composition of the gas and solid phases are limited. For complete mass- and elemental- balances, the elemental composition of the initial bio-oil and at least three of the product phases are required.

2.3.6.1 Solid formation overview

Solids that form during hydrotreating of bio-oil constitute heavy polymers and coke [101]. Coking is undesired as it can affect the catalyst performance [95]. In bio-oil hydrotreating the coke product can be excessive and must therefore be accounted for during mass balances, with coking deposits of up to 50wt% observed in experiments [95]. The formation of coke in packed beds, especially when temperatures surpass 350°C, have also been reported [91].

The catalyst used in a study with an isothermal reactor, was Pd/C and most likely NiMo/Al$_2$O$_3$ [16]. In a similar study using a non-isothermal reactor Ru/C and NiMo or CoMo/C catalysts were utilized[17]. In the isothermal reactor set-up where two separate catalyst beds were used and hydrotreating and hydrocracking occurred independently, coking was observed for the hydrotreating catalyst bed of Pd/C, in some cases so much that the experiments had to be terminated. Only slight coking occurred on the hydrocracking catalyst bed, with a minor crust at the reactor top, but no deposition on the catalyst bed [16]. For the non-isothermal reactor set-up with two sequential catalyst beds of sulphided Ru/C and NiMo or CoMo, fine powder was observed in the Ru/C bed, with coke-like material formed between the interface of the first and second catalyst bed, when NiMoS was used in the second catalyst bed [17]. In the same set-up with a CoMoS/C catalyst in the second catalyst bed, no coking was observed, however, a fine powder had formed between the catalyst

pellets. Even after filtration of the bio-oil, the powder formation occurred at the interface of the two catalysts beds [17].

 In a different study where different catalysts and their phase yields were investigated, there was no solid formation on a Pd/C catalyst for both mild hydrotreating and severe hydrotreating, although a loss of ca. 15wt% was observed for mild hydrotreating [91]. This is in contrast to the solid formed, but not quantified on the Pd/C catalyst bed in the study for an isothermal reactor set-up [16]. In a different study, the solid content for hydrotreating on a Pd/C catalyst was 1.2wt% and 1.22wt% for operating temperatures of 250°C and 300°C respectively [101]. The low coke yields were attributed to the type of catalyst, with a Pd/C catalyst giving the lowest coke yields [101].

Investigation into the effect of recycling Ru/C catalysts in a batch reactor with experimental duration of 4.3 hrs showed that solids increased from 3% to 20wt% from initial use to the third use [95]. This indicates that for continuous operation, coking might become a problem as Time on Stream (TOS) increases. Wildschut et al. [95] also investigated using different precursors for Ru/C catalyst production and found that the type of precursor has an effect on the phase yields ranging from 0-4.7% of solids. In a different study where batch hydrotreatment was carried out over 6hrs, the solids content seemed to increase over the first hour from zero to approximately 6wt% on dry basis, whereafter it stayed almost constant with a slight decrease to approximately 4wt% on dry basis for the next 5hrs, until termination of the experiment [96].

An empirical solids chemical formula of $CH_{1.5}O_{0.35}$ was obtained from elemental composition of the different phases for hydrotreating over a Ru/C catalyst for 6hours [96]. In a different study also using a Ru/C catalyst, also with beech pyrolysis oil and similar pressures and temperatures (200 bar and 350°C), the empirical formula for the solids that formed, was determined to be $CH_{1.31}O_{0.11}$ for a 4 hour experiment [91].

The reviewed literature indicates that the solid yield is highly dependent on numerous factors, including the TOS, the catalyst precursor and the type of catalyst. Empirical correlations, determined from an elemental balance, are usually used to define the chemical composition of the solids formed.

2.3.6.2 Gas composition for conventional hydrotreating catalysts

Elliott et al. [16] reported that the gases produced from the second hydrotreating reactor in a continuous set-up, where the second reactor contained conventional hydrotreating catalyst, were primarily hydrocarbons. However, in a batch set-up study by Wildschut et al. [91], the hydrocarbons only contributed 45mole% compared to the CO_2 contribution of 53mole%, as shown in Table 15. In the study by Wildschut et al. [91] raw bio-oil was used as feedstock, whereas in the study by Elliot et al. [16] hydrotreated bio-oil was used as feedstock. Baldauf et al. [27] reported gas yields for a continuous set-up using a NiMo catalyst and a CoMo catalyst respectively, see Table 15. Significant differences can be seen for the CO_2 concentrations indicated in Table 15.

Table 15 Gas composition for conventional hydrotreating catalysts

Catalyst	CoMo/Al_2O_3 [a]	NiMo/Al_2O_3 [a]	NiMo catalyst [b]	CoMo catalyst [b]
Set-up	Severe hydro-treating (batch)	Severe hydro-treating (batch)	1 stage continuous	1 stage continuous
CO_2 [mole%]	ca. 52.94	ca. 53.26	19.81	18.83
CO [mole%]	ca. 1.96	ca. 1.09	3.64	0.86
CH_4 [mole%]	ca. 33.33	ca. 31.52	42.56	37.30
C_2H_4 [mole%]	ca. 0.98	ca. 1.09	0.00	0
C_2H_6 [mole%]	ca. 7.84	ca. 8.7	22.40	25.09
C_3H_6 [mole%]	ca. 0.98	ca. 1.09	0.00	0.00
C_3H_8 [mole%]	ca. 1.96	ca. 3.26	9.76	11.38
C_4 hydrocarbon [mole%]	*	*	1.82	6.52

[a] [91] , [b] [27] , * not reported

2.4 Process Simulation Literature Background

2.4.1 Overview of techno-economic and process simulation studies for biomass to hydrocarbons and jet fuel via pyrolysis

The purpose of this study is to investigate using fast pyrolysis followed by upgrading to produce jet fuel from woody biomass. In order to do this, the literature pertaining to such a process needs to be evaluated to identify gaps and shortcomings. Modelling studies focusing on pyrolysis with hydrotreating as upgrading option to produce jet fuel, are scarce. For this reason literature studies extending to biomass pyrolysis followed by upgrading to produce hydrocarbons (of which the jet fuel is a part, although often not necessarily considered by itself as a product, but frequently expressed as a part of the naphtha/gasoline and diesel fuels) were considered.

A techno-economic analysis for bio-oil production for a stand-alone fast pyrolysis plant has been performed [104]. Literature reviews on utilizing fast pyrolysis followed by upgrading for fuel production have predicted fuel yields and have identified technological restrictions that should be addressed [84], [25]. Simulation modelling studies focusing only on fast pyrolysis, followed by bio-oil upgrading to hydrocarbon fuels, have been performed by Jones et al. [57], Wright et al. [106], Wright et al. [107] and Brown et al. [108]**.** A review of the scope and findings of the different studies mentioned follows.

In a study by Bridgwater (1996), the production of high grade chemicals and fuels via catalytic pyrolysis were discussed, hydrotreating and zeolite upgrading were considered, although no simulation modelling was performed. Recommendations included that zeolite cracking is more sensitive to the feedstock price due to smaller conversion efficiency, while capital costs are less for zeolite cracking. Furthermore, it was concluded that hydrogen supply from an existing refinery is the best short term prospective. Mass yields and energy efficiencies were only specified for the naphtha and diesel fractions, but not for the jet fuel fraction. Crude hydrocarbon mass yields were estimated at 30.5wt% (of dry wood feed) with refined hydrocarbon mass yield at 27.5wt%. Energy efficiencies for crude hydrocarbon production and refined hydrocarbon production were ca.38% and ca. 36% respectively. Bridgwater (1996) recommended further research into upgrading catalysts and into the integration of the catalytic upgrading for improved efficiency [84].

In a review on bio-oil catalytic upgrading to engine fuels, Mortensen et al. [25] also recommended that catalyst improvement and understanding of the kinetics and mechanism during upgrading still require clarification, similar to Bridgwater (1996). A summary of the technological status for zeolite cracking and hydrotreating showed that hydrotreating is currently the better option. Upgraded oil

yields for hydrodeoxygenation range between 21 to 65wt% on bio-oil [25]. Assuming a 70.7 wt% bio-oil yield on dry biomass [86], the hydrodeoxygenated bio-oil is calculated at 14.8 to 46wt%mass yield on biomass.

Ringer et al. [104], on behalf of NREL, did a techno-economic study on a large scale fast pyrolysis process. This included developing and modelling the facility in Aspen Plus®, which served as a basis for many other pyrolysis models [102], [103]. Unfortunately the final product from the model is bio-oil and some electricity exportation and upgrading to transportation fuels were not considered and modelled [104].

A techno-economic study by Anex et al. [105] considered three different pathways of producing transportation fuel; pyrolysis, gasification and biochemical pathways. Aspen Plus® process simulation software was used in the study to create detailed mass and energy balances. The plant capacity was 2000 tons of corn stover/day. Results revealed that the selling price is the most sensitive to the feedstock cost and the fuel produced from pyrolysis has the lowest gasoline equivalent. Fast pyrolysis is followed by hydroprocessing of the bio-oil, with two different scenarios considered for hydrogen production, namely purchasing hydrogen and reforming of the bio-oil to produce hydrogen. The products from the pyrolysis upgrading include naphtha and diesel range fuels with the focus on the total liquid fuel yield being reported [105]. The yields in the different fuel fractions and the specific components present in the individual fractions are not reported.

Holmgren et al. [30] considered different processing routes for the production of transportation fuels from cellulosic biomass, including pyrolysis upgrading. Experimental results reported in their study indicate fuel yields of 21wt% for the naphtha and 21wt% for the diesel range (based on the pyrolysis oil feed). No mention of process modelling is made. Other fuel fractions such as jet fuel is not reported. The minimum and maximum of the upgraded bio-oil chemical family composition is reported in terms of the paraffins, iso-paraffins, olefins, oxygenates, naphthenes and aromatics [30].

A detailed study by Jones et al. [57], investigated the hydrotreating and hydrocracking of biomass fast pyrolysis oil to produce gasoline and diesel fuels, using CHEMCAD software. The plant capacity was 2000 dry tons/day using hybrid poplar wood chips, with a total production of 76 million tons/year of gasoline and diesel. The hydrotreated pyrolysis oil had an oxygen content smaller than 2% [57]. Co-locating the pyrolysis-upgrading plant with an existing refinery could reduce the capital investment and the minimum fuel selling price. Hydrogen production was from steam reforming of the hydrotreater offgas and natural gas. The feasibility of the process is sensitive to the catalyst performance and catalyst lifetime, with the pyrolysis processing having less of an influence on the feasibility [57].

In a modelling study by Wright et al. [106], a techno-economic analysis was performed on upgrading of fast pyrolysis derived bio-oil to transportation fuels such as naphtha and diesel products, using Aspen Plus® software. The plant capacity was 2000 dry-tons/day, similar to another study by Jones et al. [57], with corn stover as feedstock; annually delivering 134 million litres of fuels (112 410 tons/year), when producing hydrogen on-site [106]. This is almost double the production reported in the study by Jones et al. [57], for a similar biomass feed capacity. Different scenarios were considered for hydrogen supply; on-site production and commercial hydrogen. The on-site hydrogen production was by means of bio-oil reforming. A sensitivity analysis for this scenario revealed that the fuel yield is a key variable for the scenario. Mass yields from this study show a 25wt% yield for

33

fuel products on the feed when hydrogen is produced on-site. When hydrogen is purchased, this yield increases to 42wt% [106]. The biomass-to-liquid fuel energy efficiency for the scenario where hydrogen is produced on-site, was 36% [106]. The focus was on naphtha and diesel as final products, with jet fuel not considered as a product. The composition of the upgraded bio-oil was modelled by C8 and C10 compounds [106], as C_8H_{18} and $C_{10}H_{22}$, without detailed final product compositions. Wright et al. [106] recommended that this process is still at the development stage, with limited system performance publicly available. It was further recommended that the catalyst performance as well as quality of bio-oil require further research, with uncertainty in the fields of bio-oil separation technology adding to the challenges [106], [107]. This is in agreement with the recommendations from Mortensen et al. [25] and Bridgwater [84].

The study by Brown et al. [108] is an updated analysis of a fast pyrolysis and hydroprocessing pathway previously investigated [107], taking into account recent advances in the technology. The plant capacity of 2000 dry tonnes/ day with a corn stover feedstock did not change from the initial study, with gasoline and diesel as final products with export electricity. Major differences between the two studies, [108] and [107], include the use of CHEMCAD software for the fast pyrolysis and hydroprocessing model. The latest study also encompassed a boiler and turbo-generator system with a heat exchanger network, which were modelled using Aspen Energy Analyser®. Further modifications include more detailed process development, such as the inclusion of a debutanizer and fuel splitters. A major difference in the assumptions is the final fuel yield, which was decreased from 58.2 MGY (million gallons per year) to 57.2 MGY. Sensitivity analysis from the study indicated that the fuel yield is the most important variable, followed by the bio-oil yield. This fits with the study by Wright et al. [106]. The sensitivity analysis in their study re-emphasized the importance of assumptions, especially the yields, due to the high sensitivity of the MFSP and hence project feasibility to yields. Final fuel products only include gasoline and diesel, with an assumed evenly split between the two fuel fractions. Jet fuel is not considered as a final fuel product and yields are not reported.

The literature available on the modelling of pyrolysis to jet fuel suggests that studies utilizing biomass to produce bio-oil, followed by hydrotreating to produce fuels, are limited. The available studies typically do not have detailed component information, making it difficult to accurately predict the true fuel yields. Additionally, it complicates determining how suitable the fuel is for its purpose and whether the fuel will meet the required specifications. The specifications of jet fuel require accurate knowledge of the oxygen and moisture content as well as the aromatic fraction, to know whether the HDO-BO and jet fractions will adhere to the strict specifications and requirements. Furthermore, in none of the available studies the jet fuel range aromatic yield is reported. This study aims to fill these gaps, by utilizing literature data to develop an Aspen Plus® simulation model that will quantify the mass and energy balances as indication of the effectiveness of converting biomass to jet fuel and jet fuel boiling range aromatics. From the simulation model, the product yields, utility requirements and certain fuel characteristics can be determined, while representing the final fuels more accurately to determine the extent of suitability of the final fuel.

2.4.2 Determining plant capacity for model
In order to determine the scale of the fast pyrolysis and hydrodeoxygenation plant, a reasonable plant capacity had to be determined, taking into account the final use of the fuel. For feedstock with a high energy density, transportation to a centralized refinery is the best option due to high capital costs of the refinery construction. However when the feedstock has a low energy density, such as

biomass with typical bulk densities of 150 kg/m^3, transportation costs to a central refinery becomes a concern (examples of energy density of fossil fuels vs biomass). This has led to an increased interest in decentralized fast pyrolysis units to produce a higher density feedstock (bio-oil with a typical density of 1200 kg/m^3) which can then be transported to a centralized refinery for upgrading [32]. Decentralized fast pyrolysis plants as big as 100 000 ton/yr. are feasible and close to commercialization [32]. Decentralized plants have both advantages and disadvantages and are summarized by Bridgwater [32]. One specific advantage is that large scale has the advantage that the production cost decreases [32], although the capacity is limited by the technology available. Bridgwater (2012) reported a production cost of 300-400Euros/ton for a 1000 dry ton/yr. facility, compared to a 60-200 euros/ton for a 500 000 ton/yr. refinery [32].

Industrial fast pyrolysis systems employing fluid beds with high capacities, are operated by Dynamotive in Canada with a maximum size of 8000kg/hr. Other types of reactors have also been used industrially; a transported bed reactor used by Ensyn in Canada capable of delivering a maximum capacity of 4000 kg/hr, an auger/screw reactor by Abritech in Canada able to produce 2083 kg/hr and a rotating cone reactor design used by BTG in the Netherlands with a maximum capacity of 2000 kg/h [32].

Commercial pyrolysis units as large as 200 tons/day have been reported to be in operation [107]. Small capacities of 100 dry ton/day have been investigated for transportable units [109], as well as larger central capacities of 500 – 550 dry ton/day (20.8 -23 dry ton/h) have been used in previous studies [110], [104]. Plant capacities as large as 2000 dry tons/day have also been used in studies [57], [107], although such large scales might experience problems sustaining the biomass requirements [110].

Jones et al. [57] used a circulating fluid bed reactor, as these reactors are used in the petroleum industry with very large throughputs and therefore potentially appropriate for large biomass feeds [57]. A CFB (circulating fluid bed) is also used in Ensyn`s RTP process and is often used in modelling studies [110], [57]. Ensyn has reported biomass throughputs of 100 dry ton/ day (4.17 dry ton/hr) for the circulating fluid bed reactor in the RTP process used in the Ontario facility in Canada [111], [112]. Wright et al. [106], [107], used a bubbling fluid bed reactor due to the large availability of data and the system utilized 4 pyrolysis reactors in parallel. Ringer et al. [104] also used a bubbling fluidized bed reactor, although heat transfer to the bed at large scale has not yet been demonstrated, even though it has been used in the chemical and petroleum industry [104]. For a bubbling fluidized bed, the feed particles need to be smaller than 2-3mm [104]. It is believed that the circulating fluid bed is the available technology that is most likely to achieve a 2000 dry ton/day capacity [57], although particle sizes need to be sufficiently small [104].

2.4.3 The definition of different efficiencies

The energy efficiency of a process is used to determine how well a process can convert energy inputs to energy available in the final products. It helps to standardize the evaluation of the effectiveness of a process, especially when comparing between different processes. Different methods of calculating the energy efficiency of a process exist. In general, the energy in the final products are compared to the energy inputs into the process. The definition most often used, is the overall process efficiency [102]. It considers the sum of thermal energies in the solid and liquid fuel products as well as the marketable electricity [102]. Previous studies have defined other forms to express the energy

efficiency in an attempt to address the differences between the quality of fuels and electricity [102], see equation 7-9.

The **Fuel Energy ratio** considers the energy present in the fuel as a fraction of the energy input in the feedstock, in this case biomass, see Equation 7, [5]. Where n_{fuel} is the fuel efficiency [%], m_{fuel} is the fuel mass [kg/h], HHV_{fuel} is the higher heating value of the fuel [MJ/kg], $m_{biomass}$ is the biomass mass [kg/h] and $HHV_{biomass}$ is the higher heating value of the biomass [MJ/kg].

$$n_{fuel} = \frac{m_{fuel}.HHV_{fuel}}{m_{biomass}.HHV_{biomass}}$$ Equation 7

However this definition does not take the energy requirements of the process into account. Even though a process might have a high energy ratio, if the process requires a large energy input, the final ratio when considering the additional energy input might be less than a process with a lower energy efficiency but a lower energy requirement. Therefore it is important to consider the electrical energy requirements of the process as well and not only the fuel energy yields, in the **Fuel and Process Energy efficiency**, see Equation 8, [5]. In this equation the net process energy is the sum of the mechanical energy and heat requirements of the process [5]. This equation does not explicitly account for electricity by-production. However, when using the correct convention for the net electricity (positive for addition to the process and negative for production by the process), it is taken into account. In equation 8 $n_{fuel+P.E}$ is the fuel and process efficiency [%], m_{fuel} is the fuel mass [kg/h], HHV_{fuel} is the higher heating value of the fuel [MJ/kg], $m_{biomass}$ is the biomass mass [kg/h], $HHV_{biomass}$ is the higher heating value of the biomass [MJ/kg] and $Net\ process\ Energy$ is the process`s mechanical energy and heat requirements.

$$n_{fuel+P.E} = \frac{|m_{fuel}.HHV_{fuel}|}{|m_{biomass}.HHV_{biomass}|+Net\ process\ Energy}$$ Equation 8

In equations 1 and 2, the energy present in by-products is not considered. A process might aim at producing a specific fuel and might be optimized for that fuel, e.g. jet fuel, yet other by-products might also be saleable products. To accommodate this, the **Liquid fuel efficiency** in Equation 9 can be used. In this case, the energy transfer to by-products is deducted from the total biomass energy. It does not take into account the fraction of the feedstock energy that reports to other by-products and converts electrical energy to thermal energy; assuming a 45% conversion efficiency by assuming direct electricity production from biomass (n_{elec}=45%), similar to previous studies, [102], [113]. Only the liquid fuel product is considered in this case as an output/product. In equation 9 , $n_{liquid\ fuel}$ is the liquid fuel efficiency [%], m_{fuel} is the fuel mass [kg/h], HHV_{fuel} is the higher heating value of the fuel [MJ/kg], $m_{biomass}$ is the biomass mass [kg/h], $HHV_{biomass}$ is the higher heating value of the biomass [MJ/kg], $m_{by-products}$ is the mass of by-products [kg/h], $HHV_{by-products}$ is the higher heating value of by-products [MJ/kg] and $E_{elect.powergen}$ is the electricity product [MJ/h].

$$n_{liquid\ fuel} = \frac{m_{fuel}.HHV_{fuel}}{m_{biomass}.HHV_{biomass} - m_{by-products}.HHV_{by-products} - \frac{E_{elect.powergen}}{n_{elec}}}$$ Equation 9

However as mentioned, some by-products might also have a market value and therefore also contribute to the overall efficiency of the processes - the thermal energy in those products is not lost. Furthermore, all fossil fuel inputs are also considered in the **Thermal Efficiency** see Equation 10, [102]. The thermal energy available in the product, as well as the thermal energy in the by-products, are considered before electricity generation. In equation 10 , $n_{thermal}$ is the thermal efficiency [%], m_{fuel} is the fuel mass [kg/h], HHV_{fuel} is the higher heating value of the fuel [MJ/kg], $m_{by-products}$

36

is the mass of by-products [kg/h], $HHV_{by-products}$ is the higher heating value of by-produts [MJ/kg] , $m_{biomass}$ is the biomass mass [kg/h], $HHV_{biomass}$ is the higher heating value of the biomass [MJ/kg], m_{fossil} is the mass of fossil fuel used [kg/h], HHV_{fossil} is the higher heating value of the fossil fuel used [MJ/kg].

$$n_{thermal} = \frac{m_{fuel}.HHV_{fuel} + m_{by-products}.HHV_{by-products\ or\ intermediate\ products}}{m_{biomass}.HHV_{biomass} + m_{fossil}.HHV_{fossil}}$$
Equation 10

When making a comparison between energy efficiencies for various processes or between papers, it is important to ensure that a similar method was used for determining the efficiency of the process. In the calculations, by-products are only considered to be products with a market value that can be sold.

Similar to Equation 8, the overall process efficiency can be determined; by also considering the thermal energy to the by-products, as well as the electrical power produced, see the **Overall Energy Efficiency** in Equation 11 [102]. The main difference between the overall efficiency and the thermal efficiency is that electricity generated is considered a product for the overall efficiency, whereas it does not contribute to the thermal efficiency. For the thermal efficiency, all by-products that can be used for heat generation are included, however these by-products are not taken into account in the overall efficiency except when it is used for steam generation and electricity production, in which case only the final product, which is electricity, is accounted for. In equation 11 , $n_{overall}$ is the overall efficiency [%], m_{fuel} is the fuel mass [kg/h], HHV_{fuel} is the higher heating value of the fuel [MJ/kg], $m_{by-products}$ is the mass of by-products [kg/h], $HHV_{by-products}$ is the higher heating value of by-produts [MJ/kg] , $E_{elect.power}$ is the exported electricity product [MJ/h], $m_{biomass}$ is the biomass mass [kg/h], $HHV_{biomass}$ is the higher heating value of the biomass [MJ/kg], m_{fossil} is the mass of fossil fuel used [kg/h], HHV_{fossil} is the higher heating value of the fossil fuel used [MJ/kg].

$$n_{overall} = \frac{m_{fuel}.HHV_{fuel} + m_{by-products}.HHV_{by-products} + E_{elec.power}}{m_{biomass}.HHV_{biomass} + m_{fossil}.HHV_{fossil}}$$
Equation 11

If the HHV of a stream cannot be measured, correlation based on the proximate or ultimate analysis can be performed. In cases where experimental results were not available, the elemental composition of the stream can be determined with the Boie-correlation, see Equation 12, for estimating an HHV. This correlation is derived from the properties of hydrocarbon fuels and the correlation accuracy has been reported to be within 1.8% [114].

HHV = 0.3517xC + 1.1626xH +0.1047S - 0.111xO
Equation 12

Where HHV is the higher heating value in MJ/kg, C, H, S and O is the carbon, hydrogen, sulphur and oxygen wt% (on a dry and ash free basis) respectively.

2.4.4 Heat Integration – Pinch Analysis
The utility cost associated with the energy requirements in a biofuel process, can make the process unviable [115]. Pinch analysis is often utilized to provide a standard method for heat integration in a process, making processes comparable [116]. A pinch analysis consists of identifying process streams that require heat, and process streams that have meaningful extra heat. Previous studies have ignored streams with heat excess between 0-2% of the available heat, where the temperatures were significantly lower than the pinch point [115]. After identification of significant hot streams and cold streams and a minimum temperatures difference (DTmin), composite curves are constructed. The cold composite curve is then manipulated to contact the hot composite curve at a unique

temperature. The minimum temperature approach (DTmin) is often optimized to account for utility-capital trade-offs, although in the absence of cost considerations, an appropriate DTmin for the system can also be obtained from literature. DTmin typically varies between 5-20°C [117]. KBS Energy services reported DTmin values as determined from past experience in the different industrial sectors, see Table 16, [118]. Since bio-oil has many heavy components, such as some lignin and oligomers, it might result in fouling of equipment before HDO. Bio-oil was considered to be similar to oil refining and a DTmin of 20-40°C was assumed. This is a conservative approach as the system is more limited with a larger DTmin, with less streams being able to provide heat to other streams. The middle of the assumed range was assumed to be the DT min for the system, at 30°C. An increase in DTmin results in an increase in the utility requirements, but a decrease in the capital cost [115].

Table 16 DTmin values for different industrial sectors

Industrial sector	DTmin values	Comments
Oil refining	20- 40 ^{o}C	Fouling in heat exchangers and relatively low heat transfer coefficients
Petrochemical	10-20 ^{o}C	Lower fouling and better heat transfer coefficients
Chemical	10-10 ^{o}C	Lower fouling and better heat transfer coefficients

From the hot composite curve and the manipulated cold composite curve to the value of DTmin apart, the hot pinch and the cold pinch temperature can be determined. This is the temperature point over which energy transfer should not occur if the hot and cold utility requirements are to be minimized [117]. Once the pinch point is determined, the heat exchanger network (HEN) is constructed, following a set of guidelines, listed below [119], [117].

    i.   Transfer across the pinch should be avoided

    ii.   The minimum approach temperature of streams entering and leaving a heat exchanger unit may not be smaller than DTmin [117]

    iii.   When streams are matched for heat exchange, mCp out of the pinch must be greater than mCp into the pinch [117], [119].

    iv.   Two streams can have only one heat exchange unit [115]

The ideal is to reach the minimum utility target, while also reducing the number of heat exchanger units to the absolute minimum [115]. The absolute minimum number of heat exchangers above or below the pinch point can be determined from Eq. 13 [117]. The pinch point divides the heat exchange area into two independent regions, therefore the absolute minimum is not always achievable [120].

Min No. exchangers = No. hot streams – No. cold streams + No. of utilities - 1   Equation 13

2.4.5 Literature on Auxiliary units for model

The auxiliary process units, in addition to the upgrading and fast pyrolysis units, are required for the plant to be independent (a stand-alone plant).

2.4.5.1 Hydrogen requirements/ production in model

a. Overview

Hydrotreating requires a source of hydrogen. Upgrading hydrogen requirements reported in literature for HDO vary. Consumptions of 100 Nm^{3}/ton for mild hydrotreating have been reported

[90]. Reported requirements for complete deoxygenation is 25 mole H_2/kg BO [90], [25]. However, in a study by Elliott et al. [16], hydrogen excess of 35-420 mole H_2/kg BO was used [25].

High pressures and a large excess of hydrogen is required in both the hydrotreating and the hydrocracking reactor, to ensure sufficient hydrogen availability [84] at the surface area of the catalyst [25]. Existing petrochemical refineries typically have hydrogen available, although in a stand-alone pyrolysis-upgrading plant, auxiliary units for hydrogen production are required.

Previous studies have considered hydrogen supply by purchasing from an external source [106], reforming a fraction of the bio-oil [106], or by reforming the hydrocarbons in the off-gas and supplementing this offgas with natural gas for sufficient hydrogen production [57]. In principle the hydrogen requirements can be derived from the aqueous phase that forms during hydrotreatment, by means of steam reforming [32]. Alternatively the aqueous phase of bio-oil can be used as feed for hydrogen production [121], [122]. Separation of the aqueous phase is accomplished by the addition of water to the raw bio-oil to produce two liquid phases: an aqueous phase composed mainly of carbohydrate derived compounds and a hydrophobic phase containing lignin-derived oligomers [123], [124].

 In one study the auto-thermal reforming of model components representing the aqueous phase in bio-oil was investigated. It was concluded that only slightly more energy is needed than for natural gas reforming, due to higher steam requirements [121]. Feed requirements for 1kmole hydrogen is 0.245 kmole simulated BO (comprised of model components of acetic acid, ethyl glycol and acetone) and 0.317 kmole natural gas [121]. UOP employs a process where the aqueous phase is used to generate hydrogen by treating it in a pre-reformer to produce syngas, which is then reacted with methane in a reformer [106]. The fraction of the aqueous phase can be up to 70% of the bio-oil weight, although only 38% of the bio-oil is needed to supply sufficient hydrogen [106]. This amounts to 61.3 wt% of the biomass designated for fuel production. In the process model, the hydrogen mass yield from the bio-oil fed for hydrogen production is only 6.73wt%.

Another alternative for hydrogen production is to process additional biomass to provide hydrogen via e.g. gasification [32]. The biomass required will be 80% of the biomass designated for bio-oil production, indicating lower efficiency than is often expressed by simple performance figures [32]. In a study where the efficiency gasification of biomass was evaluated, it was concluded that a more profitable method of utilizing biomass will be to use it in combination with natural gas [125].

A basic calculation was performed to compare the different options available, see Table 17. Hydrogen supply was calculated as the amount of hydrogen needed to recover the consumed hydrogen and hydrogen losses (via PSA efficiency of 85%), for 100g bio-oil (including moisture). This amounted to 6.2651g H_2 that had to be replenished for a 100 g (wet) bio-oil feed. The equivalent amount of biomass needed to produce the 100g bio-oil was calculated as 131.95g ≈ 132g. For the bio-oil reforming scenario reported in literature, the hydrogen requirement was estimated as 4.21wt% of the bio-oil fed. This is lower than what was used as the basis in the calculations, illustrated in Table 17 , where the yields were calculated for a hydrogen requirement of 6.2651g H_2 / 100g bio-oil fed. Another alternative for hydrogen production is to process additional biomass to provide hydrogen via gasification, although in this scenario 80% of the biomass designated for bio-oil production will be required for hydrogen production [32].

Different processes for the hydrogen supply were compared, using Table 17 as guideline. In Table 17 a significant difference compared to exists between the experimental and theoretical biomass requirements (75 g compared to 38 g biomass) when converting dry biomass via gasification and reforming to a reference quantity of hydrogen (6.265 g). According to Turn et al. [126], the difference is due to the uncontrolled decomposition and the complex molecular structure of biomass, as well as system losses and irreversabilities. The bio-oil reforming option required the largest amount of feedstock, with almost an equivalent amount of biomass for hydrogen production and for bio-oil production, at 93.23%. The natural gas option uses the smallest mass of feedstock, 11.45 %, since the hydrogen production from the feedstock is the highest at 41.44%. Although natural gas is not a renewable feedstock, the other options require between 2.5 – 8.1 times larger feedstock masses than is the case for natural gas. Furthermore, natural gas reforming is a more established technology.

Table 17 Different methods compared to produce H$_2$

Feedstock	Type of study	Process	Mass feedstock for 6.265 g H$_2$ production [g]	(wt feedstock for H$_2$/ wt biomass for Bio-oil)x 100 [%]	(Wt H$_2$ produced/ wt biomass needed for H$_2$ production) [%]	Wt feedstock/ wt natural gas
Dry biomass [a]	Experimental results	Biomass gasification	75.48	57.18	8.30	4.99
Dry biomass [a]	Theoretical Maximum in experimental results	Gasification + complete reforming (theoretical maximum)	37.97	28.77	16.50	2.51
Dry biomass [b]	Modelling study	Biomass gasification + reforming + shift reaction + clean-up via PSA	80.74	61.17	7.76	5.34
Bio-oil [c]	Modelling study	BO reforming	123. 06	93.23	5.09	8.13
Natural Gas [d]	Modelling study	Natural gas for steam reforming+ shift + clean-up via PSA	15.12	11.45	41.44	1

Calculated from [a][126], [b] [127], [c] [106], [d][57]. Calculations assumed 6.2651g H$_2$ required / 100g bio-oil fed, assuming a bio-oil yield of 59.9wt% organics from dry biomass fed, [86] and a final moisture content of 20.96wt%.

The composition of natural gas can have slight variations, see Table 18, with methane being the most prominent at 94.4-94.5 mole%. Many simulation models have represented natural gas by using methane [57], [128].

Table 18 Natural gas composition

	Typical pipeline composition [a] [mole%]	Natural gas [b] [mole%]
CH_4	94.4	94.5
C_2H_6	3.1	2.7
C_3H_8	0.3	1.5
C_4H_{10}	0.2	-
C_5H_{12}	0.1	-
CO_2	0.5	0.5
N_2	1.1	0.8
H_2S	0.0004	-

Data obtained from [129], originally presented in [a][130], [b][131]

b. Hydrogen production from natural gas

Hydrogen produced from natural gas are subjected to these steps: natural gas desulphurization, steam reforming, high and low temperature shift conversion and methanation or instead of the low temperature shift conversion and methanation, a PSA unit can be used [132], [127]. Typical refineries will remove sulphur first, by adding hydrogen to produce H_2S, which can then be removed before further downstream processing occurs. Hydrogen is added to the natural gas feed for Sulphur formation. Desulphurization is not considered in this study. This is due to the assumption of no sulphur in the feed, which is necessary for the overall mass balances on the hydrotreating and hydrocracking units. Since desulphurization was not taken into consideration, no additional hydrogen for desulphurization was required. The inclusion of such a unit will be beneficial for accuracy in more detailed modelling.

During steam reforming, light hydrocarbons are converted to hydrogen when reacted with steam in the presence of a catalyst. A nickel based catalyst is typically used and packed into tubes in the reforming furnace [127], [133]. The operating pressure ranges from 15 bar – 30 bar [127]. The high temperatures of approximately 815-871°C [127], [133], cause cracking reactions of the hydrocarbons, as well as a reaction between carbon and steam [133]. The carbon deposits onto the catalyst, although for light feeds, the carbon is removed as quickly as it is formed. The type of feedstock used is therefore limited to propane, butane, natural gas and even in some cases liquefied petroleum gas (LPG) and naphtha, with the desired feedstock boiling point less than 180 ^{o}C [133]. Steam to carbon molar ratios for the reformer range between 3-6 [132]. The steam reforming reaction, see Rxn 1, takes place in the reformer. Rxn 2 can also occur in the steam reformer [132]. After reforming the product gas is fed to shift reactors where the water-gas shift reaction occurs, see Rxn 2. The first steam reforming reaction where CO is produced is endothermic [129]. The second steam reforming reaction (shift reaction) is exothermic [129].

The steam reforming reaction:

$$CH_4 + nH_2O \; \underset{\leftarrow}{\rightarrow} \; 3H_2 + CO \qquad\qquad\qquad \text{Rxn. 1 [133]}$$

Followed by the water gas shift reaction:

$$CO + H_2O \; \underset{\leftarrow}{\rightarrow} \; CO_2 + H_2 \qquad\qquad\qquad \text{Rxn.2 [133]}$$

c. Shift Reaction

When a small quantity of hydrogen is required from the reformer product stream, with the remainder used as gas, membranes can be used to separate the hydrogen which is then fed to a PSA unit [133]. For maximum hydrogen production it is best to feed the reformer product stream to a shift reactor where more hydrogen will be produced by utilizing the CO to form additional H_2 through

41

the conversion to CO_2 [133]. In such cases reformer product gases are fed to a high temperature (HT) shift reactor and in some cases followed by a low temperature shift reactor. Typically steam-and methane-reforming plants only consist of a reformer and high temperature shift reactor, although feeding the high temperature shift products to a low temperature shift reactor will be economical due to the additional hydrogen produced [129], [134]. The shift reactors convert the water to hydrogen by changing the CO to CO_2 , see Rxn 2. The equilibrium of the shift reaction is favoured by low temperature [133]. The catalyst used in the high temperature shift reactor consists mainly of magnetite and chrome oxide and operates between 315 – 430 ^{o}C [133], or 371- 410 ^{o}C, [132]. The steam/carbon molar ratio of the shift reactor feed is important, as a too low ratio can result in the metallic iron catalysts (primarily Fe_3O_4 with Cr_2O_3) catalysing FT reactions to form hydrocarbons [133]. This can be eliminated by over-reduction done by doping the catalyst with Cu, although this also results in the catalyst being sensitive to sulphur and chlorine. Older plants used steam/carbon ratios of 5-6, while some more modern plants have ratios of 3 [133]. One of the problems associated with large steam/C ratios is the large equipment sizes required. For this reason lower steam/ C ratios (as low as 2.5), are often considered [135]. Low steam/C can increase the methane leakage, but it can be compensated for by increasing the reactor temperature, since high reforming temperature favours the steam reforming reactions [135]. Approximately 75% of the CO is converted to CO_2 in the high shift reactor [132]. The high temperature shift reactor has previously been assumed to achieve a 90% CO conversion, with an inlet temperature and pressure of 350 ^{o}C and 19 bar and with outlet temperature of 428°C and a pressure drop of 15psi [136].

Low temperature shift reactors use copper/zinc catalysts and operate at temperatures ranging between 205 -230 ^{o}C [133]. The low temperature shift reactor has been assumed to achieve a 90% CO conversion in some studies, with outlet temperature of 213°C and a pressure drop of 15psi [136]. Since low temperatures favour the equilibrium of the water-gas shift reaction, less CO and more H_2 are present in the product gas. However, the main reason for using a low temperature shift reformer is not the additional hydrogen production, but rather the lower CO content, which decreases the temperature increase in a methanator. Wet scrubbing plants use methanators for final purification, which is why it is usually economical for wet scrubbing plants to make use of a LT shift reformer, but not for plants using a PSA. In any case, any unconverted CO in the PSA offgas will be recycled to be used as reformer fuel [133].

The bulk of the reformer fuel is supplied by the PSA offgas [132]. In previous studies where the hydrogen production from biomass was investigated, the reformer was fuelled by the offgas from the PSA, as well as a small quantity of natural gas, to ensure good burner control [127]. The quantity of natural gas added represented 10% of the heating value of the PSA offgas [127]. In another study where steam reforming of natural gas was investigated, natural gas was also added to assist with burning. The natural gas supplementation contributed 4.4wt% of the total reformer fuel requirements [129]. The fraction of reformer fuel supplied by the PSA offgas should be limited to a maximum of 85% [133]. This is to minimize difficulties with burning, due to the high CO_2 content in the PSA tail gas [133]. This can be achieved either by co-feeding natural gas to the reformer for fuel, or by supplementing the other 15% with an easy combustible waste product form the refinery.

d. Additional feedstock for hydrogen production

An additional feedstock to the reformer to consider for hydrogen production, is the light refinery gas [133], although it may contain olefins and propane or heavier components [133]. Catalytic reformer gas is considered to be a good feedstock for steam reforming, with hydrotreater offgas being less desirable and Fluid Catalytic Cracking (FCC) gases being the least desirable, due to high olefin

contents [133]. Other feedstocks for reformer feed should typically have a boiling point of less than 180 ^{o}C [133]. Typical reformer feeds include propane, butane and light refinery gas or light naphtha [133]. When the light fraction have a large quantity of hydrogen present, it is considered a good alternative to natural gas co-feeding for reformer fuel as it is produced as a by-product and therefore available at low cost [133].

e. Hydrogen production heat integration

Due to high temperatures required for the reformer (approximately 870 ^{o}C), heat integration should be employed to conserve the heat from this unit. An option for heat integration includes the pre-heating of combustion air [133].   This has the advantage of reducing firing, although it can lead to an increase in the NO$_x$ formation. Heat integration can also be accomplished by generating steam [133]. The flue gas used to superheat steam is discharged into the atmosphere at approximately 150°C [132]. Other alternatives include the use of a pre-reformer, where the steam and the hydrocarbon feedstock are fed over a pre-reforming catalyst. With an increase in the extent of reforming, the temperature decreases and reheating of the gas is required before it is fed to the main reformer. However, since the main reformer is at a lower temperature (approximately 500°C) to prevent cracking, heat recovery is limited [133].   Alternatively a heat-exchange reformer can be used, where the product gas flows in the shell and the feedstock and steam flows through the tubes packed with reforming catalyst [133]. The heat-exchanger reformer can recover more heat than the pre-reformer, but it has a higher equipment cost. [133]. A heat exchanger reformer can also be combined with pre-heating of the gas to recover even more heat [133]. The overall process is an exothermic process with less steam being consumed in the plant than what can be produced [129]. This allows for steam export elsewhere in the plant/refinery or to another source close by [129].

f. Hydrogen clean-up: PSA

To purify the hydrogen stream gas clean-up is required, this can either be done using wet scrubbing or Pressure Swing Absorption (PSA). Wet scrubbing was used for plants built before 1980, to be replaced with PSA thereafter [133]. In a PSA unit gas is passed through a bed with solid adsorbents usually a mixture of activated carbon and zeolites [127], onto which most of the impurities adsorb, with the hydrogen passing through and only a small part of it being adsorbed [133]. Depressurization and purging is used to regenerate the adsorbent bed [133]. Liquids are removed prior to the PSA units, to prevent damage to the catalyst, usually by installing knock-out drum [132], with a mist eliminator [127]. PSA operating temperatures of 40 to 43°C is often employed, with low temperatures increasing the efficiency [132], [127], [125]. Feed pressures range between 14.8 -28.6 bar(a) and purge pressure between 1.2 – 1.4 bar(a) [127]. An increase in the purge gas pressure to 3.8 – 6.6 bar(a) can result in a hydrogen recovery of 60-80% [137] instead of the expected 85%.   The feed pressure to purge gas ratio should be ≥ 4 [127]. In a PSA unit, the majority of purities can be removed to desired levels, producing a cleaner hydrogen stream, with hydrogen purities ranging between 99-99.99vol% [133], see Table 19.

Table 19 PSA vs wet scrubbing product stream

	PSA	Wet scrubbing
H$_2$ purity [vol%]	99 – 99.99	95 - 97
CH$_4$ [vol%]	0.01	2 - 4
CO + CO$_2$ [vol%]	10-50	10 - 50
N$_2$ [vol%]	0.1 – 1.0	0 - 2

All data obtained from [133]

Hydrogen purity from a PSA can be even greater than 99.9vol% [127]. Industrial uses have shown that the hydrogen mole% in the stream fed to the PSA unit should exceed 70mole% for it to be economically purified in a PSA [134]. This can be achieved by recycling a portion of the purified hydrogen stream [127]. The off gas from the PSA unit is recycled and used as fuel for supply heat to the reformer. High CO_2 content in the offgas can result in combustion problems, therefore the PSA offgas is limited to contribute only 85% of the required fuel for the reformer [133]. Hydrogen losses to the offgas are approximately 15 vol% [127], but can vary between 10-20 vol% [133]. This amounts to a hydrogen recovery of 85 vol%, but values of 83 % have also been reported [132].

PSA units are usually used in steam reforming plants because of the moderate costs, high purity and easy integration into the plant [133]. Furthermore it is considered to be a less complex route [132]. It is therefore also the method of choice for this study.

It is not considered economical to use a single PSA unit to purify the product gas from steam reforming together with other hydrocarbon/hydrogen gas streams [133]. The different streams require the use of different adsorbents [133]. For this reason, different PSA systems will be used for the two different instances where it is required; one instance is after the shift reactions and the other instance is when the hydrotreating reactor gases are purified for recycling of the hydrogen.

Heat is released when adsorption occurs and required when desorption occurs, although the process can in some cases be considered to be isothermal [138]. From a reported heat duty in a previous study [127], the heat requirement was calculated to be 8.913 MJ/ton feed.

In a study where the gasification of biomass for hydrogen production was investigated, the purified hydrogen stream exits the PSA at a 99.9% purity and a temperature of $43^{o}C$ and 25Bar [125]. Spath et al. [127] used pressures of 24.8 bar and $43^{o}C$. and a purge gas pressure of 1.38 bar(a). In this study a temperature of 43 ^{o}C and pressure of 25 bar have been used. These conditions are similar to other studies [125], [127].

2.4.5.2 Distillation of hydrotreated bio-oil

A crude oil refinery is a complex system of processes [27]. Detailed distillation data for hydrotreated bio-oil is not easily found in literature, especially not for commercial scale processes where utilities and process specifications are specified. Experimental data for HDO bio-oil distillation is available in studies from Christensen et al. [15] and Baldauf et al. [27], although the distillation conditions were not reported in these laboratory scale studies, focussing on product compositions. For this reason, crude oil distillation was investigated as an alternative. Hydrotreated bio-oil differs from crude oil because it contains large quantities of cyclic components [16], as seen in Table 6. This is not expected to have a significant influence on the utilities when taking the accuracy and uncertainties of the oil components etc. into account. Design procedure for atmospheric and vacuum distillation is also empirical, due to the large range of hydrocarbons present [139].

In an oil refinery the product is fractionated into different streams according to boiling point, using a system of distillation processes. A distillation unit typically consists of a pre-flash, followed by atmospheric distillation whereafter vacuum distillation takes place [140]. In the pre-flash column, partial vaporization occurs to produce a lights fraction (referred to as lights) and naphtha, and is usually required when the feedstock has large quantities of light ends [139]. The pre-flash bottoms are then fed to the atmospheric distillation unit where additional vaporization occurs. Temperatures for atmospheric distillation flash zones are limited to approximately 370- 425 ^{o}C, to prevent cracking

44

of the feedstock [139]. The distillate streams are typically some remaining naphtha, kerosene, diesel and some atmospheric gas oil. The distillate fractions often contain some products from nearby cuts [139]. To purify the fraction for the desired cut, superheated steam is used for steam stripping, where the steam and undesired components are returned to the atmospheric distillation tower [139]. The remaining fraction, the residue, is fed to the vacuum distillation tower [140]. The feed is separated into off-gas, light- and heavy- vacuum oil and residual oil. Typical utility consumptions associated with crude oil distillation, for both the atmospheric and the vacuum distillation column, are provided in Table 67.

2.4.5.3 Combustion

Combustion is usually performed to generate heat from either a fuel source, such as natural gas, or from an undesired by-product. The heat can either be directly used in the process, or in cases where excess high quality heat is available, steam can be generated for electricity production. The ratio of air to fuel must be such that complete combustion occurs. Environmental legislation also has limits about the amount of oxygen present in the offgas, to ensure that the air was fed in excess for complete combustion and accordingly to ensure that no undesired combustor-feed components exit into the atmosphere. The product gases must contain at least 6wt% oxygen, to meet environmental standards as described in the Department of Environmental Affairs and Tourism Air Quality Act (2008), [141], [103]. Air is often pre-heated using the flue gases from combustion, to improve combustion and as a means of heat conservation. The temperature to which air is pre-heated can vary, but have been reported to range between 250 ^{o}C - 300°C [142], [143]. To pre-heat the fuel is also considered a good application of the thermal energy for conservation [136].

2.4.5.4 Cooling water and chilled water

The principle to achieve cooling in a cooling tower is evaporative cooling. Cooling water supply can range between 27-35 ^{o}C, with a return arranging between 45-52 ^{o}C [144]. Water losses can occur via evaporation, drift or windage (loss of entrained water droplets in the air) and bleed or blow down (intended purge to avoid accumulation of salts) [145]. Figure 1 shows the make-up water, W_m , the evaporation loss, W_e, the drift loss, W_d and the blow down loss W_b, with units of m^3/hr.
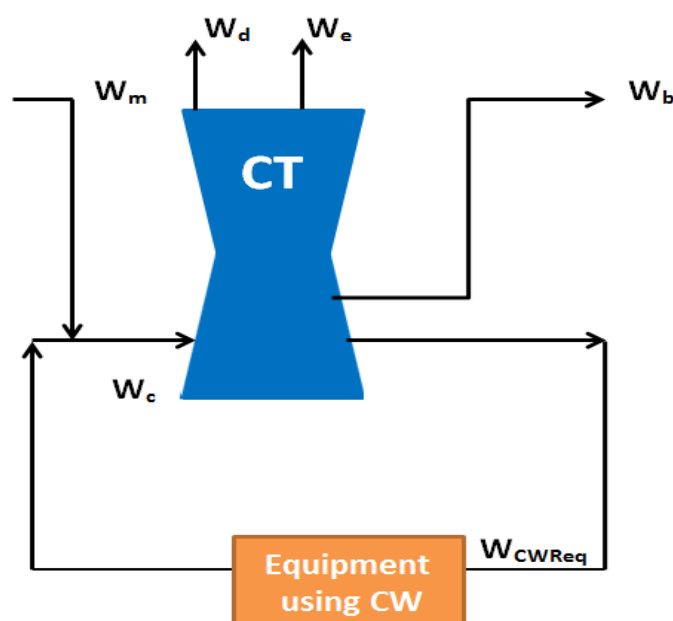
Figure 1 Cooling water flow and losses in Cooling Tower

The make-up water, used to account for losses, can be calculated from Equation 14 [146], see below:

$$W_m = W_e + W_d + W_b \qquad\qquad \text{Equation 14}$$

The quantity of water loss due to evaporation, drift and blowdown can be determined from heuristics, see Table 20.

Table 20 Losses for cooling towers*

Loss type	Quantity
Evaporation loss	1%
Drift/ windage	0.1-0.3%
Blowdown	2.5-3.0%

* Data obtained from [145], for every 100 F of cooling range

Alternatively evaporative losses can be calculated from equation 15 [146]:

$$W_e = 0.00085 \times W_c \times (T1-T2) \times 1.8 \qquad\qquad \text{Equation 15}$$

Where W_e is the evaporative loss in m^3/h, T1 is the inlet temperature in ^{o}C and T2 is the outlet temperature ^{o}C and W_c is the circulating water flow in m^3/h. The amount of circulating water, shown in Figure 1, can be determined from equation 16.

$$W_c = W_m + W_{CWReq} \qquad\qquad \text{Equation 16}$$

W_{CWReq} is the cooling water requirement of the equipment, in m^3/hr. Once the total quantity of cooling water through the cooling tower is available, the power requirements associated with it can be determined.

The power requirements is determined from the total circulating water, W_c, using equation 10. The cooling water requirements for the process, W_{CWReq}, can be determined from the simulation model. The make-up water, W_m, can be determined from equation 14, where equation 15 can be substituted into equation 14. By assuming a drift and blowdown of 0.3% and 3% respectively, the equation simplifies to equation 17. Substituting equation 16 into equation 17, simplifies to equation 18 to determine the make-up water requirement.

$$W_m = W_e + W_d + W_b$$

$$W_m = 0.00085 \times W_c \times (T1-T2) \times 1.8 + 0.3 \times W_c + 3.0 \times W_c$$

$$W_m = 0.00153 \times W_c \times (T1-T2) + 3.3\,W_c$$

$$W_m = (0.00153 \times (T1-T2) + 3.3) \times W_c \qquad\qquad \text{Equation 17}$$

$$W_m = (0.00153 \times (T1-T2) + 3.3) \times (W_m + W_{CWReq})$$

$$W_m = (0.00153 \times (T1-T2) + 3.3)/ (1-(0.00153 \times (T1-T2) + 3.3)) \times W_{CWReq} \qquad \text{Equation 18}$$

Previously cooling towers have been modelled as flash vessels in Aspen Plus®, with the effluent temperature and the evaporative loss specified [115]. This allowed for the determination of the cooling capacity and consequently power requirements, using equation 19 below [147], where COP is the Coefficient of Performance, P is the total electrical power [W] and Q is the cooling capacity [W].

$$COP = Q/Ptotal \qquad\qquad \text{Equation 19}$$

In the study by Bergensten (2009), the average annual COP of a cooling tower at base case conditions was determined at 7, to avoid having to account for seasonal differences. For chilled water

production, a variety of COP`s are reported in literature. A conservative average performance (COP) for electricity driven compressor chillers, is considered to be 3 [148].

2.4.5.5 Waste treatment and waste streams

Different waste water streams are produced in a refinery set-up. This includes oily water effluents (in storm water etc.), sour water caused by dissolved H_2S and NH_3 typically produced from the hydrocracker, gas handling, and hydrodesulphurization unit during processes such as distillation hydrotreating and hydrocracking operations and biological waste generated by the workforce [149], [149]. In this discussion, the biological waste generated by the workforce will be ignored.

Treating the pollutants from petroleum refineries are important because of the high polycyclic aromatic intents, which are considered to be toxic to the environment [150], [151]. Phenolic compounds are a major constituent in the effluents from petroleum refineries and petrochemical industries and are considered a great threat due to its stability, its ability to remain in the environment for long time periods and its toxicity [152], [153]. Phenolic components inhibit the growth of micro-organisms, with concentrations as low as 1mg/L affecting aquatic life [152]. Although a plant utilizing pyrolysis and upgrading is not a conventional refinery, the products are expected to be similar and in many cases even worse than for a typical petroleum refinery, as will be explained below.

Petroleum refinery effluents are often treated in two stages: pre-treatments steps where the oils/ grease and suspended substance content are reduced, followed by an advanced stage where the contaminants are reduced to acceptable discharge limits [153]. Pre-treatment often focuses on reducing the heterogeneous nature of the effluent and employs mechanical means followed by physiochemical means such as agglomeration, sedimentation, filtration or flotation [153], [154]. Various options for further treating exists, including advanced oxidation processes, bioremediation and combustion for heat generation [153].

Advanced oxidation processes generate hydroxyl radicals as a primary oxidizing agent [155]. The hydroxyl radical has a high oxidation potential, making it more efficient than hydrogen peroxide and ozone [155]. Although photocatalytic degradation has many advantages including its cost effectiveness and efficiency, as well as the potential to mineralise both the organic and inorganic components to nonthreatening environmental components, Diya`uddeen et al. [153] concludes that the industrial application is limited by the inadequate literature on the treatment of petroleum refinery effluent. Further research on the scale-up of waste water treatment as well as economic feasibility of this process has been proposed [155].

Bioremediation is considered to be the most widely used technique and the traditional approach [153]. Complete degradation of petroleum refinery effluents is sometimes difficult because not all persistent components are removed satisfactorily [153]. Two methods for bioremediations exist, aerobic and anaerobic digestion. Differences between anaerobic and aerobic waste-water treatment include: little excess sludge production, little nutrient requirements and no aeration energy requirements for anaerobic treatment with a further advantage that methane is produced [156], [157]. Unfortunately anaerobic bacteria are easily inhibited by many compounds and requires long start-up periods, however methane production and low electricity requirements are advantageous [156]. Some components which are known to be present in bio-oil, or produced in bio-oil upgrading, have been reported to be responsive to anaerobic technology. These include: acetaldehyde, formaldehyde, ethanol, formic acid, phenol, catechol, cresol, propanol [157].

47

The chemical oxygen demand (COD) and biological oxygen demand (BOD) of waste water streams are often used as an indication of the extent of purification that is required. The test determines the mass of oxygen (mg) required to oxidize the organic components completely to CO_2, H_2O and NH_3 for a 1L of effluent, with the COD given in mg/L. If a sample of the aqueous effluent is not available, the theoretical oxygen demand can be calculated. The theoretical oxygen demand is the theoretical demand of oxygen required for complete oxidation of the components to CO_2, H_2O and NH_3. As a simplification, the ThOD and the COD are often considered to be equal. The COD for refinery effluent limits have been summarized to range between 100– 200mg/L [153], [158], [159], [160] with phenols up to 1mg/L [149]. However, COD values as high as 1020 mg/L and phenolic concentrations ranging between 50-600 mg/L have also been reported [161], [153], [152].

2.4.5.6 Power generation

Heat recovery in a plant can be accomplished by steam generation for electricity production. High Pressure steam can be expanded in a Back pressure steam turbine (BPST) or a Condensing extraction steam turbines (CEST) to generate electricity and produce low pressure steam [103]. The low pressure steam can be utilized in the plant for process steam [103]. In a BPST no condensation occurs and the process steam is supplied at conditions close to the process heat requirements [162]. In a CEST, a portion of the steam can be extracted at intermediate pressures for process purposes and the superheat conditions are higher than for a BPST system [162], [103], [163]. The HP steam is expanded to an intermediate pressure in a high pressure turbine, followed by further expansion in an intermediate pressure turbine to a low pressure [103]. Co-generation is often used in the sugar mill industry, to produce process steam and electricity from waste heat and has also been used in fast pyrolysis process models [102–104].

Nsaful`s (2011) investigation into a sugar mill revealed that, although less HP steam can be produced in a CEST compared to a BPST (due to the higher quality of the steam used requiring more energy for superheating resulting in a smaller quantity that can be heated), the electricity produced is still higher for the CEST than for the BPST [103]. In the study, it was attributed to the low conversion efficiency from heat energy to electrical energy of the BPST compared to the CEST [103]. This was quantified as an increase in the electrical efficiency from 12.8% to 18.3% when the BPST was changed to a 82bar CEST system at 50% bagasse moisture conditions, with similar trends observed for different moisture contents [103].

Other studies in the sugar mill industry have also reported increases in electricity production when using a high pressure (40-80Bar) CEST rather than a medium pressure (15-20 Bar) turbo-alternators [164]. CEST is larger than BPST and more efficient [163]. Using a CEST also has the advantage that it can be arranged to give steam conditions similar to what the plant requires [165]. Typical boiler conditions in the sugarcane industry have been reported to range from 15-82 bar and 300-525 ^{o}C in [166], [165].

When steam expansion occurs over a very high pressure ratio, condensation can occur if the steam temperature decreases to below the saturation temperature at that specific pressure [162]. Water drops which form in the turbine can cause blade erosion to occur [162]. This can be prevented by reheating the expanded steam in the boiler before further expansion occurs [162]. This approach was followed in a study where the performance of power generation from the gasification of switchgrass was investigated [116]. The gas turbine performance was based on a General Electric MS7001FB, one of the most advanced gas turbines currently employed for commercial use in natural

gas firing [116]. In the system process heat is recovered in a heat recovery steam generator (HRSG) that generates steam which is expanded through a set of steam turbines to generate power. The steam leaving the HP steam turbine is reheated in the HRSG before feeding to the following steam turbine. The steam turbine efficiencies were reported at 75% for the HP stage, expanding from 160-36bar; at 78% for the second HP stage, expanding from 36-20.5 bar; at 82% for the intermediate stage, expanding from 20.5-3.5 bar; at 85% for the low pressure stage, expanding from 3.5-1.5 bar, and at 82% for the condensing stage where expansion from 1.5-0.05 bar occurs [116]. In this process the cooled turbine exhaust is vented to the atmosphere after leaving the HRSG at 90°C [116].

In a different study where Fischer Tropsch fuels from biomass and coal are investigated with the co-production of electricity, a HRSG generates steam at three levels, with the intermediate steam being reheated to the same supersaturated conditions as the HP steam. The three pressure stages in the steam turbine is at HP steam inlet of 124.1bar, intermediate pressure steam inlet of 23.6 bar (both at 565.6^{o}C), and the LP steam at 2.413 bar, with a low exhaust pressure of 0.0462 bar containing a vapour fraction $\geq$85% [143]. The mechanical efficiency was in all cases considered to be 0.98 and the isentropic efficiencies were 0.84, 0.89 and 0.85 for the HP, IP and LP stages [143]. Flue gas exit temperature ranges between 90 – 100°C [143]. Lower temperatures are not advisable as it may lead to corrosion due to formation of acids [116].

Steam turbine sizes are available from 100kW to larger than 250 MW and can operate over broad steam pressures from approximately 240 bar inlet steam to 0.03 bar [162], [162]. Thermodynamic efficiencies of small single stage turbines can be as low as 50%, with small multistage steam turbines having thermodynamic efficiencies that can vary from 65% (for <1000kW unit) to >90% for utility size units [162].

The excess heat is used for steam generation in a Heat Recovery Steam Generator (HRSG) in a similar manner to [116], [143]. Streams with low temperatures are used for pre-heating of the water that is vaporized in the HRSG. Heat available from streams with very low temperatures or heat transfer capacities, are rejected to cooling water utility [116]. HRSG operating pressures of 160 bar and 124 bar have been reported [116], [143]. In the previously mentioned study, [143], an nth plant approach was used [116]. In this study a more conservative 105 bar is assumed for the HRSG. This may result in less efficient electricity generation, as high pressure favours the efficiency from heat energy to electrical energy.

The extent of superheating for a CEST is typically high as it prevents condensation after expansion occurs, since condensation can be harmful to the turbine and reduces efficiency [162]. Heuristics for the extent of superheating varies between 55-85 ^{o}C [117], although in previous studies, an extent of superheating of approximately 150 ^{o}C [103], 200 ^{o}C [143] and 250 ^{o}C [116] have been used. For this study the extent of superheating was 186°C, as this allowed the expanded steam to be at steam conditions required elsewhere in the plant, for the steam reformer and distillation.

2.5 Literature Conclusions

The literature study indicates that fast pyrolysis will favour the production of bio-oil and is therefore the best suited pyrolysis for the application. Furthermore, it also indicates that moisture content, particle size and reactor temperature have been reported to have an effect on the yields and certain bio-oil characteristics. The results from experiments investigating the impact of moisture content, particle size and temperature on products are seldom statistically analysed and consequently neglect

to analyse the interactions between the (processing and operating) factors investigated. Additionally, the influence of processing and operating factors on the bio-oil chemical families, especially aromatic content, is rare in literature. This study therefore aims to address these gaps in literature by performing a structured design of experiments and by statistically analysing the data to identify interactions between the factors. It will also determine whether significant variations can be observed in the bio-oil`s chemical families, as a function of change in the factors investigated.

The literature study on upgrading processes identified hydrodeoxygenation as the best current option, due to better catalyst performance and a final product that is closer to the stringent jet fuel specifications (greater extent of deoxygenation). Although experimental results exist for the characteristics/properties of upgraded bio-oil, experimental studies rarely consider the entire process from bio-oil feedstock to a final transportation fuel, including distillation of the upgraded bio-oil, quantification of the different transportation fuel yields and analysis thereof. Very few studies have considered the production of jet fuel from bio-oil, with limited experimental information available for the processing conditions, yields and jet fuel quality.

Modelling studies for the process of bio-oil production and upgrading to transportations fuels seldom consider jet fuel as one of the final products, and tend to focus on naphtha and diesel products. The few modelling studies that did report jet fuel production from bio-oil, have not considered producing a fuel that is close to the jet fuel specifications. In addition to this, the aromatic content in the final jet fuel has also not been reported. The study will address this and will go one step further to determine the utility requirements and energy efficiency for such a plant. This will provide a holistic view of the process to produce jet fuel and jet-fuel boiling range aromatics from biomass, using fast pyrolysis and hydrotreatment upgrading processes.

3. FAST PYROLYSIS INVESTIGATION AND EXPERIMENTS

3.1 Introduction

Pyrolysis is a process by which the volumetric and energy density of biomass can be concentrated [25]. Liquid, gas and char products are always produced [32], while the product distribution differs depending on the processing conditions; specifically the residence time and the reactor temperature. Char production is favoured by long vapour residence times and low temperatures (typical of slow pyrolysis); gas production by long residence times and high temperatures and liquid production by short residence times and intermediate temperatures (typical of fast pyrolysis) [32]. Since a liquid product is desired, fast pyrolysis is the best suitable pyrolysis process, as it aims to maximize the liquid (bio-oil) yield.

The bio oil produced from fast pyrolysis is an intricate mixture of oxygenated hydrocarbons with a substantial quantity of water (A. Oasmaa & Peacocke, 2010). During fast pyrolysis the degradation reactions are "stopped" by chilling the intermediate product vapours to produce bio-oil, resulting in many reactive components in the bio-oil since the reactions were not allowed to completion (equilibrium). This contributes to the instability of bio-oil [32]. The properties of bio-oil differ from that of conventional fuels [167], [29]. Characteristics of bio-oil include a high moisture content, high acidity, high oxygen contents and chemical instability when heated [29]. Furthermore bio-oil is not miscible with mineral oils [27], [29].

Although many studies concentrate on maximizing the liquid yield, the quality of the bio-oil is sometimes ignored [168]. The desired quality will depend on the final application of the bio-oil. It is therefore important to take both the quality and quantity into account and to find conditions where these two responses correspond [168]. To manipulate the bio-oil chemistry, the thermal processing conditions can be altered or catalysts can be used [14].

Various options are available for changing the thermal processing conditions, with temperature being the most common for fast pyrolysis. Other options include the residence time and heating rate, although these cannot be manipulated directly, but needs to be adjusted indirectly via factors such as the biomass particle size, carrier gas flow rate and temperature gradients. Other parameters include the moisture content in the bio-oil and the biomass composition.

The moisture content of the biomass indicates the free water present in the biomass. During fast pyrolysis, the free water explosively vaporizes, destroying the feed particles [14]. Furthermore it can also assist in heat transfer [14]. Free moisture in the biomass feedstock requires heat of vaporization, which reduces the available heat for pyrolysis [104]. Therefore the moisture contents after drying of wet biomass, should be less than 10 wt%; preferably at 7wt% [86].

The ratio of cellulose, hemicellulose and lignin, is dependent on the biomass species and can influence the bio-oil composition [14]. Biomass with a high lignin content, tend to give lower bio-oil yields with a higher energy density, compared to biomass with a high cellulose-derived content [14]. For biomass species rich in lignin, such as bark, the bio-oil yield is typically 60-65% [14]. Pine bio-oil has been reported to contain a high phenolic content, due to the high lignin content of pine wood [25].

Literature data on the fast pyrolysis of *Pinus radiata* for a 3kg/h scale fluidized bed is available [169], although the bio-oil compositional analysis was not carried out. Other studies have investigated bio-

oil quality and composition with fluidized bed reactors at scales of ca. 60g/h for *Pinus strobus* [21], and at scales of 1kg/h and 20 kg/h for *Pinus sylvestris* [56]. According to literature, very few results from fast pyrolysis of wood biomass were statistically analysed for interactions at the scale of 1 kg/h and thus revealing the significant influence of the processing and pre-treating factors on the pyrolysis process.

The objective of this part of the study is to test the certainty of the physic-chemical properties and to understand how the variability of the processing parameters (reactor temperature and biomass particle size) and feedstock characteristics (biomass moisture content) may influence the yield and quality of fast pyrolysis products produced from *Pinus radiata* in a 1 kg/h fast pyrolysis process, on a screening basis using statistical analysis. This information will be utilized to establish the optimal pre-treatment and pyrolysis operating conditions for the pyrolysis unit in the simulation model, based on the desired bio-oil characteristics. Results from the experimental runs will be statistically analysed using Design Expert®. *Pinus radiata* will be used as feedstock, due to the high lignin content present in pine wood. A greater aromatic content is expected in the bio-oil, due to the high lignin content, which is desirable in this study.

3.2 Materials and methods

3.2.1 Experimental Design

Although a variety of variables can be manipulated to influence the pyrolysis products, the variables manipulated, as well as the ranges inspected, are restricted by the experimental set-up. The range of variables that can be manipulated, as well as the typical operating conditions for the specific pyrolysis set-up, is provided in Table 90 in Appendix B.2: Factors to influence product yields and quality in experimental set-up, page 214. The variables, further on referred to as factors, have to be capable of being manipulated independently for it to be possible to be investigated. Furthermore the range (difference between the high set-point/level and low set-point/level of a variable) that is investigated, needs to be broad enough to allow for a significant change in each of the factor`s levels. In other words, the low and high level should be wide enough apart not to have any interference due to noise or slight variations during the experiment. The factors selected were the reactor temperature, the particle size and the moisture content.

Experimental designs to determine the influence of operating conditions on the pyrolysis products reported in literature are often not defined according to a specific design of experiments (DOE) (such as the use of a fractional factorial, a full factorial or a composite design). Most literature designs are based on varying one or two parameters at a time and considering the influence of each change on the yield, compared to the previous yield. Unfortunately, with this the interaction between factors cannot easily be identified, which is why a statistical analysis of the results is proposed.

The design employed was a 2^3 design: a full factorial where 3 factors were investigated for two levels each; a high and a low level. This design is primarily appropriate for screening experiments. The levels can be observed in Table 21. The factor levels and responses were analysed using Design Expert® v.7.15 software. An ANOVA (Analysis of Variance) was performed on each response using a confidence interval of 95%. ANOVA analysis is based on the following three assumptions:
1. Independence of observations
2. Normally distributed residuals
3. Homogeneity of variance

Compliance with the ANOVA assumptions is necessary for the ANOVA analysis to be valid. Where applicable the response surfaces were fitted to give an indication of the factor`s influence on the response.

Table 21 Factors and the levels used in the experiments

Factor	Low level	High level
Temperature	450 ^{o}C	500 ^{o}C
Biomass particle size	250-850µm	1400-2000µm
Water content	4%	10%

A 2^3 factorial experiment design in Design Expert® v.7.15 software was used. Significance was considered to be at a 95% confidence interval, with a p-value <0.05. In all cases, factor abbreviations **A** refers to the moisture content [wt% wet basis], **B** to the temperature [^{o}C] and **C** to the particle size [µm].

The error associated with the biomass moisture content, the pyrolysis reactor temperature measurement and the biomass particle size, can be viewed in Appendix A.2 Drying curves determination and biomass moisture content, Appendix A.4 Temperature measurement Calibration and Section 3.3.1.2 Biomass particle size distribution and Appendix A.1 Biomass particle size distribution analysis, respectively.

A total of 13 runs were performed of which 4 runs were discarded (runs 4, 4a, 4b and 4c), due to reactor temperature control concerns. The regression equations can be used to calculate the responses for comparison with the measured values. An additional experimental run (run 1) was performed at conditions outside the set points of the 2^3 full factorial; at high temperatures and moisture contents, with an intermediate particle size. This experimental run (run 1) was used to assess the capability of the response surface to predict a response, and compared to the measured response. This is measured by the error% for run 1, compared to the error% of the other runs used for surface response development. This provides an indication of the accuracy of the response surface.

In this study, the Coefficient of Variance (CV) was used to indicate the variance of the results expressed as a percentage of the average, see Equation 20 below. The CV indicates the variance of the data, with a small CV indicating the measurements are consistent, whereas a large CV indicates a large variance in the measurement. The CV is relatively sensitive to small changes in the mean. For example, when the mean value is close to the measurement uncertainty, the coefficient of variation will increase greatly.

$$CV = \frac{standard\ deviation}{mean}\ x\ 100\%$$
Equation 20

3.2.2 Feedstock and feed preparation

Pine wood chips were selected as the feedstock for the fast pyrolysis experiments, based on its high lignin content, which is expected to lead to a high aromatic content in bio-oil. Pine (*Pinus radiata*) wood blocks were obtained from the Cape Saw Mill, situated outside Stellenbosch in the Western Cape, South Africa. A diagram showing the methodology for biomass size reduction can be viewed in Figure 2. After obtaining the desired particle sizes, biomass samples were treated to obtain the desired moisture content, prior to each run. In order to manipulate the moisture conditions in a repeatable manner, drying curves had to be constructed for each particle size fraction. The

procedure used can be viewed in Appendix A.2 Drying curves determination and biomass moisture content. Feeder calibrations were performed for each particle size class. These calibrations can be viewed in Appendix

A.3 Feeder Calibration.
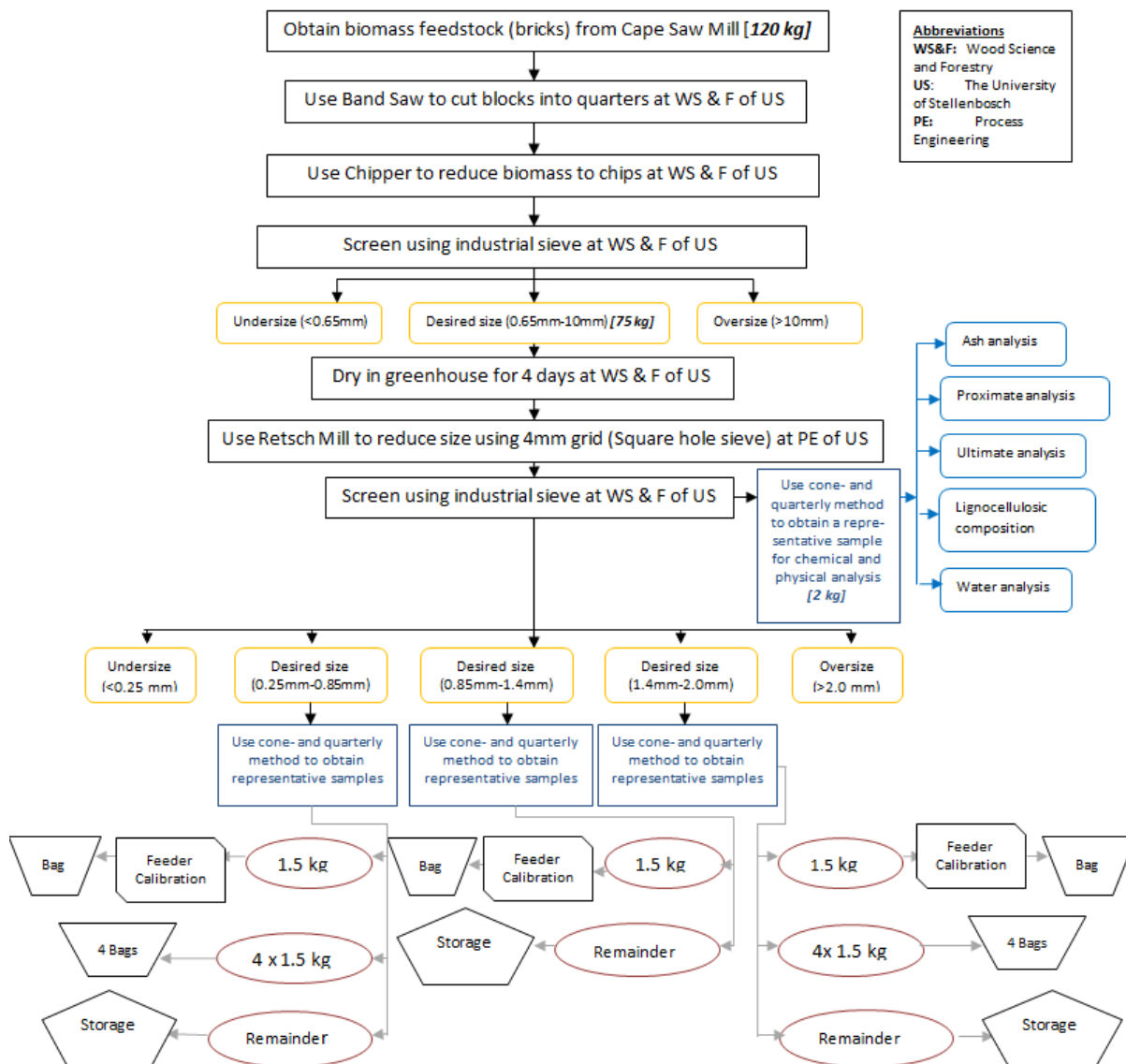
Figure 2 Biomass size reduction diagram

3.2.3 Fast pyrolysis process description and set-up

The fast pyrolysis experiments were performed at the Process Engineering Department at the University of Stellenbosch (South Africa) using a fluidized bed reactor configuration with a 1 kg/h operation capacity. A fluidized bed configuration was used for experimental work, as presented in Figure 3. A basic description of the fast pyrolysis set-up used in the experiments is provided below. A more detailed explanation can be found elsewhere [62], [68].

The prepared biomass is loaded into a hopper (H), where an attached volumetric screw feeder feeds the material to the rest of the plant. The screw feeder is turned by a variable-frequency motor (EM)

54

and controlled with an Electric Motor Controller (EMC) [62]. The feeding system is sealed off from the atmosphere during operation and a slight overpressure exists to prevent hot gases from escaping at the feed inlet [62]. The feeding pipe is connected to the reactor, which is maintained at temperatures in the range of 500 ^{o}C.

If the feeding pipe becomes warm during operation, premature decomposition of the biomass can occur, resulting in char deposits and fouling [62]. To prevent this, a water cooled jacket is positioned on the feeding pipe [62]. The pyrolysis reactor is a fluidized bed reactor (RT and RB). The reactor has a conical top (for gas exit) of 250mm and a conical bottom (for gas and biomass inlet) of 400mm. The inner diameter varies between 75-90mm, with an outer diameter of 100mm [62]. The fluidized bed is heated by placement inside a temperature-controlled oven [62], more specifically an electric furnace [170]. A PID controller is used to ensure the reactor temperatures remain at the set point [62]. The heat transfer medium in the fluidized bed is sand particles. The reactor was designed for sand particles varying between 400-600μm [62]. A weight of 400-500g of sand is used [170]. The fluidized medium used is nitrogen gas, as this is inert and reasonably priced [62]. The nitrogen gas is supplied directly from a cylinder (NC1 or NC2). A portion of the gas stream is routed to the feeder to ensure a slight overpressure and a portion of the gas stream is routed to the bottom of the fluidized reactor bed for fluidization. The gas routed to the fluidized bed is preheated. The nitrogen gas flow rate can vary between 2-3m^{3}/hr [62] and was previously used at values of 2.4-3m^{3}/hr [170] and 2.5m^{3}/hr [62].

The pyrolysis reactor and the two char pots are situated inside the electric furnace. The hot vapours and small suspended char particles are transported to the cyclones, where separation of the char solids occurred. Previous literature studies have indicated that problems occurred where only one cyclone is used. In this experimental set-up two cyclones are used in series. The first cyclone (C1) is responsible for separating the coarse particles, whereas the second cyclone (C2) is responsible for separating the fine particles from the vapour products and gases. To ensure an isothermal operation, the cyclones and char vessels (CP1 & CP2) are also situated within the oven [170]. The oven is heated before commencing with the experiment. A time period varying between 70min and 90min would allow for the reactor temperature variation to approach zero (T3-T4) and to reach a steady state, which is required before feeding of the biomass starts [170], [62].

From the cyclones, the remaining gases, aerosols and vapours are routed to a direct contacting heat exchanger. In this top part of the cooling tower (TCT), a cooled liquid, in this case Isopar G, is sprayed into the hot gases, vapours and aerosols for fast cooling. This is important as it prevents secondary reactions from occurring. Isopar G is immiscible with the bio-oil product and has other characteristics such as a high flash temperature and boiling point, which makes it favourable for this use. Thus, direct-contact cooling (quenching) occurs in the tower. The liquid formed from the condensed vapours and the isopar flow down the bottom cooling tower part (BCT) to the holdup vessel (V), where it is collected. The holdup vessel has a 25L buffer volume [62]. Continuous use of the Isopar is made possible by recycling to a heat exchanger which is a cooling water bath (CW), where the Isopar is cooled using cooling water, before re-routing it to the tower to act as cooling medium. A pump (P1) is used to pump the Isopar from the hold-up vessel to the heat exchanger. The vapours and aerosols are routed to the electrostatic precipitators, where small droplets are removed from the gas stream [62]. A two-stage Electrostatic precipitator set-up (EP1 & EP2) was used as this resulted in better separation in previous studies.

NC1	NC2	EM	EMC	H	RT	RB	C1	C2	CP1	CP2	TCT	BCT	ESP1	ESP2	CW	P1	P2	CH	V1	RH
Nitrogen cylinder 1	Nitrogen cylinder 2	Electric Motor	Electric Motor Controller	Hopper	Reactor Top	Reactor Bottom	Cyclone 1	Cyclone 2	Char Pot 1	Char Pot 2	Top Cooling Tower	Bottom Cooling Tower	Electrostatic Precipitator 1	Electrostatic Precipitator 2	Cooling Water Bath	Pump 1	Pump 2	Chiller	Bio-oil Collection Vessel	Rope Heater
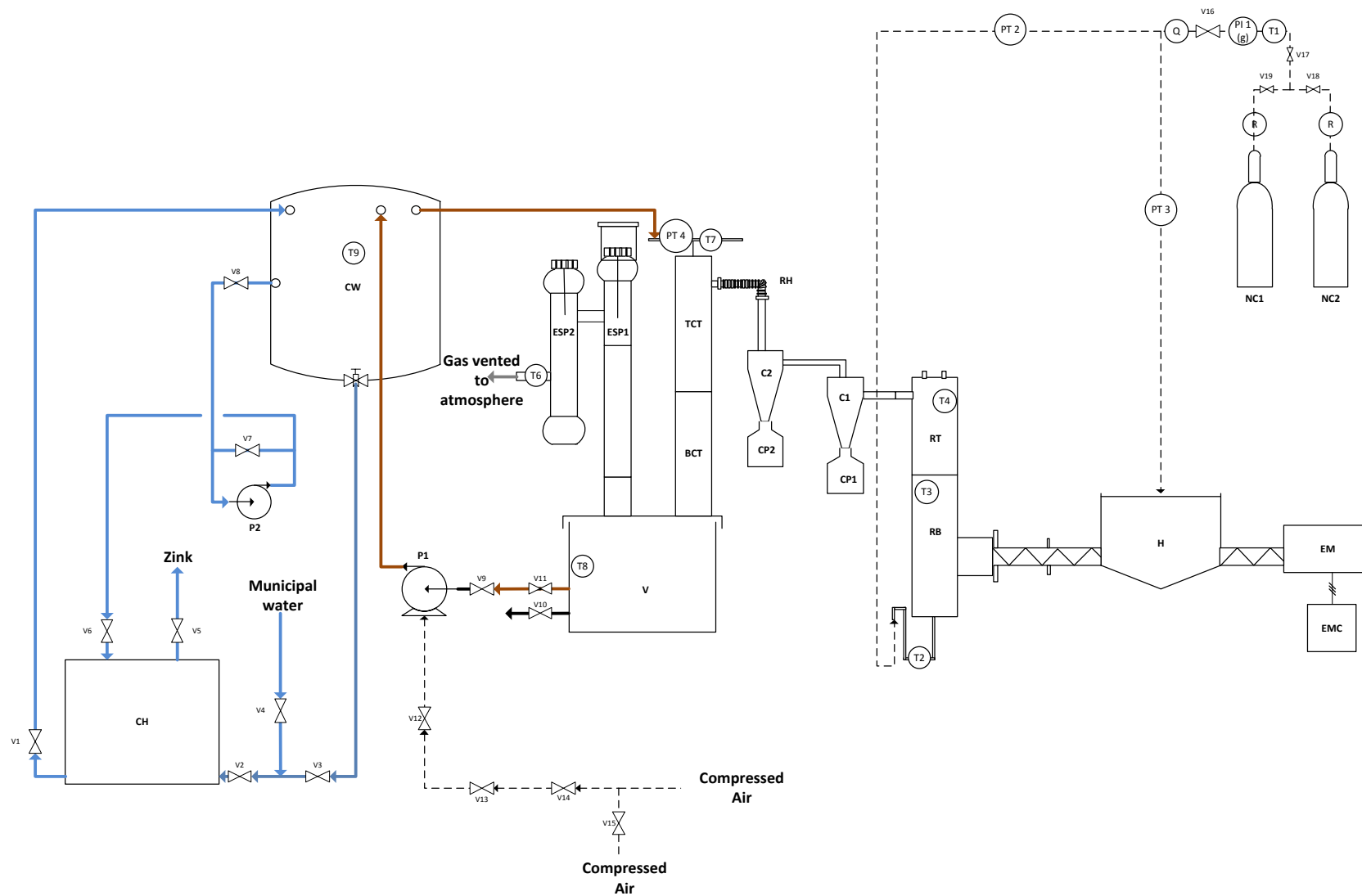
Figure 3 Experimental set-up for fast pyrolysis unit at the University of Stellenbosch

The noncondensable gases are released to the atmosphere. The bio-oil in the collection vessel is transferred to a container whereafter the Isopar and bio-oil are separated, using a conical separating flask [170]. Bio-oil is bottled and stored at 3^oC in a dark fridge. Char is removed from the char pots and stored in vacuum sealable bags.

The experimental procedure utilized can be viewed in Appendix B.3

3.2.4 Biomass analysis and characterization

The biomass was analysed to determine various physical and chemical characteristics. A particle size distribution analysis was also performed to evaluate whether the size reduction procedure was repeatable and comparable.

A representative biomass sample was obtained and stored in a temperature and humidity controlled room at least 24 hours prior to analysis. The cone-and-quarter-method was used to obtain representative samples. The analysis performed include: (i) proximate analysis, (ii) ultimate analysis, (iii) lignocellulosic analysis, (iv) calorific analysis, (v) moisture content analysis and (vi) ash analysis. In addition to the biomass sampling and analysis on the combined biomass, a biomass sample was taken at every run to analyse for moisture content and ash content, as described in Section 3.2.4.3 Ash analysis and Section 3.2.4.4 Moisture content analysis here after.

3.2.4.1   Proximate Analysis

The main purpose of the ultimate analysis is to determine the moisture content, volatiles, fixed carbon content and ash content. This can be performed using a Thermo-gravimetric Analyser (TGA) to analyse the biomass samples. The basic principle is to determine the weight loss at certain temperatures, as the temperature at which weight loss occurs, indicates the quantity of a certain material.

The samples were analysed using a Mettler Toledo TGA/DSC1 STARe system at the Department of Process Engineering at the University of Stellenbosch. Analysis was performed in duplicate. Approximately 150 mg of biomass was weighed and placed in a 900 uL ceramic crucible. The analysis starts with a drying step from room temperature to 110 ^oC, to allow for moisture removal. The sample is then further heated at a rate of 100K/min to 900^oC, with a nitrogen flow of 80 ml/min. The temperature is kept constant for 2.5 minutes where after oxygen is introduced at a flow rate of 80 ml/min for combustion purposes. The method employed is similar to ASTM E1131, however slightly more prompt.

3.2.4.2   Ultimate Analysis

The ultimate analysis is used to determine the carbon, hydrogen, nitrogen and oxygen content of the biomass. Oxygen content is often determined by difference. An elemental analyser, a Leco TruSpec micro elemental analyser, was used to analyse samples in triplicate at the Central Analytical Facilities at the University of Stellenbosch. The biomass sample is weighed (approximately 2-2.2 mg samples were used) whereafter the sample is combusted to produce CO_2, H_2O, NO_2 and SO_2 gases. The quantity of these gases is determined and used to determine the quantity of each element that was present in the biomass sample. The oxygen content was determined by difference.

3.2.4.3   Ash analysis

The ash content of the biomass was determined using two different methods. The first method has already been described – using TGA where the amount of ash present is determined as the remaining

mass. The second method was according to the procedure described in a NREL Laboratory Analytical Procedure for the Determination of Ash in Biomass, where combustion of the organic fraction occurs in a muffle furnace at $575\pm25^{o}C$, with ash as the remainder in the crucible [171]. The laboratory analytical procedure is aimed at determining the ash content, such as the mineral and inorganic content in wood.

3.2.4.4   Moisture content analysis

The water content in the biomass can also be determined using two different analysis methods. The first is by using the TGA to determine the initial moisture, as has been described. TGA analysis was used for characterisation of the raw biomass.

 The second method uses a convection oven for biomass drying at $105\pm3^{o}C$. This method is described in the Determination of Total Solids in Biomass and Total Dissolved Solids in Liquid Process Samples Laboratory Analytical Procedure as issued by NREL [172]. The convection oven method was used to determine the moisture content of the pre-treated biomass, to confirm that the correct moisture content according to the experimental design was obtained from the drying pre-treatment. Samples were analysed at the Wood Science and Forestry Department at the University of Stellenbosch.

3.2.4.5   Extractives and Lignocellulosic analysis

The extractives and lignocellulosic content in the biomass were determined using NREL LAP methods, specifically the Preparation of Samples for Compositional Analysis, Determination of Extractives in Biomass and the Determination of Structural Carbohydrates and Lignin in biomass [173–175]. The hydrolysate from the analysis was analysed on a HPLC for sugar content. For cellobiose and arabinose, a Biorad Aminex HPX-87H column, 7.8x300mm and 9 μm was used. For glucose, xylose and mannose a Waters XBridge Amide column, 4.6 x 250mm and 3.5μm was used. For the Aminex column, the analytical conditions used can be viewed in Table 22 and for the Xbridge column the analytical conditions can be viewed in Table 23.

Table 22 HPLC analysing conditions for Aminex HPX-87H column

Condition Description	Condition Value
Column Temperature	65 ^{o}C
Flow	0.6 mL/min (isocratic)
Mobile phase	0.005M H_2SO_4
Injection volume	30 μL
Detection mode	Refractive Index, Shodex RI-101, Temperature = 45°C, UV-Vis, Spectra System UV 1000, 215nm
Run time	120 minutes

Table 23 HPLC analysing conditions for Xbridge Amide column

Condition Description	Condition Value		
Column Temperature	30 ^{o}C		
Flow	0.7 mL/min		
Mobile phase A	0.01M Ammonium Acetate in 40% Acetonitrile		
Mobile phase B	0.01M Ammonium Acetate in 80% Acetonitrile		
Injection volume	10 µL		
Detection mode	Varian ELSD 380, Evap 80°C, Neb 70°C, 1.5 SLM		
Run time	43 minutes		
Gradients	Time (min)	% Mobile A	% Mobile B
	0	0	100
	28	20	80
	33	40	60
	38	0	100
	43	0	100

3.2.4.6 Calorific value analysis

The higher heating value (HHV) of a substance is the energy associated with heating the substance from a reference temperature to the temperature of combustion where-after combustion occurs and the products from combustion are cooled to the reference temperature again. The sum of the energy released or required for the three stages (heating, combustion and cooling) is the higher heating value of a substance. This can experimentally be analysed using a bomb calorimeter. Studies have also focused on developing empirical correlations to calculate the higher heating value from an elemental basis or from the results of a proximate analysis. In this study the calorific value of the biomass was determined using a bomb calorimeter at the Wood Science and Forestry Department at the University of Stellenbosch. Furthermore, the results from elemental and proximate analysis were also used to calculate the HHV.

Based on the elemental analysis, the following correlations are available in literature for HHV determination [176], [114], [177], [178] :

$$HHV \left[\frac{kJ}{kg}\right] = 35160 \times C + 116225 \times H - 11090 \times O + 6280 \times N + 10456 \times S \qquad \text{Equation 21}$$

Where C, H, O, N and S is the carbon, hydrogen oxygen nitrogen and sulphur mass fractions as determined by ultimate analysis. Equation 21, or the Boie equation, is applicable to biofuels, oil fuels and coke/char/coke fuels [176]. This equation predicted the HHV of 28 shale oils accurately with variance between measured and predicted values only ranging between 0.16-2.86% [176]. In a different study the Boie equation predicted the HHV within 1.8% - 5% of the measured HHV [176], [114], [177] .

In a different study, a correlation to determine the HHV for biomass, coals, char, liquid and gaseous materials from elemental analysis was developed, Equation 22. It is valid for C, H,O,N , S and ash ranges of: 0.00-92.25%, 0.43-25.15%, 0.00-50.00%, 0.00-5.60%, 0.00-94.08% and 0.00-71.4% respectively, with the %mass on a dry basis [114]. This correlation has been reported to have an average absolute error of 1.45% [114].

$$HHV\left[\frac{MJ}{kg}\right] = 0.3491 \times C + 1.1783 \times H - 0.1034 \times O - 0.0151 \times N + 1.1005 \times S - 0.0211A$$

<div align="right">Equation 22</div>

Equation 23, initially reported by Francis and Llyod in 1983, can also be utilized in determining the HHV from elemental analysis results using weight percentages are on a dry basis. This correlation can be used for chars and lignocellulosic waste material [177].

$$HHV\left[\frac{kJ}{kg}\right] = 357.8 \times C + 1135.6 \times H - 85.4 \times O - 54.9 \times N + 119.5 \times S - 974 \qquad \text{Equation 23}$$

The HHV can also be determined from correlations using proximate analysis data. These correlations are provided in Equations 24 and 25. Equation 24 is applicable to lignocellulosic materials and lignocellulosic-derived chars [177]. In this equation, FC is the fixed carbon and VM is the volatile matter content in weight percentage on a dry basis. The correlation deviates from experimentally determined HHV with less than 2% in most cases [177].

$$HHV\left[\frac{kJ}{kg}\right] = 354.3 \times FC + 170.8 \times VM$$

<div align="right">Equation 24</div>

Equation 25 also utilizes the proximate analysis results to calculate the HHV and is applicable to solid fuels, including char, coal and biomass [178]. The acceptable ranges for FC, VM and ASH are: 1.0-91.5%, 0.92-90.6% and 0.12-77.7% respectively [178]. The average absolute error for the correlation is 3.74% [178].

$$HHV\left[\frac{MJ}{kg}\right] = 0.3536 \times FC + 0.15598 \times VM - 0.0078 \times ASH$$

<div align="right">Equation 25</div>

All of the above equations will be used to evaluate the HHV of the biomass. The results will be compared to the experimentally determined HHV. The most accurate correlation will be used to calculate the HHV. Since the proximate and ultimate analysis were performed in at least duplicate, average values from the results will be used in the correlations.

3.2.4.7 Biomass Particle Size Distribution (PSD)

As a means of determining whether the biomass size reduction procedure is consistent and produce similar samples for the experiments, a biomass particle size distribution will be performed on each of the wood samples taken prior to the experiments. The size can only be indicated as a range in which the actual particle size falls.

A Retsch Vibratory Sieve Shaker AS 200 will be used at a 70 amplitude setting for 10 minutes. The mass of biomass remaining on each sieve, as well as the base pan, will be weighed and the cumulative mass distribution over the different size classes can be determined. For the size fraction 250 – 850 μm, the available sieve mesh sizes are: 250 μm, 300 μm, 425 μm, 500 μm, 600 μm, 710 μm and 850 μm. For the size fraction of 1400- 2000 μm, the available mesh sizes are: 1400 μm, 1600 μm, 1700 μm, 1800 μm and 2000 μm. To quantify the results, the cumulative wt% for each particle size class (250-850 μm and 1400-2000 μm) will be compared for all biomass samples from fast pyrolysis runs. Although an exact value cannot be determined for a size class, weighted averages can be used to determine the estimated average particle size. This will be performed using the average between the available sieves and multiplying it by the wt% of biomass captured between the sieves.

3.2.5 Product analysis descriptions

3.2.5.1 Water Analysis
In the study, the bio-oil water content analysis in the bio-oil will be performed using a Karl Fischer titration method similar to other studies at the Analytical Laboratory of the Process Department at the University of Stellenbosch [67], [66], [65]. A mixture of methanol and Karl-Fischer HYDRANAL composite-5 reagent was used as solvent, with an electrometric end-point method. All analyses were performed in triplicate.

3.2.5.2 Viscosity Analysis
A rheometer was used to determine the viscosity of bio-oil. The viscosity of bio-oil has been reported to vary according to the moisture content [56]. The analysis performed in this study was on an Anton Paar MCR501 Rheometer, using RHEOPLUS/32 V2.81 software. Temperature was kept at 37°C, over 4 minutes taking 30 data-points while increasing the shear rate by 3.5 1/s.   Analyses were performed in duplicate.

3.2.5.3 HHV Analysis
The bio-oil HHV can be experimentally measured using a bomb calorimeter, similar to other studies [65], [66], [67]. Correlations also exist to calculate the HHV using results from ultimate or proximate analysis. The type of fuel determines which HHV correlation is applicable. In Section 3.2.4.6 Calorific value analysis, the different HHV correlations (Equation 21 to 25) applicable to biomass were discussed. For bio-oil as fuel, Equation 21 to 25, as well as Equation 26 [179], [180] is appropriate.

$$HHV \left[\frac{kJ}{kg}\right] = 341 \times C + 1322 \times H - 120 \times O - 120 \times N + 68.6 \times S - 15.3 \times Ash \qquad \text{Equation 26}$$

The HHV of bio-oil produced in this study was experimentally determined by J Muller Laboratories, situated in Paarden Eiland in the Republic of South Africa, using a bomb calorimeter. This was only performed on a single bio-oil sample, due to cost limitations. Equation 21 to 26 were used to calculate the HHV. The calculated HHV was compared with the experimentally determined value, to establish which correlation most accurately predicts the HHV.

3.2.5.4 Density Analysis
The density of the bio-oil is an important parameter as this can influence equipment sizing on an industrial scale pyrolysis plant. A density flask can also be used to determine the density of the bio-oil. The density flask has a constant volume and is filled with the bio-oil and heated to the temperature for which the flask is calibrated. The thermometer present inside the flask is in contact with the bio-oil and indicates the temperature of the bio-oil. As the bio-oil is heated, it expands and exceeds the volume of the flask, causing it to push over the sides. From the weight of the density flask before filling with bio-oil and after filling, at the calibration temperature, the mass of bio-oil for a set volume of bio-oil can be determined and accordingly also the density of the bio-oil. Bio-oil was stored in the fridge. After swirling of the sample to insure proper mixing, the density flask was filled and the bio-oil was allowed to reach the temperature at which analysis was performed (15°C). Excess bio-oil that was pushed out of the flask due to the expansion from heating, was cleaned with acetone to insure it was not accounted for in the weighed mass. The density flask used was a calibrated 25 mL (24.873mL) flask with thermometer, obtained from Science World. Analysis was performed in duplicate, however when the standard deviation was considered to be too large, three analyses were performed.

3.2.5.5 pH Analysis

Various studies have also been performed on the pH analysis of the bio-oil, using a pH probe [67], [170]. The pH analysis performed in this study was by means of an EC620131 Eutech Instruments Glass-body pH Electrode with open pore. This electrode is known to have a wide general application range and was supplied by Wirsam. Calibration of the pH meter was performed using pH buffers of 4 and 7 as this was the commercial buffers available closest to the expected pH of the bio-oil. Approximately 50 mL of the bio-oil sample was used for analysis. After calibration the pH probe was inserted into the bio-oil until a stable reading was observed on the pH meter. The pH probe was then removed and cleaned with acetone and distilled water before analysing the next sample. Analyses were performed in duplicate and where high deviations were observed, it was analysed in triplicate.

3.2.5.6 Ultimate Analysis

The bio-oil`s carbon and hydrogen, nitrogen and sulphur content can be determined using ultimate analysis. Often oxygen is determined by difference [56]. Due to small sample sizes used in the elemental analysis, it is recommended by Oasmaa & Peacocke (2010) that the analysis be performed in, at least, triplicate. The sample does not require pre-treatment. The bio-oil samples produced in this study were analysed for carbon, hydrogen, nitrogen, sulphur and oxygen content (by difference) using a Leco TruSpec micro elemental analyser at the Central Analytical Facilities at the University of Stellenbosch. Samples were analysed in at least triplicate and where standard deviations were high, quadruple analysis were performed.

The bio-oil sample is weighed (approximately 2-2.2 mg samples were used) whereafter the sample is combusted through the entry of pure oxygen with a burn profile of 15 seconds at a furnace temperature of 1075 $^{\circ}$C to produce CO_2, H_2O, NO_2 and SO_2 gases. The oxygen content was calculated by difference. Calibration for bio-oil analysis on the elemental analyser was performed using a standard, Residual oil (AR 100), from Alpha Resources Inc. This standard has previously been used by Oasmaa et al. [181] for calibration of elemental analysis on bio-oil. The residual oil`s composition is provided below in Table 24. Difficulty with analyses was experienced for both the calibration standard and the bio-oil, due to volatility, resulting in the initial weighed mass not being similar to the mass upon entry into the elemental analyser due to evaporation of the volatile components in the sample. This was resolved by using Com-Cat Accelerator, a tungsten oxide with potassium dihydroxgen-phosphate, provided by LECO, in conjunction with the bio-oil samples. 2 mg of this reagent was added to the capsule prior to adding 2 mg of the bio-oil sample which was previously homogenised with a vortex for 30-60seconds. The capsule was closed to avoid spillages and contamination from ambient air. Standard deviations and repeatability improved with the modified method. The results from sulphur analysis were similar to, or below, the detection limit of the analyser, therefore these values were not considered trustworthy and disregarded in the results provided in Table 96 in Appendix D. The elemental analysis on a dry basis was calculated using the moisture content obtained from Karl Fischer analysis. Since the elemental analysis on a dry basis is not directly measured, no standard deviation and CV are reported.

 The analysis on the bio-char was similar to that of bio-oil, however no Com-Cat Accelerator was used and the burning profile differed slightly. The burning profile utilized consisted of 15 seconds of oxygen injection, followed by 5 seconds without gas injection, followed by another 15 seconds of oxygen injection. The furnace temperature was at 1080°C and the calibration for bio-char analysis was performed using standard AR-2781 Coal Standard, supplied by Alpha Resources Inc. The composition of the standard can be viewed in Table 24.

Table 24 Elemental composition of calibration standard: Residual Oil AR 100

Element	Composition of AR 100	Standard deviation for AR 100	Composition of AR 2781
Carbon	88.03	1.68	67.68
Hydrogen	10.49	0.36	3.97
Nitrogen	0.2	0.04	1.29
Sulphur	0.96	0.08	1.91
Oxygen	Not reported. Calculated by difference 0.32 wt%	Not reported	Not reported

3.2.5.7 GC-MS Analysis

To determine which GC-column is best suited, the results from two different columns, a HP5 and a Zebron 1701 column, were compared. Only components with a probability greater than 70% were considered in the analysis. The ZB-1701 column consists of 14% cyanopropylphenyl and 86% dimethyl polysiloxane and is considered a mid-polarity phase, general purpose column for the analysis of oxygenates and alcohols [182]. According to the Zebron datasheet, the application can include alcohols, phenols, esters, polycyclic aromatic hydrocarbons, solvents, aromatic hydrocarbons and amines [183], [184]. The HP-5MS column consists of 5%diphenyl and 95% dimethyl polysiloxane and is considered a low-polarity phase column and is considered a general purpose column for semi-volatiles and hydrocarbons [182]. In selecting the most appropriate GC-column a variety of factors were considered. The ZB 1801 column has a wide variety of acceptable applications, of which aromatic hydrocarbon analysis is one. Since the purpose of the study is to investigate the production of aromatics, the fact that the ZB-1701 column analyses for aromatic hydrocarbons, PAHs and phenols makes it suitable for analysis in the specific application for which it is required. Comparison of the responses for a major component, levoglucosan, on the different columns, indicated a peak that can be integrated more accurately on the ZB-1701 (60mx 0.25mmx0.25 µm), which was used in this study. Chromatograms can be viewed in Appendix C, Figure 44 and Figure 45.

In this study, GC-MS analysis was performed on an Agilent GC/MSD 7890A/5975C (single quadropole with Electron Ionization) with a multimode injector. Screening analysis for preliminary component identification on the GC-MS identified up to 319 components. The preliminary analyses were used to identify components with 70% or greater probability and an area% greater than 1.5% and these identified components were considered for quantification with standards on a ZB-1701 column and available standards were ordered to quantify these components. For preliminary component analysis, the area% of the components was determined relative to an internal standard as a means of improving the quality of the area% results. The instrument settings used for the preliminary analysis are provided in Table 25. From the preliminary results, components with a 60% or greater probability (according to the GC-MS library search) were used for categorizing into chemical families, see Table 43. Although the area% does not reflect quantitative data, it does however provide a relative basis for comparison of each chemical group between the different runs to indicate whether changes in experimental conditions had an influence on the distribution of chemical families. Since only components with a 60% or greater probability were considered, the cumulative area% for the components does not account for 100% of the total area%.

Quantification was performed using standards purchased from Sigma-Aldrich. A standard solution was made up and diluted to 7 different concentrations which were used for calibration purposes. Initially heptane was considered as internal standard, however it was observed that the heptane was

volatile and evaporation occurred during preparation and handling. A different internal standard, methyl-behenate, was used instead. Sample preparation included weighing 300 mg of bio-oil sample in a 2ml vial and adding 200µl of internal standard of a known concentration. 1000 µl Methanol was added followed by filtration through a 0.2µm filter into a 2ml vial. Samples were injected into the GC-MS and analysed using the instrument settings provided in Table 25. Both a SCAN and SIM (Selection Ion Mode) were used in separate analysis during component quantification. The instrument settings are provided below in Table 25.

GC-MS analyses of bio-oil were compared to that of Isopar, to ensure contamination from poor separation does not occur, and influence the component analysis results. Obvious differences between the Isopar and bio-oil were observed, see Appendix C, Figure 46, showing that overlapping of components between isopar and bio-oil does not occur; therefore any contamination will be noticeable in the GC-MS analysis on the bio-oil.

Table 25 GC-MS instrument settings

GC-MS Instrument settings			
	Preliminary analysis	**Component quantification SCAN**	**Component quantification SIM**
Injector temperature	260 °C	260 °C	260 °C
Injection volume	1 µl	1 µl	1 µl
Injection mode	Split	Split	Split
Split ratio	20:1	50:1	5:1
Split flow	26 ml/min	6.5 ml/min	6.5 ml/min
GC Mode	SCAN	SCAN	SIM
Column flow rate	1.3 ml/min	1.3 ml/min	1.3 ml/min
Carrier gas	Helium	Helium	Helium
MS transfer	280 °C	280 °C	280 °C
MS mode	Single Quadropole with electron ionization	Single Quadropole with electron ionization	Single Quadropole with electron ionization

3.2.5.8 NMR Analysis

In this study, a ^{13}C and a proton-NMR were performed. The ^{13}Carbon isotope was used as the components on which the analysis was based as well as on ^{1}Hydrogen. The same chemical shift ranges as in the studies by DeSisto et al. [21] and Ingram et al. [37] were used in this study, see Table 8 and Table 9, p.20-21. A Varian Inova NMR was used for both ^{13}C and ^{1}H analysis, with the deuterated solvent dimethyl (DMSO-d6). The preparation method was similar to that described by DeSisto et al. [21]. All the ^{1}H spectra were run at the same 45 ^{o} pulse angle, with 0.012mg Chromium (III) acetylacetonate (Cr(acac)$_3$), 64 scans and a 1 second inert-pulse delay at 25 ^{o}C. Spectra were referenced to the residual DMSO peak. All ^{13}C spectra were run at the same 90 ^{o} pulse angle with 0.012 mg Cr(acac)$_3$ and NOE enhancement suppression, full proton decoupling for 4000 scans at 1 second inert-pulse delays at 25 ^{o}C. Both the ^{1}H and ^{13}C spectra were referenced to the residual DMSO peak within the chemical shift analysed. The analysis was performed by the Central Analytical Facilities at the University of Stellenbosch. The area underneath the curve is integrated to determine the percentage of the element (carbon or hydrogen in this case) that is part of a certain functional group (in a specific chemical shift range).

To relate the proton NMR results to a volume%, Equations 4-6 were used to estimate the volume % of the paraffins, olefins and aromatics [81]. These equations have previously been used to relate the

proton NMR data to volume % of aromatics, aliphatics and olefins for bio-oil produced from oak sawdust in a slow pyrolysis set-up [81]. Results indicated that the equations were not capable of representing the fast pyrolysis bio-oil produced in this study. For this reason, results are not included.

3.2.5.9 Mass balances

Difficulty with mass balance closure for fast pyrolysis experiments have been experienced by various researchers [38]. In a study by Oasmaa et al. [56], mass balances ranged from 91-93 wt%. Acceptable mass balance closure is considered to be 90-100% [60]. The bio-oil (the liquid phase product from fast pyrolysis) consists of pyrolytic water formed during pyrolysis, the moisture which was initially present in the biomass and an organic liquid fraction. The mass yields were determined as described below.

$$M_{BM,dm}[dm] = M_{BM,wet\ feedstock\ basis}\ x\ (100 - A_{BM,oven})$$

Equation 27

$$Yield_{Gas}\ [wet\ feedstock\ basis] = \frac{M_{BM,wet\ feedstock\ basis} - M_{BO,weighed\ mass} - M_{char,weighed\ mass}}{M_{BM,wet\ feedstock\ basis}}$$

Equation 28

$$Yield_{Char}\ [wet\ feedstock\ basis] = \frac{M_{char,weighed\ mass}}{M_{BM,wet\ feedstock\ basis}}$$

Equation 29

$$Yield_{Org}[wet\ feedstock\ basis] = \frac{M_{BO,weighed\ mass} - M_{BO,weighed\ mass}x\ A_{BO,KF}}{M_{BM,wet\ feedstock\ basis}}$$

Equation 30

$$Yield_{PyrW}[wet\ feedstock\ basis] = \frac{M_{BO,weighed\ mass}x\ A_{BO,KF} - M_{BM,wet\ feedstock\ basis}\ xA_{BM,oven}}{M_{BM,wet\ feedstock\ basis}}$$

Equation 31

$$Yield_{Gas}\ [dm] = \frac{M_{BM,wet\ feedstock\ basis} - M_{BO,weighed\ mass} - M_{char,weighed\ mass}}{M_{BM,dm}}$$

Equation 32

$$Yield_{Org}[dm] = \frac{M_{BO,weighed\ mass} - M_{BO,weighed\ mass}x\ A_{BO,KF}}{M_{BM,dm}}$$

Equation 33

$$Yield_{PyrW}[dm] = \frac{M_{BO,weighed\ mass}\times A_{BO,KF} - M_{BM,wet\ feedstock\ basis}\ xA_{BM,oven}}{M_{BM,dm}}$$

Equation 34

$$Yield_{Char}\ [dm] = \frac{M_{char,weighed\ product\ mass}}{M_{BM,dm}}$$

Equation 35

Where BM is the biomass, BO is the bio-oil product, $Char$ is the char product, Gas is the noncondensable gaseous product, Org is the organic fraction in the bio-oil and $PyrW$ is the pyrolytic water formed. M refers to the mass [kg], A refers to the content of moisture determined from a certain analysis, KF refers to the moisture determined by the Karl Fisher analysis [wt%], and $oven$ refers to the moisture determined from drying in an oven [wt%]. The unit dm refers to the dry mass basis and $wet\ feedstock\ basis$ refers to the feedstock as used in the pyrolysis experiment with a pre-determined moisture content according to design of experiments (DOE).

3.2.5.10 Energy transfer to BO

The energy transfer was calculated as a fraction of the energy present in the initial biomass that was present in the liquid and char phases after pyrolysis, see Equations 36 and 37. In these equations, E

is the energy, BO is the bio-oil, BM is the biomass, HHV is the higher heating value [MJ/kg] and M is the mass [kg].

$$Energy\ transfer\ to\ BO\ =\ E_{BO}\ /E_{BM}\ =\ (HHV_{BO} \times M_{BO})/\ (HHV_{BM} \times M_{BM}) \qquad \text{Equation 36}$$

$$Energy\ transfer\ to\ Char\ =\ E_{Char}\ /E_{BM}\ =\ (HHV_{Char} \times M_{Char})/\ (HHV_{BM} \times M_{BM}) \qquad \text{Equation 37}$$

3.3 Results and Discussion

Fast pyrolysis is the process where swift thermal degradation of the biomass occurs to produce vapours that are quickly quenched to yield a liquid product. Other products include char and incondensable gases. The product yields and bio-oil quality were investigated at different experimental conditions (temperature, particle size and moisture content). This will assist in determining the significant factors that need to be optimized for optimal conditions at which a commercial fast pyrolysis plant can produce bio-oil before further upgrading to fuels, should be operated.

3.3.1 Biomass analysis and characterization

3.3.1.1 Ultimate analysis, proximate analysis, moisture, ash

The results from characterization of the biomass are provided in Table 26. The results indicated that the analysis was repeatable for moisture contents, volatile matter and fixed carbon, with CVs of less than 2%. However for the ash content, present in the smallest quantity (two orders of magnitude less than for the other materials), the CV is 27%, indicating significant variance. This is attributed to the small quantity on which even a very small standard deviation (standard deviation of only 0.06 to result in a CV of 27%) will lead to a significant deviation.

Table 26 Biomass characterization results

Proximate Analysis				
Material	**Unit**	**Average**	**Std. Dev.**	**CV [%]**
Moisture content	wt % on wet basis	11.1	0.22	1.96
Volatile matter	wt % on wet basis	73.9	0.14	0.19
Fixed carbon	wt % on wet basis	14.8	0.01	0.09
Ash content [a]	wt % on wet basis	0.2	0.06	27
Studies` results					**Literature Sources**				
Measure-ment	**Unit**	**Ave-rage**	**Std Dev.**	**CV [%]**	[b] *Pinus Radiata*	[c] *Pinus sylvestris*	[d] *Pinus strobus*	**Literature Range**	
								Min	**Max**
Ultimate Analysis									
C	dry wt%	50.4	0.16	0.3	50.1	50.5	50.1-51.8	50.1	51.8
H	dry wt%	5.7	0.03	0.5	5.6	6.4	6.1-6.3	5.6	6.3
N	dry wt%	<0.1	<0.00	5.0	0.1	<0.1	<0.5	<0.1	<0.5
O	dry wt%	43.8*	0.13	0.3	44.1	43	42.0-43.4	43	44.1
Higher Heating Value (HHV)									
HHV BC [e]	MJ/kg	19.56	-	-	-	20.4	18.04	18.04	20.4
HHV_Boie [f]	MJ/kg	19.70	-	-	19.3	20.4	20.1 -20.7	19.3	20.7
HHV_Cordero [g,h]	MJ/kg	20.08	-	-	-	-	-	-	-

* Determined by difference, [a] Determined using TGA and not the NREL LAP for the Determination of Ash in Biomass, [171], [b] calculated from [185] using 7.6% moisture, [c] [56], [d] calculated from [21] using 10% and 13% moisture content, [e] bomb calorimeter, [f] on ultimate analysis results, [g] on proximate analysis results, [h] [177]

When considering the elemental analysis, the standard deviation is small and the CV is less than 0.5 % for C, H and O. However the element present in the smallest quantity (nitrogen, whose presence is two orders of magnitude smaller than the other elements analysed), has a CV of 5.0%, indicating that there is a greater difference in the results from the analysis for nitrogen. When comparing the elemental results with literature results for different types of pine wood, all results fall within the literature range determined from previous studies [185], [56], [21], [169]. It can be concluded that the ultimate analysis results compare favourably with that of literature.

The results from the HHV correlations were compared with the experimentally determined value to determine which of the correlations most accurately predict the experimentally determined HHV, as indicated in Table 26. Correlations based on the ultimate analysis results were more accurate than the correlations based on the proximate analysis results, 19.7 MJ/kg compared to 20.08 MJ/kg respectively. This might be attributed to the accuracy of either the correlations themselves, or the ultimate and proximate analysis. In a study by Oasmaa et al. [56] the HHV of *P. sylvestris* was determined to be 20.4 MJ/kg on a dry mass basis. In another study where the HHV of *P. strobus* was tested, it was determined at 18.04 MJ/kg for 10-13 wt% moisture biomass. The HHV of the oven-dried biomass analysed in this study (19.7 MJ/kg) was lower than the reported HHV of 20.4 MJ/kg and higher than the HHV reported for biomass with moisture contents of 10-13wt%. Although slight differences occurred between the analysed value and the literature values, the HHV is within the range reported in literature. The most accurate correlation using the ultimate analysis was the Boie´s correlation and the most accurate correlation using the proximate analysis was the correlation provided by Cordero et al. [177].

The compositional characteristics of the biomass were determined using NREL Laboratory Analytical Procedures. Moisture, ash, water and ethanol extractives were determined from NREL Laboratory Procedures described earlier. The sugars and lignin content were determined using HPLC methods. Results are provided in Table 27.

Table 27 Biomass compositional characterization

Composition	Dry mass [wt%]	Normalized [wt%] [b]
Ash content [a]	0.22	0.25
Total Extractives	8.57	9.86
Water Extractives	5.17	5.96
Ethanol Extractives	3.39	3.91
Lignin	23.84	27.44
Cellulose	36.13	41.58
Glucan	36.13	41.58
Hemicellulose	18.12	20.86
Xylan	7.88	9.07
Arabinan	0.75	0.86
Mannan	9.49	10.92
Galactan	0.00	0.00
TOTAL	86.87	100.00

[a] Determined using NREL Lap for the Determination of Ash in Biomass, [171], [b] Normalized analysis results to 100 wt%

The results in Table 27 show that 13.13wt% of the dry mass cannot be accounted for from the analysis results. Repetition of the analysis yielded similar results. Similar problems were experienced in a different study where 5-17% of the material could not be identified after acid hydrolysis of the biomass feedstock [56]. The HPLC analysis on the hydrolysate showed an unknown peak emerged at

a longer retention time than the other components that were analysed for. This can possibly be a polysaccharide that was not completely hydrolysed.

The method and type of extractives are often unspecified in studies, resulting in variance and difficulty in comparison on the same basis. To ensure comparison on the same basis, the wood composition on an extractive-free basis was determined for the compositions reported in literature. Comparison with literature composition for pine wood and softwood on an extractive-free and normalized basis can be viewed in Table 28.

Cellulose was the most abundant constituent, followed by lignin and lastly hemicellulose. For all compositions, the results fall within the literature range, except for lignin. The lignin content of 30.45wt% slightly exceeds the maximum value of 29.22wt% reported in literature. However when taking the standard deviation of lignin measurements into account, the lignin is comparable to the maximum reported in literature. The greatest variation was the results of the cellulose content, with a standard deviation of 3.1wt%. The standard deviation for lignin and hemicellulose was less than for cellulose.

Table 28 Biomass component analysis comparison with literature on an extractive free basis

Composition	This study	Literature Values								
Wood type	*PR*	*PR* [c]	*PR* [d]	*Scots Pine* [e]	*Soft-wood* [f]	*PR* [g]	*Pine* [h]	*PR* [i]	*Litera-ture Min*	*Litera-ture Max*
Ash content [a] [wt%]*	0.28 ± 0.04	0.19	0.74	0.00	0.33	0.18	-	-	*0.00*	*0.74*
Lignin [wt%]*	30.45 ± 1.1	25.80	26.38	29.22	28.53	25.85	21 - 29	27.6	*21.00*	*29.22*
Cellulose [wt%]*	46.14 ± 3.1	42.03	53.19	43.55	45.83	42.11	46 - 50	50.9	*42.03*	*53.19*
Hemicelluloses [wt%]*	23.14 ± 0.9	31.99	19.68	27.23	22.56	32.05	19 - 22	19.8	*19.00*	*31.99*

* wt% based on moisture free and extractive free basis, [a] Determined using NREL Lap for the Determination of Ash in Biomass, [171], [b] Normalized analysis results to 100 wt%, [c] [185], [d] [186], [e] [187] , [f] [188], [g] [169], [h] reported in [13] as adapted from [189], [i] [190], PR= *Pinus radiata*

3.3.1.2 Biomass particle size distribution

To evaluate the biomass preparation procedure and to ensure that the biomass particle sizes for the various experimental runs were comparable, a particle size distribution was performed on the biomass of each experimental run. For the small biomass size class (250 – 850 μm), the particle size distribution was evaluated for ranges 250-300 μm, 300-425 μm, 425-500 μm, 500-600 μm, 600-710 μm, and 710-850 μm. For the large biomass size class (1400 – 2000 μm), the particle size distribution was evaluated for ranges 1400-1600 μm, 1600-1700 μm, 1700-1800 μm and 1800-2000 μm.

The biomass particle size distribution for the smaller biomass size class (250 – 850 μm) for runs 3, 6, 8 and 10 were comparable, as can be seen in Figure 40 in Appendix A.1 Biomass particle size distribution analysis. A slight difference existed for the quantity of biomass in size fraction 600-710 μm, which was slightly larger for Run 8 than it was for Runs 3, 6 and 10. All standard deviations were smaller than 1.05wt%, except for the standard deviation of particle size fraction 600-710 μm which was 5.44wt%, indicated in Table 85 in Appendix A.1 Biomass particle size distribution analysis. When considering the larger particle size class investigated (1400 – 2000 μm), the cumulative wt% for the

different size class fractions correspond well for the different runs with all standard deviations smaller than 1.7wt%, see Figure 41, in Appendix A.1 Biomass particle size distribution analysis.

Overall, the cumulative wt% corresponds well for the different experimental runs, for both the small and large particle size fractions. This indicates that the procedure used, delivered uniform particle size distribution and particle size classes between the different experimental runs were comparable.

3.3.2 Product yields

When considering the best operating and pre-processing conditions for a fast pyrolysis facility and the objective of this study, two aspects should be considered, the final product yield (organic fraction of the bio-oil) and the quality of the product (with regards to BO moisture content, viscosity, HHV, density, pH, elemental composition of C,H,N and component composition). The yields from the experimental runs and the physio-chemical results from the fuel products were statistically analysed to determine significance of the factors investigated and the optimal conditions at which the factors should be operated. The regression equations can be used to calculate the responses for comparison with the measured values.

The factors influencing the phase yields were investigated and the significant factors identified using ANOVA analysis. The significant factors, the regression model`s R^2 and regression equation are provided in Table 30. The assumptions made with the ANOVA analysis were validated for the char yield fraction, the gas yield fraction, the organic phase fraction and the pyrolytic fraction. Results from run 4 are not included due to problems experienced during the run.

Yields from this study and other literature studies are summarized in Table 29. These results are discussed in detail in Section 3.3.2.

Table 29 Comparison of product yields between study and literature for fast pyrolysis

	This study	**[21]**	**[37]**	**[191]**
	Wt% (dm)	**Wt% (dm)**	**Wt% (dm)**	**Wt% (dm)**
Char yield	11.2 − 15.3	13.3 − 18.7	18.6 − 21.5	18 − 22
Gas yield	27.2 − 36.2	21.1 − 27.6		27 − 38
Organic liquid yield	39.8 − 52.1	NR	NR	NR
Pyrolytic water yield	6.1 − 17.4	NR	NR	NR
Liquid yield	56 − 68	71 − 76	51.8 − 54.1	49 − 54

NR- not reported, cannot be calculated with available literature

3.3.2.1 Phase yield: Char

3.3.2.1.1 Experimental data

The char yield ranged from 11.2-15.3wt% (dm basis, at 488°C, 3.7wt% moisture and 250-850µm, and 491°C, 4.0wt% moisture and 1400-2000µm respectively) and 10.5-14.7wt% (wet feedstock basis), see Table 94 in Appendix D. The literature results in Table 29 show that pyrolyzing *P. strobus* in a fluidized bed reactor with 60g/h capacity, resulted in a char yield of 13.3-18.7wt% (dry feedstock basis) at 500°C [21]. When pine wood was pyrolysed in an auger reactor with 1kg/h capacity, the char yields ranged between 18.6-21.5wt% (dry feedstock basis), [37]. The auger reactor set-up typically has slower heating rates and longer solid residence times [21], favouring char production by secondary reactions such as repolymerization [37], [68], [191], [62], [32].

3.3.2.1.2 Statistical analysis

The statistical analysis indicated that the moisture content, particle size and the interaction between the aforementioned were significant factors influencing char yield. The surface model, described in Table 30, had a good fit, with R^2 and adjusted R^2 values of 0.9756 and 0.9573 respectively. The surface plot of the model depicts a twisted plane, see Figure 4. This is due to the significant interaction existing between the particle size and moisture content. The surface plot indicated that the largest char yield was obtained at low moisture content and large particle sizes. For high moisture contents, the particle size does not influence the char yield as much as at low moisture contents. This can be observed from the steeper gradient on the 4wt% moisture plane compared to the 10wt% moisture plane. Furthermore, the char yield increases with an increase in particle size. This might be due to either of two reasons: (1) incomplete volatilization of the lignocellulosic content in the particle due to insufficient heat transfer throughout the particle, or alternatively (2) a lower heating gradient exists throughout the particle, which will affect the kinetics of the formation of volatiles. The lower heat gradient results in a slower heating rate, which promotes secondary reactions such as repolymerization, followed by an increase in char yield, similar to the reasoning behind increased char yields from auger reactors. This is supported by the increase in the carbon content of the char with an increase in particle size, as depicted in Figure 24.

When considering the response surface model for the char yield, the error between predicted and actual values ranged from -2.81% to 2.62%, shown in Table 30. When the response surface was used to predict the response of run 1 (an additional experimental run at a particle size of level 0), the response surface model under-predicted the yield with 14.73%. The large error% indicates that the response surface model can only be trusted within approximately 20% accuracy.

In a different study, it was found that the char yield decreased with an increase in pyrolysis reactor temperature over temperatures of 400, 500 and 600 $^{\circ}$C [21], while in this study, temperature did not have a significant effect. This may be attributed to the small temperature range and increment investigated (450 and 500°C), compared to large temperature increases of 100 $^{\circ}$C investigated in previous mentioned study. The high char yield at low temperatures can be the result of incomplete or un-pyrolysed biomass [21]. The temperature is not a significant factor, while the particle size is; therefore external particle heat transfer is not limiting, but intra-particle heat transfer is. In another study, performed on the same experimental setup, but using *Eucalyptus grandis* as biomass, it was concluded that neither the particle size, nor the reactor temperature was significant within a 95% confidence interval. However for a 90% confidence interval, the reactor temperature was found to be significant - with an increase in reactor temperature resulting in a decrease in the overall char yield [79].
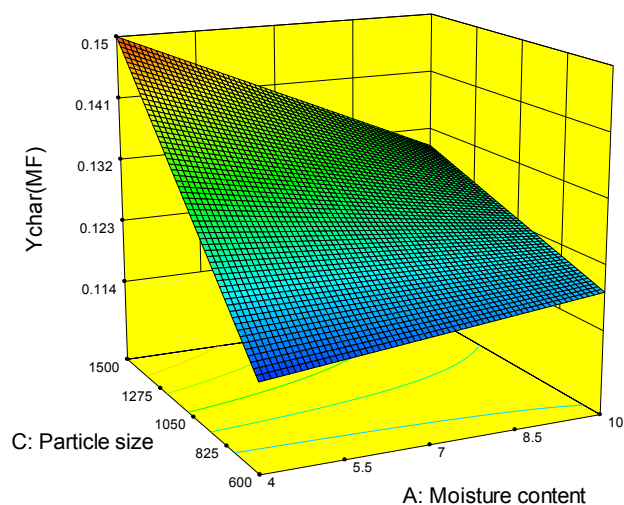
Figure 4 Surface plot of regression model for the char yield

Table 30 Significant factors influencing product yields

Quality analysed [Y]	Significant factors	R^2	R^2 adjusted	Regression equation in terms of actual factors
Char yield fraction	A: Moisture content C: Particle size AC: Moisture content and particle size interaction	0.9756	0.9573	$Y[mf] = 0.0758 + 3.681 \times 10^{-3} \times A + 5.8540 \times 10^{-5} \times C - 4.7226 \times 10^{-6} \times A \times C$
Gas yield	B: Temperature C:Particle Size BC: Temperature and particle size interactions	0.8200	0.6849	$Y[mf] = 1.2628 - 2.0208 \times 10^{-3} \times B - 1.2849 \times 10^{-3} \times C + 2.7089 \times 10^{-6} \times B \times C$
Organic phase	C: Particle size	0.8383	0.7170	$Y[mf] = 0.5635 - 2.397 \times 10^{-3} \times A - 1.0987 \times 10^{-4} \times C + 4.93 \times 10^{-6} \times A \times C$
Pyrolytic water	B: Temperature C:Particle Size	0.7992	0.7189	$Y[mf] = 0.7210 - 1.429 \times 10^{-3} \times B + 5.167 \times 10^{-5} \times C$

A: Moisture content, B: Temperature, C: Particle size

3.3.2.2 Phase yield: Gas

3.3.2.2.1 Experimental data

The gas yield obtained in this study was 25-33%, based on the wet biomass feed, and 27-36wt% based on the dry biomass feed (at 465°C, 9.5wt% moisture and 1400-2000μm, and at 493°C, 9.2wt% moisture and 1400-2000μm respectively), see Table 94 in Appendix D. In a study where *P. radiata* sawdust was pyrolysed in a bubbling fluidized bed, the gas yield ranged between ca.27-38wt% (dry feed basis) over a temperature range of 450-500°C [191]. In another study, the gas yield for a 60g/hr fluidized bed reactor, with *P. strobus* as feedstock, was 19-24wt% (wet basis) and 21.1-27.6wt% (dry biomass feed) [21]. These literature results are provided in Table 29. The gas yield from this study is higher than the gas yields where *P. strobus* was used as feedstock [21], yet comparable to yields

using *P. radiata* as feedstock [191]. Higher gas yields may indicate an increase in secondary reactions such as cracking. Due to the experimental set-up in this study, all errors of losses are compounded in the gas yield, as the gas yield was determined by difference from a mass balance in this study. Other studies with all measured yields, had indicated that total mass balance closure is extremely difficult and 90% closure is within acceptable limits, with mass losses of 10% having been reported [60]. The total gas yield calculated in this study therefore includes the error from yield measurements used in the mass balance. A significant change in the guaiacol to catechol with temperature increase has been reported for pine wood [21]. This is the result of O-CH$_3$ homolysis where the methoxy functional group is converted to a hydroxyl group, while producing methane [21]. This is due to secondary reactions occurring from the primary products produced in bio-oil and has been found to increase with temperature, which will also explain the increase in gas yield with reactor temperature [21]. Secondary decomposition from guaiacols to catechols is followed by further reactions to phenols [55].

3.3.2.2.2 Statistical analysis

The main factor influencing the gas yield is the interaction term between the temperature and the particle size. In order for the data to be hierarchical, the factors causing the interaction need to be included in the ANOVA analysis. The temperature and particle size were included, even though these factors are not significant within a 95% confidence interval. The influence of the interaction term is indicative of the interdependence between the temperature and particle size. The model indicated a good fit, with a respective R^2 and adjusted R^2 value of 0.8200 and 0.6849.

When considering the surface plot, Figure 5, it shows that the highest gas yield is obtained at high temperature and large particle size, with the lowest gas yield at low temperature and large particle sizes. The twisted lane is a result of the interaction between the temperature and the particle size. The combination of temperature and particle size can be related to the heating rate and vapour residence time respectively.

At larger particle sizes, the temperature has a greater effect on the gas yield compared to small particle sizes, as can be seen by the steeper gradient and the minimum and maximum char yields on the particle size high level plane (1500um). Larger biomass particle sizes will have a longer residence time in the fluidized bed reactor, allowing more time for secondary reactions. In addition to this, the route for the volatilized lignocellulosic material might be longer, before leaving the inner structure of the biomass particle, resulting in extended vapour residence times in contact with the char [24] – enhancing secondary reactions [32]. Long vapour residence times have been known to result in secondary cracking of the vapour to noncondensable gases , thereby increasing the overall gas yield at the expense of the char and organic liquid fraction phase [32].

The deviation for the gas yield has an error% below 5% for Runs 2-10, with the largest deviation at 4.68 % error, see Table 30. For experimental run 1, the run not used to develop the response surface, the response surface results in the largest error for all runs, an error of 14.9%. The high error% indicates that the response surface model is less capable of predicting the gas yield at conditions not initially used for model regression.

Another study on *P. radiata* reported that the gas yield increased significantly (from ca. 25 to ca. 37wt% on a wet basis) with an increase in reactor temperature from 450 to 500 ^{o}C, i.e. 723K to 773K [191]. This was due to secondary reactions at higher temperatures [191]. It was also reported that particle sizes, ranging from 0.7-1mm, had limited influence on the product distribution. This is unlike

the results observed in this study, which indicated that the particle size was indeed significant. This can be due to differences in particle size ranges investigated. For a small particle range significant changes might not be observable [191].
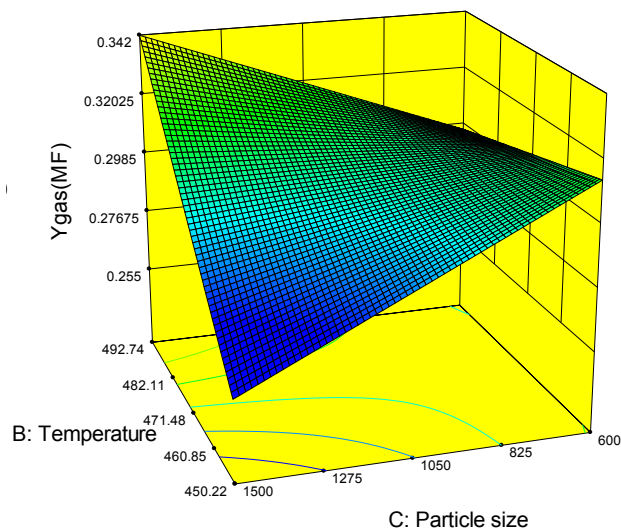
Figure 5 Surface plot of regression model for the gas yield

3.3.2.3 Phase yield: Organic Liquid

3.3.2.3.1 Experimental data

The organic liquid yield obtained in this study varied between 39.8-52.1 wt% (dm basis, at 457°C, 4.1wt% moisture and 1400-2000µm, and at 488°C, 3.7wt% moisture and 250-850µm), see Figure 6 and Table 94 in Appendix D. The organic liquid yield is lower than what has been reported for pine sawdust (*P. sylvestris*) where the organic liquid yield was 62wt% (dry feed) for a 20 kg/h unit [56]. The total liquid yield (organic fraction and water present in BO) obtained in another study where *P. strobus* was pyrolysed in a fluidized bed reactor with a 60g/h capacity, ranged between 71-76% (dry feed basis) at 500 ^{o}C, as indicated in Table 29 [21]. DeSisto et al. [21] also found temperature influenced the liquid yield, with an increase from 400 to 500°C resulting in a slight increase in the liquid yield; increasing the temperature further to 600 ^{o}C resulted in a significant decrease in liquid yield. This might be due to secondary reactions becoming more significant, which has been reported for temperatures around 650°C [192]. In this study the total liquid yields obtained at similar temperatures (around 500 ^{o}C) were lower at 56-68 wt% (dry feed basis), compared to the previous mentioned study 71-76 wt% [21]. However in another study where the effect of reaction conditions on *P. radiata* derived bio-oil was investigated, a limited change was observed in the total liquid yield for a temperature increase from 400 to 450 ^{o}C of only ca. 1-2wt%, while a further increase in the temperature to 500°C resulted in a decrease of approximately ca. 6wt%, to 45wt% (wet feed basis) [191]. When converted to a dry feed basis, the total liquid yield varied between 49-54 wt%, provided in Table 29. This is slightly lower than liquid yields obtained in this study. Differences in liquid product yields for the different studies might be a result of contact between the hot vapour and the char product and extended residence times [32]. The biomass ash content can also influence product yields, by acting as a catalyst to enhance secondary reactions. However, comparison between the biomass ash content in this study and the biomass ash content in the studies with lower and higher

73

liquid yields respectively, showed agreement (0.2wt% in this study, compared to 0.2-0.3wt% in literature) [191], [21].

 The liquid yields obtained in this study fall between the lower reported values of 49-54wt% (dry feed basis) from a study by Park et al. [191] and the higher reported values of 71-76wt% (dry feed basis) from a study by DeSisto et al. [21]. The temperature was not found to have a significant influence on the organic liquid yield in this study, indicating that a 50 ^{o}C temperature variation does not have a significant influence on the reactions that produce the organic liquid product. From an energy perspective, it will be beneficial to operate at the lower temperature investigated, as the temperature does not have a significant influence on the organic yield, although other bio-oil characteristics need to be evaluated before this can be concluded.

3.3.2.3.2 Statistical analysis

For the organic liquid yield response, the particle size is significant according to the ANOVA analysis. The maximum organic yield is achieved at small particle sizes. In a study by Niu and Liu [193] the biomass particle size influenced the decomposition kinetics for pine-branch biomass, with an increase in particle size resulting in an increase in the activation energy. This observation was related to the negative correlation between ash content and particle size, with the small particles containing a higher ash content and having a smaller activation energy for decomposition [193]. At certain conditions, the lower activation energy of small particle sizes can enhance decomposition reactions to produce greater organic yields, compared to larger biomass particle sizes. The organic yield decreases with an increase in the particle size at both the high and the low moisture contents investigated, according to the surface response model as indicated in Figure 6 below. The R^2 value for the model to the data is 0.8383 with an adjusted R^2 value of 0.7170 and a small predicted R^2 of 0.353, see Table 30.

From the surface plot it can be seen that the moisture content has an effect on the organic yield which is greater at larger particle sizes (according to the steeper gradient on the 1500 μm plane in comparison with the gradient on the 600 μm plane). It appears that the influence of moisture content is minor at small particle sizes, presumably due to easier devolatilization of water occurring at smaller particle sizes. The predicted maximum organic liquid fraction is 0.504g/g moisture-free (MF) biomass. The reactor temperature did not have a significant impact on the organic liquid yield. Other studies have indicated that the reactor temperature had a significant impact on the total liquid yield within a 95% confidence interval for *Eucalyptus grandis* over a temperature range of 440-530 ^{o}C [79]. Another study has also reported that the liquid yield is influenced by the reactor temperature, with an increase in liquid yield from 400°C to 500 ^{o}C, and a decrease in liquid yield from 500°C to 600 ^{o}C for *P. radiata* in a fluidized bed reactor [21].

The greatest error% was 5.73% and the greatest under-prediction was -4.89%. The regression model under-predicted the organic yield for run 1 (the run not included in the full factorial) with 8.5%, see Table 94 in Appendix D.
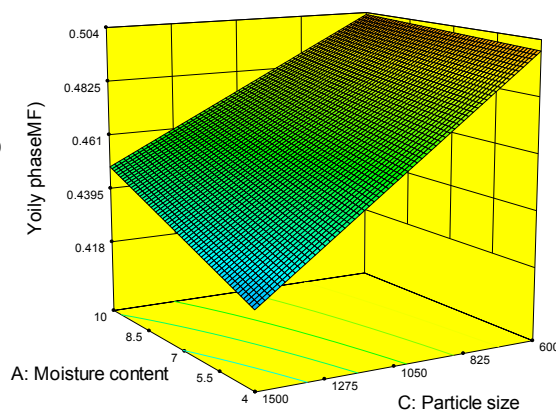
Figure 6 Surface plot of regression model for the organic liquid phase

3.3.2.4 Phase yield: Pyrolytic water

3.3.2.4.1 Experimental data

Most studies only report the liquid product, but fail to report on the pyrolytic water formed. In this study, the pyrolytic water ranged between 6.1wt% - 17.4wt% (dm basis, at 478°C, 9.4wt% moisture and 250-850μm, and at 456°C, 4.1wt% moisture and 1400-2000μm respectively), as can be seen in Table 94 in Appendix D. Pyrolytic water yields for fast pyrolysis have been reported at approximately 12wt% on a dry feed basis [32].

3.3.2.4.2 Statistical analysis

The pyrolytic water refers to the water that forms as a result of the pyrolysis process (including secondary reactions) and does not include the moisture present in the feedstock [194]. The significant factors identified in ANOVA analysis were the temperature and particle size. The lowest pyrolytic water is produced at high temperatures and small particle sizes. The surface plot of the response model, Figure 7, indicated that an increase in the particle size resulted in an increase in the pyrolytic water, while a decrease in the temperature also resulted in an increase in the pyrolytic water. The model had a R^2 value of 0.7992 and an adjusted R^2 value of 0.7189. Particle size has also been reported to be an important parameter in controlling the pyrolytic water [195]. In another study on the effect of particle size on the fast pyrolysis of Australian oil mallee woody biomass, two types of pyrolysis water were reported – low temperature pyrolytic water and high temperature pyrolytic water. Low temperature pyrolytic water was regarded as a swift process, such as the dehydration of certain biomass structures, and was independent of the temperature and particle size at low temperatures. From previous work, the high temperature pyrolytic water was thought to be the product from secondary cracking reactions and dependent on the temperature [194], [195]. High temperature pyrolytic water was also reported to be influenced by heating rate and the extent of inter- and intra- particle reactions (and consequently also by particle size) [194]. This agreed with the outcome observed in this study, where temperature and particle size have a significant effect on the pyrolytic water yield – indicating that the changes in pyrolytic water observed is similar to that of high temperature pyrolytic water and consequently from secondary reactions. Furthermore at high temperatures, the change in gas yield and pyrolytic water yield seems to correspond. It appears that

the pyrolytic water can be used as a reference point to measure the extent of secondary reactions [194].

The regression model for the pyrolytic water content has the largest error range compared to the regression models for the other product phase yields. It varies between 14.33% and -34.58%, showing that the model over-predicts in some cases and under-predicts in other cases for the experimental runs on which the regression model was developed. For the experimental run which was not part of the full factorial(run 1), the error% is 33.40, indicating that the model is not capable of accurately predicting the pyrolytic water phase, see Table 94 in Appendix D.
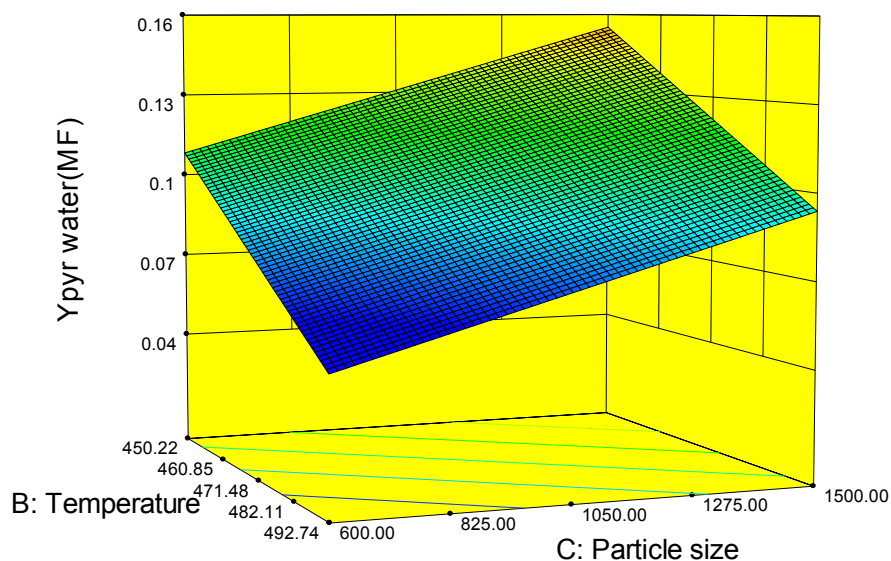
Figure 7 Surface plot of regression model for the pyrolytic water phase

3.3.2.5 Conclusions

The preferred pre-treatment and operating conditions to maximize the primary product (organic liquid fraction) yield, were evaluated. Particle size had a statistically significant influence on the organic liquid yield, with maximisation of the organic liquid yield achieved at small particle sizes. Neither biomass moisture content nor reactor temperature had a statistically significant influence on the organic liquid yield. Temperature significantly affected the pyrolytic water formation, with an increase in temperature lowering the pyrolytic water yield.

3.3.3 Product analysis and characterization

Bio-oil characteristics and their dependence on operating conditions were determined for moisture content, viscosity, HHV, density, pH, elemental composition, and chemical composition as determined by GC-MS and NMR analyses. Results from run 4 are not included due to problems experienced during the run. The experimental results, predicted results (from the response surface model) and the error between these values, are provided in Table 95 to Table 102 in Appendix D. A summary of literature results for BO moisture content, viscosity, density, pH and HHV is provided in Table 40, on p.86.

3.3.3.1 Bio-oil Moisture analysis

3.3.3.1.1 Experimental data

The average moisture content of the bio-oil ranged between 18.7 - 35.3 wt%, at conditions of 488°C, 3.7wt% moisture and 250-850μm, and at 456°C, 4.1wt% moisture and 1400-2000μm, respectively. The standard deviation of the measurements was low, and CV varied between 0.279%-1.440%, indicating the good repeatability of the measurements, see Table 31. Literature results for BO moisture content are summarized in Table 40 on p.86. Fast pyrolysis experiments on *P. radiata* at slightly lower temperature (400 ^{o}C) and a particle size of approximately 0.7mm, produced bio-oil with 28.8wt% moisture [191]. The test run at the most similar conditions (temperature, particle size and moisture contents of 450°C, 0.25-0.85mm and 4wt% moisture respectively) produced bio-oil with a minimum moisture content of 21.75wt%. Another study utilizing a 1 kg/h fluidized bed reactor with *P. sylvestris* as feedstock produced bio-oil at moisture contents of 15.9-17.8wt% at 4.5wt% feedstock moisture, 525°C reactor temperature and particle sizes less than 2mm [56]. For a 7 ton/day fluidized-bed pilot plant using pine sawdust the moisture content in the liquid product was 26 wt% [17]. When pine harvesting residue was pyrolysed in a 20kg/h process development unit (PDU), the moisture content in the bio-oil was 24wt% [17]. Most of the results obtained in this study compared well with the experimental results available in literature, with only a few of the results being higher than the maximum reported in literature for pine wood (28.8wt%). Minimum moisture content (18.7wt%) for this study is in reasonable agreement with the minimum values reported in literature for pine wood (15.9wt%).

Table 31 Moisture content of BO produced in experimental runs

Run nr	Moisture content [wt%] Measurement 1	Moisture content [wt%] Measurement 2	Moisture content [wt%] Measurement 3	Avg wt% moisture	Std deviation	CV [%]
Run 1	24.5	24.5	24.9	24.6	0.28	1.14
Run 2	33.6	33.1	33.5	33.4	0.23	0.68
Run 3	26.9	26.6	26.3	26.6	0.29	1.08
Run 5	31.8	31.5	31.5	31.6	0.18	0.57
Run 6	25.7	25.9	25.9	25.8	0.09	0.34
Run 7	23.1	23.7	23.6	23.4	0.29	1.26
Run 8	18.9	18.5	18.7	18.7	0.18	0.96
Run 9	35.4	35.2	35.2	35.3	0.10	0.28
Run 10	22.0	21.4	21.9	21.8	0.31	1.44
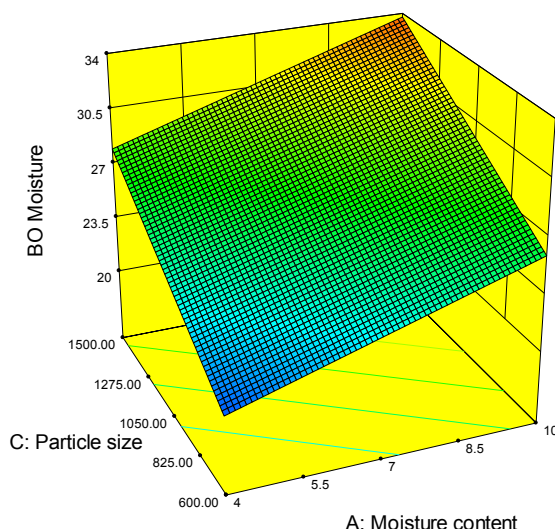
Figure 8 Three dimensional surface for BO moisture content as a function of moisture content and particle size

3.3.3.1.2 Statistical analysis

The maximum error% for the BO moisture content was 10.41% for runs 2-10, however for run 1, which was not utilized in the regression curve development, the error was highest at 14.5%, see Table 95 in Appendix D. This indicates the regression model is only applicable in the range of factors investigated in this study. The model`s R^2 and R^2 adjusted are acceptable at 0.875 and 0.7813 respectively, see Table 32. The feed biomass moisture content had a significant effect on the BO moisture content, as expected when considering a simple component balance on the process. An increase in the biomass feed moisture content resulted in an increase in the bio-oil moisture content. Furthermore, the particle size also had a significant impact on the BO moisture content, with larger biomass particles resulting in higher moisture contents in the bio-oil. This has also been reported elsewhere, for mallee wood [195] and is likely due to the increased vapour residence times at larger particle sizes. At longer residence times when the vapour is residing in the particle and possibly in contact with some char (formed by the degradation), secondary reactions can occur. This will increase cracking and potentially also moisture formation [196], [192]. Maximum moisture is present in the bio-oil at high particle sizes and high biomass moisture feeds, see Figure 8.

Table 32 Regression model and significant factors as determined by ANOVA analysis for Bio-oil moisture content

Quality analysed [Y]	Significant factors	R^2	R^2 adjusted	Regression equation in terms of actual factors
BO moisture content	A: Moisture content C: Particle size	0.8750	0.7813	Y [%][a]= 89.3701+0.9535xA-0.1645xB +8.6625x10^{-3}x C

[a]wt water/(wt bio-oil including moisture) x 100%, A: Moisture content, B: Temperature, C: Particle size

3.3.3.2 Viscosity Analysis

3.3.3.2.1 Experimental data

The average dynamic viscosity of the bio-oils produced in this study ranged between 10.9-48.9mPa.s, at an analysis temperature of 37°C. The operating conditions for the minimum and maximum values were respectively at 456°C, 4.1 wt% moisture and 1400-2000µm, and 488°C,

3.7wt% moisture and 250-850µm. The standard deviations were small and the CV varied between 0.39 – 4.16%, indicating the good repeatability of the analysis, see Table 33. Reported viscosity analyses vary in terms of the temperature at which the runs are performed, therefore direct comparison is not always possible. Literature results for BO viscosity are summarized in Table 40 on p.86. The viscosity for a study where pine wood derived bio-oil was analysed at 40°C showed a viscosity of 20.5 mPa.s [56]. In yet another study, the dynamic viscosity for bio-oil derived from fast pyrolysis of pine sawdust in a 7 ton/day unit, the dynamic viscosity at 40°C was measured at 22.6 mPa.s [17]. In the study by Elliott et al. [17], the viscosity of the top phase bio-oil, produced from pine harvesting residue, was also analysed and found to be 42.9 mPa.s. The range of viscosities measured in this study exceeds both the lower limit and the higher limit of the values that have been reported in literature for pine wood. However, typical viscosity measurements for wood-derived bio-oil vary between 40-100 mPa.s at 40°C, which is in agreement with the upper limit of the measured values from this study [32]. Due to the instability of bio-oil, an increase in viscosity occurs with time [33]. The time delay between fast pyrolysis experiments and the bio-oil`s viscosity analysis, can influence the viscosity and might be the reason for the differences between this study and literature results.

It has been reported that the bio-oil`s viscosity increases with an increase in reactor temperature, with the viscosity doubling from 400°C to 500°C and tripling with a reactor temperature increase from 500°C to 600°C [21]. In this study, the effect of reactor temperature was not observed to be significant within the 95% confidence interval, compared to the other factors investigated.

It has been reported that the moisture content in the bio-oil correlates with the viscosity of the bio-oil [56], [29]. This is also noticeable in Figure 10 which depicts the correlation between the bio-oil moisture content and the viscosity of the bio-oil in this study, showing that an increase in bio-oil moisture content reduces the dynamic viscosity. This study has indicated that the biomass moisture content influences the moisture content of the bio-oil. This confirms the statistical observation that the biomass moisture content has a significant effect on the viscosity of the bio-oil.

Table 33 Viscosity of BO produced in experimental runs

Run nr	Avg Viscosity [mPa.s] Measurement 1	Avg Viscosity [mPa.s] Measurement 2	Avg Viscosity [mPa.s]	Std deviation	CV [%]
Run 1	25.9	26.0	25.9	0.10	0.39
Run 2	14.0	13.9	14.0	0.10	0.73
Run 3	26.6	26.3	26.5	0.26	0.97
Run 5	14.4	13.9	14.2	0.30	2.14
Run 6	25.7	25.2	25.4	0.39	1.52
Run 7	29.5	27.8	28.6	1.19	4.16
Run 8	49.6	48.3	48.9	0.91	1.86
Run 9	10.9	10.8	10.9	0.12	1.08
Run 10	33.9	32.8	33.4	0.84	2.53
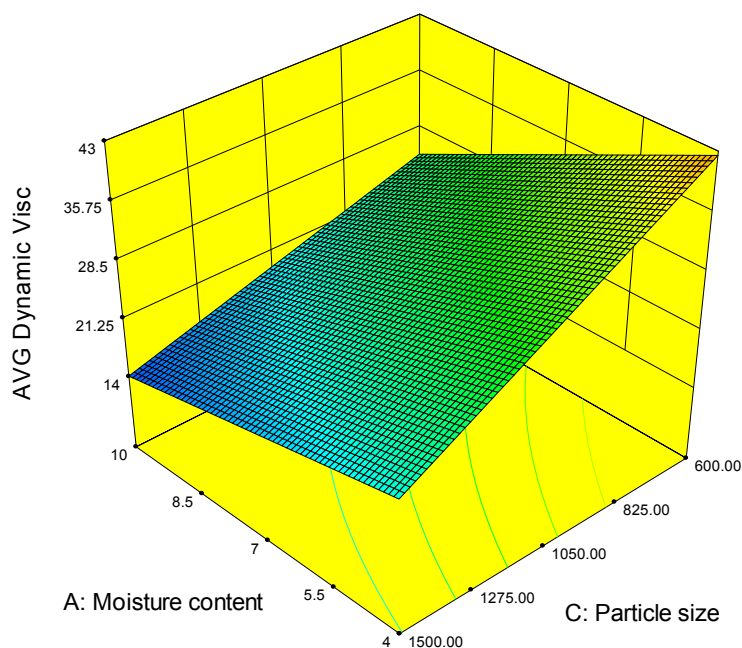
Figure 9 Three dimensional plot indicating moisture content and particle size effects on Dynamic viscosity
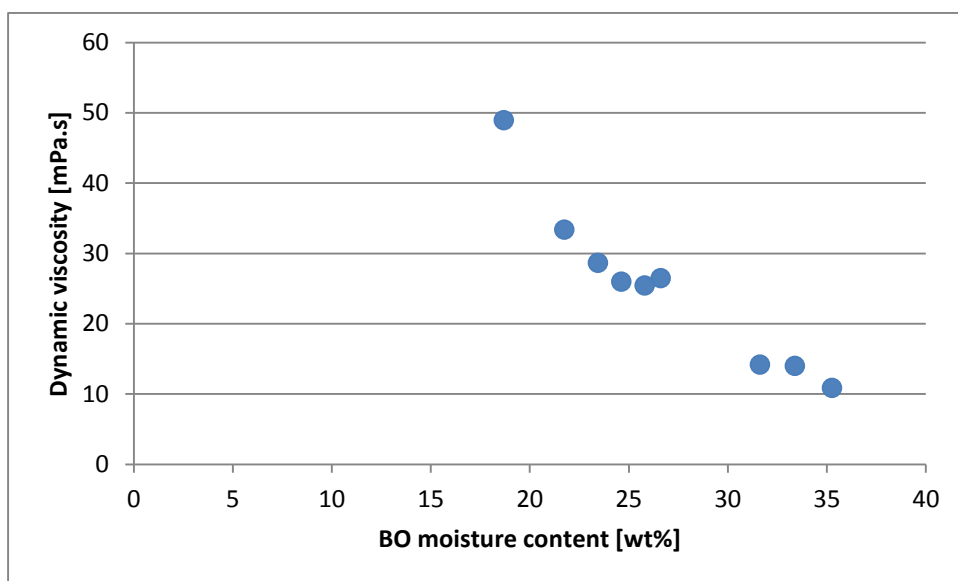
Figure 10 Dependence of viscosity on BO moisture content

3.3.3.2.2 Statistical analysis

When considering the BO dynamic viscosity, it can be seen that the regression model has a good R^2 and adjusted R^2 indicating a good fit to the data, see Table 34. The error between predicted and measured values ranged from -6.0 to 11.4%, for the experimental results used in the ANOVA, however for run 1, the error was much larger at -25.1%, see Table 95. This indicates that the capability of the model to predict the dynamic viscosity outside conditions for which the regression model was developed, is very limited. The moisture content and particle sizes were identified as having a significant contribution in influencing the BO dynamic viscosity. The viscosity decreased with an increase in moisture content and an increase in the particle size, see Figure 9. This is expected to be due to the moisture content in the biomass, as a higher moisture content in the bio-oil will result in a less viscous bio-oil. This is further supported by the observation that for the conditions which enhances the moisture content in bio-oil (large particle sizes and high biomass moisture contents),

80

the same conditions significantly affect the dynamic viscosity by lowering it. In another study investigating the effect of reactor temperature and particle size on *Eucalyptus grandis* derived bio-oil, using the same experimental set-up as this study, the particle size was found to have a significant effect on viscosities (within a 95% confidence interval) [79].

Table 34 Regression model and significant factors as determined by ANOVA analysis for Bio-oil Viscosity

Quality analysed [Y]	Significant factors	R2	R2 adjusted	Regression equation in terms of actual factors
BO dynamic viscosity	A: Moisture content C: Particle size	0.9898	0.9641	Y [mPa.s]= -299.3888 + 37.1056 x A +0.7821 x B – 0.0303 x C -0.0864 x A x B +1.7760 x 10-3A x C

A: Moisture content, B: Temperature, C: Particle size

3.3.3.3 HHV Analysis

3.3.3.3.1 Experimental data

The HHV values for bio-oils calculated in this study ranged between 19.3- 23.6 MJ/kg (respectively at 10wt% biomass moisture, and at 4 wt% biomass moisture), shown in Table 95 on p.223. It has been reported that the moisture content in the bio-oil correlates with the heating value of the bio-oil [56], [29]. Typical HHV values for wood derived bio-oil is 17 MJ/kg (as produced) [32]. Other studies have reported experimentally determined HHV results of 22 MJ/kg for the same feedstock, pyrolysed in a bubbling fluidized bed reactor with a 180g/h feed rate [191], as can be seen in the literature summary in Table 40 on p.86. In the study by DeSisto et al. [21], *P. strobus* was pyrolysed at different temperatures. It was observed that an increase in the pyrolysis temperature resulted in an increase in the HHV of the produced bio-oil, with the most prominent increase occurring from 400°C to 500 ^{o}C corresponding to an increase from 19.27 MJ/kg to 24.73 MJ/kg[21]. The results obtained in this study agree well with the HHV range found in literature for pine wood at 16.9 – 25.96 MJ/kg.
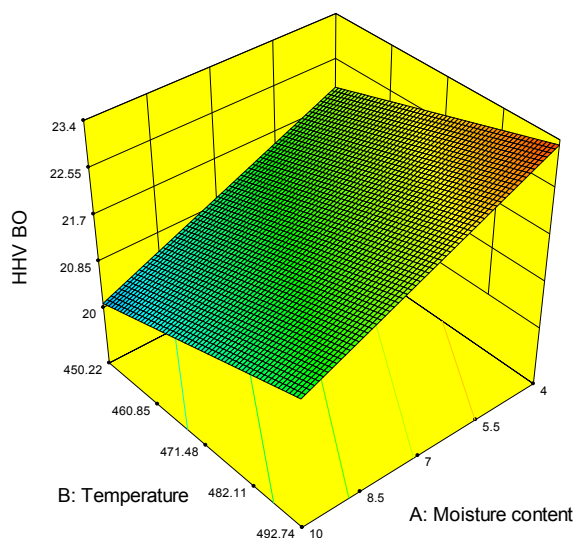
Figure 11 Three dimensional plot indicating BO HHV as a function of moisture content and temperature

3.3.3.3.2 Statistical analysis

The model fitted to the experimental data had R^2 and R^2 adjusted values of 0.6575 and 0.5205 respectively, see Table 35. The error % for predicted values ranged from -7.86% to 6.82% as indicated in Table 95 in Appendix D. The highest error was observed for run 1, which was excluded during model fitting. Overall, the error% is acceptable for screening purposes, as was the objective.

When considering the bio-oil HHV, it showed that only the moisture content of the biomass feed was identified as a significant factor for a 95% confidence interval. This is expected as an increase in the feed moisture had been indicated to result in an increase in moisture content in the BO and an increase in the moisture content of the BO will result in a decrease in the HHV of the bio-oil. It has previously been reported that an increase in temperature should lead to an increase in the HHV of the bio-oil [195], [21]. The pyrolysis temperature was not identified as being a significant factor within a 95% confidence interval in the current study. In a previous study neither the reactor temperature of the particle size was determined to have a significant influence on the HHV of the bio-oil for *E. grandis* within a 90% confidence interval [79].

Table 35 Regression model and significant factors as determined by ANOVA analysis for Bio-oil HHV

Quality analysed [Y]	Significant factors	R^2	R^2 adjusted	Regression equation in terms of actual factors
HHV BO	A: Moisture content	0.6575	0.5205	Y [MJ/kg] [a] = 10.2033 -0.3315 x A + 0.0293 x B

[a]dry basis, A: Moisture content, B: Temperature, C: Particle size

3.3.3.4 Density Analysis

3.3.3.4.1 Experimental data

The average density for the bio-oils produced in this study ranged from 1201-1251kg/m^3 measured at 15°C, respectively for operating conditions of 456°C and 1400-2000μm, and 488°C and 250-850μm. In all cases the standard deviation was small and the CV was very small ranging between 0.006% - 0.050%, as indicated in Table 36. The density range reported in this study is in good agreement with densities of bio-oil produced from pine sawdust at a 1 kg/h fluidized bed unit and a 20 kg/h process development unit, with densities of 1240-1250 kg/m^3 and 1200 kg/m^3 respectively. Densities as low as 1180 kg/m^3 and 1190 kg/m^3 have also been measured for pine sawdust, pyrolysed with a fluidized bed reactor set-up and an auger set-up respectively [17], [21]. A summary of the literature density results are provided in Table 40 on p.86. It has been reported that the bio-oil moisture content correlates with the density [56]. For this study the biomass moisture content did not have a significant effect on the density for a 95% confidence interval. However, the same factors that are significant in influencing the pyrolytic water, are significant for the density. At conditions which enhance the pyrolytic water formed (a combination of maximum particle size and minimum temperature, as employed in Runs 2 and 9), the density is minimum, and conversely. This can indicate that the moisture from biomass present in the bio-oil, does not necessarily have the main influence on the density, but rather the reactive water, which is formed during pyrolysis.

Table 36 Density of BO produced in experimental runs

	Density [kg/m³] measurement 1	Density [kg/m³] measurement 2	Density [kg/m³] measurement 3	Average density	Std Deviation	CV [%]
Run 1	1221.54	1221.43	-	1221.49	0.077	0.006
Run 2	1202.75	1202.93	-	1202.84	0.128	0.011
Run 3	1236.09	1235.64	-	1235.87	0.318	0.026
Run 5	1214.36	1214.59	-	1214.48	0.159	0.013
Run 6	1234.47	1234.48	-	1234.47	0.009	0.001
Run 7	1231.81	1232.16	-	1231.98	0.247	0.020
Run 8	1250.25	1251.13	-	1250.69	0.623	0.050
Run 9	1201.91	1200.77	1201.07	1201.25	0.587	0.049
Run 10	1242.99	1241.86	1242.33	1242.39	0.563	0.045
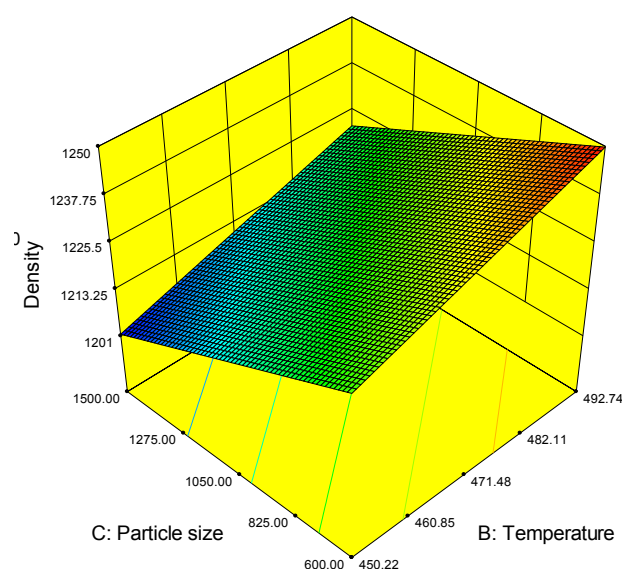
Figure 12 Three dimensional surface for BO density as a function of temperature and particle size

3.3.3.4.2 Statistical analysis

The regression model for the BO density gives a good prediction and had an R^2 and adjusted R^2 of 0.93 and 0.87 respectively, see Table 37. The error was always small, ranging from -0.5 to 0.6%, see Table 95 in Appendix D. The error for run 1, was 0.3%, within the error range of the experimental runs used for ANOVA analysis.

Significant factors were the temperature and the particle size; with an increase in the temperature resulting in an increase in the density and an increase in the particle size resulting in a decrease in the density. The change in density as a function of temperature and the pyrolytic water yield as a function of temperature is inversely proportional, with an increase in temperature decreasing the pyrolytic water yield (see Figure 7), and increasing the density (Figure 12). Since water has a lower density than bio-oil, a decrease in the density with an increase in water (which occurs at lower temperatures, Figure 7) is expected. It is interesting to note that the biomass moisture content did not have a significant influence on the BO density, for a 95% confidence interval. The decrease in

83

density with an increase in particle size corresponds to the effect particle size has on the BO moisture content.

The temperature will enhance/favour the decomposition of certain components (e.g. cellulose degrades between at 275 – 350°C [41], [24]. At higher temperatures the cellulose experiences more degradation, although lignin is known to experience degradation over a wider range, but up to even higher temperatures. Cellulose is known to produce anhydrosugars [197], [198]. These sugars are polar compounds similar to water, which might also contribute to the increase in the density [198].

Table 37 Regression model and significant factors as determined by ANOVA analysis for Bio-oil density

Quality analysed [Y]	Significant factors	R^2	R^2 adjusted	Regression equation in terms of actual factors
BO Density	B: Temperature C: Particle Size	0.9283	0.8745	Y [kg/m^3]= 1046.3585 – 2.1014 x A +0.4806 x B-0.0311 x C

A: Moisture content, B: Temperature, C: Particle size

3.3.3.5 pH analysis

3.3.3.5.1 Experimental data

The average pH ranged between 2.16-2.77, indicating the bio-oil is acidic. The minimum and maximum pH values were respectively obtained at operating conditions of 465°C, 9.5wt% moisture and 1400-2000µm, and at 456°C, 4wt% moisture and 1400-2000µm. The standard deviation was small, with small CVs of 0-0.643%, see Table 38. The upper limit of the pH range agrees with reported literature pH values for pine wood, which ranges from 2.3 to 2.79 for (bubbling) fluidized bed reactors [191], [21]. For an auger reactor, the pH was determined as 3.1 [37]. A summary of the literature pH results discussed is provided in Table 40 on p.86. Typical wood derived bio-oil pH is approximately 2.5 [32]. Some of the pH values measured in this study is lower than the pH range found in literature. The model showing the BO pH as a function of moisture content and temperature, is presented in Figure 13.

Table 38 pH of BO produced in experimental runs

Run nr	pH 1st measurements	pH 2nd measurement	Average pH	Std deviation	CV [%]
1	2.28	2.26	2.27	0.014	0.623
2	2.15	2.16	2.16	0.007	0.328
3	2.20	2.22	2.21	0.014	0.640
5	2.29	2.29	2.29	0.000	0.000
6	2.19	2.21	2.20	0.014	0.643
7	2.24	2.24	2.24	0.000	0.000
8	2.31	2.31	2.31	0.000	0.000
9	2.77	2.77	2.77	0.000	0.000
10	2.20	2.21	2.21	0.007	0.321
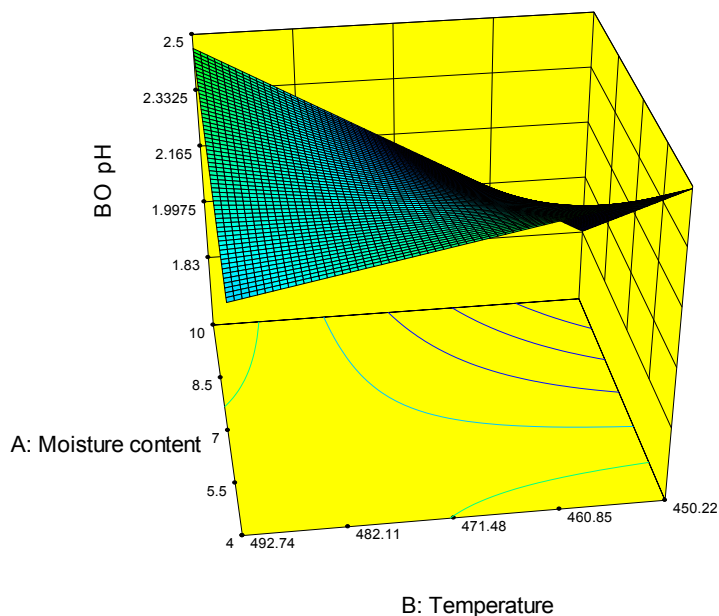
Figure 13 Three dimensional surface showing BO pH as a function of temperature and moisture content

3.3.3.5.2 Statistical analysis

The statistical analysis on the BO showed that none of the factors investigated had a significant effect within a 95% confidence interval. It has previously also been reported that the particle size and reactor temperature were not considered to be significant at a 95% confidence interval for *Eucalyptus grandis* bio-oil [79]. In the study by DeSisto et al. [21], the pH increased with an increase in reactor temperature. For this study, the R^2 value was high at 0.9491, with the adjusted R^2 value at 0.6438, see Table 39. The error ranged from -3.26% to 3.78% for experimental runs 2-10, see Table 95 in Appendix D. For run 1, the error% is 3.02%, which is within the error range for the results used to develop the statistical response model. This indicates that the regression model can most likely be used to predict a response for conditions other than what was used for model development.

Table 39 Regression model and significant factors as determined by ANOVA analysis for Bio-oil pH

Quality analysed [Y]	Significant factors	R^2	R^2 adjusted	Regression equation in terms of actual factors
BO's pH	None	0.9491	0.6438	$Y = 1.4424 -1.5477 \times A +1.2276 \times 10^{-3} \times B +9.2440 \times 10^{-3} \times C +3.3013 \times 10^{-3} \times A \times B -4.6557 \times 10^{-5} \times A \times C -1.8543 \times 10^{-5} \times B \times C$

A: Moisture content, B: Temperature, C: Particle size

Table 40 Comparison with literature for BO properties and characteristics

Source		This study	[191]	[56]			[17]		[21]			[37]	
Feedstock		*Pinus radiata*	*Pinus radiata*	*Pinus sylvestris*	*Pinus sylvestris*	Pine wood	Pine sawdust	Pine harvesting residue	*Pinus strobus*			Pine wood	
Reactor		1 kg/h fluidized bed reactor	228 g/h bubbling fluidized bed	1 kg/h fluidized bed reactor	20 kg/h Process development Unit	NR	7 tons/day fluidized bed reactor	20 kg/h process development unit	60 g/h fluidized bed reactor			1 kg/h auger reactor	
Conditions		BM Moisture 3-10wt%, particle sizes 0.25-2mm, reactor temperature 450-500 ^{o}C.	BM moisture <1 wt%, 400 ^{o}C, particle size 0.7m	BM moisture 4 - 4.4 wt%, 525 ^{o}C, particle size <2mm	BM moisture 4.5 wt%, 520 ^{o}C, particle size <2mm	NR	NR	NR	400 ^{o}C	500 ^{o}C	600 ^{o}C	450 ^{o}C, 2-4 mm particle sizes, 6-8% moisture	
BO Moisture Content [wt%]		18.70 - 35.27	28.8 wt%	15.9- 17.8 wt%	17wt%	23.9 wt%	26 wt%	24wt%	NR	NR	NR	16wt%	
Viscosity	Temperature [^{o}C]	37°C	NR	50 ^{o}C	50 ^{o}C	40 ^{o}C	40 ^{o}C	40 ^{o}C	25 ^{o}C	25 ^{o}C	25 ^{o}C	25 ^{o}C	50 ^{o}C
	mPa.s	10.86- 48.92	NR	28.52-35	33	20.5	22.6	42.9 [b]	11100 [c]	226000 [c]	62200 [c]	200 - 264	51 - 154
Density	Temperature [^{o}C]	15 ^{o}C	NR	15 ^{o}C	15 ^{o}C	15 ^{o}C	15 ^{o}C	15 ^{o}C	-	-	-	15 ^{o}C	
	kg/m^3	1201-1250	NR	1240-1250	1200	1206	1180	1180 [b]	NR	NR	NR	1190	
pH		2.16-2.77	2.3	2.4	2.4	2.7	NR	NR	2.26 [c]	2.66 [c]	2.79 [c]	3.1	
HHV [MJ/kg]		19.3-23.6	22 [a]	18.2-18.9	18.7	16.9	NR	NR	19.27 [c]	24.73 [c]	25.96 [c]	21.9 [a]	

NR – not reported, [a] experimentally determined, [b] top phase, [c] ESP fraction

3.3.3.6 Ultimate analysis on BO

3.3.3.6.1 Experimental data

The C, H, N elemental results obtained for this study are provided (on a dry basis) in Table 96 in Appendix D. The CVs for the analyses were mostly below 15%, although deviations occurred for the nitrogen measurement at runs 3 and 7. High deviations were attributed to the heterogeneity of the samples.

Literature results are provided in Table 41. The carbon content range in this study ranged from 34.6 to 44.3wt% (including moisture) and 52.1 – 56.3wt% (excluding moisture). The carbon content range (excluding moisture) compared well with the range found for pine-derived bio-oils in literature, 53 to 62.7wt%. Hydrogen content (excluding moisture) ranged from 4.7 to 6.7 wt% in this study. The lowest value of the hydrogen in this study (4.7wt%) was lower than reported in literature, with minimum literature values on a similar basis reported at 6.4wt%. When considering the results from each run in Table 96 in Appendix D, only a single run had a hydrogen content of less than 6wt%, run 3. This run also had a high CV of 18.3wt% (including moisture), possibly due to sampling effects. When considering the ratio of H/C vs the O/C on a molar basis, it can be seen that the results from Run 3 is the most scattered from the other results, see Figure 14. The nitrogen content (excluding moisture), ranged from 0.1-0.2wt% and compared well with the literature range of 0.1-0.3wt%, even though some of the CV values were high (> 15%). The oxygen content, calculated by difference, ranged from 36.9 – 42.8wt% (excluding moisture). This is 2.3wt% higher than the maximum of 40.5 wt% reported in literature. The errors for the analyses on C, H and N are compounded in the oxygen content as a result of calculating it by difference. This can also result in greater inaccuracies with the oxygen results and might contribute to the greater oxygen content compared to literature. Only runs 2 and 3 had substantial deviations from literature.
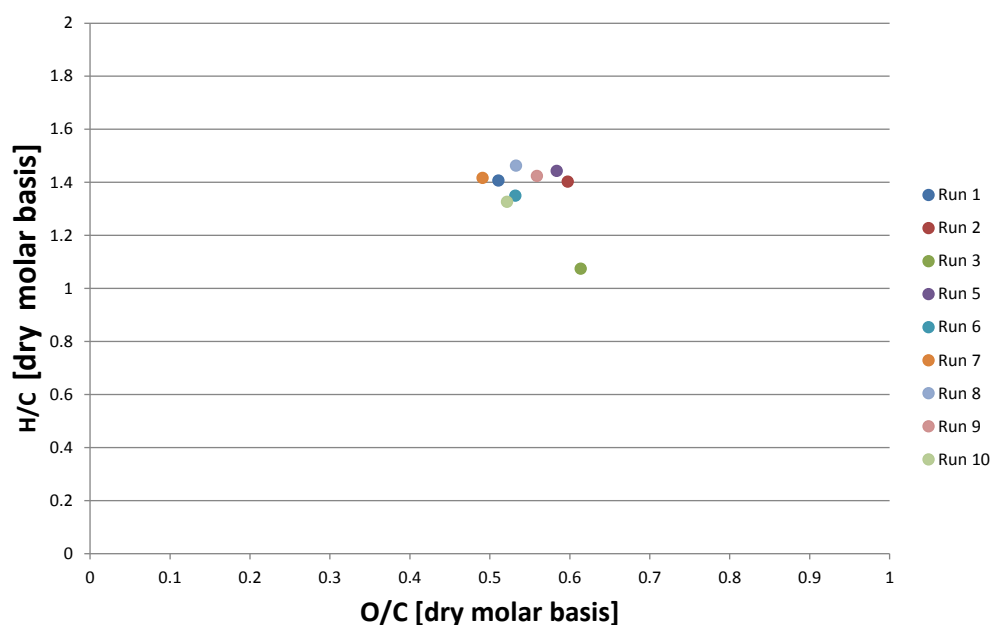
Figure 14 Diagram of H/C to O/C

Table 41 Elemental analysis of bio-oil compared to literature

Source	This study		[191]	[56]			[17]				[21]			[37]	
Feedstock	Pinus radiata		*Pinus radiata*	*Pinus sylvestris*	*Pinus sylvestris*	Pine wood	Pine sawdust		Pine harvesting residue		*Pinus strobus*			Pine wood	
Reactor	Fluidized bed reactor		Bubbling fluidized bed (228g/h)	1 kg/h fluidized bed reactor	20 kg/h Process develop-ment Unit	NR	7 tons/day Fluidized bed reactor		20 kg/h Process development unit		60g/h Fluidized bed reactor,			1 kg/h Auger reactor	
Conditions	Moisture contents 3-10wt%, particle sizes 0.25-2mm, reactor temperatures 450-500 ^{o}C		BM moisture <1 wt%, 400C, particle size 0.7mm	BM moisture 4 -4.4 wt%, 525C, particle size <2mm	BM moisture 4.5 wt%, 520C, particle size <2mm	NR	NR		NR		400°C	500°C	600°C	450 ^{o}C, 2-4 mm Particle sizes, 6-8% moisture	
	Wt% (incl.m)	Wt% (excl.m)	NR	Wt% (incl.m)	Wt% (incl.m)	Wt% (incl.m)	Wt% (incl.m)	Wt% (excl.m)	Wt% (incl.m)	Wt% (excl.m)	NR	NR	NR	Wt% (incl.m)	Wt% (excl.m)
C	34.6 - 44.3	52.1-56.3	56.0	44.8-46.2	45.7	40.6	38.8	53.0	43.9	55.1	57.9	59.2	62.7	52.6	62.7
H	6.4-8.1	4.7 - 6.7	5.6	7	7	7.6	7.7	6.4	7.6	6.7	6.5	6.6	6.2	7.5	6.8
O	48.0 - 57.3	36.9-42.8	36.7	46.7-48.1	47.2	51.7	53.4	40.5	48.2	37.8	35.5	34.2	31.1	39.5	30.1
N	0.1- 0.2	0.1 -0.2	1.7	<0.1	<0.1	<0.1	0.09	0.1	0.26	0.3	0.1	<0.5	<0.5	0.1	0.1

NR: not reported, incl.m: including moisture, excl.m: excluding moisture

3.3.3.6.2 Statistical analysis

An ANOVA analysis on the carbon, hydrogen and oxygen in the bio-oil (on a moisture free basis) was performed, see Table 42. According to the ANOVA analysis, none of the factors investigated had a significant influence on the carbon and hydrogen content of the bio-oil. The moisture content of the biomass was significant in influencing the oxygen content of the bio-oil. This is not the result of moisture transfer from the biomass to the bio-oil, as the elemental analysis used for ANOVA analysis was based on the moisture free bio-oil.

Table 42 Regression model and significant factors as determined by ANOVA analysis for different Bio-oil elemental analysis response

Elemental content[Y]	Significant factors	R^2	R^2 adjusted	Regression equation in terms of actual factors
C in BO[a]	None	0.5940	0.2895	Y [wt%]= 55.4936 -0.1205*A+9.0100x 10^{-4}x C -2.3589x 10^{-4}x A x C
H in BO [a]	None	0.6532	-0.2138	Y [wt%]= 3.2216 -1.9441*A+7.4729 x 10^{-3}x B +6.6857 x 10^{-3}x C +3.7955 x10^{-3}x A x B -1.3351 x 10^{-5}x B x C
O in BO [a]	Moisture content	0.6537	0.5151	Y [wt%]= 51.6023 + 0.5198x A- 0.0325xB

[a] Elemental composition analysed on a moisture-free basis, A: Moisture content, B: Temperature, C: Particle size

The R^2 and R^2 adjusted for the carbon present in BO, was 0.5940 and 0.2895 respectively, indicating the regression model does not fit all the data well. This is also observed when considering the error% in Table 97 in Appendix D, which ranges from -4.71 to 2.62%. The regression model was capable of predicting the carbon content of run 1 sufficiently, with an error% of only -0.81% even though this run was not used for model regression purposes.

The R^2 and R^2 adjusted for the hydrogen present in BO, was 0.6532 and -0.2138 respectively, indicating a poor fit of the regression model to predict the bio-oil`s hydrogen content. This is also indicated by the large range of error%, from -7.23 to 14.62%. The error% for run 3 is very high (14.62%), as this run had a large CV for the hydrogen analysis, indicated in Table 96 in Appendix D, which is likely to increase the error%.

R^2 and R^2 adjusted values for oxygen present in the bio-oil was 0.6537 and 0.5151 respectively. The error% ranged from -2.82% to 7.74wt%. The biomass moisture content was found to influence the oxygen present in the bio-oil (moisture free basis). An increase in biomass moisture content results in an increase in the oxygen content of the BO, for both low and high temperature levels, see Figure 15. An increase in the temperature results in a reduction in the oxygen content of the BO. Minimum oxygen content (37.7wt %) is achieved at high temperatures and low moisture contents, whereas high oxygen content (41.6wt %) in the BO occurs at high moisture contents and low temperatures. Figure 15 depicts the decrease in oxygen for a decrease in biomass moisture content and an increase in reactor temperature experienced in this study. This agreed with literature where a decrease in the oxygen content of the bio-oil was observed with an increase in the reactor temperature, experienced for a 60g/h fluidized bed reactor with *P. strobus* as feedstock, see Table 41 [21]. It also agrees with a study on mallee wood [195].
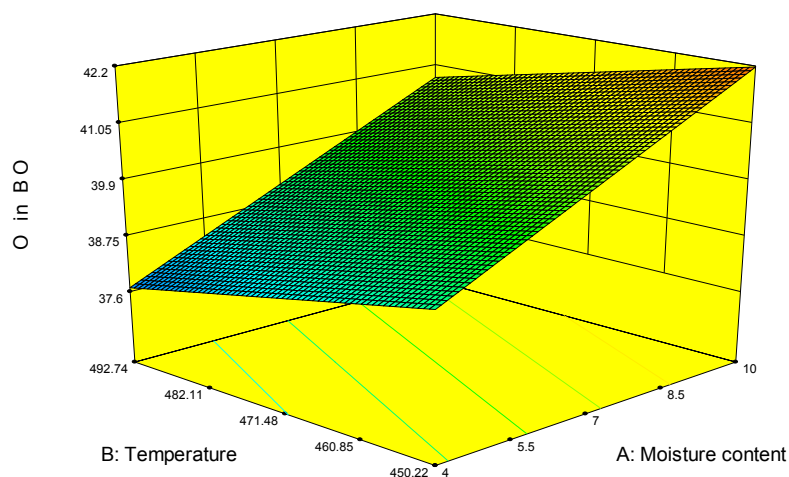
Figure 15 Surface response for regression model on the oxygen content of BO (moisture free basis)

3.3.3.7 GC-MS analysis

GC-MS analysis results were used to qualitatively examine the effect of changes in process conditions on the chemical families. Certain bio-oil components were also analysed on a quantitative basis.

3.3.3.7.1 Experimental data - Chemical families

The results from GC-MS were used for qualitatively examining whether the changes in process conditions influence the chemical family groups detected in the bio-oil. Previous studies have reported this for Eucalyptus wood [79] and for pine wood [21]. In this study the analysis was performed using the area% results from the GC-MS analysis (with an internal standard of methyl-behenate) as an indication of the quantity of the component in bio-oil, relative to the internal standard. This approach assumes a universal detector response, however it cannot be used for determining the absolute concentration of a component in the bio-oil [199]. A similar approach has been used for investigating the chemical families in bio-oil in other studies [77]. The inaccuracy associated with assuming the responses for different components are similar in GC-MS analysis and that the area% can be related to a quantity is evident when considering the large difference in the area% and the actual quantity of levoglucosan present in the bio-oil.

Chemical families were grouped according to aldehydes, ketones, phenols and aromatics, sugars, furans, acids, alcohols, alkanes, alkenes and hetero-components, where hetero-components referred to components containing an element that is not carbon, hydrogen or oxygen. Only components with a probability greater than 60% (as determined by the GC-MS analysis software) were considered in the qualitative analysis of the GC-MS results for chemical families. Results for the chemical families and the unidentified area can be viewed in Table 43. In a study where beech oil was analysed using 2D GC-FID, the chemical families were reported using the area% (similar to this study) [199]. The area% of acids and furans present in the beech oil samples was 8.3% , and 5.3% respectively [199], all of which agreed with the ranges observed in Table 43 of this study. The sugar content for beech oil and pine oil was reported at 21.4% and 34.44% respectively, which is at the limits of the ranges observed in this study [199], [200]. Beech oil contained 18.7% of ketones and aldehydes combined [199], which is slightly lower than the range of 18.9% obtained in this study.

Table 43 Semi-qualitative composition of bio-oil in terms of chemical family group as determined by GC-MS

Run nr	Aldehydes [Area%]	Ketones [Area%]	Phenols and aromatic [Area%]	Sugars [Area%]	Furans [Area%]	Acids [Area%]	Alcohols [Area%]	Alkane [Area%]	Alkene [Area%]	Hetero-com-pound [Area%]	Un-Identi-fied [Area%]
1	5.70	14.81	18.56	20.17	7.43	7.92	0.14	2.01	0.06	0.35	22.85
2	5.52	14.88	17.86	24.35	5.07	9.62	0.11	1.05	0.15	1.71	19.68
3	5.26	18.31	7.50	25.01	6.74	10.87	1.22	1.41	0.00	1.04	22.64
5	4.78	16.01	6.94	33.82	7.86	8.03	0.54	1.61	0.03	1.69	18.69
6	5.35	18.15	12.48	23.16	8.22	8.39	0.49	1.82	0.12	0.24	21.58
7	4.37	14.54	10.18	30.24	7.27	8.27	0.52	1.40	0.00	1.39	21.82
8	5.13	16.22	17.64	24.45	7.06	6.50	0.14	1.85	0.18	1.85	18.98
9	6.13	14.21	7.39	32.34	4.90	10.04	0.64	1.58	0.02	4.11	18.64
10	5.89	16.53	15.29	23.14	6.80	10.21	0.03	1.21	0.13	0.69	20.08
Min	*4.37*	*14.21*	*6.94*	*20.17*	*4.90*	*6.50*	*0.03*	*1.05*	*0.00*	*0.24*	*18.64*
Max	*6.13*	*18.31*	*18.56*	*33.82*	*8.22*	*10.87*	*1.22*	*2.01*	*0.18*	*4.11*	*22.85*

Min-minimum, Max-maximum

3.3.3.7.2 Experimental data - Quantified components

Quantified results for the different runs are reported in Table 44. A comparison with literature values are given in Table 45.

Due to poor calibration of the standards of furfural and 5-hydroxymethyl-furfural, with the GC-MS, analysis using HPLC was also performed. The results obtained by GC-MS and HPLC for both furfural and 5-hydroxymethyl-furfural, differed with an order of a magnitude, see Table 44. The results for the maximum quantified values indicated that levoglucosan is the most prominent component (4.9wt%), followed by acetic acid (2.6wt%), formic acid (1.1wt%) and coniferyl aldehyde (0.54wt%). The results indicate that bio-oil consists of many components present in small quantities.

The quantified components were compared with values from literature, see Table 45. A literature range was compiled for the components whose concentrations were available in literature. This was used for comparison with the quantified range for the same component (as determined from experimental runs 1-3 and 5-10). In most cases, the experimental ranges fell within the range observed in literature, except a small deviations observed for 2 methoxy-4 vinylphenol, where the maximum quantity determined in this study (0.0247wt %) was less than the minimum reported in literature (0.06wt %). The vapour residence time and the biomass particle residence time influence the extent of degradation [32]. The biomass constituents, such as ash content, also influence the extent of degradation [24], [32]. These variables are expected to contribute to slight variations in component concentrations.

The maximum levoglucosan quantity in this study was 4.9wt%, which falls within the reported literature range of 1wt% to 13.7% [45], [21]. When considering the area% quantification for levoglucosan, the quantities varied between 16.93 area% and 31.42 area%, which compares favourably with reported literature values of 23.9area% [199].

Table 44 Quantified components in bio-oil using GC-MS and HPLC

Components	Quantity of component [wt% of BO]										
	Run 1	Run 2	Run 3	Run 5	Run 6	Run 7	Run 8	Run 9	Run 10	*MIN*	*MAX*
2-Methyltetrahydrofuran	0.0189	0.0181	0.0203	0.0210	0.0203	0.0199	0.0193	0.0206	0.0184	*0.0181*	*0.0210*
Isobutyl alcohol (1-Propanol, 2-methyl)	0.1165	0.1959	0.2203	0.2282	0.1481	0.3232	0.4695	0.2015	0.1980	*0.1165*	*0.4695*
Ethylbenzene	0.0029	0.0028	0.0031	0.0032	0.0031	0.0030	0.0029	0.0031	0.0028	*0.0028*	*0.0032*
Cumene (Benzene, (1-methylethyl)-)	0.0047	0.0043	0.0048	0.0050	0.0048	0.0047	0.0045	0.0049	0.0043	*0.0043*	*0.0050*
1-Hexanol	0.0341	0.0328	0.0366	0.0378	0.0371	0.0367	0.0348	0.0376	0.0345	*0.0328*	*0.0378*
4-Hydroxy-4-methyl-2-pentanone	0.0281	0.0268	0.0302	0.0313	0.0304	0.0296	0.0287	0.0308	0.0274	*0.0268*	*0.0313*
Anisole	0.0068	0.0064	0.0073	0.0075	0.0073	0.0071	0.0070	0.0074	0.0067	*0.0064*	*0.0075*
Benzyl alcohol	0.0438	0.0415	0.0467	0.0485	0.0469	0.0458	0.0444	0.0473	0.0424	*0.0415*	*0.0485*
Ethyl levulinate	0.0418	0.0389	0.0440	0.0455	0.0441	0.0432	0.0416	0.0447	0.0397	*0.0389*	*0.0455*
Guaiacol (2-methoxy Phenol)	0.1972	0.2961	0.0933	0.0983	0.1446	0.1945	0.2363	0.1429	0.1705	*0.0933*	*0.2961*
Creosol {2-Methoxy-4-methylphenol}	0.2145	0.3612	0.0963	0.1095	0.1442	0.1968	0.2464	0.1773	0.1731	*0.0963*	*0.3612*
2,3-Dimethylphenol	0.0107	0.0123	0.0060	0.0073	0.0077	0.0089	0.0099	0.0095	0.0072	*0.0060*	*0.0123*
Eugenol (4-Allyl-2-methoxyphenol)	0.0563	0.0831	0.0348	0.0377	0.0410	0.0460	0.0573	0.0610	0.0472	*0.0348*	*0.0831*
2-Methoxy-4-propylphenol (4-propyl guaiacol)	0.0353	0.0266	0.0199	0.0192	0.0188	0.0190	0.0194	0.0270	0.0198	*0.0188*	*0.0353*
2,6-Dimethoxyphenol (syringol)	0.0226	0.0182	0.0197	0.0202	0.0196	0.0191	0.0186	0.0198	0.0177	*0.0177*	*0.0226*
Vanillin	0.1991	0.2571	0.2452	0.2321	0.2336	0.2113	0.2608	0.2874	0.2464	*0.1991*	*0.2874*
Dibenzyl ether (Benzene, 1,1'-[oxybis(methylene)]bis-)	0.0229	0.0099	0.0093	0.0093	0.0088	0.0085	0.0082	0.0092	0.0079	*0.0079*	*0.0229*
Levoglucosan (1,6-Anhydro-B-D-glucose)	4.9379	4.4514	3.2202	4.1331	3.1059	4.0212	3.1800	3.6565	3.3697	*3.1059*	*4.9379*
4-Hydroxy-3-methoxycinnamaldehyde (coniferyl aldehyde)	0.3176	0.4112	0.3811	0.4164	0.3441	0.3068	0.3290	0.5403	0.3427	*0.3068*	*0.5403*
1,3 cyclopentanedione	0.1806	0.1645	0.1150	0.1097	0.2057	0.2305	0.1731	0.1106	0.2143	*0.1097*	*0.2305*
2(5H)-furanone	0.3252	0.3124	0.3359	0.2987	0.3677	0.3711	0.4115	0.3244	0.4150	*0.2987*	*0.4150*
Phenol	0.0803	0.0610	0.0433	0.0587	0.0716	0.0859	0.0820	0.0407	0.0619	*0.0407*	*0.0859*
2 methoxy-4 vinylphenol (4 vinyl guaiacol)	0.0175	0.0159	0.0148	0.0136	0.0163	0.0195	0.0247	0.0141	0.0185	*0.0136*	*0.0247*
Isoeugenol	0.0299	0.0238	0.0166	0.0132	0.0210	0.0292	0.0441	0.0202	0.0375	*0.0132*	*0.0441*
Acetovanillone	0.0815	0.0626	0.0752	0.0587	0.0791	0.0805	0.0925	0.0604	0.0955	*0.0587*	*0.0955*

Apocynin (acetovanillone)	0.0087	0.0077	0.0076	0.0080	0.0084	0.0084	0.0082	0.0080	0.0078	*0.0076*	*0.0087*
Formic Acid	0.9739	0.9120	1.0983	0.8528	1.1200	1.1130	1.0534	0.7474	0.9828	*0.7474*	*1.1200*
Acetic Acid	2.4198	2.5744	1.9878	1.9194	2.0410	2.6215	2.2688	2.1254	2.4431	*1.9194*	*2.6215*
Furfural (2 furaldehyde) [a]	0.2344	0.2895	0.1432	0.1622	0.1906	0.2384	0.2642	0.2013	0.1901	*0.1432*	*0.2895*
Furfural (2 furaldehyde) [b]	0.0299	0.0204	0.0094	0.0090	0.0166	0.0231	0.0258	0.0096	0.0208	*0.0090*	*0.0299*
5-(Hydroxymethyl)-furfural [a]	0.3848	0.3961	0.4845	0.5229	0.4474	0.4792	0.4851	0.4997	0.3987	*0.3848*	*0.5229*
5-(Hydroxymethyl)-furfural [b]	0.0571	0.0430	0.0548	0.0503	0.0531	0.0551	0.0541	0.0452	0.0525	*0.0430*	*0.0571*

[a] Quantified using GC-M C, [b] Quantified using HPLC

Table 45 Component concentration in bio-oil for current study compared with literature

Component / Literature source / Biomass feed and Conditions:	This study MIN wt%	This study MAX wt%	Pine sawdust in a fluidized bed reactor [a,j] [°C] 400	500	600	Beech flakes using rotating cone reactor [b,l]	Beech flakes using rotating cone reactor [c]	Pine wood in an auger reactor [d]	Southern pine wood heated at 350°C for 30min [e]	Pinus sylvestris [f]	Pine wood as feedstock [g,k]	Composition of bio-oil [h]	Mallee wood in fluidized bed reactor at 500°C [i]	Literature MIN	Literature MAX
Ethylbenzene	0.0028	0.0032					ND							0.0000	
Furfural (2 furaldehyde)	0.1432 [m] 0.0090 [n]	0.2895 [m] 0.0299 [n]					ND	0.47	0.34			0.1-1.1	x	0.1000	1.1100
Guaiacol (2-methoxy Phenol)	0.0933	0.2961	0.24	0	0.01			0.39	0.41				x	0.0000	0.4100
Creosol (2-Methoxy-4-methylphenol)	0.0963	0.3612				1.4									1.4
2,3-Dimethylphenol	0.0060	0.0123					ND	0.01						0.0000	0.0100
Eugenol (4-Allyl-2-methoxyphenol)	0.0348	0.0831	0.25	0.17	0.03			0.19	0.22			0.1-2.3		0.0300	2.3000
2-Methoxy-4-propylphenol (4-propyl guaiacol)	0.0188	0.0353						0				0.1-0.4		0	0.4
5-(Hydroxymethyl)-furfural	0.3848	0.5229						0	0.99					0.0000	0.9900
Vanillin	0.1991	0.2874	0.33	0.43	0.12			0.24	0.35					0.1200	0.4300
Levoglucosan (1,6-Anhydro-B-D-glucose)	3.1059	4.9379	13.7	12.7	23.8	23.9	0.429	14.2	4.86		3.05	0.4-1.4	x	0.4000	23.7900
2(5H)-furanone	0.2987	0.4150				3.2		0	1.1				x	0.0000	3.2000
Phenol	0.0407	0.0859	0.02	0.02	0.1		ND	0.77	0.04			0.1-3.8	x	0.0000	3.8000
2 methoxy-4 vinylphenol (4 vinyl guaiacol)	0.0136	0.0247	0.77	0.52	0.06									0.0600	0.7700
Isoeugenol	0.0132	0.0441	0.19	0.15	0	0.6	0.006	0.62	0.51			0.1-7.2		0.0000	7.2000
Acetovanillone	0.0587	0.0955	0.19	0.15	0			0.16						0.0000	0.1900
Formic Acid	0.7474	1.1200								1.2	1.14	0.3-9.1		0.3000	9.1000
Acetic Acid	1.9194	2.6215					0.691		1.87	2.2	2.59	0.5-12	x	0.5000	12.0000

[a][21], [b][199], [c][77], [d][37], [e][201], [f][56], [g][200], [74], [h][202], [i][101], [j] Detected in toluene and ethyl acetate fraction, [k] converted from dry basis to wet basis, [l] based on area%, [m] quantified using GC-MS , [n] quantified using HPLC, x- present, ND – not detected, MIN- minimum, MAX - maximum

3.3.3.7.3 Statistical analysis

The chemical families were grouped according to: aldehydes, ketones, phenols and aromatics, sugars, furans, acids, alcohols, alkanes, hetero-components. Results in Table 43 were statistically analysed, using Design Expert software, to determine which of the factors investigated had a significant influence on the chemical families within a 95% confidence interval. None of the factors investigated had a significant effect on the aromatics, not even within a 90% confidence interval, yet some of the factors did significantly influence the presence of aldehydes, ketones, sugars, furans, acids and alkanes in the bio-oil, within a 95% confidence interval.

Table 46 Regression model and significant factors as determined by ANOVA analysis for different chemical families in Bio-oil

Elemental content [Y]	Significant factors	R^2	R^2 adjusted	Regression equation in terms of actual factors
Aldehydes	B: Temperatures AB: Moisture content and Temperature BC: Temperature and Particle size	0.9961	0.9863	Y [wt%]= 13.9534 -2.2502 xA-0.0180 x B+0.0156 x C +4.7334 x10^{-3} x A x B - 3.3137 x10^{-5} x B x C
Ketones	C: Particle Size	0.9476	0.9083	Y [wt%]= 16.2946 + 0.3636 x A - 1.7242 x 10^{-3} x C – 1.0675 x 10^{-4} x A x C
Sugars	B: Temperatures C: Particle Size	0.6366	0.4912	Y [wt%]= -7.4389 +0.0588 x B +6.1417 x 10^{-3}x C
Furans	B: Temperature	0.8556	0.6631	Y [wt%]= 16.8780 -6.6059 x A -0.0190 x B -1.2287 x 10^{-3} x C +0.0140 x A x B
Acids	B: Temperature	0.8317	0.6073	Y [wt%]=41.5239 +0.4742 x A -0.0761x B+2.3671 x 10^{-3} X C -3.0025 x10^{-4}x A x C
Alkanes	B: Temperature	0.9356	0.7744	Y [wt%]= -5.8909 -2.3487 x A +0.0164 x B +0.0126 x C+4.9051 x 10^{-3}x A x B - 2.6972 x 10^{-5} x B x C

A: Moisture content, B: Temperature, C: Particle size

The temperature and interaction of moisture content with temperature (AB), as well as the interaction between temperature and the particle size, were significant within a 95% confidence interval according to the ANOVA analysis for the presence of aldehydes. This analysis indicated that the R^2 and R^2 adjusted, were 0.9961 and 0.9863 respectively, indicating the good representation of the data by the surface response model. The error% for all runs used for regression model development was within -2.1wt% and 0.2wt%, however for run 1, the error was much greater at -10.3 wt%, see Table 98 in Appendix D. This indicated that the regression model should be used with caution when operating at other conditions than the experimental conditions. According to the surface response of the regression model depicted in Figure 16, the aldehyde content increased with a decrease in temperature. Aldehyde content was maximized at low temperature and low moisture content and minimized at high temperatures and low moisture contents. Aldehydes in bio-oil are known to be reactive [203]. The reactions that occur during bio-oil aging is suspected to be reactions of aldehydes [51]. It has also been reported that phenols degrade to aldehydes and acids [81]. During bio-oil aging, the reactions comprise of aldehydes reacting to form hydrates, water, resins, dimers, acetals and hemiacetals [51]. Other studies have also reported that the increase in stability after hydrotreatment can be observed as aldehydes and sugars are reduced to form alcohols [33]. When considering the probable reactions that cause bio-oil degradation, most of the reactions have

the organic acid or the aldehyde in the bio-oil participating in the reaction to form a more stable product. This shows that the organic acids and aldehydes are unstable products in the bio-oil [204], [13]. Low contents of aldehydes will therefore be desirable in terms of improved fuel stability. It has also been reported that the aldehydes, unsaturated oxygenates and furans are the major threats of toxicity [205], [72].
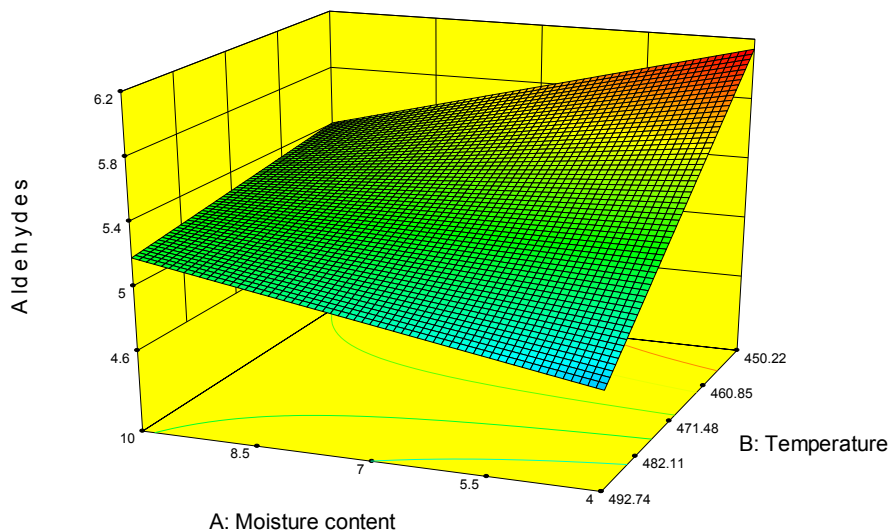
Figure 16 Regression model for chemical family of aldehydes in bio-oil

From the ANOVA analysis, it was determined that the particle size had a significant influence on the quantity of ketones present in the bio-oil. The regression model accurately described the data points, with a R^2 and an adjusted R^2 value of 0.9476 and 0.9083 respectively. This was also confirmed by the minor error% range of -3.9 to 3.9wt%, see Table 98 in Appendix D. The regression model was less accurate for run 1, and thus less capable of predicting at conditions other than the experimental conditions used for regression model development. An increase in the particle size results in a decrease in the ketone quantity, see Figure 17. Certain ketones (1-hydroxy-2-propanone) have been noted to be a primary tar product [192]. A reduction in the ketones might therefore be the result of secondary reactions caused by the greater particle size (e.g. ketones could be reacting with volatiles that are trapped inside the particle).
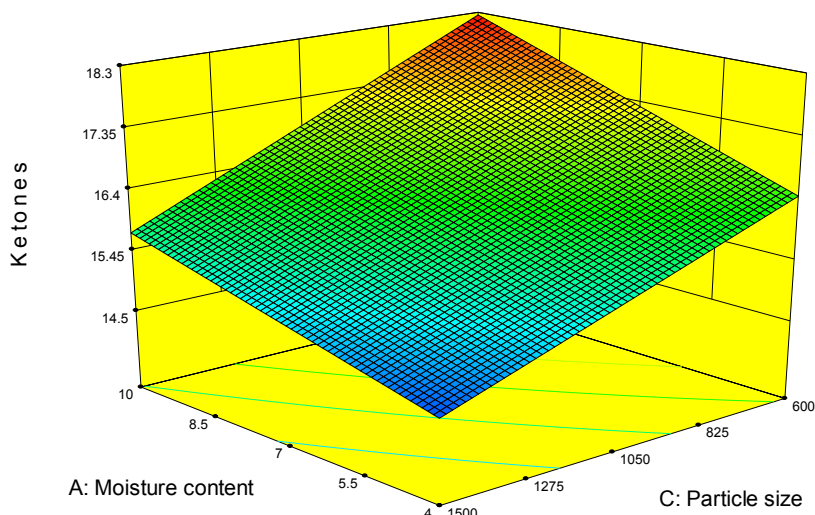
Figure 17 Regression model for chemical family of ketones in bio-oil

The regression model predicted the R^2 and R^2 adjusted associated with the sugars in the bio-oil at values of 0.6366 and 0.4912 respectively. The error % of the regression model ranged between -10.2 to 21.3wt%, indicating the large variation in accurately predicting the amount of sugars. The regression model predicted even worse for the data point not included in the development of the regression mode, with an error% of 39wt%, indicating that the regression model cannot be used for prediction of the sugar quantity in bio-oils. The sugar content in bio-oil was influenced by both temperature and particle size. The most significant sugar present, according to GC-MS analysis, was levoglucosan as reported previously [37], [206]. Previous studies have observed an increase in the levoglucosan content with increasing reactor temperature [21], [201], [206]. Cellulose has been reported to degrade into a mixture of pyrolysis water and sugars, due to the ratio of cellulose/(sugars and product water) being similar for different experiments [56]. Figure 18 shows that the sugars levels increase with an increase in reactor temperature for both small and large particle sizes. Levoglucosan is derived from cellulose pyrolysis, together with other pyrolysis products such as furans. Levoglucosan can also degrade to produce furans, but this was not observed under pyrolysis conditions [206]. It was found that the levoglucosan has a good thermal stability and only after 600 ^{o}C was degrading sufficient to produce furan products [206]. This has the implication that at low temperatures, the furans that are produced, are from the cellulose and not from secondary reactions of the levoglucosan [206]. It can therefore be concluded that the levoglucosan had not experienced further degrading to furans as the experimental temperatures were equal to/ less than 500 ^{o}C.
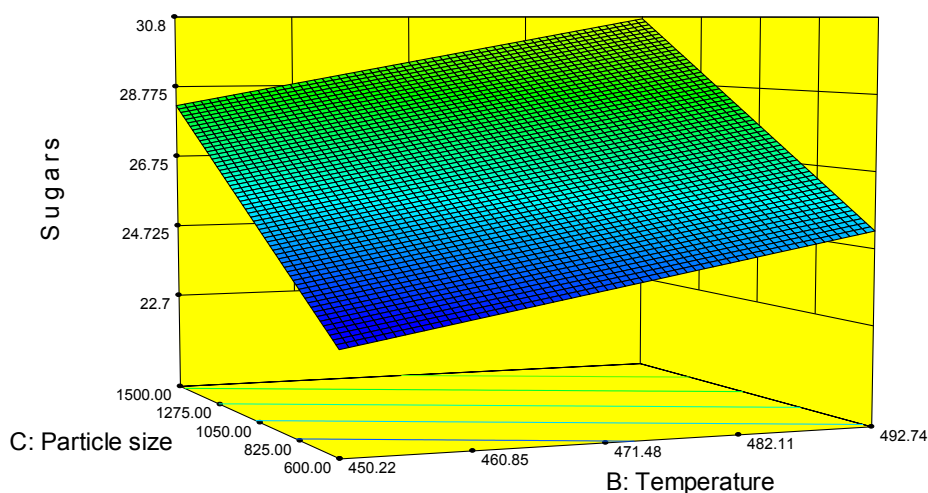
Figure 18 Chemical family of sugars in bio-oil

The acid content in the bio-oil was significantly influenced by the temperature, according to the ANOVA analysis. The ANOVA analysis on pH, representing strong acids, indicated that none of the factors was significant. This difference might partially be due to the poor detection capacity of the GC-MS for the most prominent acids present in the bio-oil, formic and acetic acids. Furthermore, some of the organic acids, such as acetic acid, are considered to be weak acids and will therefore not dissociate completely which explains the insignificant effect on the pH measurements. The R^2 and adjusted R^2 values for the acids chemical family was 0.8317 and 0.6073 respectively, indicating an acceptable fit. When considering the performance of the regression model to predict the acid content of the bio-oil, the error% varied between -7.6% and 11.1% for all reported runs, indicating the limited capability of the regression model to accurately predict the acid content, as can be seen in Table 99 in Appendix D. When considering the regression model, the maximum acids are obtained at low temperatures for both high and low particle sizes, see Figure 19. At low temperatures and small particle sizes, minimum acid content is achieved. Some of the acids, such as acetic acid, originate from the carbohydrates present in the wood [37]. It has been reported that the acids, alcohols, ketones and aldehydes are likely to be formed from the decomposition of oxygenates, sugars and furans [13]. It has been proposed that the formation of acetic acids might be due to dehydration – hydration reactions from acetaldehyde [45].

Hemicelluloses have been reported to degrade into gases and acids [56], and furfural [37], with degradation temperatures of between 473-623 K [191]. This is in agreement with the maximum yield observed at the low temperature of 450°C in this study, see Figure 19, as the hemicellulose will completely have degraded by this temperature to its primary products. Another study has also reported that acids dominate more at 400°C, as opposed to 500°C and 600°C [21], further confirming the ANOVA results from this study. In another study based on oak sawdust, a decrease in the acids (acetic and formic acid) were observed for an increase in temperature from 400 to 500°C [81]. Organic acids, as well as elements in the char, can act as catalyst during bio-oil storage and aging [51]. Some studies have also reported that acids can react with alcohols to form water and esters [72], although no significant decrease in the acid content was observed during more than a year of bio-oil storage [51].
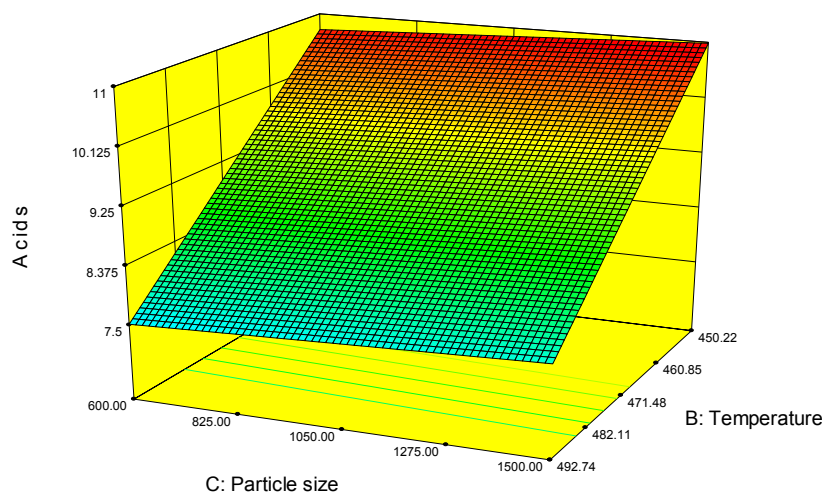
Figure 19 Chemical family of acids in bio-oil

Alkanes are typically not present in bio-oil in high concentrations. In this study, Isopar G, which is rich in linear and branched alkanes, was used as quenching medium. Due to differences in polarity, the bio-oil and the isopar are not miscible, however some contamination can occur in which case the bio-oil will have a greater alkane content than is expected. This might have influenced the alkane content in the bio-oil, which was investigated with control GC-MS runs with Isopar G, to confirm a small risk of contamination. According to the ANOVA analysis, only temperature had a significant effect on the alkane content. The R^2 and adjusted R^2 values are 0.9386 and 0.7744 respectively, according to Table 46. The error% associated with the alkanes in the bio-oil ranges between -4.2 to 13.2% for all runs excluding run 1, as can be seen in Table 99 in Appendix D. For run 1 the error% was -8.9%. Previous studies have reported no alkanes present in bio-oil derived from fast pyrolysis of mixed wood [16]. The alkane content increased with an increase in temperature, both at small and large particle sizes, see Figure 20.
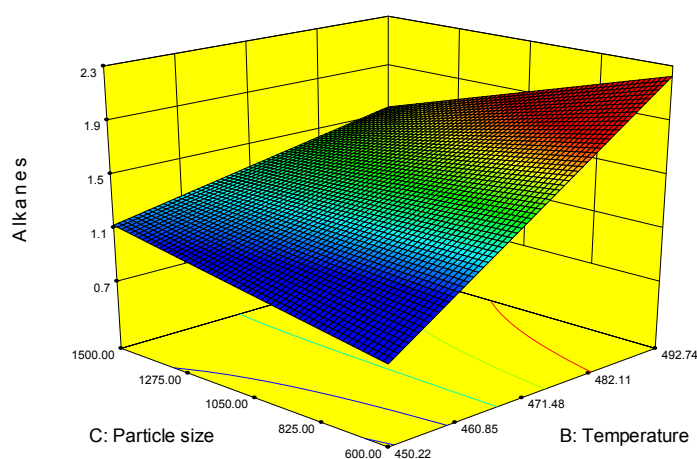
Figure 20 Chemical family of alkanes in bio-oil

99

3.3.3.8 NMR analysis

3.3.3.8.1 Experimental data – ^{13} C analysis

The results for the $^{13\text{-}}$C NMR analysis are provided in Table 47. The ^{13}C NMR shifts used in this study, are similar to previous studies [21], [37]. The 54-84 ppm region of the spectra, which contain methoxy- and hydroxy-bound carbons, contained the greatest amount of carbons, with 43.9 to 53.0% of carbons present in this particular group. The total aromatic range (110-163 ppm) contained 10.8 to 18.4 % of all carbons. Different types of aromatic carbons are present in different sections of the spectra, with guaiacyl carbons ranging from 112-125 ppm, whereas syringyl carbons range from 110-112ppm and general aromatic carbons range from 125 - 163ppm. The combined aromatic carbons are provided in the last column of Table 47. The carbohydrate carbon range contained 11.6 to 16.6 % of all carbons and the carbonyl type of carbons contained 8.6 to 11.1% of all carbons. Therefore a high quantity of carbons are present in the methoxy/hydroxy carbon range (54- 85ppm), the aromatic carbon range (110-163 ppm) and in the carbonyl section of the spectra, which includes carbons in ketones.

Guaiacyl carbons were present in quantities that were one to two orders of magnitude greater than syringyl carbons, shown in Table 47. Approximately 90% of softwood lignin (*P. radiata* is a softwood) is comprised of coniferyl alcohol, with sinapyl alcohol and p-coumaryl as the remaining 10% [54]. When considering the structures of these compounds, it seems appropriate that the guaiacyl (which closely resembles coniferyl alcohol) carbons are more abundant than the syringol carbons (which closely resembles sinapyl alcohol), as observed in the results from this study.

The experimental ranges obtained from this study were compared to ranges reported in literature, see Table 48. The carbonyl compounds compared well with the literature range. The carbohydrate range was close to the literature reported range, with the upper limit from this study (16.6% carbons) exceeding the upper limit of 15.1% carbons reported in literature Table 47. In a previous study the carbohydrate carbons were observed to increase with an increase in temperature [21]. This correlation was not observed from the NMR data in this study. However, it does correlate with results from another analysis (GC –MS), to be discussed later.

Table 47 ¹³C NMR results for experimental runs

Type of group/ description	Carbonyl compounds	Total aromatic carbons			Carbo-hydrate type carbons	Methoxy, Hydroxy bound compounds	Primary, secondary, tertiary & quaternary alkyl carbons	Secondary & tertiary carbons	Mostly primary & some secondary carbons		Inte-grated total	Sum total aromatic carbons
		General aromatic carbons	Guaiacyl compounds	Syringyl compounds								
Chemical Shift Range [ppm]	215-163	163-125	125-112	112-110	110-84	84-54	54-34	34-24	24-6	6-1		163-110
Run 1	11.048	7.535	10.515	0.366	12.234	43.913	2.818	5.974	5.596	0.000	*100*	18.416
Run 2	9.376	5.798	5.763	0.174	14.594	50.229	2.105	6.488	5.473	0.000	*100*	11.735
Run 3	9.098	4.824	6.271	0.246	15.833	51.112	2.726	5.302	4.520	0.068	*100*	11.342
Run 5	8.703	5.162	6.907	0.232	16.560	49.473	2.354	5.601	4.971	0.036	*100*	12.301
Run 6	8.640	5.208	8.166	0.474	15.265	49.779	1.062	5.849	5.557	0.000	*100*	13.848
Run 7	8.838	6.233	10.415	0.287	14.653	45.830	1.683	5.977	6.083	0.000	*100*	16.935
Run 8	9.219	5.350	8.689	0.161	15.564	49.508	0.251	5.864	5.393	0.000	*100*	14.200
Run 9	8.692	3.951	6.622	0.261	14.172	52.951	2.371	6.045	4.911	0.024	*100*	10.834
Run 10	10.279	8.478	9.195	0.437	11.578	45.105	2.536	6.495	5.896	0.000	*100*	18.110
MIN	*8.640*	*3.951*	*5.763*	*0.161*	*11.578*	*43.913*	*0.251*	*5.302*	*4.520*	*0.000*		*10.834*
MAX	*11.048*	*8.478*	*10.515*	*0.474*	*16.560*	*52.951*	*2.818*	*6.495*	*6.083*	*0.068*		*18.416*

A comparison between the results from this study and reported literature values is provided in Table 48. The maximum aromatic content in this study (18.4% of carbons) was lower than the minimum reported in other studies [(22.6% of carbons), [21]]. Repeatability of the analysis on runs 1 and 10 indicated a standard deviation of only 0.1%, indicating good repeatability of the analysis. The carbons present in the alkyl carbon region (1-54 ppm) were lower than was reported in literature, with the maximum obtained in this study (14.9%) close to the minimum reported in literature [14.8% carbons, [21]]. However, when taking the standard deviation for runs 1 and 10 into account (0.9 and 1.9% respectively), the value is comparable with literature [21]. The chemical shift range from 135-165ppm mainly represents non-protonated aromatic carbons and includes phenolic and phenoxyl compounds (150-165ppm) and alkyl-substituted aromatics (135-150ppm) [207]. In a study where the bio-oil was fractionated by ethyl acetate to a lignin-rich fraction, the alkyl carbons were observed to be greater in the lignin-rich fraction. It was credited to the aliphatic chains cross-linking the phenolic groups in lignin [37]. The carbons present in the aromatic (and phenolic) chemical shift range and the alkyl carbon chemical shift range, are greatly contributed by the lignin in biomass. Possible reasons for the lower percentage of carbons in the 1-54 ppm range obtained in this study, compared to literature, might be due to differences in lignin quantities in the biomass. Unfortunately the comparable literature study, [21], does not report the biomass lignin content, making comparison impossible. Alternatively, it can be due to more extensive cracking of the lignin in this study. More extensive cracking should be unlikely, as the literature study used for comparison utilized an auger reactor which has longer residence times and which should therefore be prone to more extensive cracking. However, comparison of the gas yields indicate a higher gas yield for this study; 27-36wt% compared to 19-24wt% in the study by DeSisto et al. [21], showing this to be a likely cause.

A trade-off seems to exist between the aromatic-and alkyl carbons (110-163 ppm, 1-54 ppm) and the methoxy carbons (54-84ppm) when comparing the experimental results with literature results. In this study, a smaller fraction of the carbons is present in aromatic and alkyl hydrocarbons compounds compared to literature, and a greater fraction of the carbons is present in the methoxy/hydroxy chemical shift range, compared to literature (Table 48). The methoxy/hydroxy fraction has been reported to show a significant decrease with an increase in reactor temperature, whereas the aromatic fractions show an increase with an increase in reactor temperature [21]. This seems to support the trade-off that can exist between the methoxy/hydroxy carbons and the aromatic carbons. The increase in aromatic content was attributed to the greater stability of the lignin-derived products at high temperatures compared to the cellulose-derived products [21].

The carbonyl carbons (163-215 ppm) region includes carbons present in aldehydes and ketones. In a study where the bio-oil was fractionated to a lignin-rich fraction by ethyl acetate fractionation, it was observed that the carbons present in the carbonyl spectra were greater in the whole bio-oil [37]. This was attributed to the fact that more of the cellulose and hemicelluloses derived components are present in the whole bio-oil than in the lignin rich fraction [37]. GC-MS results obtained in this study, show a decrease in aldehydes for an increase in reactor temperature, see Figure 16. In another study a decrease in carbonyl carbons for an increase in reactor temperature was also observed [21]. A similar trend could not be observed from the NMR results in this study.

The quantified GC-MS results indicated that levoglucosan was the most prominent compound and the chemical family results indicated that sugars were the most common chemical family, followed by aromatics and phenols, followed by ketones. Direct quantitative comparison between sugars measured by GC-MS and the carbons in the carbohydrate region measured by ^{13}C NMR, is not

102

possible, due to the differences in measuring units (area% compared to % of carbons). The high fraction of aromatic- and phenolic carbons, measured by GC-MS, agrees with the high quantity of carbons present in the methoxy/hydroxy carbon range (54- 85ppm) and the aromatic carbon range (110-163 ppm) measured by ^{13}C NMR. The [13] C NMR results indicated that a large amount of carbons is also present in the carbonyl section of the spectra, which includes carbons in ketones. This large amount of carbons is comparable to the quantity of ketones measured by GC-MS. The comparison between the GC-MS and NMR results in this study shows agreement on the high contents of aromatic/phenolic components and ketones in bio-oil.

According to statistical analyses, none of the factors investigated had a significant effect (within a 95% confidence interval) on the integrated ^{13}C NMR responses for different chemical shifts. In a previous study the carbohydrate carbons were observed to increase with an increase in temperature [21]. Although this has not been observed in the ^{13}C NMR results of this study, the results from DeSisto et al. [21] correlated well with the GC-MS results for the sugar chemical family, which showed that an increase in reactor temperature increased the presence of the sugar chemical family.

Table 48 ^{13}C NMR results comparison with literature

Type of group/ description	Carbonyl compounds	Total aromatic carbons			Carbohydrate type carbons	Methoxy, Hydroxy bound compounds	Primary, secondary, tertiary & quaternary alkyl carbons	Secondary & tertiary carbons	Mostly primary & some secondary carbons	
		General aromatic carbons	Guaiacyl carbons	Syringyl carbons						
Chemical Shift Range [ppm]	**215-163**	**163-125**	**125-112**	**112-110**	**110-84**	**84-54**	**54-34**	**34-24**	**24 to 6**	**6 to 1**
Fast pyrolysis of pine sawdust in fluidized bed reactor at 400°C [e]	8.4	22.6			13.5	38.2	17.2			
								10.3	6.7	
Fast pyrolysis of pine sawdust in fluidized bed reactor at 500°C [e]	7	24.3			15.1	38.9	14.8			
								8.2	6.4	
Triplicate results for fast pyrolysis of pine sawdust in fluidized bed reactor at 500°C, 13LPM, 40mL bed volume [e]	6.0-7.2	33.0-36.7			2.9-6.4	33.5-34.9	18.0-20.3			
								8.4-9.5	6.1-6.8	
Pyrolysis if pine wood in an auger reactor at 450°C [f]	11.8	48.4			5.8	16.1	17.9			
								8.5	9.4	
MIN from study	*8.640*	*3.951[a]*	*5.763[b]*	*0.161[c]*	*11.578*	*43.913*	*0.251*	*5.302*	*4.520*	
		10.834[d]					*11.509[a]*			
MAX from study	*11.048*	*8.478[a]*	*10.515[b]*	*0.474[c]*	*16.560*	*52.951*	*2.818*	*6.495*	*6.083*	
		18.413[d]					*14.927[a]*			

[a] individual run`s minimum for specific spectra (163-125ppm), [b] individual run`s minimum for specific spectra(125-112ppm), [c] individual run`s minimum for specific spectra(112-110ppm), [d] individual run`s minimum for specific spectra (163-110ppm), [e] [21], [f] [37]

3.3.3.8.2 Experimental data – Proton (^{1}H) NMR analysis

The ^{1}H NMR (proton NMR) results are provided in Table 49. It has previously been reported that the overlapping of the protons in the chemical shift ranges for protons complicates quantification and interpretation of the results [37]. According to the results, the methoxy hydrogens, present in the 3-4.2 ppm region of the spectra, are the most common, with 54.0 to 66.7% of all hydrogen present in a methoxy group. The 4.2-6.4 ppm range, which includes phenolic protons, was the second largest accounting for 7.8 to 24.3 % of all protons.

Comparison with literature indicated that the methoxy protons and phenolic OH and non-conjugated olefinic protons contents, corresponding respectively to chemical shift ranges of 3-4.2 ppm and 4.2-6.4 ppm, were greater than those reported in literature, see Table 50. While the presence of protons in other chemical shift ranges (8-10ppm, 6.8-8 ppm, 6.4-6.8ppm, 1.6-2.2 ppm and 0-1.6 ppm) were found to be lower than those reported in literature (Table 88).

The proton NMR results were consistent with the ^{13}C NMR results, indicating that the methoxy group is the most prominent, with the protons in the methoxy group and the carbons in the methoxy/hydroxyl carbons as the highest for all functional groups (54.0 to 66.7% of all hydrogen and 43.9 to 53.0% of all carbons). The proton NMR results for the 4.2-6.4 ppm section of the spectra, which included phenolic protons, were in agreement with the results from ^{13}C NMR, which indicated that the aromatic range (110-163 ppm), which contains phenolic and phenoxyl compounds (150-165ppm) [207], was the second largest, see Table 48. GC–MS results also indicated that levoglucosan was the most prominent compound and the sugar fraction the most common chemical family, followed by phenols and ketones. According to the chemical family analysis on GC-MS data, the phenolic group was the second most abundant in the bio-oil. This agreed with the proton NMR and with the ^{13}C NMR results discussed earlier in this paragraph.

105

Table 49 ^{1}H NMR results for experimental runs

Chemical Shift Range [ppm]	10-8 [a]	8-6.8 [a]	6.8-6.4 [a]	6.4-4.2 [a]	4.2-3 [a]	3-2.2 [a]	2.2-1.6 [a]	1.6-0 [a]	Integrated total ^{1}H-NMR
	Aldehyde protons, lower field aromatic protons [a]	Aromatic protons, olefinic protons conjugated to carbonyls [a]	Olefinic protons conjugated to carbonyls [a]	Phenolic OH functionality, non-conjugated olefinic protons [a]	Methoxy protons [a]	α-located protons to ketones, carboxyl groups, aldehydes and benzylic protons [a]	Aliphatic protons [a] and aliphatic hydroxyls	Aliphatic protons [a]	Total
Group type	-CHO, -COOH, downfield ArH	ArH, HC=C (conjugated)	HC=C (uncon-jugated)	=CHO, ArOH, HC=C (nonconju-gated)	CH3O-, -CH2O-	CH3Ő-, CH3-Ar, -CH2Ar	-CH2-, aliphatic OH	-CH3, -CH2-	
Run 1	0.721	0.344	3.227	13.498	61.190	7.531	9.678	3.810	100
Run 2	0.414	0.061	1.644	7.818	66.707	8.492	10.071	4.792	100
Run 3	0.773	0.682	2.895	11.800	61.472	8.356	8.684	5.338	100
Run 5	0.559	0.580	2.336	15.974	63.411	6.282	7.631	3.229	100
Run 6	0.748	0.737	2.985	16.469	58.897	7.452	8.662	4.050	100
Run 7	0.471	0.774	3.677	19.522	53.947	7.490	9.516	4.602	100
Run 8	0.704	0.971	4.661	14.779	61.381	6.274	7.965	3.265	100
Run 9	0.452	1.747	2.326	24.252	58.676	4.182	6.095	2.270	100
Run 10	0.781	0.470	3.437	13.391	54.849	9.258	11.620	6.194	100
MIN from study	*0.414*	*0.061*	*1.644*	*7.818*	*53.947*	*4.182*	*6.095*	*2.270*	
MAX from study	*0.781*	*1.747*	*4.661*	*24.252*	*66.707*	*9.258*	*11.620*	*6.194*	

[a] Obtained from [37]

Table 50 ^{1}H NMR results comparison with literature

Chemical Shift Range [ppm]	10-8	8-6.8	6.8-6.4	6.4-4.2	4.2-3	3-2.2	2.2-1.6	1.6-0
Group type	-CHO, -COOH, downfield ArH	ArH, HC=C (conjugated)	HC=C (unconjugated)	=CHO, ArOH, HC=C (non-congugated)	CH3O-, -CH2O-	CH3Ő-, CH3-Ar, -CH2Ar	-CH2-, aliphatic OH	-CH3, -CH2-
Group description	Aldehyde protons, lower field aromatic protons [a]	Aromatic protons, olefinic protons conjugated to carbonyls [a]	Olefinic protons conjugated to carbonyls [a]	Phenolic OH functionality, non-conjugated olefinic protons [a]	Methoxy protons [a]	α-located protons to ketones, carboxyl groups, aldehydes and benzylic protons [a]		Aliphatic and hydroxyl protons [a]
Pine wood used for pyrolysis on auger reactor [a]	2.63	4.35	5.3	16.54	37.56	9.04	13.69	10.88
Fast pyrolysis oil from beech wood, supplied by BTG [b]	0.9	Aromatic [b]		9	26.3	6.4	Aliphatic [b]	
		3.3	4.4				32.7	17.0
MIN from study	*0.414*	*0.061*	*1.644*	*7.818*	*53.947*	*4.182*	*6.095*	*2.270*
MAX from study	*0.781*	*1.747*	*4.661*	*24.252*	*66.707*	*9.258*	*11.620*	*6.194*

[a] Obtained from [37], [b] according to [91]

106

3.3.3.8.3 Statistical analysis

According to the ANOVA analysis on the proton NMR data, only the aldehyde, lower field aromatics protons (8-10ppm) and the olefinic protons, conjugated to carbonyls (6.4-6.8ppm), were significantly influenced within a 95% confidence interval by the factors investigated in the study. The aldehydes and lower field aromatic protons were significantly influenced by the particle size, and the olefinic protons conjugated to carbonyls, were significantly influenced by the moisture content and the temperature. Previous studies have reported difficulties with quantification of results due to overlapping of shift ranges [37].

The R^2 and adjusted R^2 for the regression model for the aldehyde protons and lower field aromatics, were 0.9066 and 0.8910 respectively, see Table 51. The error% associated with the regression model ranges between -16.9 and 14.7%, see Table 100 in Appendix D, indicating the large variation on the regression model`s results. The protons present in the 8-10 ppm chemical shift range were significantly influenced by the particle size. An increase in the particle size resulted in a decrease in the aldehyde protons and low field aromatic protons, see Figure 21. In a study by Oasmaa and Kuoppala (2003), aldehydes have been linked to contribute to aging of the bio-oil, due to the participation in condensation reactions, which results in a decrease in the aldehyde concentration [51]. It is possible that the decrease in protons for the 8-10 ppm section of the spectra was due to a greater extent of poly-condensation reactions experienced at larger particle sizes. The ANOVA on the aldehyde family detected by GC-MS, did not indicate that the particle size was a significant factor, but rather that the temperature was significant, with an increase in temperature resulting in a decrease in the aldehydes. The reason for the discrepancy between the GC-MS and ^{1}H NMR analysis can be due to the limitations associated with lumping techniques, or due to the different types of protons (aldehyde protons and lower field aromatic protons) being measured within the 8-10 ppm chemical shift range and not only aldehydes as in the GC-MS analysis. The decreasing trend in aldehydes agreed with results from NMR results from another study where a decrease in the carbonyl carbons was observed for an increase in reactor temperature [21]. The significant influence of particle size on the 8-10ppm chemical shift range (as identified by ANOVA) might therefore reflect on the effect of the particle size on the low field aromatic protons. This has not been reported in literature and cannot be confirmed from the available results.

Table 51 Regression model and significant factors as determined by ANOVA analysis for NMR results

Spectra [ppm]	Significant factors	R^2	R^2 adjusted	Regression equation in terms of actual factors
Aldehyde protons and lower field aromatic protons [10-8 ppm]	C:Particle size	0.9066	0.8910	Y [wt%]= 0.9178 -2.8320x 10^{-4} x C
% Olefinic protons conjugated to carbonyls [6.8-6.4 ppm]	A: Moisture content B: Temperature C:Particle size	0.9837	0.9714	Y [wt%]= -9.4983 $-$ 0.2112 x A + 0.0320 x B -1.1731 x 10^{-3} x C

A: Moisture content, B: Temperature, C: Particle size
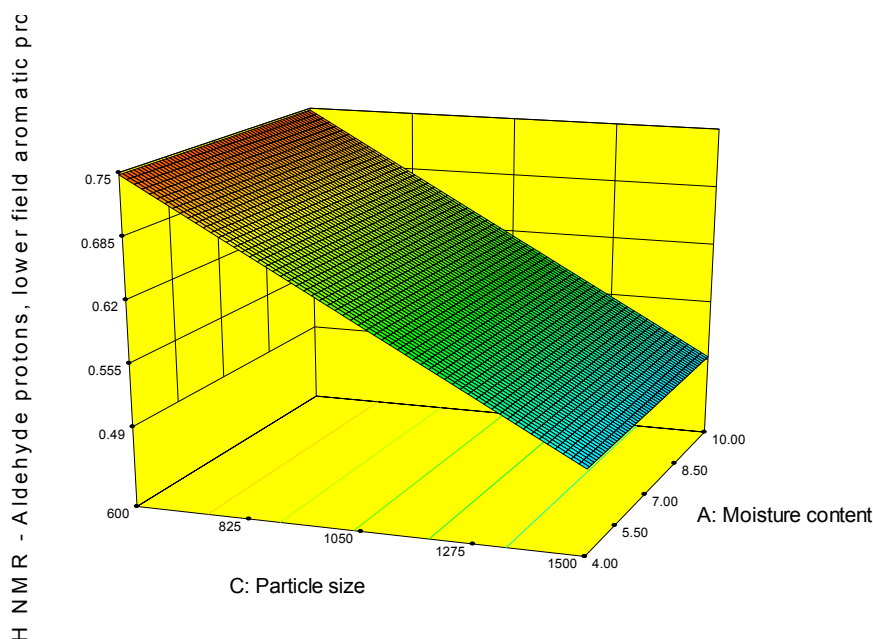
Figure 21 Protons in spectra 8 – 10 ppm

The R^2 and adjusted R^2 for the regression model for the olefinic protons conjugated to carbonyl, were 0.9837 and 0.9714 respectively, see Table 51. The error% ranged from -5.6 to 6.5% for the experimental runs used to derive the regression model. For run 1, the error% was greatest at -15.2%, indicating that the regression model was not as accurate at other conditions. According to ANOVA analysis, all three factors investigated were significant. An increase in reactor temperature increased the fraction of protons present in the 6.4-6.8ppm range of the spectra, whereas an increase in moisture content and particle size decreased the fraction of protons present in the 6.4-6.8ppm range, see Figure 22 and Figure 23. The conditions that maximized protons in the 6.4-6.8ppm region of the spectra (high temperature, low moisture content and small particle sizes), all enhance heat transfer to and through the biomass particle.

From the ^{13}C NMR analysis in a study by DeSisto et al. [21], the methoxy/hydroxy carbon fraction was shown to decrease significantly with an increase in reactor temperature, whereas the aromatic fractions increased with an increase in reactor temperature. The increase in aromatic content was attributed to the greater stability of the lignin-derived products at high temperatures compared to the cellulose-derived products [21]. In a ^{1}H NMR analysis performed in a study where the effect of temperature on the fast pyrolysis of lignin was investigated, aromatic protons were considered to have a chemical shift of 5.5-8.0 ppm in a proton NMR analysis on bio-oil [208]. It was determined that the methoxy functional groups are reactive and temperature sensitive, due to the methoxylated phenols drastically decreasing with an increase in temperature as a result of demethylation [208]. The same trend for the methoxy/ hydroxyl fraction and aromatic fraction was not detected in either the ^{1}H NMR or the ^{13}C NMR analyses in this study.
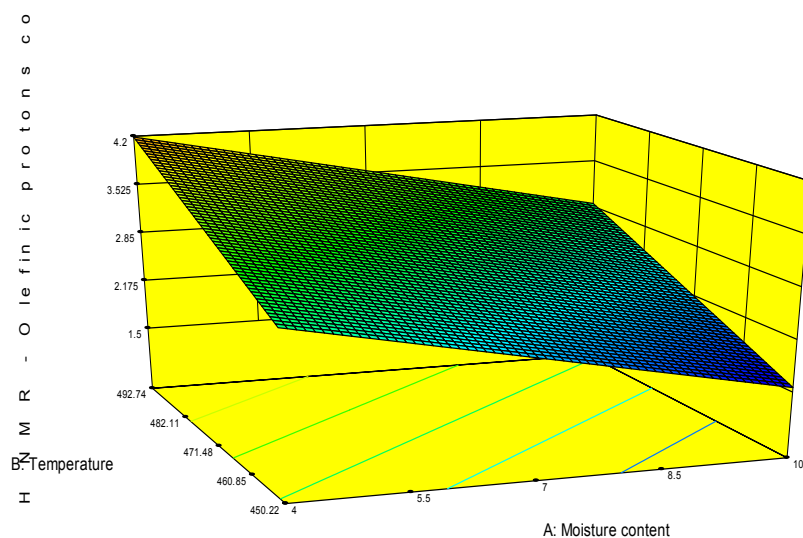
Figure 22 Protons in spectra 6.4 – 6.8 ppm as a function of moisture content and temperature
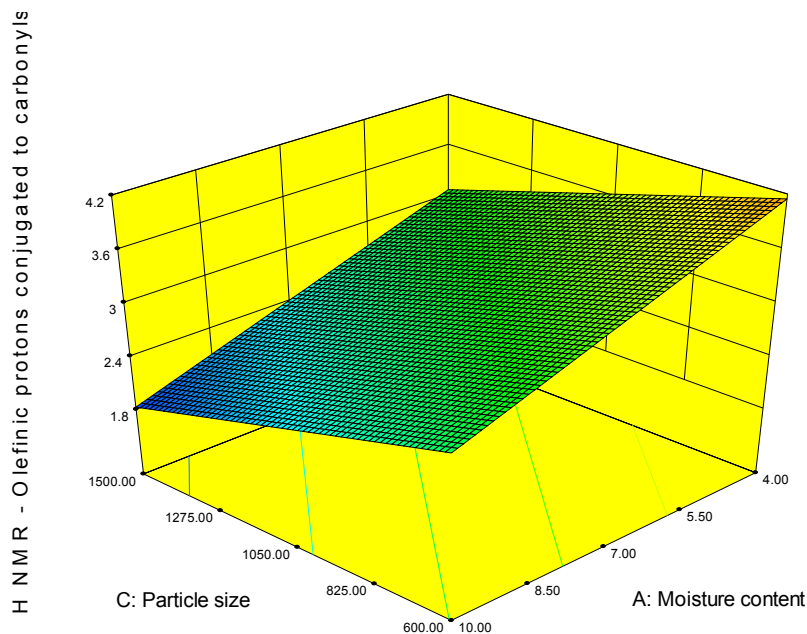
Figure 23 Protons in spectra 6.4 – 6.8 ppm as a function of moisture content and particle size

3.3.3.9 Ultimate analysis on Bio Char

3.3.3.9.1 Experimental data

The elemental analysis of bio-char was performed in duplicate (Table 52). Sulphur contents had high standard deviations and CVs and were close to the detection limit. Sulphur is seldom reported in literature and due to the large CV values obtained, was thus excluded from the present study. In most cases the nitrogen was below detection limit and therefore not reported. Oxygen was calculated by difference. The CV for carbon was low and ranged between 0.087% and 2.144%. The CV for hydrogen was acceptable (less than 10%) and ranged from 0.058% to 8.739%. The deviation in the oxygen content was the greatest of the elements reported. This was expected since the oxygen is calculated by difference and includes the compounded errors from carbon, hydrogen and the omission of nitrogen and sulphur analysis. The CV for oxygen ranged from 0.530% to 11.137%.

109

Table 52 Elemental analysis of bio-char

Sample name	C [wt%] [c]	H [wt%] [c]	O [wt%] [a,b,c]
Run 1	83.53 ± 1.04	2.61 ± 0.16	13.86 ± 0.88
CV [%]	1.244	6.226	6.325
Run 2	83.84 ± 0.58	2.47 ± 0.13	13.69 ± 0.45
CV [%]	0.692	5.407	3.260
Run 3	80.89 ± 0.07	2.62 ± 0.06	16.49 ± 0.13
CV [%]	0.087	2.346	0.802
Run 5	83.66 ± 0.30	2.42 ± 0.12	13.93 ± 0.40
CV [%]	0.355	4.946	2.899
Run 6	82.21 ± 1.15	2.37 ± 0.20	15.42 ± 0.95
CV [%]	1.393	8.256	6.160
Run 7	82.44 ± 1.12	2.36 ± 0.21	15.21 ± 0.99
CV [%]	1.450	8.739	6.504
Run 8	81.67 ± 0.08	2.58 ± 0.16	15.76 ± 0.08
CV [%]	0.095	6.251	0.530
Run 9	81.80 ± 1.75	2.44 ± 0.00	15.76 ± 1.76
CV [%]	2.144	0.058	11.137
Run 10	81.00 ± 0.10	2.89 ± 0.20	16.11 ± 0.30
CV [%]	0.122	6.974	1.865

[a] calculated by difference, [b] ignoring sulphur and nitrogen contents, [c] ± standard deviation

The carbon contents of the biochar produced in this study ranged from 80.89 – 83.84 wt%, see Table 52. A comparison with literature is provided in Table 53. The carbon range compares well with the range reported in literature, with carbon contents of 71.91 and 74.10wt% reported at 400 ^{o}C and 500°C for *P. strobus,* as well as with the carbon content of 82.8wt% reported for *P. radiata* at 400 ^{o}C. The hydrogen content range of 2.35 – 2.89wt% achieved in this study was lower than the range of 3.00 – 4.77 wt% available in literature for comparable conditions; see Table 41 and Table 53.

Literature values for the oxygen content in char vary from 14.2 to 23.33 wt% for the similar temperatures, see Table 53. The oxygen content for the char produced in this study, 13.69 to 16.49wt%, was less than the range of 21.5 to 23.33wt% reported at 500°C and 400°C for *P. strobus*. However, it is comparable with the oxygen content in the char produced from *P. radiata* at 400°C. The lower limit of the experimental runs were slightly lower than the minimum oxygen content in bio-char reported in literature, although with the oxygen measurements` standard deviation of 0.083 to 1.755 wt% taken into account, the reported values and results from this study compare well.

Table 53 Elemental analysis of bio-char compared to literature

Source	This study	Literature			
Feedstock	*Pinus radiata*	*Pinus strobus* [b]			*Pinus radiata* [c]
Reactor	Fluidized bed reactor	Fluidized bed reactor, 60g/hr			Bubbling fluidized bed (228g/hr)
Conditions	Moisture contents 3-10wt%, particle sizes 0.25-2mm, reactor temperatures 450-500°C.	400°C	500°C	600°C	BM moisture <1 wt%, 400°C, particle size 0.7mm,
C [wt%]	80.89-83.84	71.91	74.10	86.42	82.80
H [wt%]	2.35-2.89	4.77	4.40	3.21	3.00
O[a] [wt%]	13.69-16.49	23.33	21.50	10.36	14.20

[a] calculated by difference, [b] obtained from [21], [c] obtained from [191]

3.3.3.9.2 Statistical analysis

ANOVA analysis on the carbon, hydrogen and oxygen present in the char was performed, see Table 54. According to an ANOVA analysis, the particle size had a significant impact on the carbon and oxygen content of the char. None of the factors investigated had a significant influence on the hydrogen content of the char. The R^2 and R^2 adjusted values for the regression model of the carbon content in the char were both acceptable at 0.8910 and 0.7465 respectively. The error associated with the model prediction was low and ranged from -0.77 to 0.71%, confirming the good fit even for data not used in development of the regression model (run 1), see Table 101 in Appendix D.

The carbon present in the char increased with an increase in the particle size, see Figure 24. This was expected to be due to the larger particle sizes having a longer residence time in the reactor, which leads to secondary reactions. Longer residence times and secondary reactions such as repolymerization is known to promote the formation of char, which contributes to the measured carbon content [68], [191].

The regression model for predicting the hydrogen content was less, with the R^2 and R^2 adjusted values 0.7505 and 0.5634 respectively. The error associated with predicting the hydrogen content ranged between -7.38 and 7.02%, see Table 101 in Appendix D. The model for oxygen present in the char fitted the data sufficiently, with R^2 and R^2 adjusted values of 0.7579 and 0.5764. The error ranged from -5.46 to 8.45%, see Table 101 in Appendix D.

The regression model indicated that particle size had a significant influence on the oxygen in the char. Figure 25 depicts that high particle sizes and high moisture contents minimized the oxygen content, whereas small particle sizes at both high and low moisture contents maximized the oxygen in the char. The decrease of oxygen with an increase in particle size and moisture content indicated that the secondary reactions result in the formation of oxygenated compounds, which evolve during the degradation of the carbonaceous structure of the char. Furthermore, the initial moisture is beneficial to carbonization of the solid material. It is interesting to note that statistically the particle size only has an effect on the elemental distribution in the char products, but not on the bio-oil`s elemental distribution.

Table 54 Regression model and significant factors as determined by ANOVA analysis for different Char elemental analysis response

Elemental content[Y]	Significant factors	R^2	R^2 adjusted	Predicted R^2	Regression equation in terms of actual factors
C in Char	C: Particle Size	0.8910	0.7456	0.4865	Y [wt%]= 74.2238 -0.1717xA - 0.0159 x B - 5.4790x 10^{-4}x C +2.9866x 10^{-4}x A x C
H in Char	None	0.7505	0.5634	-0.3649	Y [wt%]= 10.0808 -0.0156x B − 4.2705 x 10^{-3}x C +8.6385 x 10^{-6}x B x C
O in Char [a]	C:Particle size	0.7579	0.5764	0.0036	Y [wt%]= 14.3118 +0.1467 x A +1.6394x 10^{-4}x C-2.4470 x 10^{-4}x A x C

[a] Calculated by difference, neglecting sulphur and nitrogen, A: Moisture content, B: Temperature, C: Particle size
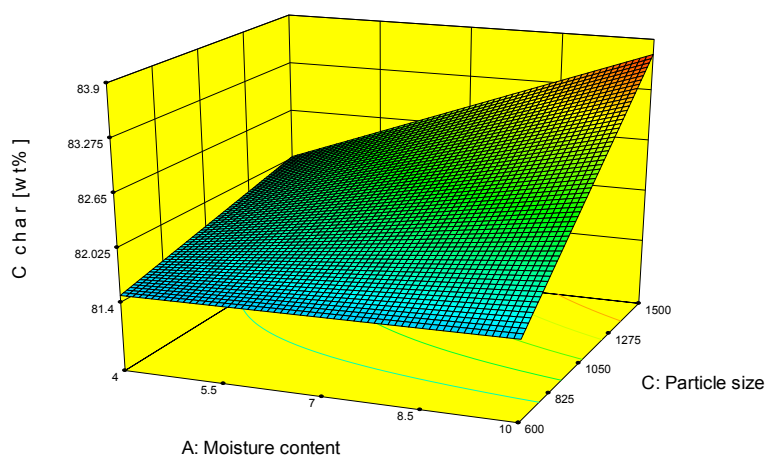
Figure 24 Carbon content in char
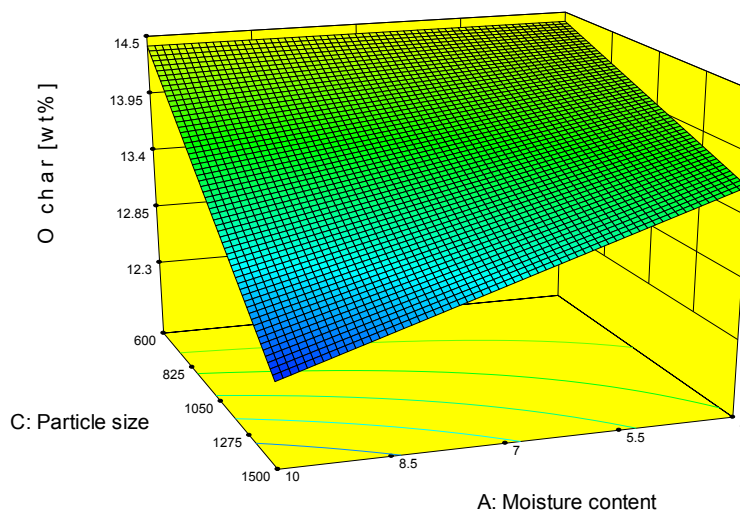
Figure 25 Oxygen content in char

3.3.3.10 Char HHV

3.3.3.10.1 Experimental data

The HHV of char was calculated based on the elemental analysis of the char, combined with the Boie correlation, which provided the most accurate prediction of the HHV as indicated in Table 55. HHV results are reported in Table 102 in Appendix D.

Table 55 Comparison for different correlations to calculate Bio-char HHV

Run nr.	Experimentally determined [MJ/kg]	Boie correlation [a] [MJ/kg]	Channiwala correlation [b] [MJ/kg]	Proximate Analysis correlation [c] [MJ/kg]	Proximate Analysis correlation [d] [MJ/kg]
3	30	29.93	28.87	31.27	31.01

[a] Equation 21 in this study, obtained from [176], [b] Equation 22 in this study, obtained from [114], [c] Equation 24 in this study, obtained from [177], [d] Equation 25 in this study, obtained from [178]

In this study, the HHV of the char varied between 29.93 and 31.22 MJ/kg, which compared well with literature. In a study by DeSisto et al. [21], the HHV of char at 400°C and 500°C, was 28.50 and 28.05 MJ/kg respectively. Other literature studies have reported char produced from fast pyrolysis of corn cobs at 500°C, with a HHV of 30.0MJ/kg [209]. In a different study char produced from fast pyrolysis of pine wood at 400°C and 450°C, had a HHV of 31.7 MJ/kg (dry basis) [210].

The significant factors that influenced the char HHV proved to be the particle size and the interaction between the moisture content and particle size. The interaction between the moisture content and the particle size results in a twisted surface response, see Figure 26. The HHV is maximized at large particle sizes and high moisture contents. This is expected to be due to incomplete pyrolysis/volatilization, resulting in a portion of the organic material remaining in the solid phase: at high moisture contents, more energy is required for the vaporization of free moisture, resulting in less heat available for volatilization of the organic content and a greater portion of the organic material remains in the solid phase. The HHV of organics still trapped in the carbonaceous matrix can contribute to increase the HHV of the char [211]. At lower moisture contents, less energy is required for vaporization of free moisture and therefore more energy is available for the volatilization of the organic content, resulting in a larger transfer of the organic content to the bio-oil phase. Furthermore the conditions for maximizing the HHV is similar to the conditions at which the carbon in the char is maximized (high moisture contents and large particle sizes, see Figure 24).

A slight decrease in the char HHV was reported from 400°C to 500°C, although an increase occurred from 500°C to 600°C [21]. In a different study where the statistical significance of reactor temperature was investigated, it was concluded that the reactor temperature was significant within a 95% confidence interval, with an increase in reactor temperature resulting in a decrease in char HHV [79]. In this study the pyrolysis reactor temperature was not found to be significant.
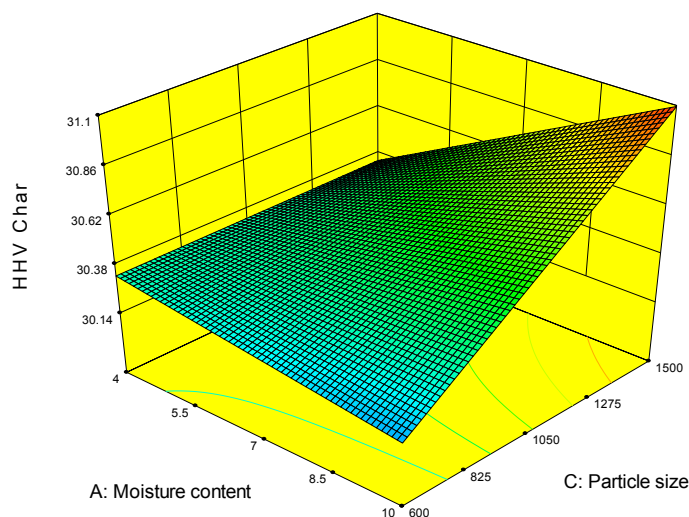
Figure 26 Three dimensional surface indicating effect of particle size and moisture content on char HHV

3.3.3.10.2 Statistical analysis

The R^2 and R^2 adjusted are 0.9132 and 0.8481 as indicated in Table 56. Overall, the char HHV could be predicted well, with the error% ranging between -0.74 and 0.65% for the runs considered in the ANOVA analysis, see Table 102 in Appendix D. For run 1 (not considered), the error was highest at -1.79%, which is still an acceptable error%.

Table 56 Regression model and significant factors as determined by ANOVA analysis for HHV of char

Quality analysed	Significant factors	R^2	R^2 adjusted	Regression equation
HHV char	C: Particle Size AC: Moisture content & Particle size interaction	0.9132	0.8481	Y [MJ/kg] ^{a}= 30.8641 -0.1357 x A -6.8020 x 10^{-4}x C +1.7387 x 10^{-4}x A x C

^{a}dry basis, A: Moisture content, B: Temperature, C: Particle size

3.3.3.11 Energy content and transfer

3.3.3.11.1 Energy transfer to BO

The energy transfer is used to describe the energy present in the BO phase (energy transfer to BO) and the char phase (energy transfer to char), as a fraction of the energy that was present in the initial biomass. The energy transfer to the BO ranged between 45-61%, as indicated in Table 102 in Appendix D. The energy transfer to the BO is only significantly influenced by the particle size, with the R^2 at 0.5455 and the adjusted R^2 at 0.4698, see Table 57. The surface plot indicated that the energy transfer to the BO is highest at small particle sizes with a linear decrease as the particle size increases, as can be seen in the response surface, see Figure 27. This was attributed to better heating of the smaller particle sizes, which reduces the time the vapour spends travelling to the outside of the particle. In addition to this, smaller particle sizes will result in a shorter distance the product vapours at the particle inside needs to travel to reach the outer part of the particle. It also prevents/minimizes cracking of large organic molecules, which condenses and contributes to the energy content of the bio-oil. The error% in predicting the energy transfer ranged from -7.68 to 12.69% for runs 2-10, see Table 102 in Appendix D. For run 1, the error was highest at -15.06%; showing that the regression model is less accurate for the experimental conditions not used for development of the regression model.
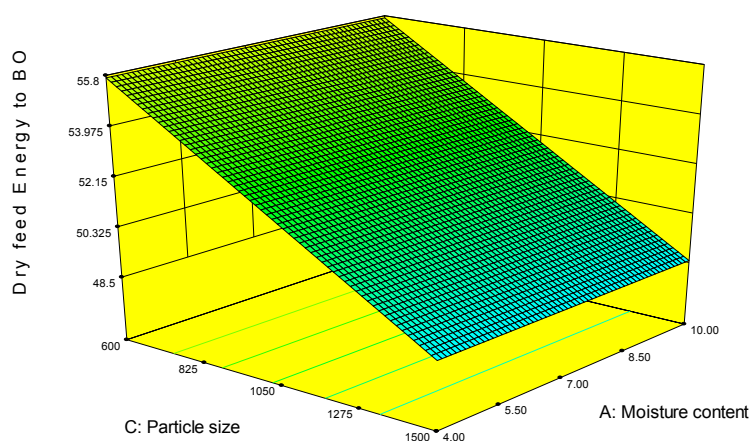
Figure 27 Three dimensional plot indicating the effect of particle size on the energy transfer from BM to BO

3.3.3.11.2 Energy transfer to char

The char contained approximately 25% and the product gas approximately 5% of the energy present in the feedstock [32]. The energy present in the char for this study ranged between 17.33 and 23.72%, see Table 102 in Appendix D. The maximum obtained in this study is still slightly lower than the 25% approximation [32].

Only the particle size was significant in influencing the energy transfer to the char. The R^2 was 0.8187 and the adjusted R^2 was 0.7885, see Table 57. An increase in the particle size results in an increase in the energy transfer from the biomass to the char, see Figure 28. These results agree with the HHV of char, as was expected, although there was no interaction between the moisture content and the particle size as was observed for the char HHV. The error% ranged from -5.76 to 8.62% for runs 2-10 and was the highest for run 1, at -13.76%, see Table 102 in Appendix D. This indicated that the regression model was not capable of predicting the results at experimental conditions other than those used for regression model development.
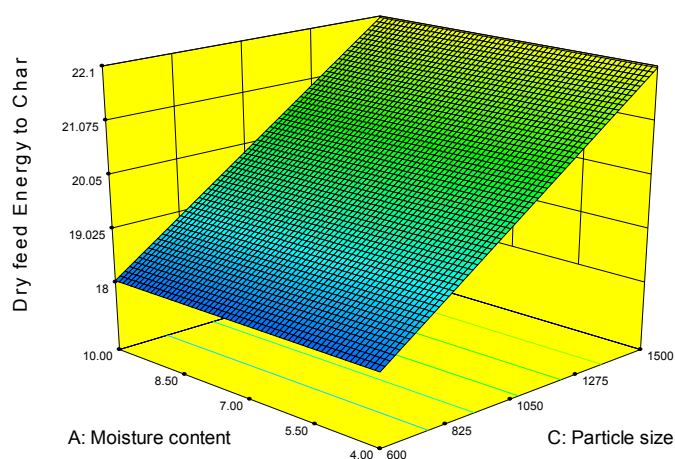
Figure 28 Three dimensional plot indicating the effect of particle size on the energy transfer in the biomass (on a dry basis) to char

Table 57 Regression model and significant factors as determined by ANOVA analysis for Energy related responses

Quality analysed	Significant factors	R^2	R^2 adjusted	Regression equation
Energy to BO	C: Particle Size	0.5455	0.4698	Y [%] [a]= 60.4793 -7.9365 x 10^{-3} x C
Energy to Char	C: Particle size	0.8187	0.7885	Y [%] [b] = 15.3301 +4.4941 x 10^{-3} x C

[a] % of energy in dry biomass to bio-oil, [b] % of energy in dry biomass to char, A: Moisture content, B: Temperature, C: Particle size

3.4 Experimental conclusions

In this study, the yield and quality of bio-oil produced by fast pyrolysis of South African *Pinus radiata,* at different feedstock pre-treatment conditions and operating conditions, were assessed. A statistical design was utilized for screening and assessing significant factors.

Maximum organic yield occurred at small particle sizes (0.25 – 0.85 mm), high temperatures (500°C) and low moisture contents. The small particle size allowed for rapid heat transfer and shorter residence time of the volatilized product within the particle. Although high temperatures did not have a significant effect on the organic yield, it reduced the pyrolytic water formation and produced a higher quality bio-oil. Low moisture content levels did not influence the pyrolytic water formation or the organic liquid yield, although it minimized the free moisture transfer to the bio-oil from the biomass.

Specific bio-oil characteristics were assessed to evaluate the bio-oil quality. The moisture content in the bio-oil was significantly increased by higher biomass moisture contents and larger particle sizes. The dynamic viscosity of the bio-oil was significantly increased by lower feedstock moisture contents and smaller particle sizes. The same factors which increased the moisture content in the bio-oil, affected the viscosity, since it enhanced the moisture causing the viscosity to decrease. The HHV of the bio-oil was significantly decreased by an increase in the moisture content in the biomass, with such moisture directly transferred to the bio-oil. The bio-oil density was significantly increased by an increase in temperature and a decrease in biomass particle size. The opposite trends were observed for the formation of pyrolytic water, which increased with low temperatures and large particle sizes. The density was not significantly affected by the biomass moisture content or by the same factors that affected the bio-oil moisture content. This could indicate that the biomass moisture present in the bio-oil is not necessarily the main influence on the density, but rather the reactions which enhance pyrolytic water formation. The pH was not significantly influenced by the biomass moisture content, the biomass particle size or the reactor temperate.

In terms of chemical composition, the carbon and hydrogen content in the bio-oil were not significantly influenced by the biomass moisture content, particle size or temperature. Only the oxygen content in the bio-oil was significantly influenced by one of the factors investigated – the moisture content of the biomass. The oxygen content in the bio-oil (moisture free basis) increased with an increase in biomass moisture content.

Quantified GC-MS data indicated that bio-oil is comprised of many components present in small quantities. Neglecting water, levoglucosan was present in the largest quantity (up to 4.9wt%), followed by acetic- and formic acid (2.6 wt% and 1.2wt% respectively), with all other quantified components present in <1wt%. Quantified GC-MS results compared well with ranges reported in literature, with the exception of 2 methoxy-4 vinylphenol, whose maximum quantity determined in this study was less than the minimum reported in literature.

The area percentages of GC-MS chromatogram peaks were used as indication of the effect of processing conditions on product quantities of chemical families. Statistical analysis indicated that the reactor temperature, particle size and the moisture content did not have a significant influence on the bio-oil aromatic content, within a 95% confidence interval. However, these factors did have a significant influence on the aldehydes, ketones, sugars, furans, acids and alkanes content of bio-oil, within a 95% confidence interval. The aldehyde quantity was significantly affected by the temperature and interaction of moisture content with temperature (AB), as well as the interaction between temperature and the particle size. Aldehydes were maximized at low temperature and low moisture content and minimized at high temperatures and low moisture contents. Due to aldehydes` reactive nature, low concentrations are desirable for a more stable bio-oil. An increase in the particle size decreased the ketone quantity, possibly because of greater heat transfer limitations. The sugar content was significantly increased by an increase in reactor temperature at both small and large particle sizes, similar to previous reports. A decrease in reactor temperature significantly increased the acid content in the bio-oil. Other literature studies have also observed that acid quantities are favoured at low temperatures [21], [81]. This is expected to be the result of hemicellulose degradation, as it agrees with the temperatures at which maximum acids are produced [56], [37], [191]. The alkane content is significantly influenced by the reactor temperature, with an increase in temperature, both at small and large particle sizes, resulting in an increase in the alkane content. Alkanes are not commonly present in bio-oil and might have been partially contaminated from the Isopar G used as a cooling medium, even with precautions taken.

None of the factors investigated had a significant effect (within a 95% confidence interval) on the chemical shift spectra from the ^{13}C NMR analyses. The ^{13}C NMR analyses indicated the highest quantity of carbons are present in the methoxy/hydroxy carbon range (54- 85ppm), followed by the aromatic carbon range (110-163 ppm) and the carbonyl chemical shift range. The aromatic carbon range (110-163 ppm) contained between 10.8 and 18.4% of all carbons present in the bio-oil. Guaiacyl carbons are much more common compared to syringyl carbons (5.7-10.5% vs 0.2-0.5%). This was attributed to softwood`s lignin structure. The carbonyl carbon content and the carbohydrate content were comparable with literature, whereas the total aromatics and alkyl carbons were less than reported in literature. A trade-off existed between the aromatic- and alkyl carbons (110-163 ppm, 1-54 ppm) and the methoxy carbons (54-84ppm) when comparing the experimental results with reported literature results.

Agreement between the GC-MS and ^{13}C NMR results existed on the high contents of aromatic/ phenolic components and a high content of ketones in bio-oil, however according to statistical analyses, none of the factors investigated had a significant effect on the ^{13}C NMR responses for different chemical shift ranges.

The ^{1}H NMR analyses indicated that the methoxy hydrogens were the most common, 54.0 to 66.7% of all hydrogens, followed by the 4.2-6.4 ppm region, which included phenolic protons and non-conjugated olefinic protons, accounting for 7.8 to 24.3 % of all protons. The methoxy protons and phenolic and non-conjugated olefinic proton contents were larger than reported in literature, while the presence of protons in other ranges (8-10ppm, 6.8-8 ppm, 6.4-6.8ppm, 1.6-2.2 ppm and 0-1.6 ppm) was found to be lower. The proton NMR corresponded with the ^{13}C NMR results that indicated that the methoxy group was the most prominent. The protons present in the 4.2-6.4 ppm region (which included phenolic protons), were in agreement with the results from ^{13}C NMR which indicated that the aromatic range (110-163 ppm), which contained phenolic and phenoxyl compounds (150-

117

165ppm), was the second largest. The GC-MS results, which indicated the phenolic group was the second most abundant, resembled the NMR results.

Statistical analysis on the proton analysis indicated that the aldehyde - and lower field aromatic-proton spectra, was a function of the particle size, with an increase in particle size resulting in a decrease in the protons present in the spectra. This was not detected by GC-MS analysis and can be due to limitations associated with lumping techniques, or due to the different types of protons (aldehyde protons and lower field aromatic protons) being measured within the 8-10 ppm chemical shift range. The olefinic protons conjugated to carbonyls chemical shift region, was a function of all the factors investigated. The conditions which maximized protons in the olefinic protons conjugated to carbonyls region, all enhance heat transfer to and through the biomass particle.

The carbon and oxygen contents in pyrolysis char was significantly affected by particle size. Small particle sizes decrease the carbon remaining in the char and increase the char`s oxygen content. None of the factors investigated had a significant influence on the hydrogen content in the char. A small particle size fraction maximized the energy transfer from the biomass to the bio-oil and minimized the energy transfer to the char, thereby reducing energy losses from the biomass to by-products.

The conclusions from the experimental and statistical work, can be integrated and used to guide to a general conclusion of the effect of the factors investigated on the bio-oil yield and quality. Particle size had a significant influence on the organic liquid yield and the energy transfer to the bio-oil. At small particle sizes, organic liquid yield and energy transfer to the bio-oil increased. Low biomass moisture contents reduced the moisture content in the bio-oil and improved the bio-oil HHV. Although temperature did not have a statistically significant influence on the organic liquid yield, operation at high temperatures lowered the pyrolytic water formation and increased the HHV. Temperature had a significant effect on many of the chemical families, specifically on the sugar, acid and aldehyde concentration and should be selected according to the specific chemical family on which the focus is. Maximum organic liquid production were obtained at small particle sizes, low moisture contents and high temperatures.

From the work in this chapter, the optimal operating conditions to produce a bio-oil product that will be best suited for upgrading to jet fuel, can be identified. Due to upscaling factors, exact values from the experimental results will not necessarily be feasible to implement on a large scale. For this reason, the results from the experimental work will be used as guideline to identify the best operating conditions for a large scale pyrolysis facility from literature, which will then be used in the fast pyrolysis and upgrading model in Chapter 5.

4. METHODOLOGY FOR MASS BALANCE AND PROCESS SIMULATION DEVELOPMENT

4.1 Introduction

In this part of the study, the effectiveness of upgrading bio-oil to jet fuel (Pyrolysis to jet) is investigated, from mass and energy balances. A simplified block flow diagram of the overall pyrolysis to jet process can be viewed in Figure 29, with the blocks corresponding to the different unit operations in the Aspen® simulation. The figure shows that the overall process can be divided into a fast pyrolysis process, followed by a bio-oil upgrading process. The fast pyrolysis process is indicated by the green dash line and the upgrading process by the blue dash line in Figure 29.
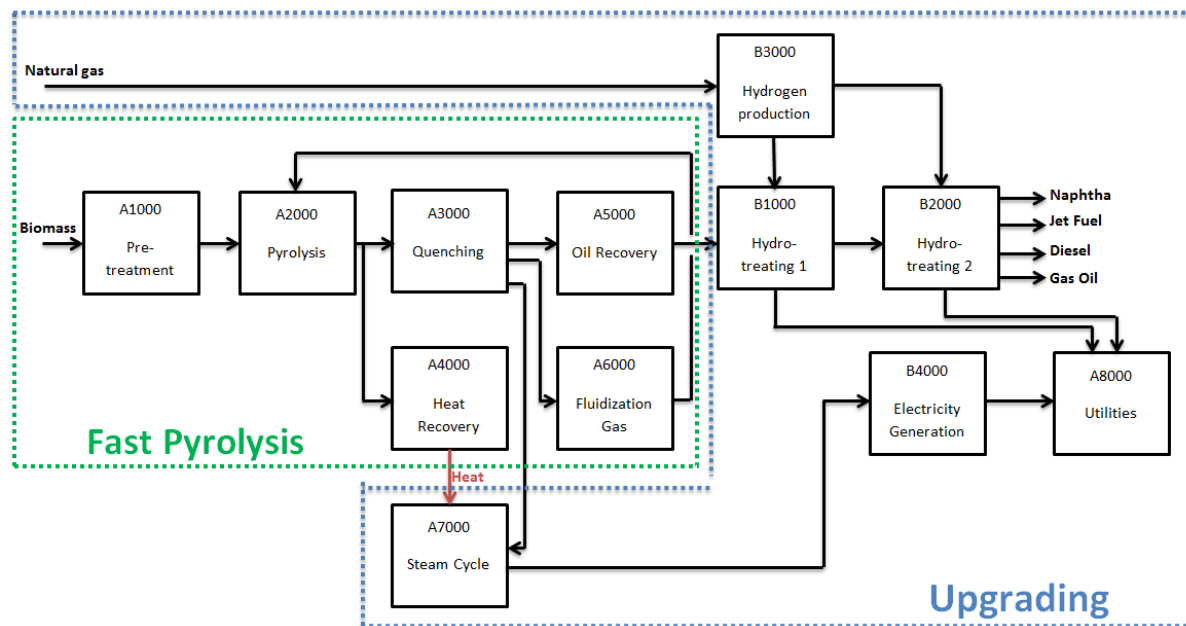
Figure 29 Block flow diagram for the fast pyrolysis and upgrading process simulation

An existing fast pyrolysis process simulation was modified to accommodate the biomass selected in this study (pine wood chips). Results from the experimental study are used as guide to determine the best pre-treatment conditions (moisture content of biomass and particle size) and reactor operating condition (with the final product taken into account), from the available literature ranges. The model was developed further to include the upgrading process, through the addition of hydrotreating units (B1000, B2000) and a hydrogen production facility (B3000). The steam cycle, electricity generation and utility units were modified according to the PTJ process` requirements. This part of the study also investigated the utility requirements associated with such a process and determined the energy efficiency of the process to benchmark against other process routes to aid in comparison with these different options available.

The model was developed in Aspen Plus® v.7.1, and upgrading processing conditions, yields and mass balances were based on experimental data reported in literature. Operating conditions and yields for the hydrotreating process were mostly based on experimental literature by Elliott et al. [16] and final fuel specifications and compositions were mostly based on experimental data reported by Christensen et al. [15]. Care was taken to select experimental data capable of producing the jet fuel that is closest to meeting the strict jet fuel specifications, and where the final jet fuel components` composition and elemental composition was well-defined in the reported experimental data.

Other studies focusing on the production of fuel from pyrolysis and hydrotreating have been performed. Very few of these studies paid attention to the jet fuel fraction with regards to yield (which is important in quantifying the effectiveness of the process), the product composition, and the process elemental balance (which is important to know, to determine how close to the final specifications the final fuel is). This study will aim to do that.

4.2 Methodology for mass balance and process simulation

The effectiveness of the process was investigated by considering mass and energy balances and the utility requirements, using Aspen Plus® v7.1 software. The process consisted of a fast pyrolysis unit that produces char, gas and bio-oil. Literature indicated that the most feasible option for producing high quality transportation fuels is through hydrodeoxygenation rather than zeolite cracking [25]. The bio-oil is upgraded in a hydrotreating facility via hydrodeoxygenation.

Ringer et al. [104] developed a fast pyrolysis simulation using Aspen Plus ® software. This simulation has been widely used as basis for other fast pyrolysis simulations [102], [103]. Their simulation was initially developed for wood chips and modified for sugarcane bagasse [102], [103], [104]. A fraction of the bio-oil is used to generate heat to keep the pyrolysis reactor temperature at the set temperature (500°C). The remainder is upgraded to transportation fuels.

4.2.1. Enhancing the key characteristics in bio-oil

Maintaining some of the key characteristics of the fast pyrolysis process, such as high heating rates and short residence times, is challenging when scaling up from bench to commercial scale [86]. Therefore, the guidelines from the experimental work in this study (Chapter 3) were combined with literature data to account for scale-up effects.

From the statistical analysis performed in Section 3.3, the best conditions at which a plant can operate was determined based on the following objectives: obtain a high organic yield and secondly obtain a high quality bio-oil best suited for a fuel. According to the statistical analysis, the highest organic yield was obtained at small particle sizes. The best utilization of the energy contained in the biomass occurs at small particle sizes, with the greatest quantity of energy transferred to the liquid phase. The lower particle size range in the fast pyrolysis experiments ranged between 0.25-0.8 mm, since this allowed for an evenly spaced particle size range distribution (to accommodate the different particle size levels in the statistical design) within the pyrolysis reactor`s designed particle size range. Literature models representing large scale pyrolysis facilities use biomass particle sizes ranging from <2mm-5mm [86], [57]. The lower end of the range reported in literature was chosen - particles smaller than 2mm.

The fast pyrolysis experiments indicated that a lower biomass moisture content is preferred as it increased the bio-oil HHV and decreased the moisture content in the bio-oil. Moisture content levels for biomass in the experiments were 4 wt% and 10 wt%. Recommended moisture contents for large scale pyrolysis facilities range between 7 - 10 wt% [107], [86], [57], [56]. The lower end of the literature range (7wt%) was selected for the model.

For bio-oil quality, the most important characteristics identified were a high energy content (HHV), a low acid content (to protect equipment against corrosion), low aldehyde content [aldehydes are suspected to be reactive and be responsible for bio-oil aging [203], [51]], and a low pyrolytic water content (as this is expected to be partially due to secondary reactions). Although a higher reactor

temperature (500 ^{o}C compared to 450 ^{o}C) did not have a significant influence on the organic oil yield, it does influence the quality of the bio-oil, with the higher temperature of 500 ^{o}C, favouring a higher HHV, a lower acid and aldehyde content and a lower pyrolytic water content. The reactor used in the model therefore operates at 500 ^{o}C, as this will result in more favourable bio-oil characteristics.

4.2.2. Plant Capacity

When considering the capacity of a plant, it is important to consider the feedstock availability, as a too large capacity will result in a too high feedstock requirement, which might not be sustainable or available in close vicinity. Previous studies have also observed that the plant capacity has an influence on the feasibility of a process [212].

The fast pyrolysis unit capacity was determined by considering two scenarios: (1) the kerosene fraction of the hydroprocessed pyrolysis oil (HPO) produced make up 10 vol% (adhering to IATA`s ambitious goals of 10% renewable fuels by 2017, [5]) of and existing gas to liquid (GTL) refinery`s kerosene fraction. (2) The blend of HPO kerosene with an existing GTL refinery is such that the minimum aromatic limit is obtained. It was assumed that the fast pyrolysis plant will assist a 38000 barrels per day GTL plant that produces approximately 19-20wt% GTL kerosene relative to other products. This is similar to the LOTIN YO`L GTL plant to be commissioned in Uzbekistan, capable of producing 38 000 barrels per day [213], with product distributions similar to that of 304 000 ton kerosene of 1 573 2000 ton total products [214], or 25 000 barrels of 140 000 barrels per day like in Shell`s Pearl GTL in Qatar [215]. The blending ratios will differ, depending on the final fuel`s properties.

The required plant capacity, according to the kerosene demands, is summarized in Table 58. The density of the jet fraction distilled from the HDO bio-oil is not reported by Christensen et al. [15], therefore a density for the jet fraction of the HDO-BO had to be assumed. A density of 826.6 kg/m^3 was assumed, as this was the average of the final HPO mixed wood density (850 kg/ m^3 [16]) and that of the average conventional jet fuel containing the approximately 19 vol% aromatics of 803.22 kg/m^3 [216]. The density of the fuels has a large impact on the calculations and the quantity of biomass required in Table 58.

For scenario 1, where the HDO JF will contribute 10vol% of renewable fuel to a 304 000 tonnes/yr. GTL refinery, 184 tonnes wet biomass/hr is required, or an equivalent of 2200 dry tonnes biomass/day. This will only contribute an estimated 3.36vol% aromatics to the final blend. For scenario 2, where the goal is to blend the jet fraction from HDO with the jet fuel from a 304 000tonnes/yr. refinery, until the final jet fuel has a 8vol% aromatic content, 846 wet tonnes biomass/hr is required, or the equivalent of 10 149 dry tonnes/day. The maximum plant capacity investigated for a pyrolysis plant, is up to 2000 dry tonnes/day [57], as feedstock availability [110] and available technology can become a problem. Taking this into account, it is clear that blending the jet fraction of HDO to obtain 8vol% aromatics in the final jet fuel for a 304 000tonnes/yr. GTL refinery, is currently not feasible due to excessive biomass requirements. A 10vol% renewable fuel goal is currently more realistic. However for a smaller GTL refinery, blending up to 8vol% aromatics might be practical, as a smaller quantity of jet distillate from the HDO will be required.

From the calculations, the most realistic option in terms of biomass availability, was to produce 10vol% renewable fuel to add to an existing GTL refinery. However, this will still only contribute an estimated 3.36vol% aromatics.

Table 58 Biomass requirements in determining plant capacity

	10 vol% renewable fuels	% for aromatics to meet min spec of 8vol% after blend
GTL kerosene [tonnes/yr.] [m^3/yr.]^a	304 000 413 324	304 000 413 324
Volume HPO kerosene [m^3/yr.]	45 925	210 942
Estimated density of HPO jet fraction [kg/m^3] ^{b}	826.6	826.6
Mass HPO kerosene fraction [tonnes/yr.]	37 962	174 367
Total [tonnes/yr.]	341 962	478 367
Aromatics in HPO kerosene fraction [wt%] ^{c}	19.98	19.98
Aromatic in blended kerosene from GTL & HPO [wt%]	2.22	7.28
Aromatic in blended kerosene from GTL & HPO [vol%] ^{d}	3.36	8.00
Required dry biomass ^{e} [tonnes/yr.] [tonnes/day]^f [tonnes/hr]	784 394 2210 92	3 602 867 10149 423
Required wet biomass ^{g} [tonnes/yr.] [tonnes/day]^f [tonnes/hr]	1 568 788 4419 184	7 205 733 20298 846

^{a} assume average GTL kerosene fraction density of 735.5 kg/m3 [217], ^{b} assumed as average density of total HPO from mixed wood [16] & maximum upper density of conventional JF from Ontario as determined in World Fuel Sampling Program [216], ^{c} from mass balances and selected components determined from [15], ^{d} assuming wt% to vol% conversion for diesel fuel in [218], ^{e} calculated from kerosene yield by [15] , HPO yield by [16] and bio-oil yield by [86], ^{f} assuming 355 operational days, g moisture content of 50wt%

The final plant capacity selected for this study was 184 wet tonnes/h, with biomass supplied at 50wt% moisture content [109], [219], [56], [57], [86]. This is the equivalent of approximately 2200 dry tons/day or 783 840 dry tons/yr. This was set as the maximum, due to biomass availability within an acceptably close region to the central plant which might become a problem for larger capacities [110]. The capacity investigated in this study is close to the 2000 dry tons/yr. investigated in other studies [57],[107]. Operational time of 355 days/yr. is considered, which is comparable to another study [110].

4.2.3 Fast Pyrolysis process simulation overview

An existing fast pyrolysis model was adapted to accommodate the desired plant capacity and feedstock. Statistical analysis results, from Section 3.3 Results and Discussion, were used to enhance more favourable characteristics in the bio-oil. In this study, the fast pyrolysis model was extended to include an upgrading part. A brief description of the fast pyrolysis model and the modifications made are provided below.

Since the aim of the upgraded bio-oil is to be an aromatic-rich source in the jet fuel range, a feedstock with a high lignin content, that will yield a high aromatic content, was selected. Lignin is considered as a building block for high value aromatics [55] due to its aromatic nature [43]. Pine wood chips were selected as the feedstock for the fast pyrolysis process, because of its high lignin content potentially leading to a high aromatic content, with the aromatic contribution in lignin products after hydrotreating being estimated at 65% [13]. A more detailed discussion of the feedstock can be viewed in Section 3.2.4 Biomass analysis and characterization. The biomass

composition was determined from experimental analysis on *Pinus radiata* wood, using NREL standards [171], [174], [175].

A simplified block flow diagram and a simplified Process Flow Diagram (PFD), which summarizes the fast pyrolysis and upgrading process model, can be viewed in Figure 30 and Figure 35 respectively. The fast pyrolysis process is indicated by the shaded blocks in Figure 30. The fast pyrolysis plant aimed at producing bio-oil and utilizing excess heat for the co-production of electricity via steam generation. The fast pyrolysis section consists of 5 main processing areas: feed pre-treatment (A1000), pyrolysis (A2000), product recovery (A3000, A5000, A6000), heat recovery (A4000) and steam generation. A brief description of the modified fast pyrolysis model is provided below. A more detailed description on the original fast pyrolysis model is provided elsewhere [104].
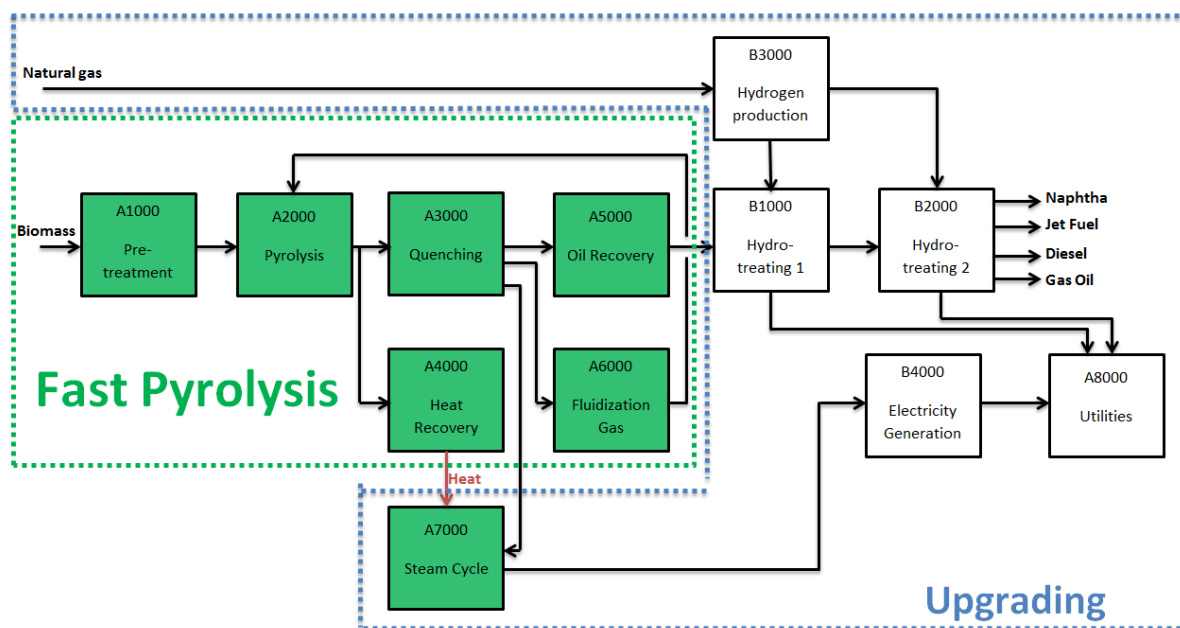
Figure 30 Simplified block flow diagram indicating fast pyrolysis units in process simulation

In the feed handling and pre-treatment section, unit A1000, the wood chip sizes are reduced to <2mm (see Section 4.2.1. Enhancing the key characteristics in bio-oil, for particle size selection). The wood particles are dried using air pre-heated from heat in the second condenser (HX-3002+) in A3000 where the bio-crude vapours are cooled. A final moisture content of 7wt% was targeted (see Section 4.2.1. Enhancing the key characteristics in bio-oil), while the simulation achieved 7.28wt%. The fine particles are then fed to the pyrolysis section, unit A2000, where pyrolysis occurs in a fluidized bed (PY-2001). The pyrolysis reactor was modelled as a yield reactor (RYield) where the product yields can be specified. The bio-oil composition differed from previous Aspen Plus® models, due to this study`s focus on the aromatic content in the final fuel, which was not considered in previous pyrolysis models. The bio-oil composition was determined from literature and will be discussed in Section 4.2.4.4 Review of experimental results for distillate fractions of HDO, and Section 4.2.4.5 Review of chemical reactions occurring through hydrotreating. Due to this, the pyrolysis reactor yields from past models also had to be modified.

In a study by Badger et al. [109], a transportable fast pyrolysis unit of 100 dry ton/day was investigated for pine wood chips as feedstock, with a bio-oil yield of 60wt% of the products . Data from a pilot plant of Renewable Oil International ® was used. Bridgwater reported commercial scale production of 59.9 wt% organics and 10.8wt% process water [86], amounting to a total of 70wt% bio-

oil. Due to the complexity of the bio-oil composition in this study, in combination with the recycle streams present in the simulation model, exact yield values were difficult to obtain and yield ranges were identified from literature. The model aimed to achieve pyrolysis yields reported for large scale operation [86], as it was believed to have a better representation of the scale-up effect that will occur in a commercial plant and to biomass of similar type (Pinus families). The modified yield ranges are presented in Table 59.

The fluidizing medium in the pyrolysis reactor is noncondensable gases from the Electrostatic Precipitator (ES-3001) in unit A6000, which was heated using heat from char and bio-oil combustion in (CB-4001) in the heat recovery unit, unit A4000. Sufficient heat in the fluidizing gas is important as this ensures the pyrolysis reactor operates at 500°C, using a design specification (PY2001T) to determine the fraction of final bio-oil product that needs to be combusted. The gas composition was modified from the previous studies to represent experimental data obtained for the fast pyrolysis of pine wood at 500°C [21].

The hot vapours, char and non-condensable gases from the pyrolysis reactor are separated in high efficiency cyclones (CY-2001) in unit A2000 to a char stream and a gaseous and vapour stream. The hot vapour and noncondensable gases are rapidly cooled in unit A3000 (HX-3001+ and HX-3002+) where the heat removed, is used to heat water for steam generation (sent for further heating in A7000) and for heating the air used for biomass drying (fed to the pre-treatment section in unit A1000). After cooling of the vapour and noncondensable gases stream, the aerosols are removed in the scrubber (SC-3001) followed by a wet Electrostatic Precipitator (ESP-3001). Fluidizing gas leaving the ESP, is sent to a flash drum (FL-6001) in unit A6000, where any remaining vapours are removed and the final cleaned noncondensable gases are compressed and heated for recycling as heating medium in the pyrolysis reactor. A fraction of the noncondensable gases are fed to the combustor as a bleed stream. The bio-oil from the scrubber, the ESP, and the flash drum (FL-6001), is then combined in a tank (T-5001) in the oil recovery section (unit A5000) and cooled before a fraction of the bio-oil is recycled to the scrubber. A fraction of the remaining bio-oil is combined with the char stream from the cyclone (CY-2001) in unit A2000, whereafter it sent to the combustor (CB-4001) in unit A4000 for heat generation to heat the fluidizing gas. The bio-oil fraction is controlled by a design specification (PY2001T). The remaining bio-oil is sent for upgrading in the HDO area (Unit B1000 – B3000).

In reality the combustor and the pyrolysis reactor will be integrated into a single piece of equipment, although here it is separated for modelling purposes [104]. The combustor is modelled as a stoichiometric reactor (RStoic) with the software determining the combustion reactions and final products and assuming adiabatic operation. The excess heat from the combustor is exported for steam generation. The air supply to the combustor is regulated by a design specification (AIRCOM-P). The amount of air required is set such that the product gases exiting the combustor contain at least 6wt% oxygen. This is to ensure complete combustion and also to meet environmental standards as described in the Department of Environmental Affairs and Tourism Air Quality Act (2008), [141], [103].

The steam cycle section (A7000) and the utilities section (A8000) from the process model by Nsaful (2012), were modified to allow integration of the new HDO plant into the existing pyrolysis plant.

Table 59 Literature parameters compared to pyrolysis model parameters

Characteristic/ assumption	Reference Value	Reference	Model Value
Feed	Wood chips (3-45mm)	[104]	Wood chips (3-45mm)
Ground particles	<2mm – 5mm	[104], [86]	<2mm
Wood composition* (*Pinus radiata*) [wt% dry basis]	Cellulose : 0.41243 Lignin : 0.27217 Xylan : 0.08999 Arabinan : 0.00856 Mannan : 0.10831 Galactan : 0.00000 Extractives : 0.09863 Ash : 0.00992	Experimentally determined	Cellulose : 0.41243 Lignin : 0.27217 Xylan : 0.08999 Arabinan : 0.00856 Mannan : 0.10831 Galactan : 0.00000 Extractives : 0.09863 Ash : 0.00992
Moisture content Biomass as-received **Dried biomass to PY-2001** [wt% wet basis]	50% 7% -8% (<10%)	[104], [56], [220] [104], [57], [107], [56], [86]	50% 7.28 wt%
Pyrolysis reactor	500 ^{o}C	[104]	500 ^{o}C
Yields from pyrolysis* [wt% dry biomass fed] **Organics** **Water** **Char** **Gases**	59.9 – 64.0 10.0-10.8 12.0- 16.2 12.0- 13.1	[104], [56],[86] [57], [104] ,[86] [56], [104] ,[86] [56], [104] ,[86]	60.23 10.62 16.01 13.13
Gas composition* [wt% of gas] **CO** **CO_2** **CH_4**	41.3 55.8 2.8	[21]	41.1 55.5 3.3
Gas to feed ratio [wt:wt]	2.75 : 1 gas to feed 2.57:1 gas to feed	[104] [102]	2.4: 1
Grinding power demand	50kWh/dried ton	[104]	50kWh/dried ton

* wt% not adding up to 100% is the result of rounding off efforts

4.2.4 Hydrotreating and hydrocracking process simulation development

Due to this study`s focus on jet fuel and jet-fuel range aromatics, only literature where the final jet fuel and jet-fuel range aromatic yields were reported, could be considered as basis for the process mass balance. Unfortunately relevant literature sources did not have a complete mass balance available. Therefore a methodology that would allow the establishment of a mass balance had to be developed, as a complete mass balance with a known jet fuel yield and jet fuel-range aromatic yield was necessary to model the upgrading section of the PTJ process. The methodology described hereafter in Section 4.2.4.1 to 4.2.4.5 was followed to get to a mass balance, which was used for modelling the hydrotreating units, UB1000 and UB2000, indicated in Figure 31. The schematic diagram, Figure 32, explains the approach described in Section 4.2.4.1 to 4.2.4.5.

125
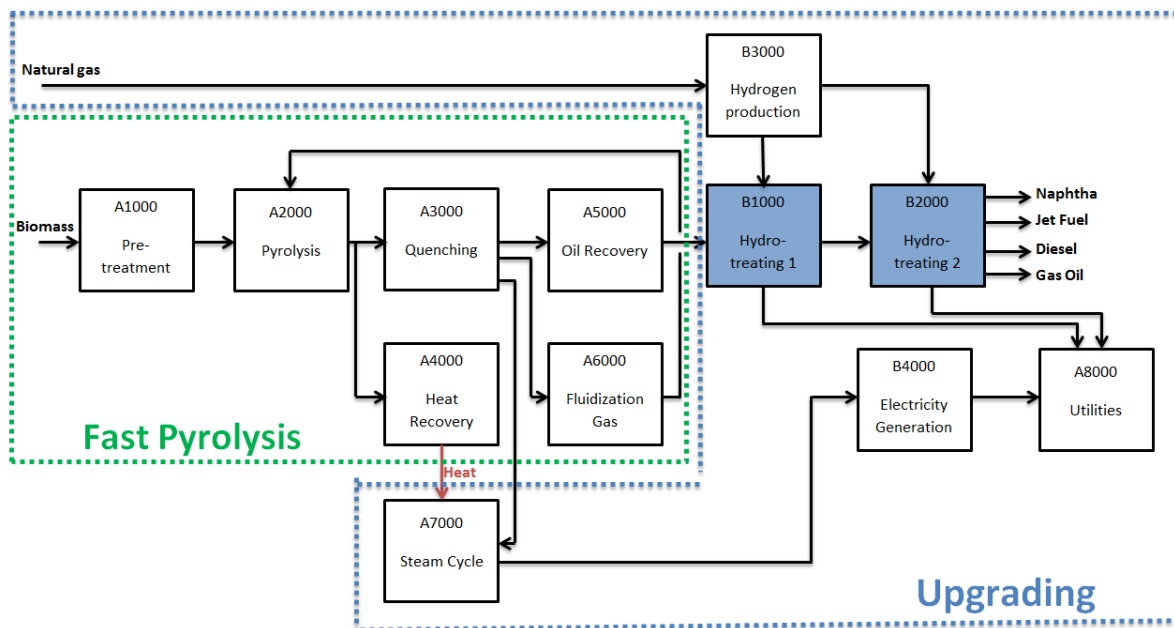
Figure 31 Simplified block flow diagram indicating upgrading units in process simulation

Figure 32 Diagram explaining methodology followed in going from experimental data to process model
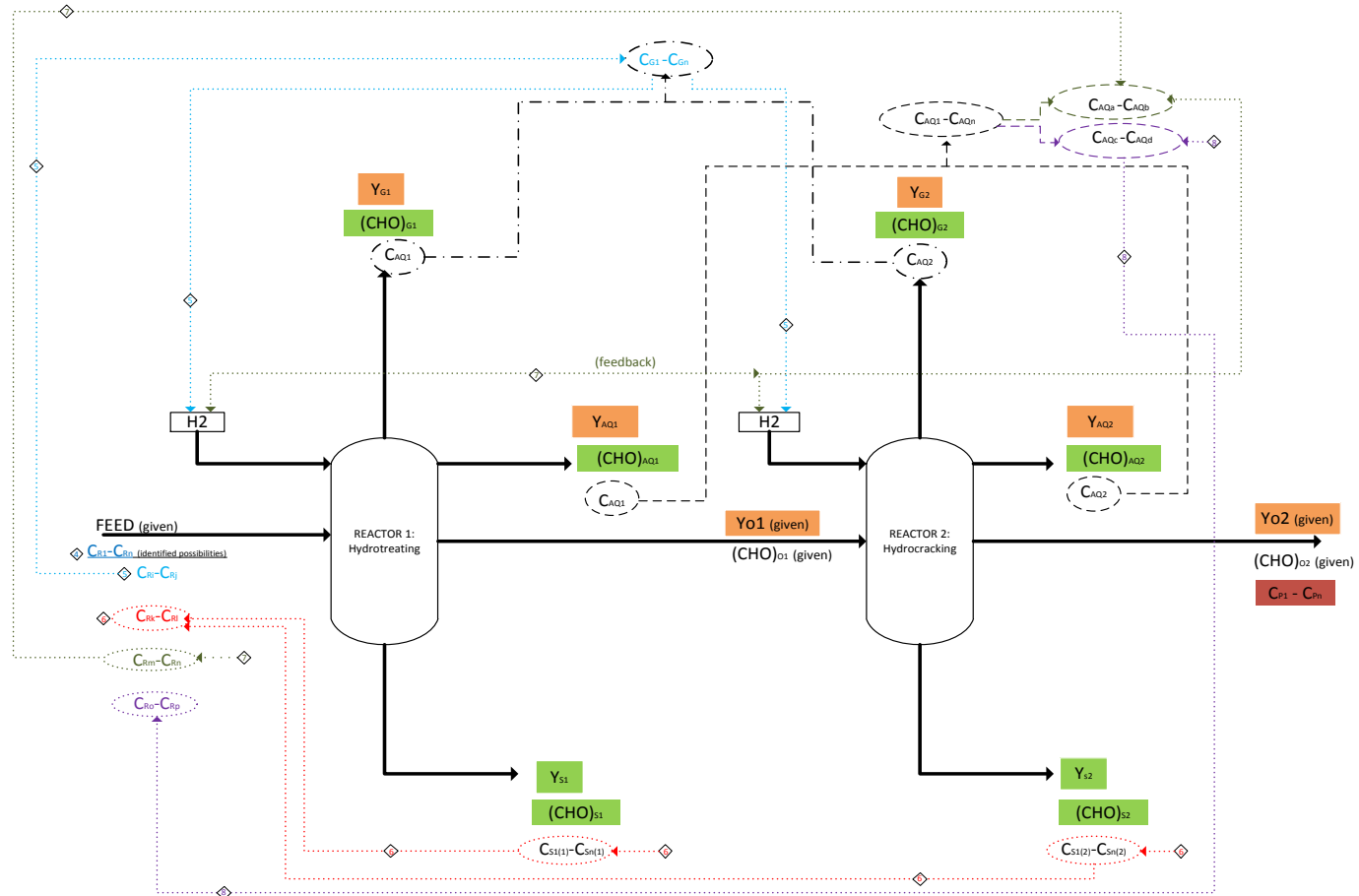
1. Determine from literature data: Y_{G1}, Y_{G2}, Y_{AQ1}, Y_{AQ2}, Y_{O1}, Y_{O2}
2. Determine from literature and assumptions: $(CHO)_{AQ1}$, $(CHO)_{AQ2}$, $(CHO)_{G1}$, $(CHO)_{G2}$, Y_{S1}, Y_{S2}, $(CHO)_{S1}$, $(CHO)_{S2}$
3. Determine and select components: C_{P1}-C_{Pn} in oily 2
4. Identify possible C_{R1}-C_{Rn} from literature
5. Select components C_{Ri}-C_{Rj} to give desired C_{G1}-C_{Gn} and modify H2 consumed and H2O formed
6. Select components $C_{S1(1)}$-$C_{Sn(1)}$ and $C_{S1(2)}$ – $C_{Sn(2)}$ from literature, CHO requirements and modify C_R to get C_{Rk}-C_{Rl}
7. Select components from C_{Rm}-C_{Rn} (iteratively) to get desired H2 consumption, modify C_{AQa}- C_{AQb} accordingly and modify H2O formed.
8. Select other components such that AQ composition meets the calculated CHO requirements: C_{AQc}– C_{AQd} and modify C_R to C_{Ro}-C_{Rp}

4.2.4.1 Selection of experimental data

Catalytic hydrotreating was selected as the upgrade method. Since this study focuses on producing an aromatic-rich jet fuel, the chemical end products from the hydrotreating were particularly important. Due to the study`s focus on the aromatic content and elemental composition of the jet fuel boiling range, an upgraded fuel fraction, which most closely matched the desired aromatic rich jet fuel, was identified in literature [15]. From there the processing conditions employed to produce this was investigated as a possibility for the fundamental literature basis in this study. Considerations when determining an appropriate final product was: the process parameters (temperature, pressure, catalyst type used); sufficient data for mass balances (phase yields, hydrogen consumption); and distilled HDO-BO into cuts similar to that in a typical refinery (lights, naphtha, jet, diesel, gas oil). Composition information required was the oxygen and moisture contents before and after HDO, a quantified value of the aromatic content present in the jet fraction, as well as identified aromatic components in the jet fraction. On this basis, experimental data from Christensen et al. [15] and Elliott et al. [16] were identified as the most suitable, as their studies complied with the requirements mentioned above. Furthermore the whole bio-oil had to be upgraded and the biomass feed had to be from a woody biomass. Literature data from Christensen et al. [15] and Elliott et al. [16] was used as it complied with all these requirements.

The upgrading literature reported by Elliott et al. [16], was used to determine phase yields (oil, aqueous, gas and solid), as well as the operating conditions used for upgrading of the bio-oil in the hydrotreating and hydrocracking reactors. The literature from Christensen et al. [15] was used to determine the components present in the final upgraded bio-oil and the yield of each fuel fraction (lights, naphtha, jet, diesel, gas oil) as fraction of the total upgraded bio-oil produced. The experimental results from their study, [15], are therefore only applicable to the final fuel, which is the oil phase after the second reactor, and does not contain information regarding the aqueous, gas, solid or oil phase after the first reactor, nor the gas, solids and aqueous phase after the second reactor – only information relating to the final oil phase is reported.

4.2.4.2 Hydrotreating and hydrocracking set-up and configuration used in the simulation

Elliott et al. [16] investigated the hydroprocessing of fast pyrolysis derived bio-oil using different process conditions and bio-oil from different biomass on a fixed bed set-up. Their study aimed at developing process technology that will convert bio-oil into a petroleum refinery feedstock. A two-stage reactor set-up compared to a non-isothermal reactor set-up was initially considered. The results indicated that both systems effectively processed the bio-oil. Bio-oils, similar to what were produced in the studies by Elliott et al. [16] and Elliott et al. [17], were analysed by Christensen et al. [15], who investigated the oxygenated compound present in oil distillate fractions. The oil distillate fractions were classified as: lights, naphtha, jet, diesel and gas oil. The aromatic carbon % in the oil distillate fractions was also reported, along with GC-MS results for the different fractions [221]. Combining these two papers provided sufficient data for complete mass balances.

As mentioned, two upgrading configurations were investigated by Elliott et al. [16]: a single non-isothermal reactor and a two-stage reactor. In the two-stage configuration, phase separation occurs to produce two liquid phases - an aqueous and an oil phase. The phase separation between the first and second hydroprocessing stages allows for smaller processing units downstream, as the oil is more concentrated. When two separate reactors are used, there is more variability for regeneration of the catalyst. Elliott et al. [16] noted that the first reactor experienced catalyst deactivation, after as little as 3 to 40hrs on stream, although not observed in the second reactor. The first catalyst bed

128

had experienced coking, resulting in pressure build up and eventually termination of the runs, whereas the second catalyst bed also experienced some coking, but not on the catalyst itself and it did not require termination of the runs [16]. The two catalyst beds do not experience the same extent of coking. When one reactor is used, the first catalyst bed might require catalyst regeneration before the second bed does. A coking problem was indeed observed in runs on pine bio-oil on the non-isothermal reactor [17].

Although a single reactor set-up will likely be preferred in future, requiring fewer processing steps/units, a two-stage reactor set-up was used in the process model, as it will be easier to control and maintain the integrity of the catalyst based on current technology available. The process model`s set-up was similar to a previous two-stage experimental set-up used [16]. In the first reactor mainly hydrotreating occurs. It operates at optimum process conditions of 340 ^{o}C, 2000 psig (137.9bar) and a a liquid hourly space velocity (LHSV) of 0.28 L/L/h, with a Pd/C catalyst, patented by Batelle [16]. Excess hydrogen at flow rates of 10 000 SCF/bbl was used, which correlates to 13.7-15.2wt% of the BO fed. The second reactor aims at hydrocracking. Processing conditions were close to conventional hydrocracking conditions, at 400°C, 2000 psig (137.9bar), a LHSV of 0.4 L/L/h, and a conventional hydrotreating catalyst, provided by UOP. A patent describing the same process specifies that the catalyst used in the second reactor is a sulfided nickel and molybdenum on alumina support catalyst, provided by UOP [222].

4.2.4.3 Hydrotreating and hydrocracking experimental results used in simulation

In both the hydrocracking and hydrotreating reactors, two liquid phases (an oil and an aqueous phase) are produced, together with gaseous and solid phases. In order to obtain the phase yields, mass balances were performed on experimental results from the upgrading of mixed wood bio-oil, as reported in literature [16]. This correlates with step 1 in Figure 32, which stipulates that the mass yield of gas, aqueous phase and oil from the first hydrotreating reactor (Y_{G1}, Y_{AQ1} and Y_{O1}), as well as the mass yield of gas, aqueous and oil yield from the second reactor (Y_{G2}, Y_{AQ2} and Y_{O2}), are calculated from literature by Elliott et al. [16].

Data used for the mass balances are provided in Table 60 and were obtained from mixed wood experiments [16]. The elemental composition of the feed, hydrotreated oily phase and the hydrocracked oily phase were also provided in literature. The available literature for these experiments does not report quantified values of solids or coke.

Table 60 Literature data used for mass balances*

Stream	Composition						Yields			H$_2$ Con-sumed [L/L feed]	Iso-therm
	C	H	O	N	S	Mois-ture [wt% wet basis]	Oil yield [g/g dry feed]	Aqueous yield [g/g wet feed]	Gas yield [g/g carbon feed]		
Feed	57.7 [a]	6.2 [a]	33.7 [a]	0.2 [a]	-	20.96 [b]	-	-	-	-	-
Hydro-treating [b]	75.5	9.4	12.3	0.6	0.01	2.7	0.62	0.48	0.062	205	+6°C
Hydro-cracking	86.8	12.9	0.4	< 0.06	0.01	0.01	0.61	0.24	0.087	290	+16°C

*Data obtained from [16], [a] wt% dry basis, [b] wt% wet basis

Overall the degrees of freedom were too much for complete mass and components balance without making assumptions. This correlates with step 2 of Figure 32. Since the elemental composition of the aqueous phases, gases and the solids [$(CHO)_{AQ1}$, $(CHO)_{G1}$, $(CHO)_{S1}$ respectively] were not reported for either the first or second reactor products [$(CHO)_{AQ2}$ $(CHO)_{G2}$, $(CHO)_{S2}$], this had to be assumed from literature. Furthermore, the solid yields from the first and second reactor (Y_{S1} and Y_{S2}) had to be calculated as indicated in step 2 of Figure 32. The assumptions and literature data are discussed below. The hydrotreating reactor and its products are considered first.

For the hydrotreating reactor, solid yields were calculated as the difference between the bio-oil feed and hydrogen consumed and the sum of the oil, gas and aqueous phase (in other words, the remainder to close the mass balance). The hydrogen consumption was assumed to be reported at STP, amounting to a consumption of 1.5665gH_2/100g bio-oil fed. The solid yield (Y_{S1}) calculated was 1.66wt%. To complete the elemental balances, the solid composition was assumed to be $C_1H_{1.34}O_{0.16}$, as described in the elemental derived reaction over a Pd/C catalyst [91].

The gas composition, $(CHO)_{G1}$, for the hydrotreating over Pd/C was reported by Elliott et al. [16], at values of 96-98% H_2, 1-4% CO_2 and <1% CH_4 and <0.1% higher hydrocarbon gases. Gas composition in other studies also utilizing a Pd/C catalyst and also experiencing mild hydrotreating reported yields of 89.16mole%, 9.64mole%, 1.81mole% for H_2, CO_2 and CO respectively [91]. The hydrogen content in the product gas for the study by Wildschut et al. [91] was smaller, and combined with a larger content of CO_2, compared to the study by Elliott et al. [16]. For this reason, the minimum H_2 and the maximum CO_2, in the range provided by Elliott et al. [16], were assumed. The assumed gas composition was: 96mole% H_2, 2.9mole% CO_2, 1mole% CO and 0.1mole% C_2H_6. Since the gas yield and the mole% of the gas components are known, the hydrogen content can be determined. Hydrogen was reported to be fed at an excess of 10 000 SCF/bbl [16] and elsewhere as 2 standard m^3/L bio-oil [17]. This amounts to approximately 13.73 – 15.42 g H_2 in excess/100g bio-oil fed. The initial bio-oil elemental composition and the intermediate oil`s composition [the product from the first reactor, $(CHO)_{o1}$] are given in literature [16]. With all the yields and the elemental composition of all the phases except the aqueous phase available, the elemental balance could be completed to determine the elemental composition of the aqueous phase. The oil and aqueous phase separate from each other and no special separation techniques have been reported to be necessary. The reason for phase separation is due to the changes in the olefinic, carbonyl and aromatic characteristics, leading to less hydrophilic compounds. This disturbs the balance in the single phase product, resulting in separate phases forming [34].

Different assumptions had to be considered to complete mass balances on the hydrocracking reactor, due to too many degrees of freedom. Different approaches to resolve this included: (1) assuming no solid formation (Elliott et al. [16] reported a solid crust forming in the second reactor, while Baldauf et al. [27] reported a gum-like substance to form on a NiMo catalyst [16], [27]); (2) the solid content was fixed as the remainder to close the mass balance and assuming a fixed solids composition of $C_1H_{1.38}O_{0.21}$ from the average of studies performed on Pd/C and Ru/C [96], [91]- since empirical coke compositions on $NiMo/Al_2O_3$ catalyst could not be found in literature. These assumptions were initially combined with an assumed gas composition estimated from the study by Baldauf et al. [27], but did not yield satisfactory mass balance closures. The third approach (3) assumed a carbon content of 0.6wt% in the aqueous phase, as values of 0.5-0.6wt% was typically obtained for the non-isotheral process [16], [17]. The ratio of H to O was fixed at 2:1 to represent water, although this resulted in the quantity of oxygen exceeding the amount of oxygen entering in the hydrotreated oil, and the assumption was abandoned. The last approach considered, approach

(4), provided satisfactory mass balances. The amount of free oxygen that will form water - in other words not the oxygen present in water, but the oxygen to be removed from the oxygenated compounds via hydrogen to form water in the aqueous phase, was assumed from literature [27]. The total mass of water could be calculated by adding the mass of water present in the hydrotreated bio-oil and the mass of water that will form from the 70% of free oxygen to water. This is at the limit of the lower end of the range found in the study by Baldauf et al. [27] on $CoMo/Al_2O_3$ and $NiMo/Al_2O_3$ with a range of 70.75-85.96 wt% and corresponds to water yield of 21-25.5 wt% [27]. An empirical composition of $C_6H_{10}O_{0.4}$ was determined for the hydrocarbon components present in the aqueous phase forming after hydrocracking.

The gas composition was assumed according to the literature range in Table 15, as 22mole% CO_2, 3mole% CO, 43mole% CH_4, 22.5mole% C_2H_6, 8 mole% C_3H_8 and 1.5mole% C_4H_{10} on a hydrogen free basis. Differences existed between the reported gas yields from different studies, with the major difference that the one study utilized a continuous set-up, whereas the other study utilized a batch set-up [27], [91]. Results from Elliott et al. [16] correlated with the results from the continuous reactor set-up that showed that gases were primarily of a hydrocarbon nature. The gas composition used in the model was therefore similar to that of the continuous study`s results, as this agreed better with qualitative results from Elliott et al. [16] and the continuous reactor operation is more likely to be utilized in a plant. From literature, the hydrogen consumption was determined to be 1.5037 g H_2/100g bio-oil fed. The final mass balance based on 100g bio-oil can be viewed in the Appendix E, where Table 103 indicates the mass balance on the hydrotreating reactor before the oil phase from the hydrotreating reactor is fed to the hydrocracking reactor, with the hydrocracking reactor`s mass balance provided in Table 104.

A summary of the assumptions that were made to determine phase yields and the elemental composition (steps 1 and 2 in Figure 32) of the different phases from literature [16] are:
1. The sulphur and nitrogen will be ignored from the mass balances, due to too many degrees of freedom and limited information available in literature
2. Where summation of C, H , O content did not add up to 100wt%, values were normalized
3. Solids yield for hydrotreating determined as the remainder of the mass balance for closure
4. Empirical composition for the solids formed during hydrotreating was $C_1H_{1.34}O_{0.16}$
5. Gas composition for hydrotreating : 96mole% H_2, 2.9mole%CO_2, 1mole% CO and 0.1mole% C_2H_6
6. 70wt% of free oxygen transferred to the aqueous phase as water for the hydrocracking reactor
7. The remainder of the aqueous phase from hydrocracking comprised of a component with empirical formula of $C_6H_{10}O_{0.4}$
8. Gas composition for hydrocracking : 22mole%H_2, 3mole%CO, 43mole%CH_4, 22.5mole% C_2H_6, 8mole% C_3H_8, 1.5mole% C_4H_{10}

4.2.4.4 Review of experimental results for distillate fractions of HDO

Even though mass and elemental yields have been determined for the upgrading process, the final product characteristic also had to be investigated to determine the quantity of aromatics present in the jet fraction. This corresponds to step 3 in Figure 32, which focuses on identifying model components (C_{P1} –C_{Pn}) to represent the final product - the oil phase after hydrocracking from bio-oil hydrotreating literature.

Model compounds are typically used to represent bio-oil since it contains hundreds of compounds. Rather than choosing model compounds to represent the bio-oil and using them to determine the final jet yield, it was decided to select a number of components present in each of the final distillate fractions from experimental data, [15] and [221] as far as possible, and to work backwards, to determine the probable bio-oil components that could have produced these components after hydrotreating and hydrocracking, see Figure 33. The reason for this approach is the focus on producing aromatics within the jet fuel boiling range from the upgraded bio-oil. It is important to know the aromatic components present in the final upgraded fuel as well as the yield of each component, to be able to determine which of the aromatic components will fall within the jet fuel boiling range. Working backward from the GC-MS experimental information of the jet fuel fractions, the aromatic content in the jet fuel boiling range can be accurately specified in the model. Final upgraded bio-oil compounds were selected from supplementary information provided in a paper by Christensen et al. [221].
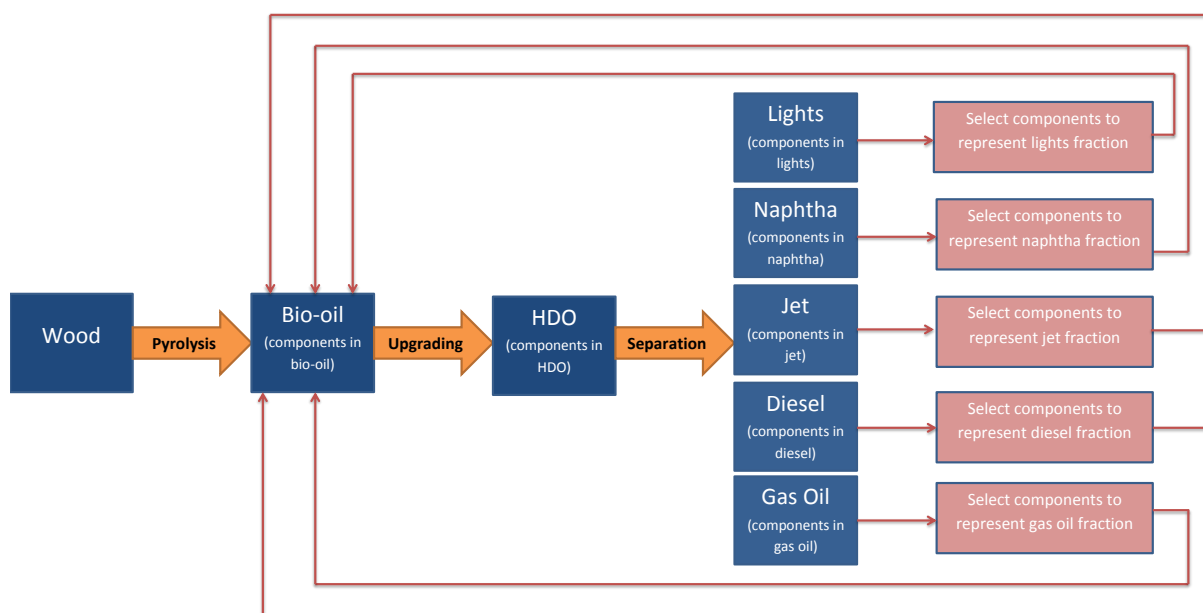
Figure 33 Methodology for final HDO component selection and determining bio-oil composition from it

Christensen et al. [15] analysed oxygenated compounds in different levels of oxygen containing bio-oils, using a variety of techniques including TAN, GC-MS, HPLC, ^{13}C NMR, simulated distillation and actual distillation. The bio-oils were produced using the same experimental set-up and conditions, reported by Elliott et al. [16], and on which the mass balance data was based. The bio-oils investigated had oxygen contents of 8.2wt% (High oxygen content, HOC), 4.9 wt% (medium oxygen content, MOC) and 0.4wt% oxygen (low oxygen content, LOC) [15]. The oils were distilled and the distillate fractions analysed for elemental composition. The oxygen content in the jet fractions of both the HOC and MOC was very high, resulting in a low hydrogen plus carbon composition, at 88.8wt% and 94.0wt% for HOC and MOC respectively, indicated in Table 61. According to SPK standards in ASTM D7566, hydrogen and carbon content must be > 99.5wt%, see Table 13. Even the LOC has a too high oxygen content, resulting in a hydrogen plus carbon content of only 99.3wt%, which is too low according to SPK standards, yet it is the closest to the required jet fuel product. Therefore, the LOC hydrotreated bio-oil was selected as the best options for SPK.

Table 61 Oxygen present in HOC, MOC and LOC hydrotreated and hydrocracked bio-oil

	HOC	MOC	LOC
Jet fraction`s hydrogen + carbon [wt%]	88.8	94.0	99.3
Jet fraction`s oxygen content [wt%]	11.9	6.6	0.7

All data obtained from [15]

Elliott et al. [16] concluded that the final products produced after hydrotreating and hydrocracking are similar, although bio-oils derived from different biomass species were used. This indicated that although mixtures of hydrocracked bio-oil were used for providing the LOC, this would not have a significant impact on the bio-oil composition. The products after hydrocracking were mainly cyclic hydrocarbons [16]. The results from Elliott et al. [16] for mixed wood compared favourably to that of Christensen et al. [15] for the LOC, see Table 62, with only 0.3wt% difference in the carbon and hydrogen content. This indicated that the bio-oil components determined from Christensen et al. [15] could indeed be used to represent the hydrotreated and hydrocracked bio-oil from Elliott et al. [16], as these oils were expected to be similar and the processing conditions used to produce the LOC, are comparable to the conditions used in the specific study by Elliott et al. [16].

Table 62 Comparison of hydrotreated and hydrocracked bio-oil for mixed wood to LOC

	C [wt%]	H [wt%]	N [wt%]	S [wt%]	O [wt%]
Hydrotreated & hydrocracked mixed wood bio-oil [a]	86.6	12.9	<0.06	0.01	0.4
LOC [b]	86.9	12.6	0.02	0.01	0.44

[a][16], [b][15]

A crude oil refinery is a complex system of processes [27], therefore simplifications had to be made in the modelling of the process. This is even more the case for bio-oil as hundreds of components are present. To simplify the complexity of the distillate fraction compositions, only a few model components were selected to represent each category, see Table 64.

 The elemental composition of the final product fractions` , experimentally determined for C, H,O, N and S composition, was reported in literature [15]. Component analysis, using GC-MS, were also performed in the study by Christensen et al. [15], and results were reported as supporting literature [221]. To simplify the overall elemental balances, the experimental GC-MS identified components from their study were categorized into aliphatics, (branched and linear), cyclics, deoxygenated aromatics and oxygenated aromatics [15]. The H/C and O/C ratios for each of these categories were determined, assuming the area% as being similar to the wt%. Elemental balances were also categorized into aliphatics, oxygenated aromatics and oxygen-free aromatics for each of the distillate fractions from HDO.

The following procedure was followed for the naphtha, jet, diesel and gas oil fractions: each fraction was categorized into alkanes (linear and branched), cyclics, oxygenated aromatics and oxygen-free aromatics. Elemental composition balances on the separate categories were performed. The overall fraction`s elemental composition, as well as the wt% of aromatic carbons, determined from ^{13}C NMR, was reported in literature for all distillate fractions [15] and is provided in Table 63. The minimum numbers of components were selected to represent the oxygenated aromatic category. Since oxygen was assumed to be present only as part of an aromatic component, the quantity of oxygenated aromatics had to be such that all oxygen was represented by it. Once the model component for oxygenated aromatic was identified, the C and H present in these components and

accordingly the entire oxygenated aromatic stream, could be determined. Since the wt% of carbons that are aromatic was available from ^{13}C NMR analysis, the remaining aromatic carbons are present in the oxygen-free aromatics.

The H/C ratio for the oxygen-free aromatics could be calculated from the GC-MS results provided [15], see Table 63. From the carbon content in the oxygen-free aromatics calculated, the hydrogen present could be determined using the H/C ratio. With the elemental composition of both the oxygenated aromatics and the oxygen-free aromatics being calculated and the overall fraction`s elemental composition provided, the elemental composition of the aliphatic part could be calculated. Once the elemental composition of the aliphatics, oxygenated aromatics and oxygen-free aromatics were calculated, the H/C ratio could be calculated for the aliphatics, oxygenated aromatics and oxygen-free aromatics. This was used to select applicable components from the GC-MS data to represent the aliphatic, oxygenated aromatic and oxygen-free aromatics in the naphtha, jet, diesel and gas oil fractions. When a single component with a similar H/C ratio was not available from the identified components in that specific distillate fraction, a component with a higher H/C ratio and a component with a lower H/C ratio were selected. In such cases the ratio of the higher H/C to the lower H/C was such that the combined composition resembled the desired H/C.

Table 63 Data used for elemental balances & component selection

	Feed [a, b] [Wt%]			wt% aromatic carbons [b]	H/C molar ratio for Oxygen-free aromatics from GC-MS data [c]
	C	H	O		
Lights	85.22	14.48	0.30	7.1	1.1846
Naphtha	86.39	13.31	0.30	13.1	1.2232
Jet	87.00	12.30	0.70	20.0	1.2924
Diesel	88.14	11.37	0.50	29.4	1.1847
Gas oil	88.16	11.44	0.40	27.8	0.8442

[a] normalized to ignore S and N, [b][15], [c] calculated from [221]

This overall approach was similar for naphtha, jet, diesel and gas oil, but not for the lights fraction. For the oxygenated aromatics in the jet fraction, two oxygenated aromatic components were assumed, both identified from experimental results provided by GC-MS analysis in the study by Christensen et al. [221]. The calculations for the lights fraction were slightly different. Oxygen was assumed to be present in the aromatic and in the aliphatic categories (and not only in the aromatic fraction as for naphtha, jet, diesel and gas oil). The lightest oxygenated aromatic is phenol, with a boiling point of approximately 181°C. However, the light fraction had a boiling range of up to 71°C. From this it is clear that phenol will be more likely to elute in the naphtha fraction where the boiling point is from 71°C to 182°C. However, about a third of the oxygen present in the lights fraction does elute as phenol, with 0.79wt% of the lights being phenols [15]. As a modelling precaution to prevent separation problems in distillation, a lighter non-aromatic oxygen-containing component was selected - tetrahydrofuran. According to literature, furans have a low hydrodeoxygenation reactivity [28], therefore it is a reasonable assumption that complete hydrodeoxygenation of the oxygen present in the tetrahydrofuran did not occur. Phenols were assumed to contain a third of the oxygen, with the remainder of the oxygen present in tetrahydrofuran. This results in the elemental composition of the oxygenated aromatics, as well as the oxygenated aliphatics, being completely specified. Since the wt% of carbons that are aromatic is specified and the H/C ratio for the oxygen-free aromatics was determined from GC-MS data, the hydrogen content of the aromatic segment can

be determined. The oxygen-free aliphatic composition can be determined from an overall elemental balance.

The general assumptions made in performing elemental balances to allow for selecting components for each category in the oily fraction (the final oil product/ distillate fractions) and the assumptions made when selecting the components to represent each category in the distillate fraction, are summarized below:

1. GC-MS results [221] reporting area% for the components identified in the fractions, will be the equivalent of wt%

2. Sulphur and nitrogen were ignored and feed compositions normalized accordingly. The nitrogen and sulphur contents are very low, at maximum values of 0.03wt% and 0.031wt% respectively. This assumption was made to decrease the degrees of freedom to allow for mass balance calculations and component selection.

3. Model component or components to represent each of the categories (oxygenated aromatics, oxygen-free aromatics and aliphatics) in each of the distillate fractions (lights naphtha, jet, diesel, gas oil), were assumed, see Table 64.

   a. These assumed components were selected based on the following criteria: components identified by the GC-MS analysis and listed in the study by Christensen et al. [221], that had a H/C or O/C value close to the average calculated for each category in each distillate fraction, were selected in the oxygenated aromatic category in the specific distillate fraction given.

   b. If no single component was close to the average calculated H/C ratio, a combination of components that will make up the desired H/C ratio was selected. If no such a combination could be made from the experimental GC-MS results, literature and availability in Aspen Plus® databank was used to identify possible components.

   c. For the oxygen-free aromatics and aliphatics components in the lights, naphtha, jet, diesel and gas oil, model components with a similar H/C ratio to the average value calculated from the experimental GC-MS data ratio, were selected.

   d. No oxygenated-aromatic components were identified in either the diesel or the gas oil fractions by GC-MS, [221]. For the diesel fraction, dibenzofuran was selected. Dibenzofuran has been reported to be present in bio-oil and to have a high resistance to hydrotreating [28]. For the gas oil fraction, dinonylphenol was assumed, as this was the heaviest oxygenated-aromatic component that is likely to resist hydrodeoxygenation due to its phenolic nature, which was available in the Aspen Plus® databank.

In all cases where components were selected, preference was given to components present in the GC-MS data, as this is experimental data proving the components presence in the specific fuel fraction. Unfortunately, not all components identified by GC-MS agreed with the experimentally measured H/C ratio and not all components were available in the databank. In such cases similar components with similar boiling points that were available in the databank were considered. The H/C ratios, as calculated from the elemental compositions provided in literature, can be viewed in Table 64. The components selected to represent each specific fraction are also listed. Ethylbenzene is present in both the lights and naphtha fraction as an oxygen-free aromatic component. Ethylbenzene has a H/C ratio of 1.250 and was therefore selected since both benzene and toluene have a H/C ratio lower than required to meet the H/C ratio of the lights and naphtha fractions (H/C for benzene is 1 and H/C for toluene is 1.143, compared to the required H/C ratios for the lights and naphtha fractions of 1.1846 and 1.2232 respectively, see Table 63). By selecting ethylbenzene in conjunction

135

with another oxygen-free aromatic component with a lower H/C ratio, the desired H/C ratio could be obtained by varying the ratio of the two oxygen-free aromatic components relative to each other.

Table 64 Components selected in final fractions

Distillate fraction	Category	Calculated H/C [moles]	Calculated O/C [moles]	Selected model component name	Chemical formula	H/C [moles]	O/C [moles]
Lights	Oxygenated aliphatic	2.000	0.250	Tetrahydrofuran	C4H8O	2.000	0.250
	Aliphatics (oxygen free)	2.092	-	Hexane	C6H14	2.333	-
				Cyclohexane	C6H12	2.000	-
	Oxygenated aromatics	1.000	0.167	Phenol	C6H6O	1.000	0.167
	Oxygen-free aromatics	1.185	-	Toluene	C7H8	1.143	-
				Ethylbenzene	C8H10	1.250	-
Naphtha	Aliphatics	1.933	-	Methyl- cyclohexane	C7H14	2.000	-
				1,3 cyclohexadiene	C6H8	1.333	-
				3 methyl heptane	C8H18	2.250	-
	Oxygenated aromatics	1	0.167	Phenol	C6H6O	1.000	0.167
	Oxygen-free aromatics	1.223 [a]	-	m-xylene (1,3 dimethyl benzene)	C8H10	1.250	-
				Ethylbenzene	C8H10	1.250	-
				Indane	C9H10	1.111	-
Jet	Aliphatics	1.785	-	Decalin (decahydronaphthalene)	C10H18	1.800	-
				Octahydro-1H indene	C9H16	1.778	-
	Oxygenated aromatics	1.264	0.123	p-cresol	C7H8O	1.143	0.143
				2 ethyl, 4 methyl phenol	C9H12O	1.333	0.111
	Oxygen-free aromatics	1.292 [a]	-	n-propyl benzene	C9H12	1.333	-
				Tetralin	C10H12	1.200	-
Diesel	Aliphatics	1.721	-	Tetradecane	C14H30	2.143	-
				Hexadecahydro fluoranthene	C16H26	1.625	-
	Oxygenated aromatics	0.667	0.083	Dibenzofuran	C12H80	0.667	0.083
	Oxygen-free aromatics	1.185 [a]	-	1,2- diphenylethane	C14H14	1.000	-
				Cyclohexylbenzene	C12H16	1.333	-
Gas Oil	Aliphatics	1.715	-	Octadecahydro-naphthacene	C18H30	1.667	-
				Tetracosane	C24H50	2.083	-
	Oxygenated aromatics	1.75	0.042	2, 4 dinonylphenol	C24H42O	1.750	0.042
	Oxygen-free aromatics	0.844 [a]	-	Fluoranthene	C16H10	0.625	-
				2,4 diphenyl-4-methylpentene	C18H20	1.111	-

[a] determined from GC-MS data in [15]

4.2.4.5 Review of chemical reactions occurring through hydrotreating

In step 4 of Figure 32, model compounds to represent the raw bio-oil had to be identified. To determine the initial components present in bio-oil, the reactions that typically occur during hydrotreating and hydrocracking, were considered based on the model components representing the final product (C_{P1}-C_{Pn}). Reactants that were identified as precursors to each of the selected final

136

products are listed in Table 64. Assumptions that were made in order to simplify the calculations and the procedure include:

    a.   The type of catalyst does not influence the reaction that occurs and hydrotreating reactions are independent of the catalyst.

    b.   All reactants identified for each of the different categories react to completion. Some components selected to represent a category, do not undergo any reactions (indane in the aromatic oxygen-free naphtha fraction and fluoranthene in the aromatic oxygen-free diesel fraction).

    c.   All components are equally likely to react in the hydrotreating and the hydrocracking reactor, with no preference given to which is more susceptible to hydrotreating and hydrocracking. In other words, this approach does not consider the likelihood of reactions as a function of their chemical family or operating conditions. E.g. olefins and alcohols react at lower temperatures around 150 $^\circ$C and 200°C respectively, whereas dibenzofuran react at 400°C. From the operating conditions, where the first reactor operates at a lower temperature, it is expected that the olefins and alcohols will react, but not the dibenzofuran. The dibenzofuran is only expected to react in the second reactor, at 405°C. This assumption considers dibenzofuran and olefins to have the same chance of reacting in the first reactor and second reactor.

Many reactions produce gas and water and other aqueous products during hydrotreating and hydrocracking, while consuming hydrogen. As mentioned previously, the hydrogen consumption for hydrotreating and hydrocracking are reported [93]. The aqueous and solid yields have been calculated. The gas yield has also been calculated, as well as the exact gas composition. The initial bio-oil components identified were selected based on:

    a.   Precursor reactants reported in literature for the products selected in the final distillate fraction. E.g. cyclohexane is typically the product of the hydrotreating of benzene; the final product in the oxygen-free aliphatic of the lights fraction is cyclohexane, but the initial bio-oil component in the bio-oil (before hydrotreating) was most likely benzene.

    b.   Typical bio-oil components, as found in literature (and experimental results performed in this study, see Section 3.2.5.7 GC-MS Analysis and Section 3.2.5.8 NMR Analysis.

    c.   Proposed reaction based on analogies with reaction reported in literature.

As mentioned, numerous potential components were identified as possible precursors (reactants), from the criteria mentioned above (step 4 of Figure 32). Considering so many reactions complicates the stream and future calculations, therefore key components were selected on the following basis:

    a.   As a means to simplify the calculations, the first gas phase and the second gas phase were examined together, as if it was a single phase. From the list of reactants identified, reactants that produced the components in the combined gas phase were selected in such a ratio that the desired gas composition was obtained. Since these hydrotreating reactions use hydrogen and produce water as product, the hydrogen consumption and water formed had to be modified to account for this, as stated in step 5 of Figure 32.

    b.   In the next step in Figure 32, step 6, stipulates that the raw bio-oil components that are responsible for solid phase formation be selected as a part of the raw bio-oil components. For the first solid phase produced (after hydrotreating), components likely to result in solid phase formation were selected and the ratio of the reactants determined according to the empirical chemical composition ($C_1H_{1.34}O_{0.16}$). The second solid phase forming after hydrocracking, proved to be more difficult to find typical bio-oil components to represent this phase due to the small oxygen content, which was calculated from mass and elemental balances. A combination of heavy components was selected to represent this. The ratio of

heavy components was selected to comply with the empirical chemical composition determined ($C_1H_{1.309}O_{0.007}$).

c. At this stage of the methodology, step 7 in Figure 32 is followed. The gaseous and solid phases are already completely specified and the raw bio-oil components contributing/eluting to these two phases selected. The hydrogen requirements and water formation have been adjusted to account for the reactions the selected raw bio-oil components undergo to form the gaseous and solid phases. The final oil`s component composition has already been selected. The total hydrogen consumption is known, as well as the hydrogen consumption of the raw bio-oil components that produce by-products contributing to the solid and gaseous phases. In other words, the remainder of hydrogen will be utilized by raw bio-oil components to form products present in the final oil. This remaining hydrogen quantity was used to select the raw bio-oil composition from all the identified possible raw bio-oil components, as the different raw bio-oil components consume different quantities of hydrogen in the chemical reaction to produce the final product pathway. This will be better explained by an example: for a final product of cyclohexane, the initial raw bio-oil component could have been phenol or benzene. However, phenol to cyclohexane requires 4 moles of hydrogen, whereas benzene to cyclohexane requires only three moles of hydrogen. Therefore the combination of selected raw bio-oil components had to be such that the overall hydrogen requirements agreed with that of the literature reported values.

d. The next step in Figure 32, is step 8. To simplify the calculations, the first and the second aqueous phases were examined together, as if it was a single phase. First the total hydrogen consumption [as determined from literature [93]] for all the reactions occurring had to be met, by adapting the selected chemical reactions to produce the carbon components in the aqueous phase. This was accomplished by selecting typical bio-oil components that produce carbon components that are soluble in the aqueous phase after hydrotreating. The ratio of these initial bio-oil components was determined such that the total hydrogen requirements were met. Secondly the composition of the aqueous phase had to be modified to represent the calculated elemental composition in the aqueous phase by selecting two components based on their chemical formula (2,2`-oxybis-propanedioc acid and 2-(3,4-dihydroxy-5-oxo-2H-furan-2-yl)-2-hydroxy-acetic acid).

e. Since the two aqueous phases and the two gaseous phases were treated as a single aqueous and a single gas phase in determining the initial reactants in bio-oil, specific reactions occurring in the hydrotreating and in the hydrocracking reactors were not specified. The distribution of these reactions was determined using SOLVER in Excel. The hydrogen consumption (1.5665g/100g bio-oil in hydrotreating reactor and 1.5037 g/100g bio-oil in the hydrocracking reactor) and the gases released from each of the reactors were optimized for by changing the extent of reaction of all of the identified reactions within the first reactor. This has the implication that the oil going to the hydrocracking reactor will not have the same composition as that of the literature data [16]. This is indicated by the comparison between the literature data and the data used for the simulation model, see Table 65. Consequently, the oil fed to the hydrocracker in the model will have more carbon than the reported experimental data, though overall gas, aqueous, solids and oil yields will not be affected. Future studies should consider alternative approaches, where the aqueous phases are not treated as a single aqueous phase.

Table 65 Comparison for aqueous phase from hydrotreating reactor to hydrocracking reactor (based on the mass of bio-oil fed)

Component	C [wt%]	H [wt%]	O [wt%]
Mass balances from Literature [a]	6.4347	3.6909	37.6044
Model	9.2024	4.8294	37.5954

[a] [16]

The above procedure describes how the components for all phases have been identified and selected. The final mass closure was 99.36%. Acceptable mass balance limits for pyrolysis processes and upgrading experiments are reported to be 90-100% [60], this is within acceptable error. A summary of the chemical reactions and final components are provided in Table 66. Components to represent the diesel and gas oil fractions were especially difficult to obtain from literature. This is due to the typical analysis techniques (GC-MS) not being adequate for analysis of heavier components, typically present in the diesel and gas oil fractions. GC-MS depends on the sample being vaporized, which becomes difficult with heavy components. For much of the component selection in the diesel and gas oil fractions, the C/H and O/H ratios, determined from literature [221], were used as basis for component selection. Few components are reported in the heavy fractions in literature, therefore similar components to what have been reported in other heavy fuel fractions, were selected. Furthermore, very few of these reported components appear in the Aspen Plus® databank, therefore comparable components were selected from the databank.

Table 66 Chemical reactions in hydrotreating and hydrocracking reactor

Rxn No.	Stoichiometric Reaction	Reference Reaction	Reference Bio-oil compound	Component information	Reference Final compound
1	ACETACID + 2 H_2 → ETHAN-01 + H_2O	Reported reaction [43]	GLYCO-01: [223], [74], [199]	ACETACID: acetic acid $C_2H_4O_2$	ETHAN-01: proposed from bio-oil compound and reaction
				ETHAN-01: ethanol C_2H_6O	
				GLYCO-01: glycolic acid $C_2H_4O_3$	
2	GLYCO-01 + 3 H_2 → ETHAN-01 + 2 H_2O	Analogy to acetic acid converted to ethanol [43]	GLYCO-01: [223], [74]	GLYCO-01: glycolic acid $C_2H_4O_3$	ETHAN-01:proposed from bio-oil compound and reaction
				ETHAN-01: ethanol C_2H_6O	
3	FURFURAL + 4 H_2 → + TETRA-01 + METHA-01	Reported reaction [224]	FURFURAL: [43], [37], [101]	FURFURAL : furfural $C_5H_4O_2$	Proposed Reaction
				TETRA-01 : tetrahydrofuran C_4H_8O	
				METHA-01: Methanol CH_4O	
4	BENZOATE + 2 H_2 → TOLUENE + 2 CH_4 + CO_2	Proposed reaction	BENZOATE: [28]	BENZOATE: Methyl 2,5 - dimethyl benzoate $C_{10}H_{12}O_2$	TOLUENE: [221] in GC-MS data for LOC
				TOLUENE: Toluene C_7H_8:	
5	METHPHEN + 5 H_2 → TOLUENE + 2 CH_4 + 2 H_2O	Proposed hydrogenation reaction	METHPHEN: [28]	METHPHEN: 2,3 Dimethyl, 5 methoxy phenol $C_9H_{10}O_2$	TOLUENE: [221] in GC-MS data for LOC

				TOLUENE: Toluene C_7H_8	
6	ETHYLGUA + 3 H_2 → ETHYL-01 + CH_4 + 2 H_2O	Proposed reaction, analogy similar to guaiacol to catechol reaction [28], followed by a conversion of catechol to phenol [28], and phenol to benzene [28]	ETHYLGUA: [43],[37], [21], [201]	ETHYLGUA: 4 Ethyl guaiacol $C_9H_{12}O_2$ ETHYL-01: Ethylbenzene C_8H_{10}	ETHYL-01 :[221] in GC-MS data for LOC
7	N-HEP-01 $_2$+ H_2 → N-HEX-01 + H_2O + CO	Analogy to decanoic acid forming nonane [28]	N-HEP-01: [15]	N-HEP-01: N-heptanoic acid $C_7H_{14}O_2$ N-HEX-01: N-Hexane C_6H_{14}	N-HEX-01:[221] in GC-MS data for LOC
8	MESHEPTA + H_2 → N-HEX-01 + CH_4 + CO_2	Analogy to methyl laurate forming n-undecane [225]	Proposed compound, heptanoic compounds have been reported [199] and acids found in BO [43]	MESHEPTA: Heptanoic acid methyl ester $C_8H_{16}O_2$ N-HEX-01: N-Hexane C_6H_{14}	N-HEX-01:[221] in GC-MS data for LOC
9	BENZOFUR + 7 H_2 → CYCLO-01 + H_2O + ETHAN-02	Benzofuran forms benzene [226], [227]. Benzene forms cyclohexane [43]	BENZOFUR: lignin model compound [54], [28]	BENZOFUR: Benzofuran C_8H_6O CYCLO-01: Cyclohexane C_6H_{12} ETHAN-02: Ethane C_2H_6	CYCLO-01:[221] in GC-MS data for LOC
10	TRIMEBEN + 9 H_2 → CYCLO-01 + 3 CH_4 + 3 H_2O	Proposed reaction based on hydrotreating of guaiacol to catechol, to phenol to benzene to cyclohexane [43], [228]	TRIMEBEN: [101]	TRIMEBEN: Trimethoxybenzene $C_9H_{12}O_3$ CYCLO-01: Cyclohexane C_6H_{12}	CYCLO-01:[221] in GC-MS data for LOC
11	PHENOL + 4 H_2 → CYCLO-01 + H_2O	Reported reaction [43]	[199], [201], [21], [37]	PHENOL: Phenol C_6H_6O CYCLO-01: Cyclohexane C_6H_{12}	CYCLO-01:[221]
12	TRIMEBEN + 5 H_2 → PHENOL + 3 CH_4 + 2 H_2O	Proposed reaction based on hydrotreating of guaiacol to catechol to phenol [43], [228]	TRIMEBEN: [101]	TRIMEBEN: Trimethoxybenzene $C_9H_{12}O_3$ PHENOL: Phenol C_6H_6O	PHENOL: [15] in GC-MS data for LOC
13	2:4-X-01 + H_2 → M-XYL-01 + H_2O	Proposed reaction	2:4-X-01 : [43], [37]	2:4-D-01: 2,4-Diphenyl-4-methylpentene $C_{18}H_{20}$ M-XYL-01: M-Xylene C_8H_{10}	M-XYL-01: [221] in GC-MS data for LOC
14	O-ETH-01 + H_2 → ETHYL-01+ H_2O	Proposed reaction	O-ETH-01: [37]	O-ETH-01: O-Ethylphenol $C_8H_{10}O$ ETHYL-01: Ethylbenzene C_8H_{10}	ETHYL-01: [221] in GC-MS data for LOC

140

15	ETHYLGUA + 3 H_2 → ETHYL-01 + 2 H_2O + CH_4	Proposed reaction. Analogous to guaiacol to catechol [28] and catechol to phenol to benzene [28]	[43], [202]	ETHYLGUA: 4 Ethyl guaiacol $C_9H_{12}O_2$ ETHYL-01: Ethylbenzene C_8H_{10}	ETHYL-01: [221] in GC-MS data for LOC
16	4PROPGUA + 6 H_2 → METHY-01 + PROPA-01 + 2 H_2O	Proposed reaction to form methylphenol, [28]. Similar to reaction reported for o-ethyl-phenol to ethyl-cyclohexane [28],[226]	4PROPGUA: [202], Monomer of lignin [54], [202]	4PROPGUA: 4-Propylguaiacol $C_{10}H_{14}O_2$ METHY-01: Methylcyclohexane C_7H_{14} PROPA-01: Propane C_3H_8	METHY-01: [221] in GC-MS data for LOC
17	HMBENZAC + 4 H_2 → 1:3-C-01 + CH_4 + CO_2 + 2 H_2O	Proposed reaction. COOH is decarboxylated [225],[43] to form guiaiacol, followed by catechol formation [28], followed by proposed reaction to form 1,3 cyclohexadiene.	HMBENZAC: [28]	HMBENZAC: 4-Hydroxy 3-methoxy benzoic acid $C_8H_8O_4$ 1:3-C-01: 1,3-Cyclohexadiene C_6H_8	Proposed compound
18	METOCTAC → 3-MET-01 + CO_2	Proposed reaction similar to carboxylic acids` reaction [43]	3-MET-01: Proposed carboxylic acids component [43]	METOCTAC: 4 Methyl octanoic acid $C_9H_{18}O_2$ 3-MET-01: 3-Methylheptane C_8H_{18}	3 MET-01: [221] in GC-MS data for LOC
19	2:6-D-01 + 2 H_2 → P-CRE-01 + 2 ISOBU-01	Reported reaction [28], [229]	2:6-D-01: [28], [229]	2:6-D-01: 2,6-Di-tert-butyl-p-cresol $C_{15}H_{24}O$ P-CRE-01: P-Cresol C_7H_8O ISOBU-01: Isobutane C_4H_{10}	2:6-D-01: [28], [229]
20	4PROPGUA + 2 H_2 → P-CRE-01 + PROPA-01 + H_2O	Reported reaction [28]	4PROPGUA : lignin monomer [54], [202]	4PROPGUA: 4-Propylguaiacol $C_{10}H_{14}O_2$ P-CRE-01: P-Cresol C_7H_8O PROPA-01: Propane C_3H_8	
21	CONIFALC + 4 H_2 → ETMEPHEN + CH_4 + 2 H_2O	Proposed reaction	CONIFALC: found in softwood lignin [54]	CONIFALC: Coniferyl alcohol $C_{10}H_{12}O_3$ ETMEPHEN: 2 Ethyl, 4 methyl phenol $C_9H_{12}O$	ETMEPHEN: analogy to 2-ethyl-6-methyl phenol in jet fraction [221]
22	ISOEUGEN + 4 H_2 → N-PRO-02 + CH_4 + 2 H_2O	Proposed hydrogenation to 4-propyl-guaiacol, [28]	ISOEUGEN: [202], eugenol found in bio-oil [43] p.1050, [37], [28]	ISOEUGEN: Isoeugenol $C_{10}H_{12}O_2$	N-PRO-02: [221]

		to p-propylphenol, followed by proposed hydrogenation reaction to n-propylbenzene		N-PRO-02: N-propylbenzene C_9H_{12}	
23	NAPHT-01 + 2 H_2 → 1:2:3-01	Reported reaction [28], [230]	NAPTH-01: [43], [37]	NAPHT-01: Naphthalene $C_{10}H_8$	1:2:3-01: [221] in Jet fraction
				1:2:3-01: 1,2,3,4-Tetrahydro-naphthalene $C_{10}H_{12}$	
24	NAPHT-01 + 5 H_2 → CIS-D-01	Reported reaction [28], [230]	NAPHT-01: [43], [37], [202]	NAPHT-01: Naphthalene $C_{10}H_8$	CIS-D-01: [221] in GC-MS data for LOC
				CIS-D-01: Cis -decalin $C_{10}H_{18}$	
25	INDAN-01 + 3 H_2 → 1HINDANE	Proposed hydrogenation reaction	INDAN-01: [221] in GC-MS data for LOC	INDAN-01: Indane C_9H_{10}	1HINDANE: [221] in jet fraction
				1HINDANE: Trans- octahydro-1H-Indene C_9H_{16}	
26	PHENKETO + 4 H_2 → 1:2-D-01 + 3 H_2O	Propose hydrogenation reaction	PHENKETO: compound found to be a typical component derived from lignin [43]	PHENKETO: Benzyl 2,4 Dihydroxy-phenyl ketone $C_{14}H_{12}O_3$	1:2-D-01: [221]
				1:2-D-01: 1,2-Diphenylethane $C_{14}H_{14}$	
27	XANTHENE + 6 H_2 → CYCLO-02 + CH_4 + H_2O	Proposed hydrogenation reaction	XANTHENE: considered to be a model compound [28], [229]	XANTHENE: Xanthene $C_{13}H_{10}O$	CYCLO-02: [221]
				CYCLO-02: Cyclohexylbenzene $C_{12}H_{16}$	
28	P-DECANO + H_2 → N-TET-01 + CO_2 + CH_4	Proposed reaction from decanoic acid [28]	Proposed reactant	P-DECANO: Methylpentadecanoate $C_{16}H_{32}O_2$	N-TET-01: [221]
				N-TET-01: N-tetradecane $C_{14}H_{30}$	
29	FLUOR-01 + 8 H_2 → HYDFLUOR	Proposed hydrogenation reaction	FLUOR-01: [202], [221]	FLUOR-01: Fluoranthene $C_{16}H_{10}$	Proposed reaction and proposed product
				HYDFLUOR: Hexadecahydro-fluoranthene $C_{16}H_{26}$	
30	DNONDBEN + H_2 → DINON-01 + H_2O	Proposed reaction	Proposed component based on H/C and O/C ratio`s	DNONDBEN: 4,5 Dinonyl 1,2 benzenediol $C_{24}H_{42}O_2$	Proposed component based on H/C and O/C ratio`s
				DINON-01: Dinonylphenol $C_{24}H_{42}O$	
31	NAPHT-02+ 9 H_2 → HYDNAPH	Proposed reaction	Proposed compound which might be the result of repolymerization of lignin derived compounds [54]	NAPHT-02: Naphthacene $C_{18}H_{12}$	Proposed component
				HYDNAPH: Octadecahydro-naphthacene $C_{18}H_{30}$	
32	PENTACOS + H_2 → N-TET-02 + CO_2 + ETHAN-02	Proposed reaction analogous to methyl laurate [225]	Proposed compound	PENTACOS: Ethyl pentacosa-noate $C_{27}H_{54}O_2$	N-TET-02 : Proposed bio-oil compound & proposed reaction

142

#				N-TET-02: N-tetracosane $C_{24}H_{50}$	
				ETHAN-02: Ethane C_2H_6	
33	0.545886 LEVOGLUC + 1.161296 4METGUA + 9.715441 ETHYLANI → COKE1	LEVOGLUC: [231] ETHYLGUA : [55], [28], [43] [101]	ETHYLANI: [43], LEVOGLUC : [231] ETHYLGUA: [55]	LEVOGLUC: Levoglucosan $C_6H_{10}O_5$	
				4METGUA: 4 – Methyl guaiacol $C_8H_{10}O_2$	
				ETHYLANI: Ethyl anisole $C_9H_{12}O$	
				ETHYLGUA: 4 Ethyl guaiacol $C_9H_{12}O_2$	
34	0.3131404 $C_{22}H_{20}O$ + 0.1262399 $C_{21}H_{24}O_4$ + 5.0255485 C18H28 → COKE2	Empirical chemical composition	$C_{21}H_{24}O_4$: [54]		
UNREACTING COMPONENTS					
	2:4-D-01			2:4-D-01: 2,4-Diphenyl-4-methylpentene $C_{18}H_{20}$	[221]
	FUMAR-01			FUMAR-01: Fumaric acid $C_4H_4O_4$	Proposed component based on H/C and O/C ratio
	1, 2 B-01			1:2-B-01: 1,2-Benzenediol $C_6H_6O_2$	[37], [199]

4.2.5 Auxiliary units for the hydrotreating facility

The BO upgrading process requires additional supporting units/equipment. This includes: a unit that can produce hydrogen (which is a reactant in the hydrotreating process), equipment that can purify recycled hydrogen to minimize reactant losses, a distillation column that can separate the final fuels into their respective fuel fractions and a waste treatment section to treat waste products. Figure 34 indicates where the auxiliary units are present in the Aspen Plus® process simulation. In the process simulation, hydrogen production and purification occurs in unit B3000 and distillation occurs in unit B2000 after hydrotreating. The auxiliary units are discussed in more details in Section 4.2.5.1 to Section 4.2.5.4.
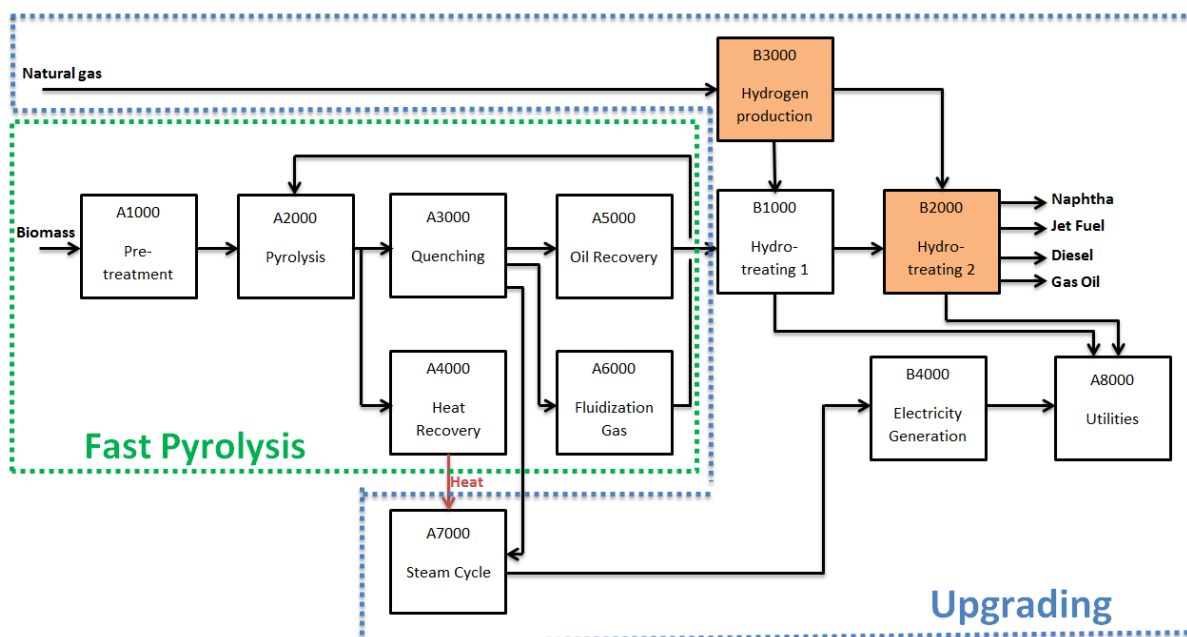
Figure 34 Simplified block flow diagram indicating where auxiliary units/ equipment are present

4.2.5.1 Hydrogen supply

High pressures and a large excess of hydrogen are required in both the hydrotreating and the hydrocracking reactor, to ensure sufficient hydrogen availability at the surface area of the catalyst [84], [25]. In an existing petrochemical refinery, hydrogen supply will be available, while in a stand-alone biomass pyrolysis-upgrading facility this is not the case. A stand-alone facility is more rigorous and considers the worst-case scenario; thereby critically assessing the viability of the process.

The different hydrogen supply options were discussed in detail in Section 2.4.5.1 Hydrogen requirements/ production in model, a. Overview, on p.38. Natural gas reforming uses the smallest mass of feedstock (11.45%) and is considered an established technology [133]. Although natural gas is not a renewable feedstock, the other options require between 2.5 – 8.1 times more feedstock compared to the natural gas option. Hence, hydrogen production from natural gas reforming was used in the simulation model. The natural gas composition can vary slightly, however methane contributes more than 90mole%, see Table 18, therefore methane was used to represent the natural gas in the process model. Natural gas reforming typically consists of feed desulphuring, reforming, followed by shift reactions, however in this simulation, desulphurizing was not considered. The H_2 production in the simulation model was based on literature [132], [57].

The reformer fuel is supplied by the PSA offgas [132], together with at least 15% fuel from a different source to insure good burner quality control since the high CO_2 content in the PSA offgas can result in combustion issues [127]. Additional fuel for this process is supplied by the lights from the distillation column and is supplemented with natural gas to complete the required 15% non-PSA offgas fuel source. Only a high temperature shift reactor is employed in this study, since a low temperature shift reactor is not needed when using a PSA unit, as any unconverted CO will be used as fuel for the reformer [133]. For the high temperature shift reactor it was assumed that no CH_4 will react and that the conversion of CO to CO_2 is 75%, similar to what has been reported in literature [132].

The yields used in the simulation were based on literature by Parkash (2003), [132] which corresponds closely to other literature sources [57]. A modification to the steam/C ratio was made (6.67 compared to 3.99 [132]), by decreasing the excess water, for a better representation of modern

144

refinery operation, discussed in detail in Section 2.4.5.1 Hydrogen requirements/ production in model, b. Hydrogen production from natural gas, on p.41. Since the steam/C ratio is also important for downstream processing, the steam/C feed was such that the steam/C ratio to the shift converter is at 3, to eliminate problems previously discussed (high hydrocarbon formation etc.). All yields based on C_xH_y were the same, with the only difference being the quantity of excess water. Furthermore, the ratio of water converted relative to the C_xH_y was similar to other literature [132], with a calculated steam/C ratio of 4.45 (corresponding to a value of 4.99 for mass H_2O fed/ mass C_xH_y fed) used in this study. The steam/C ratio used in this study falls within the range described in literature [132], [57].

Different methods of heat recovery can be employed to conserve heat from the unit with typical options including pre-heating air, steam generation, using a pre-reformer, using a heat exchange reformer, or using a heat exchange reformer with air preheating [133]. Since the pyrolysis unit in this simulation produces steam for the co-production of electricity, steam generation was selected as the most suitable option. After the shift reactor, the product stream is once again cooled to almost ambient temperature and excess water is removed before it is sent to the purification unit [135], [127].

4.2.5.2 Auxiliary units for the hydrotreating facility: Hydrogen clean-up

The process and configuration downstream from the HT shift reactor vary depending on the purification operation used. Typical purification operations include wet scrubbing and PSA [133]. In steam reforming plants, PSA units are usually employed due to the moderate costs, high purity and easy integration into the plant [133]. Furthermore, it is considered to be a less complex route [132].

In a PSA unit gas is passed through a bed with solid adsorbents, usually a mixture of activated carbon and zeolites, onto which most of the impurities adsorb. The hydrogen passes through and only a small part of it adsorbs [127], [133]. Hydrogen losses in the offgas are approximately 15 vol% [127], but can range from 10-20 vol% [133]. To prevent damage to the catalyst, liquids are removed prior to the catalyst bed, using a knock-out drum [132] with a mist eliminator [127]. Low temperatures increase the efficiency and operating temperatures vary between 40 - 43°C [132], [127], [125]. The adsorbed components are desorbed by decreasing the pressure, to allow adsorbed gas impurities to be purged from the PSA. The ratio of feed pressure to purge gas pressure should be $\geq$ 4 [127]. Typical operating pressures range from 14.8 -28.6 bar(a), with purge pressures ranging between 1.2-1.4 bar(a) [127]. The hydrogen recovery is sensitive to the purge gas pressure and can decrease from 85% to 60-80% for a purge gas ranging from to 3.8 – 6.6 bar (a) [137]. A single PSA unit to purify the product gas from steam reforming, as well as other hydrocarbon/hydrogen gas streams, is not considered to be economical [133], since the different streams require the use of different adsorbents [133]. For this reason, different PSA systems will be used for the two different instances where it is required; one instance is after the shift reactions and then the other instance is when the hydrotreating reactor gases are purified for recycling of the hydrogen. Heat is released when adsorption occurs and required when desorption occurs and the process can in some cases be considered to be isothermal [138]. From a reported heat duty in a previous study [127], the heat requirement was calculated to be 8.9133 MJ/ton feed.

4.2.5.3 Distillation

Detailed distillation data for hydrotreated bio-oil in literature is limited, especially for a commercial scale process where operating conditions and utility requirements are specified. Laboratory scale studies have been performed by Christensen et al. [221] and Baldauf et al. [27], although their focus was on the type of products, and the distillation conditions were not reported.

An attempt was made to model the distillation of the bio-oil fraction to obtain yields similar to that of Christensen et al. [15], since the model components were selected from the experimental data of distilled bio-oil. This indicated that a rather complex distillation system was necessary to obtain the same fractionation as was obtained from the experimental yields. Since that was not within the scope of the study, the distillation unit was modelled using a separator (SEP) in Aspen Plus®, with the yields specified according to the literature data from Christensen et al. [15]. A single separator was used to represent the atmospheric distillation and the vacuum distillation units.

Since distillation conditions were not reported for the experimentally determined fuel fractions [15], literature on the utility consumption of crude oil distillation was considered to determine the utility requirements. One of the major differences between the distillation of crude oil and HDO bio-oil, is the large quantity of cyclics present in HDO bio-oil [16], see Table 6. However, this is not expected to have a significant influence on the estimated utilities in the simulation model. Furthermore the design procedure for atmospheric and vacuum distillation is often empirical, as a result of the large range of hydrocarbons present in oil [139]. This justifies using utilities requirements for crude oil distillation from literature [139]. Utilities from literature , [139], was used and scaled according to the oil feeds, see Table 67.

The utilities associated with distillation were calculated in calculator block, DISTIL. This accounted for the electricity, steam, distilled water, fuel and cooling water utilities.

Table 67 Utilities for integrated atmospheric- and vacuum-distillation column

Utility	Value
Fuel [kJ/ton feed]	633 034
Steam [kJ/ton feed]	94 955
Electricity [kW.hr/ton feed]	8.7
Distilled water [L/ton feed]	90.9
Cooling water [L/ton feed]	1409.3

Data obtained and calculated from [139]

4.2.5.4 Waste treatment

Waste water is not generated during the fast pyrolysis process, however during hydrotreating and hydrocracking, liquid phase separation occurs to produce an oily and an aqueous phase. The aqueous phase is a waste product since the oily phase is the main desired product. The composition and properties of the aqueous phase is not well-known, since uses within the process (e.g. as water feed for reforming to produce hydrogen) have not been explored. Since the exact composition and properties are unknown, it is difficult to determine which waste treatment option will be best suited. From the calculated mass and elemental balances, components present in the aqueous phase were identified, although this was only based on elemental composition and not a true indication of the actual components. Since certain processes, especially the ones where micro-organisms are utilized, are very sensitive to the component composition, it is difficult to determine which option will be best suited. From the knowledge available on the aqueous waste product, the elemental composition, the feasibility of each of the different water treating options can be investigated. To determine which of the identified options will be best suited, the COD was determined.

The ThOD and the COD were considered to be equal in order to determine the best option for waste water treating. The calculated ThOD or COD for the combined aqueous effluent from hydrotreating and hydrocracking reactors, was calculated to be 626 990 mg O_2/L effluent. This is extremely high considering other reported COD values for a refineries are at 1020 mg O_2/L [161], and is due to the

high carbon transfer to the aqueous phases during upgrading, indicated in Table 75 on p.169. Dilution of the waste streams with other process water streams were also considered. This decreased the COD slightly, although it was still extremely high at 291 346 mg O_2/L effluent. Due to the high COD values calculated, other industries were investigated to determine typical COD values and the waste water treatment methods used in the industry. These industries included brandy distilleries and the pulp and paper industry, since these industries are expected to have similar components to that expected in the aqueous effluent (expected components are polar components that are present in bio-oil, such as phenols). The maximum COD measurements in the distillery industry were for cane molasses stillage, with values ranging from 65 000 − 100 000 mg/L, as reported by [232], [233]. Brown paper is reported to have CD flows ranging from 20 000- 80 000 mg O_2/L effluent [234]. This is still much less than the values obtained in the aqueous effluent from the hydrotreating and hydrocracking. The combination of the high ThOD or COD values, and the uncertainty with regards to the exact components and their concentrations [e.g. high phenolic content can be toxic to micro-organisms, [152]], complicates identifying which option will be best suited. Another option that does not require detailed knowledge of the components is combustion of the effluent water. To determine whether the aqueous phase will be combustible, it was simulated in Aspen Plus®. This was achieved using an adiabatic Gibbs Reactor (RGIBBS), with possible products as H_2O, CO_2, CO, O_2, CH_4, Ar and N_2. The Flash point was determined to be -170°C using this approach and the FLPT-Tag function in Aspen Plus®. Since the outlet temperature is larger than the flash point temperature, it can be concluded that the aqueous effluent will indeed be combustible. The heat generated from this can be used for additional steam production. Even though this seems to be the best option, the aqueous effluent waste water was not combusted in the final model.

4.3 Conclusion

With the methodology described in this section, a complete mass balance could be developed to account for the PTJ process from bio-oil production, to the final fuels. This was used as an input into the PTJ process simulation in Aspen Plus®.

5. PROCESS SIMULATION

5.1 Introduction

In this part of the study, the final Aspen process simulation is discussed. This includes discussing the changes made to the previous fast pyrolysis model (Section 5.2), as well as the process flow and the details of the new units B1000, B2000, B3000, B4000, A7000 and A8000, in Sections 5.3.1 to 5.3.6. The results from the Aspen simulation is provided and discussed in Section 5.4, with regards to the mass balance and yields, energy balance and efficiencies, utility requirements and waste products. The Aspen Plus® input report can be viewed in Appendix E.16 Process simulation input file. The properties for the BO and jet fuel from the simulation are also evaluated against experimental data and the jet fuel specifications. The results are used to evaluate the possibilities and opportunities for the pyrolysis to jet process, which is summarized in the conclusions (Section 5.5).

5.2 Fast pyrolysis unit

A block flow diagram of the process can be viewed below, in Figure 35. The original model by Ringer et al. [104] was modified by Leibbrandt (2010) to investigate the feasibility of the fast pyrolysis of sugarcane bagasse to liquid biofuels in South Africa [102]. Thereafter the model was modified by Nsaful (2012) to investigate different energy conversion processes of sugarcane bagasse [103]. The fast pyrolysis model was further modified to consider pine wood and to align the model with the focus of this study – the components present in the bio-oil. After modification to the fast pyrolysis section, additions were made to include the upgrading part. The modifications made to the previous fast pyrolysis model are listed below.

1. The biomass type was changed from sugarcane bagasse to pine wood with the appropriate lignin, extractives, ash, cellulose and sugar contents, see Table 59, p.114 .
2. The plant capacity was modified to represent the calculated requirements of a SPK plant as addition to a GTL facility, using a multiplication block (MULT1001).
3. The product yields (char, bio-oil and gases) were slightly modified to a range determined from literature, see Table 59, p.114 .
4. The gas composition and bio-oil composition were also modified. The gas composition was determined from literature for pine biomass, at experimental conditions of 500°C [21], see Table 59, on p.114. The bio-oil composition was modified to resemble the raw bio-oil that would have produced the upgraded bio-oil composition after hydrotreating and hydrocracking, see Section 4.2 on p. 120. The modifications to the gas and bio-oil compositions were made by changing the yields in the pyrolysis reactor (PY-2001) to represent the newly determined composition given in Table 68, p.151.
5. The steam cycle was modified to produce steam at 500$^{\mathrm{o}}$C and 105 bar, using a system of HP, MP and LP turbines. The final steam temperature was increased to 500$^{\mathrm{o}}$C, rather than 400$^{\mathrm{o}}$C, because it decreases condensation after expansion through the LP turbine and increases efficiency [165].
6. The previous design specification, BFWFLOW, calculated the quantity of water that will produce HP steam at 400 $^{\mathrm{o}}$C from the available heat. The design specification was modified to BFWATER, which calculates the quantity of water that must be added to the steam cycle to produce steam at 500$^{\mathrm{o}}$C.
7. Design specification, AIRCOMB (renamed AIRCOM-P) determines the air feed to combustion (stream 4002A). The previous design specification was modified to ensure the quantity of air is such that at least 6wt% oxygen is present in the product gas (stream 4005) as a result of excess air fed. This ensures complete combustion and is required to meet environmental

standards as described in the Department of Environmental Affairs and Tourism Air Quality Act (2008), [141].

8. Design specification, ASHQUENC, was modified to accommodate the larger ash stream as a result of increased plant capacity, as well as an increase in the ash content in the biomass.

9. The utility section (A8000) was modified to account for additional electrical (power) utilities required by the upgrading section in the model (B1000, B2000 and B3000).

The model developed by Leibbrandt (2010) and Nsaful (2012) covered only fast pyrolysis. The aim of this study is to investigate upgrading bio-oil to jet fuel, therefore the following additions were required:

1. A hydrotreating unit (B1000), including its auxiliary equipment, was added.
2. A hydrocracking unit (B2000), including its auxiliary equipment, was added.
3. A hydrogen production (via natural gas steam reforming) and gas clean-up unit was added (B3000).
4. An electricity generation unit was added (B4000) using a condensing extraction steam turbine set-up.
5. In the utilities section (A8000), additional utilities (cooling water, natural gas and steam) were added.
6. Components were added to the Aspen Plus® simulation, see marked (*) components in Table 68, and the properties for these components were estimated using the TDE function in Aspen Plus®. This was required because some of the selected bio-oil components were not available in the software databanks. Other unavailable properties were estimated using Aspen Plus® property estimation function.

| PY-2001 Pyrolysis Reactor | CY-2001 Cyclone | SC-3001 Scrubber | ES-3001 Electrostatic Precipitator | R-B1001 Hydrotreating Reactor | F-B1002 Flash Drum | S-B1001 Decanter | R-B2001 Hydrocracking Reactor | F-B2001 Flash Drum | S-B2001 Decanter | D-B2001 Distillation | R-B3001 Reforming Reactor | R-B3002 Gas Shift Reactor | PS-B3001 Pressure Swing Absorption | PS-B3002 Pressure Swing Absorption |

Figure 35 Basic Process Flow Diagram with main equipment

Table 68 PY-2001 yields

Name in databank	True name	Chemical formula	Calculated PY-2001 yield for simulation
H2O	WATER	H_2O	0.2345
ACETACID	ACETIC ACID	$C_2H_4O_2$	0.0178
PHENOL	PHENOL	C_6H_6O	0.0029
FURFURAL	FURFURAL	$C_5H_4O_2$	0.0004
N-HEP-01	N-HEPTANOIC-ACID	$C_7H_{14}O_2$	0.0043
2:4-X-01	2,4-XYLENOL	$C_8H_{10}O$	0.0057
O-ETH-01	O-ETHYLPHENOL	$C_8H_{10}O$	0.0016
INDAN-01	INDANE	C_9H_{10}	0.0341
2:6-D-01	2,6-DI-TERT-BUTYL-P-CRESOL	$C_{15}H_{24}O$	0.0018
NAPHT-01	NAPHTHALENE	$C_{10}H_8$	0.0166
DIBEN-01	DIBENZOFURAN	$C_{12}H_8O$	0.0030
FLUOR-01	FLUORANTHENE	$C_{16}H_{10}$	0.0344
2:4-D-01	2,4-DIPHENYL-4-METHYLPENTENE-1	$C_{18}H_{20}$	0.0032
NAPHT-02	NAPHTHACENE	$C_{18}H_{12}$	0.0223
GLYCO-01	GLYCOLIC-ACID	$C_2H_4O_3$	0.1511
FUMAR-01	FUMARIC-ACID	$C_4H_4O_4$	0.0137
1:2-B-01	1,2-BENZENEDIOL	$C_6H_6O_2$	0.0002
2,2PROPA	*PROPANEDIOC ACID, 2,2`-OXYBIS-	$C_6H_6O_9$	0.1158
FURACETA	*2-(3,4-DIHYDROXY-5-OXO-2H-FURAN-2-YL)-2-HYDROXY-ACETIC ACID	$C_6H_6O_7$	0.0405
LEVOGLUC	*LEVOGLUCOSAN	$C_6H_{10}O_5$	0.0009
4METGUA	*4-METHYLGUAIACOL	$C_8H_{10}O_2$	0.0016
ETHYLANI	*4-ETHYL ANISOLE	$C_9H_{12}O$	0.0134
BENZOATE	*METHYL 2,5-DIMETHYLBENZOATE	$C_{10}H_{12}O_2$	0.0019
METHPHEN	*2,3-DIMETHYL-5-METHOXYPHENOL	$C_9H_{10}O_2$	0.0006
ETHYLGUA	*ETHYL GUAIACOL	$C_9H_{12}O_2$	0.0029
MESHEPTA	*HEPTANOIC ACID METHYL ESTER	$C_8H_{16}O_2$	0.0119
BENZOFUR	*BENZOFURAN	C_8H_6O	0.0306
TRIMEBEN	*TRIMETHOXYBENZENE	$C_9H_{12}O_3$	0.0059
4PROPGUA	*4 PROPYL GUAIACOL	$C_{10}H_{14}O_2$	0.0148
HMBENZAC	*4-HYDROXY-3-METHOXYBENZOIC ACID	$C_8H_8O_4$	0.0463
METOCTAC	*4 METHYL OCTANOIC ACID	$C_9H_{18}O_2$	0.0594
CONIFALC	*CONIFERYL ALCOHOL	$C_{10}H_{12}O_3$	0.0028
ISOEUGEN	*ISOEUGENOL	$C_{10}H_{12}O_2$	0.0085
PHENKETO	*BENZYL 2,4 DIHYDROXYPHENYL KETONE	$C_{14}H_{12}O_3$	0.0074
XANTHENE	*XANTHENE	$C_{13}H_{10}O$	0.0086
P-DECANO	*METHYL PENTADECANOATE	$C_{16}H_{32}O_2$	0.0101
DINONPHE	*DINONYLPHENOL	$C_{24}H_{42}O_2$	0.0034
PENTACOS	*ETHYL PENTACOSANOATE	$C_{27}H_{54}O_2$	0.0040
C22H20O	*3-[1,1'-BIPHENYL]-4-YL-1,2,3,4-TETRAHYDRO-1-NAPHTHOL	$C_{22}H_{20}O$	0.0042
C18H28	*1,4-DICYCLOHEXYLCYCLOHEXA-1,3-DIENNE	$C_{18}H_{28}$	0.0548
C21H24O4	*2-METHOXY-4-[(2S,3R)-7-METHOXY-3-METHYL-5-[(1E)-2-BUTENYL]-2,3-DIHYDRO-1-	$C_{21}H_{24}O_4$	0.0019

151

	BENZOFURAN-2-YL]PHENOL		
ETMEPHEN	*2-ETHYL,4-METHYL PHENOL	$C_9H_{12}O$	0
1HINDANE	*1H-INDENE,OCTAHYDRO-, TRANS	C_9H_{16}	0
HYDFLUOR	*HEXADECAHYDROFLUORANTHENE	$C_{16}H_{26}$	0
HYDNAPH	*OCTADECAHYDRONAPHTHACENE	$C_{18}H_{30}$	0
Total			*1.0000*

* Not available in Aspen Plus®. User defined components with properties estimated using TDE function in Aspen Plus®. All other unavailable properties estimated using Aspen Plus® property estimation

5.3 Upgrading unit

5.3.1 Hierarchy B1000 – Hydrotreating Section

The process flow for B1000 can be viewed in Section E.12 Unit B1000 – Hydrotreating 1, p.256. The bio-oil product (stream 5006) from the fast pyrolysis unit is pumped (P-B1001) to a pressure of 2000psig (138.91bar), whereafter it is heated in a heat exchanger (HXB10010) to around 340°C, before entering the hydrotreating reactor (R-B1001). These conditions are similar to experimental conditions [16]. Hydrogen is fed in excess at 13.2wt% of the moisture-free BO fed. The hydrotreating reactor was modelled as a stoichiometric reactor (RStoic) in Aspen Plus®, with the pressure specified at 2000 psig and as adiabatic. The chemical reactions occurring were also specified, as indicated in Table 69. The HDO reactions are exothermic [92], [16], resulting in a temperature increase in the reactor. The heat exchanger (HXB1001) supplies sufficient heat to ensure that the final reactor temperature agrees with literature data indicating a value around 340 °C [16]. The heat to HXB1001 is supplied by cooling of the high temperature shift reactor (R-3002) products, from 369.7 °C to 157 °C, using HXB3003. This heat integration between HXB1001 and HXB3003 was determined from the pinch analysis. Heat exchanger HXB1001 together with R-B1001 represent an actual reactor where the temperature will be kept at a set- value, with the duty supplied to the HXB1001 equal to the net energy required to keep the reactor at the set-point.

As mentioned earlier, the extent of the chemical reactions in the different reactors (R-B1001, R-B2001) were determined to optimize for the hydrogen consumption and the gas composition closest to experimental data, by changing the fractional conversion of each reaction until the sum of the errors squared were minimized. The chemical reactions together with the fractional conversion can be viewed in Table 69. Overall, it was assumed that all reactions proceed to completion, except for indane and fluoranthene, see Section 4.2.4.5 Review of chemical reactions occurring through hydrotreating, p.136. All reactants (excluding indane and fluoranthene) that do not react to completion in R-B1001 will react to completion in R-B2001. The components selected to represent coking on the catalyst reacted to form pseudo components - coke 1 and coke 2, with properties similar to that of char in Aspen Plus®.

Table 69 Extent of reactions in R-B1001 and R-B2001

Rxn No.	Fractional conversion in R-B1001	Stoichiometric Reaction (component names in simulation)	Component information
1	2.9200E-04	ACETACID + 2 H_2 → ETHAN-01 + H_2O	ACETACID: acetic acid ($C_2H_4O_2$)
			ETHAN-01: ethanol (C_2H_6O)
			GLYCO-01: glycolic acid ($C_2H_4O_3$)
2	1.0000E+00	GLYCO-01 + 3 H_2 → ETHAN-01 + 2 H_2O	GLYCO-01: glycolic acid ($C_2H_4O_3$)
			ETHAN-01: ethanol (C_2H_6O)
3	2.4843E-01	FURFURAL + 4 H_2 → + TETRA-01 + METHA-01	FURFURAL : furfural ($C_5H_4O_2$)
			TETRA-01 : tetrahydrofuran (C_4H_8O)

152

			METHA-01: methanol (CH_4O)
4	1.7441E-01	BENZOATE + 2 H_2 → TOLUENE + 2 CH_4 + CO_2	BENZOATE: methyl 2,5 -dimethyl benzoate ($C_{10}H_{12}O_2$)
			TOLUENE: toluene (C_7H_8)
5	2.1910E-01	METHPHEN + 5 H_2 → TOLUENE + 2 CH_4 + 2 H_2O	METHPHEN: 2,3 dimethyl, 5 methoxy phenol ($C_9H_{10}O_2$)
			TOLUENE: toluene (C_7H_8)
6	2.2585E-01	ETHYLGUA + 3 H_2 → ETHYL-01 + CH_4 + 2 H_2O	ETHYLGUA: 4 ethyl guaiacol ($C_9H_{12}O_2$)
			ETHYL-01: ethylbenzene (C_8H_{10})
7	0.0000E+00	N-HEP-01 $_2$+ H_2 → N-HEX-01 + H_2O + CO	N-HEP-01: n-heptanoic acid ($C_7H_{14}O_2$)
			N-HEX-01: n-hexane (C_6H_{14})
8	2.1064E-05	MESHEPTA + H_2 → N-HEX-01 + CH_4 + CO_2	MESHEPTA: heptanoic acid methyl ester ($C_8H_{16}O_2$)
			N-HEX-01: n-hexane (C_6H_{14})
9	3.6142E-02	BENZOFUR + 7 H_2 → CYCLO-01 + H_2O + ETHAN-02	BENZOFUR: benzofuran (C_8H_6O)
			CYCLO-01: cyclohexane (C_6H_{12})
			ETHAN-02: ethane (C_2H_6)
10	3.8380E-02	TRIMEBEN + 9 H_2 → CYCLO-01 + 3 CH_4 + 3 H_2O	TRIMEBEN: trimethoxybenzene ($C_9H_{12}O_3$)
			CYCLO-01:cyclohexane (C_6H_{12})
11	3.0763E-01	PHENOL + 4 H_2 → CYCLO-01 + H_2O	PHENOL: phenol (C_6H_6O)
			CYCLO-01: cyclohexane (C_6H_{12})
12	6.2815E-02	TRIMEBEN + 5 H_2 → PHENOL + 3 CH_4 + 2 H_2O	TRIMEBEN: trimethoxybenzene ($C_9H_{12}O_3$)
			PHENOL: phenol (C_6H_6O)
13	3.2901E-01	2:4-X-01 + H_2 → M-XYL-01 + H_2O	2:4-D-01: 2,4-diphenyl-4-methylpentene ($C_{18}H_{20}$)
			M-XYL-01: m-xylene (C_8H_{10})
14	2.7108E-01	O-ETH-01 + H_2 → ETHYL-01+ H_2O	O-ETH-01: o-ethylphenol ($C_8H_{10}O$)
			ETHYL-01: ethylbenzene (C_8H_{10})
15	2.1947E-01	ETHYLGUA + 3 H_2 → ETHYL-01 + 2 H_2O + CH_4	ETHYLGUA: 4 ethyl guaiacol ($C_9H_{12}O_2$)
			ETHYL-01: ethylbenzene (C_8H_{10})
16	0.0000E+00	4PROPGUA + 6 H_2 → METHY-01 + PROPA-01 + 2H_2O	4PROPGUA: 4-propylguaiacol ($C_{10}H_{14}O_2$)
			METHY-01: methylcyclohexane (C_7H_{14})
			PROPA-01:propane (C_3H_8)
17	5.8776E-01	HMBENZAC + 4 H_2 → 1:3-C-01 + CH_4 + CO_2 + 2 H_2O	HMBENZAC: 4 hydroxy 3 methoxy benzoic acid ($C_8H_8O_4$)
			1:3-C-01: 1,3-cyclohexadiene (C_6H_8)
18	1.0000E+00	METOCTAC → 3-MET-01 + CO_2	METOCTAC: 4 methyl octanoic acid ($C_9H_{18}O_2$)
			3-MET-01: 3-methylheptane (C_8H_{18})
19	0.0000E+00	2:6-D-01 + 2 H_2 → P-CRE-01 + 2 ISOBU-01	2:6-D-01: 2,6-di-tert-butyl-p-cresol ($C_{15}H_{24}O$)
			P-CRE-01: p-cresol (C_7H_8O)
			ISOBU-01: isobutene (C_4H_{10})
20	0.0000E+00	4PROPGUA + 2 H_2 → P-CRE-01 + PROPA-01 + H_2O	4PROPGUA: 4-propylguaiacol ($C_{10}H_{14}O_2$)
			P-CRE-01: p-cresol (C_7H_8O)
			PROPA-01: propane (C_3H_8)
21	2.9689E-01	CONIFALC + 4 H_2 → ETMEPHEN + CH_4 + 2 H_2O	CONIFALC: coniferyl alcohol ($C_{10}H_{12}O_3$)
			ETMEPHEN: 2 ethyl, 4 methyl phenol ($C_9H_{12}O$)
22	9.1514E-02	ISOEUGEN + 4 H_2 → N-PRO-02 + CH_4 + 2 H_2O	ISOEUGEN: isoeugenol ($C_{10}H_{12}O_2$)
			N-PRO-02: n-propylbenzene (C_9H_{12})

153

23	2.5123E-01	NAPHT-01 + 2 H_2 → 1:2:3-01	NAPHT-01: naphthalene ($C_{10}H_8$)
			1:2:3-01: 1,2,3,4-tetrahydronaphthalene ($C_{10}H_{12}$)
24	2.4462E-01	NAPHT-01 + 5 H_2 → CIS-D-01	NAPHT-01: naphthalene ($C_{10}H_8$)
			CIS-D-01: cis –decalin ($C_{10}H_{18}$)
25	2.2240E-01	INDAN-01 + 3 H_2 → 1HINDANE	INDAN-01: indane (C_9H_{10})
			1HINDANE: trans- octahydro- 1H-Indene (C_9H_{16})
26	1.0000E+00	PHENKETO + 4 H_2 → 1:2-D-01 + 3 H_2O	PHENKETO: benzyl 2,4 dihydroxyphenyl ketone ($C_{14}H_{12}O_3$)
			1:2-D-01: 1,2-diphenylethane ($C_{14}H_{14}$)
27	8.4447E-02	XANTHENE + 6 H_2 → CYCLO-02 + CH_4 + H_2O	XANTHENE: xanthene ($C_{13}H_{10}O$)
			CYCLO-02: cyclohexylbenzene ($C_{12}H_{16}$)
28	1.6815E-02	P-DECANO + H_2 → N-TET-01 + CO_2 + CH_4	P-DECANO: methylpentadecanoate ($C_{16}H_{32}O_2$)
			N-TET-01: n-tetradecane ($C_{14}H_{30}$)
29	1.8365E-01	FLUOR-01 + 8 H_2 → HYDFLUOR	FLUOR-01: fluoranthene ($C_{16}H_{10}$)
			HYDFLUOR: hexadecahydro fluoranthene ($C_{16}H_{26}$)
30	3.1137E-01	DNONDBEN + H_2 → DINON-01 + H_2O	DNONDBEN: 4,5 dinonyl 1,2 benzenediol ($C_{24}H_{42}O_2$)
			DINON-01: dinonylphenol ($C_{24}H_{42}O$)
31	2.2997E-01	NAPHT-02+ 9 H_2 → HYDNAPH	NAPHT-02: naphthacene ($C_{18}H_{12}$)
			HYDNAPH: octadecahydro-naphthacene ($C_{18}H_{30}$)
32	1.0000E+00	PENTACOS + H_2 → N-TET-02 + CO_2 + ETHAN-02	PENTACOS: ethyl pentacosanoate ($C_{27}H_{54}O_2$)
			N-TET-02: n-tetracosane ($C_{24}H_{50}$)
			ETHAN-02: ethane (C_2H_6)
33	1.0000E+00	0.545886 LEVOGLUC + 1.161296 4METGUA + 9.715441 ETHYLANI → COKE1	LEVOGLUC: levoglucosan($C_6H_{10}O_5$)
			4METGUA: 4 methyl guaiacol ($C_8H_{10}O_2$)
			ETHYLANI: ethyl anisole ($C_9H_{12}O$)
			ETHYLGUA: 4 ethyl guaiacol ($C_9H_{12}O_2$)
34	0.0000E+00	0.3131404 $C_{22}H_{20}O$ + 0.1262399 $C_{21}H_{24}O_4$ + 5.0255485 C18H28 → COKE2	

At the exit of the hydrotreating reactor (R-B1001), the phases formed are: an oily phase, an aqueous phase, a gas phase and a solid phase [16]. The gases are separated from the other products using a flash drum. However, due to light component transfer to the vapour phase, the product stream (B1004) needs to be cooled in HXB1002+ before flashing in F-B1001. The pressure loss for HXB1002+ was specified as 0.62Bar [144]. The desired flash temperature determines the extent to which cooling in HX-B1002+ is required. The best conditions for F-B1001 can be viewed in Appendix E.2 Validation of flash conditions in Unit B1000 and B2000. The liquid hydrocarbon components most susceptible to vapour transfer were identified to be: hexane, cyclohexane and tetrahydrofuran. A maximum transfer of 10% for these components was set as the limit for transfer to the gaseous phase. However, since conversion of hexane was so small in R-B1001 (indicated in Table 69), the hexane was ignored in determining the optimal flash conditions. A pressure similar to that in R-B2001, approximately 104 Bar, is advantageous since the feed to R-B2001 is already at the desired pressure. The flash column was modelled as an adiabatic flash (FLASH2) in Aspen Plus®, with a set pressure of 104 Bar and an outlet temperature of 57°C. The vapour stream leaving F-B1001 contains some light hydrocarbons and a large quantity of hydrogen, due to the high excess hydrogen fed. The gases leaving in stream B1007 are purified in a Pressure Swing Absorption (PSA) unit, PS-B3002,

together with the gaseous phase from the hydrocracking reactor (R-B2001), to purify the vapour phase for a hydrogen recycle stream [133].

The liquid hydrotreating products form two phases - an aqueous and an oily phase [16], [90], [16]. After separation of the gas phase, the aqueous phase and the oily phase are separated, using a decanter. Difficulty to reconcile the experimental data with that of the simulation model was experienced for phase separation when the separator (S-B1001) was modelled as a decanter (DECANTER/ H-DRUM). Different property methods and different decanter unit specifications were investigated, yet similar separation to the experimental results was still not obtained. The decanter was therefore modelled as a separator block (SEP) in the simulation. Since experimental data verifying the simple phase separation after hydrotreating exists, this approach is justified. The inability of the decanter to accurately predict the phase separation was attributed to the complex mixture present, along with an inability to predict the interactions between the components present. The separator`s split fractions were specified to coincide with the calculated values from mass balances on literature data [16]. A design specification, SHYD1H2O, was used to ensure the water fraction in stream B1010 is at 0.27, by changing the block variable (flow frac) in separator S-B1001, in order to comply with literature data. The aqueous phase, stream B1009, has a high organic content and requires wastewater treatment. Different treatment options were discussed in Section 4.2.5.4 Waste treatment, although detailed waste water treatment was not modelled.

Many hydrotreating and hydrocracking studies report the formation of a solid phase or coke formation on the catalyst [95], [91] ([16], [17]. Hydroprocessing catalysts require regeneration to eliminate coke [97]. This results in a non-steady state operation for the coke mass balance, as it is not removed with the product streams, but only once the catalyst is regenerated. This was modelled as a solid pseudo component, coke1, leaving the hydrotreating reactor (R-B1001). However, this will have downstream consequences as a solid will be present for downstream processing, which is not the situation for actual circumstances. To eliminate this problem, a separator (S-B1002) was used to remove the solids formed, for modelling purposes. This separator was also modelled as a SEP unit in the simulation, with a specified separation of coke1. The pseudo components used for modelling purposes exit in stream B1012. The catalyst in R-B1001 is a Pd/C catalyst [16]. Pd/C has been reported to be the best catalyst for mild hydrotreating, due to the products` low oxygen content and high oil yield [91]. The hydrotreated oil (stream B1011) is fed to the hydrocracking unit, B2000.

5.3.2 Hierarchy B2000 – Hydrocracking section

In hierarchy B2000, hydrotreated bio-oil from the hydrotreating unit is pre-heated in HXB2001 to approximately 109°C, see Section E.13 Unit B2000 – Hydrotreating 2, p.260. The heat is supplied by cooling the product stream leaving the hydrocracking reactor (R-B2001) in HXB2003. Heat integration between HXB2001 and HXB2003 was determined from the pinch analysis. Excess hydrogen is fed to R-B2001 in stream B2003, at approximately 15.3wt% of the bio-oil feed stream (B2002). The hydrocracking reactor operates at 103 Bar(a) (1500 psig) and 405°C, similar to reported experimental conditions [16], and was modelled as a stoichiometric reactor (RStoic) with a set pressure of 150 psig and specified reactions. The chemical reactions and the fractional conversion are reported in Table 69. The fractional conversion reported is for R-B1001, but all reactions were assumed to go to completion, therefore the remainder of the fractional conversion is for R-B2001, except for Fluoranthene and Indane, which are also two of the final product components. These two components had fractional conversions of 0.866 and 0.934 in this reactor, R-B2001, respectively. The HDO reaction is exothermic with an overall reaction heat in the range of 2.4MJ/kg [92]. Reactor R-B2001 was modelled as an adiabatic reactor. The lower pre-heating temperature of 109°C and the

155

higher operating temperature of 405°C, compared to 339°C and 340°C for R-B1001, indicated that the reactions occurring in the hydrocracking reactor were more exothermic. This agreed with experimental results where the relative exotherm vs. set-point for hydrotreating was +6°C for the hydrotreating reactor, compared to +16°C for the hydrocracking reactor [16]. Excess hydrogen is supplied at approximately 15.3 wt% of the feed, similar to the calculated experimental excess of 13.7-15.2wt% [16], [17]. The product stream from R-B2001 is cooled in a series of heat exchangers as determined from the pinch analysis. The heat removed from the first heat exchanger, HXB2002+, is used for steam generation, followed by the second heat exchanger, HXB2003, where the heat is used to pre-heat the reactor feed. This correlates to a product cooling from 369.7^{o}C to 352.8^{o}C. The heat removed from the third heat exchanger, HX2004+, is used for heating water for steam generation, where the product stream is cooled to 55°C. The product stream, B2007, is cooled using cooling water in HXB2005+ to the final temperature required in the flash drum, F-B2001.

The processing conditions of flash drum (F-B2001), were determined in a similar manner to F-B1001, see Appendix E.2 Validation of flash conditions in Unit B1000 and B2000 for the sensitivity analysis. The components most prone to transfer to the vapour phase were identified to be: benzene, hexane, cyclohexane and tetrahydrofuran. A high pressure suppresses transfer of light components to the vapour phase. The operating conditions for the flash drum (F-B2001) are 100 Bar and 50°C and it was modelled as an adiabatic flash drum (FLASH2). The light components are removed from the product mixture in the flash drum, with the noncondensables and other gases exiting in stream B2009. Due to the excess hydrogen feed to R-B2001, the gas exiting F-B2001 is rich in hydrogen and needs to be purified before the hydrogen can be recycled. The gas is routed to PS-B3002, to be purified together with the gas from the first reactor, stream B1007. The remaining liquid product, which is a mixture of the aqueous and oily phases, are separated from each other using a decanter, S-B2001, modelled as a separation block, SEP, in Aspen Plus®. Similar difficulties to what was experienced and discussed with S-B1001 occurred, hence selecting a SEP block rather than a DECANTER.

The aqueous stream, stream B2012, contains dissolved hydrocarbons and must be sent to waste water treatment for further treating, similar to the aqueous phase from the hydrotreating reactor in stream B1009 in hierarchy B1000. To simulate the solids forming on the catalyst, a pseudo component was used, coke2, with similar properties to that of char in Aspen Plus®. Since this will typically deposit on the catalyst, removal from the product streams will not be required in an actual plant. Catalyst regeneration will be used for coke removal from the catalyst.

The solids formed in R-B2001, coke2, had to be removed as to avoid inaccurate estimation of properties downstream. This was done using SEP unit S-B2002, whose only purpose is to remove coke2 as a modelling amendment. The oil phase, stream B2014, contains hydrocarbons with wide boiling point ranges. In order to obtain the desired petrochemical fractions, it is distilled. Accurate distillation of a complex mixture like the one in stream B2014, is very difficult, as can be seen looking at crude oil refineries. Oil refineries often have a pre-flash, followed by atmospheric distillation and then by vacuum distillation [140]. The desired boiling point separation is achieved by pump-back and pump-around refluxes with integrated reheating [139]. An actual distillation unit was modelled as a pre-flash and a distillation unit, where the distillation unit represents the combined atmospheric and vacuum distillation unit. The separation achieved in the distillation unit (D-B2001) for each product stream was specified based on experimental distillation results [15]. The pre-flash, (F-B2002), was modelled as a FLASH2 block and the distillation unit, D-B2001, as a SEP block in the simulation. The light components are removed in the pre-flash via stream B2015 and the hydrocarbon liquid in stream B2016 is sent for distillation, to produce the desired distillate fractions: light fraction (stream

B2017), naphtha (stream B2018), kerosene (stream B2019), diesel (stream B2020) and gas oil (stream B2021). The light fraction is sent to the combustor, CB-B3001, to be burnt together with other fuel sources for heat supply to the reformer, R-B3001. The utilities for the pre-flash, atmospheric distillation and vacuum distillation were obtained and modified from literature for a crude oil refinery [139]. The separation achieved in the distillation column was specified in the SEP block, based on the experimental data from Christensen et al. [15], for the specific component group. Deviations in the yields from D-B2001 from experimental data, is due to a fraction of the bio-oil being combusted to supply heat for the pyrolysis reactor.

5.3.3 Hierarchy B3000 – Hydrogen production

Due to the excessive hydrogen requirements for a hydrotreating plant, an additional unit aims only at providing the required hydrogen to the downstream process. Ideally the feedstock should also be from a renewable source, although an investigation into different scenarios to provide hydrogen for hydrotreating and hydrocracking (provided in Table 17 on p.40), revealed that natural gas reforming was identified as the best option due to higher yields. Although natural gas is not a renewable feedstock, the other options require between 2.5 – 8.1 times larger feedstock masses than is the case for natural gas, see Section 2.4.5.1 Hydrogen requirements/ production in model.

Natural gas was represented as methane gas in accordance with previous modelling studies [57], [128]. Natural gas and steam are sent to the reformer, R-B3001, where they are partially converted to CO, CO_2 and H_2O, via the steam reforming reaction, see Rxn 1. The natural gas feed was assumed to be at room temperature (25^oC) and already pressurized (25.83 bar); typical for the transportation of natural gas in a long distance pipeline. The natural gas is heated to 371 ^{o}C in HXB3008-, before being fed to the reformer, using heat obtained from cooling the combustor effluents in heat stream QHXB3008 [139]. A design specification, TNGEXIT, is used to ensure the required natural gas feed pre-heating is provided in HXB3008-. This is achieved by manipulating the temperature to which cooling of the combustor offgas occurs in HXB3008+. The reformer was modelled as a yield reactor, RYIELD, due to the complexity when the temperature and steam ratios are considered in detail. Heat for the reforming reaction is obtained from cooling of the effluent, stream B3037, in heat exchanger HXB3007+. A design specification, TREFEXIT, is used to insure that the exit temperature of the reformer in stream B3006, is at 857^oC, similar to literature [139]. This is achieved by manipulating the temperature to which the combusted products are cooled in HXB3007+. The initial selected value and the range within which design specifications TNGEXIT and TREFEXIT are specified, are important to prevent convergence difficulties.

The operating yields were calculated from literature [139], see Table 70. The steam/C feed to R-B3001 was such that the ratio of steam/C ratio to the shift converter (R-B3002) is at 3 (mole basis) to represent a modern day facility and to avoid hydrocarbon formation problems, see Section 2.4.5.1 Hydrogen requirements/ production in model, subsection c. Shift Reaction, on p.41. This resulted in a steam/C ratio of 4.45 (moles) which corresponds to a value of 4.99 for mass H_2O fed/mass C_xH_y fed. This falls within the range for steam/C_xH_y ratio reported in literature of 4.48 – 7.50 (mass basis) [57], [139]. The pressure drop over the reforming reactor was set as 2.068 bar as was reported in literature [127]. The steam is obtained from the steam produced by heat integration and exits the CEST after the HP stage, via stream B4005.

Table 70 Reforming reactor R-B3001 product stream composition

Component	Product stream composition* [wt of component/ wt of total product stream]
CH_4	0.0191
H_2	0.0666
H_2O	0.5647
CO	0.1011
CO_2	0.2485

*Calculated from [139]

The reformer product, stream B3006, is cooled to 350°C in HXB3001, before it enters the high temperature shift reactor, R-B3002 [127]. The heat from HXB3001 is used to generate steam for electricity production in area A7000. The reactor was modelled as an adiabatic stoichiometric reactor, RSTOIC, with the following reaction specified: CO + H_2O → CO_2 + H_2. A fractional conversion of 75mole% (CO basis) was assumed [139]. A pressure loss of 0.414 bar was assumed, which is the average obtained from literature [139], [57].

The product streams from R-B3002 consist of unreacted CH_4 and steam, as well as products of CO, CO_2 and H_2. To purify the hydrogen, a Pressure Swing Adsorption technology is used. Adsorption is an exothermic process and is therefore favoured by low temperatures. The products stream is cooled in a series of heat exchangers from HXB3002 to HXB3005+ before it is sent for clean-up. The degree to which the products are cooled was determined from pinch analysis. To prevent adsorption and damage to the adsorbent, moisture is removed from the stream before it is fed to the PSA, in F-B3001. The flash drum was modelled as an adiabatic flash drum, FLASH2, with a set temperature of 43°C. The gaseous stream is fed to the PSA vessels, PS-B3001, for H_2 purification. The hydrogen content in the feed stream to the PSA, stream B3014, exceeds the recommended minimum of 70mole% [127], with a value of 79mole%, indicating that sufficient separation and a high degree of purification are possible. The PSA vessels were modelled as a single separation unit, SEP, with 85% of the H2 present in the feed recovered at a 99.99-100% purity [127]. The offgas, stream B3015, exits at a pressure of 0.37 bar(g) and is used as fuel to the combustor for heat generation [127]. The pure hydrogen stream, B3016, is then fed to a compressor, CP-B3003. It is not considered economical to use a single PSA unit to purify the product gas from steam reforming and hydrocarbon/hydrogen gas streams together, due to different adsorbent requirements [133]. The gaseous product from hydrotreating and hydrocracking, streams B3018 and B3017 respectively, is therefore purified in PS-B3002. The gaseous products need to be cooled to increase the adsorption efficiency. Cooling water is used for this purpose, in HXB3006-, to cool the PS-B3002 feed to 43°C. The processing conditions and yields for PS-B3001 and PS-B3002 are similar. The hydrogen purity in the feed stream to the PSA, PS-B3002, exceeds the recommended minimum of 70mole% [127], at a value of 98mole%. The offgas is combusted in CB-3001 for heat and the purified hydrogen is routed to CB-3003 to boost the pressure to the required pressure for hydrocracking, 104. 43 bar. The required amount of hydrogen is split at SP-B3001, at a ratio of 0.36, as calculated from the excess hydrogen feed required. Stream B3027 is routed to the hydrocracking reactor, R-B2001, and the remainder of the hydrogen is sent to CP-B3004, where it is compressed to 138.9 bar before it is routed to the hydrotreating reactor, R-B1001, in stream B3026. Compressor CP-B3003 and CP-B3004 were modelled as isentropic compressors, with isentropic efficiencies of 0.82 and set discharge pressures of 1500psig and 2000psig respectively.

The combustor provides the required heat to the reforming reactor, R-B3001. The fuel sources for the combustor, CB-B3001, comprise of PSA offgas, streams B3015 and stream B3022, the light fraction from distillation, stream B3030, and natural gas, stream B3026. The combustor was modelled as an adiabatic reactor, RSTOIC, and set to generate combustion reactions. The PSA offgas is limited to contribute only 85% of the required fuel to fuel the reformer [133], as a result of potential burning problems. For this reason additional fuel in the form of distillation lights and natural gas are combusted together with the PSA offgas. A design specification, NGFUEL, was used to ensure this criteria is met even when some other process values such as PSA offgas and the distillate lights may change, by varying the mass flow-rate of the natural gas fuel, stream B3028. The air to the combustor is determined from a design specification, AIRCOM-H, to ensure that the oxygen present in the flue gas is at least 6 wt%, to comply with environmental regulations [141], [103]. To conserve the heat generated during combustion, a series of heat exchangers is used, HXB3007+ to HX-B3012. The air feed to the combustor, stream B3035, is preheated in HXB3011- to 250°C, similar to other studies where air was pre-heated to 250-300°C, [142], [143]. This is achieved by cooling the combustor products in stream B3041. A design specification, TAIRCOM, determines the temperature to which the combustor products in stream B3042 are cooled, in order to supply sufficient heat to the air feed heater, HXB3011-. A summary of the assumptions for the hydrogen production unit, are listed below:

  i.   The sulphur removal process can be ignored
  ii.   The yields will be similar to what was reported [132], even though the steam/ C molar ratio was changed
  iii. 75% of the CO is converted in the HT shift reactor
  iv.   No other chemical reactions will occur in the HT shift reactor.
  v.   Residue formation on the catalyst can be ignored.
  vi.   Yields and operating conditions for the reformer & HTS are similar to conditions reported by [132].

5.3.4 Hierarchy A7000 – Steam cycle

The steam cycle was developed together with the pinch analysis, where either high quality excess heat, or large heat availability, was reserved for use to heat water for steam production to eventually generate electricity. The steam cycle consists of water preheating in streams 7001, 7003, 7006, 7009 and 7012, which utilizes high availabilities of process heat at low quality that are then fed to a steam boiler, where further heating is possible due to the high quality heat available. The water is pre-heated (with low quality heat) in parallel to ease the logistics and decrease piping costs on the plant, but more importantly, to allow for water heating to be accomplished without the risk of inadequate temperature difference should some of the process streams go off specification. Pre-heating occurs in HX-3001-, HXB3004-, HXB2004, HXB1002 and HXB3012, whereafter it is mixed before being fed to the steam boiler. Mixing is required to obtain a uniform temperature. The steam boiler is modelled as HXB3001-, HXB3009-, HX4003- and HX4002-, coupled to HXB3001, HXB3009, HX4002+ and HX4003+ respectively, in a similar manner as was used in the previous model [103].

Assumptions include that the water to be heated, is supplied at 25°C and 1.01 bar. The water is then pumped to a final pressure of 105 bar, this is done to avoid unnecessary repetitive vaporization during pre-heating. Partial or total vaporization will result in a larger pipe size which will lead to additional costs. All low quality water flow rates were determined to ensure that the pre-heated water is below the point of vaporization, which occurs at 314°C for 105 bar water. The total heat available in the steam cycle was used to determine the quantity of water that can be heated to 500°C. Set flow rates for streams 7003, 7006, 7009 and 7012 were determined, to produce pre-

159

heated water below the point of vaporization. The flow-rate of an additional stream, stream 7001, is determined from a design specification, BFWATER. It determines the quantity of additional water required to produce steam at 500°C and 105 bar, by utilizing all the heat that is available in the steam boiler by changing the flow-rate of stream 7001 and determining if the final steam temperature is at 500°C. A total quantity of 382 tons/h of HP steam is produced in the steam cycle. Closed loop cycles are often used for electricity purposes, although in this model an open loop system was considered. Should a closed loop system be desired, make up water will have to be added since some of the steam is used in the process. Additional utility requirements for cooling of the LP steam to re-use as water feed for steam generation will also have to be considered, which will have an impact on the cooling water requirements.

5.3.5 Hierarchy B4000 – Electricity Generation

Electricity can be produced as a co-product due to high process temperatures and excess heat. The excess heat is used for steam generation in A7000. Electricity is generated from the superheated steam in unit B4000. The superheated steam at 105 bar and 500°C, and is expanded in a series of turbines. The extent of superheating is 186°C, which corresponds to the literature range of 150°C to 250°C [103], [143] and [116]. The system used is a Condensing Extraction Steam Turbine (CEST) system. This system was selected since it is more efficient than the BPST and has the advantage that it can be arranged to give steam conditions similar to what the plant requires [163], [165], [162]. The CEST system consists of three turbines, the HP turbine, the MP turbine and the LP turbine, units T-B4001, T-B4002 and T-B4003 respectively. The interstage conditions were determined such that the steam requirements of the plant can be met, while simultaneously ensuring that the final product does not contain a vapour fraction >85wt% [143]. The HP turbine expands the steam to 49 bar and 400°C, followed by steam extraction for the steam reformer and distillation. The remainder is expanded in a MP turbine to 10 Bar (typical of MP steam, [117]) and 225°C, followed by final expansion in a LP turbine to 2 Bar (typical of LP steam [117]) and 120.3^{o}C. All turbines had a mechanical efficiency of 0.98 [143] with the isentropic efficiency of 0.84 [143], 0.85 and 0.85 [102] for the HP, MP and LP steam turbines respectively. The vapour fraction at the LP exit is at 97%, larger than the lower limit of 85% used elsewhere [143]. The LP steam produced can possibly be used elsewhere in the plant as utility.

5.3.6 Hierarchy A8000 – Utilities

The net utilities of the plant are the difference between the requirements and the generated utilities. The net value was determined by combining the individual utility streams in a Mixer units, MIXER, in Aspen Plus®, similar to what was done previously [103]. This approach was followed for the following utilities: Work (electricity), cooling water, distillation water, HP steam, fuel and LP steam.

5.3.6.1 Utilities: Cooling water and chilled water

The cooling water tower was assumed to supply CW at 27°C and receive hot cooling water between 45-52°C [144]. The cooling water flow rate is the sum of all the cooling water returned from the equipment. This includes streams CWA5001O, CWB2005O, CWB3005O, CWB3006O and CWDIST. The flow rates for streams CWB2005O, CWB3005O and CWB3006O are calculated in design specifications CW2005, CW3005 and CW3006 respectively. These design specifications function in a similar manner. The temperature of the returned cooling water will either be at the CWR temperature, since the mass flow of the cooling water can be manipulated to ensure this occurs, or it will be at a temperature 10°C less than the hot inlet temperature (due to a minimum temperature approach of 10°C being the limit). The design specifications manipulate the flow rates (CWB2005I, CWB3005I, CWB3006I) to ensure the temperature of the cooling water outlet (cold outlet) is either equal to the

assumed CWR temperature, or equal to 10°C less than the process stream inlet (hot in), whichever one is at a lower temperature. In all of the design specifications mentioned above, the minimum temperature approach of 10°C was lower and preference was given to this limit.

The cooling water required for distillation was determined from literature at 310 imperial gallons/ton fed for distillation [139], or equivalently 1.4m^{3}/ton distillation feed. The cooling water requirements for distillation, stream CWDIST, is calculated in calculator block, DISTIL. The calculated value is based on the feed stream B2016. For conversion from volume to mass cooling water, a water density of 992.026 kg/m^{3} was used, corresponding to the supply cooling water conditions in the plant.   A total of 21.47 ton/hr of cooling water is required for distillation purposes.

The cooling water losses occur due to vaporization, drift and blowdown. The CW loss due to drift and blowdown, can be assumed at 0.3% and 3% of circulated water, respectively, from Table 20. The make-up water required can then be determined from Equation 18 with the cooling water requirements for the process available from the simulation model, in stream HOTCW. This equation is used in calculator block, W-CW, to calculate the make-up water, stream MAKEUPCW at 6.88 tons/h. The evaporation loss, EVAPLOSS, is incorporated into the model by calculating the vapour fraction in cooling tower, CWT-8001, in calculator block W-CW. This is calculated as the evaporation loss divided by the circulating flow, stream CWCIRC. The cooling tower is modelled as a flash vessel, FLASH2 in Aspen Plus®, with specified outlet temperature of 27°C and the vapour fraction calculated in W-CW. The other losses, drift and blowdown, are accounted for in stream DRIFLOSS and BLOWDOWN at 0.353 tons/h and 3.528 tons/h respectively. The CWUTIL stream is the cooled water supplying the plants` cooling water requirements, excluding losses, and it must be equal to stream HOTCW at 110.68 tons/h. The cooled water is fed to process equipment and is returned in streams CWA5001O, CWB3006O, CWB3005O, CWB2005O and CWDIST.

To ensure that all vapours are removed and that only noncondensable gases remain, the bio-oil is cooled with chilled water, CHW6001I, to minimize the noncondensable gases. The chilled water enters at 4°C [103] and experiences a temperature rise of 8°C [104]. As a conservative approach, a water loss similar to that of the cooling water was assumed, amounting to 6.2wt%. The total chilled water that needs to be refrigerated (CHW), is the sum of the chilled water required, stream CHW6001I and the 6.2wt% loss, stream CHWLOSS, giving a total of 191.16 tons/h. HX-8003 is only used for modelling purposes to calculate the duty for cooling the water from the returned 12°C to the supply temperature of 4°C. The duty, QCHW, is used in calculator block, W-CHW, to determine the electrical requirements, WCHW, assuming a conservative performance with a COP of 3 [148].

5.3.6.2 Utilities: Electricity

The net power of the plant is the power difference between the power required to run equipment such as compressors, pumps, the WESP, the grinding and the electricity generated by the expansion turbines. The net value was determined by combining all work streams in MX-8001.

The electrical requirements for all equipment utilizing electricity were considered. This includes the following work streams from compressors or fans: WCPA3001, WCPA4001, WCPA6001, WCPB3001, WCPB3002, WCPB3003 and WCPB3004 as well as work requirements from pumps: WPA5001, WPA7001, WPA7002, WPA7003, WPA7004, WPA7005, WPA7006 and WPB1001. Since distillation and its utilities were not modelled in detail but on a mass feed basis, an additional electricity requirement for distillation had to be considered in work stream WDISTIL. The cooling of returned cooling water also has associated electricity requirements for the equipment, such as the pumps and

fans associated with the cooling process; represented by work stream WCW. Other equipment that will have a significant electricity requirement were identified as the Electrostatic Precipitator ES-3001 and grinding of the wood feedstock in work streams WESP and WGRIND respectively.

The distillation electricity requirement, WDISTIL, accounts for the electricity requirements of pumps and is determined in a calculator block, DISTIL. The electricity requirements for a unit containing both an atmospheric and a vacuum distillation column is reported at 8.7 kWh/ton fed, calculated on a stream B2016 feed basis [139]. This amounted to an electricity requirement of 0.134 MW.

The electricity requirement for grinding, WGRIND, was determined with a calculator block, W-GRIND, and the electricity requirement for the WESP was determined from a calculator block, W-ESP.

The power demand associated with grinding was taken into account at a value of 50kWh/dried ton for final sizes of <2 mm [104]. This was determined using a calculator block (W-GRIND). The calculator block used the dried biomass flow-rate in stream 1005 to determine the electricity requirements in stream WGRIND, at 4.96 MW. The electricity requirements for the Electrostatic Precipitator was calculated at 5.17×10^{-4} kW/actual cubic feet per minute fed, corresponding to 1.095KJ/actual m^3 [104]. The gas fed to ES-3001 in stream A3005 is 133.3 km^3/hr. The electrostatic precipitator`s electricity requirements could therefore be determined as 0.041 MW. The actual gas flow was imported as a fixed value into the design specification, since the software imports the standard conditions volumetric flow rate. The implication is that should the flow rate to ES-3001 change, the actual volumetric flow rate in calculator block, WGRIND, should be changed manually.

The cooling water and chilled water electricity requirements, WCW and WCHW, were calculated in calculator blocks, W-CW and W-CHW respectively. The power requirements for cooling water are typically associated with fans and pumps [145]. To determine the power requirements associated with the cooling tower and the process of cooling and transporting the water, equation 19 was used and an average COP of 7 was assumed, similar to previous studies [147], [115]. The power requirements (stream WCW) were calculated to be 0.015 MW. The chilled water electricity requirement was determined in a similar manner to that of the cooling water, with an assumed COP of 3 [148]. This resulted in a power requirement of 0.30 MW in stream WCHW.

An electricity contribution was made by the turbines in the following streams: WTB4001, WTB4002 and WTB4003. This resulted in a 19.9 MW, 28.7 MW and 21.9 MW contribution respectively. A net electricity co-product of 46 MW is available to be put onto the grid or sold.

5.3.6.3 Utilities: Steam HP

The utility steam for a combined atmospheric and vacuum distillation unit is reported at 0.09mmBTU/ton distillation feed or equivalently 94.955 MJ/ton distillation feed [139]. The corresponding mass will depend on the conditions of the steam, although the steam conditions were not specified in the literature source. To determine the mass of steam required, steam at 400°C and 49 bar was assumed, as this corresponds to the conditions of the expanded steam leaving the HP turbine. The utility steam duty was calculated in calculator block, DISTIL, and exported to QDISTA. The exit temperature of the steam was assumed to be at 263°C as this is slightly above the saturation temperature of 49 bar steam. In order to determine the mass flow quantity of steam that corresponds to the calculated heating duty, QDISTA, a design specification, QSTMDIST, was used. This design specification varies the split fraction (in S-B4002) of steam exiting the HP turbine in stream B4004, and that is to be sent to distillation. Accordingly, this changes the mass flow of steam

162

in stream STMDIST, the feed to a virtual HX-8001. The split fraction is varied until the heat stream QSTMDISC, equals the calculated heat in stream QSTMDISB. The heat duty in stream QSTMDISC is determined from a temperature decrease in HX-8001 from 400°C to 263°C. This is simply a method to determine the mass steam requirement and not a representation of the actual plant. The steam utility was calculated to be 5.82 tons/h. The steam requirement is obtained from splitting the steam leaving the HP turbine, with stream B4005 used for distillation heating purposes.

5.3.6.4 Utilities: LP Steam

After expansion through the turbines, the LP gas can be used as heating utility in the process or condensed to water to be used in the steam cycle. In this model, the LP steam is used as heating utility. One of the main opportunities available in the process to utilize the LP steam, is for heating utility in the PSA`s, PS-B3001 and PS-B3002. An operating pressure and duty requirement of 8.9133 MJ/ton feed has been reported [127]. The required duty, stream QPSAA, was calculated in calculator block: PSA. The energy requirements associated with a PSA unit consisting of four vessels, were reported by Spath et al. [127] to be 8333BTU/kg feed, this was normalized to the feed in order to use this for utility calculations in this model. The duty was calculated based on the combined PSA feed, streams B3021 and B3014, and amounted to 343 MJ/hr. To determine the equivalent amount of LP steam required, a design specification, QPSA, was used. A fraction of the LP steam, stream B4008, is used to provide duty for the PSA. The calculator block determines the duty provided in the heat exchanger, HX-8002, and manipulates the stream split fraction in S-8002, to have the duty available from cooling in the heat exchanger equal to the requirements for the PSA (stream QPSAC equal QPSAB). The heat exchanger is used to calculate the steam requirements for the PSA systems. In the heat exchanger the steam condenses to form water at 2 bar and 115°C. The quantity of LP steam required was determined as 0.174 ton/hr. The remaining LP steam, LPTOT, is 330 tons/h.

5.3.6.5 Utilities: Fuel

The fuel utilities only include the natural gas required for heat (combustion). It does not include the natural gas required for reforming, as it is a reactant in reforming. Fuel is required for distillation and for combustion of the PSA offgas.

 The fuel requirements for distillation have been reported as 633 MJ/ton feed to distillation [139]. Since the fuel is reported on an energy basis, conversion to a mass basis is needed. This was accomplished by simulating a virtual combustor, CB-8001, where the natural gas, stream FUELDIS, is fed at 25°C and 1 atm to be combusted with an excess of air, AIRDIS, to insure a 6wt% of oxygen present in the flue gas. The combustor was modelled as a RSTOIC reactor with the combustion reaction automatically calculated. In literature, the cold streams leaving the furnace are typically at 371°C, [139], although as a safety factor, a 35°C minimum temperature was added, to yield an exit temperature of 406°C. For modelling purposes, the virtual combustor will be operated at 406°C and heat is removed to insure this. The heat available, stream QFLDISC, must equal the required duty for distillation, 633 MJ/ton distillation feed. This is accomplished by changing the quantity of fuel required, stream FUELDIS, in design specification QFLDIST, such that heat stream QFLDISC equals QFLDISB. The quantity of fuel required was calculated to be 0.27 tons/h.

As mentioned, fuel is also required for supplementing the PSA offgas to provide heat for hydrogen production. The PSA off-gases and the distillation light stream are combusted in CB-3001, however the contribution of PSA offgas is limited due to combustion problems. For this reason, the available PSA offgas needs to be supplemented with natural gas, in stream B3028. The quantity of this stream is calculated from design specification, NGFUEL, as previously discussed. However, this fuel requirement also needs to be included in the total fuel requirements. A calculator block, DISTIL, sets

FUELH2PR equal to stream B3028. The fuel requirement to supplement the PSA offgas for hydrogen production is accounted for in the total fuel requirements by adding stream FUELH2PR to FUELDIST. The total fuel requirement is the combined distillation and fuel for combustion to produce hydrogen requirements. Stream FUELTOT represents this total with a value of 2.644tons/h.

5.3.6.6 Utilities: Distilled water

From literature, the quantity of distilled water for distillation purposes has been reported as 20 imperial gallons/ton feed to distillation or equivalently 0.0909m^3/ton feed to distillation [139]. The quantity of distilled water was calculated in calculator block, DISTIL, and based on a distillation feed stream B2016. The conditions of the distilled water is not specified in the literature source, therefore a density of 970.5 kg/m^3, corresponding to water at 49°C and 1.03 bar, was assumed. Total distilled water requirements were calculated to be 1.4 tons/h.

5.4 Results and Discussion

5.4.1 Model verification

The model is verified by comparing the yields and operating parameters of the main equipment in the simulation model to the experimental literature on which the model was based. Generally a deviation of 10% on a mass balance basis is acceptable [60].

Table 71 demonstrates the deviations on the major equipment`s (R-B1001 and R-B2001) operating conditions. The deviation on the overall phase yield and fuel yields are less than 10%, indicating that the model and the literature data compare favourably. A minor deviation is observed for the temperature in R-B2001, with a 5.6^{o}C temperature difference. A design specification was initially used to fix the reactor temperature at 405°C, however it had to be removed during heat integration, resulting in a slight deviation of the reactor temperature. The greatest deviation occurred for the excess hydrogen fed to R-B2001, with a deviation over 9%. Literature reports the excess hydrogen to the hydrotreating reactor, but not to the hydrocracking reactor. It was assumed that similar excess requirements will be needed for both reactors, based on the moisture free feed. Since this value is only an assumed value, a larger deviation is acceptable. Due to non-ideal phase separation occurring in the flash drums, F-B1001 and F-B2001, the components that were specifically selected to represent a certain group (aromatic, aliphatic etc.) in a specific phase (gas, liquid etc.) do not elute as desired. This results in the phase yields deviating from the literature values - the cyclohexane flashes in the flash drums and does not elute as an aliphatic light component, which is the category for which it was initially selected, causing the product yield for aliphatic lights to be less than the literature values. In order to validate the model, based on the components selected, ideal separation was assumed and the phase yields for this case were considered. Deviations for the simulation model ranged from 2.3 to 7.6% for aqueous phase and gas phase respectively, although for the case assuming ideal separation, the maximum deviation from the calculated literature values is 4.5% for the solids, with the final product oil deviating only 3%. However, due to complicated phase separation taken into account by the Aspen Plus® software (which was not accounted for in the determination of component selection), this deviation increased to 5.2% for the actual simulation.

The distillate fractions` yields show the highest deviation for naphtha, at 7.4%. This is attributed to some of the naphtha components eluting in the flash columns with the gases, causing the amount of these components to be distilled to decrease, resulting in a decreased quantity eluting in the naphtha fraction. An example of this, is 1,3 cyclohexadiene and the 3 methyl heptane. The other distillate fraction yields are all below 5%, which are considered to be an acceptable deviation.

164

Table 71 Model verification for operating conditions for hydrotreating upgrading process

	Experimental data from literature used as basis for simulation model		Simulation Model	Deviation
	Christensen et al. [15]	Elliott et al. [16]		
R-B1001				
R-B1001 Temperature	-	340° C	339.7^{o}C	0.1%
R-B1001 Pressure	-	2000psig (138.91bar)	2000psig (138.91bar)	0%
H$_2$ consumed [%wt H$_2$/ wt BO fed]	-	1.57[a]	1.57	0.3%
H$_2$ consumed [%wt H$_2$/ wt moisture free BO fed]	-	1.99[a]	2.05	3.0%
H$_2$ excess fed (R-B1001) [%wt excess/wt BO fed]	-	13.74[a]	13.24	3.6%
H$_2$ excess fed (R-B1001) [%wt excess/wt moisture free BO fed]	-	17.38[a]	17.30	0.5%
R-B2001				
R-B2001 Temperature	-	405°C	399.4^{o}C	1.4%
R-B2001 Pressure	-	1500 psig	1500 psig (104.435bar)	0%
H$_2$ consumed [%wt H$_2$/ wt oily phase from hydrotreating fed]		3.07[a]	3.21	4.5%
H$_2$ consumed (R-B2001) [%wt H$_2$/ wt moisture free oily phase from hydrotreating fed]	-	3.15[a]	3.30	4.6%
H$_2$ excess fed (R-B2001) [%wt excess/wt oily phase from hydrotreating fed]	-	16.92[a]	15.34	9.4%
H$_2$ excess fed (R-B2001) [%wt excess/wt moisture free oily phase from hydrotreating fed]	-	17.38[a]	15.78	9.2%
OVERALL PHASE YIELDS				
Wt% Gas produced [wt gas/(wt bio-oil+ H$_2$ consumed)]	-	6.02[a]	6.48 / 5.77[b]	7.6% / 4.2%[b]
Wt% Aqueous phase produced [wt aqueous /(wt bio-oil+ H$_2$ consumed)]	-	57.98[a]	59.31 / 59.43[b]	2.3% / 2.5%[b]
Wt% Solids produced [wt solids/(wt bio-oil+ H$_2$ consumed)]	-	7.78[a]	7.46 / 7.42[b]	4.0% / 4.5%[b]
Wt% Final Oil produced [wt oil/(wt bio-oil+ H$_2$ consumed)]	-	28.22[a]	26.74 / 27.38[b]	5.2% / 3.0%[b]
OVERALL HYDROCARBON PHASE FUEL FRACTION YIELDS [wt% based on BO feed stream]				
Fraction yields : Lights	4.03	-	3.92	2.8%
Fraction yields : Naphtha	8.77	-	8.12	7.4%
Fraction yields : Jet	6.39	-	6.11	4.3%
Fraction yields : Diesel	5.98	-	5.74	4.1%
Fraction yields : Gas oil	3.12	-	3.76	4.1%

[a] Calculated from [16], [b] Values calculated if intended /ideal separation was achieved in process units in simulation model, [c] Calculated on lights and pre-flash lights

In Table 72, the elemental composition of the distillate fuel fractions from the simulation model are compared with experimental results reported in literature. Comparison of this indicates whether appropriate components were selected to represent the different fractions. From Table 72, a deviation can be seen between the model and the literature data`s oxygen content in the distillation lights. The main reason for the discrepancies, is due to the gases (formed during hydrocracking) dissolving in the product stream of R-B2001; especially a large quantity of CO_2 and a smaller fraction of the CH_4. These gases cannot be removed using flash drum, F-B2002, as they are dissolved. Almost 5% of the CO_2 present in the R-B2001 product enters the distillation feed in stream B2016. When ignoring the dissolved gases' contribution to the lights distillation fraction, the elemental composition closely resembles that of literature, with a difference as little as 0.1wt% for C and H. The H/C ratio`s also compare well. Differences between the simulation model and the literature for the O/C ratio of the lights are significant, although when excluding the dissolved gases in the lights distillation fraction, the ratio is the same as literature, at 0.003. Other characteristics include the aromatic C%, which also compares favourably; the jet, diesel and gas oil are comparable up to 0.01. Slightly larger differences are observed for the lights and the naphtha fraction, with differences of 0.12 and 0.03 respectively, corresponding to deviations of only 1.7% and 0.2%.

Table 72 Model verification of the distillate fractions` yields

Characteristics	Lights		Naphtha		Jet		Diesel		Gas Oil	
	[a]	Model [c]	[a]	Model [c]	[a]	Model [c]	[a]	Model [c]	[a]	Model [c]
C	85.2	84.09 (85.08) [b]	86.3	86.39	87.0	87.00	88.1	88.13	88.2	88.16
H	14.5	14.37 (14.61) [b]	13.3	13.37	12.3	12.30	11.4	11.37	11.4	11.44
O	0.3	1.53 (0.31) [b]	0.3	0.24	0.7	0.70	0.5	0.49	0.4	0.40
Water	-	0	-	0	-	0	-	0	-	0
H/C [mole]	2.04	2.036 (2.046) [b]	1.85	1.844	1.70	1.685	1.55	1.537	1.55	1.547
O/C [mole]	0.003	0.014 (0.003) [b]	0.003	0.002	0.006	0.006	0.004	0.004	0.003	0.003
Aromatic C% [mass basis]	7.1	6.98	13.1	13.07	20.0	20.01	29.4	29.40	27.8	27.80
Aliphatic C% [mass basis]	92.9	93.02	86.9	86.93	80.0	79.97	70.6	70.60	72.2	72.20

[a] Experimental value normalized from [15], [b] calculated excluding gases formed in hydrotreating or hydrocracking process, [c] From Aspen Plus® simulation model, - not reported

Overall it can be concluded that the simulation model is a good representation of experimental data obtained for the process, since deviations are in all cases less than 10%.

5.4.2 Mass balances – overall yields and consumption

A summarized mass balance of the simulation model can be viewed in Table 73. The additional natural gas fed for the PSA offgas combustion and the air supply for combustion are not accounted for in the summarized mass balance. More detailed mass balances are provided in Appendix E. By-products such as char, pyrolysis offgas and upgrading offgas are used for heating purposes. The lights and pre-flash lights streams are also used for heating purposes in this model.

Table 73 Summarized mass balance for model

Mass flow description	Unit: tons/h
FEED	
Biomass (dry)	92.0
Natural Gas feed for H_2 production	9.2
Water in biomass	92.0
Steam	45.8
Air (drying)	728.7
FUEL PRODUCTS	
Bio-oil	16.7
Total pre-flash lights & lights	2.2
Naphtha	4.5
Jet	3.4
Diesel	3.2
Gas Oil	2.1
DIRECT* WASTE PRODUCT STREAMS	
Offgas (from pyrolysis)	12.1
Offgas (from upgrading)	5.4
Offgas (from H_2 production)	51.6
Char	14.7
Total waste water (from upgrading)	34.1
Total coke (from upgrading)	4.3
Moisture & drying air	813.4

*Before combustion /utilization of waste streams

Since the pre-lights and lights streams are used for heat generation, these streams are not accounted for in the total fuel products. From Table 73 the total fuel products amount to 29.9 tons/h (excluding pre-lights and lights) for a 92 dry ton/hr facility, which is a 32.5 wt% (dry wood basis) and 16.3% (as received biomass moisture content of 50wt%) yield of fuel products. The aromatic and aliphatic fractions of the final product distillate fractions are reported in Table 74. The focus of this study is the jet fuel production and the aromatic content present in it. In the simulation model a total of 3.4 tons/h of the jet fraction is produced, with the maximum possible yield at 4.6 tons/h. This corresponds to yield of 3.7wt% of dry biomass converted to jet fuel, with the maximum possible at 5wt% (dry biomass). In the simulation model, the aromatic jet fuel stream produced is 0.7 tons/h, with the maximum achievable of 0.9 tons/h, had a fraction of the bio-oil not been used for heat generation. The jet fuel aromatic product, produced in the simulation model, is only 0.76wt% of the total dry biomass feed and can yield a theoretical maximum of 0.97wt% of the dry biomass feed. The low jet fuel yield and the low jet fuel boiling range aromatic yield, respectively 3.7wt% and 0.67wt% on dry biomass feed, show this process has a low selectivity for converting biomass solely to jet fuel and jet fuel boiling range aromatics.

For a more effective use of the biomass, it is necessary to utilize the other fuel fractions in order to minimize waste and to maximize profit. The naphtha (4.9wt% on dry biomass basis), diesel (3.5wt% on dry biomass basis) and gas oil (2.3wt% on dry biomass basis) fuel fractions therefore also need to be considered as final products to increase the effectiveness of this process. However, if the naphtha, diesel and gas oil fractions do not meet the required specifications, they will require further upgrading (which will add to the utility requirements), or should be utilized for heat application to produce electricity. The total fuel yield is 16.7wt% on a dry biomass basis**.** The maximum achievable

fuel is 22.7wt% of the dry biomass. This is low and can only be justified if the final product value compensates for this low yield.

The maximum achievable is lower than the reported mass yield of 27.5wt% for refined hydrocarbons [84]. A noteworthy difference between the study by Bridgwater (1996) and this study, is the extent of hydrodeoxygenation. The extent of hydrodeoxygenation for the study by Bridgwater (1996) was 98%, although in this study, hydrodeoxygenation of 99.1% was used. Previous studies have reported yields of 31.6wt% of bio-naphtha (98% deoxygenated) and 28.4wt% diesel/refined bio-naphtha [58]. This is significantly higher than the maximum determined in this model (22.7wt%). Differences are attributed to two factors; the bio-oil yield for their study was 80.4wt% (on dry basis) compared to 78.7wt% (on a dry basis) for this model, and secondly the extent of hydrotreating is less. The bio-naphtha is only 98% hydrotreated compared to 99.1% in this study. The non-hydrocarbon content in the final product in the kerosene fraction should be as close as possible to 0.00wt%, as the ASTM D7566-11 Specification for FT-SPK or HEFA-SPK requires hydrocarbons to be present from 99.5wt% to 100wt%. This roughly translates to a maximum possible oxygen content of 0.05wt% (based on a simple mass balance and ignoring any other fuel specifications). The reported mass ratio for the production of HDO from hardwood, is ca. 28% [5]. This is near the value calculated in this model.

When considering the waste produced, excluding the air used for drying and the biomass moisture removed, the waste amounts to 122.1 ton/h for a 92 dry tons/h (184 wet tons/h) facility, see Table 73. The waste from hydrogen production performed on site (this includes unreacted steam, CO, CO_2 and CH_4 removed when purifying the hydrogen) is the largest contributor at 42.2%. Hydrogen from a supplier can reduce the amount of waste generated, however operating costs and feedstock costs will increase. The second largest contributor to waste is the waste water at 30.3%. This can be attributed to the following: (1) water being present in the initial biomass fed, (2) pyrolytic water formation during pyrolysis and (3) much of the oxygen reduction is removed in the form of water. Unfortunately the water contains a large amount of dissolved hydrocarbons. This can be seen when looking at a carbon balance on the process, see Table 75.

Table 74 Aromatic and aliphatic yields for distillate fractions

Distillate fraction	Model			Maximum		
	Aromatic [ton/h]	Aliphatic [ton/h]	Total* [ton/h]	Aromatic [ton/h]	Aliphatic [ton/h]	Total [ton/h]
Pre-flash lights and lights	0.1	2.1	2.2	0.2	2.7	2.9
Naphtha	0.6	4.0	4.5	0.8	5.5	6.3
Jet	0.7	2.7	3.4	0.9	3.7	4.6
Diesel	0.5	2.7	3.2	0.7	3.7	4.3
Gas Oil	0.6	1.5	2.1	0.8	2.1	2.8

* Difference between total and the sum of aromatics and aliphatics is due to rounding off

In the pyrolysis section, Section 3.2.4.6 Calorific value analysis, the Boie correlation accurately calculated the HHV of the bio-oil, indicating that the carbon content can be used as an indication of the energy in the fuel [114]. A carbon balance was performed as indication of the energy distribution. Unfortunately the carbon transfer to fuel products is quite limited at 36.2wt%, with the carbon transfer to the waste streams at 63.8wt%. The carbon present in the aqueous waste streams, is 10.8wt% of the total carbon entering the process. It is the equivalent of 12.2wt% of all the carbon

entering in the dry biomass. Table 75 shows that the largest loss of carbon is through the char produced from pyrolysis, at 24wt%. Although this does not contribute towards the final fuel products, it is still useful in that it can provide heat, which is a necessity for pyrolysis and for natural gas reforming. The offgas products from natural gas reforming also have a significant carbon waste at 11.9wt%. Similar to char, the 10.6wt% carbon lost in the gases (pyrolysis by-product, hydrotreating by-product) can be used for generating heat required in the process. Almost half (54%) the carbon present in the waste/by-products can be used for heat generation; this corresponds to 34.6wt% of the total carbon feed.

The biomass supplies 88.1% of the carbon (reactant) feedstock in the process, with the remainder supplied by natural gas for reforming. A comparison with literature indicates that the ratio of carbon in biomass to the natural gas fed, is similar with reported values of 88% and 12% carbon in the biomass and natural gas feedstock's respectively [57]. However, differences between this model and literature studies were observed for the carbon transfer to the fuel- and waste-products. In a study by Jones et al. [57], the total fuel pool contained 55% of the carbon and the waste products only contained 45% of carbon fed [57]. This difference is the result of differences observed at the pyrolysis unit exhaust, which contain 23% of carbon fed, whereas in this study`s model, the total carbon waste for pyrolysis unit is 31.4%. Another significant difference is the amount of carbon lost in the waste water produced from upgrading; with 0wt% and 10.8wt% for the study by Jones et al. [57] and this study respectively. The reformer exhaust was reported to contain 20wt% carbon fed. However, in this study it only contains 11.9wt% of the carbon fed.

Table 75 Carbon balance on model

Material Stream	Wt% C
FEED = 100.0%	
Biomass Feed (dry)	88.1
Natural gas (for H_2 production)	11.9
FUEL PRODUCTS = 36.2 %	
Bio-oil	13.0
Pre-flash lights	0.1
Lights	3.1
Naphtha	6.8
Jet	5.1
Diesel	4.9
Gas Oil	3.2
WASTE PRODUCTS = 63.8 %	
Pyrolysis Char	24.0
Pyrolysis Gases	7.4
Hydrotreating Gas	1.2
Hydrotreating Aqueous	8.5
Hydrotreating & hydrocracking coke	6.4
Hydrocracking Gas	2.0
Hydrocracking Aqueous	2.3
Natural gas (for H_2 production) offgas products	11.9

Looking at the overall results of the mass balance, the mass yields of jet fuel and jet fuel boiling range aromatics show the process is not selective towards the conversion to jet fuel and jet fuel aromatics. Utilization of the remainder of the fuel fraction will increase the effectiveness of the process,

although even the maximum achievable yield for this process is still low. Except for the mass balances, energy efficiency should also be considered, as a low fuel yield is not necessarily indicative of a poor energy transfer to the fuel. The energy efficiency will take both the mass yields and the energy content of the final fuels into account and is a better indication of the effectiveness of the process, see Section 5.4.6 Energy Efficiency.

5.4.3 Comparison of simulated fuel properties with experimental properties and jet fuel specifications

Estimated bio-oil properties from the simulation were compared to experimentally determined bio-oil properties from Section 3.3.3 Product analysis and characterization, to indicate how well the model represents bio-oil. In addition to this, the estimated jet fuel properties from the simulation were compared to jet fuel specifications (ASTM D7566 and DEF STAN 91-91).

The density, the moisture content and the HHV from the simulation model were compared to the results from the experimental bio-oil analysis and characterization, see Table 76. The simulated bio-oil`s HHV was slightly higher compared to the experimentally produced bio-oil (24.3 MJ/kg compared to 19.3-23.6 MJ/kg). The simulated bio-oil`s density of 1209kg/m^3 was within the experimentally determined bio-oil densities of 1201-1251kg/m^3, presented in Section 3.2.5.4 Density Analysis. The moisture content of the simulated bio-oil and the experimentally produced bio-oil compared well, since the simulated bio-oil moisture content of 23.5wt% falls within the experimental range of 18.7-35.3wt%, reported in Section 3.3.3.1 Bio-oil Moisture analysis.

Table 76 Comparison between experimentally determined bio-oil properties and simulated bio-oil properties

Property	Units	Experimental bio-oil	Simulated bio-oil
Density	kg/m^3	1201-1251	1209[b]
HHV[a]	MJ/kg	19.3-23.6	24.3
Moisture	wt%	18.7-35.3	23.5

[a] Determined using the Boie correlation (Equation 12), [b] Determined as weighted contribution of individual components

Since the jet fuel from pyrolysis is not an approved fuel, the exact specifications it should meet is unclear. For a blend with conventional fuel, the final blend (consisting of both pyrolysis derived jet fuel and conventional fuel) will probably have to meet the SSJF specifications. In addition, it is expected that the pyrolysis derived jet fuel portion will have to meet the SPK specifications. The FSJF specifications are only applicable to a specific approved fuel (produced by Sasol), although its specifications give an indication of additional requirements. The required specifications for SSJF, SPK and FSJF were therefore considered, as it gives an indication of where the properties of the PTJ differ from other acceptable properties. Blending the pyrolysis derived jet fuel with conventional fuel to produce a SSJF will produce a final fuel with different properties compared to the simulated properties of the pyrolysis derived jet fuel.

Simulated jet fuel properties were obtained using Aspen Plus® property estimation D86 and FLPT-API to determine the distillation temperature for 10%, 50% and 90% recovered (D86-10, D86-50 and D86-90) and the flash point. The density was determined based on the weight contribution of each component, using reference densities from AspenPlus® and literature [235]. The results in Table 77 show the density from the simulated jet fuel fraction is higher than the SSJF specifications allow. The flash point was greater (42.4^{o}C) than the required minimum value of 38°C, yet smaller than the maximum of 50°C applicable to FSJF. Additional specifications only applicable to SPK fuel are the

170

distillation gradient between the distillation temperature for 50% recovered and 10% recovered (T50-T10) and the distillation gradient between the distillation temperature for 90% recovered and 50% recovered (T90-T50). Results for these properties indicated that the distillation gradient between the distillation temperatures for T50-T10 was lower than the required 15°C, at 0.7°C and the distillation temperature for T90-T50 was lower than the required 40°C, at 27.5°C. This is the result of having a limited number of model components with a narrow range of boiling points. When blending the PTJ-SPK with a conventional jet fuel with a broad boiling range, or with components more towards the diesel range, the distillation gradients will improve and then it might be possible to meet the SSJF specification. Should a fully synthetic jet fuel be pursued, and blending of PTJ-SPK and FT-SPK/HEFA-SPK be allowed, the distillation gradients might also improve. Ongoing research is in progress to consider the effect of distillation ranges on the lean blowout (LBO) of a gas turbine combustor [236]. Some studies have suggested that there is no correlation between the distillation gradients (T50-T10, T90-T10) and the LBO [236]. Should this be the case, then the specifications might become less strict in future.

The calculated LHV of 42.2 MJ/kg was lower than the minimum SSJF requirement of 42.8 MJ/kg. However, by blending with conventional fuel, the minimum requirement for a SSFJ can be met.

Table 77 Comparison between simulated properties of jet fuel fraction and jet fuel specifications

Property/ Specification	Units	Kerosene fraction (stream B2019)	SSJF [a]	SPK [a]	SSJF [b]	FSJF [b]
Density	kg/m^3	890.7 [c]	775-840 [d]		775-840 [d]	
D86-10	$^{\circ}$C	155.32 [e]	≤205		≤205	
D86-50	$^{\circ}$C	156.05 [f]	report		report	
D86-90	$^{\circ}$C	182.79 [g]	report		report	
T50-T10	$^{\circ}$C	0.7	-	≥15	≥15	≥10
T90-T10	$^{\circ}$C	27.5	-	≥40	≥40	≥40
Flashpoint	$^{\circ}$C	42.4 [h]	≥38		≥38	≤50
LHV	MJ/kg	42.2 [i]	≥42.8		≥42.8	

[a] [11] [b] [10], [c] Determined from weight contribution of individual component densities, [d] at 15 $^{\circ}$C, [e] Determined using D86-10 property estimation in Aspen Plus®, [f] Determined using D86-50 property estimation in Aspen Plus®, [g] Determined using D86-90 property estimation in Aspen Plus®, [h] Determined using property estimation FLPT-API in Aspen Plus®, [i] Determined LHV from HHV (Boie correlation)

The PTJ-SPK`s properties indicate that the jet fuel will not be able to meet the current SPK-specifications. However, should PTJ-SPK be approved, it will receive a different set of specifications, due to the difference in aromatic nature of PTJ-SPK, compared to the other SPK fuels. By blending the PTJ-SPK with conventional jet fuel, the final blend should be able to meet some of the SSJF specifications. A blend of PTJ-SPK and HEFA/FT-SPK will allow for a fully synthetic jet fuel that meets the aromatic and density requirements. Although the exact specifications for a PTJ-SPK is not available at present, the final SSJF and FSJF will not change and therefore it is worthwhile to examine the properties of a PTJ-SPK-and-conventional fuel blend, as well as a PTJ-SPK-and-FT/HEFA-SPK blend.

Although this does not have approval at the moment, a fully synthetic jet fuel can be produced by blending the PTJ-SPK (with a 20vol% aromatic content) with FT-SPK or HEFA-SPK (assuming no aromatics). Assuming the blend is in such a ratio as to meet the 8vol% aromatics in the final fuel, the PTJ-SPK contribution will be 40%. Such a blend will increase the LHV of the final fuel to 43.3 MJ/kg (assuming a LHV and density of 44.1 MJ/kg and 762 kg/m^3 for FT/ HEFA-SPK, [19]). This blend will

meet the current minimum criteria of 42.8 MJ/kg applicable to a FSJF. Such a blend will also be beneficial towards the final fuel density, since the high PTJ-SPK density and the low FT/HEFA-SPK density will complement each other to produce a fuel with a final density of 813.5 kg/m^3, which is within a current accepted limits (for SSJF).

5.4.4 Pinch Point Analysis Results

Heat integration has previously been done on the fast pyrolysis model [102–104].The heat integration using pinch analysis was therefore only performed on the HDO section, according to the methodology and fixed procedure described in literature [119], [117] and Section 2.4.4 Heat Integration – Pinch Analysis. In systems that are not closely situated, direct heat transfer might not be acceptable [237]. Since the fast pyrolysis and the HDO plants will in practice not be closely situated, performing heat integration between them will not be considered. The cold and hot composite curves show a cross at approximately 50.02^{o}C, see Figure 36. This is physically impossible and must be remedied by shifting of the cold composite curve to the right [117]. This is represented by the shifted cold composite in the diagram, which was shifted 247 262.7 MJ/h to the right to achieve the assumed DTmin of 30°C, as is used in the oil refining industry [118]. The hot pinch point can be observed at 370°C (to be exact, 369.7^{o}C), as can be seen in Figure 36. Excess heat is available to fulfil the requirements of the cold streams. Above and below the pinch point there are large quantities of excess heat that require external cooling, see Figure 37. Rather than cooling the hot streams using cooling water utilities, the excess heat that needs to be removed can be used for steam generation to allow co-production of electricity. Initially only the high temperature heat (at temperatures above the pinch point) was considered for steam production. This is similar to previous biofuel studies with co-generation and pinch point analysis [115], as shown in Figure 36 .
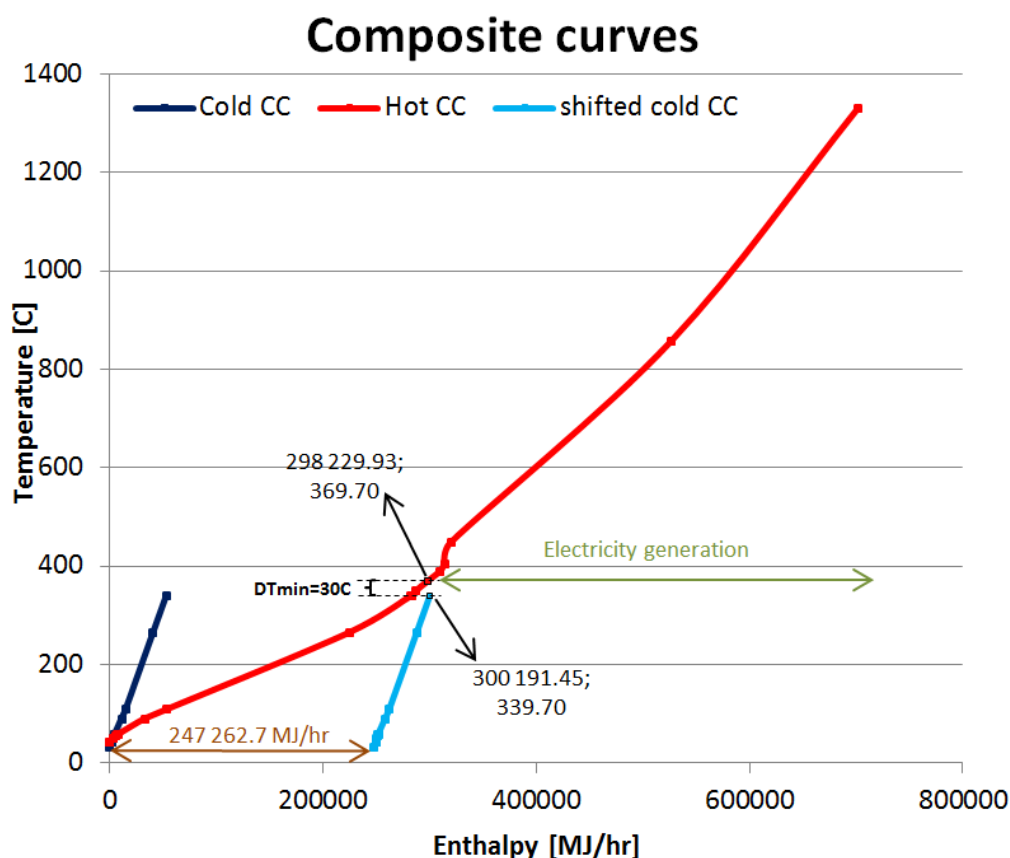
Figure 36 Composite curves of hot and cold streams
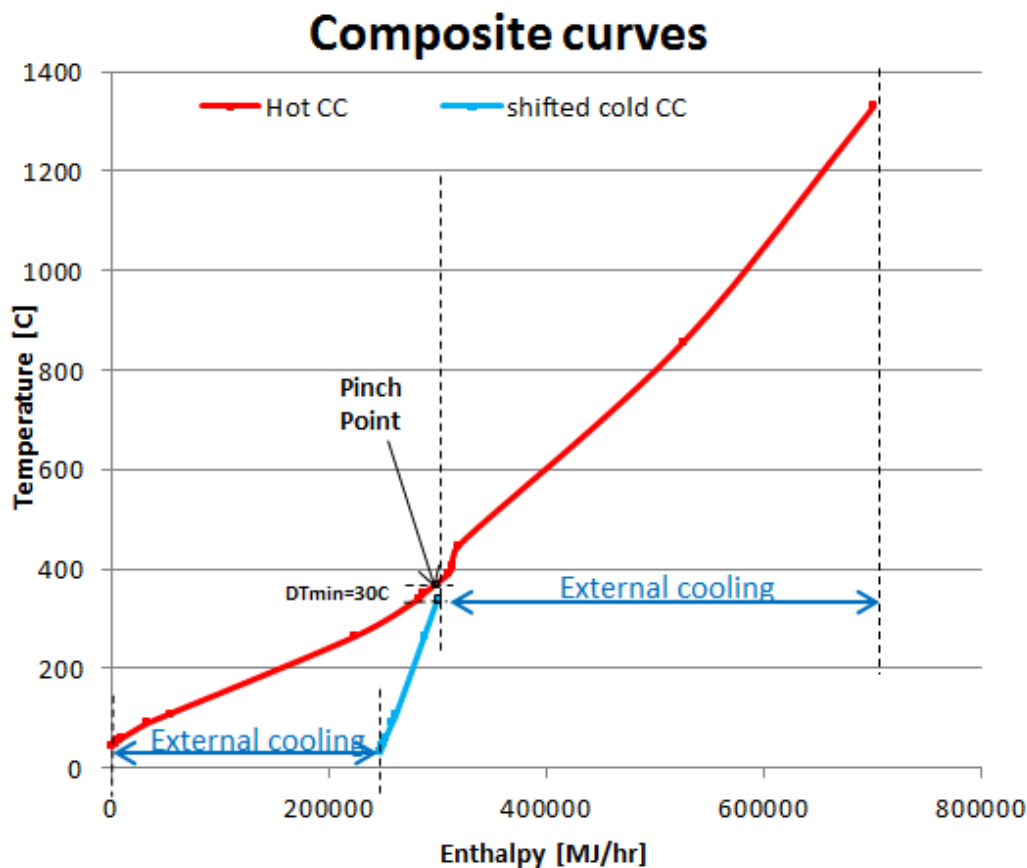
Figure 37 Composite curve external cooling requirements

The Heat Exchanger Network (HEN) was constructed using the prescribed guidelines from Section 2.4.4 Heat Integration – Pinch Analysis. A grid diagram was used to design the HEN. When constructing the composite curves, simplified values for the specific heat capacity at constant pressure (C_p) were used. From this, the temperature of the hot stream after heating the selected cold stream could be determined. Once this is applied in the simulation, the temperatures are not exactly the same as calculated using simplified specific heat capacity values, because detailed specific heat capacity values are used in the simulation software; true temperatures are indicated in brackets in Figure 38 and Figure 39. Rather than using cooling water as utility to decrease the temperature of high temperature streams, it is used for steam generation, see Figure 38. To investigate whether this approach, where low grade heat is utilized for water (steam) pre-heating, is worthwhile, two comparative scenarios were investigated. The only difference was that the low grade heat from process streams was used for initial steam pre-heating. In other words, the quantity of the same quality (500°C and 105 bar) steam that could be generated differed. The CEST system was exactly the same for both scenarios. The difference in amount of steam generated resulted in a difference in the amount of electricity generated. The results from this investigation were used to decide on the use of the cooling utilities vs water pre-heating on which the rest of the model was built.

Had electricity generation not been considered, the cooling utility would have amounted to 177 230kW. This can be reduced to 67 396 kW when the high temperature streams above the pinch and QHXB3002 below the pinch, further on referred as Case 1, are considered for steam production, see Table 78.

Duty stream in Aspen	Stream name	mCp [kW/K]	Enthalpy [kW]			Hot Pinch [C]	369.7				Enthalpy [kW]
QHXB3009	H1	102.73						447.9		1330.9	90706.85
QHXB3001	H2	37.70	742.76	350						857	18372.93
					353.70 C / (352.83)						
QHXB(2002 -2005)	H3	35.79	11443.25	50						405	1263.52
QHXB(3002-3005)	H4	83.73	27354.06	43	200.94C / (156.99)					390.2	1716.43
QHXB1002	H5	97.19	27503.55	57		340					
QHXB3012	H6	87.58	15327.21	90		265					
QHXB3006	H7	41.30	470.82	43.3		54.7					

						Cold pinch [C]	339.7		Above pinch [kW]	112802.48
									Below pinch [kW]	742.76
QHXB1001	C1	45.79	14129.94	31.1	339.7				Total for steam gen [kW]	113545.24
QHXB2001	C2	11.36	572.48	58.9	109.3				Cooling water utility [kW]	67396.47

Figure 38 Grid diagram for HEN (including steam production and large CW utility)

Even when considering all hot streams above the pinch and QHCB3002, the cooling water utility is still 3 143 tons/h. Circulation of the cooling water also has associated electrical requirements due to the use of pumps and fans used in cooling towers. In an attempt to decrease the cooling water utility further, steam generation from the streams above the pinch and QHXB3002, as well as streams QHXB2002, QHXB3003, QHX1002 and QHXB3012 were considered, further on referred to as case 2. Not utilizing the heat available in these streams for water pre-heating (to eventually use for steam generation), will result in a loss of 62 031 kW. A comparison between case 1 and case 2 indicated that the electricity generation increased with 15.4 MW, or 28.07% with a mere 90.3 tons/h of cooling water, which is only 2.87% of the CW requirements of 3 143 tons/h in case 1, see Table 78. Case 2 (compared to case 1) required two additional heat exchange units, see Figure 39. A trade-off exists between the capital cost of the two additional heat exchangers and its electrical requirements (e.g. pumping) for steam generation in case 2, and the higher operating cost of the larger CW utility (pumping, fans, etc.) and a higher capital cost to build a larger capacity cooling tower in case 1. These two cases need to be considered in detail to determine which case will be the best. Since capital cost is not considered in this study, the lower operating cost was selected (case 2). This investigation indicated that the use of low-grade heat for water pre-heating, for steam generation, was a viable option in terms of energy conservation.

Table 78 Comparison of small and large CW utility cases

	Case 1: Large CW utility	Case 2: Small CW utility
Streams considered	Hot streams above pinch + QHXB3002	Hot streams above pinch + QHXB3002 + QHXB2002 + QHXB3003+ QHX1002+ QHXB3012
Cooling requirements [kW]	67 396	1 655
Required CW (excluding distillation & Fast pyrolysis unit) [tons/h]	3 143	90.3
Heat used for steam production [kW]	113 545	175 576
Mass steam (@105bar, 500°C) [tons/h]	301.9	381.4
Electricity generated		
Electricity generated turbine 1 [MW]	15.68	19.81
Electricity generated turbine 2 [MW]	22.24	28.64
Electricity generated turbine 3 [MW]	16.94	21.81
Total electricity generated [MW]	*54.86*	*70.26*
Comparison from Case 1 to Case 2		
CW in case 2/ CW in case 1 [%]	2.87 %	
Increase in electricity generated [MW]	15.40	
Increase in electricity generated [%]	28.07 %	

In Figure 39 the final heat exchange network can be seen. Cold stream QHXB1001 is heated by stream QHXB3003, as the mC_p of the stream leaving the pinch is larger than that of the stream into the pinch and QHXB3003 is able to supply all the required heat for the cold stream. Cold stream QHX2001 is heated by QHX2002 for the same reasons. Although the remaining heat in QHXB3003 would also have been a sufficient supply of heat, preference was given to QHXB2001 as it is closely situated in the plant, where the product stream can be used to heat the inlet. Cooling water is used to cool streams QHXB2002 and QHX3003 to the final temperature. Since QHXB3004 is already at a low temperature with a small enthalpy, it will not be used for steam production and is cooled with cooling water. The final cooling water utility required was 1655kW or 90.3 tons/h for the available cooling water. The cooling water supply temperature was assumed to be at 27°C and the return temperature to the cooling tower at 49°C [117].

Duty stream in Aspen	Stream name	mCp [kW/K]	Enthalpy [kW]				Hot Pinch [C]	369.7				Enthalpy [kW]
QHXB3009	H1	102.73							447.9	1330.90	90706.85	
QHXB3001	H2	37.70	742.76	350						857.00	18372.93	
QHXB(2002-2005)	H3	35.79	11443.25	50	353.70 C / (352.83)					405.00	1263.52	
				55C								
QHXB(3002-3005)	H4	83.73	27354.06	43	200.94C / (156.99)					390.20	1716.43	
				55C								
QHXB1002	H5	97.19	27503.55	57		340						
QHXB3012	H6	87.58	15327.21	90		265						
QHXB3006	H7	41.30	470.82	43.3		54.7						
							Cold pinch	339.7				
QHXB1001	C1	45.79	14129.94	31.1		339.7						
QHXB2001	C2	11.36	572.48	58.9		109.3						

ABOVE PINCH [kW]	112802.48
Below pinch (QHXB3002)	742.76
Below pinch (QHXB2002)	10660.44
Below pinch (QHXB3003)	8539.46
Below pinch (QHXB1002)	27503.55
Below pinch (QHXB3012)	15327.21
BELOW PINCH [kW]	62773.42
Total for steam gen [kW]	175575.90
Cooling water utility [kW]	1654.53

Figure 39 Grid diagram for HEN (incl steam production & small CW utility)

5.4.5 Utilities

Both the utilities required and the utilities produced are summarized in Table 79. The utilities are the total required for the plant of 92 dry tons/h biomass with natural gas reforming for hydrogen production. A large amount of 330 ton/h LP steam is produced. Depending on detailed plant design, this can either be condensed for a closed steam power generation loop, or alternatively used in the plant as LP steam. The amount of power required, 24.0 MW, is approximately a third of the power produced from the turbines. The equipment type with the largest power requirement is compressors and fans, contributing to 70.28% of the total power consumption due to high pressure operation at over 100 bar, see Table 80. The second largest contributor is the grinding requirements. This corresponds with literature reporting grinding to be an energy-intensive process [106], [86].

Table 79 Utilities associated with the facility

Required	
Power	24.0 MW
Fuel	2.64 ton/h
Steam	5.82 ton/h
Cooling water	110.68 ton/h
Process water	1.10 ton/h
Chill water	179.68 ton/h
Distilled water	1.36 ton/h
Cooling water make-up	6.88 ton/h
Chill water make-up	11.51 ton/h
Produced	
Power	70.42 MW
LP Steam	330.39 ton/h

Table 80 Equipment and unit power requirements expressed as a % of total power requirements

Equipment / Unit	% of total power consumption
Pumps	7.01
Compressors/ fans	70.28
Grinding	20.67
Cooling water (chill water and cooling water)	1.32
Distillation	0.56
Electrostatic Precipitator	0.17

The water make-up requirements of the plant will depend on the configuration and extent of water and heat integration in the system, complicating detailed comparison with other systems. A simple comparison between the water make-up requirements for this system and for another literature model can be viewed, Table 81. The make-up water includes the process requirement water (for reforming, distillation and ash removal), loss of cooling water in the cooling towers, the loss of chilled water during cooling and the estimated water lost when cooling the steam from the electricity generation cycles down. The simulation model`s water requirement is 4.3 m^3 water/m^3 products (naphtha, jet and diesel distillation fractions). In the study by Jones et al. [57], the hot bio-oil is cooled with recycled bio-oil, therefore a chilled water make up is not required in their study. When neglecting the chilled water make-up, the water make-up requirements amount to 2.9 m^3/m^3 products. This is similar to water make-up requirements reported in Jones et al. [57], with a difference of less than 5%.

The power requirements for the pyrolysis module have been reported to be 40 kWh/oven dry ton of feedstock, similar to that of an atmospheric gasifier [86]. This amounts to 3.7 MW for the pyrolysis module. Grinding power requirement estimates were determined from a 50 kWh/oven dry ton feedstock basis, as reported in a previous study [104]. The power requirement for the pyrolysis part of the model is 11.5 MW (sum of WPA5001, WCPA3001, WCPA6001, WCPA4001, WPA7006, WPGRIND, WESP and WCHW); the discrepancy is due to the high power requirements for biomass grinding and for compression of the fluidizing gas.

Table 81 Make up water requirements

Water demand	Simulation model [a, b]	Literature [c]
Water make-up	4.3 [m^3 water/m^3 products]	-
Water make-up	2.9 [m^3 water/m^3 products] [d]	3.0 [gal water/gal product]

[a] Assumptions include chilled water loss at 6.2 wt%, water loss of 4.3wt% for the power cycle steam cooling as obtained from Table 20 and density of water at 997kg/m^3 , [b] Products are considered to be naphtha, jet and diesel fractions, [c] [57], [d] Excluding chill water make-up

5.4.6 Energy Efficiency

The efficiency definitions considered in this study were discussed in Section 2.4.3 . Where the HHV of streams were not available, the Boie correlation was used for estimating it as it was the most accurate, see Section 3.3.1.1 Ultimate analysis, proximate analysis, moisture, ash, on p.66. A previous study has shown that the omission of utility demands can result in an over-estimation of the energy efficiency of up to 5% [115]. This study addresses both the utility requirements and is based on experimental validated jet fraction yields from the hydrodeoxygenation of fast pyrolysis bio-oil.

Energy efficiency can be evaluated at different points in the model e.g. the pyrolysis section only. When considering the whole process, jet fuel or the final fuels (from the distillation fractions) can be considered as the final products. For equation 10 ($n_{thermal}$) and equation 11 ($n_{overall}$) this will not make a difference, however for equation 7 (n_{fuel}) and equation 8 ($n_{fuel+P.E}$), it will make a difference as it does not consider the energy present in by-products, whereas equations 10 and 11 do. The efficiencies depend on the final product, i.e. there will be a difference between considering only jet fuel as the final product with the other liquid fuels as by-products, compared to considering all fuelsfrom distillation and pre-flashing as final products. In the process a small amount of natural gas is fed to aid in combustion of the PSA offgas in CB-3001, due to a high CO_2 concentration resulting in combustion problems [133]. However, should experiments determine that the CO_2 concentration does not cause a combustion problem, the additional natural gas can be neglected as an energy

input. For this reason, both cases (one where natural gas is fed to aid in combustion and one where natural gas for fuel combustion is not considered) were considered in determining the energy efficiency, as shown in Table 82. Efficiencies were determined for the cases where natural gas is fed and where it is not fed for combustion purposes, for different final products - bio-oil, jet fuel and fuel products, with results summarized in Table 82.

Table 82 Energy efficiency of process [a]

Final product	n_{fuel}	$n_{fuel+ P.E}$	$n_{liquid\ fuel}$	$n_{thermal}$	$n_{overall}$	n_{fuel}	$n_{fuel+ P.E}$	$n_{liquid\ fuel}$	$n_{thermal}$	$n_{overall}$
Bio-oil	71.6	-	-	85.3	-	-				
	Excluding natural gas for combustion purposes					**Including natural gas for combustion purposes**				
Jet Fuel	8.5	7.1	19.2	60.0	37.3	6.6	6.7	11.7	56.8	35.3
Fuel products	38.6	42.5	48.1	60.0	37.3	30.1	39.4	34.1	56.8	35.3

[a] Experimental values for biomass, char and bio-oil are 19.56 MJ/kg, 30 MJ/kg and 17.8 MJ/kg respectively. Other HHV values were calculated using the Boie correlation and the elemental composition in the simulation model streams.

The **Fuel and process energy efficiency** ($n_{fuel+ P.E}$), **Liquid fuel efficiency** ($n_{liquid\ fuel}$) and the **Overall efficiency** ($n_{overall}$) were not calculated for the fast pyrolysis process alone. This is because of an integrated steam cycle and electricity generation system, making the electricity generation contribution from the fast pyrolysis process indistinguishable. The electricity production is required according to the definitions for these efficiencies. The energy efficiency for the bio-oil production varies between 71-85%, depending on the energy efficiency definition used. The char and gas produced during fast pyrolysis can be utilized for energy requirements within the process and contributes to the **Thermal efficiency** ($n_{thermal}$) of the process, causing it to be 13.7% larger than the **Fuel efficiency** (n_{fuel}). In this study, the **Thermal efficiency** was determined at 85.3% with bio-oil as the final product, considering both char and gas as by-product/intermediate product contributions. This is higher than in the previous study with bagasse as feedstock, where the **Thermal efficiency** was calculated at 70% [102].

There is no difference between the **Thermal efficiency** for jet fuels and fuel products, because the by-products are included in the definition of the **Thermal efficiency** (60.0% excluding natural gas and 56.8% including natural gas), shown in Table 82. This is also the case for the **Overall efficiency** for jet fuel and the fuel products (37.3% excluding natural gas and 35.3% including natural gas).

The **Fuel efficiency** (n_{fuel}) for fuel products in this study, was calculated at 30.1-38.6%. This compares well with another study where bio-oil is reformed to produce hydrogen, with a reported biomass to liquid fuel efficiency of 36% [107]. However it is less than some other literature sources have reported. A **Fuel efficiency**, also called fuel energy ratio, for HDO produced from hardwood, have been reported at approximately 52% [5]. Results from this study is also less than the processing efficiency (comparable to the **Fuel efficiency** in this study) of 53.7% reported for a pyrolysis process with hydrogen production and corn stover as feedstock [105].

In this study, the **Fuel and process energy efficiency** ($n_{fuel+ P.E}$) for fuel products was calculated at 39.4-42.5wt%. This is lower than reported values of ca. 66% [5] for the **Fuel and process energy efficiency**, which takes the net process energy into account.

In the study by Leibbrandt (2010), it was estimated that the **Liquid fuel efficiency** ($n_{liquid\ fuel}$) can decrease by 9-15% should the bio-oil be upgraded to transportation fuel with a comparable quality

to bio-ethanol [102], [13]. From this, the refined bio-oil ***Liquid fuel efficiency*** was projected to decrease to 52% [102]. This is higher than the value of 34.1-48.1% projected from this model for fuel products, for the same efficiency definition ($n_{liquid\,fuel}$).

The ***Fuel efficiency*** (n_{fuel}), ***Liquid fuel efficiency*** ($n_{liquid\,fuel}$) and ***Fuel and process energy efficiency*** ($n_{fuel+\,P.E}$), determined in the study are slightly lower than other literature estimates [102], [5], [105]. The experimentally determined hydrodeoxygenated bio-oil yields that were used in this study, and obtained from literature [15], are lower than other reported values [5].

The ***Thermal efficiencies*** of 60% (neglecting natural gas for combustion purposes) and 56.8% (including natural gas for combustion purposes) were obtained for fuel products in this study. It has been suggested that crude bio-oil will be a promising replacement of residual fuels, whereas gasification followed by FT synthesis is believed to be a more favourable replacement for transportation fuels [102]. A decrease in the thermal process energy efficiency was projected, from 70% to approximately 55%, when upgrading bio-oil [102]. Another study has reported a processing efficiency (similar to the ***Thermal efficiency*** in this study) of 76.7%, for a pyrolysis process with hydrogen production and corn stover as feedstock [105]. The ***Thermal efficiencies*** in this study (56.8%-60%) are within the range reported in literature [102], [105].

The biggest influence of co-feeding natural gas to aid with combustion characteristics is seen on the ***Fuel efficiency*** and ***Liquid fuel efficiency*** (8.5% decrease in ***Fuel efficiency*** and 14% decrease in ***Liquid fuel efficiency*** when considering fuel products). The natural gas for combustion characteristics does not add to the fuel produced and can be considered as an energy expense. A smaller effect is seen on the ***Fuel and process energy efficiency***, the ***Thermal efficiency*** and the ***Overall efficiency***, as these definitions take into account the heat produced from combustion of the additional natural gas. The efficiency decrease is only 3.1%, 3.2% and 2.0% respectively.

To determine how energy efficient the process in this study is, it can be compared with other processes, see Section 5.4.7 Energy efficiencies of alternative routes for producing renewable SPK.

5.4.7 Energy efficiencies of alternative routes for producing renewable SPK

The different options available for producing renewable jet fuel, as well as the reported commercial readiness of each of these processes, were discussed in Section 2.1.2 Renewable jet fuel technologies available and their commercial readiness. These included the Fischer Tropsch process, Hydroprocessed Esters and Fatty Acids process (also known as HRJ), the Alcohol to jet process, the Pyrolysis to jet process (or hydrodeoxygenated bio-oil) and the FRJ process. According to a study on the commercial readiness of these processes, FT and HEFA are the furthest developed, followed by ATJ, then pyrolysis and upgrading and lastly FRJ [23]. FRJ will not be considered for comparison in this section.

From the ***Overall energy efficiency*** of the processes, the ability of each process to transfer the energy present in the biomass to the energy available in the products, can be measured and compared. A comparison between the efficiency for different pathways (FT-SPK, HEFA-SPK, ATJ-SPK and HDO-SPK production) can be viewed in Table 83. Different definitions for energy efficiency are used throughout literature. For comparison with other pathways, the energy efficiency needs to be determined in a similar manner, therefore some of the energy efficiency definitions used in Table 83 differ from those reported in Table 82. For this reason, the energy efficiency definition utilized is indicated in Table 83. Unfortunately the jet fraction is not individually reported in some studies, with

179

reported efficiencies considering all of the fuel products. Such reported efficiencies can still provide a rough indication, as the jet fraction overlaps with the naphtha and diesel fraction boiling points. It still gives the maximum efficiency limit since any further processing (to achieve separation to jet fuel), will result in a decrease in energy efficiency.

When considering the FT-SPK pathway with wood as feedstock, the efficiency with only jet fuel as the final product has been reported at 25% [238]. When considering the energy transfer to the other products as well, the efficiency increases to 46% and can even increase to 79% when considering heat production [238]. Other literature sources for FT processing from biomass have reported product efficiencies ranging between 16-49% [239], [23], [240], which can increase to 23.5-52.5% when including electricity production [239], [23]. Another study has reported that the Gasification and Fischer Tropsch process (GFT) of sugarcane bagasse resulted in an overall efficiency of 50.6%, including electricity production, and 46.4% when neglecting electricity production [115]. The energy efficiencies for a biomass to liquid (BTL) system with a recycle of unconverted syngas has been reported at 50.2% [143]. A comparison between the literature efficiencies can be viewed in Table 83. According to a study reported by IATA [5], the energy efficiency from hardwood (or nearly any biomass) for the production of FT synthetic fuel, is ca. 78%, which is significantly higher than other literature ranges, where only fuel production (excluding electricity generation), is considered. Efficiencies reported by Ekbom et al. [238] and IATA [5] are very optimistic compared to the literature range of 23.5-52.5%, for efficiencies where product energies and electricity generation are considered [239], [23]. A possible reason for the high efficiency of 79% can be due to the consideration of heat production rather than the conventional electricity co-generation, which will neglect to account for energy losses in the electricity generation process. High overall efficiencies are expected for the FT pathway, due to the complete utilization of all the products from the FT process to produce fuels, whereas in the case of hydrotreated bio-oils, only the liquid fraction of the bio-oil can be used, with the char and gases not contributing to the final fuel product [5].

An alternative to gasification and the Fischer Tropsch process is to hydro-process esters and fatty acids to produce fuels. For this process, jet fuel efficiencies are significantly less than what was reported for FT-SPK (25wt%), at 6%. This efficiency is however comparable to the same efficiency definition calculated in this study for the HDO-process (6.6-8.5%). Liquid product efficiencies are reported at 38%, which is comparable with the lower limit of FT-SPK efficiencies reported. The wide product distribution seems to contribute significantly to the low jet fuel efficiency for HEFA-SPK.

When considering the Alcohol-to-jet pathway (ATJ), different means of producing the alcohols are available, including gasification and biochemical routes. Jet fuel efficiencies for indirect gasification followed by alcohol production, have been reported at 29%, comparable to the 25% from the FT process [241], [23]. Other literature sources have not reported the jet fuel efficiency, but have focused on ethanol and gasoline production and had not considered the further upgrading requirements for converting the products to jet fuel. Therefore, the jet fuel efficiency will be less than the efficiencies determined for ethanol and gasoline production. Gasoline production efficiency was reported at 37.7% [242] and ethanol production efficiency at 40% [243]. When considering the ethanol and electricity production using a biochemical pathway (and dilute acid treatment), the efficiency was reported at 44.1% [105].

In a different study where biological models for biofuel production were considered, the liquid fuel efficiency (liquid products) for Simultaneous Saccharification and Fermentation was 38.8% and 43.6% for Fermentation and Separate Hydrolysis [115]. The overall efficiency for production of liquid fuels

for the HDO process in this study (35.2% to 47.8%) is comparable to that of the efficiencies calculated for the biological processes in the study by Petersen (2012). Biological routes were reported to be less energy efficient compared to thermochemical routes (BTL and pyrolysis), in a study where bagasse was used as feedstock, with liquid fuel efficiencies reaching a maximum of 41% [102].

For the hydrodeoxygenation of bio-oil, investigated in this study, the results showed a jet fuel efficiency range between 6.6-8.5% (depending on the definition used), as indicated in Table 83. This is comparable with that of HEFA-SPK (6%). When including the energy present in the other products produced, the efficiency increases to 30.0-38.5% and when including the electricity produced, the efficiency increases further to 37.2-47.8%, reported in Table 83. When considering the additional hydrogen fed for combustion purposes, the efficiency decreases to 35.2%. Other studies looking at hydrotreating bio-oil have reported higher product efficiencies (liquid fuels + fuel gas) of 53.7% [105]. Products included naphtha and diesel range stock; however further treating will be required to separate the jet fraction from the naphtha and diesel which will decrease the reported efficiency to less than 53.7% [105].

When considering the results in Table 83, the efficiency for jet fuel production for HEFA-SPK and for HDO-SPK compares very well (6.6-8.5% for HDO process compared to 6% for HEFA process). However, it is significantly smaller than the 25% for FT-SPK and the 29% efficiency for dilute acid pre-treatment and co-fermentation to produce alcohols which is upgraded to jet fuel. When considering the jet fuel as well as the by-products, comparison between the different pathways` efficiencies indicate the efficiency determined in this study is much less than the efficiency reported by Anex et al. [105]. Their study reported the highest efficiency (53.7%) among the different pathways when considering fuel products [105]. A similar efficiency determined in this study for the HDO process was 38.5% (neglecting hydrogen production feedstock) which is similar to what has been determined for HEFA-SPK (38%). The efficiency for the HDO process, considering jet fuel and by-products (30.0-38.5%, depending on natural gas requirements for hydrogen production) falls within the broad range that was observed in literature for the FT-SPK pathway of 16-49%, see Table 83. The energy efficiency of ATJ-SPK is slightly higher than the efficiency of the HDO-SPK (40-45% or 37.7-42.6% vs. 38.5%), although the ATJ-SPK efficiency does not take into account the upgrading from ethanol to jet fuel and the separation of products to obtain a pure jet fraction. These processing conditions will decrease the product efficiency for the ATJ-SPK pathway causing it to be closer to the efficiencies determined in this study for HDO-SPK.

Reported ranges vary significantly among different literature sources, making comparison between the possible process routes difficult. The process efficiencies for HDO-SPK obtained in this study were lower than another study had indicated [105]. When considering the other literature efficiencies for HDO-SPK [105], the efficiencies for FT-SPK and HDO-SPK are comparable, and are more efficient than HEFA-SPK. However, when comparing the efficiency results from this study with efficiencies for other processes, and neglecting optimistic efficiencies [5], [238], the maximum process efficiency from the FT-SPK literature range is slightly higher than the other processes. Results from this study show the FT-SPK process is slightly more efficient, with the HEFA-SPK and the HDO-SPK process efficiencies being quite similar. Since the energy efficiencies of the HDO-SPK process are comparable with that of HEFA-SPK and FT-SPK, its ability to produce aromatic rich SPK gives it an advantage.

Table 83 Comparison between efficiencies for different routes for producing renewable jet fuel

FT-SPK				HEFA-SPK		ATJ-SPK								HDO-SPK						
[238]		Other literature sources [a, b, c, e]		[212], [23]		[241], [23]		[242] [LHV basis]		[243] [LHV basis]		[105] [HHV basis]		This study						[105]
Wood chips		Wood residue [a, b], Biomass [c] Corn stover [e]		Vegetable oil		Corn stover (dilute acid pre-treatment, co-fermentation)		Southern Pine wood (indirect gasification, GTL)		Poplar wood (gasification , methanol synthesis)		Corn stover (biochemical pathway)		Woody (pine) biomass						Corn stover
Defini-tion	Eff	Defini-tion	Eff	Defini-tion	Eff	Defini-tion	Eff	Defini-tion	Eff	Defini-tion	Eff	Defini-tion	Eff	Defini-tion	Eff	Defini-tion	Eff	Defini-tion	Eff	Defini-tion	Eff
Jet/ BM	25%	*	*	Jet / BM	6%	Jet/ BM	29%	EtOH/ BM	40%	Gasoline / BM	37.7%			Jet/ BM	8.5% [d]	Jet/ (BM + NG for H$_2$ prodn)	6.6% [e]				
(Jet + prod) / BM	46%	Liquid Prod/ BM	16% [a,b], 49% [c]	Liquid Prod/ BM	38%			(EtOH + Liquid Prod) / BM	45%	(Gasoline + LPG) /BM	42.6%			(Jet + prod)/ BM	38.5% [d]	(Jet + prod) /(BM + NG for H$_2$ prodn)	30.0% [e]			(Liquid fuels+ Fuel gas)/ BM	53.7%
(Jet + prod + heat)/ BM	79%	All prod/ BM [a,b] or All prod + net electr/ BM [e]	23.5% [a,b], 49% [a,b], 52.5% [e]	**	**							(EtOH+ electr) / BM	44.1%	(Jet + prod + net electr) / BM	47.8% [d]	(Jet + prod net electr)/ (BM + NG for H$_2$ prodn)	37.2% [e]	(Jet + prod + net electr)/ (BM + NG for H$_2$ prodn+ NG for comb)	35.2% [e]	(Liquid fuels +Fuel gas+ char)/ BM	76.7%

BM= biomass, EtOH= Ethanol, Electr= electricity, prod=products, prodn = production, NG= natural gas, comb = combustion, LPG= liquefied petroleum gas, Eff= efficiency * No Jet A1 production,**No electricity production, [a][239], [b][23], [c][240], [d] excluding natural gas for combustion purposes, [e] including natural gas for combustion purposes, [d] excluding natural gas for combustion purposes, [e][105]

5.4.8 Final outlet streams disposed to environment

The waste product streams reported in Table 73 include the immediate waste streams. These streams still have an intrinsic value, as they can be combusted for heat to enable steam generation and consequently power production. The final product streams that will be disposed to the environment is therefore not all the waste streams generated by the process, as that will be inefficient use of available energy. The final outlet streams disposed to the environment are reported in Table 84.

Table 84 Final outlet streams disposed to the environment*

Stream number	STREAMS IN SIMULATION MODEL[a]									TOTAL OUTLET STREAMS	TOTAL WASTE[b]
	1004	4015	4014	4010	B1009	B2012	B2015	B3043	B3013		
Stream description	Air & moisture from BM	Water from Water & Ash	Ash from Water & Ash	Flue gas from CB-4001	Aqueous waste (R-B1001)	Aqueous waste (R-B2001)	Pre-flash lights	Flue gas from CB-B3001	Reformer & shift reactor waste		
N2	546.799	0.000	0.000	311.626	0.000	0.000	0.000	208.757	0.000	1067.182	520.383
O2	167.522	0.000	0.000	32.185	0.000	0.000	0.000	18.485	0.000	218.192	50.670
H2	0.000	0.000	0.000	0.000	0.000	0.000	0.003	0.000	0.005	0.008	0.008
CO	0.000	0.000	0.000	0.000	0.000	0.000	0.000	0.000	0.022	0.022	0.022
CO2	0.291	0.000	0.000	93.980	0.000	0.000	0.023	41.907	3.088	139.289	138.998
H2O	89.581	1.102	0.000	14.841	16.846	2.027	0.000	35.639	28.209	188.245	98.664
CH4	0.000	0.000	0.000	0.000	0.000	0.000	0.006	0.000	0.038	0.044	0.044
AR	9.254	0.000	0.000	5.275	0.000	0.000	0.000	3.534	0.000	18.063	8.809
N-HEX-01	0.000	0.000	0.000	0.000	0.000	0.000	0.002	0.000	0.000	0.002	0.002
CYCLO-01	0.000	0.000	0.000	0.000	0.000	0.000	0.003	0.000	0.000	0.003	0.003
METHY-01	0.000	0.000	0.000	0.000	0.000	0.000	0.001	0.000	0.000	0.001	0.001
1:3-C-01	0.000	0.000	0.000	0.000	0.000	0.000	0.003	0.000	0.000	0.003	0.003
3-MET-01	0.000	0.000	0.000	0.000	0.000	0.000	0.001	0.000	0.000	0.001	0.001
FUMAR-01	0.000	0.000	0.000	0.000	0.051	0.713	0.000	0.000	0.000	0.764	0.764
1:2-B-01	0.000	0.000	0.000	0.000	0.002	0.009	0.000	0.000	0.000	0.011	0.011
ETHAN-01	0.000	0.000	0.000	0.000	4.891	0.722	0.000	0.000	0.000	5.613	5.613
2,2PROPA	0.000	0.000	0.000	0.000	6.458	0.000	0.000	0.000	0.000	6.458	6.458
FURACETA	0.000	0.000	0.000	0.000	0.664	1.593	0.000	0.000	0.000	2.257	2.257
METHA-01	0.000	0.000	0.000	0.000	0.002	0.002	0.000	0.000	0.000	0.004	0.004
ETHAN-02	0.000	0.000	0.000	0.000	0.000	0.027	0.008	0.000	0.000	0.035	0.035
PROPA-01	0.000	0.000	0.000	0.000	0.000	0.040	0.004	0.000	0.000	0.044	0.044
ISOBU-01	0.000	0.000	0.000	0.000	0.000	0.016	0.001	0.000	0.000	0.017	0.017
ASH	0.000	0.000	0.912	0.000	0.000	0.000	0.000	0.000	0.000	0.912	0.912
TOTALS	*813.447*	*1.102*	*0.912*	*457.907*	*28.914*	*5.149*	*0.055*	*308.322*	*31.362*	*1647.170*	*833.723*

* Aqueous waste streams are treated as the final aqueous waste product and combustion thereof is not considered in these reported values, [a] All values in [ton/h], [b] Ignore air & moisture from BM drying

All the final outlet streams are reported above, although not all of these streams are waste streams. For example, the air that was used to dry the biomass contains moisture, but this is not a waste product, therefore totals including and excluding the air and biomass moisture are presented in Table 84. Since air was fed in excess to assure complete combustion and a 6wt% oxygen contribution

in the offgas, large quantities of nitrogen and oxygen are also emitted. The gas outlet streams are the greatest with a total of greenhouse gases emitted (only CO_2, CO and CH_4), at 136.207 ton/h excluding water vapour (streams 1004, 4010, B2015 and B3043) and 276.268 ton/h including water vapour (only CO_2, CO, CH_4 and H_2O in streams 1004, 4010, B2015 and B3043). The aqueous waste streams (streams B1009, B2012 and B3013) amount to 65.425 ton/hr. The solid waste (ash) formed is removed with water to form a suspension of 2.014ton/h (streams A4014 and A4015).

5.5 Conclusions from process simulation

The literature study on hydrodeoxygenation of bio-oil indicated that upgrading literature for hydrodeoxygenated bio-oil that can comply with (or are close to) the stringent specifications for SSJF or FSJF, are limited. Studies on the upgrading of bio-oil often do not report all the necessary information such as temperatures, pressures, yields and catalysts to be able to build a simulation model. The most applicable literature was from a study by Elliott et al. [16] and a study by Christensen et al. [15].

The experimental work in this study (Chapter 3) was used as guideline to identify the best operating conditions from literature data for a commercial scale fast pyrolysis unit aiming to produce bio-oil for upgrading to jet fuel. This approach allowed for scale-up effects to be accounted for, while enhancing conditions that will lead to favourable bio-oil characteristics for jet fuel production. The best operating conditions was determined based on the following objectives: a high organic yield and a high quality bio-oil best suited for a fuel. A high quality bio-oil was defined based on the following criteria: a high energy content (HHV), a low acid content, a low aldehyde content and a low pyrolytic water content. It was concluded that small particle sizes are favourable due to increased energy transfer to the bio-oil and increased organic liquid yields. Lower biomass moisture contents are preferred as it decreased the bio-oil moisture content and increased bio-oil HHV. For fuel stability, a high reactor temperature level was optimal, to limit the aldehyde concentration and to minimize the acid content. The combination of small particle sizes, low moisture contents and high reactor temperatures also produced the maximum organic liquid yield and was therefore optimal for the application of upgrading the bio-oil to a fuel.

Based on published experimental studies, it is difficult for upgraded bio-oil to meet the stringent jet fuel specifications, in particular the low TAN and high carbon and hydrogen requirements. If the requirements were less severe, it will be easier to meet, however the integrity of the fuel cannot be compromised due to safety implications.

The upgrading part of the simulation model reflected the literature data well, with deviations on the hydrogen utilization, hydrotreating reactor operating conditions, overall phase yields, final fuel stream yields and the elemental composition (carbon, hydrogen and oxygen) and component types (aromatic/aliphatic) within 10% from literature.

The jet fuel yield was 3.7wt% based on a dry biomass basis and 1.85 wt% on a selected 'wet' (50% moisture) feedstock basis. The total yield of jet-fuel boiling range aromatics was 0.76wt% (based on dry wood feed) with a maximum of 0.97wt% possible. The low jet fuel yield (mass based) and the low jet fuel boiling range aromatic yield (mass based), show a low effectiveness for this process to convert the biomass to the desired final jet fuel products. Other fuels that were also produced, included naphtha, diesel and gas oil, with yields of 4.9wt%, 3.5wt% and 2.3wt% (dry biomass basis)

respectively. Fuels other than jet fuel were not evaluated against the industry specifications applicable to each. To make the pyrolysis-to-jet process more worthwhile, the naphtha, diesel and gas oil fuel fractions should also be considered as sellable fuel products. This will increase the total fuel products to 16.7wt% (dry feedstock basis), with a maximum achievable of 22.7wt% (dry feedstock basis). This might require additional upgrading to comply with petrol and diesel specifications, affecting product yields and incurring further costs. Alternatively these fuel fractions can be used for electricity generation. The maximum fuel yields obtained in this study are lower than other literature sources report [84], [58]. This was attributed to higher bio-oil yields and a smaller extent of hydrodeoxygenation for the other studies in literature.

Comparison between the estimated properties for the simulated bio-oil and the properties of the experimentally produced and analysed bio-oil, indicated that the HHV, moisture content and density for the simulated bio-oil and the experimental bio-oil were similar. Since the PTJ-SPK specifications are not yet available, an evaluation was made against current SPK specifications. The distillation gradients were lower than the minimum required value. Unfortunately this is partly due to a limitation of the simulation model, due to few representative components selected within a similar boiling range, which biased the results. The LHV of PTJ-SPK was lower than the minimum requirement for SSJF and FSJF. The smaller distillation gradients and the low LHV can both be addressed by blending the PTJ-SPK with a conventional fuel with a wide distillation range or with a heavy HEFA-SPK. PTJ-SPK contained approximately 20vol% aromatics and a high density – properties which are lacking for the other SPK fuels. This provides an opportunity for a fully synthetic jet fuel by blending PTJ-SPK and FT/HEFA-SPK in a 40:60 ratio to meet the 8vol% aromatic specification.

The carbon content in a fuel can be related to the energy in a fuel [114]. Carbon transfer to fuel products is small (almost half) compared to the transfer to waste/ by-product streams; 36.2wt% compared to 63.8 wt% respectively. Almost half of the carbon present in the waste streams (54%) can be utilized for heat generation purposes (electricity generation). The greatest carbon loss is to char during pyrolysis (24wt%) and almost an eighth of the carbon present in the biomass is transferred to the aqueous waste streams produced during upgrading of the bio-oil.

The direct waste streams from the process, before combustion for energy recovery, amounted to 122.1 ton/h for a 184 wet tons/h facility (including char, aqueous waste water from upgrading, offgas from pyrolysis, upgrading and hydrogen production, while excluding the air used for drying and the biomass moisture removed). The greatest contribution to the final waste streams was from gases. The total greenhouse gas emissions were 136 ton/h (excluding water vapour) and 276 ton/h (including water vapour). Aqueous waste streams were second greatest at 65 ton/h with solids in suspension being the smallest waste stream at 2 ton/h. Some of the waste streams produced, especially the aqueous waste streams from the reactors during upgrading, can be combusted for electricity generation because it is rich in hydrocarbons.

Two scenarios were investigated during pinch point analysis; utilizing only high grade quality heat and utilizing both low and high grade quality heat. A significant improvement of 28% increase in electricity generation (from 55 to 70 MW) occurred when utilizing both low and high grade quality heat. It also resulted in a significant reduction in cooling water from 3143 to 90 tons/h (excluding fast pyrolysis and distillation units).

The process produced HP steam for power generation and LP steam. Utility requirements included: power/electricity, fuel, cooling water, process water, chill water, make-up water and steam at values of 24 MW, 3 ton/h, 111 ton/h, 1 ton/h, 180 ton/h, 18 ton/h and 6 ton/h respectively. Utilities produced included electricity at 70 MW and LP steam of 330 ton/h. The process generated almost 3 times more power than it consumed, making electricity generation a viable by-product. Compressors and fans utilized the most power due to the high pressure at which the hydrotreating and hydrocracking reactors operate.

The *Fuel efficiency* for pyrolysis was 71.6%, however when considering the contribution of the gas and char by-products, indicated by the *Thermal efficiency,* the efficiency increased to 85.3%, which is higher than the reported *Thermal efficiency* of 70% for a bagasse pyrolysis process [102]. A small quantity of natural gas supplements the PSA offgas combustion to assist with combustion characteristics, and efficiencies were determined both with and without natural gas as supplement to PSA offgas [133]. The *Thermal efficiency* for the entire process was 60% and 56.8% respectively (without and with the addition of natural gas for combustion characteristics), for both jet fuel and fuel products. Upgrading the bio-oil to liquid fuels resulted in a *Liquid fuel efficiency* of 48.1% (when natural gas is not necessary for combustion purposes) and 34.1% (when natural gas is used for combustion purposes). When only jet fuel is considered as final product, the *Liquid fuel efficiency* decreased to 19.2% (when natural gas is not necessary for combustion purposes) and 11.7% (when natural gas is used for combustion purposes). The decrease in efficiency from the *Thermal efficiency* to *Liquid fuel efficiency*, indicated that the energy is not concentrated in the desired final jet fuel product, but that much of the energy in the biomass is transferred to other by-products and waste streams. The reduction in the *Liquid fuel efficiency* from considering all liquid fuels as products, compared to only considering the jet fuel as product, is due to the lack of a high jet fuel selectivity from the process, resulting in a high production of by-product fuels. This simulation model predicted lower energy efficiencies for the *Fuel efficiency* and the *Liquid fuel efficiency* for fuel products, than literature results (30.1-48.1% compared to 52-53.7%) [102], [5], [105]. The overall *Thermal efficiency* from this study (56.8%-60%) falls within the literature range of 55-76.7% [102], [105].

The energy efficiency results indicate that the inclusion of the other fuel fractions (not just jet fuel) as fuel product will be beneficial for the process to be more efficient, since the inclusion of the other fuel fractions significantly increased the *Liquid fuel efficiency* of the process from 11.7% to 34.1% (when natural gas is used for combustion purposes). Experimental results should confirm whether the addition of natural gas is required for combustion properties, as this will reduce the energy efficiency of the process. Much of the energy which is not concentrated in the jet fuel, or the other fuel fractions, can be utilized as thermal energy.

From the product yields determined in this study, the process efficiencies could be determined, from which comparison with other processes were possible in order to gage the PTJ-SPK process. The efficiency ranges reported in literature for different processes of producing renewable jet fuel (FT-SPK, HEFA-SPK, ATJ-SPK and PTJ-SPK) are broad, even within a single process; complicating direct comparison, as jet fuel is seldom considered as an individual product. Comparison indicated that the FT-SPK pathway is the most efficient. The ATJ-SPK method has a lower efficiency than the FT-SPK method to produce the intermediate ethanol-product and gasoline, although uncertainty in the efficiency for converting to jet fuel makes benchmarking this pathway difficult. The efficiencies of the HEFA-SPK process and the efficiencies determined in this study for the PTJ-SPK process were

reasonably similar. The advantage of the PTJ-SPK process is the production of aromatic-containing SPK, whereas the FT-SPK pathway does not.

6. OVERALL CONCLUSIONS

This part of the study combines the conclusions drawn from the experimental fast pyrolysis study and the conclusions drawn from the modelling of the integrated fast pyrolysis and bio-oil upgrading process.

6.1 Experimental Conclusions

The effect of changes in the moisture content, particle size and reactor temperature on product yields, bio-oil quality and bio-oil properties were investigated. Statistical analyses were performed and statistical correlations developed to identify the statistically significant factors affecting the product yields, bio-oil quality and properties. The results and conclusions from experimental work were used as guideline to identify the best operating conditions to produce a product that will be best suited for upgrading to jet fuel.

The statistical analysis of fast pyrolysis experiments indicated that the organic liquid yield was significantly affected by particle size; with a small particle size increasing the organic liquid yield. Small particle sizes allow for rapid heat transfer and minimum residence time of the volatilized product within the particle, ensuring high organic liquid yields by reducing the extent of secondary reactions. The maximum organic yield occurred at small particle sizes (0.25 – 0.85 mm), high temperatures (500°C) and low moisture contents.

Statistical analyses on the bio-oil properties indicated that the bio-oil moisture content was significantly influenced by the biomass moisture content and the particle size, with a decrease in biomass moisture content and particle size reducing the bio-oil moisture content. The viscosity was significantly affected by the same factors influencing the bio-oil moisture content, however with an opposite tendency, due to an increase in the bio-oil moisture decreasing the bio-oil viscosity. The HHV of the bio-oil decreased with an increase in biomass moisture content, due to moisture transfer from the biomass to the bio-oil. The bio-oil density was significantly increased by an increase in temperature and a decrease in biomass particle size. An opposite tendency was observed for the formation of pyrolytic water, which increased with low temperatures and large particle sizes. The biomass moisture content and the same combination of factors that affected the bio-oil moisture content, did not have a significant influence on the bio-oil density. This could indicate that the main influence on the density is not the bio-oil moisture, but rather the reactions which enhance pyrolytic water formation. The bio-oil`s oxygen content (moisture-free) was significantly increased by an increase in the biomass moisture content. The carbon and hydrogen contents of the bio-oil were not significantly influenced by any of the factors investigated. The pH was also not significantly influenced by any of the factors.

GC-MS analyses confirmed that bio-oil contains a large variety of components, with water being the most abundant component, followed by the sugar levoglucosan, acetic acid and formic acid. Other quantified components were present in small quantities of less than 1wt%. Statistical analysis on GC-MS results indicated that the sugar, acid and alkane chemical families in bio-oil were significantly affected by reactor temperature. The aldehyde content was significantly affected by reactor temperature, by the interaction between temperature and moisture content and by the interaction between temperature and particle size. The aromatic content in bio-oil was not significantly affected by any of the factors investigated, according to statistical analysis of GC-MS and ^{13}C NMR results. Statistical analysis on the ^{13}C NMR results indicated that none of the factors investigated had a

significant effect on the ^{13}C NMR responses for any of the chemical shift ranges. Statistical analysis on ^{1}H NMR results indicated that the quantity of hydrogens in the aldehyde chemical shift range was significantly affected by the particle size. This differed from the GC-MS results. Differences can be due to the limitations of lumping techniques, or alternatively due to the different types of protons (aldehyde protons and lower field aromatic protons) being measured within the 8-10 ppm chemical shift range. The ^{1}H NMR results also indicated that the olefinic protons conjugated to carbonyls range was significantly affected by all factors investigated.

Both ^{13}C NMR results and ^{1}H NMR results showed that the methoxy functional groups were the most prominent, with the protons in the methoxy group and the carbons in the methoxy/hydroxyl carbons as the highest for all functional groups. The proton NMR results for the 4.2-6.4 ppm range, which included phenolic protons, were in agreement with the results from ^{13}C NMR, which indicated that the aromatic range (110-163 ppm), containing phenolic and phenoxyl compounds, was the second largest. Furthermore, this agreed with GC–MS results which also indicated that phenols and aromatics were the second largest chemical family.

The conclusions from the experimental and statistical work were integrated and used to lead to a general conclusion on the effect of the factors investigated on the bio-oil yield and quality. Particle size had a significant influence on the organic liquid yield and the energy transfer to the bio-oil, with a small particle size increasing the organic liquid yield and favouring energy transfer to the bio-oil. Low biomass moisture contents enhanced the bio-oil HHV and reduced the bio-oil moisture content. Temperature did not have a statistically significant influence on the organic liquid yield, although high temperatures lowered the pyrolytic water formation and increased the HHV. Temperature had a significant effect on many of the chemical families, specifically on the sugar, acid and aldehyde concentration, however it did not affect the aromatic chemical family. Maximum organic liquid production was obtained at small particle sizes, low moisture contents and high temperatures. These conclusions served as a guideline to select appropriate literature operating conditions for the fast pyrolysis process unit, which was developed in Chapter 4 and 5.

6.2 Process Simulation Conclusion

Literature for bio-oil hydrodeoxygenation, with the aim of producing jet fuel, is limited. The characteristics and composition of the final fractionated hydrodeoxygenated bio-oil are seldom considered in literature studies and rarely reported in literature. Studies on the upgrading of bio-oil often do not report all the necessary information such as temperatures, pressures, yields and catalysts to allow for the construction of a complete simulation model from a single literature source. The most applicable bio-oil hydrodeoxygenation literature was from a study by Elliott et al. [16] and a study by Christensen et al. [15]. The aim of the simulation modelling was to evaluate the process of producing an aromatic rich jet fuel fraction from bio-oil.

An Aspen Plus® simulation model was developed for the process of producing bio-oil from fast pyrolysis and upgrading it to a final jet fuel. The experimental work in this study (Chapter 3) was used as guideline to identify the most suitable operating conditions from literature, to be used in the simulation model (developed in Chapter 4 and 5) for a commercial scale fast pyrolysis unit producing bio-oil for upgrading to jet fuel. This approach allowed for upscaling effects to be accounted for, while enhancing the conditions that lead to favourable bio-oil characteristics for jet fuel production. The best operating conditions were determined with the intent to obtain a high organic yield and a

high quality bio-oil, best suited for a fuel. The criteria used for a high quality fuel was: a high energy content (HHV), a low acid content, a low aldehyde content and a low pyrolytic water content. The combination of small particle sizes, low moisture contents and high reactor temperatures was optimal for the application of upgrading the bio-oil to a fuel. Small particle sizes increased organic liquid yields and energy transfer to the bio-oil. Lower biomass moisture contents decreased the bio-oil moisture content and increased the bio-oil HHV. A high reactor temperature decreased fuel instability by limiting the aldehyde concentration and minimized the acid content. The combination of small particle sizes, low moisture contents and high reactor temperatures also produced the maximum organic liquid yield. These processing and operating conditions were used in the simulation model`s fast pyrolysis unit.

Mass and energy balances from the simulation model were used to estimate product yields, utility requirements and waste products. The process produced a jet fuel at a yield of 3.7wt% (dry biomass feed) and a jet fuel aromatic yield of 0.76wt% (dry biomass feed). Other fuels were also produced, including naphtha, diesel and gas oil, at yields of 4.9wt%, 3.5wt% and 2.3wt% (dry biomass basis) respectively. Comparison of the different fuel yields indicated that the process was not selective towards jet fuel production.

Only 36.2wt% of the carbon in biomass was transferred to fuel products with remainder lost to by-product/waste streams. The greatest carbon loss was to char during pyrolysis (24wt%) and approximately 11wt% of the biomass carbon was transferred to aqueous waste streams produced during bio-oil upgrading. The greatest contribution to the final waste streams was from gases. The total greenhouse gas emissions were 136 ton/h (excluding water vapour) or 276 ton/h when including water vapour. Aqueous waste streams were second greatest at 65 ton/h. The solids in suspension waste stream was the smallest at 2 ton/h.

By using both low and high grade quality heat in the heat integration, a significant increase of 28% in electricity generation was accomplished, from 55 to 70 MW, accompanied by a significant reduction in cooling water requirements from 3143 to 90 ton/h (excluding fast pyrolysis and distillation units). The process produced almost 3 times more electricity than it consumed (24MW), making electricity generation a viable by-product. Other utility requirements included: fuel, cooling water, process water, chill water, make-up water and steam at values of 3 ton/h, 111 ton/h, 1 ton/h, 180 ton/h, 18 ton/h and 6 ton/h respectively. LP steam was produced at 330 ton/h.

The density, moisture content and HHV of the simulated bio-oil were similar to experimental results. Comparison of the PTJ-SPK properties with current SPK specifications indicated that the distillation gradients were lower than minimum allowed values. This was partly due to a limited number of components selected for modelling purposes, all within a similar boiling range. PTJ-SPK had a high density compared to conventional jet fuel and synthesized paraffinic kerosene and contained approximately 20vol% aromatics.

The *Thermal efficiency* for the entire process was 56.8%. When neglecting thermal energy in the by- and intermediary-products, the *Liquid fuel efficiency* decreased to 34.1%, taking into account all final liquid fuels. The decrease from *Thermal efficiency* to *Liquid fuel efficiency* indicated the energy content of the biomass was not concentrated into the liquid fuel products, but was present in many of the other streams, including the waste streams. When only jet fuel is considered as final fuel, the

Liquid fuel efficiency decreased further to 11.7%. The *Thermal efficiency* for the PTJ pathway was within the range reported in literature. The *Liquid fuel efficiency*, with all final fuels considered as products, is lower than literature estimates. Compared to other options for producing a renewable jet fuel, Fischer Tropsch, Hydroprocessed Esters and Fatty Acids and Alcohol to jet, the results from this simulation indicated the Pyrolysis to jet process is less efficient than the Fischer Tropsch process, yet its efficiency is comparable with the Hydroprocessed Esters and Fatty Acids pathway. The Pyrolysis to jet option has the advantage of producing aromatic-containing SPK, which is a shortcoming in the Fischer Tropsch to jet fuel process.

From the product yields and energy efficiency results, it can be concluded that a pyrolysis-to-jet plant will need to include naphtha and diesel production, or electricity production, or both. Because PTJ-SPK has a high aromatic content and a high density, it can complement HEFA/FT-SPK by supplying aromatics and by increasing the density. This provides an opportunity for a renewable fully synthetic jet fuel that meets the jet fuel specifications. The required pyrolysis plant size to compliment a 304 000 tonnes/yr. FT-SPK facility by blending in a 60:40 volume ratio to obtain 8vol% aromatics in the final fuel, is 6 410 000 dry tonnes biomass/yr. (770 dry tonnes biomass/h) (assuming 95% operational time, FT-SPK density of 762 kg/m^3) [214], [19]. At such high capacities, biomass availability becomes limited and unfeasible [110]. The plant capacity that was investigated in this study (92 dry tonnes/h) will only contribute 10vol% to a 304 000 tonnes/yr. FT-SPK facility.

Based on a jet fuel specification criteria for SSJF and FSJF, PTJ-SPK is expected to be a viable option. However, based on feedstock availability, the PTJ process is not a promising option due to low PTJ-SPK yields, resulting in very high biomass requirements. Although this study focused on *Pinus radiata,* it might be possible to produce bio-oil from the waste cellulosic material created by the production of HEFA. By using a combination of fresh biomass feed and cellulosic waste material (from HEFA production), the fresh biomass requirement will decrease, making the PTJ-SPK process more viable. Improving the bio-oil yield from fast pyrolysis and the HDO from the hydrodeoxygenation of bio-oil will also reduce the biomass requirements, thereby increasing the feasibility of a HEFA/FT-SPK and PTJ-SPK blend to produce a FSJF.

7. OVERALL RECOMMENDATIONS

Recommendations for future work on the fast pyrolysis experimental set-up and the modelling are provided below.

7.1 Fast pyrolysis experiments

The screening experimental investigation was aimed at identifying whether the particle size, moisture content and reactor temperature influence specific parameters of the final bio-oil product used for further processing. The recommendations made hereafter, focus on improving the detail from the results obtained in this study.

1. The experimental set-up utilized did not stably control the reactor temperature above 500°C, therefore the study was limited to a maximum reactor temperature of 500°C. It is recommended that the temperature control be improved to obtain a faster response and that the experiments be performed over a greater reactor temperature range of 450-550°C.
2. Organic yields were slightly lower than other experimental studies have reported. It is therefore recommended to investigate the residence time of the hot vapour and biomass particles within the reactor.
3. It is recommended that future studies focus on identifying which of the parameters investigated are the most significant for an industrial scale pyrolysis unit with bio-oil as feedstock, followed by hydrotreating. Detailed surface response models should be developed for these parameters, using the results from this study to identify which factors to include in the design.
4. Due to the screening nature of the experiments, a basic 2^3 level factorial was used. The preliminary response surface models deviated from the results obtained from the additional run (run 1 that was not part of the design of experiments). It is therefore recommended that a more detailed Design of Experiment, that will allow for centre points (e.g., centre composite design), be utilized in future work, in order to be able to accurately determine the response surface at central conditions. This will make the conclusions from the experimental section more robust.

7.2 Process Simulation

The model used in this study serves as a basis for further studies on the effectiveness and utility requirements. Design that is more detailed will increase the accuracy of the model and should be considered for future research.

1. The following recommendations mainly focus on increasing the detail for simplified units or processes used in this model:
   a. Take the product dependency on the type of catalyst into account during component selection.
   b. Replacing the yield reactor (for steam reforming) with a Gibbs free reactor to take the thermodynamic equilibrium into account.
   c. Extend the compression of hydrogen gas to a multistage compression unit with intercooling stages, as this is more realistic of what will be used in practice.

> d. The excess heat from the combusted char can be used to pre-heat the fluidizing gas as this will increase the bio-oil yield, although the amount of steam available to produce (excess) electricity will be reduced.
> e. A wider set of model components should be considered in future studies. This will allow more accurate and robust simulation of the final jet fuel properties. Data availability might however prove to be a problem.
> f. The distillation unit should be developed in more detail, with optimized reflux ratios to obtain the desired separation. Experimental literature for this is scarce and further growth in this research field should be considered.
> g. Adapt the model to include the sulphur balance and units associated with separation thereof for a better resemblance with an actual refinery.
> h. Using the LP steam as feed to the steam cycle, which will decrease the boiler feed water requirements and reduce the excess LP steam.

2. It is recommended that the model be adapted to include a sensitivity analysis, evaluating the effect an increase in the pyrolysis bio-oil yield and the hydrodeoxygenation product oil yield will have on the final jet fuel yield and the aromatic content in the jet fuel yield.

7.3 PTJ process route

The following recommendations aim to suggest means to improve the PTJ process`s effectiveness, based on the results from this study.

1. Limited upgrading literature was available for a final product that can be expected to meet, or be close to, the jet fuel requirements. Experimental studies should be performed to confirm which of the minimum requirements the jet fuel (derived from bio-oil) should meet, are not adhered to. This will identify future focus areas for research on hydrodeoxygenation of bio-oil with jet-fuel applications in mind.
2. A low jet fuel mass yield and jet fuel boiling range aromatic yield was observed for the PTJ pathway. Future research into improving the bio-oil yield from pyrolysis and the oil yields from hydrodeoxygenation of the bio-oil, will contribute to make the PTJ pathway more viable. This will also improve the opportunity to produce a FSJF by blending PTJ-SPK and FT/HEFA-SPK due to lower biomass requirements.
3. The possibility of producing a fully synthetic jet fuel by blending HEFA-SPK and PTJ-SPK, using the waste cellulosic material from HEFA production as feed to the pyrolysis process, should be investigated.
4. It is recommended to do a study to determine the yields from the upgrading process at which the process will be feasible. By evaluating how far the current upgrading technology is from delivering a feasible yield, estimation on the future feasibility of hydrodeoxygenation of bio-oil from fast pyrolysis can be made.
5. It is further recommended that a detailed economic study be performed to be used as baseline study to investigate options for improvement. An alternative approach could be to convert the bio-oil into chemicals and some fuel, or to convert the other fuel fractions (gasoline and diesel) into chemicals through further processing. A smaller quantity of speciality chemicals can have a higher selling price, with a higher earning potential, even if produced quantities are small. However, to produce chemicals will require additional separation processes, resulting in additional capital and operation costs. The economic study can also be used to determine the financial incentive needed for the process to be feasible.

6. Once sufficient information on co-refining processes are available to detail the product yields and compositions from co-refining, it is recommended that a co-refining facility including pyrolysis, hydrotreating and FT processes should be evaluated as a possibility for the PTJ process. This is due to the possibility of higher yields that might be achievable in co-refining systems.

REFERENCES

[1]   S. Sgouridis, P. A. Bonnefoy, and R. J. Hansman, "Air transportation in a carbon constrained world: Long-term dynamics of policies and strategies for mitigating the carbon footprint of commercial aviation," *A Collection of Papers:Transportation in a World of Climate Change*, vol. 45, no. 10, pp. 1077-1091, 2011.

[2]   Intergovernmental Panel on Climate Change, "Aviation and the Global Atmosphere," no. Cambridge University Press, 1999.

[3]   K. Maniatis, M. Weitz, and A. Zschocke, "2 million tons per year : A performing biofuels supply chain for EU aviation," no. June. pp. 1-27, 2011.

[4]   IATA, "IATA 2012 Report on Alternative Fuels," 2012.

[5]   IATA, "IATA 2009 Report on Alternative Fuels," 2009.

[6]   IATA, "IATA 2010 Report on Alternative Fuels," Canada, 2010.

[7]   IATA, "IATA 2011 Report on Alternative Fuels," Canada, 2011.

[8]   News24, "SAA , Boeing look to tobacco for jet fuel," Cape Town, Aug-2014.

[9]   N. Odendaal, "SAA to test biofuel flight next year," *Creamer Media`s Engineering News*, Dec-2014.

[10]   UK Ministry of Defence, "Defence Standard 91-91 : Turbine Fuel, Aviation Type, Jet A-1," vol. Issue 6. 2008.

[11]   ASTM International Standards Worldwide Subcommittee:D02.J0.06, "Standard Specification for Aviation Turbine Fuel Containing Synthesized," 2011.

[12]   A. De Klerk, *Fischer-Tropsch Refining*. Wiley Online Library, 2011.

[13]   G. W. Huber, S. Iborra, and A. Corma, "Synthesis of transportation fuels from biomass: chemistry, catalysts, and engineering.," *Chemical reviews*, vol. 106, no. 9, pp. 4044-98, Sep. 2006.

[14]   D. Mohan, C. Pittman, and P. H. Steele, "Pyrolysis of Wood/Biomass for Bio-oil: A Critical Review," *Energy & Fuels*, vol. 20, no. 3, pp. 848-889, May 2006.

[15]   E. D. Christensen, G. M. Chupka, J. Luecke , T. Smurthwaite, T. L. Alleman, K. Iisa, J. Franz, D. C. Elliott, and R. L. McCormick, "Analysis of Oxygenated Compounds in Hydrotreated Biomass Fast Pyrolysis Oil Distillate Fractions," *Energy & Fuels*, vol. 25, no. 11, pp. 5462-5471, Nov. 2011.

[16]   D. C. Elliott, T. R. Hart, G. G. Neuenschwander, L. J. Rotness, and A. H. Zacher, "Catalytic Hydroprocessing of Biomass Fast Pyrolysis Bio-oil to Produce Hydrocarbon Products," *Environmental Progress & Sustainable Energy*, vol. 28, no. 3, pp. 441-449, 2009.

[17]   D. C. Elliott, T. R. Hart, G. G. Neuenschwander, L. J. Rotness, M. V. Olarte, A. H. Zacher, & Y. Solantausta, "Catalytic Hydroprocessing of Fast Pyrolysis Bio-oil from Pine Sawdust," *Energy & Fuels*, 2012.

[18]   J. Sandquist and M. B. Guell, "Overview of Biofuels for Aviation," *Chemical Engineering Transactions*, vol. 29, pp. 1147-1152, 2012.

[19]   E. Corporan, T. Edwards, L. Shafer, M. J. DeWitt, C. Klingshirn, S. Zabarnick, Z. West, R. Striebich, J. Graham, and J. Klein, "Chemical , Thermal Stability , Seal Swell , and Emissions Studies of Alternative Jet Fuels," *Energy & fuels*, vol. 25, pp. 955-966, 2011.

[20]   G. R. Wilson, T. Edwards, E. Corporan, and R. L. Freerks, "Certification of Alternative Aviation Fuels and Blend Components," *Energy & Fuels*, vol. 27, no. 2, pp. 962-966, Feb. 2013.

[21]   W. J. DeSisto, N. Hill, S. H. Beis, S. Mukkamala, J. Joseph, C. Baker, T. Ong, E. A. Stemmler, M. C. Wheeler, B. G. Frederick, A. van Heiningen, "Fast Pyrolysis of Pine Sawdust in a Fluidized-Bed Reactor," *Energy & Fuels*, vol. 24, no. 4, pp. 2642-2651, Apr. 2010.

[22]   J. I. Hileman, D. S. Ortiz, J. T. Bartis, H. M. Wong, P. E. Donohoo, M. A. Weiss, and I. A. Waitz, "Near-Term Feasibility of Alternative Jet Fuels," 2009.

[23]   B. M. Guell, M. Bugge, R. S. Kempegowda, A. George, and S. M. Paap, "Benchmark of conversion and production technologies for synthetic biofuels for aviation," Norway, 2012.

[24]   P. Basu, *Biomass gasification and pyrolysis: practical design and theory*. Academic Press, 2010.

[25]   P. M. Mortensen, J. D. Grunwaldt, P. A. Jensen, K. G. Knudsen, and A. D. Jensen, "A review of catalytic upgrading of bio-oil to engine fuels," *Applied Catalysis A: General*, vol. 407, pp. 1-19, Nov. 2011.

[26]   J. C. Mankins, "Technology readiness assessments: A retrospective," *Acta Austronautica*, vol. 65, no. 9–10, pp. 1216- 1223, 2009.

[27]   W. Baldauf, U. Balfanz, and M. Rupp, "Upgrading of flash pyrolysis oil and utilization in refineries," *Biomass and Bioenergy*, vol. 7, no. 1–6, pp. 237-244, 1994.

[28]   E. Furimsky, "Catalytic hydrodeoxygenation," *Applied Catalysis A: General*, vol. 199, no. 2, pp. 147-190, Jun. 2000.

[29]   A. Oasmaa and C. Peacocke, "Properties and fuel use of biomass-derived fast pyrolysis liquids," *Vtt Publications*, 2010.

[30]   J. Holmgren, R. Marinangeli, P. Nair, D. Elliott, and R. Bain, "Consider upgrading pyrolysis oils into renewable fuels," *Hydrocarbon Processing*, vol. 87, no. 9, 2008.

[31]   A. Oasmaa and S. Czernik, "Fuel Oil Quality of Biomass Pyrolysis Oils-State of the Art for the End Users," *Energy &Fuels*, vol. 13, pp. 914-921, 1999.

[32]   A. V. Bridgwater, "Review of fast pyrolysis of biomass and product upgrading," *Biomass and Bioenergy*, vol. 38, pp. 68-94, 2012.

[33]   A. Oasmaa, E. Kuoppala, and D. C. Elliott, "Development of the Basis for an Analytical Protocol for Feeds and Products of Bio-oil Hydrotreatment," *Energy & Fuels*, vol. 26, no. 4, pp. 2454-2460, Apr. 2012.

[34]   D. C. Elliott, "Historical Developments in Hydroprocessing Bio-oils," *Energy & Fuels*, vol. 21, no. 3, pp. 1792-1815, May 2007.

[35]   D. Sutton, "Refining 101." Marathon Petroleum Company LP, 2012.

[36]   US Department of Energy, "Petroleum & other liquids," 2013. [Online]. Available: http://www.eia.gov/dnav/pet/pet_pnp_pct_dc_nus_pct_a.htm. [Accessed: 01-Jan-2014].

[37]   L. Ingram, D. Mohan, M. Bricka, P. Steele, D. Strobel, D. Crocker, B. Mitchell, J. Mohammed, K. Cantrell, and C. U. Pittman, "Pyrolysis of wood and bark in an auger reactor: Physical properties and chemical analysis of the produced bio-oils," *Energy & Fuels*, vol. 22, no. 1, pp. 614-625, 2008.

[38]   A. S. Kalgo, "The Development and Optimisation of a Fast Pyrolysis Process for Bio-oil Production," Aston University, 2011.

[39]   A. V. Bridgwater, "Principles and practice of biomass fast pyrolysis processes for liquids," *Journal of Analytical and Applied Pyrolysis*, vol. 51, pp. 3-22, 1999.

[40]   H. Yang, R. Yan, H. Chen, D. H. Lee, and C. Zheng, "Characteristics of hemicellulose, cellulose and lignin pyrolysis," *Fuel*, vol. 86, no. 12–13, pp. 1781-1788, Aug. 2007.

[41]   J. V. Kumar and B. C. Pratt, "Compositional analysis of some renewable biofuels.," *American Laboratory*, vol. 28, no. 8, pp. 15-20, 1996.

[42]   D. Lv, M. Xu, X. Liu, Z. Zhan, Z. Li, and H. Yao, "Effect of cellulose, lignin, alkali and alkaline earth metallic species on biomass pyrolysis and gasification," *Gasification: Fundamentals and application*, vol. 91, no. 8, pp. 903-909, 2010.

[43]   H. Wang, J. Male, and Y. Wang, "Recent Advances in Hydrotreating of Pyrolysis Bio-Oil and Its Oxygen-Containing Model Compounds," *ACS Catalysis*, vol. 3, no. 5, pp. 1047-1070, May 2013.

196

[44]   T. B. Reed, *Encyclopedia of biomass Thermal Conversion: Kinetics of char gasification reactions above 500C (Chapter 7)*, 3rd Editio. Biomass Energy Foundation Press, 2002, p. II-289.

[45]   J. Piskorz, D. Radlein, and D. S. Scott, "On the mechanism of the rapid pyrolysis of cellulose," *Journal of Analytical and Applied Pyrolysis*, vol. 9, no. 2, pp. 121-137, Jan. 1986.

[46]   J. P. Diebold and A. V. Bridgwater, "Overview of fast pyrolysis of biomass for the production of liquid fuels," in *Developments in Thermochemical Biomass Conversion*, A. V. Bridgwater and D. G. B. Boocock, Eds. Blackie Academic & Professional, 1997, pp. 5-27.

[47]   C. Branca, P. Giudicianni, and C. Di Blasi, "GC/MS Characterization of Liquids Generated from Low-Temperature Pyrolysis of Wood," *Industrial & Engineering Chemistry Research*, vol. 42, no. 14, pp. 3190-3202, Jul. 2003.

[48]   A. . Bridgwater, S. Czernik, and J. Piskorz, "An overview of fast pyrolysis," in *Progress in Thermochemical Biomass Conversion*, A. Bridgwater, Ed. Oxford, UK: Blackwell Science Ltd, 2008.

[49]   D. Radlein, "The production of chemicals from fast pyrolysis of bio-oils," in *Fast Pyrolysis of Biomass: A Handbook*, Vol.1 ed., Newbury, UK: CPL Press, 1999, p. 164.

[50]   K. Kudo and E. Yoshida, "The decomposition process of wood constituents in the course of carbonization I: the decomposition of carbohydrate and lignin in Mizunara.," *Journal of the Japan Wood Research Society*, vol. 42, no. 16, pp. 125-127, 1957.

[51]   a. Oasmaa and E. Kuoppala, "Fast Pyrolysis of Forestry Residue. 3. Storage Stability of Liquid Fuel," *Energy & Fuels*, vol. 17, no. 4, pp. 1075-1084, Jul. 2003.

[52]   D. Mohan, C. U. (Jnr) Pittman, and P. H. Steele, "Pyrolysis of wood/biomass for bio-oil: a critical review," *Energy and Fuels*, vol. 20, no. 3, pp. 848-889, 2006.

[53]   E. J. Soltes and T. J. Elder, *Pyrolysis*. CRC Press, 1981.

[54]   J. Zakzeski, P. C. A. Bruijnincx, A. L. Jongerius, and B. M. Weckhuysen, "The catalytic valorization of lignin for the production of renewable chemicals.," *Chemical reviews*, vol. 110, no. 6, pp. 3552-99, Jun. 2010.

[55]   E. Dorrestijn, L. J. J. Laarhoven, I. W. C. E. Arends, and P. Mulder, "The occurrence and reactivity of phenoxyl linkages in lignin and low rank coal," *Journal of Analytical and Applied pyrolysis*, vol. 54, pp. 153-192, 2000.

[56]   A. Oasmaa, Y. Solantausta, V. Arpiainen, E. Kuoppala, and K. Sipilä, "Fast Pyrolysis Bio-Oils from Wood and Agricultural Residues," *Energy & Fuels*, vol. 24, no. 2, pp. 1380-1388, Feb. 2010.

[57]   S. B. Jones, C. Valkenburg, C. W. Walton, D. C. Elliott, J. E. Holladay, D. J. Stevens, C. Kinchin, and S. Czernik, "Production of gasoline and diesel from biomass via fast pyrolysis, hydrotreating and hydrocracking: a design case," Pacific Northwest National Laboratory, United States of America, 2009.

[58]   M. Cottam and A. V. Bridgwater, "Techno-economic modelling of biomass flash pyrolysis and upgrading systems," *Biomass and Bioenergy*, vol. 7, no. 1–6, pp. 267-273, 1994.

[59]   Y. C. Chen, Y. N. Pan, and K. H. Hsieh, "Process Optimization of Fast Pyrolysis Reactor for Converting Forestry Wastes into Bio-Oil with the Taguchi Method," *Procedia Environmental Sciences*, vol. 10, pp. 1719-1725, 2011.

[60]   R. Fahmi, a. V. Bridgwater, I. Donnison, N. Yates, and J. M. Jones, "The effect of lignin and inorganic species in biomass on pyrolysis oil yields, quality and stability," *Fuel*, vol. 87, no. 7, pp. 1230-1240, Jun. 2008.

[61]   D. Meier and O. Faix, "State of the art of applied fast pyrolysis of lignocellulosic materials-a review," *Bioresource Technology*, vol. 68, no. 1, pp. 71-77, 1999.

[62]   T. J. Hugo, "Pyrolysis of Sugarcane Bagasse," University of Stellenbosch, 2010.

[63]   J. Joubert, M. Carrier, R. Stahl, and J. H. Knoetze, "Fast Pyrolysis of Eucalyptus grandis," 2011, no. 1998.

[64]   D. Elliott, "Analysis and comparison of biomass pyrolysis / gasification condensates: Final report, report No PNL-5943," Richland, Washington, 1986.

[65]   H. S. Heo, H. J. Park, J. Yim, J. M. Sohn, J. Park, S. Kim, C. Ryu, J. Jeon, and Y. Park, "Influence of operation variables on fast pyrolysis of Miscanthus sinensis var. purpurascens.," *Bioresource technology*, vol. 101, no. 10, pp. 3672-7, May 2010.

[66]   S. Kim, S. Jung, and J. Kim, "Fast pyrolysis of palm kernel shells: influence of operation parameters on the bio-oil yield and the yield of phenol and phenolic compounds," *Bioresource technology*, vol. 101, no. 23, pp. 9294-300, Dec. 2010.

[67]   R. Li, Z. Zhong, B. Jin, X. Jiang, C. Wang, and A. Zheng, "Influence of reaction conditions and red brick on fast pyrolysis of rice residue (husk and straw) in a spout-fluid bed," *The Canadian Journal of Chemical Engineering*, vol. 9999, Aug. 2011.

[68]   M. Carrier, J. Joubert, S. Danje, T. Hugo, J. Görgens, and J. Knoetze, "Impact of the lignocellulosic material on fast pyrolysis yields and product quality," *BIORESOURCE TECHNOLOGY*, vol. 150, pp. 129-138, 2013.

[69]   R. A. Hague, "The pre-treatment and pyrolysis of biomass for the production of liquids for fuels and speciality chemicals," Aston University, 1998.

[70]   D. J. Nowakowski, A. V. Bridgwater, D. C. Elliott, D. Meier, and P. de Wild, "Lignin fast pyrolysis: Results from an international collaboration," *Journal of Analytical and Applied Pyrolysis*, vol. 88, no. 1, pp. 53-72, 2010.

[71]   H. Aubin and C. Roy, "Study on the corrosiveness of wood pyrolysis oils," *Fuel Science and Technology International*, vol. 8, no. 1, pp. 77-86, 1990.

[72]   L. Qiang, L. Wen-Zhi, and Z. Xi-Feng, "Overview of fuel properties of biomass fast pyrolysis oils," *Energy Conversion and Management*, vol. 50, no. 5, pp. 1376-1383, May 2009.

[73]   D. a. Bulushev and J. R. H. Ross, "Catalysis for conversion of biomass to fuels via pyrolysis and gasification: A review," *Catalysis Today*, vol. 171, no. 1, pp. 1-13, Aug. 2011.

[74]   R. H. Venderbosch and W. Prins, "Fast pyrolysis technology development," *Biofuels, Bioproducts and Biorefining*, vol. 4, no. 2, pp. 178-208, 2010.

[75]   A. Oasmaa and D. Meier, "Norms and standards for fast pyrolysis liquids," *Journal of Analytical and Applied Pyrolysis*, vol. 73, no. 2, pp. 323-334, Jun. 2005.

[76]   T. Milne, F. Agblevor, M. Davis, S. Deutch, and D. Johnson, *Developments in thermochemical biomass conversion*. London: Blackie Academic & Professional, 1997, p. 409.

[77]   J. H. Marsman, J. Wildschut, F. Mahfud, and H. J. Heeres, "Identification of components in fast pyrolysis oil and upgraded products by comprehensive two-dimensional gas chromatography and flame ionisation detection," *Journal of chromatography. A*, vol. 1150, no. 1–2, pp. 21-7, May 2007.

[78]   E. Park, B. Kang, and J. Kim, "Recovery of Oils With High Caloric Value and Low Contaminant Content By Pyrolysis of Digested and Dried Sewage Sludge Containing Polymer Flocculants," *Energy & Fuels*, vol. 22, no. 2, pp. 1335-1340, Mar. 2008.

[79]   J. Joubert, "Pyrolysis of Eucalyptus grandis," University of Stellenbosch, 2013.

[80]   M. E. Myers, J. Stollstelmer, and A. M. Wims, "Determination of Hydrocarbon-Type Distribution and Hydrogen / Carbon Ratio of Gasolines by Nuclear Magnetic Resonance Spectrometry," *Analytical Chemistry*, vol. 47, no. 12, 1975.

[81]   A. Sınağ, B. Uskan, and S. Gülbay, "Detailed characterization of the pyrolytic liquids obtained by pyrolysis of sawdust," *Journal of Analytical and Applied Pyrolysis*, vol. 90, no. 1, pp. 48-52, Jan. 2011.

[82]   H. S. Joo and J. A. Guin, "Continuous upgrading of a plastics pyrolysis liquid to an environmentally favorable gasoline range product," *Fuel Processing Technology*, vol. 57, no. 1, pp. 25-40, Aug. 1998.

[83]   F. Ateş, E. Pütün, and A. E. Pütün, "Fast pyrolysis of sesame stalk: yields and structural analysis of bio-oil," *Journal of Analytical and Applied Pyrolysis*, vol. 71, no. 2, pp. 779-790, Jun. 2004.

[84]   A. V. Bridgwater, "Production of high grade fuels and chemicals from catalytic pyrolysis of biomass," *Catalysis Today*, vol. 29, pp. 285-95, 1996.

[85]   J. C. Serrano-Ruiz and J. A. Dumesic, "Catalytic routes for the conversion of biomass into liquid hydrocarbon transportation fuels," *Energy & Environmental Science*, vol. 4, no. 1, p. 83, 2011.

[86]   A. V. Bridgwater, A. J. Toft, and J. G. Brammer, "A techno-economic comparison of power production by biomass fast pyrolysis with gasification and combustion," *Renewable and Sustainable Energy Reviews*, vol. 6, no. 3, pp. 181-248, Sep. 2002.

[87]   A. . Bridgwater, "Catalysis in thermal biomass conversion," *Applied Catalysis A,*, vol. 116, no. 1–2, pp. 5-47, 1994.

[88]   F. De Miguel Mercader, M. J. Groeneveld, S. R. Kersten, C. Geantet, G. Toussaint, N. W. J. Way, C. J. Schaverien, and K. J. A. Hogendoorn, "Hydrodeoxygenation of pyrolysis oil fractions: process understanding and quality assessment through co-processing in refinery units," *Energy & Environmental Science*, vol. 4, no. 3, p. 985, 2011.

[89]   M. C. Samolada, W. Baldauf, and I. A. Vasalos, "Production of a bio-gasoline by upgrading biomass flash pyrolysis liquids via hydrogen processing and catalytic cracking," *Fuel*, vol. 77, no. 14, pp. 1667-1675, Nov. 1998.

[90]   R. H. Venderbosch, A. R. Ardiyanti, J. Wildschut, A. Oasmaa, and H. J. Heeres, "Stabilization of biomass-derived pyrolysis oils," *Journal of Chemical Technology & Biotechnology*, vol. 85, no. 5, pp. 674-686, May 2010.

[91]   J. Wildschut, F. H. Mahfud, R. H. Venderbosch, and H. J. Heeres, "Hydrotreatment of Fast Pyrolysis Oil Using Heterogeneous Noble-Metal Catalysts," *Industrial & Engineering Chemistry Research*, vol. 48, no. 23, pp. 10324-10334, Dec. 2009.

[92]   J. Wildschut, "Pyrolysis oil upgrading to transportation fuels by catalytic hydrotreatment," Rijksuniversiteit Groningen, 2009.

[93]   D. C. Elliott and T. R. Hart, "Catalytic Hydroprocessing of Chemical Models for Bio-oil," *Energy & Fuels*, vol. 23, no. 2, pp. 631-637, Feb. 2009.

[94]   Y. Wang, T. He, K. Liu, J. Wu, and Y. Fang, "From biomass to advanced bio-fuel by catalytic pyrolysis/hydro-processing: Hydrodeoxygenation of bio-oil derived from biomass catalytic pyrolysis," *Bioresource technology*, vol. 108, pp. 280-4, Mar. 2012.

[95]   J. Wildschut, I. Melián-Cabrera, and H. J. Heeres, "Catalyst studies on the hydrotreatment of fast pyrolysis oil," *Applied Catalysis B: Environmental*, vol. 99, no. 1–2, pp. 298-306, Aug. 2010.

[96]   J. Wildschut, M. Iqbal, F. H. Mahfud, I. M. Cabrera, R. H. Venderbosch, and H. J. Heeres, "Insights in the hydrotreatment of fast pyrolysis oil using a ruthenium on carbon catalyst," *Energy & Environmental Science*, vol. 3, no. 7, p. 962, 2010.

[97]   P. Dufresne, "Hydroprocessing catalysts regeneration and recycling," *Applied Catalysis A: General*, vol. 322, pp. 67-75, Apr. 2007.

[98]   ASTM International Standards Worldwide Subcommittee:D02.J0.01, "Standard Specification for Aviation Turbine Fuels," D1655–11b ed., 2011, pp. 1-16.

[99]   P. T. Williams and P. A. Horne, "Characterisation of oils from the fluidised bed pyrolysis of biomass with zeolite catalyst upgrading," *Biomass and Bioenergy*, vol. 7, no. l–6, pp. 223-236, 1994.

[100] X. Y. Guo, Y. J. Yan, and T. C. Li, "Influence of catalyst type and regeneration on upgrading of crude bio-oil through catalytical thermal cracking," *The Chinese Journal of Process Engineering*, vol. 4, no. 1, pp. 53-58, 1994.

[101] R. Gunawan, X. Li, C. Lievens, M. Gholizadeh, W. Chaiwat, X. Hu, D. Mourant, J. Bromly, and C. Li, "Upgrading of bio-oil into advanced biofuels and chemicals. Part I. Transformation of GC-detectable light species during the hydrotreatment of bio-oil using Pd/C catalyst," *Fuel*, vol. 111, pp. 709-717, Sep. 2013.

[102] N. H. Leibbrandt, "Techno-economic study for sugarcane bagasse to liquid biofuels in South Africa: A comparison between Biological and Thermochemical process routes," University of Stellenbosch, 2010.

[103] F. Nsaful, "Process modelling of sugar mill biomass to energy conversion processes and energy integration of pyrolysis," University of Stellenbosch, 2012.

[104] M. Ringer, V. Putsche, and J. Scahill, "Large-Scale Pyrolysis Oil Production: A Technology Assessment and Economic Analysis," 2006.

[105] R. P. Anex, A. Aden, F. K. Kazi, J. Fortman, R. M. Swanson, M. M. Wright, J. Satrio, R. C. Brown, D. E. Daugaard, A. Platon, G. Kothandaraman, D. D. Hsu, and A. Dutta, "Techno-economic comparison of biomass-to-transportation fuels via pyrolysis, gasification, and biochemical pathways," *Fuel*, vol. 89, p. S29-S35, Nov. 2010.

[106] M. M. Wright, J. A. Satrio, R. C. Brown, D. E. Daugaard, and D. D. Hsu, "Techno-Economic Analysis of Biomass Fast Pyrolysis to Transportation Fuels," 2010.

[107] M. M. Wright, D. E. Daugaard, J. A. Satrio, and R. C. Brown, "Techno-economic analysis of biomass fast pyrolysis to transportation fuels," *Fuel*, vol. 89, p. S2-S10, Nov. 2010.

[108] T. R. Brown, R. Thilakaratne, R. C. Brown, and G. Hu, "Techno-economic analysis of biomass to transportation fuels and electricity via fast pyrolysis and hydroprocessing," *Fuel*, vol. 106, pp. 463-469, Apr. 2013.

[109] P. Badger, S. Badger, M. Puettmann, P. Steele, and J. Cooper, "Techno-economic analysis: Preliminary assessment of pyrolysis oil production costs and material energy balances associated with transportable fast pyrolysis systems," *BioResources*, vol. 6, no. 1, pp. 34-47, 2011.

[110] D. Iribarren, J. F. Peters, and J. Dufour, "Life cycle assessment of transportation fuels from biomass pyrolysis," *Fuel*, vol. 97, pp. 812-821, Jul. 2012.

[111] Ensyn, "Key RTP Facilities," 2012. [Online]. Available: http://www.ensyn.com/technology/key-rtp-facilities/. [Accessed: 12-Jan-2014].

[112] Ensyn, "Overview Unique, Patented and Proprietary," 2012. [Online]. Available: http://www.ensyn.com/technology/overview/. [Accessed: 12-Jan-2014].

[113] C. Hamelinck, G. van Hooijdonk, and A. Faaij, "Ethanol from lignocellulosic biomass: techno-economic performance in short-, middle-and long-term," *Biomass and Bioenergy*, vol. 4, no. 28, pp. 384-410, 2005.

[114] S. A. Channiwala and P. P. Parikh, "A unified correlation for estimating HHV of solid , liquid and gaseous fuels," *Fuel*, vol. 81, pp. 1051-1063, 2002.

[115] A. M. Petersen, "Comparison of the technical, financial risk and life cycle assessments of various processing options of sugarcane," University of Stellenbosch, 2012.

[116] H. Jin, E. D. Larson, and F. E. Celik, "Performance and cost analysis of future , commercially mature gasification-based electric power generation from switchgrass," *Biofuels, Bioproducts and Biorefining*, pp. 142-173, 2009.

[117] R. Turton, R. C. Bailie, W. B. Whiting, and J. A. Shaeiwitz, "Pinch Technology," in *Analysis, Synthesis and Design of Chemical Processes*, Third Edit., Westford, Massachusetts: Pearson Education, Inc., 2010, pp. 521- 581.

[118] KBC Energy services, "Pinch Technology Introduction." .

[119] Linnhoff March, "Introduction to Pinch Technology," 1998.

[120] F. A. Perrins, Ed., "Fourth European Symposium on Computer Aided Process Engineering," in *ESCAPE 4: A three-day symposium No. 507*, 1994.

[121] E. Vagia and A. Lemonidou, "Thermodynamic analysis of hydrogen production via autothermal steam reforming of selected components of aqueous bio-oil fraction," *International Journal of Hydrogen Energy*, vol. 33, no. 10, pp. 2489-2500, May 2008.

[122] E. Vagia and A. Lemonidou, "Thermodynamic analysis of hydrogen production via steam reforming of selected components of aqueous bio-oil fraction," *International Journal of Hydrogen Energy*, vol. 32, no. 2, pp. 212-223, Feb. 2007.

[123] J. Piskorz, D. . Scott, and D. Radlein, *Pyrolysis Oils from Biomass*, vol. 376. Washington, DC: American Chemical Society, 1988.

[124] S. Chernik, D. Wang, D. Montane, and E. Chornet, *Developments in thermochemical biomass conversion*. London: Blackie Academic & Professional, 1996, pp. 672-686.

[125] M. K. Cohce, M. a. Rosen, and I. Dincer, "Efficiency evaluation of a biomass gasification-based hydrogen production," *International Journal of Hydrogen Energy*, vol. 36, no. 17, pp. 11388-11398, Aug. 2011.

[126] S. Turn, C. Kinoshita, and D. Ishimura, "An Experimental Investigation of Hydrogen Production from Biomass Gasification," *International Journal Hydrogen Energy*, vol. 23, no. 8, pp. 641-648, 1998.

[127] P. Spath, A. Aden, T. Eggeman, M. Ringer, B. Wallace, and J. Jechura, "Biomass to Hydrogen Production Detailed Design and Economics Utilizing the Battelle Columbus Heated Gasifier," 2005.

[128] S. B. Jones, C. Valkenburg, C. W. Walton, D. C. Elliott, J. E. Holladay, D. J. Stevens, C. Kinchin, and S. Czernik, "Design Case Summary: Production of Gasoline and Diesel from Biomass via Fast Pyrolysis , Hydrotreating , and Hydrocracking," 2009.

[129] P. L. Spath and M. K. Mann, "Life Cycle Assessment of Hydrogen Production via Natural Gas Steam Reforming Life Cycle Assessment of Hydrogen Production via Natural Gas Steam Reforming," Cola]orado, 2001.

[130] J. G. Lacson, *Chemical Economics Handbook Product Review: Natural Gas*, Volume 4. Menlo Park, CA: SRI International, 1999, p. Section 229.2000.

[131] SRI International, "Options for Refinery Hydrogen." Menlo Park, CA, 1994.

[132] S. Parkash, "Hydrogen Production and Recovery," in *Refinery Processes Handbook*, 2003.

[133] R. A. Meyers, "Hydrogen Production," in *Handbook of Petroleum Refining Processes*, Third., McGraw-Hill Education, 2004.

[134] M. K. Mann, "Technical and Economic Assessment of Producing Hydrogen by Reforming Syngas from the Battelle Indirectly Heated Biomass Gasifier Technical and Economic Assessment of Producing Hydrogen by Reforming Syngas from the Battelle Indirectly Heated Biomass Gasifi," Colorado, 1995.

[135] N. R. Udengaard, "Hydrogen production by steam reforming of hydrocarbons," *Division of Fuel Chemistry, American Chemical Society (pre-print papers)*, vol. 49, no. 2, pp. 906-907, 2004.

[136] J. C. Molburg and R. D. Doctor, "Hydrogen from Steam-Methane Reforming with CO 2 Capture Hydrogen from Steam-Methane Reforming with CO2 Capture," Illinois, 2003.

[137] S. M. Leiby, "Options for Refinery Hydrogen," Menlo Park, CA, 1994.

[138] C. a. Grande, "Advances in Pressure Swing Adsorption for Gas Separation," *ISRN Chemical Engineering*, vol. 2012, pp. 1-13, 2012.

[139] S. Parkash, "Refinery Distillation," in *Refinery Processes Handbook*, Gulf Professional Publishing, 2003, pp. 1-28.

[140] R. K. More, V. K. Bulasara, R. Uppaluri, and V. R. Banjara, "Optimization of crude distillation system using aspen plus: Effect of binary feed selection on grass-root design," *Chemical Engineering Research and Design*, vol. 88, no. 2, pp. 121-134, Feb. 2010.

[141] Department of Environmental Affairs and Tourism, "AQA implementation: Listed activities and minimum emission standards." Republic of South Africa, 2008.

[142] F. Nsaful, J. F. Görgens, and J. H. Knoetze, "Comparison of combustion and pyrolysis for energy generation in a sugarcane mill," *Energy Conversion and Management*, vol. 74, pp. 524-534, Oct. 2013.

[143] T. G. Kreutz, E. D. Larson, G. Liu, and R. H. Williams, "Fischer-Tropsch Fuels from Coal and Biomass," no. August. Pittsburgh, Pennsylvania, 2008.

[144] R. Turton, R. C. Bailie, W. B. Whiting, and J. A. Shaeiwitz, "Utilizing experience-based principles to confirm the sustainability of a process design," in *Analysis, Synthesis and Design of Chemical Processes*, Third Edit., Westford, Massachusetts: Pearson Education, Inc, 2010, pp. 363-391.

[145] G. J. Suppes, "Heuristics in Chemical Engineering." Butterworth-Heinemann, 2002.

[146] D. W. Green and R. H. Perry, *Perry`s Chemical Engineers Handbook*, 8th ed. McGraw-Hill, 2007, pp. 12-21.

[147] B. Bergsten, "Evaporative Cooling Tower and Chilled Beams Evaporative Cooling Tower and Chilled Beams," Chalmers University of Technology, 2009.

[148] L. Trygg and S. Amiri, "European perspective on absorption cooling in a combined heat and power system – A case study of energy utility and industries in Sweden," *Applied Energy*, vol. 84, no. 12, pp. 1319-1337, Dec. 2007.

[149] S. Parkash, "Refinery Water Systems," in *Refining Processes Handbook*, S. Parkash, Ed. Burlington: Gulf Professional Publishing, 2003, pp. 242-269.

[150] H. Wake, "Oil refineries: a review of their ecological impacts on the aquatic environment," *Estuarine, Coastal and Shelf Science*, vol. 62, no. 1–2, pp. 131-140, Jan. 2005.

[151] H. E. Tatem, B. a. Cox, and J. W. Anderson, "The toxicity of oils and petroleum hydrocarbons to estuarine crustaceans," *Estuarine and Coastal Marine Science*, vol. 6, no. 4, pp. 365-373, Apr. 1978.

[152] G. S. Veeresh, P. Kumar, and I. Mehrotra, "Treatment of phenol and cresols in upflow anaerobic sludge blanket (UASB) process: a review.," *Water research*, vol. 39, no. 1, pp. 154-70, Jan. 2005.

[153] B. H. Diya'uddeen, W. M. A. W. Daud, and a. R. Abdul Aziz, "Treatment technologies for petroleum refinery effluents: A review," *Process Safety and Environmental Protection*, vol. 89, no. 2, pp. 95-105, Mar. 2011.

[154] M. H. El-Naas, S. Al-Zuhair, A. Al-Lobaney, and S. Makhlouf, "Assessment of electrocoagulation for the treatment of petroleum refinery wastewater.," *Journal of environmental management*, vol. 91, no. 1, pp. 180-5, Oct. 2009.

[155] J. E. F. Moraes, F. H. Quina, C. A. O. Nascimento, D. N. Silva, and O. Chiavone-Filho, "Treatment of saline wastewater contaminated with hydrocarbons by the photo-Fenton process.," *Environmental science & technology*, vol. 38, no. 4, pp. 1183-7, Feb. 2004.

[156] G. Lettinga, L. W. H. Pol, I. W. Koster, W. M. Wiegant, W. J. De Zeeuw, A. Rinzema, P. C. Grin, R. E. Roersma, and S. W. Hobma, "High-Rate Anaerobic Waste-Water Treatment Using the UASB Reactor under a Wide Range of Temperature Conditions," *Biotechnology and Genetic Engineering Reviews*, vol. 2, no. 1, pp. 253-284, Oct. 1984.

[157] R. E. Speece, "Anaerobic biotechnology for industrial wastewater treatment," *Environmental Science & Technology*, vol. 17, no. 9, p. 416A-427A, 1983.

[158] F. Ma, J. Guo, L. Zhao, C. Chang, and D. Cui, "Application of bioaugmentation to improve the activated sludge system into the contact oxidation system treating petrochemical wastewater.," *Bioresource technology*, vol. 100, no. 2, pp. 597-602, Jan. 2009.

[159] M. L. Hami, M. a. Al-Hashimi, and M. M. Al-Doori, "Effect of activated carbon on BOD and COD removal in a dissolved air flotation unit treating refinery wastewater," *Desalination*, vol. 216, no. 1–3, pp. 116-122, Oct. 2007.

[160] F. V. Santos, E. B. Azevedo, G. L. Sant Anna Jr., and M. Dezotti, "Photocatalysis as a tertiary treatment for petroleum refinery wastewaters," *Brazilian Journal of Chemical Engineering*, vol. 23, no. 04, pp. 451-460, 2006.

[161] A. Coelho, A. V. Castro, M. Dezotti, and G. L. Sant'Anna, "Treatment of petroleum refinery sourwater by advanced oxidation processes.," *Journal of hazardous materials*, vol. 137, no. 1, pp. 178-84, Sep. 2006.

[162] Energy and Environmental Analysis, "Technology Characterization : Steam Turbines," Virginia, 2008.

[163] W. Alonso-Pippo, C. a. Luengo, F. F. Felfli, P. Garzone, and G. Cornacchia, "Energy recovery from sugarcane biomass residues: Challenges and opportunities of bio-oil production in the light of second generation biofuels," *Journal of Renewable and Sustainable Energy*, vol. 1, no. 6, p. 063102, 2009.

[164] J. M. Ogden, S. Hochgreb, and M. Hylton, "Steam economy and cogeneration in cane sugar factories," *International Sugar Journal*, vol. 92, no. 1099, pp. 131-140, 1990.

[165] C. Mbohwa and S. Fukuda, "Electricity from bagasse in Zimbabwe," *Biomass and Bioenergy*, vol. 25, no. 2, pp. 197-207, Aug. 2003.

[166] J. M. Quevauvilliers, "Implications for cogeneration industry: description of an advanced cogeneration plant." Quatre Bornes, Mauritius, 2001.

[167] A. Oasmaa, A. Kalli, C. Lindfors, D. C. Elliott, D. Springer, C. Peacocke, and D. Chiaramonti, "Guidelines for Transportation, Handling, and Use of Fast Pyrolysis Bio-Oil. 1. Flammability and Toxicity," 2012.

[168] M. Garcia-Perez, S. Wang, J. Shen, M. Rhodes, W. J. Lee, and C. Li, "Effects of Temperature on the Formation of Lignin-Derived Oligomers during the Fast Pyrolysis of Mallee Woody Biomass," *Energy & Fuels*, vol. 22, no. 3, pp. 2022-2032, 2008.

[169] B. Kang, K. H. Lee, H. J. Park, Y. Park, and J. Kim, "Fast pyrolysis of radiata pine in a bench scale plant with a fluidized bed: Influence of a char separation system and reaction conditions on the production of bio-oil," *Journal of Analytical and Applied Pyrolysis*, vol. 76, no. 1–2, pp. 32-37, Jun. 2006.

[170] S. Danje, "Physical and chemical analyses of pine saw dust bio-oils." Stellenbosch, South Africa, 2012.

[171] A. Sluiter, B. Hames, R. Ruiz, C. Scarlata, J. Sluiter, and D. Templeton, "Determination of Ash in Biomass Laboratory Analytical Procedure (LAP)," 2008.

[172] A. Sluiter, B. Hames, D. Hyman, C. Payne, R. Ruiz, C. Scarlata, J. Sluiter, D. Templeton, and J. Wolfe, "Determination of Total Solids in Biomass and Total Dissolved Solids in Liquid Process Samples Biomass and Total Dissolved Solids in Liquid Process Samples (NREL/TP-510-42621)," 2008.

[173] B. Hames, R. Ruiz, C. Scarlata, A. Sluiter, J. Sluiter, and D. Templeton, "Preparation of Samples for Compositional Analysis Laboratory Analytical Procedure (LAP)," 2008.

[174]   A. Sluiter, B. Hames, R. Ruiz, C. Scarlata, J. Sluiter, D. Templeton, and D. Crocker, "Determination of Structural Carbohydrates and Lignin in Biomass Laboratory Analytical Procedure (LAP)," 2011.

[175]   A. Sluiter, R. Ruiz, C. Scarlata, J. Sluiter, and D. Templeton, "Determination of Extractives in Biomass Laboratory Analytical Procedure (LAP)," 2008.

[176]   K. Annamalai, J. M. Sweeten, and S. C. Ramalingam, "Estimation of gross heating values of biomass fuels," *American Society of Agricultural Engineers*, vol. 30, no. 4, pp. 1205-1208, 1987.

[177]   T. Cordero, F. Marquez, J. Rodriguez-Mirasol, and J. J. Rodriguez, "Predicting heating values of lignocellulosics and carbonaceous materials from proximate analysis," *Fuel*, vol. 80, no. 11, pp. 1567-1571, Sep. 2001.

[178]   J. Parikh, S. Channiwala, and G. Ghosal, "A correlation for calculating HHV from proximate analysis of solid fuels," *Fuel*, vol. 84, no. 5, pp. 487-494, Mar. 2005.

[179]   T. A. Milne, A. H. Brennan, and B. H. Glenn, *Source Book of methods of analysis for biomass and biomass conversion processes*. London: Elsevier Applied Science, 1990.

[180]   P. C. A. Bergman, H. Boerrigter, R.N.J Coman, J. van Doorn, A. van der Drift, S. Eenkhoorn, P. A. Geelhoed-Bonouvrie, P. G. T. Heere, D. Hoede, J. H. A. Kriel, R. Korbee, C. M. van der Meijden, M. Mozaffarian, J. P. A. Neeft, S. V. B. van Paasen, L. P. L. M. Rabou, J. H. Reith, H,. den uil, H. M. van Veen, H. J. M Visser, E. van Zessen, and R.W. R Zwart, "Contribution ECN Biomass to the '12th European conference and technology exhibition on biomass for energy, industry and climate protection'," Amsterdam, The Netherlands, 2002.

[181]   A. Oasmaa, E. Leppamaki, P. Koponen, J. Levander, and E. Tapola, *Physical characterisation of biomass-based pyrolysis liquids : Application of standard fuel oil analyses*. Espoo: JULKAISIJA – UTGIVARE – PUBLISHER, 1997.

[182]   Restek Corporation, "GC Columns," 2008. [Online]. Available: http://www.chromspec.com/pdf/e/rk10.pdf. [Accessed: 07-Jun-2012].

[183]   Agilent Technologies, "DB-1301 and DB-1701," 2012. [Online]. Available: http://www.thomassci.com/Equipment/Gas-Chromatography-Columns/_/DB-1301-and-DB-1701/#. [Accessed: 05-Jun-2012].

[184]   Zebron, "ZB-1701 GC Columns." [Online]. Available: http://www.brechbuehler.ch/fileadmin/redacteur/pdf/columns-sampleprep/gc-columns/ZB-1701.pdf. [Accessed: 05-Jun-2012].

[185]   H. J. Park, H. S. Heo, J. Jeon, J. Kim, R. Ryoo, K. Jeong, and Y. Park, "Highly valuable chemicals production from catalytic upgrading of radiata pine sawdust-derived pyrolytic vapors over mesoporous MFI zeolites," *Applied Catalysis B: Environmental*, vol. 95, no. 3–4, pp. 365-373, Apr. 2010.

[186]   J. M. Aguilera and R. S. Martin, "Steam Hydrolysis of Pine (Pinus radiata) Sawdust," *Biomass*, vol. 8, pp. 301-313, 1985.

[187]   A. Kilpeläinen, H. Peltola, A. Ryyppö, and S. Kellomäki, "Scots pine responses to elevated temperature and carbon dioxide concentration: growth and wood properties.," *Tree physiology*, vol. 25, no. 1, pp. 75-83, Jan. 2005.

[188]   F. Cherubini, "The biorefinery concept: Using biomass instead of oil for producing energy and chemicals," *Energy Conversion and Management*, vol. 51, no. 7, pp. 1412-1421, Jul. 2010.

[189]   G. P. Towler, A. R. Oroskar, and S. E. Smith, "Development of a sustainable liquid fuels infrastructure based on biomass," *Environmental Progress*, vol. 23, no. 4, pp. 334-341, Dec. 2004.

[190]   A. I. Hohlberg, J. M. Aguilera, E. Agosin, and R. San Martin, "Catalyzed Flash Pretreatments Improve Saccharification of Pine (Pinus radiata) Sawdust," *Biomass*, vol. 18, pp. 81-93, 1989.

[191]   H. J. Park, Y. Park, and J. S. Kim, "Influence of reaction conditions and the char separation system on the production of bio-oil from radiata pine sawdust by fast pyrolysis," *Fuel Processing Technology*, vol. 89, no. 8, pp. 797-802, Aug. 2008.

[192]   P. Morf, P. Hasler, and T. Nussbaumer, "Mechanisms and kinetics of homogeneous secondary reactions of tar from continuous pyrolysis of wood chips," *Fuel*, vol. 81, pp. 843-853, 2002.

[193]   H. Niu and N. Liu, "Effect of Particle Size on Pyrolysis Kinetics of Forest Fuels in Nitrogen," *Fire Safety Science*, vol. 11, pp. 1393-1405, 2014.

[194]   J. Shen, X. Wang, M. Garcia-Perez, D. Mourant, M. J. Rhodes, and C. Li, "Effects of particle size on the fast pyrolysis of oil mallee woody biomass," *Fuel*, vol. 88, no. 10, pp. 1810-1817, Oct. 2009.

[195]   M. Garcia-Perez, X. S. Wang, J. Shen, M. J. Rhodes, F. Tian, W. Lee, H. Wu, and C. Li, "Fast Pyrolysis of Oil Mallee Woody Biomass: Effect of Temperature on the Yield and Quality of Pyrolysis Products," *Industrial & Engineering Chemistry Research*, vol. 47, no. 6, pp. 1846-1854, Mar. 2008.

[196]   D. K. Shen, S. Gu, K. H. Luo, S. R. Wang, and M. X. Fang, "The pyrolytic degradation of wood-derived lignin from pulping process.," *Bioresource technology*, vol. 101, no. 15, pp. 6136-46, Aug. 2010.

[197]   J. Piskorz, D. Radlein, D. Scott, and S. Czernik, "Pretreatment of wood and cellulose of sugars by fast pyrolysis for production," *Journal of Analytical and Applied Pyrolysis*, vol. 16, pp. 127-142, 1989.

[198]   X. Sang, I. Gensch, W. Laumer, B. Kammer, C. Y. Chan, G. Engling, A. Wahner, H. Wissel, and A. Kiendler-Scharr, "Stable Carbon Isotope Ratio Analysis of Anhydrosugars in Biomass Burning Aerosol Particles from Source Samples," *Environmental Science & Technology*, vol. 46, no. 6, pp. 3312-3318, 2012.

[199]   J. H. Marsman, J. Wildschut, P. Evers, S. de Koning, and H. J. Heeres, "Identification and classification of components in flash pyrolysis oil and hydrodeoxygenated oils by two-dimensional gas chromatography and time-of-flight mass spectrometry.," *Journal of chromatography. A*, vol. 1188, no. 1, pp. 17-25, Apr. 2008.

[200]   A. Oasmaa, E. Kuoppala, S. Gust, and Y. Solantausta, "Fast Pyrolysis of Forestry Residue. 1. Effect of Extractives on Phase Separation of Pyrolysis Liquids," *Energy & Fuels*, vol. 17, no. 1, pp. 1-12, Jan. 2003.

[201]   Q. Fu, D. S. Argyropoulos, D. C. Tilotta, and L. A. Lucia, "Products and Functional Group Distributions in Pyrolysis Oil of Chromated Copper Arsenate (CCA)-Treated Wood, as Elucidated by Gas Chromatography and a Novel 31 P NMR-Based Method," *Industrial & Engineering Chemistry Research*, vol. 46, no. 16, pp. 5258-5264, Aug. 2007.

[202]   S. Fernando, S. Adhikari, C. Chandrapal, and N. Murali, "Biorefineries: Current Status, Challenges, and Future Direction," *Energy & Fuels*, vol. 20, no. 4, pp. 1727-1737, Jul. 2006.

[203]   Y. Tang, W. Yu, L. Mo, H. Lou, and X. Zheng, "One-Step Hydrogenation–Esterification of Aldehyde and Acid to Ester over Bifunctional Pt Catalysts: A Model Reaction as Novel Route for Catalytic Upgrading of Fast Pyrolysis Bio-Oil," *Energy & Fuels*, vol. 22, no. 5, pp. 3484-3488, Sep. 2008.

[204]   J. P. Diebold, "A Review of the Chemical and Physical Mechanisms of the Storage Stability of Fast Pyrolysis Bio-Oils A Review of the Chemical and Physical Mechanisms of the Storage Stability of Fast Pyrolysis Bio-Oils," Colorado, 2000.

[205]   J. Diebold, "A review of the toxicity of biomass pyrolysis liquids formed at low temperatures," 1997.

[206]   Q. Lu, X. Yang, C. Dong, Z. Zhang, X. Zhang, and X. Zhu, "Influence of pyrolysis temperature and time on the cellulose fast pyrolysis products: Analytical Py-GC/MS study," *Journal of Analytical and Applied Pyrolysis*, vol. 92, no. 2, pp. 430-438, Nov. 2011.

[207] K. Mao, G. J. Kennedy, S. M. Althaus, and M. Pruski, "Determination of the Average Aromatic Cluster Size of Fossil Fuels by Solid-State NMR at High Magnetic Field," *Energy and Fuels*, vol. 27, pp. 760-763, 2013.

[208] S. Zhou, M. Garcia-Perez, B. Pecha, S. R. A. Kersten, A. G. McDonald, and R. J. M. Westerhof, "Effect of the Fast Pyrolysis Temperature on the Primary and Secondary Products of Lignin," *Energy & Fuels*, vol. 27, no. 10, pp. 5867-5877, Oct. 2013.

[209] C. A. Mullen, A. A. Boateng, N. M. Goldberg, I. M. Lima, D. A. Laird, and K. B. Hicks, "Bio-oil and bio-char production from corn cobs and stover by fast pyrolysis," *Biomass and Bioenergy*, vol. 34, no. 1, pp. 67-74, 2010.

[210] D. Mohan, C. U. Pittman, M. Bricka, F. Smith, B. Yancey, J. Mohammad, P. Steele, M. F. Alexandre-Franco, V. Gomez-Serrano, and H. Gong, "Sorption of arsenic , cadmium , and lead by chars produced from fast pyrolysis of wood and bark during bio-oil production," *Journal of Colloid and Interface Science*, vol. 310, pp. 57-73, 2007.

[211] M. Carrier, T. Hugo, J. Gorgens, and H. Knoetze, "Comparison of slow and vacuum pyrolysis of sugar cane bagasse," *Journal of Analytical and Applied Pyrolysis*, vol. 90, no. 1, pp. 18-26, 2011.

[212] M. N. Pearlson, "A Techno-Economic and Environmental Assessment of Hydroprocessed Renewable Distillate Fuels by," 2011.

[213] Sasol, "Uzbekistan brand launch Oltin Yo`L GTL," 2012. [Online]. Available: http://www.sasol.com/media-centre/media-releases/uzbekistan-brand-launch-oltin-yol-gtl. [Accessed: 14-Oct-2013].

[214] Middle East North Africa Financial Network (MENAFN), "Sasol Limited intends to reduce its stake in GTL-project in Uzbekistan," 2013. [Online]. Available: http://www.menafn.com/0a3137a9-c97d-445e-941b-1358c10ae752/Sasol-Limited-intends-to-reduce-its-stake-GTLproject-Uzbekistan?src=main. [Accessed: 14-Oct-2013].

[215] R. Teo, "Shell making strides with GTL technology," 2013. [Online]. Available: http://www.theborneopost.com/2013/03/11/shell-making-strides-with-gtl-technology/. [Accessed: 14-Oct-2013].

[216] O. J. Hadaller and J. M. Johnson, "World Fuel Sampling Program," 2006.

[217] C. A. Moses, "Comparitive study of semi-synthetic jet fuels," New Braunfels, Texas, 2008.

[218] California Air Resources Board, *The California Diesel Fuel Regulations*. California: California Air resources Board, 2004.

[219] A. Kumar, J. B. Cameron, and P. C. Flynn, "Biomass power cost and optimum plant size in western Canada," *Biomass and Bioenergy*, vol. 24, no. 6, pp. 445-464, Jun. 2003.

[220] J. G. Brammer and A. V. Bridgwater, "Drying technologies for an integrated gasification bio-energy plant," *Renewable and Sustainable Energy Reviews*, vol. 3, pp. 243-289, 1999.

[221] E. D. Christensen, G. Chupka, J. Luecke , T. Smurthwaite, T. L. Alleman, K. Iisa, J. A. Franz, D. C. Elliott, and R. L. McCormick, "Supporting Information for: Analysis of Oxygenated Compounds in Hydrotreated Biomass Fast Pyrolysis Oil Distillate Fractions," 2011. [Online]. Available: http://pubs.acs.org/doi/suppl/10.1021/ef201357h/suppl_file/ef201357h_si_001.pdf.

[222] M. J. Mccall and T. A. Brandvold, "Fuel and Fuel blending components from biomass derived pyrolysis oil," U.S. Patent US 20090253948A12009.

[223] A. V. Bridgwater, S. Czernik, and J. Piskorz, "An overview of fast pyrolysis," in *Progress in Thermochemical Biomass Conversion*, A. V. Bridgwater, Ed. Blackwell Science, 2001, pp. 977-997.

[224] D. C. Elliott, J. Hu, T. R. Hart, and G. G. Neuenschwander, "Paladium catalyzed hydrogenation of bio-oils and organic compounds," U.S. Patent US007956224B22011.

[225] B. Donnis, R. G. Egeberg, P. Blom, and K. G. Knudsen, "Hydroprocessing of Bio-Oils and Oxygenates to Hydrocarbons. Understanding the Reaction Routes," *Topics in Catalysis*, vol. 52, no. 3, pp. 229-240, Jan. 2009.

[226] M. Edelman, M. Maholland, R. Baldwin, and S. W. Cowley, "Vapor-phase catalytic hydrodeoxygenation of benzofuran," *Journal of Catalysis*, vol. 111, no. 2, 1988.

[227] L. Artok, O. Erbatur, and H. H. Schobertb, "Reaction of dinaphthyl and diphenyl ethers at liquefaction conditions," *Fuel Processing Technology*, vol. 47, no. 2, pp. 153-176, 1996.

[228] V. N. Bui, G. Toussaint, D. Laurenti, C. Mirodatos, and C. Geantet, "Co-processing of pyrolisis bio oils and gas oil for new generation of bio-fuels: Hydrodeoxygenation of guaïacol and SRGO mixed feed," *Catalysis Today*, vol. 143, no. 1–2, pp. 172-178, 2009.

[229] S. R. Kirby, C. Song, and H. H. Schobert, "No TitleHydrodeoxygenation of O-containing polycyclic model compounds using a novel organometallic catalyst precursor," *Catalysis Today*, vol. 31, no. 1–2, pp. 121-135, 1996.

[230] C. Li, Z. Xu, Z. Cao, B. C. Gates, and L. Petrakis, "Hydrodeoxygenation of 1-naphthol catalyzed by sulfided Ni-Mo/γ-Al2O3: Reaction network," *AIChE Journal*, vol. 31, no. 1, pp. 170-174, 1985.

[231] J. Wildschut, J. Arentz, C. B. Rasrendra, R. H. Venderbosch, and H. J. Heeres, "Catalytic Hydrotreatment of Fast Pyrolysis Oil : Model Studies on Reaction Pathways for the Carbohydrate Fraction," *Environmental Progress & Sustainable Energy*, vol. 28, no. 3, pp. 450-460, 2009.

[232] W. Hiatt, A. Carr, and J. Andrews, "Anaerobic digestion of rum distillery wastes," *Engneering Bulletin Purdue University, Engineering Extension Series*, vol. 142, pp. 966-976, 1973.

[233] G. J. Sheehan and P. F. Greenfield, "Utilisation, treatment and disposal of distillery wastewater," *Water Research*, vol. 14, pp. 257-277, 1980.

[234] European IPPC Bureau, "Integrated Pollution Prevention and Control : Draft Reference Document on Best Available Techniques in the Pulp and Paper Industry," 2010.

[235] D. R. Lide, Ed., *CRC Handbook of Chemistry and Physics, Internet Version 2005*. Boca Raton, FL: CRC Press, 2005.

[236] C. A. Moses, "Jet Fuel 'Aromatics effects' and 'Distillation Slope' Research Survey," New Braunfels, Texas, 2012.

[237] K. H. Chew, J. J. Klemes, S. R. W. Alwi, and Z. A. Manan, "Industrial implementation issues of Total Site Heat Integration," *Applied Thermal Engineering*, vol. 61, pp. 17-25, 2013.

[238] T. Ekbom, C. Hjerpe, M. Hagström, and F. Hermann, "Förstudie för biobaserat flygbränsle för Stockholm-Arlanda Flygplats," Stockholm, 2009.

[239] K. Yamashita and L. Barreto, "Biomass gasification for the co-production of Fischer-Tropsch liquids and electricity," Laxenburg, 2004.

[240] R. M. Swanson, A. Platon, J. a. Satrio, and R. C. Brown, "Techno-economic analysis of biomass-to-liquids production based on gasification," *Fuel*, vol. 89, p. S11-S19, Nov. 2010.

[241] D. Humbird, R. Davis, L. Tao, D. Kinchin, D. Hsu, A. Aden, P. Schoen, J. Lukas, B. Olthof, M. Worley, D. Sexton, and D. Dudgeon, "Process Design and Economics for Biochemical Conversion of Lignocellulosic Biomass to Ethanol," 2011.

[242] A. Dutta, M. Talmadge, J. Hensley, M. Worley, D. Dudgeon, D. Barton, P. Groenendijk, D. Ferrari, B. Stears, E. Searcy, C. Wright, and J. R. Hess, "Techno-economics for conversion of lignocellulosic biomass to ethanol by indirect gasification and mixed alcohol synthesis," *Environmental Progress & Sustainable Energy*, vol. 31, no. 2, pp. 182-190, Jul. 2012.

[243] S. D. Phillips, J. K. Tarud, M. J. Biddy, and A. Dutta, "Gasoline from Wood via Integrated Gasification , Synthesis , and Methanol-to- Gasoline Technologies," Colorado, 2011.

Appendix A : Biomass and Experimental Preparation

A.1 Biomass particle size distribution analysis

In Figure 40 the smaller size class (250 – 850 µm) was analysed. It can be seen that the quantity of biomass in size fraction 600-710 µm was slightly larger for Run 8 than it was for the other runs and simultaneously the quantity in size fraction 710-850 µm was slightly less for Run 8 than it was for Runs 3, 6 and 10. The standard deviation for particle size fraction 600-710 µm was greatest, at 5.44wt%, with all other standard deviations smaller than 1.05wt%, see Table 85.
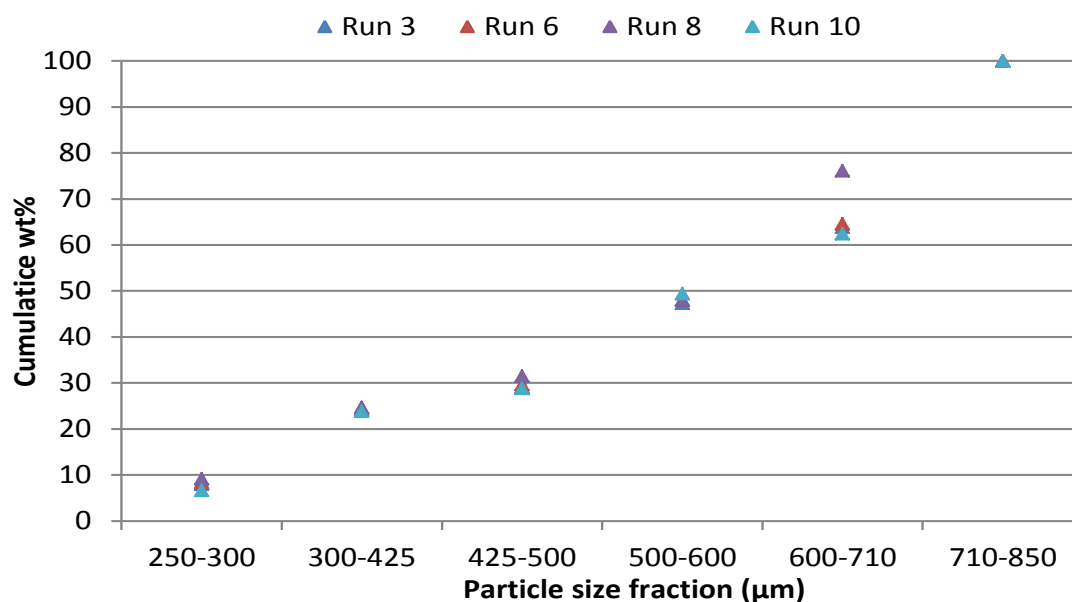
Figure 40 Particle Size Distribution of particle size class 250-850 µm for runs 3, 6, 8, and 10

When considering the larger particle size class investigated, see Figure 41, the cumulative wt% for the different size class fractions correspond well for the different runs. The majority (between 70.6-75.0%) of the particle size class consists of particles in the range of 1400-1600 µm, which is at the lowest end of the overall particle size class. An even distribution over the entire particle size range was not obtained. Over 70wt% of the particles were within the 1400-1600 µm size range, however all samples used for fast pyrolysis runs had a similar distribution.

The standard deviation was smaller than 2.3wt% for all particles size classes ranging between 1400-2000 µm. The larger size class had smaller CVs and standard deviations compared to the smaller particle size class, see Table 85. The maximum CV for the small particle size class was 11.37% followed by 8.16%. The maximum CV for the large particle size class was 2.27%. This might partly be attributed to the fact that fewer sieves intervals (due to limited sieve size availability within the 1400-2000 µm particle size range) were used in the large particle size class, which broadens the size intervals in the particle size class. This can hide possible deviations that might have been visible were the sieve intervals smaller. With fewer sieves (and larger particle size ranges), the weight of biomass in a particle size class will most likely be greater compared to when there are more equally distributed particle size ranges. Measurements with small numerical values tend to have greater CVs, as mentioned earlier. This can also explain why the sieve intervals with small biomass contents (e.g. 250-300 µm with a cumulative average of 8.02wt%) had greater CVs.

208

Table 85 Particle Size distribution for experimental runs

Particle Size fraction	Runs [cumulative wt%]				Average cumulative wt%	Std. dev. for average cumulative wt%	CV [%] for average cumulative wt%
SMALL: 250 to 850 µm particle size class:	Run 3	Run 6	Run 8	Run 10			
250-300	8.0	8.3	9.2	6.6	8.0	0.9	11.4
300-425	24.1	24.6	24.6	23.8	24.3	0.3	1.4
425-500	29.1	29.6	31.5	28.8	29.7	1.1	3.5
500-600	47.3	48.0	48.0	49.4	48.2	0.8	1.6
600-710	63.8	64.6	76.1	62.4	66.7	5.4	8.2
710-850	100.0	100.0	100.0	100.0			
LARGE: 1400 - 2000 µm particle size class:	Run 2	Run 5	Run 7	Run 9	Average cumulative wt%	Std. dev. for average cumulative wt%	CV [%] for average cumulative wt%
1400-1600	70.6	73.3	75.0	74.3	73.3	0.7	0.9
1600-1700	82.9	83.3	85.4	85.3	84.2	1.0	1.2
1700-1800	90.6	91.1	92.2	92.0	91.5	0.4	0.5
1800-2000	100.0	100.0	100.0	100.0			
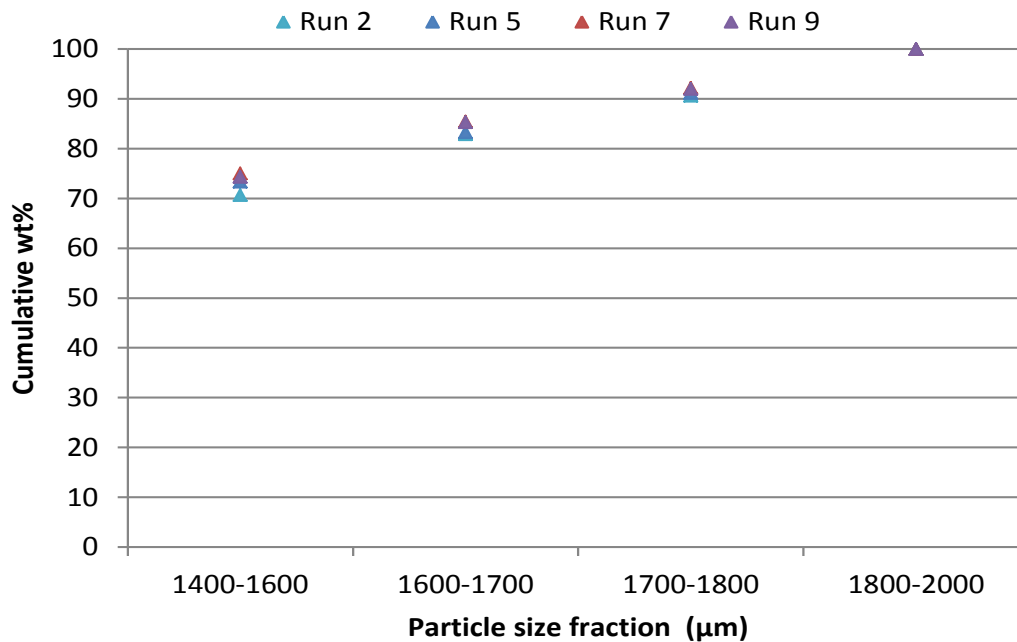
Figure 41 Particle Size Distribution of particle size class 1400-2000 µm for runs 2, 5, 7 and 9

A.2 Drying curves determination and biomass moisture content

The drying curves are oven specific and therefore all biomass samples had to be treated in the same convection oven. The drying curves` development procedure is described hereafter.

1. Samples of 1.5 kg of the biomass for each size class were used. The 1.5 kg of biomass was left in the conditioning room at Wood Science and Forestry at the University of Stellenbosch for 24 hours prior to drying. The conditioning room is temperature and humidity controlled to ensure moisture contents of wood at 10wt% (on dry biomass).

2. After 24 hours in the conditioning room, the biomass sample was loaded into a pre-heated oven (at 103°C), while starting a stop watch. A sample was taken at 0 min (at the time of loading the biomass).These samples were left to cool in a desiccator before storage in a vacuum bag for moisture content analysis.

3. Biomass samples were taken at time intervals of: 5 min, 10 min, 15 min, 20 min, 30 min, 40 min, 50 min, 60 min , 70 min, 80 min and 90 min.   Samples were left to cool in a desiccator before storage in a vacuum bag for moisture content analysis.

4. After 90 min, drying was terminated. Biomass samples taken during the drying time were analysed for moisture content in a different oven using the Convection Oven Method in NREL Laboratory Analytical Procedure for Determination of Total Solids in Biomass and Total Dissolved Solids in Liquid Process Samples [172].

5. Moisture content analysis results were used to plot the moisture content as a function of time in the oven. A regression curve was fitted to the data to obtain a mathematical equation to determine the drying time required to obtain a specific moisture content; curves can be viewed in Figure 42.

6. This procedure (steps 1-5) was performed for particle size classes of 250-850 µm, 850- 1400 µm and 1400- 2000 µm in duplicate for each particle size class. Averages from the duplicate runs were used for regression curve determination. The regression curves were used to determine the amount of time that the specific size fraction had to be dried in the convection oven to obtain the desired moisture content, according to the specific experiment`s requirements.
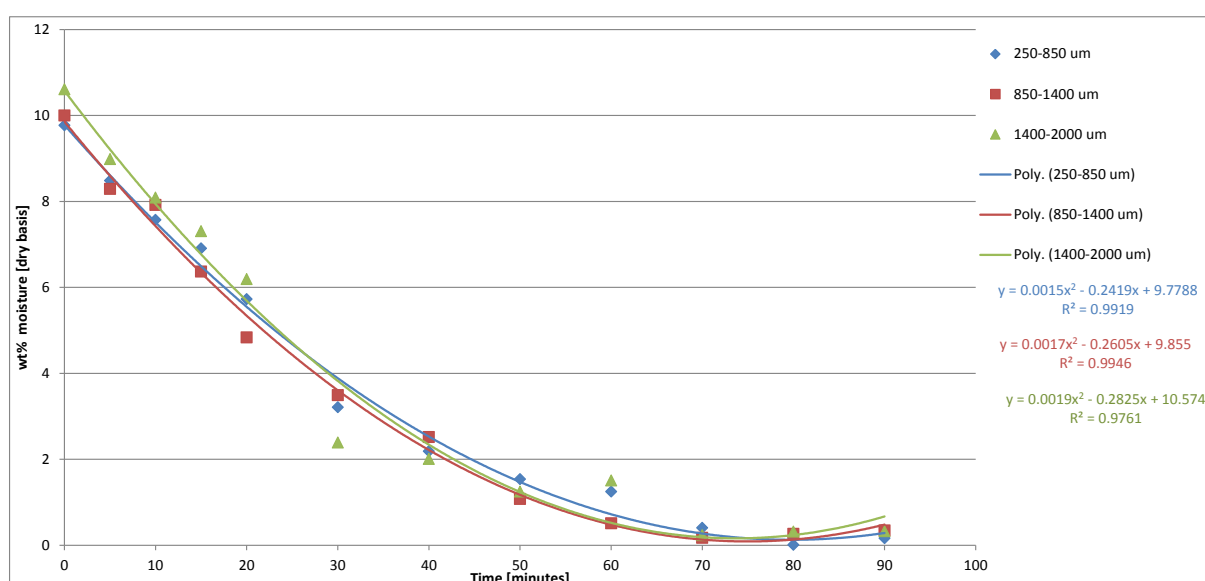
Figure 42 Drying curves

Although the drying curves assisted in manipulating the moisture content to close to the desired value, the exact desired value was seldom obtained. Since the moisture content in the biomass could be measured, this error could be accounted for in analysis of the results. A comparison between desired and actual moisture contents are provided in Table 86. The error% ranged between -2.6 and 11.7%.

Table 86 Comparison between desired and actual biomass moisture contents using drying curves for biomass preparation for runs

Run Nr	Desired Moisture content [wt% on a wet basis]	Actual moisture content [wt% on a wet basis]	Error%[a]	Std dev
1	10.0	9.42	5.8	0.41
2	10.0	9.50	5.0	
3	10.0	10.26	-2.6	
5	10.0	9.19	8.1	
6	10.0	9.37	6.3	
7	4.0	4.03	-0.7	0.26
8	4.0	3.73	6.8	
9	4.0	4.10	-2.4	
10	4.0	3.53	11.7	

[a]Error% =(Desired value- Actual value)/Desired value x 100%, Std dev= standard deviation

A.3 Feeder Calibration

The screw feeder was calibrated for each particle size fraction investigated. The biomass exiting the screw feeder in 5 minutes for a certain screw feeder rate was recorded and used to determine the biomass that would have exited the screw feeder in 60 minutes to determine the feed rate. Calibrations were performed in duplicate and average values were used for curve fitting to the feed rates determined at different screw feed rate settings. From the curve fitted to the data, the screw feeder rate could be determined to obtain a 1kg/h feed for a specific particle size fraction. Results are provided in Figure 43. The screw feed rate for each particle size required for a 1000g/h biomass feed rate are provided in Table 87.
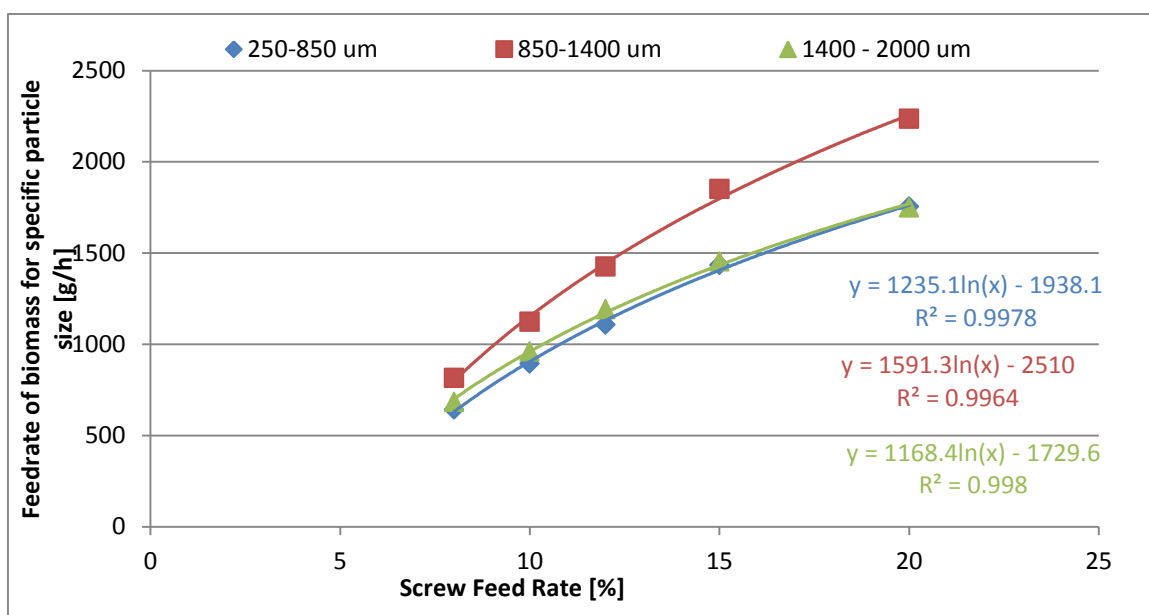
Figure 43 Screw Feeder Calibration Curves

Table 87 Feed rate as a function of screw feed rate settings

Particle size	250-850 µm	850-1400 µm	1400-2000 µm
Screw Feed Rate [%]	10.8	9.1	10.35
Biomass feed rate [g/h]	1000.3	1000.5	1000.4

A.4 Temperature measurement Calibration

The temperature probes measuring the reactor temperature were calibrated by SA Metrology at 450 and 550 ^{o}C. Results are provided in Table 88.

Table 88 Error associated with temperature measurement and regulation during pyrolysis

	Offset at 450 ^{o}C	Offset at 550 ^{o}C	Error
Probe: T2	1.3	1.4	± 1.4 ^{o}C
Probe: T3	0.1	0.9	± 0.9 ^{o}C
Probe: T4	2.7	2.7	± 2.7 ^{o}C

Appendix B: Experimental information

B.1: Factors to influence product yields and quality in literature

Table 89 Summary of the process conditions and investigated ranges for bio-oil production via fast pyrolysis from literature

Factor / Variable		Typical Value/ Range used	Optimum value of factor	Source
Reactor Temperature		500-800 ^{o}C	*	[42]
		480-529 ^{o}C	*	[32]
		425-557 ^{o}C	*	[37]
		450-600 ^{o}C	*	[27]
		400- 650 ^{o}C	500 ^{o}C	[58]
		450,470,500 ^{o}C	500 ^{o}C	[59]
		-	500 ^{o}C	[38]
Hot vapour residence time		*	*	[24]
		1s	*	[32]
		<1s	*	[27]
		<1s – 2s	*	[38]
		1.6s	*	[62]
Heating Rate		*	*	[24]
		>100 - 1000 ^{o}C/min	*	[37]
Particle size		1mm	*	[42]
		0.25-2mm	0.25-1mm	[63]
		1mm	*	[24]
		<2 – 3mm	*	[32]
		<1 – 3mm	*	[37]
		0.425mm, 1.7mm, 3.35mm	3.35mm	[59]
		2-3mm	*	[38]
Moisture content		*	*	[32]
		<10%	*	[59]
		<10%	*	[38]
Type of biomass		*	*	[32]
		*	*	[38]
Feedstock composition	**Ash content**	*	*	[42]
	Ash content	*	*	[32]
	Lignin content	*	*	[42]
	Cellulose content	*	*	[42]
	Char separation	*	*	[32]

*Not reported

B.2: Factors to influence product yields and quality in experimental set-up

All possible factors which could be influential to the product yield and product characteristics for the specific experimental set-up are provided in Table 90. Not all of these factors could be manipulated independently and with accuracy, therefore it had to be disregarded from possible statistical analysis. Furthermore, not all of these factors were considered to have a significant influence on the product yield and characteristics according to the literature study. This was used as basis for identification and selection of the final factors for the study.

Table 90 Potential factors and operating conditions for Fluidized Bed Fast Pyrolysis Unit

Expected influence on pyrolysis process to influence pyrolysis products	Type of process parameter	Factor	Typical operating range [62]
Influence on reactor temperature	Internal	Reactor temperature	428-526 ^{o}C
Influence on the vapour residence time	Internal	Nitrogen flow rate	2.5 m^3/hr
Influence on the heat transfer and vapour residence time	Internal	Biomass Feed rate	0.9kg/hr
Influence on cooling rate and hence secondary reactions	Internal	Temperature of coolant	10-12 C ^{o}C
	Internal	Coolant flow rate	1L/min (min) – 12L/min (max) 2-3 L/ min (typical)
Influences on heating rate	External	Biomass Particle size	>250 µm – 2mm
	External	Biomass water content	<10wt%
	External	Heat transfer medium (sand) particle size	400-600 µm
Influences feedstock composition	External	Ash content in the biomass	Not investigated

B.3: Experimental Run Protocol

The experimental procedure as followed for all experiments is provided below, see Table 91. It is based on the procedures described in the studies of Hugo (2010) , Danje (2012) and Joubert (2011), [62], [170], [63]. The experimental set-up for the procedure described below, can be viewed in Figure 3, in Section 3.2.3 Fast pyrolysis process description and set-up on p.54.

Table 91 Preparation for experiment on day before run

Nr.	Steps	Check	Important
DAY BEFORE RUN		
1	Place biomass samples to be used in conditioning room 24 hours prior to commencing with drying for experimental run.		→ Spread biomass out evenly
2	Calibrate feeder for biomass with specific particle size, moisture content according to the feeder configuration.	→ Run continuously for 5 minutes in triplicate and use average as flow rate.	→ Use same mass of biomass as would be used in experiments. → Distribute biomass in similar way as would be done in experiments if multi-inlet configuration is used (e.g. equal amounts in all three compartments). → Avoid bridging by using rods to move biomass – take care with height of rods as it can damage screw if it gets stuck.
3	Sieve sand, use400-500gram of size fraction 0.4-0.6mm		
4	Vacuum clean furnace.		→ Take care to vacuum elements properly as carbon residue can cause hotspots and element melting.
5	Weigh sections: • RB • RT • TCT • LCT • ESP CT1 • ESP CT2 • ESP Teflon connection	→ Note the fittings included in original weighing of each unit.	→ When equipment parts have an inconvenient shape, make use of bucket to weigh component. Weigh bucket, tare scale, and place equipment inside to determine weigh of equipment.
6	Assemble plant & sensors • Assemble cooling and condensation sections, using Vaseline and builder's tape as leak prevention measures. • Insert RB into furnace Zone 3. • Connect RFP to reactor bottom inlet – make sure bottom two bolts are inserted before RFP is inserted, because once RFP is	→ Make sure ESP wires are centred. → Use Vaseline on all Teflon seals. → Make sure gasket in place. → Make sure reactor does not touch	

215

	inserted it is very difficult to insert bolts. • Attach RFP to RB by inserting other bolts and tightening with a spanner. • Connect RB to gas (nitrogen) feeding line and tighten with spanners. • Insert thermocouple T2 into feeding line opening and spray nickel spray before tightening with a spanner (but not too tightly). • Place weighed sand inside RB. • Place top part of reactor on and spray Nickel spray before tightening until cyclone position is at desired point. • Insert thermocouples T3 and T4 and use Nickel spray at connections before tightening with spanner (not too tightly). • Attach cyclones and spray Nickel spray before tightening with spanners.	elements. → Make sure thermocouple T2 does not touch elements. → Make sure all hot connections between different parts are sprayed with nickel spray. → Make sure all thermocouple cables and furnace cables are out of furnace. → Make sure char pots and bottom plugs are inserted at cyclones` bottoms and have been sprayed with Nickel spray.	
7	Test for leaks at Nitrogen flow rate of 8m^3/hr	→ Check for leaks at fittings and in piping.	→ Ensures there are no leaks in the system.
8	• Place glass fibre insulation on zone 3 top ridge. Also, place on top of feeding pipe and nitrogen inlet pipe. • Lower furnace. • Connect cyclone exit and cooling tower, using HVFL with rope heater. • First insert side most difficult to tighten. Use Nickle spray on hot vapour feeding line cyclone exit connection. Use spanners to tighten firmly. • After making sure condensation and furnace sections connect properly, disconnect HVFL and TCT.	→ Ensure fibre glass insulation is evenly distributed and covers RFP and GFL. → Make sure all thermocouple cables and furnace cables are out of furnace.	→ Even distribution of fibre glass prevents heat losses from the oven.

Table 92 Experimental procedure on day of run

DURING THE RUN			
Nr.	Steps	Check	Important
1	Prepare biomass sample`s moisture content by drying specific sample in		→ Pre-heat convection oven prior to biomass

216

	convection oven for the pre-determined time to obtain desired moisture content (see Figure 42). After drying allow samples to cool under vacuum.		drying.
2	Start oven.		→ Wait for oven to reach equilibrium temperature (between 1-1.5hrs).
3	Add biomass to feeder • For compartment feeder, loosen bolts and remove Perspex plate, insert biomass in desired configuration. Place rubber back and Perspex plate on top. Insert bolts and tighten using spanners.	→ Seal rubber with Vaseline.	→ Take sample for ash and water analysis.
4	Start extractor fan.	→ Switch on at main switchboard.	

When oven is close to set point (approximately 30min before commencing with run or 100 ^{o}C from Set point)

5	Test ESP``s and test Isopar pump - switch both off after testing.	→ Make sure ESP`s do not experience shortages/ crackling sounds. → Make sure isopar leakages from cooling bath is insignificant.	→ Isopar is flammable and high voltages are generated in ESP, leakages can be very dangerous.
6	Test connection between HVFL and TCT. Disconnect after testing.	→ This is important to make sure that the condensation section and the furnace can be properly connected, as it is much more difficult to connect these sections properly when the HVFL is hot.	→ When disconnecting, take care to move as little as possible. Turn the HVFL slightly towards window to prevent CT from heating up.
7	Start cooling section – open chiller water → open V5 & V8.	→ Chiller hose must be in sink.	
8	Load biomass	→ The biomass loading differs depending on the experimental conditions investigated.	→ Take care to choose biomass loading at a time which will not compromise the experimental conditions investigated.
9	Flush system with N_2	→ 3min at 0.5 m^3/hr	
10	Attach HVFL pipe with rope heater to TCT and tighten using spanners.	→ Testing to ensure proper fitting will have eliminated connection problems.	→ Use heat resistant gloves as the HVFL is very hot. → One cannot attach HVFL earlier in the procedure, as the hot gases will cause the condensation section to become hot. Some of the isopar

217

			components can also start to volatilize, leading to isopar losses.
11	Switch chiller on by pressing 'Cooling' on control panel.		→ Typical water temperature is 6 ^{o}C. The temperature indicated on the chiller should be close to 6 ^{o}C after running for a while. The lowest possible temperature is 4 ^{o}C for water. (If colder temperatures are desired, use glycol solution).
12	Start isopar pump . (by adjusting compressed air flow → V12).	→ Line pressure P4 = 1.8-3 kPa	→ Should be done approximately 15min before starting with run.
13	Start rope heater.	→ Set point is 400 ^{o}C.	→ Should be done approximately 10min before starting with run.
14	Once oven is at set temperature, start N$_2$ flow, by opening V19 & V17 OR V18 & V17.	→ P1 = +/- 300 kPa → Set on control panel = 2.4-4 m^3/hr	→ This is done to maintain the fluidization bed and to ensure it is stable once feeding starts.
15	Monitor T3 and T4.	→ Temperature difference is 10 ^{o}C.	
16	Start ESP`s.	→ ESP 1= 15kV → ESP2= 12kV	→ Earth wire connected. → No shocking or crackling sounds– this will be the result of the wire touching the sides .
17	Start jacket cooling water at RFP.	→ Ensure jacket hose is in sink.	
18	Check for problems in system e.g. Leaks, low/high pressure/ low/high temperatures		
19	Insert flash drive.		
20	Start feeder at calibrated feeding rate.	→ Check for bridging & flow obstructions.	→ Ensure feeder pressure is higher than reactor pressure (P3>P2). → Make sure rods do not get caught in screw feeder.
21	Monitor process during experiment.		
	When biomass is completely fed		
22	When all biomass has been fed, continue feeding for at least 10 minutes (to get rid of all biomass that can still be in screw section).		
23	Switch off ESP.	→ Little gas must be in the ESP when they are switched off – only	

Nr.	Steps	Check	Important
			then has all biomass been pyrolysed. If this is the case, continue with process.
24	Switch furnace off.	→ At the manual switch on orange control box.	
25	Switch off rope heater.		→ The HVFL must be removed therefore the pipe should start to cool asap otherwise removing it is difficult.
26	Reduce N_2 flow rate on control panel.	→ 0.5 m³/hr	→ Maintain inert atmosphere.
27	Stop chiller on control panel and close water tap ➔V 5.		
28	Switch off isopar pump by closing compressed air ➔ V12.		
29	Redirect gas flow from HVFL- insert pipe to point to extractor fan.	→ Use high temperature resistant gloves to remove pipe.	→ Pipe is very hot! → Maintain N_2 flow (0.5 m³/hr).
30	Remove flash disc.		→ Press 'Remove USB' on control panel, otherwise file will be corrupted.
31	When T3 is lower than 300 °C, remove furnace top.	→ Usually 3 hours after end of run.	→ Maintain N_2 flow (0.5 m³/hr)
32	When T3 is lower than 100 °C, switch off N_2 flow .	→ Usually after 1 hr from opening furnace.	→ Maintain N_2 flow (0.5 m³/hr)
33	Stop jacket cooling water.		
34	Leave until cool enough to handle.		

*The time at which the biomass loading occurs, can differ depending on the experimental conditions. If one of the experimental conditions investigated is the effect at different moisture contents, then the biomass needs to be fed closely before commencing with the run. Take care to choose biomass loading at a time which will not compromise the experimental conditions investigated.

Table 93 Experimental procedure after run is completed

AFTER THE RUN			
Nr.	Steps	Check	Important
1	Dissemble and weighing cooling section.	→ Weigh dirty condenser components.	→ Take care to correlate equipment with initial weighing configuration. → The weights are used to determine product yields.
2	Clean cooling section.	→ Use Acetone to squirt into cooling tower etc. → And collect all acetone and bio-oil in bucket.	→ Weigh bucket before-hand.
3	Collect oil from condenser by tilting bio-oil collection bucket and opening V10.		→ Allow isopar and bio-oil to settle in conical flask to settle before separating.
4	Remove isopar and clean/wash bio-oil collection bucket with acetone.		→ Take precaution to remove all of the bio-oil and acetone after

219

			→ washing bucket. → Vapours can be removed by vacuum cleaning at lowest setting.
5	Dissemble reactor.	→ Weigh dirty reactor.	→ Take care to correlate equipment with initial weighing configuration.
6	Make necessary replacements for the next run (e.g. Nitrogen cylinder, isopar etc.).		
7	Order items needed.	→ N_2, isopar, sand, gasket, acetone, Nickel spray, Vaseline, plumber`s tape.	

Appendix C: GC MS Analysis

Take note that the scales on Figure 44 and Figure 45 differ.
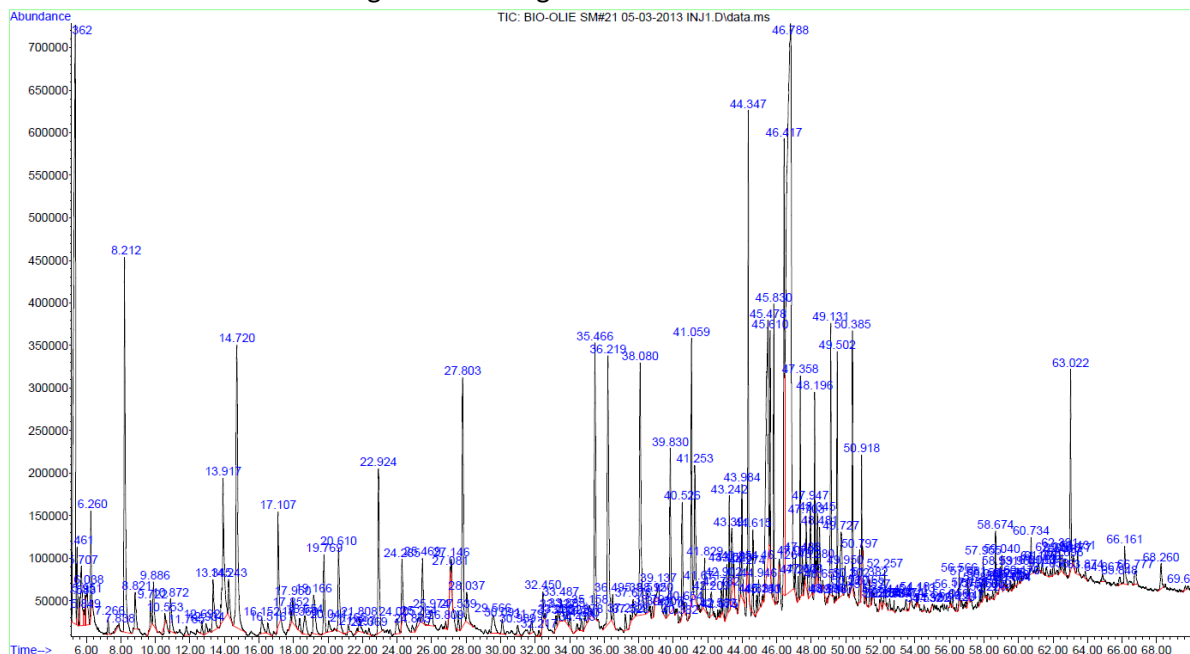
Figure 44 Chromatogram of bio-oil samples on HP-5 GC-MC column
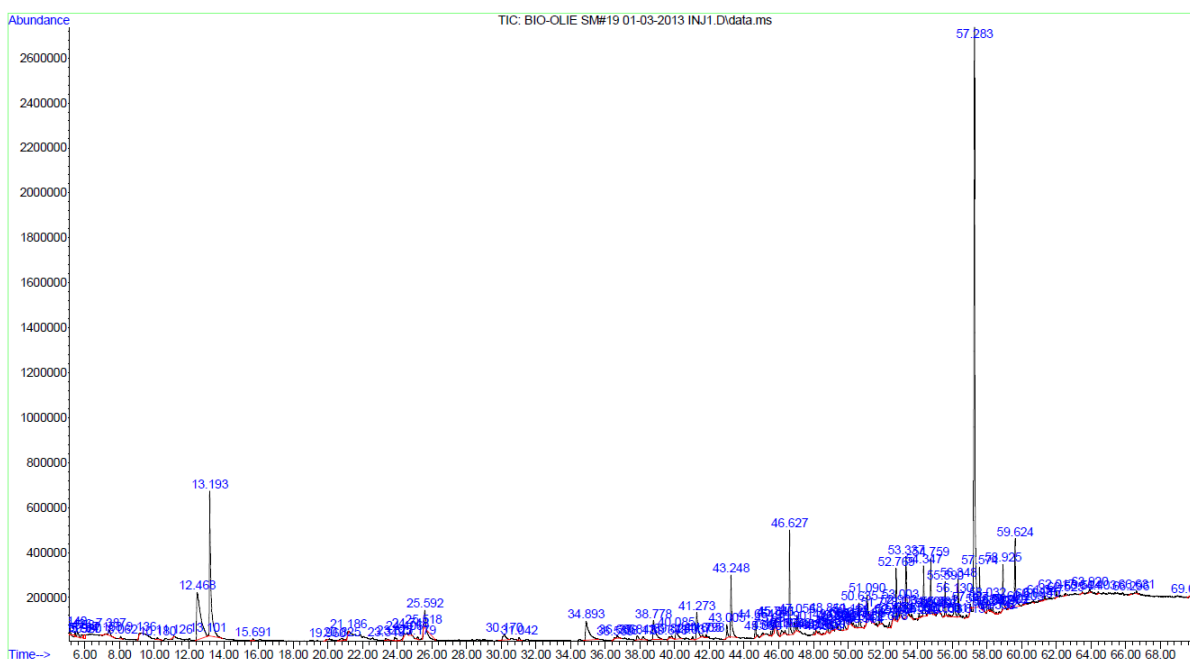
Figure 45 Chromatogram of bio-oil samples on ZB-1701 GC-MC column
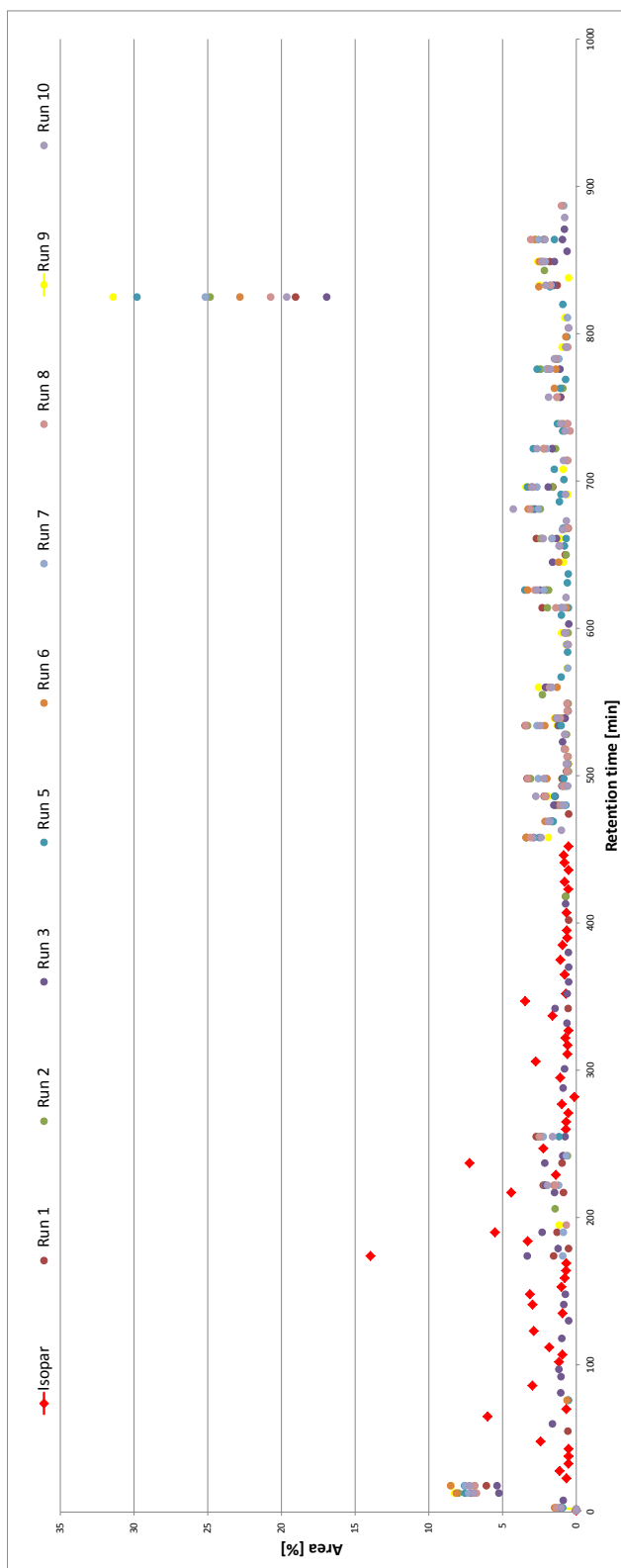
Figure 46 Comparison of isopar and bio-oil results

Appendix D: Experimental and Statistical Results

Table 94 Experimental responses, predicted responses and %error for phase yields*

Factor A: Moisture content level	Factor B: Temperature level	Factor C: Particle Size level	Run Nr	Factor A: Moisture content level	Factor B: Temperature level	Factor C: Particle Size level	Pred	Exp	% ER	Pred	Exp	% ER	Pred	Exp	% ER	Pred	Exp	% ER
							Char fraction yield [dm]			Gas fraction yield [dm]			Organic phase fraction yield [dm]			Pyrolytic water fraction yield [dm]		
1	-1	1	2	9.5	465.36	1563.861	0.132	0.14	-2.39	0.284	0.27	4.75	0.442	0.46	-4.89	0.137	0.13	6.63
1	-1	-1	3	10.3	472.00	594.021	0.120	0.12	2.55	0.305	0.31	-3.00	0.504	0.50	0.47	0.077	0.07	14.33
1	1	1	5	9.2	492.74	1570.000	0.133	0.13	2.62	0.345	0.36	-4.68	0.440	0.42	5.73	0.098	0.09	7.06
1	1	-1	6	9.4	478.13	591.074	0.119	0.12	-2.81	0.303	0.31	-3.01	0.503	0.51	-0.37	0.068	0.06	12.74
-1	1	1	7	4.0	491.58	1563.779	0.152	0.15	-0.18	0.343	0.33	4.45	0.413	0.43	-3.87	0.099	0.09	10.65
-1	1	-1	8	3.7	488.07	574.372	0.113	0.11	1.11	0.298	0.29	4.17	0.502	0.52	-3.66	0.053	0.08	-34.58
-1	-1	1	9	4.1	456.66	1565.330	0.152	0.15	0.09	0.265	0.28	-3.72	0.413	0.40	3.77	0.149	0.17	-14.38
-1	-1	-1	10	3.5	450.22	595.303	0.114	0.11	-0.67	0.314	0.31	2.09	0.500	0.48	3.99	0.108	0.10	11.61
1	*1*	*0*	*1*	*9.4*	*485.78*	*1125.0*	0.126	0.15	-14.73	0.316	0.28	14.87	0.470	0.51	-8.5	0.085	0.06	33.40

*Pred= predicted using response surface model, Exp. = experimentally measured and measured, %ER= % error calculated as : %ER= (Exp-Pred)/Exp x100%, dm- dry mass

Table 95 Experimental responses, predicted responses and %error for bio-oil quality *

Factor A: Moisture content level	Factor B: Temperature level	Factor C: Particle Size level	Run Nr	Factor A: Moisture content level	Factor B: Temperature level	Factor C: Particle Size level	Pred	Exp	% ER	Pred	Exp	% ER	Pred	Exp	% ER	Pred	Exp	% ER	Pred	Exp	% ER
							BO Moisture content [wt%]			BO density [kg/m^3]			BO dynamic viscosity [mPa.s]			BO HHV [MJ/kg]			BO pH		
1	-1	1	2	9.5	465.36	1563.861	35.42	33.40	6.05	1201.41	1202.84	-0.12	14.11	13.96	1.02	20.69	21.05	-1.71	2.18	2.16	0.93
1	-1	-1	3	10.3	472.00	594.021	26.66	26.61	0.17	1233.17	1235.87	-0.22	24.88	26.47	-6.00	20.63	19.31	6.82	2.14	2.21	-3.26
1	1	1	5	9.2	492.74	1570.000	30.67	31.63	-3.03	1215.04	1214.48	0.05	13.80	14.16	-2.50	21.59	21.47	0.58	2.27	2.29	-0.89
1	1	-1	6	9.4	478.13	591.074	24.77	25.81	-4.02	1238.07	1234.47	0.29	27.08	25.43	6.49	21.11	22.38	-5.71	2.28	2.20	3.78
-1	1	1	7	4.0	491.58	1563.779	25.89	23.45	10.41	1225.51	1231.98	-0.52	27.26	28.63	-4.78	23.27	23.62	-1.46	2.26	2.24	0.74
-1	1	-1	8	3.7	488.07	574.372	17.61	18.70	-5.84	1255.23	1250.69	0.36	49.86	48.92	1.92	23.27	22.74	2.34	2.29	2.31	-0.86

-1	-1	1	9	4.1	456.66	1565.330	31.72	35.27	-10.07	1208.54	1201.25	0.61	12.10	10.86	11.42	22.23	21.97	1.18	2.75	2.77	-0.55
-1	-1	-1	10	3.5	450.22	595.303	23.84	21.75	9.58	1236.79	1242.39	-0.45	32.09	33.35	-3.79	22.22	22.46	-1.06	2.21	2.21	0.38
1	*1*	*0*	*1*	*9.4*	*485.78*	*1125.0*	28.19	24.62	14.49	1225.04	1221.49	0.29	19.43	25.95	-25.11	21.31	23.13	-7.86	2.34	2.27	3.02

*Pred= predicted using response surface model, Exp. = experimentally measured and measured, %ER= % error calculated as : %ER= (Exp-Pred)/Exp x100%

Table 96 Elemental analysis of bio-oils

Run Nr.	Experimentally determined (including moisture) [wt%]				Calculated (excluding moisture)[wt%]			
	C	**H**	**N**	**O**[a]	**C**	**H**	**N**	**O**[a]
RUN 1	41.83 ±0.36	7.70 ±0.08	0.11 ±0.00	50.36 ±0.61	55.497	6.553	0.147	37.802
CV [%]	0.853	0.985	0.057	1.205	-	-	-	-
RUN 2	34.73 ± 0.86	7.82 ± 0.38	0.12 ± 0.01	57.33 ± 1.31	52.142	6.142	0.176	41.540
CV [%]	2.465	4.872	8.869	2.293	-	-	-	-
RUN 3	38.41 ± 2.52	6.44 ± 1.18	0.10 ±0.02	55.06 ±3.76	52.332	4.721	0.130	42.817
CV [%]	6.567	18.342	18.463	6.835	-	-	-	-
RUN 5	35.94 ± 1.11	7.90 ± 0.56	0.10 ± 0.01	56.07 ±1.74	52.568	6.371	0.141	40.920
CV [%]	3.095	7.111	6.960	3.100	-	-	-	-
RUN 6	40.66 ± 0.40	7.50 ± 0.22	0.09 ± 0.01	51.76 ± 0.85	54.800	6.210	0.124	38.866
CV [%]	0.992	2.877	12.814	1.632	-	-	-	-
RUN 7	43.10 ± 0.24	7.75 ± 0.20	0.100 ± 0.03	49.04 ± 0.54	56.307	6.699	0.131	36.863
CV [%]	0.546	2.576	26.648	1.093	-	-	-	-
RUN 8	44.26 ± 0.60	7.53 ± 0.12	0.16 ± 0.01	48.05 ± 0.80	54.443	6.688	0.199	38.670
CV [%]	1.359	1.568	8.853	1.665	-	-	-	-
RUN 9	34.64 ± 2.53	8.09 ± 0.45	0.14 ± 0.01	57.14 ± 3.04	53.509	6.398	0.208	39.885
CV [%]	7.297	5.507	4.349	5.313	-	-	-	-
RUN 10	43.48 ± 0.43	7.39 ± 0.14	0.11 ± 0.01	49.02 ± 0.70	55.566	6.332	0.143	37.959
CV [%]	0.989	1.906	5.819	1.424	-	-	-	-

[a] calculated by difference

Table 97 Experimental responses, predicted responses and %error for BO elemental composition *

Factor A: Moisture content level	Factor B: Temperature level	Factor C: Particle Size level	Run Nr	Factor A: Moisture content level	Factor B: Temperature level	Factor C: Particle Size level	Pred	Exp	*% ER*	Pred	Exp	*% ER*	Pred	Exp	*% ER*
							C in BO			H in BO			O in BO		
							[wt% (moisture free BO basis)]			[wt% (moisture free BO basis)]			[wt% (moisture free BO basis)]		
1	-1	1	2	9.5	465.36	1563.9	52.3	52.1	0.24	5.7	6.1	-6.39	41.4	41.5	-0.26
1	-1	-1	3	10.3	472.00	594.0	53.4	52.3	1.97	5.4	4.7	14.62	41.6	42.8	-2.82
1	1	1	5	9.2	492.74	1570.0	52.4	52.6	-0.29	6.4	6.4	0.35	40.4	40.9	-1.32
1	1	-1	6	9.4	478.13	591.1	53.6	54.8	-2.20	5.8	6.2	-7.23	40.9	38.9	5.36
-1	1	1	7	4.0	491.58	1563.8	54.9	56.3	-2.42	6.8	6.7	1.09	37.7	36.9	2.36
-1	1	-1	8	3.7	488.07	574.4	55.1	54.4	1.14	6.6	6.7	-0.95	37.7	38.7	-2.53
-1	-1	1	9	4.1	456.66	1565.3	54.9	53.5	2.62	6.7	6.4	4.61	38.9	39.9	-2.46
-1	-1	-1	10	3.5	450.22	595.3	55.1	55.6	-0.81	6.2	6.3	-2.77	38.8	38.0	2.27
1	*1*	*0*	*1*	*9.4*	*485.78*	*1125.0*	52.9	55.5	-4.71	6.1	6.6	-6.43	40.7	37.8	7.74

*Pred= predicted using response surface model, Exp. = experimentally measured and measured, %ER= % error calculated as : %ER= (Exp-Pred)/Exp x100%

225

Table 98 Experimental responses, predicted responses and %error for chemical families of aldehydes, ketones and sugars in BO*

Factor A: Moisture content level	Factor B: Tempe-rature level	Factor C: Particle Size level	Run Nr	Factor A: Moisture content level	Factor B: Tempe-rature level	Factor C: Particle Size level	Pred	Exp	% ER	Pred	Exp	% ER	Pred	Exp	% ER
							Aldehydes in BO			Ketones in BO			Sugars in BO		
							[wt% (moisture free BO basis)]			[wt% (moisture free BO basis)]			[wt% (moisture free BO basis)]		
1	-1	1	2	9.5	465.36	1563.9	5.4	5.5	-2.1	15.5	14.9	3.9	29.5	24.4	21.3
1	-1	-1	3	10.3	472.00	594.0	5.3	5.3	0.2	18.4	18.3	0.2	24.0	25.0	-4.2
1	1	1	5	9.2	492.74	1570.0	4.7	4.8	-1.8	15.4	16.0	-3.9	31.2	33.8	-7.8
1	1	-1	6	9.4	478.13	591.1	5.3	5.4	-0.5	18.1	18.2	-0.3	24.3	23.2	4.9
-1	1	1	7	4.0	491.58	1563.8	4.3	4.4	-0.8	14.4	14.5	-1.0	31.1	30.2	2.7
-1	1	-1	8	3.7	488.07	574.4	5.1	5.1	-1.3	16.4	16.2	1.3	24.8	24.5	1.4
-1	-1	1	9	4.1	456.66	1565.3	6.1	6.1	-0.5	14.4	14.2	1.3	29.0	32.3	-10.2
-1	-1	-1	10	3.5	450.22	595.3	5.8	5.9	-1.0	16.3	16.5	-1.2	22.7	23.1	-1.9
1	*1*	*0*	*1*	*9.4*	*485.78*	*1125.0*	5.1	5.7	-10.3	16.6	14.8	12.4	28.0	20.2	39.0

*Pred= predicted using response surface model, Exp. = experimentally measured and measured, %ER= % error calculated as : %ER= (Exp-Pred)/Exp x100%

Table 99 Experimental responses, predicted responses and %error for chemical families of furans, acids and alkanes in BO

Factor A: Moisture content level	Factor B: Tempe-rature level	Factor C: Particle Size level	Run Nr	Factor A: Moisture content level	Factor B: Tempe-rature level	Factor C: Particle Size level	Pred	Exp	% ER	Pred	Exp	% ER	Pred	Exp	% ER
							Furans in BO			Acids in BO			Alkanes in BO		
							[wt% (moisture free BO basis)]			[wt% (moisture free BO basis)]			[wt% (moisture free BO basis)]		
1	-1	1	2	9.5	465.36	1563.9	5.3	5.1	3.6	9.9	9.6	2.5	1.2	1.1	13.2
1	-1	-1	3	10.3	472.00	594.0	7.2	6.7	6.8	10.0	10.9	-7.6	1.4	1.4	1.0
1	1	1	5	9.2	492.74	1570.0	8.3	7.9	5.3	7.8	8.0	-3.3	1.7	1.6	7.7
1	1	-1	6	9.4	478.13	591.1	7.9	8.2	-4.0	9.3	8.4	11.1	1.7	1.8	-4.2
-1	1	1	7	4.0	491.58	1563.8	6.7	7.3	-7.4	7.8	8.3	-5.3	1.4	1.4	-0.5
-1	1	-1	8	3.7	488.07	574.4	7.7	7.1	9.7	6.9	6.5	5.6	2.0	1.9	5.9
-1	-1	1	9	4.1	456.66	1565.3	5.4	4.9	10.3	10.5	10.0	4.5	1.6	1.6	1.0
-1	-1	-1	10	3.5	450.22	595.3	6.5	6.8	-4.1	9.7	10.2	-4.8	1.3	1.2	4.8
1	*1*	*0*	*1*	*9.4*	*485.78*	*1125.0*	8.1	7.4	9.1	8.5	7.9	7.4	1.8	2.0	-8.9

*Pred= predicted using response surface model, Exp. = experimentally measured and measured, %ER= % error calculated as : %ER= (Exp-Pred)/Exp x100%

226

Table 100 Protons in spectra 10-8ppm and 6.8-6.4ppm for experimental run, predicted values and error%

Factor A: Moisture content level	Factor B: Temperature level	Factor C: Particle Size level	Run Nr	Factor A: Moisture content level	Factor B: Temperature level	Factor C: Particle Size level	Pred	Exp	*% ER*	Pred	Exp	*% ER*
							Aldehyde protons & Lower field aromatics [10-8 ppm]			Olefinic protons conjugated to carbonyls [6.8-6.4 ppm]		
							Protons in 8-10ppm/(all protons in BO)			Protons in 6.8-6.4ppm/(all protons in BO)		
1	-1	1	2	9.5	465.36	1563.9	0.5	0.4	14.7	1.6	1.6	-5.6
1	-1	-1	3	10.3	472.00	594.0	0.7	0.8	-3.0	2.7	2.9	-5.3
1	1	1	5	9.2	492.74	1570.0	0.5	0.6	-15.4	2.5	2.3	6.5
1	1	-1	6	9.4	478.13	591.1	0.8	0.7	0.3	3.1	3.0	4.8
-1	1	1	7	4.0	491.58	1563.8	0.5	0.5	0.8	3.5	3.7	-3.5
-1	1	-1	8	3.7	488.07	574.4	0.8	0.7	7.3	4.7	4.7	0.0
-1	-1	1	9	4.1	456.66	1565.3	0.5	0.5	5.0	2.4	2.3	3.7
-1	-1	-1	10	3.5	450.22	595.3	0.7	0.8	-4.1	3.5	3.4	0.8
1	*1*	*0*	*1*	*9.4*	*485.78*	*1125.0*	0.6	0.7	-16.9	2.7	3.2	-15.2

*Pred= predicted using response surface model, Exp. = experimentally measured and measured, %ER= % error calculated as : %ER= (Exp-Pred)/Exp x100%

Table 101 Elemental composition of char for experimental run, predicted values and error%

Factor A: Moisture content level	Factor B: Temperature level	Factor C: Particle Size level	Run Nr	Factor A: Moisture content level	Factor B: Temperature level	Factor C: Particle Size level	Pred	Exp	*% ER*	Pred	Exp	*% ER*	Pred	Exp	*% ER*
							C in Char			H in Char			O in Char		
							[wt%]			[wt%]			[wt%]		
1	-1	1	2	9.5	465.36	1563.9	83.6	83.8	-0.32	2.4	2.5	-1.70	12.3	12.3	0.35
1	-1	-1	3	10.3	472.00	594.0	81.5	80.9	0.71	2.6	2.6	-0.75	14.4	15.3	-5.46
1	1	1	5	9.2	492.74	1570.0	83.9	83.7	0.33	2.4	2.4	-1.82	12.4	12.4	-0.35
1	1	-1	6	9.4	478.13	591.1	81.5	82.2	-0.81	2.5	2.4	7.02	14.4	13.5	7.02
-1	1	1	7	4.0	491.58	1563.8	82.4	82.4	-0.08	2.4	2.4	0.86	13.6	13.6	0.11
-1	1	-1	8	3.7	488.07	574.4	81.7	81.7	0.00	2.4	2.6	-5.56	14.4	14.2	1.95
-1	-1	1	9	4.1	456.66	1565.3	81.8	81.8	0.05	2.4	2.4	0.25	13.6	13.6	-0.03
-1	-1	-1	10	3.5	450.22	595.3	81.1	81.0	0.10	2.8	2.9	-2.04	14.4	14.8	-2.69
1	*1*	*0*	*1*	*9.4*	*485.78*	*1125.0*	82.9	83.5	-0.77	2.4	2.6	-7.38	13.3	12.2	8.45

*Pred= predicted using response surface model, Exp. = experimentally measured and measured, %ER= % error calculated as : %ER= (Exp-Pred)/Exp x100%

227

Table 102 Experimental responses, predicted responses and %error with regards to energy transfer *

Factor A: Moisture content level	Factor B: Temperature level	Factor C: Particle Size level	Run Nr	Factor A: Moisture content level	Factor B: Temperature level	Factor C: Particle Size level	Pred	Exp	% ER	Pred	Exp	% ER	Pred	Exp	% ER
							HHV Char			Energy to BO			Energy to Char		
1	-1	1	2	9.5	465.36	1563.861	31.09	31.14	-0.16	48.07	50.03	-3.92	22.36	21.56	3.72
1	-1	-1	3	10.3	472.00	594.021	30.13	29.93	0.65	55.76	49.50	12.65	18.00	17.84	0.89
1	1	1	5	9.2	492.74	1570.000	31.06	31.01	0.16	48.02	45.69	5.10	22.39	20.61	8.62
1	1	-1	6	9.4	478.13	591.074	30.15	30.38	-0.74	55.79	57.82	-3.52	17.99	18.97	-5.21
-1	1	1	7	4.0	491.58	1563.779	30.35	30.39	-0.13	48.07	51.88	-7.35	22.36	23.72	-5.76
-1	1	-1	8	3.7	488.07	574.372	30.34	30.32	0.08	55.92	60.57	-7.68	17.91	17.33	3.37
-1	-1	1	9	4.1	456.66	1565.330	30.36	30.32	0.12	48.06	44.73	7.44	22.36	23.58	-5.14
-1	-1	-1	10	3.5	450.22	595.303	30.35	30.34	0.02	55.75	55.21	0.99	18.01	17.76	1.39
1	*1*	*0*	*1*	*9.4*	*485.78*	*1125.0*	30.66	31.22	-1.79	51.55	60.69	-15.06	20.39	23.64	-13.76

*Pred= predicted using response surface model, Exp. = experimentally measured and measured, %ER= % error calculated as : %ER= (Exp-Pred)/Exp x100%

Appendix E: Process Flow Diagrams for Modelling

E.1 Basis for mass balance from literature

Table 103 Mass balance from literature for hydrotreating reactor [a]

	Feed to hydrotreating reactor [g for 100g raw BO feed (wet basis)]					H_2 consumed[b]	Oil yield [g wet oil/100g wet BO]x100%					Gas yield [g wet base]				Aqueous yield [g wet base]				Solids [g wet base]			
	Total stream [g]	C [g]	H [g]	O [g]	H_2O [g]	[g H_2/100g BO fed]	Total stream [g]	C [g]	H [g]	O [g]	H_2O [g]	Total stream [g]	C [g]	H [g]	O [g]	Total stream [g]	C [g]	H [g]	O [g]	Total stream [g]	C [g]	H [g]	O [g]
Mass	100.000	46.728	7.366	45.906	20.960	1.566	49.005	38.064	4.739	6.201	1.323	2.897	0.973	0.092	1.833	48.000	6.435	3.961	37.604	1.665	1.256	0.141	0.268

[a] Based on 100g bio-oil feed calculated from [16], [b] In hydrotreating reactor

Table 104 Mass balance from literature for hydrocracking reactor [a]

	Feed to hydrocracking reactor [g for 100g feed (wet basis)]					H_2 consumed [b]	Oil yield [g wet oil/100g wet BO]x100%					Gas yield [g wet base]				Aqueous yield [g wet base]					Solids [g wet base]			
	Total stream [g]	C [g]	H [g]	O [g]	H_2O [g]	[g H_2/100g raw BO fed]	Total stream [g]	C [g]	H [g]	O [g]	H_2O [g]	Total stream [g]	C [g]	H [g]	O [g]	Total stream [g]	C [g]	H [g]	O [g]	H_2O [g]	Total stream [g]	C [g]	H [g]	O [g]
Mass	49.005	38.064	4.739	6.201	1.323	1.504	29.086	25.214	3.756	0.116	0.003	3.312	1.990	0.451	0.871	11.761	5.271	1.329	5.161	5.285	6.350	5.590	0.708	0.052

[a] Based on 100g bio-oil feed calculated from [16], [b] In hydrocracking reactor

E.2 Validation of flash conditions in Unit B1000 and B2000

The Figures (Figure 47 to Figure 50) below indicate the transfer of the components most susceptible to flashing to the vapour phase (hexane, cyclohexane and tetrahydrofuran) at different flashing pressures. Maximum transfer of 10% benzene to the vapour phase was considered as acceptable. However since conversion of hexane was so small in R-B1001, see Table 69, only benzene and cyclohexane transfer were considered in determining the optimal flash conditions. Optimal conditions were selected at approximately 57°C and 104 bar for F-B1001. The sensitivity analysis on the flash drum in Unit B2002, F-B2001, hexane was the most volatile, see Figure 51 to Figure 55. A transfer fraction smaller than 10% (0.1 fraction) was used as guide to determine the best operating temperature of 50°C.
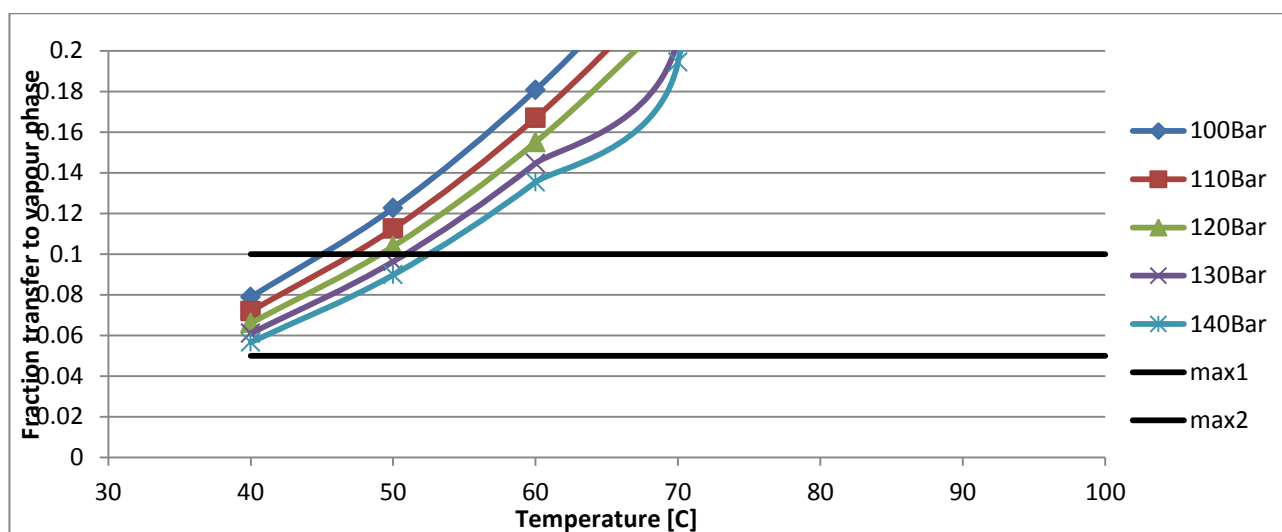
Figure 47 Hexane transfer to vapour phase in F-B1001 at different flash pressures
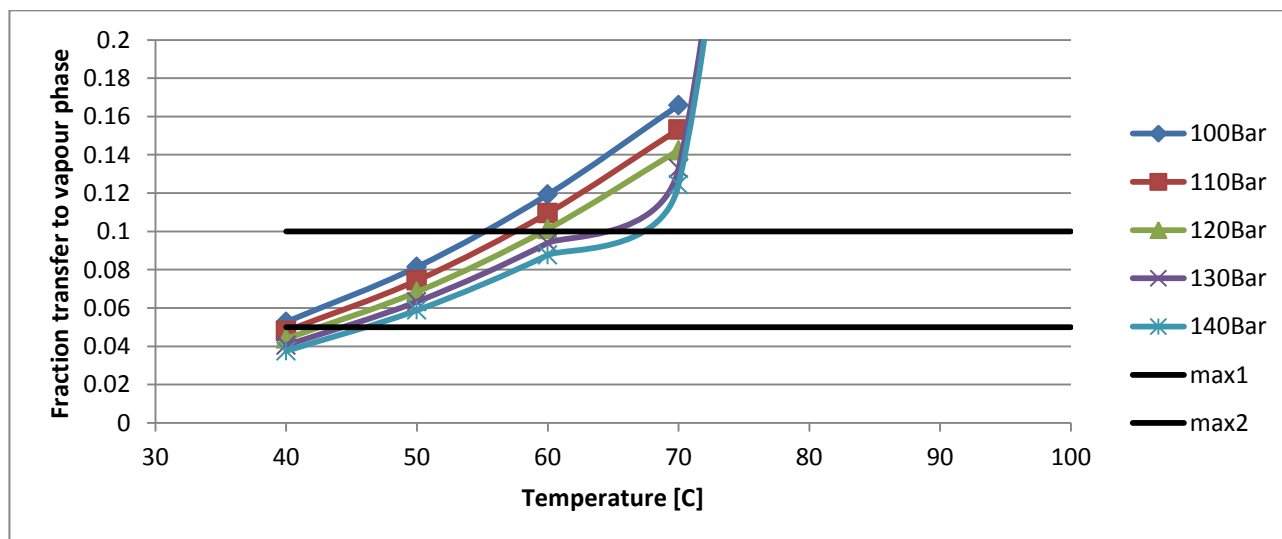
Figure 48 Cyclohexane transfer to vapour phase in F-B1001 at different flash pressures

230
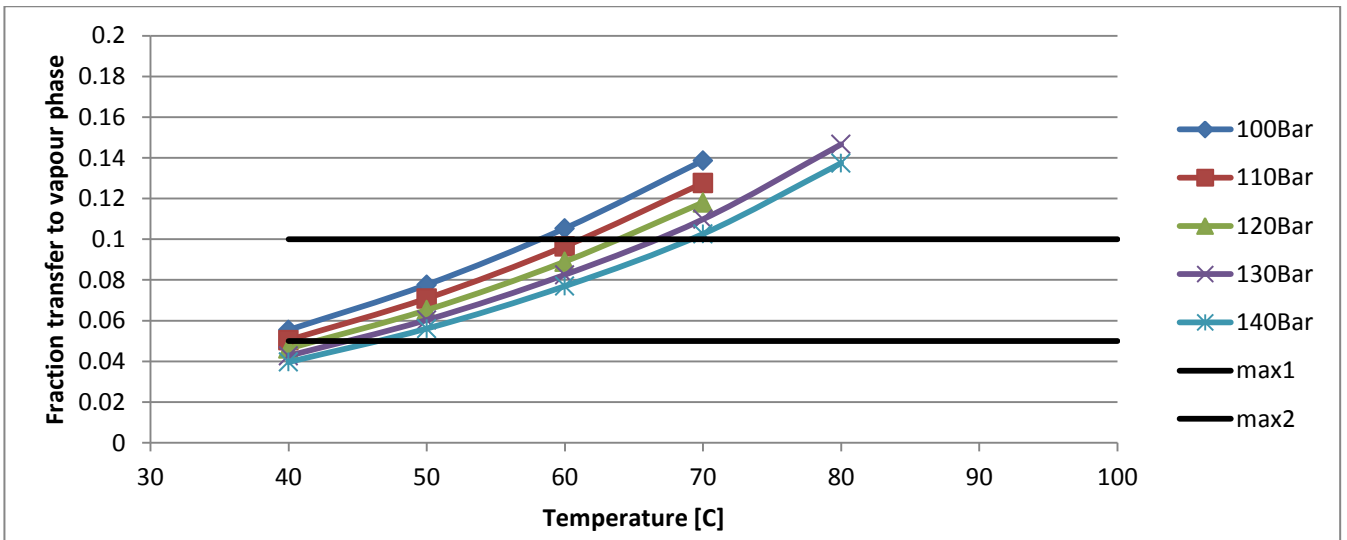
Figure 49 Tetrahydrofuran transfer to vapour phase in F-B1001 at different flash pressures
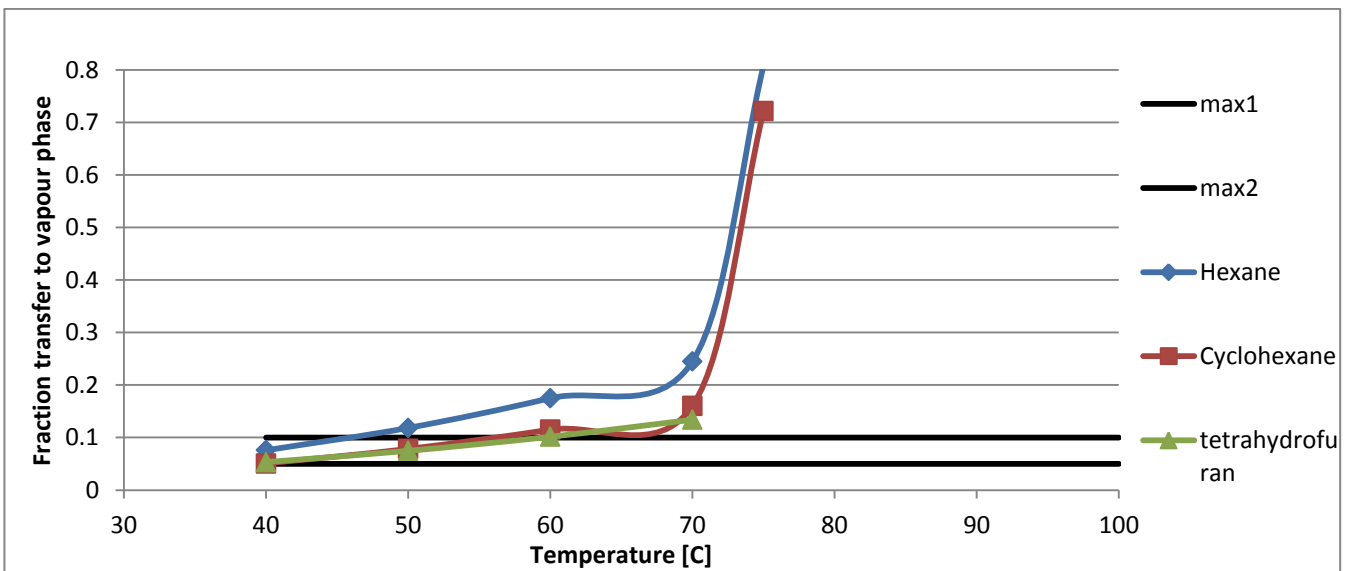
Figure 50 Transfer of hexane, cyclohexane and tetrahydrofuran to vapour phase in F-B1001 at 104 Bar
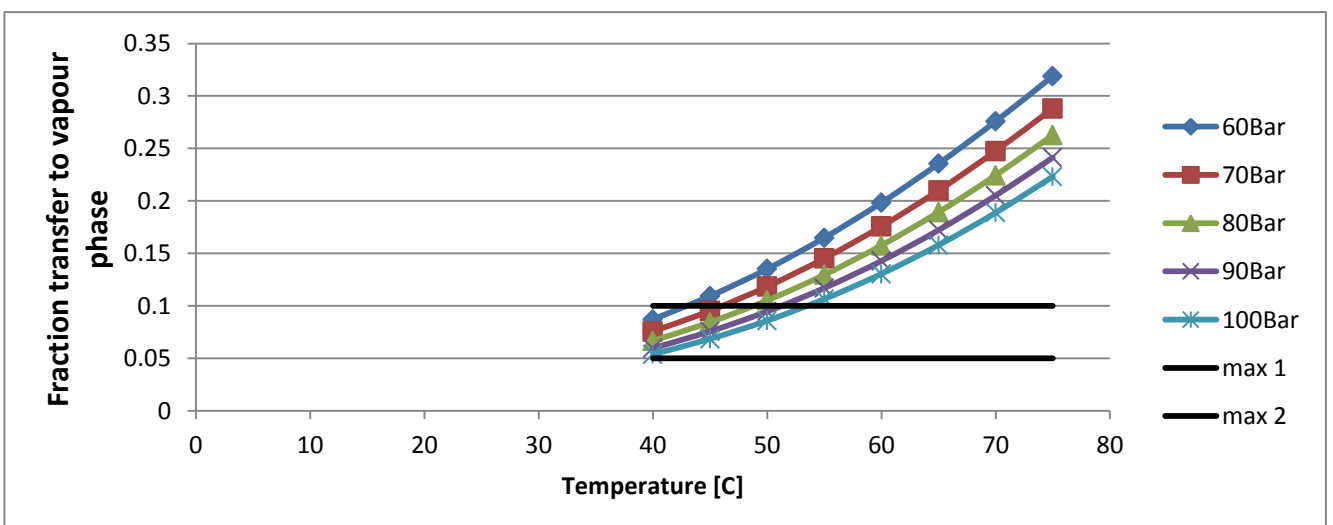
Figure 51 Hexane transfer to vapour phase in F-B2001 at different flash pressures

231
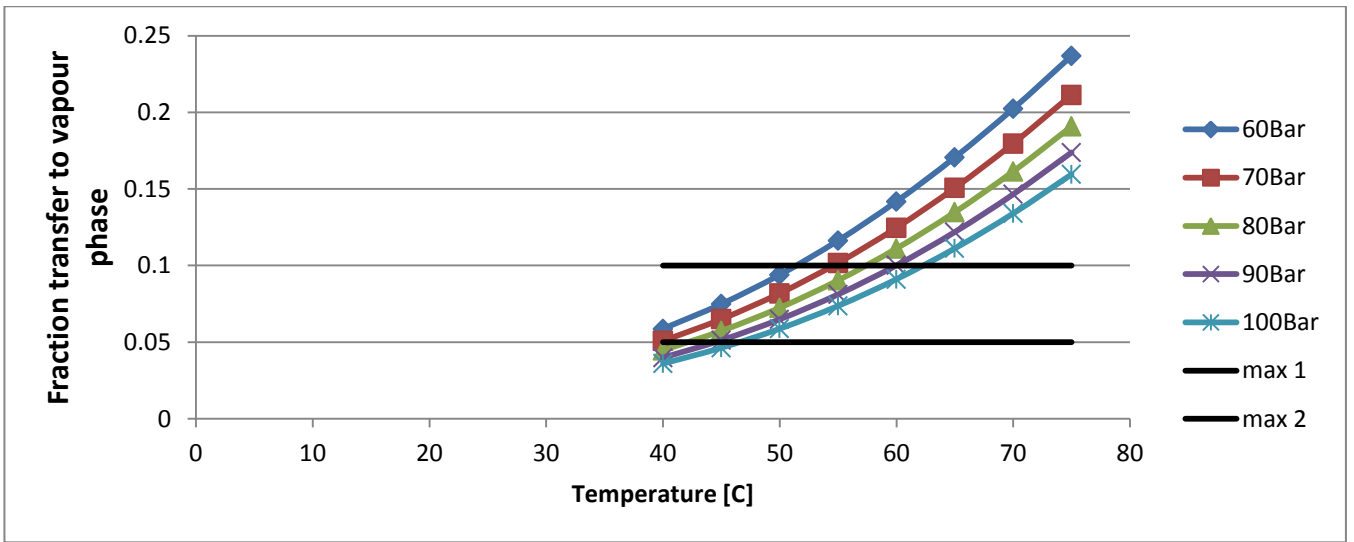
Figure 52 Cyclohexane transfer to vapour phase in F-B2001 at different flash pressures
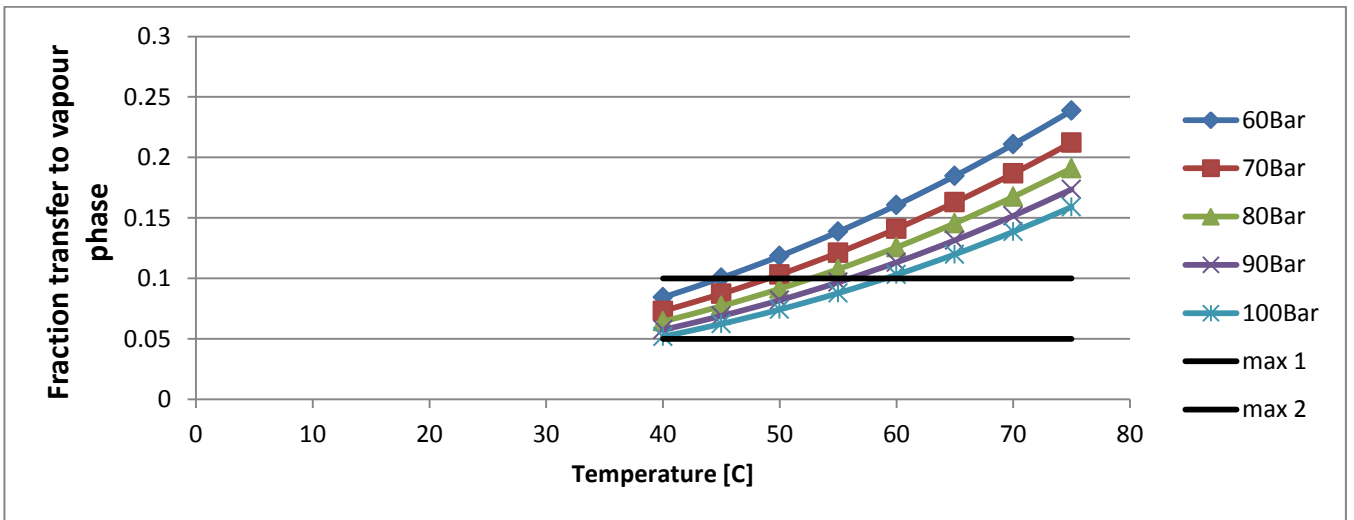
Figure 53 Tetrahydrofuran transfer to vapour phase in F-B2001 at different flash pressures
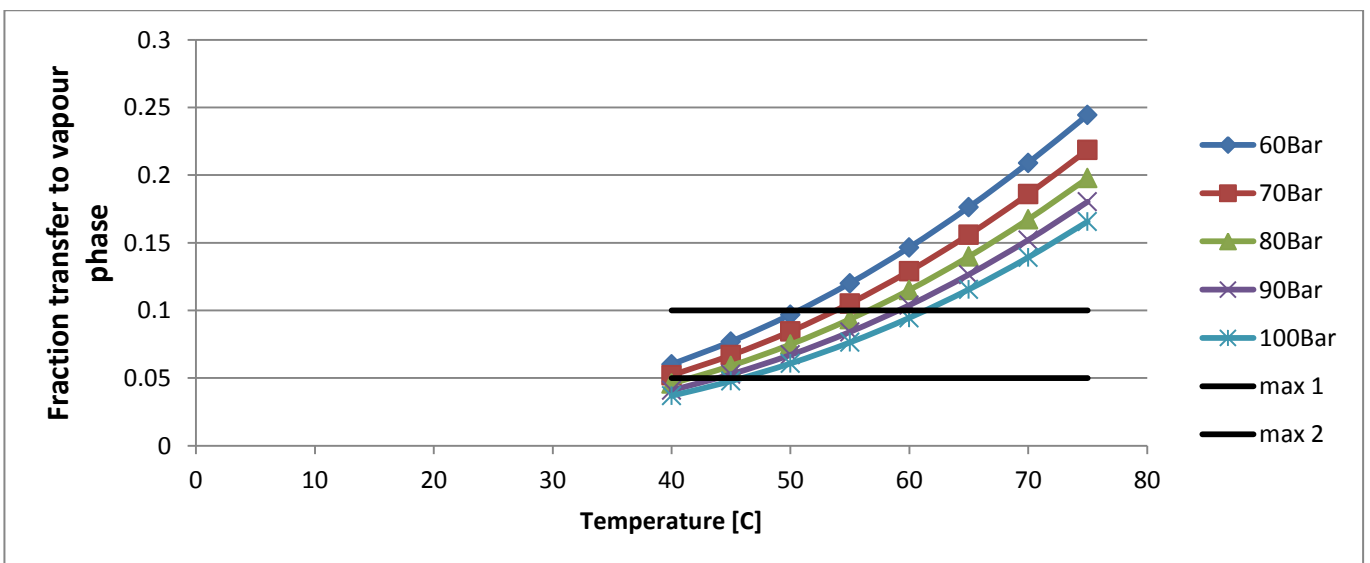
Figure 54 Benzene transfer to vapour phase in F-B2001 at different flash pressures
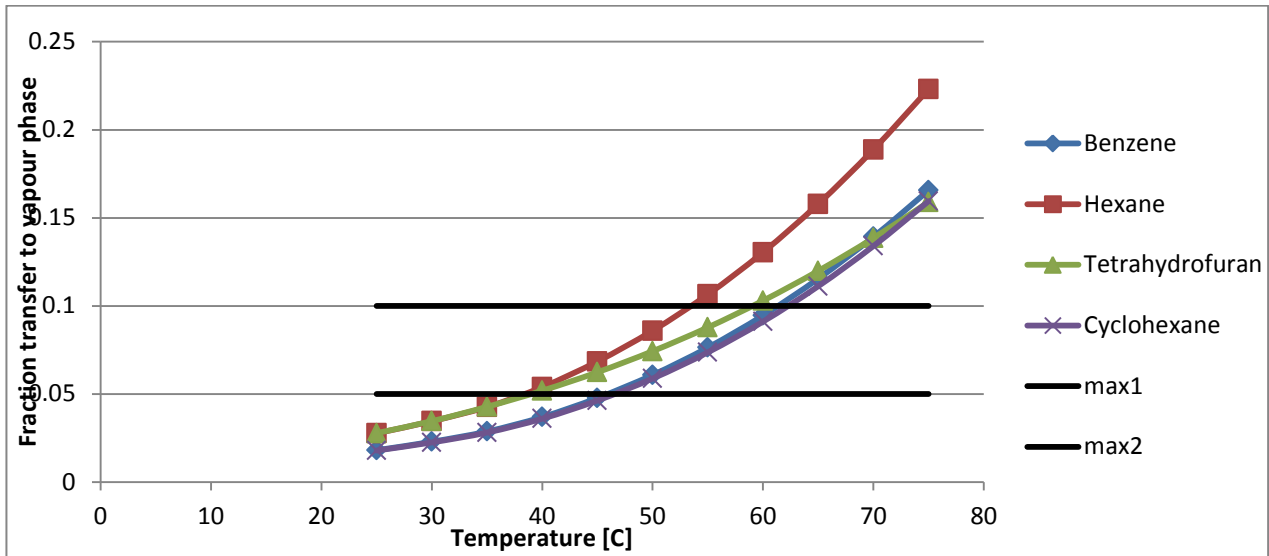
Figure 55 Transfer of hexane, cyclohexane and tetrahydrofuran to vapour phase in F-B2001 at 100 Bar

E.3 Overall
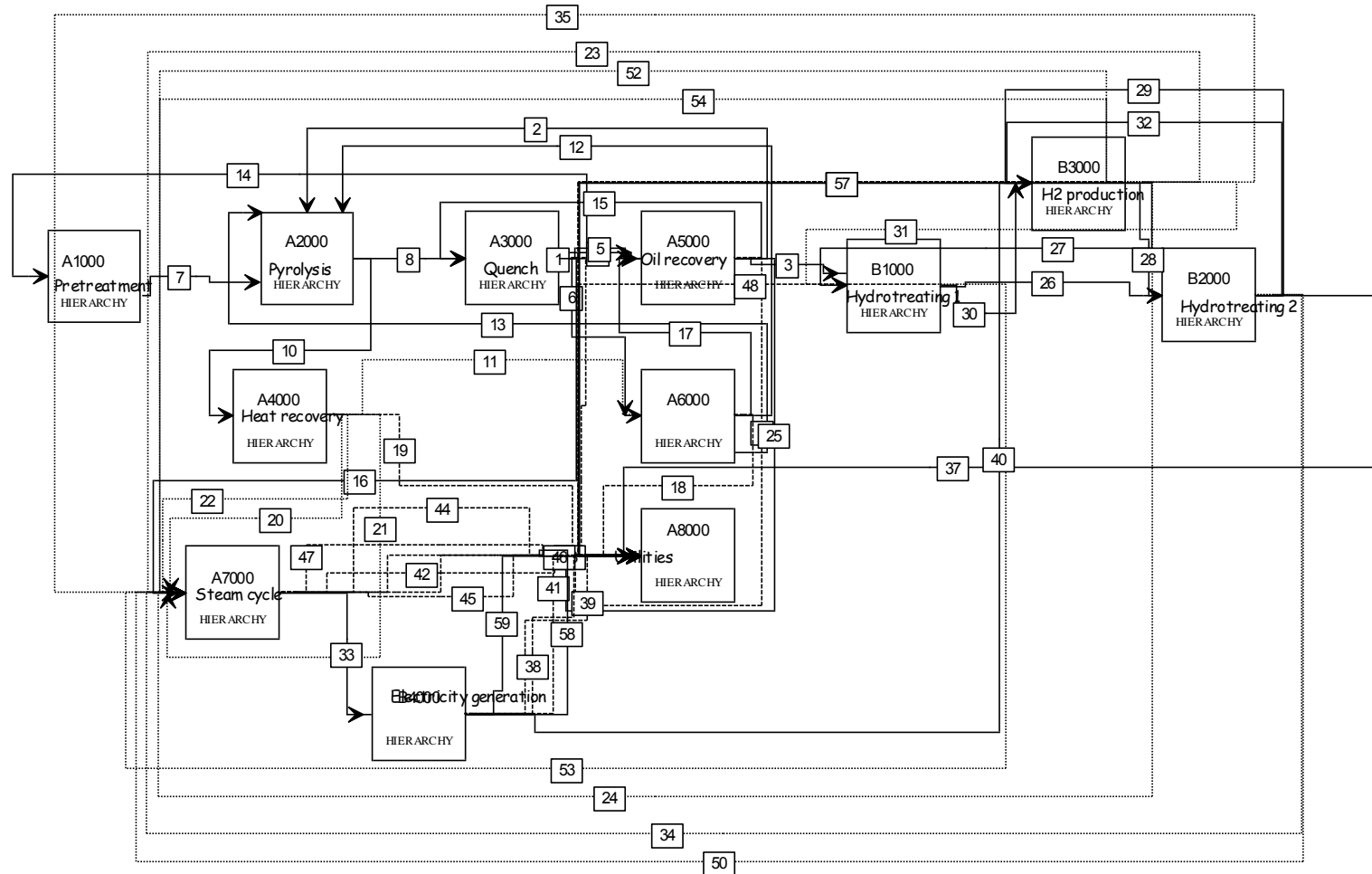
Figure 56 Overall Block Flow diagram of pyrolysis and upgrading Process

E.4 Unit A1000 – Pre-treatment
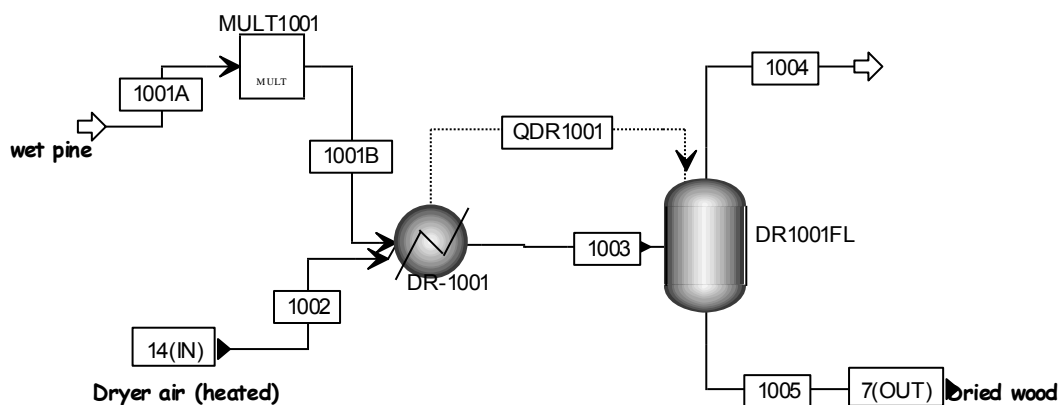
Figure 57 Process Flow Diagram of Unit A1000 – Pre-treatment

Table 105 Mass Balances for Unit A1000 – Pre-treatment

	1001A	1001B	1002	1003	1004	1005
Total Mass Flow tons/h	89.863	184.000	728.689	912.689	813.448	99.241
Temperature C	25.000	25.000	356.100	110.000	67.700	67.700
Pressure bar	1.379	1.379	1.020	1.379	1.379	1.379
MIXED						
Mass Flow tons/h	49.363	101.074	728.689	829.763	813.448	16.315
Vapor Frac	0.000	0.000	1.000	0.996	1.000	0.000
Enthalpy GJ/hr	-601.580	-1231.774	164.774	-1019.913	-1057.803	-11.883
Mass Flow tons/h						
N2	0.000	0.000	546.808	546.808	546.799	0.009
O2	0.000	0.000	167.526	167.526	167.522	0.003
CO2	0.000	0.000	0.291	0.291	0.291	0.000
H2O	44.932	92.000	4.809	96.809	89.581	7.229
AR	0.000	0.000	9.254	9.254	9.254	0.000
EXTRACT	4.432	9.074	0.000	9.074	0.000	9.074
CISOLIDS						
Mass Flow tons/h	40.500	82.926	0.000	82.926	0.000	82.926
Enthalpy Gcal/hr	-63.888	-130.814		-129.454		-130.173
Enthalpy GJ/hr	-267.307	-547.326		-541.636		-544.644
Mass Flow tons/h						
ASH	0.446	0.912	0.000	0.912	0.000	0.912
CELLULOS	18.531	37.944	0.000	37.944	0.000	37.944
LIGNIN	12.229	25.040	0.000	25.040	0.000	25.040
XYLAN	4.043	8.279	0.000	8.279	0.000	8.279
ARABINAN	0.385	0.788	0.000	0.788	0.000	0.788
MANNAN	4.866	9.964	0.000	9.964	0.000	9.964

Table 106 Duty/ heat Streams for Unit A1000 to A6000

	A1000. QDR1001	A3000. QHX3001	A3000. QHX3002	A4000. QCB-4001	A4000. QHX4001	A4000. QHX4002	A4000. QHX4003	A4000. QHX4004	A5000. QHX5001	A6000. QHX4001	A6000. QHX6001
QCALC MJ/hr	-52815	15372	225278	0	245442	227938	97495	172208	574	245442	4914
TBEGIN C	62.91	500.02	465.00	133.46	1592.95	1141.00	700.00	500.00	28.69	1592.95	27.84
TEND C	110.00	465.00	28.00	1592.95	1141.00	700.00	500.00	120.00	25.00	1141.00	7.00

E.5 Unit A2000 – Pyrolysis
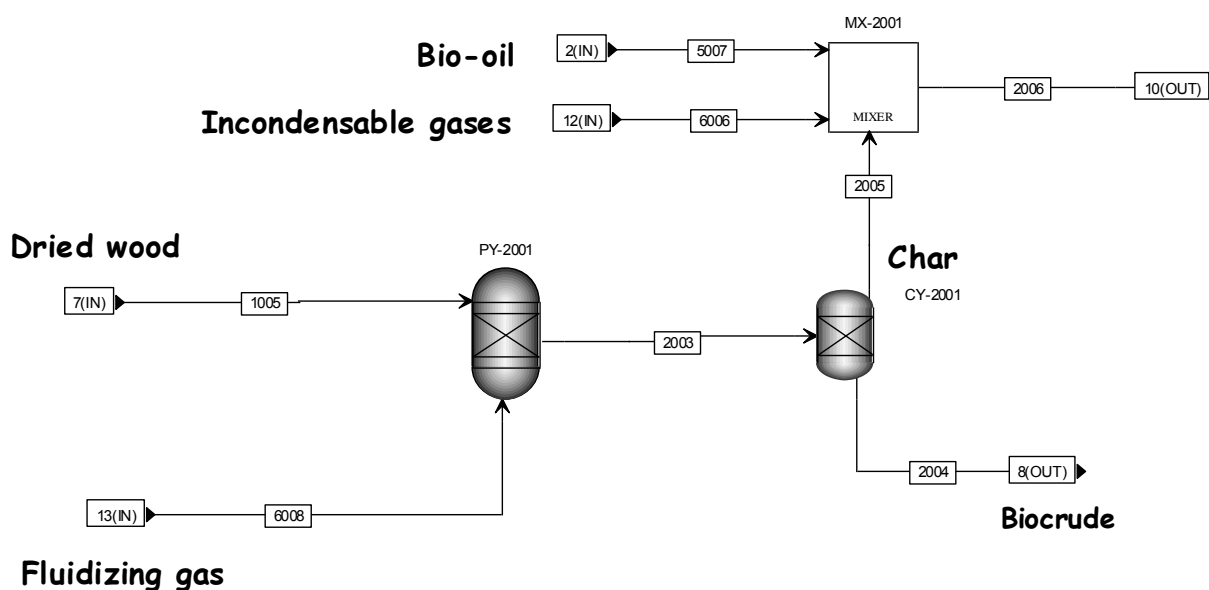
Figure 58 Process Flow Diagram of Unit A2000 – Pyrolysis

Table 107 Mass Balances for Unit A2000 – Pyrolysis

	1005	2003	2004	2005	2006	5007	6006	6008
Total Mass Flow tons/h	99.241	356.088	341.358	14.730	43.486	16.653	12.103	256.846
Temperature C	67.700	500.000	500.000	500.000	92.600	25.000	93.400	949.800
Pressure bar	1.379	1.379	1.379	1.379	1.379	2.758	3.103	3.103
MIXED								
Mass Flow tons/h	16.315	341.358	341.358	0.000	28.756	16.653	12.103	256.846
Vapor Frac	0.000	1.000	1.000		0.752	0.000	1.000	1.000
Enthalpy GJ/hr	-11.883	-1864.780	-1864.780		-173.247	-107.688	-73.249	-1309.203
Mass Flow tons/h								
N2	0.009	0.000	0.000	0.000	0.000	0.000	0.000	0.000
O2	0.003	0.000	0.000	0.000	0.000	0.000	0.000	0.000
CO	0.000	110.637	110.637	0.000	4.979	0.000	4.979	105.659
CO2	0.000	149.351	149.351	0.000	6.721	0.000	6.721	142.630
H2O	7.229	17.002	17.002	0.000	3.907	3.906	0.001	0.019

CH4	0.000	8.936	8.936	0.000	0.402	0.000	0.402	8.534
ACETACID	0.000	1.289	1.289	0.000	0.296	0.296	0.000	0.000
PHENOL	0.000	0.210	0.210	0.000	0.048	0.048	0.000	0.000
FURFURAL	0.000	0.027	0.027	0.000	0.006	0.006	0.000	0.000
EXTRACT	9.074	0.000	0.000	0.000	0.000	0.000	0.000	0.000
N-HEP-01	0.000	0.314	0.314	0.000	0.072	0.072	0.000	0.000
2:4-X-01	0.000	0.415	0.415	0.000	0.095	0.095	0.000	0.000
O-ETH-01	0.000	0.116	0.116	0.000	0.027	0.027	0.000	0.000
INDAN-01	0.000	2.467	2.467	0.000	0.567	0.567	0.000	0.001
2:6-D-01	0.000	0.133	0.133	0.000	0.031	0.031	0.000	0.000
NAPHT-01	0.000	1.202	1.202	0.000	0.276	0.276	0.000	0.000
DIBEN-01	0.000	0.218	0.218	0.000	0.050	0.050	0.000	0.000
FLUOR-01	0.000	2.490	2.490	0.000	0.573	0.573	0.000	0.000
2:4-D-01	0.000	0.233	0.233	0.000	0.053	0.053	0.000	0.000
NAPHT-02	0.000	1.617	1.617	0.000	0.372	0.372	0.000	0.000
GLYCO-01	0.000	10.945	10.945	0.000	2.517	2.517	0.000	0.002
FUMAR-01	0.000	0.992	0.992	0.000	0.228	0.228	0.000	0.000
1:2-B-01	0.000	0.014	0.014	0.000	0.003	0.003	0.000	0.000
2,2PROPA	0.000	8.387	8.387	0.000	1.929	1.929	0.000	0.000
FURACETA	0.000	2.932	2.932	0.000	0.674	0.674	0.000	0.000
LEVOGLUC	0.000	0.065	0.065	0.000	0.015	0.015	0.000	0.000
4METGUA	0.000	0.118	0.118	0.000	0.027	0.027	0.000	0.000
ETHYLANI	0.000	0.973	0.973	0.000	0.224	0.224	0.000	0.000
BENZOATE	0.000	0.136	0.136	0.000	0.031	0.031	0.000	0.000
METHPHEN	0.000	0.042	0.042	0.000	0.010	0.010	0.000	0.000
ETHYLGUA	0.000	0.208	0.208	0.000	0.048	0.048	0.000	0.000
MESHEPTA	0.000	0.864	0.864	0.000	0.199	0.199	0.000	0.000
BENZOFUR	0.000	2.219	2.219	0.000	0.510	0.510	0.000	0.000
TRIMEBEN	0.000	0.430	0.430	0.000	0.099	0.099	0.000	0.000
4PROPGUA	0.000	1.070	1.070	0.000	0.246	0.246	0.000	0.000
HMBENZAC	0.000	3.356	3.356	0.000	0.772	0.772	0.000	0.000
METOCTAC	0.000	4.299	4.299	0.000	0.989	0.989	0.000	0.000
CONIFALC	0.000	0.202	0.202	0.000	0.046	0.046	0.000	0.000
ISOEUGEN	0.000	0.612	0.612	0.000	0.141	0.141	0.000	0.000
PHENKETO	0.000	0.538	0.538	0.000	0.124	0.124	0.000	0.000
XANTHENE	0.000	0.623	0.623	0.000	0.143	0.143	0.000	0.000
P-DECANO	0.000	0.729	0.729	0.000	0.168	0.168	0.000	0.000
DNONDBEN	0.000	0.245	0.245	0.000	0.056	0.056	0.000	0.000
PENTACOS	0.000	0.287	0.287	0.000	0.066	0.066	0.000	0.000
C18H28	0.000	3.969	3.969	0.000	0.913	0.913	0.000	0.000
C21H24O4	0.000	0.139	0.139	0.000	0.032	0.032	0.000	0.000
C22H20O	0.000	0.304	0.304	0.000	0.070	0.070	0.000	0.000
CISOLIDS								
Mass Flow tons/h	82.926	14.730	0.000	14.730	14.730	0.000	0.000	0.000
Enthalpy GJ/hr	-544.644	-0.950		-0.950	-8.640			

Mass Flow tons/h								
CHAR	0.000	13.818	0.000	13.818	13.818	0.000	0.000	0.000
ASH	0.912	0.912	0.000	0.912	0.912	0.000	0.000	0.000
CELLULOS	37.944	0.000	0.000	0.000	0.000	0.000	0.000	0.000
LIGNIN	25.040	0.000	0.000	0.000	0.000	0.000	0.000	0.000
XYLAN	8.279	0.000	0.000	0.000	0.000	0.000	0.000	0.000
ARABINAN	0.788	0.000	0.000	0.000	0.000	0.000	0.000	0.000
MANNAN	9.964	0.000	0.000	0.000	0.000	0.000	0.000	0.000

E.6 Unit A3000 – Quench
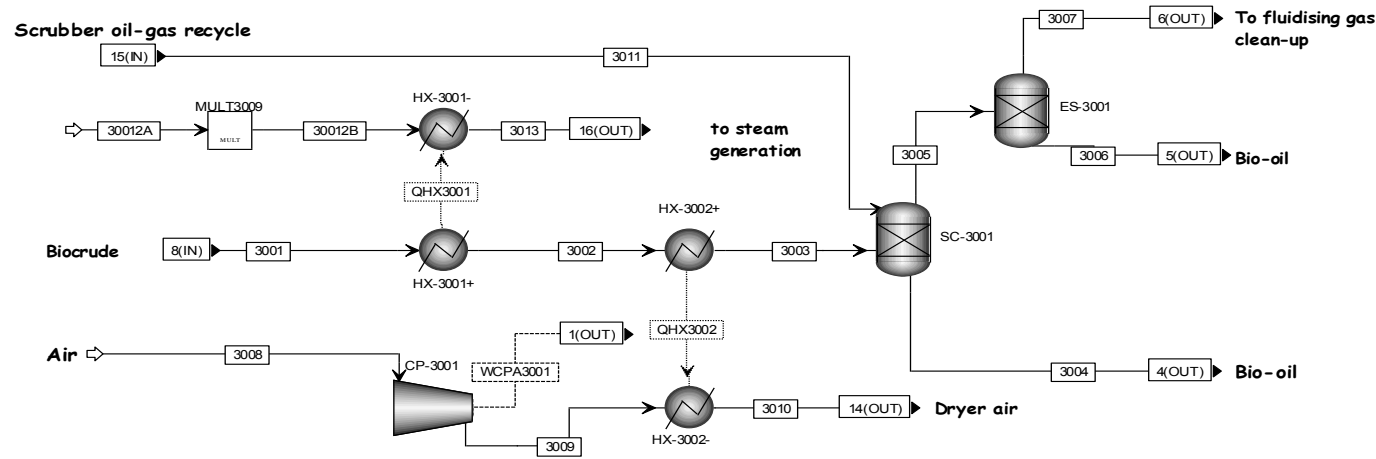
Figure 59 Process Flow Diagram of Unit A3000 – Quenching in Pyrolysis Process

Table 108 Mass Balances for Unit A3000 – Quenching in Pyrolysis Process

	3001	3002	3003	3004	3005	3006	3007	3008	3009	3010	3011	3013	30012A	30012B
Total Mass Flow tons/h	341.358	341.358	341.358	52.187	301.895	32.937	268.958	728.689	728.689	728.689	12.724	29.000	2.900	29.000
Temperature C	500.000	465.000	28.000	27.800	27.800	27.800	27.800	25.000	25.800	356.100	25.000	196.900	80.000	80.000
Pressure bar	1.379	1.379	1.379	1.379	1.379	1.379	1.379	1.014	1.020	1.020	2.758	40.000	1.379	1.379
Vapor Frac	1.000	1.000	0.869	0.000	0.889	0.000	1.000	1.000	1.000	1.000	0.000	0.000	0.000	0.000
Enthalpy GJ/hr	-1864.780	-1880.139	-2105.267	-210.623	-1975.342	-339.653	-1643.697	-60.886	-60.350	164.774	-82.651	-395.681	-41.104	-411.040
MIXED														
Mass Flow tons/h														
N2	0.000	0.000	0.000	0.000	0.000	0.000	0.000	546.808	546.808	546.808	0.000	0.000	0.000	0.000
O2	0.000	0.000	0.000	0.000	0.000	0.000	0.000	167.526	167.526	167.526	0.000	0.000	0.000	0.000
CO	110.637	110.637	110.637	0.000	110.637	0.000	110.637	0.000	0.000	0.000	0.000	0.000	0.000	0.000
NO2	0.000	0.000	0.000	0.000	0.000	0.000	0.000	0.000	0.000	0.000	0.000	0.000	0.000	0.000

CO2	149.351	149.351	149.351	0.000	149.351	0.000	149.351	0.291	0.291	0.291	0.000	0.000	0.000	0.000
H2O	17.002	17.002	17.002	0.000	19.999	19.979	0.020	4.809	4.809	4.809	2.997	29.000	2.900	29.000
H3N	0.000	0.000	0.000	0.000	0.000	0.000	0.000	0.000	0.000	0.000	0.000	0.000	0.000	0.000
CH4	8.936	8.936	8.936	0.000	8.936	0.000	8.936	0.000	0.000	0.000	0.000	0.000	0.000	0.000
AR	0.000	0.000	0.000	0.000	0.000	0.000	0.000	9.254	9.254	9.254	0.000	0.000	0.000	0.000
ACETACID	1.289	1.289	1.289	1.213	0.303	0.303	0.000	0.000	0.000	0.000	0.227	0.000	0.000	0.000
PHENOL	0.210	0.210	0.210	0.198	0.049	0.049	0.000	0.000	0.000	0.000	0.037	0.000	0.000	0.000
FURFURAL	0.027	0.027	0.027	0.026	0.006	0.006	0.000	0.000	0.000	0.000	0.005	0.000	0.000	0.000
N-HEP-01	0.314	0.314	0.314	0.296	0.074	0.074	0.000	0.000	0.000	0.000	0.055	0.000	0.000	0.000
2:4-X-01	0.415	0.415	0.415	0.391	0.098	0.098	0.000	0.000	0.000	0.000	0.073	0.000	0.000	0.000
O-ETH-01	0.116	0.116	0.116	0.109	0.027	0.027	0.000	0.000	0.000	0.000	0.020	0.000	0.000	0.000
INDAN-01	2.467	2.467	2.467	2.322	0.581	0.580	0.001	0.000	0.000	0.000	0.435	0.000	0.000	0.000
2:6-D-01	0.133	0.133	0.133	0.125	0.031	0.031	0.000	0.000	0.000	0.000	0.023	0.000	0.000	0.000
NAPHT-01	1.202	1.202	1.202	1.131	0.283	0.283	0.000	0.000	0.000	0.000	0.212	0.000	0.000	0.000
DIBEN-01	0.218	0.218	0.218	0.205	0.051	0.051	0.000	0.000	0.000	0.000	0.038	0.000	0.000	0.000
FLUOR-01	2.490	2.490	2.490	2.343	0.586	0.585	0.001	0.000	0.000	0.000	0.439	0.000	0.000	0.000
2:4-D-01	0.233	0.233	0.233	0.219	0.055	0.055	0.000	0.000	0.000	0.000	0.041	0.000	0.000	0.000
NAPHT-02	1.617	1.617	1.617	1.521	0.380	0.380	0.000	0.000	0.000	0.000	0.285	0.000	0.000	0.000
GLYCO-01	10.945	10.945	10.945	10.301	2.575	2.573	0.003	0.000	0.000	0.000	1.931	0.000	0.000	0.000
FUMAR-01	0.992	0.992	0.992	0.934	0.233	0.233	0.000	0.000	0.000	0.000	0.175	0.000	0.000	0.000
1:2-B-01	0.014	0.014	0.014	0.013	0.003	0.003	0.000	0.000	0.000	0.000	0.002	0.000	0.000	0.000
2,2PROPA	8.387	8.387	8.387	7.894	1.973	1.972	0.002	0.000	0.000	0.000	1.480	0.000	0.000	0.000
FURACETA	2.932	2.932	2.932	2.759	0.690	0.689	0.001	0.000	0.000	0.000	0.517	0.000	0.000	0.000
LEVOGLUC	0.065	0.065	0.065	0.061	0.015	0.015	0.000	0.000	0.000	0.000	0.011	0.000	0.000	0.000
4METGUA	0.118	0.118	0.118	0.111	0.028	0.028	0.000	0.000	0.000	0.000	0.021	0.000	0.000	0.000
ETHYLANI	0.973	0.973	0.973	0.916	0.229	0.229	0.000	0.000	0.000	0.000	0.172	0.000	0.000	0.000
BENZOATE	0.136	0.136	0.136	0.128	0.032	0.032	0.000	0.000	0.000	0.000	0.024	0.000	0.000	0.000
METHPHEN	0.042	0.042	0.042	0.039	0.010	0.010	0.000	0.000	0.000	0.000	0.007	0.000	0.000	0.000
ETHYLGUA	0.208	0.208	0.208	0.196	0.049	0.049	0.000	0.000	0.000	0.000	0.037	0.000	0.000	0.000
MESHEPTA	0.864	0.864	0.864	0.814	0.203	0.203	0.000	0.000	0.000	0.000	0.153	0.000	0.000	0.000

BENZOFUR	2.219	2.219	2.219	2.088	0.522	0.521	0.001	0.000	0.000	0.000	0.391	0.000	0.000	0.000
TRIMEBEN	0.430	0.430	0.430	0.405	0.101	0.101	0.000	0.000	0.000	0.000	0.076	0.000	0.000	0.000
4PROPGUA	1.070	1.070	1.070	1.007	0.252	0.252	0.000	0.000	0.000	0.000	0.189	0.000	0.000	0.000
HMBENZAC	3.356	3.356	3.356	3.159	0.790	0.789	0.001	0.000	0.000	0.000	0.592	0.000	0.000	0.000
METOCTAC	4.299	4.299	4.299	4.046	1.012	1.011	0.001	0.000	0.000	0.000	0.759	0.000	0.000	0.000
CONIFALC	0.202	0.202	0.202	0.190	0.047	0.047	0.000	0.000	0.000	0.000	0.036	0.000	0.000	0.000
ISOEUGEN	0.612	0.612	0.612	0.576	0.144	0.144	0.000	0.000	0.000	0.000	0.108	0.000	0.000	0.000
PHENKETO	0.538	0.538	0.538	0.507	0.127	0.127	0.000	0.000	0.000	0.000	0.095	0.000	0.000	0.000
XANTHENE	0.623	0.623	0.623	0.587	0.147	0.147	0.000	0.000	0.000	0.000	0.110	0.000	0.000	0.000
P-DECANO	0.729	0.729	0.729	0.686	0.172	0.171	0.000	0.000	0.000	0.000	0.129	0.000	0.000	0.000
DNONDBEN	0.245	0.245	0.245	0.231	0.058	0.058	0.000	0.000	0.000	0.000	0.043	0.000	0.000	0.000
PENTACOS	0.287	0.287	0.287	0.271	0.068	0.068	0.000	0.000	0.000	0.000	0.051	0.000	0.000	0.000
C18H28	3.969	3.969	3.969	3.735	0.934	0.933	0.001	0.000	0.000	0.000	0.700	0.000	0.000	0.000
C21H24O4	0.139	0.139	0.139	0.130	0.033	0.033	0.000	0.000	0.000	0.000	0.024	0.000	0.000	0.000
C22H20O	0.304	0.304	0.304	0.304	0.000	0.000	0.000	0.000	0.000	0.000	0.000	0.000	0.000	0.000

E.7 Unit A4000 – Heat Recovery
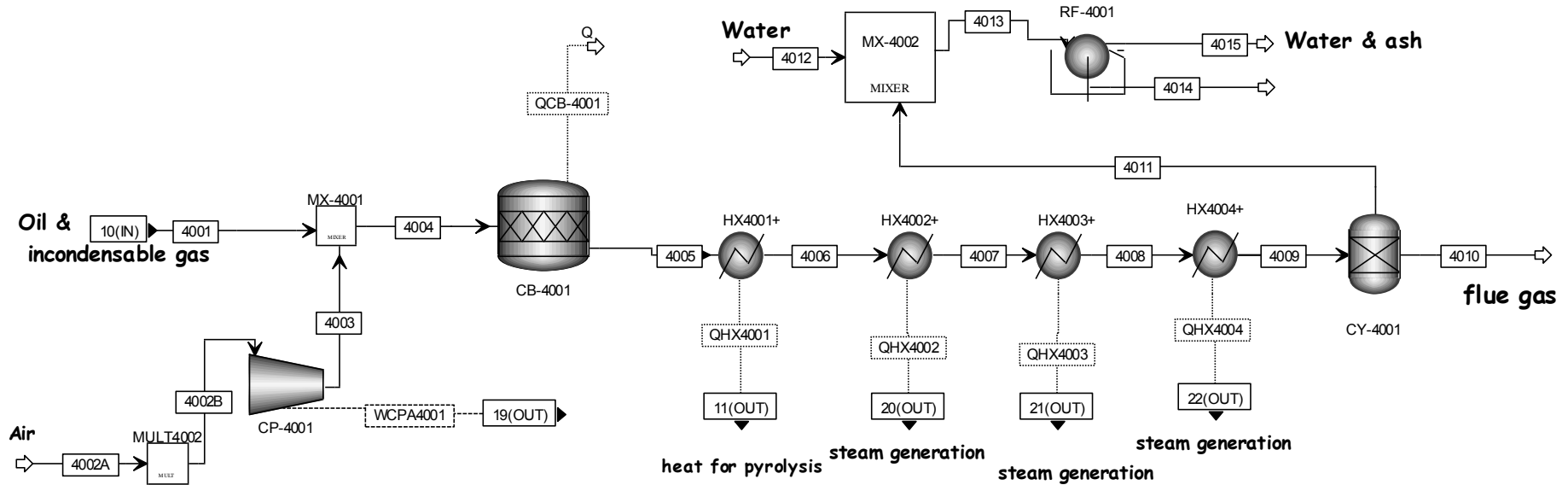
Figure 60 Process Flow Diagram of Unit A4000 – Heat Recovery

Table 109 Mass Balances for Unit A4000 – Heat Recovery

	4001	4002A	4002B	4003	4004	4005	4006	4007	4008	4009	4010	4011	4012	4013	4014	4015
Total Flow tons/h	43.486	182.838	415.335	415.335	458.822	458.819	458.819	458.819	458.819	458.819	457.907	0.912	1.102	2.014	0.912	1.102
Temperature C	92.610	150.000	150.000	151.124	133.458	1592.950	1141.000	700.000	500.000	120.000	120.000		25.000	40.000		40.000
Pressure bar	1.379	1.014	1.014	1.020	14.800	1.020	1.020	1.020	1.020	1.020	1.020	1.020	1.379	1.020		1.020
MIXED																
Total Flow tons/h	28.756	182.838	415.335	415.335	444.092	457.907	457.907	457.907	457.907	457.907	457.907	0.000	1.102	1.102	0.000	1.102
Vapor Frac	0.752	1.000	1.000	1.000	0.996	1.000	1.000	1.000	1.000	1.000	1.000		0.000	0.000		0.000
Enthalpy GJ/hr	-173.360	5.615	12.755	13.188	-160.690	-160.690	-405.760	-633.340	-730.680	-902.600	-902.600		-15.848	-15.789		-15.789
Mass Flow tons/h																

N2	0.000	137.184	311.626	311.626	311.626	311.626	311.626	311.626	311.626	311.626	311.626	0.000	0.000	0.000	0.000	0.000
O2	0.000	42.035	95.486	95.486	95.486	32.185	32.185	32.185	32.185	32.185	32.185	0.000	0.000	0.000	0.000	0.000
CO	4.979	0.000	0.000	0.000	4.979	0.000	0.000	0.000	0.000	0.000	0.000	0.000	0.000	0.000	0.000	0.000
CO2	6.721	0.091	0.208	0.208	6.928	93.980	93.980	93.980	93.980	93.980	93.980	0.000	0.000	0.000	0.000	0.000
H2O	3.907	1.207	2.741	2.741	6.648	14.841	14.841	14.841	14.841	14.841	14.841	0.000	1.102	1.102	0.000	1.102
CH4	0.402	0.000	0.000	0.000	0.402	0.000	0.000	0.000	0.000	0.000	0.000	0.000	0.000	0.000	0.000	0.000
AR	0.000	2.322	5.275	5.275	5.275	5.275	5.275	5.275	5.275	5.275	5.275	0.000	0.000	0.000	0.000	0.000
ACETACID	0.296	0.000	0.000	0.000	0.296	0.000	0.000	0.000	0.000	0.000	0.000	0.000	0.000	0.000	0.000	0.000
PHENOL	0.048	0.000	0.000	0.000	0.048	0.000	0.000	0.000	0.000	0.000	0.000	0.000	0.000	0.000	0.000	0.000
FURFURAL	0.006	0.000	0.000	0.000	0.006	0.000	0.000	0.000	0.000	0.000	0.000	0.000	0.000	0.000	0.000	0.000
BENZENE	0.000	0.000	0.000	0.000	0.000	0.000	0.000	0.000	0.000	0.000	0.000	0.000	0.000	0.000	0.000	0.000
N-HEP-01	0.072	0.000	0.000	0.000	0.072	0.000	0.000	0.000	0.000	0.000	0.000	0.000	0.000	0.000	0.000	0.000
2:4-X-01	0.095	0.000	0.000	0.000	0.095	0.000	0.000	0.000	0.000	0.000	0.000	0.000	0.000	0.000	0.000	0.000
O-ETH-01	0.027	0.000	0.000	0.000	0.027	0.000	0.000	0.000	0.000	0.000	0.000	0.000	0.000	0.000	0.000	0.000
INDAN-01	0.567	0.000	0.000	0.000	0.567	0.000	0.000	0.000	0.000	0.000	0.000	0.000	0.000	0.000	0.000	0.000
2:6-D-01	0.031	0.000	0.000	0.000	0.031	0.000	0.000	0.000	0.000	0.000	0.000	0.000	0.000	0.000	0.000	0.000
NAPHT-01	0.276	0.000	0.000	0.000	0.276	0.000	0.000	0.000	0.000	0.000	0.000	0.000	0.000	0.000	0.000	0.000
DIBEN-01	0.050	0.000	0.000	0.000	0.050	0.000	0.000	0.000	0.000	0.000	0.000	0.000	0.000	0.000	0.000	0.000
FLUOR-01	0.573	0.000	0.000	0.000	0.573	0.000	0.000	0.000	0.000	0.000	0.000	0.000	0.000	0.000	0.000	0.000
2:4-D-01	0.053	0.000	0.000	0.000	0.053	0.000	0.000	0.000	0.000	0.000	0.000	0.000	0.000	0.000	0.000	0.000
NAPHT-02	0.372	0.000	0.000	0.000	0.372	0.000	0.000	0.000	0.000	0.000	0.000	0.000	0.000	0.000	0.000	0.000
GLYCO-01	2.517	0.000	0.000	0.000	2.517	0.000	0.000	0.000	0.000	0.000	0.000	0.000	0.000	0.000	0.000	0.000
FUMAR-01	0.228	0.000	0.000	0.000	0.228	0.000	0.000	0.000	0.000	0.000	0.000	0.000	0.000	0.000	0.000	0.000
1:2-B-01	0.003	0.000	0.000	0.000	0.003	0.000	0.000	0.000	0.000	0.000	0.000	0.000	0.000	0.000	0.000	0.000
2,2PROPA	1.929	0.000	0.000	0.000	1.929	0.000	0.000	0.000	0.000	0.000	0.000	0.000	0.000	0.000	0.000	0.000
FURACETA	0.674	0.000	0.000	0.000	0.674	0.000	0.000	0.000	0.000	0.000	0.000	0.000	0.000	0.000	0.000	0.000
LEVOGLUC	0.015	0.000	0.000	0.000	0.015	0.000	0.000	0.000	0.000	0.000	0.000	0.000	0.000	0.000	0.000	0.000
4METGUA	0.027	0.000	0.000	0.000	0.027	0.000	0.000	0.000	0.000	0.000	0.000	0.000	0.000	0.000	0.000	0.000
ETHYLANI	0.224	0.000	0.000	0.000	0.224	0.000	0.000	0.000	0.000	0.000	0.000	0.000	0.000	0.000	0.000	0.000
BENZOATE	0.031	0.000	0.000	0.000	0.031	0.000	0.000	0.000	0.000	0.000	0.000	0.000	0.000	0.000	0.000	0.000

METHPHEN	0.010	0.000	0.000	0.000	0.010	0.000	0.000	0.000	0.000	0.000	0.000	0.000	0.000	0.000	0.000	0.000
ETHYLGUA	0.048	0.000	0.000	0.000	0.048	0.000	0.000	0.000	0.000	0.000	0.000	0.000	0.000	0.000	0.000	0.000
MESHEPTA	0.199	0.000	0.000	0.000	0.199	0.000	0.000	0.000	0.000	0.000	0.000	0.000	0.000	0.000	0.000	0.000
BENZOFUR	0.510	0.000	0.000	0.000	0.510	0.000	0.000	0.000	0.000	0.000	0.000	0.000	0.000	0.000	0.000	0.000
TRIMEBEN	0.099	0.000	0.000	0.000	0.099	0.000	0.000	0.000	0.000	0.000	0.000	0.000	0.000	0.000	0.000	0.000
4PROPGUA	0.246	0.000	0.000	0.000	0.246	0.000	0.000	0.000	0.000	0.000	0.000	0.000	0.000	0.000	0.000	0.000
HMBENZAC	0.772	0.000	0.000	0.000	0.772	0.000	0.000	0.000	0.000	0.000	0.000	0.000	0.000	0.000	0.000	0.000
METOCTAC	0.989	0.000	0.000	0.000	0.989	0.000	0.000	0.000	0.000	0.000	0.000	0.000	0.000	0.000	0.000	0.000
CONIFALC	0.046	0.000	0.000	0.000	0.046	0.000	0.000	0.000	0.000	0.000	0.000	0.000	0.000	0.000	0.000	0.000
ISOEUGEN	0.141	0.000	0.000	0.000	0.141	0.000	0.000	0.000	0.000	0.000	0.000	0.000	0.000	0.000	0.000	0.000
PHENKETO	0.124	0.000	0.000	0.000	0.124	0.000	0.000	0.000	0.000	0.000	0.000	0.000	0.000	0.000	0.000	0.000
XANTHENE	0.143	0.000	0.000	0.000	0.143	0.000	0.000	0.000	0.000	0.000	0.000	0.000	0.000	0.000	0.000	0.000
P-DECANO	0.168	0.000	0.000	0.000	0.168	0.000	0.000	0.000	0.000	0.000	0.000	0.000	0.000	0.000	0.000	0.000
DNONDBEN	0.056	0.000	0.000	0.000	0.056	0.000	0.000	0.000	0.000	0.000	0.000	0.000	0.000	0.000	0.000	0.000
PENTACOS	0.066	0.000	0.000	0.000	0.066	0.000	0.000	0.000	0.000	0.000	0.000	0.000	0.000	0.000	0.000	0.000
C18H28	0.913	0.000	0.000	0.000	0.913	0.000	0.000	0.000	0.000	0.000	0.000	0.000	0.000	0.000	0.000	0.000
C21H24O4	0.032	0.000	0.000	0.000	0.032	0.000	0.000	0.000	0.000	0.000	0.000	0.000	0.000	0.000	0.000	0.000
C22H20O	0.070	0.000	0.000	0.000	0.070	0.000	0.000	0.000	0.000	0.000	0.000	0.000	0.000	0.000	0.000	0.000
CISOLIDS																
Total Flow tons/h	14.730	0.000	0.000	0.000	14.730	0.912	0.912	0.912	0.912	0.912	0.000	0.912	0.000	0.912	0.912	0.000
Enthalpy GJ/hr	-8.645				-8.129	-8.126	-8.506	-8.861	-9.016	-9.302		-9.302		-9.361	-9.361	
Mass Flow tons/h																
CHAR	13.818	0.000	0.000	0.000	13.818	0.000	0.000	0.000	0.000	0.000	0.000	0.000	0.000	0.000	0.000	0.000
ASH	0.912	0.000	0.000	0.000	0.912	0.912	0.912	0.912	0.912	0.912	0.000	0.912	0.000	0.912	0.912	0.000

E.8 Unit A5000 – Oil Recovery
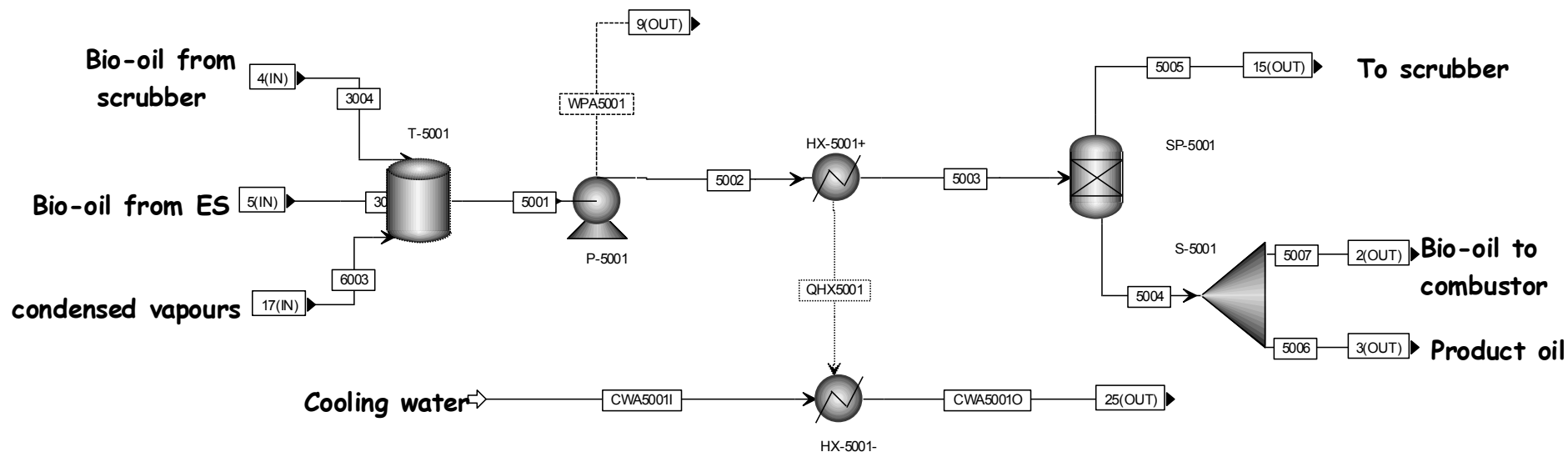
Figure 61 Process Flow Diagram of Unit A5000 – Oil Recovery in Pyrolysis Process

Table 110 Mass Balance for Unit A5000 – Oil Recovery in Pyrolysis Process

	3004	3021	5001	5002	5003	5004	5005	5006	5007	6003	CWA5001I	CWA5001O
Total Mass Flow tons/h	52.187	32.937	85.133	85.133	85.133	72.409	12.724	55.755	16.653	0.009	16.319	16.319
Temperature C	27.800	27.800	28.700	28.700	25.000	25.000	25.000	25.000	25.000	7.000	21.100	31.100
Pressure bar	1.379	1.379	1.793	2.758	2.758	2.758	2.758	2.758	2.758	1.379	1.034	1.034
Vapor Frac	0.000	0.000	0.000	0.000	0.000	0.000	0.000	0.000	0.000	0.000	0.000	0.000
Enthalpy GJ/hr	-210.623	-339.653	-550.313	-550.309	-550.882	-468.231	-82.651	-360.539	-107.688	-0.033	-234.835	-234.262
MIXED												
Mass Flow tons/h												
H2O	0.000	19.979	19.979	19.979	19.979	16.982	2.997	13.076	3.906	0.000	16.319	16.319
ACETACID	1.213	0.303	1.516	1.516	1.516	1.289	0.227	0.993	0.296	0.000	0.000	0.000

PHENOL	0.198	0.049	0.247	0.247	0.247	0.210	0.037	0.162	0.048	0.000	0.000	0.000
FURFURAL	0.026	0.006	0.032	0.032	0.032	0.027	0.005	0.021	0.006	0.000	0.000	0.000
N-HEP-01	0.296	0.074	0.370	0.370	0.370	0.314	0.055	0.242	0.072	0.000	0.000	0.000
2:4-X-01	0.391	0.098	0.488	0.488	0.488	0.415	0.073	0.319	0.095	0.000	0.000	0.000
O-ETH-01	0.109	0.027	0.136	0.136	0.136	0.116	0.020	0.089	0.027	0.000	0.000	0.000
INDAN-01	2.322	0.580	2.902	2.902	2.902	2.467	0.435	1.899	0.567	0.000	0.000	0.000
2:6-D-01	0.125	0.031	0.156	0.156	0.156	0.133	0.023	0.102	0.031	0.000	0.000	0.000
NAPHT-01	1.131	0.283	1.414	1.414	1.414	1.202	0.212	0.926	0.276	0.000	0.000	0.000
DIBEN-01	0.205	0.051	0.256	0.256	0.256	0.218	0.038	0.168	0.050	0.000	0.000	0.000
FLUOR-01	2.343	0.585	2.929	2.929	2.929	2.490	0.439	1.917	0.573	0.001	0.000	0.000
2:4-D-01	0.219	0.055	0.274	0.274	0.274	0.233	0.041	0.179	0.053	0.000	0.000	0.000
NAPHT-02	1.521	0.380	1.902	1.902	1.902	1.617	0.285	1.245	0.372	0.000	0.000	0.000
GLYCO-01	10.301	2.573	12.875	12.875	12.875	10.944	1.931	8.427	2.517	0.001	0.000	0.000
FUMAR-01	0.934	0.233	1.167	1.167	1.167	0.992	0.175	0.764	0.228	0.000	0.000	0.000
1:2-B-01	0.013	0.003	0.016	0.016	0.016	0.014	0.002	0.011	0.003	0.000	0.000	0.000
2,2PROPA	7.894	1.972	9.867	9.867	9.867	8.387	1.480	6.458	1.929	0.002	0.000	0.000
FURACETA	2.759	0.689	3.449	3.449	3.449	2.932	0.517	2.257	0.674	0.001	0.000	0.000
LEVOGLUC	0.061	0.015	0.076	0.076	0.076	0.065	0.011	0.050	0.015	0.000	0.000	0.000
4METGUA	0.111	0.028	0.139	0.139	0.139	0.118	0.021	0.091	0.027	0.000	0.000	0.000
ETHYLANI	0.916	0.229	1.145	1.145	1.145	0.973	0.172	0.749	0.224	0.000	0.000	0.000
BENZOATE	0.128	0.032	0.161	0.161	0.161	0.136	0.024	0.105	0.031	0.000	0.000	0.000
METHPHEN	0.039	0.010	0.049	0.049	0.049	0.042	0.007	0.032	0.010	0.000	0.000	0.000
ETHYLGUA	0.196	0.049	0.245	0.245	0.245	0.208	0.037	0.160	0.048	0.000	0.000	0.000
MESHEPTA	0.814	0.203	1.017	1.017	1.017	0.864	0.153	0.665	0.199	0.000	0.000	0.000
BENZOFUR	2.088	0.521	2.609	2.609	2.609	2.218	0.391	1.708	0.510	0.000	0.000	0.000
TRIMEBEN	0.405	0.101	0.506	0.506	0.506	0.430	0.076	0.331	0.099	0.000	0.000	0.000
4PROPGUA	1.007	0.252	1.259	1.259	1.259	1.070	0.189	0.824	0.246	0.000	0.000	0.000
HMBENZAC	3.159	0.789	3.948	3.948	3.948	3.356	0.592	2.584	0.772	0.001	0.000	0.000
METOCTAC	4.046	1.011	5.058	5.058	5.058	4.299	0.759	3.310	0.989	0.001	0.000	0.000
CONIFALC	0.190	0.047	0.237	0.237	0.237	0.202	0.036	0.155	0.046	0.000	0.000	0.000

ISOEUGEN	0.576	0.144	0.720	0.720	0.720	0.612	0.108	0.472	0.141	0.000	0.000	0.000
PHENKETO	0.507	0.127	0.634	0.634	0.634	0.538	0.095	0.415	0.124	0.000	0.000	0.000
XANTHENE	0.587	0.147	0.733	0.733	0.733	0.623	0.110	0.480	0.143	0.000	0.000	0.000
P-DECANO	0.686	0.171	0.858	0.858	0.858	0.729	0.129	0.561	0.168	0.000	0.000	0.000
DNONDBEN	0.231	0.058	0.289	0.289	0.289	0.245	0.043	0.189	0.056	0.000	0.000	0.000
PENTACOS	0.271	0.068	0.338	0.338	0.338	0.287	0.051	0.221	0.066	0.000	0.000	0.000
C18H28	3.735	0.933	4.669	4.669	4.669	3.969	0.700	3.056	0.913	0.001	0.000	0.000
C21H24O4	0.130	0.033	0.163	0.163	0.163	0.139	0.024	0.107	0.032	0.000	0.000	0.000
C22H20O	0.304	0.000	0.304	0.304	0.304	0.304	0.000	0.234	0.070	0.000	0.000	0.000

E.9 Unit A6000 – Recycle
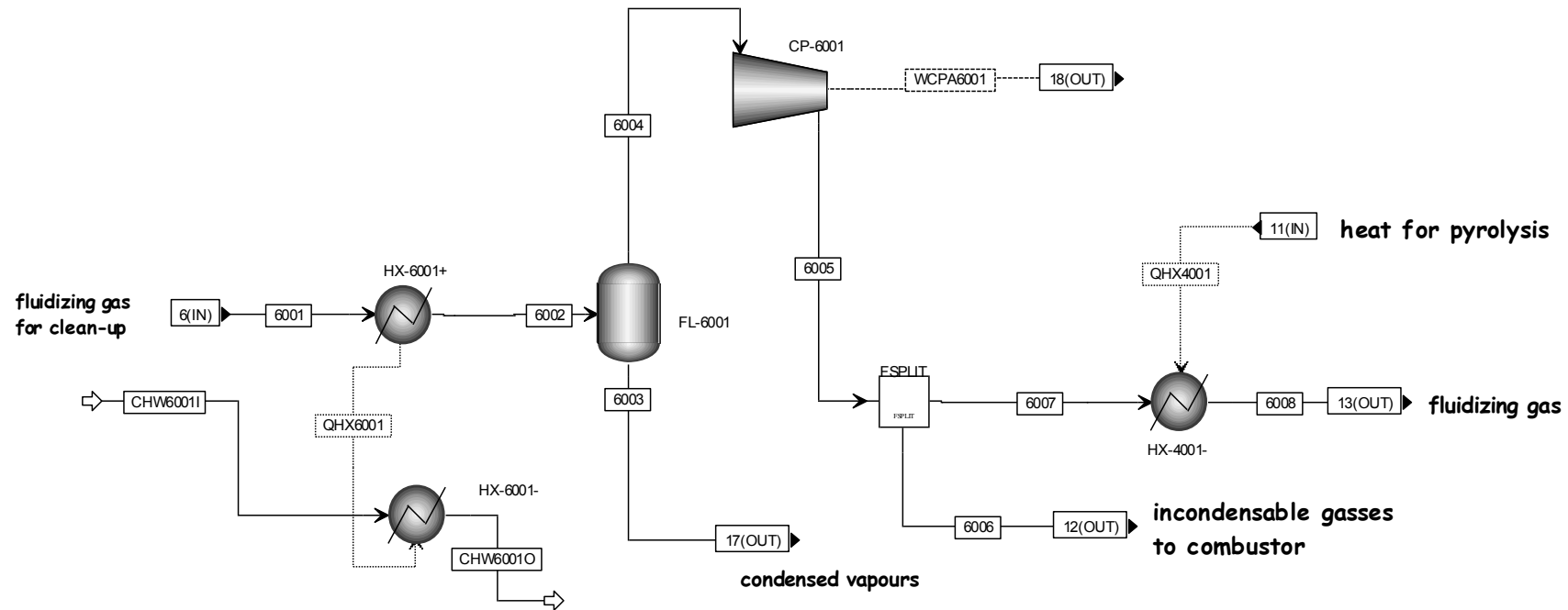
Figure 62 Process Flow Diagram of Unit A6000 – Recycling in Pyrolysis Process

Table 111 Mass balances for Unit A6000 – Recycling in Pyrolysis Process

	6001	6002	6003	6004	6005	6006	6007	6008	CHW6001I	CHW6001O
Total Mass Flow tons/h	268.958	268.958	0.009	268.949	268.949	12.103	256.846	256.846	179.677	179.677
Temperature C	27.800	7.000	7.000	7.000	93.400	93.400	93.400	949.800	4.000	12.000
Pressure bar	1.379	1.379	1.379	1.379	3.103	3.103	3.103	3.103	1.034	1.034
Vapor Frac	1.000	1.000	0.000	1.000	1.000	1.000	1.000	1.000	0.000	0.000
Enthalpy GJ/hr	-1643.697	-1648.609	-0.033	-1648.575	-1627.731	-73.249	-1554.486	-1309.207	-2596.067	-2591.155
MIXED										
Mass Flow tons/h										
CO	110.637	110.637	0.000	110.637	110.637	4.979	105.658	105.658	0.000	0.000
CO2	149.351	149.351	0.000	149.351	149.351	6.721	142.630	142.630	0.000	0.000
H2O	0.020	0.020	0.000	0.020	0.020	0.001	0.019	0.019	179.677	179.677
CH4	8.936	8.936	0.000	8.936	8.936	0.402	8.534	8.534	0.000	0.000
INDAN-01	0.001	0.001	0.000	0.001	0.001	0.000	0.001	0.001	0.000	0.000
FLUOR-01	0.001	0.001	0.001	0.000	0.000	0.000	0.000	0.000	0.000	0.000
GLYCO-01	0.003	0.003	0.001	0.002	0.002	0.000	0.002	0.002	0.000	0.000
2,2PROPA	0.002	0.002	0.002	0.000	0.000	0.000	0.000	0.000	0.000	0.000
FURACETA	0.001	0.001	0.001	0.000	0.000	0.000	0.000	0.000	0.000	0.000
BENZOFUR	0.001	0.001	0.000	0.001	0.001	0.000	0.000	0.000	0.000	0.000
HMBENZAC	0.001	0.001	0.001	0.000	0.000	0.000	0.000	0.000	0.000	0.000
METOCTAC	0.001	0.001	0.001	0.000	0.000	0.000	0.000	0.000	0.000	0.000
C18H28	0.001	0.001	0.001	0.000	0.000	0.000	0.000	0.000	0.000	0.000

E.10 Unit A7000 – Steam Cycle
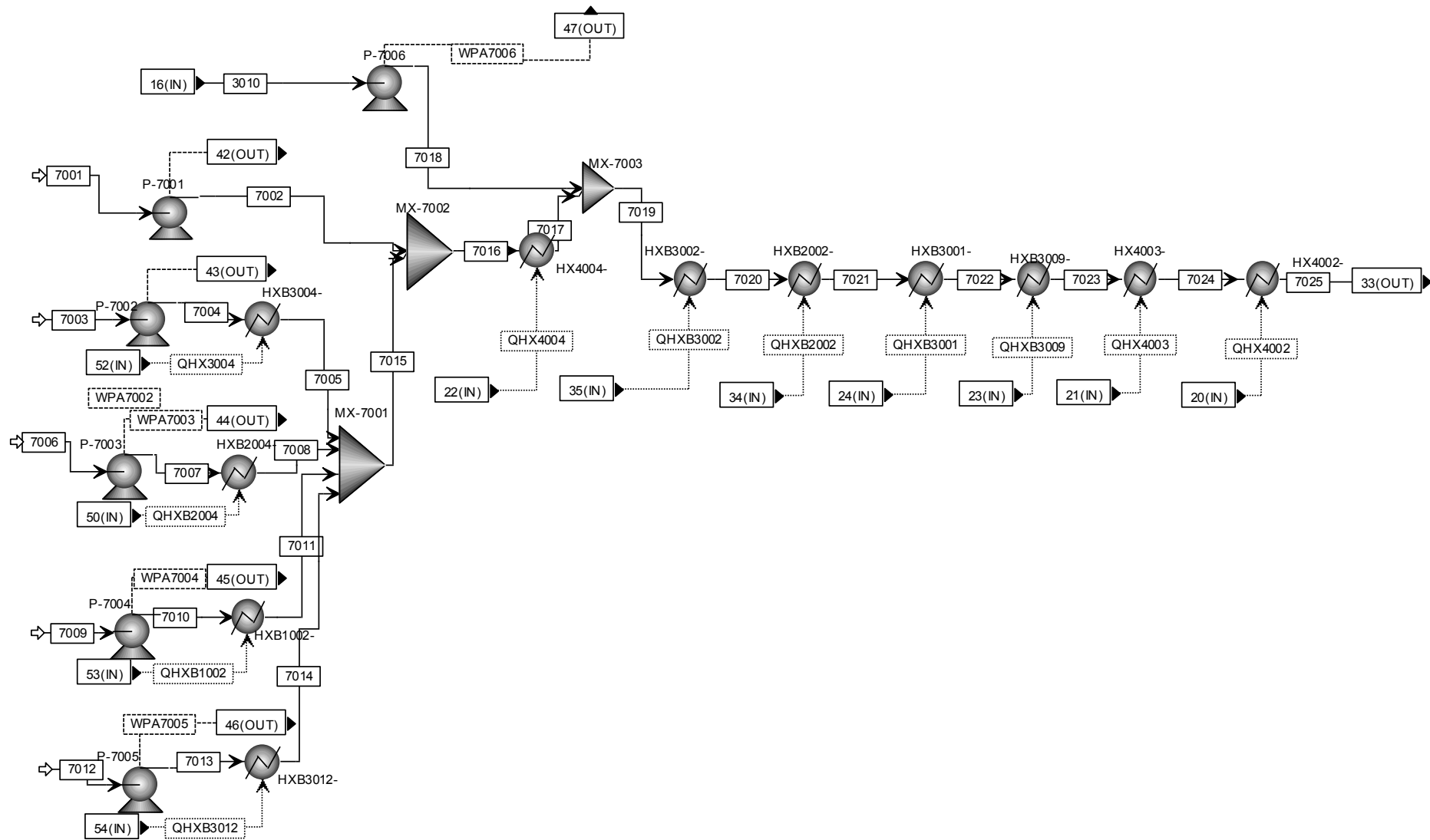
Figure 63 Process Flow Diagram of Unit A7000 – Steam Cycle

Table 112 Mass Balances for streams 7001-7012 of Unit A7000 – Steam Cycle

	3010	7001	7002	7003	7004	7005	7006	7007	7008	7009	7010	7011	7012
Mass Flow tons/h	29.000	85.168	85.168	117.000	117.000	117.000	26.000	26.000	26.000	65.000	65.000	65.000	60.000
Temperature C	196.900	25.000	29.000	25.000	28.800	134.700	25.000	30.000	311.400	25.000	29.200	313.500	25.000
Pressure bar	40.000	1.013	105.000	1.013	105.000	105.000	1.013	105.000	105.000	1.013	105.000	105.000	1.013
Vapor Frac	0.000	0.000	0.000	0.000	0.000	0.000	0.000	0.000	0.000	0.000	0.000	0.000	0.000
Enthalpy GJ/hr	-395.681	-1224.4	-1223.21	-1682.03	-1680.46	-1631.78	-373.786	-373.33	-334.226	-934.463	-933.513	-834.327	-862.582
Mass Flow tons/h													
H2O	29.000	85.168	85.168	117.000	117.000	117.000	26.000	26.000	26.000	65.000	65.000	65.000	60.000

Table 113 Mass Balances for streams 7013-7025 of Unit A7000 – Steam Cycle

	7013	7014	7015	7016	7017	7018	7019	7020	7021	7022	7023	7024	7025
Mass Flow tons/h	60.000	60.000	268.000	353.168	353.168	29.000	382.168	382.168	382.168	382.168	382.168	382.168	382.168
Temperature C	29.200	232.800	229.700	190.900	270.600	199.300	265.900	266.800	268.200	291.800	314.500	314.500	500.000
Pressure bar	105.000	105.000	105.000	105.000	105.000	105.000	105.000	105.000	105.000	105.000	105.000	105.000	105.000
Vapor Frac	0.000	0.000	0.000	0.000	0.000	0.000	0.000	0.000	0.000	0.000	0.567	0.787	1.000
Enthalpy GJ/hr	-861.691	-806.349	-3606.67	-4829.88	-4657.79	-395.317	-5053.11	-5050.44	-5046.86	-4978.1	-4649.42	-4551.99	-4324.2
Mass Flow tons/h													
H2O	60.000	60.000	268.000	353.168	353.168	29.000	382.168	382.168	382.168	382.168	382.168	382.168	382.168

Table 114 Duty/ heat Streams for Unit A7000

	A7000. QHX3004	A7000. QHX4002	A7000. QHX4003	A7000. QHX4004	A7000. QHXB1002	A7000. QHXB2002	A7000. QHXB2004	A7000. QHXB3001	A7000. QHXB3002	A7000. QHXB3009	A7000. QHXB3012
QCALC MJ/hr	48720.03	227938.20	97494.59	172207.82	99252.26	3581.98	39129.80	68805.74	2667.02	328906.84	55379.72
TBEGIN C	156.99	1141.00	700.00	500.00	339.73	399.38	352.83	856.97	390.24	1333.90	265.11
TEND C	55.00	700.00	500.00	120.00	57.00	369.70	55.00	350.00	369.70	447.95	90.00

E.11 Unit A8000 – Utilities
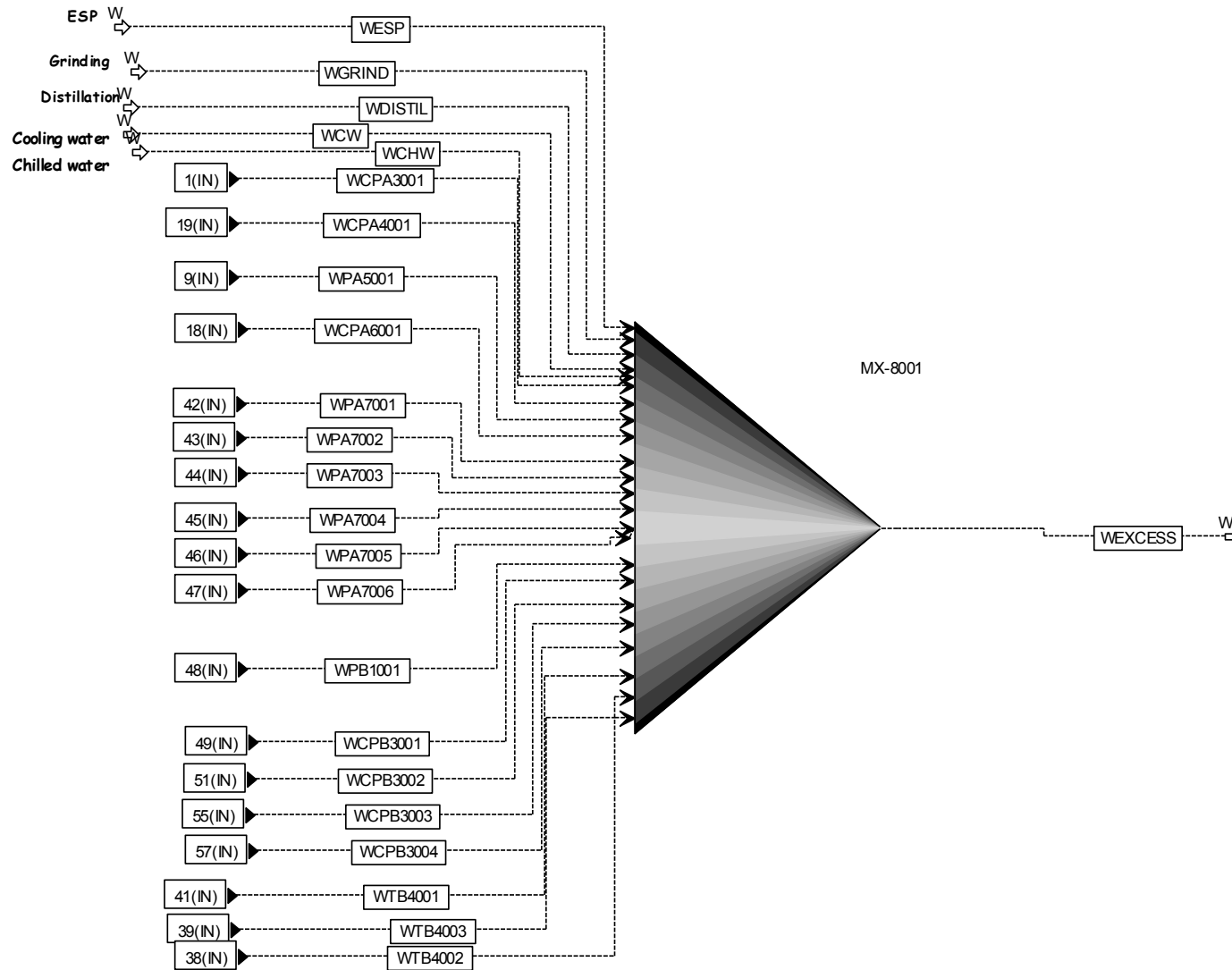
Figure 64 Energy (power) balance in Unit A8000 - Utilities
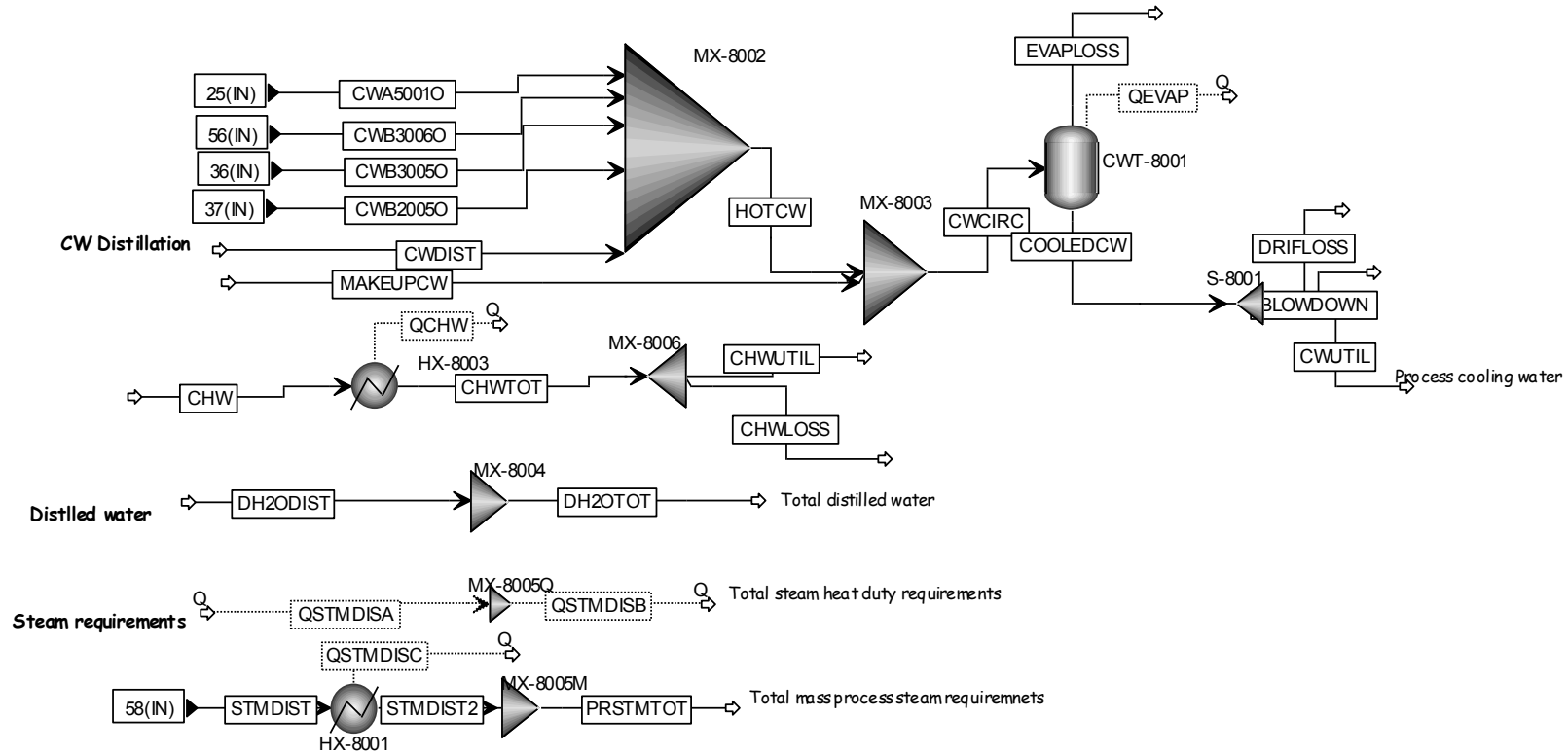
Figure 65 Cooling water, distilled water and steam requirement balances in Unit A8000 - Utilities
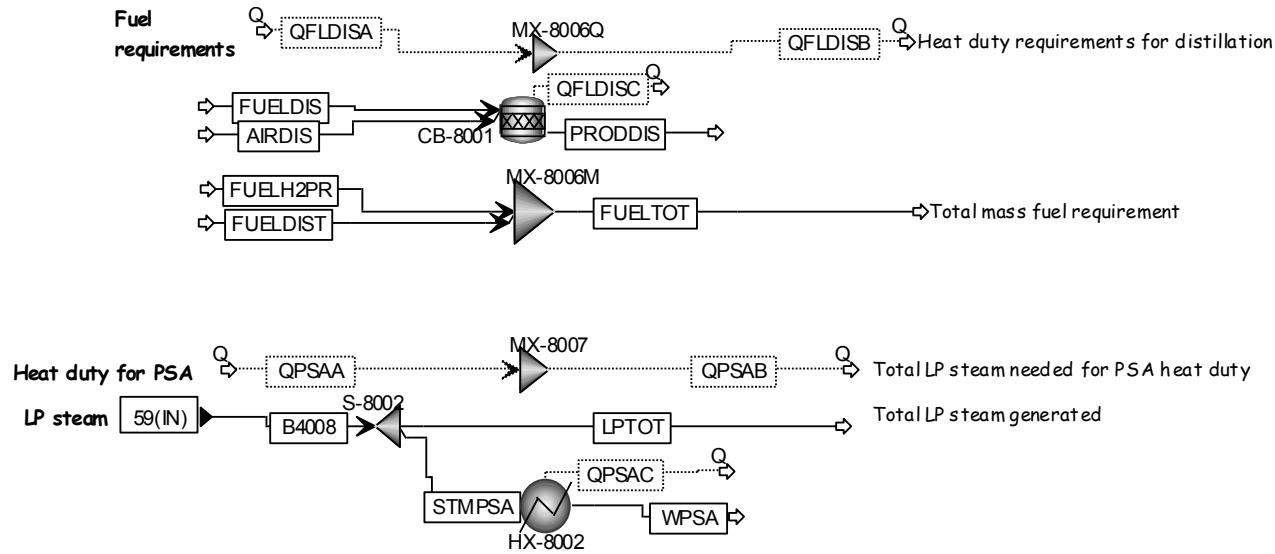
Figure 66 Fuel requirements and LP steam requirement balances in Unit A8000 - Utilities

Table 115 Mass Balances for Unit A8000 – Utilities Part 1

	AIRDIS	B4008	BLOWDOWN	CHW	CHWLOSS	CHWTOT	CHWUTIL	COOLEDCW	CWA5001O	CWB2005O	CWB3005O
Total Flow tons/h	6.487	330.559	3.528	191.187	11.509	191.187	179.678	114.564	16.320	8.370	37.363
Temperature C	25.000	120.272	27.000	12.000	7.000	7.000	7.000	27.000	31.127	45.000	45.000
Pressure bar	1.013	2.000	0.036	1.034	1.034	1.034	1.034	0.036	1.034	1.030	1.030
Vapor Frac	1.000	0.970	0.000	0.000	0.000	0.000	0.000	0.000	0.000	0.000	0.000
Enthalpy GJ/hr	-0.548	-3991.600	-50.734	-2759.000	-166.290	-2762.300	-2596.000	-1647.300	-234.420	-119.820	-534.850
MIXED											
Mass Flow tons/h											
N2	4.867	0.000	0.000	0.000	0.000	0.000	0.000	0.000	0.000	0.000	0.000
O2	1.491	0.000	0.000	0.000	0.000	0.000	0.000	0.000	0.000	0.000	0.000
CO2	0.003	0.000	0.000	0.000	0.000	0.000	0.000	0.000	0.000	0.000	0.000

253

H2O	0.043	330.559	3.528	191.187	11.509	191.187	179.678	114.564	16.320	8.370	37.363
CH4	0.000	0.000	0.000	0.000	0.000	0.000	0.000	0.000	0.000	0.000	0.000
AR	0.082	0.000	0.000	0.000	0.000	0.000	0.000	0.000	0.000	0.000	0.000

Table 116 Mass Balances for Unit A8000 – Utilities Part 2

	CWB3006O	CWCIRC	CWDIST	CWUTIL	DH2ODIST	DH2OTOT	DRIFLOSS	EVAPLOSS	FUELDIS	FUELDIST
Total Flow tons/h	27.162	117.564	21.469	110.683	1.355	1.355	0.353	3.001	0.272	0.272
Temperature C	44.691	43.695	49.000	27.000	49.000	49.000	27.000	27.000	25.000	25.000
Pressure bar	1.030	1.030	1.030	0.036	1.030	1.030	0.036	0.036	1.013	1.013
Vapor Frac	0.000	0.000	0.000	0.000	0.000	0.000	0.000	1.000	1.000	1.000
Enthalpy GJ/hr	-388.840	-1683.500	-307.020	-1591.500	-19.378	-19.378	-5.074	-36.528	-1.147	-1.147
MIXED										
Mass Flow tons/h										
N2	0.000	0.000	0.000	0.000	0.000	0.000	0.000	0.000	0.000	0.000
O2	0.000	0.000	0.000	0.000	0.000	0.000	0.000	0.000	0.000	0.000
CO2	0.000	0.000	0.000	0.000	0.000	0.000	0.000	0.000	0.000	0.000
H2O	27.162	117.564	21.469	110.683	1.355	1.355	0.353	3.001	0.000	0.000
CH4	0.000	0.000	0.000	0.000	0.000	0.000	0.000	0.000	0.272	0.272
AR	0.000	0.000	0.000	0.000	0.000	0.000	0.000	0.000	0.000	0.000

Table 117 Mass Balances for Unit A8000 – Utilities Part 3

	FUELH2PR	FUELTOT	HOTCW	LPTOT	MAKEUPCW	PRODDIS	PRSTMTOT	STMDIST	STMDIST2	STMPSA	WPSA
Total Flow tons/h	2.372	2.644	110.684	330.385	6.880	6.759	5.821	5.821	5.821	0.174	0.174
Temperature C	25.000	25.000	43.682	120.272	43.900	406.000	262.721	399.692	263.000	120.272	115.000
Pressure bar	1.013	1.013	1.030	2.000	1.030	1.013	49.000	49.000	49.000	2.000	2.000
Vapor Frac	1.000	1.000	0.000	0.970	0.000	1.000	1.000	1.000	1.000	0.970	0.000
Enthalpy GJ/hr	-9.994	-11.141	-1584.900	-3989.500	-98.516	-11.416	-68.483	-67.022	-68.480	-2.107	-2.450

254

MIXED											
Mass Flow tons/h											
N2	0.000	0.000	0.000	0.000	0.000	4.867	0.000	0.000	0.000	0.000	0.000
O2	0.000	0.000	0.000	0.000	0.000	0.406	0.000	0.000	0.000	0.000	0.000
CO2	0.000	0.000	0.000	0.000	0.000	0.750	0.000	0.000	0.000	0.000	0.000
H2O	0.000	0.000	110.684	330.385	6.880	0.654	5.821	5.821	5.821	0.174	0.174
CH4	2.372	2.644	0.000	0.000	0.000	0.000	0.000	0.000	0.000	0.000	0.000
AR	0.000	0.000	0.000	0.000	0.000	0.082	0.000	0.000	0.000	0.000	0.000

Table 118 Work streams for Unit A8000 – Utilities Part 1

STREAM	WCPA3001	WPA5001	WCPA6001	WCPA4001	WTB4002	WTB4003	WTB4001	WPA7001	WPA7002	WPA7003	WPA7004	WPA7005
POWER MW	0.149	0.002	5.793	0.120	-28.709	-21.858	-19.853	0.332	0.436	0.127	0.264	0.247

Table 119 Work streams for Unit A8000 – Utilities Part 2

STREAM	WPA7006	WPB1001	WCPB3001	WCPB3002	WCPB3003	WCPB3004	WESP	WGRIND	WDISTIL	WCW	WCHW	WEXCESS
POWER MW	0.101	0.173	0.082	0.001	9.137	1.587	0.041	4.962	0.134	0.015	0.302	-46.415

Table 120 Duty/ heat Streams for Unit A8000

	A8000. QCHW	A8000. QEVAP	A8000. QFLDISA	A8000. QFLDISB	A8000. QFLDISC	A8000. QSTMDISA	A8000. QSTMDISB	A8000. QSTMDISC
QCALC MJ/hr	3260.91	374.79	9721.25	9721.25	9721.25	1458.19	1458.19	1458.19
TBEGIN C	12.00	43.69			25.00			399.69
TEND C	7.00	27.00			406.00			263.00

E.12 Unit B1000 – Hydrotreating 1
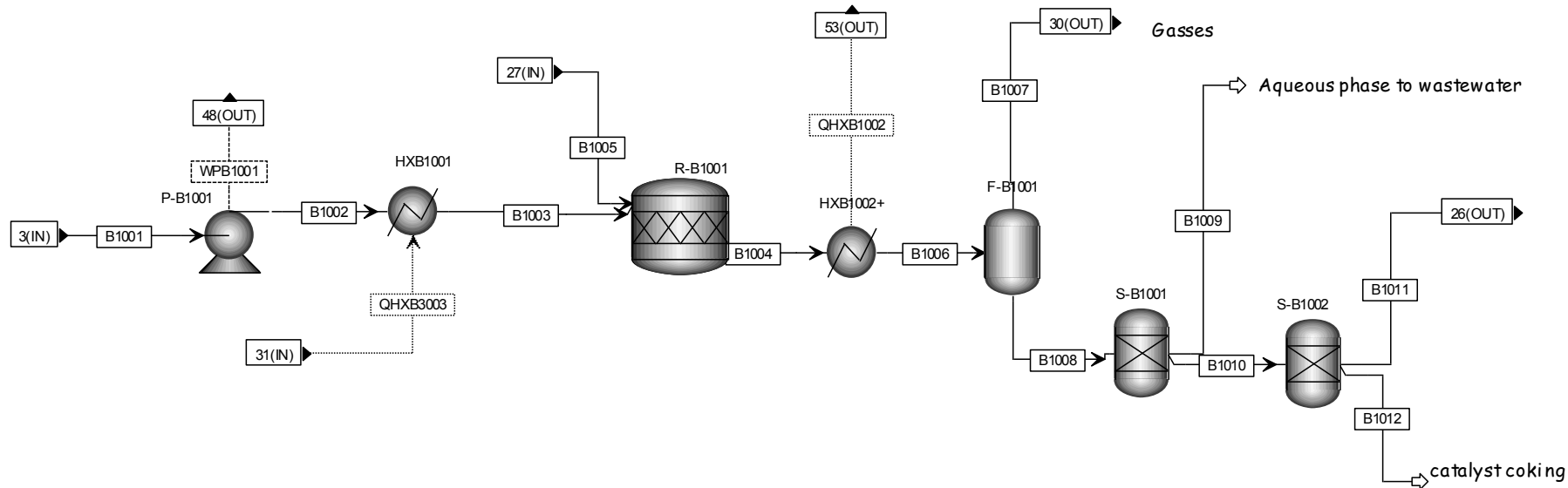
Figure 67 Process Flow Diagram for Unit B1000 – Hydroptreating Stage 1

Table 121 Mass balances for Unit B1000 – Hydroptreating Stage 1

	B1001	B1002	B1003	B1004	B1005	B1006	B1007	B1008	B1009	B1010	B1011	B1012
Mass Flow tons/h	55.755	55.755	55.755	64.010	8.255	64.010	9.136	54.874	28.914	25.960	25.070	0.890
Temperature C	25.000	31.100	339.700	339.700	289.900	57.000	56.900	56.900	58.900	58.900	58.900	58.900
Pressure bar	2.758	138.908	138.908	138.908	138.908	138.288	104.000	104.000	104.000	104.000	104.000	104.000
Vapor Frac	0.000	0.000	0.000	0.976	1.000	0.742	1.000	0.000	0.000	0.005	0.005	0.000
Enthalpy GJ/hr	-360.539	-359.916	-309.085	-280.378	28.706	-379.564	-9.071	-370.493	-317.737	-52.798	-50.367	-2.431
MIXED												
Mass Flow tons/h												
H2	0.000	0.000	0.000	7.382	8.255	7.382	7.377	0.005	0.000	0.005	0.005	0.000
CO2	0.000	0.000	0.000	1.348	0.000	1.348	1.243	0.106	0.000	0.106	0.106	0.000

H2O	13.076	13.076	13.076	17.570	0.000	17.570	0.021	17.549	16.846	0.703	0.703	0.000
CH4	0.000	0.000	0.000	0.171	0.000	0.171	0.168	0.003	0.000	0.003	0.003	0.000
ACETACID	0.993	0.993	0.993	0.992	0.000	0.992	0.010	0.983	0.000	0.983	0.983	0.000
PHENOL	0.162	0.162	0.162	0.117	0.000	0.117	0.000	0.117	0.000	0.117	0.117	0.000
TOLUENE	0.000	0.000	0.000	0.015	0.000	0.015	0.001	0.014	0.000	0.014	0.014	0.000
FURFURAL	0.021	0.021	0.021	0.016	0.000	0.016	0.000	0.016	0.000	0.016	0.016	0.000
TETRA-01	0.000	0.000	0.000	0.004	0.000	0.004	0.000	0.004	0.000	0.004	0.004	0.000
N-HEP-01	0.242	0.242	0.242	0.242	0.000	0.242	0.000	0.242	0.000	0.242	0.242	0.000
2:4-X-01	0.319	0.319	0.319	0.214	0.000	0.214	0.000	0.214	0.000	0.214	0.214	0.000
O-ETH-01	0.089	0.089	0.089	0.065	0.000	0.065	0.000	0.065	0.000	0.065	0.065	0.000
INDAN-01	1.899	1.899	1.899	1.477	0.000	1.477	0.003	1.474	0.000	1.474	1.474	0.000
2:6-D-01	0.102	0.102	0.102	0.102	0.000	0.102	0.000	0.102	0.000	0.102	0.102	0.000
NAPHT-01	0.926	0.926	0.926	0.698	0.000	0.698	0.000	0.698	0.000	0.698	0.698	0.000
DIBEN-01	0.168	0.168	0.168	0.168	0.000	0.168	0.000	0.168	0.000	0.168	0.168	0.000
FLUOR-01	1.917	1.917	1.917	1.565	0.000	1.565	0.000	1.565	0.000	1.565	1.565	0.000
2:4-D-01	0.179	0.179	0.179	0.179	0.000	0.179	0.000	0.179	0.000	0.179	0.179	0.000
NAPHT-02	1.245	1.245	1.245	0.958	0.000	0.958	0.000	0.958	0.000	0.958	0.958	0.000
ETHYL-01	0.000	0.000	0.000	0.046	0.000	0.046	0.001	0.045	0.000	0.045	0.045	0.000
CYCLO-01	0.000	0.000	0.000	0.092	0.000	0.092	0.010	0.082	0.000	0.082	0.082	0.000
M-XYL-01	0.000	0.000	0.000	0.091	0.000	0.091	0.001	0.091	0.000	0.091	0.091	0.000
1:3-C-01	0.000	0.000	0.000	0.724	0.000	0.724	0.030	0.693	0.000	0.693	0.693	0.000
3-MET-01	0.000	0.000	0.000	2.390	0.000	2.390	0.027	2.363	0.000	2.363	2.363	0.000
N-PRO-02	0.000	0.000	0.000	0.032	0.000	0.032	0.000	0.031	0.000	0.031	0.031	0.000
1:2:3-01	0.000	0.000	0.000	0.038	0.000	0.038	0.000	0.038	0.000	0.038	0.038	0.000
CIS-D-01	0.000	0.000	0.000	0.205	0.000	0.205	0.000	0.205	0.000	0.205	0.205	0.000
1:2-D-01	0.000	0.000	0.000	0.331	0.000	0.331	0.000	0.331	0.000	0.331	0.331	0.000
CYCLO-02	0.000	0.000	0.000	0.036	0.000	0.036	0.000	0.036	0.000	0.036	0.036	0.000
N-TET-01	0.000	0.000	0.000	0.007	0.000	0.007	0.000	0.007	0.000	0.007	0.007	0.000
DINON-01	0.000	0.000	0.000	0.056	0.000	0.056	0.000	0.056	0.000	0.056	0.056	0.000
N-TET-02	0.000	0.000	0.000	0.183	0.000	0.183	0.000	0.183	0.000	0.183	0.183	0.000

GLYCO-01	8.427	8.427	8.427	0.000	0.000	0.000	0.000	0.000	0.000	0.000	0.000	0.000
FUMAR-01	0.764	0.764	0.764	0.764	0.000	0.764	0.000	0.764	0.051	0.713	0.713	0.000
1:2-B-01	0.011	0.011	0.011	0.011	0.000	0.011	0.000	0.011	0.002	0.009	0.009	0.000
ETHAN-01	0.000	0.000	0.000	5.105	0.000	5.105	0.214	4.891	4.891	0.000	0.000	0.000
2,2PROPA	6.458	6.458	6.458	6.458	0.000	6.458	0.000	6.458	6.458	0.000	0.000	0.000
FURACETA	2.257	2.257	2.257	2.257	0.000	2.257	0.000	2.257	0.664	1.593	1.593	0.000
LEVOGLUC	0.050	0.050	0.050	0.000	0.000	0.000	0.000	0.000	0.000	0.000	0.000	0.000
4METGUA	0.091	0.091	0.091	0.000	0.000	0.000	0.000	0.000	0.000	0.000	0.000	0.000
ETHYLANI	0.749	0.749	0.749	0.001	0.000	0.001	0.000	0.001	0.000	0.001	0.000	0.001
BENZOATE	0.105	0.105	0.105	0.087	0.000	0.087	0.000	0.087	0.000	0.087	0.087	0.000
METHPHEN	0.032	0.032	0.032	0.025	0.000	0.025	0.000	0.025	0.000	0.025	0.025	0.000
ETHYLGUA	0.160	0.160	0.160	0.125	0.000	0.125	0.000	0.125	0.000	0.125	0.125	0.000
MESHEPTA	0.665	0.665	0.665	0.665	0.000	0.665	0.001	0.665	0.000	0.665	0.665	0.000
BENZOFUR	1.708	1.708	1.708	1.646	0.000	1.646	0.001	1.645	0.000	1.645	1.645	0.000
TRIMEBEN	0.331	0.331	0.331	0.315	0.000	0.315	0.000	0.315	0.000	0.315	0.315	0.000
4PROPGUA	0.824	0.824	0.824	0.824	0.000	0.824	0.000	0.824	0.000	0.824	0.824	0.000
HMBENZAC	2.584	2.584	2.584	1.065	0.000	1.065	0.000	1.065	0.000	1.065	1.065	0.000
METOCTAC	3.310	3.310	3.310	0.000	0.000	0.000	0.000	0.000	0.000	0.000	0.000	0.000
CONIFALC	0.155	0.155	0.155	0.109	0.000	0.109	0.000	0.109	0.000	0.109	0.109	0.000
ISOEUGEN	0.472	0.472	0.472	0.428	0.000	0.428	0.000	0.428	0.000	0.428	0.428	0.000
PHENKETO	0.415	0.415	0.415	0.000	0.000	0.000	0.000	0.000	0.000	0.000	0.000	0.000
XANTHENE	0.480	0.480	0.480	0.439	0.000	0.439	0.000	0.439	0.000	0.439	0.439	0.000
P-DECANO	0.561	0.561	0.561	0.552	0.000	0.552	0.000	0.552	0.000	0.552	0.552	0.000
DNONDBEN	0.189	0.189	0.189	0.130	0.000	0.130	0.000	0.130	0.000	0.130	0.130	0.000
PENTACOS	0.221	0.221	0.221	0.000	0.000	0.000	0.000	0.000	0.000	0.000	0.000	0.000
ETMEPHEN	0.000	0.000	0.000	0.035	0.000	0.035	0.000	0.035	0.000	0.035	0.035	0.000
1HINDANE	0.000	0.000	0.000	0.444	0.000	0.444	0.001	0.443	0.000	0.443	0.443	0.000
HYDFLUOR	0.000	0.000	0.000	0.380	0.000	0.380	0.000	0.380	0.000	0.380	0.380	0.000
HYDNAPH	0.000	0.000	0.000	0.309	0.000	0.309	0.000	0.309	0.000	0.309	0.309	0.000
C18H28	3.056	3.056	3.056	3.056	0.000	3.056	0.000	3.056	0.000	3.056	3.056	0.000

C21H24O4	0.107	0.107	0.107	0.107	0.000	0.107	0.000	0.107	0.000	0.107	0.107	0.000
C22H20O	0.234	0.234	0.234	0.234	0.000	0.234	0.000	0.234	0.000	0.234	0.234	0.000
METHA-01	0.000	0.000	0.000	0.002	0.000	0.002	0.000	0.002	0.002	0.000	0.000	0.000
ETHAN-02	0.000	0.000	0.000	0.032	0.000	0.032	0.028	0.004	0.000	0.004	0.004	0.000
COKE1	0.000	0.000	0.000	0.889	0.000	0.889	0.000	0.889	0.000	0.889	0.000	0.889

Table 122 Duty/ heat Streams for Unit B1000 to B2000

	B1000. QHXB1002	B1000. QHXB3003	B2000. QHXB2002	B2000. QHXB2003	B2000. QHXB2004	B2000. QHXB2005
QCALC MJ/hr	99252.26	50867.82	3581.98	2072.08	39129.80	537.42
TBEGIN C	339.73	369.70	399.38	369.70	352.83	55.00
TEND C	57.00	156.99	369.70	352.83	55.00	50.00

259

E.13 Unit B2000 – Hydrotreating 2
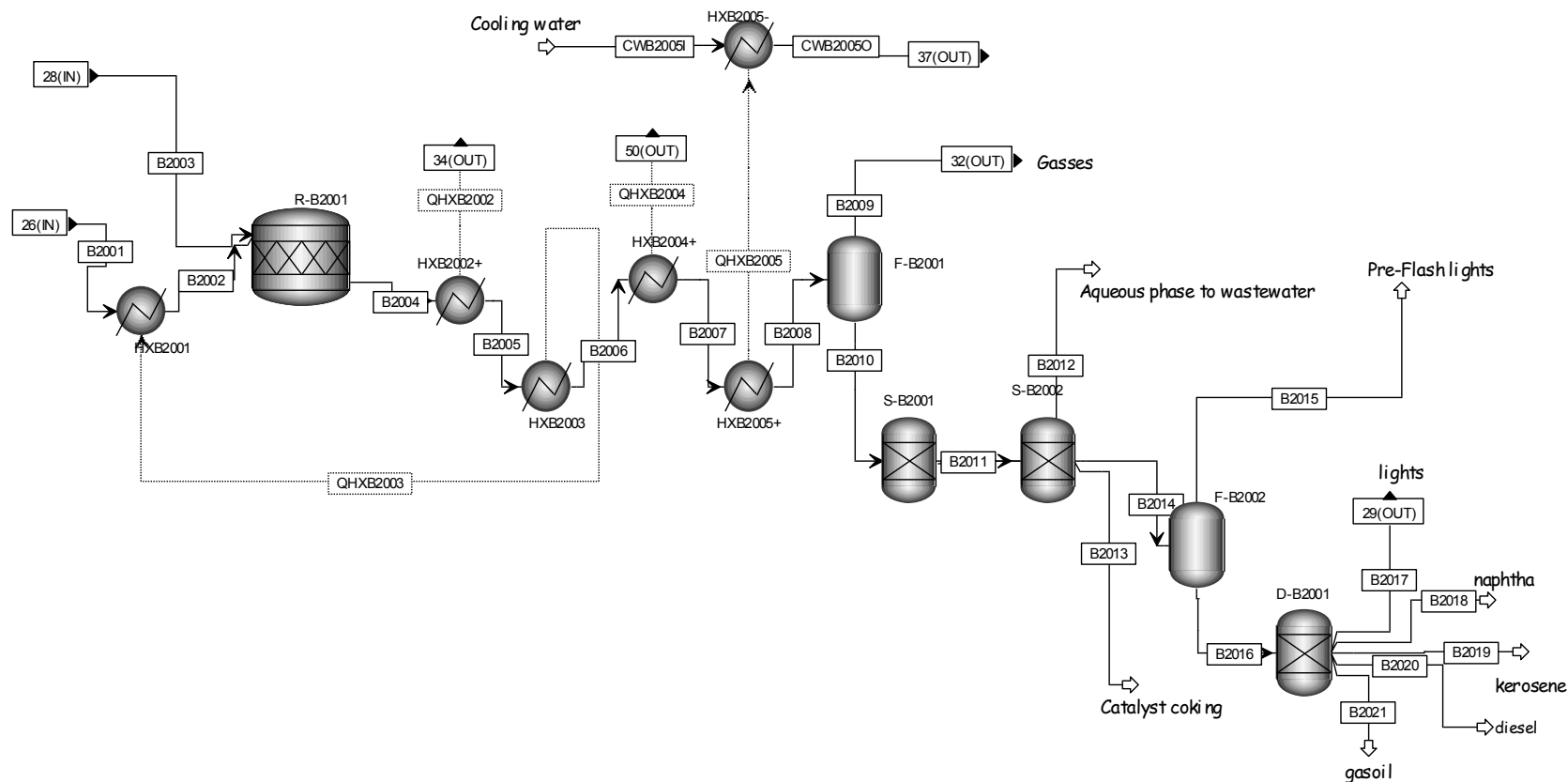
Figure 68 Process Flow Diagram for Unit B2000 – Hydroptreating Stage 2

Table 123 Mass Balances for Unit B2000 – Hydroptreating Stage 2, Part 1

	B2001	B2002	B2003	B2004	B2005	B2006	B2007	B2008	B2009	B2010	B2011
Mass Flow tons/h	25.070	25.070	4.644	29.714	29.714	29.714	29.714	29.714	5.756	23.959	18.808
Temperature C	58.900	109.600	237.400	399.400	369.700	352.800	55.000	50.000	50.500	50.500	50.400
Pressure bar	104.000	104.000	104.435	104.435	103.815	103.815	103.815	103.815	100.000	100.000	100.000

Vapor Frac	0.005	0.006	1.000	0.991	0.988	0.987	0.877	0.877	1.000	0.000	0.004
Enthalpy GJ/hr	-50.367	-48.296	12.937	-35.363	-38.940	-41.012	-80.115	-80.651	-7.607	-73.044	-25.937
MIXED											
Mass Flow tons/h											
H2	0.005	0.005	4.644	3.845	3.845	3.845	3.845	3.845	3.843	0.003	0.003
CO	0.000	0.000	0.000	0.052	0.052	0.052	0.052	0.052	0.052	0.000	0.000
CO2	0.106	0.106	0.000	0.705	0.705	0.705	0.705	0.705	0.646	0.059	0.059
H2O	0.703	0.703	0.000	2.037	2.037	2.037	2.037	2.037	0.010	2.027	0.000
CH4	0.003	0.003	0.000	0.429	0.429	0.429	0.429	0.429	0.421	0.009	0.009
ACETACID	0.983	0.983	0.000	0.000	0.000	0.000	0.000	0.000	0.000	0.000	0.000
PHENOL	0.117	0.117	0.000	0.078	0.078	0.078	0.078	0.078	0.000	0.078	0.078
TOLUENE	0.014	0.014	0.000	0.078	0.078	0.078	0.078	0.078	0.002	0.076	0.076
FURFURAL	0.016	0.016	0.000	0.000	0.000	0.000	0.000	0.000	0.000	0.000	0.000
TETRA-01	0.004	0.004	0.000	0.015	0.015	0.015	0.015	0.015	0.001	0.014	0.014
N-HEP-01	0.242	0.242	0.000	0.000	0.000	0.000	0.000	0.000	0.000	0.000	0.000
2:4-X-01	0.214	0.214	0.000	0.000	0.000	0.000	0.000	0.000	0.000	0.000	0.000
O-ETH-01	0.065	0.065	0.000	0.000	0.000	0.000	0.000	0.000	0.000	0.000	0.000
INDAN-01	1.474	1.474	0.000	0.097	0.097	0.097	0.097	0.097	0.000	0.097	0.097
2:6-D-01	0.102	0.102	0.000	0.000	0.000	0.000	0.000	0.000	0.000	0.000	0.000
NAPHT-01	0.698	0.698	0.000	0.000	0.000	0.000	0.000	0.000	0.000	0.000	0.000
DIBEN-01	0.168	0.168	0.000	0.168	0.168	0.168	0.168	0.168	0.000	0.168	0.168
FLUOR-01	1.565	1.565	0.000	0.210	0.210	0.210	0.210	0.210	0.000	0.210	0.210
2:4-D-01	0.179	0.179	0.000	0.179	0.179	0.179	0.179	0.179	0.000	0.179	0.179
NAPHT-02	0.958	0.958	0.000	0.000	0.000	0.000	0.000	0.000	0.000	0.000	0.000
ETHYL-01	0.045	0.045	0.000	0.189	0.189	0.189	0.189	0.189	0.001	0.187	0.187
N-HEX-01	0.000	0.000	0.000	0.557	0.557	0.557	0.557	0.557	0.049	0.509	0.509
CYCLO-01	0.082	0.082	0.000	1.447	1.447	1.447	1.447	1.447	0.086	1.361	1.361
M-XYL-01	0.091	0.091	0.000	0.277	0.277	0.277	0.277	0.277	0.002	0.275	0.275
METHY-01	0.000	0.000	0.000	0.470	0.470	0.470	0.470	0.470	0.015	0.456	0.456

1:3-C-01	0.693	0.693	0.000	1.201	1.201	1.201	1.201	1.201	0.042	1.159	1.159
3-MET-01	2.363	2.363	0.000	2.363	2.363	2.363	2.363	2.363	0.021	2.342	2.342
P-CRE-01	0.000	0.000	0.000	0.068	0.068	0.068	0.068	0.068	0.000	0.068	0.068
N-PRO-02	0.031	0.031	0.000	0.345	0.345	0.345	0.345	0.345	0.001	0.344	0.344
1:2:3-01	0.038	0.038	0.000	0.151	0.151	0.151	0.151	0.151	0.000	0.151	0.151
CIS-D-01	0.205	0.205	0.000	0.840	0.840	0.840	0.840	0.840	0.000	0.839	0.839
1:2-D-01	0.331	0.331	0.000	0.331	0.331	0.331	0.331	0.331	0.000	0.331	0.331
CYCLO-02	0.036	0.036	0.000	0.422	0.422	0.422	0.422	0.422	0.000	0.422	0.422
N-TET-01	0.007	0.007	0.000	0.434	0.434	0.434	0.434	0.434	0.000	0.434	0.434
DINON-01	0.056	0.056	0.000	0.181	0.181	0.181	0.181	0.181	0.000	0.181	0.181
N-TET-02	0.183	0.183	0.000	0.183	0.183	0.183	0.183	0.183	0.000	0.183	0.183
FUMAR-01	0.713	0.713	0.000	0.713	0.713	0.713	0.713	0.713	0.000	0.713	0.000
1:2-B-01	0.009	0.009	0.000	0.009	0.009	0.009	0.009	0.009	0.000	0.009	1:2-0.000
ETHAN-01	0.000	0.000	0.000	0.754	0.754	0.754	0.754	0.754	0.032	0.722	0.000
FURACETA	1.593	1.593	0.000	1.593	1.593	1.593	1.593	1.593	0.000	1.593	0.000
BENZOATE	0.087	0.087	0.000	0.000	0.000	0.000	0.000	0.000	0.000	0.000	0.000
METHPHEN	0.025	0.025	0.000	0.000	0.000	0.000	0.000	0.000	0.000	0.000	0.000
ETHYLGUA	0.125	0.125	0.000	0.000	0.000	0.000	0.000	0.000	0.000	0.000	0.000
MESHEPTA	0.665	0.665	0.000	0.000	0.000	0.000	0.000	0.000	0.000	0.000	0.000
BENZOFUR	1.645	1.645	0.000	0.000	0.000	0.000	0.000	0.000	0.000	0.000	0.000
TRIMEBEN	0.315	0.315	0.000	0.000	0.000	0.000	0.000	0.000	0.000	0.000	0.000
4PROPGUA	0.824	0.824	0.000	0.000	0.000	0.000	0.000	0.000	0.000	0.000	4P0.000
HMBENZAC	1.065	1.065	0.000	0.000	0.000	0.000	0.000	0.000	0.000	0.000	0.000
CONIFALC	0.109	0.109	0.000	0.000	0.000	0.000	0.000	0.000	0.000	0.000	0.000
ISOEUGEN	0.428	0.428	0.000	0.000	0.000	0.000	0.000	0.000	0.000	0.000	0.000
XANTHENE	0.439	0.439	0.000	0.000	0.000	0.000	0.000	0.000	0.000	0.000	0.000
P-DECANO	0.552	0.552	0.000	0.000	0.000	0.000	0.000	0.000	0.000	0.000	0.000
DNONDBEN	0.130	0.130	0.000	0.000	0.000	0.000	0.000	0.000	0.000	0.000	0.000
ETMEPHEN	0.035	0.035	0.000	0.117	0.117	0.117	0.117	0.117	0.000	0.117	0.117
1HINDANE	0.443	0.443	0.000	1.890	1.890	1.890	1.890	1.890	0.004	1.886	1.886

HYDFLUOR	0.380	0.380	0.000	1.843	1.843	1.843	1.843	1.843	0.000	1.843	1.843
HYDNAPH	0.309	0.309	0.000	1.344	1.344	1.344	1.344	1.344	0.000	1.344	1.344
C18H28	3.056	3.056	0.000	0.006	0.006	0.006	0.006	0.006	0.000	0.006	0.006
C21H24O4	0.107	0.107	0.000	0.000	0.000	0.000	0.000	0.000	0.000	0.000	0.000
C22H20O	0.234	0.234	0.000	0.000	0.000	0.000	0.000	0.000	0.000	0.000	0.000
METHA-01	0.000	0.000	0.000	0.005	0.005	0.005	0.005	0.005	0.001	0.005	0.002
ETHAN-02	0.004	0.004	0.000	0.423	0.423	0.423	0.423	0.423	0.368	0.054	0.027
PROPA-01	0.000	0.000	0.000	0.219	0.219	0.219	0.219	0.219	0.138	0.081	0.040
ISOBU-01	0.000	0.000	0.000	0.054	0.054	0.054	0.054	0.054	0.022	0.032	0.016
COKE2	0.000	0.000	0.000	3.390	3.390	3.390	3.390	3.390	0.000	3.390	3.390

Table 124 Mass Balances for Unit B2000 – Hydroptreating Stage 2, Part 2

	B2012	B2013	B2014	B2015	B2016	B2017	B2018	B2019	B2020	B2021	CWB2005I	CWB2005O
Mass Flow tons/h	5.151	3.397	15.411	0.055	15.357	2.131	4.525	3.406	3.198	2.096	8.370	8.370
Temperature C	50.400	50.400	50.400	50.300	50.300	50.300	50.300	50.300	50.300	50.300	27.000	45.000
Pressure bar	100.000	100.000	100.000	3.771	3.771	3.771	3.771	3.771	3.771	3.771	1.030	1.030
Vapor Frac	0.000	0.000	0.004	1.000	0.000	0.043	0.000	0.000	0.000	0.000	0.000	0.000
Enthalpy GJ/hr	-47.137	-9.648	-16.288	-0.251	-16.037	-3.782	-4.489	-3.824	-2.364	-1.569	-120.273	-119.738
MIXED												
Mass Flow tons/h												
H2	0.000	0.000	0.003	0.003	0.000	0.000	0.000	0.000	0.000	0.000	0.000	0.000
CO	0.000	0.000	0.000	0.000	0.000	0.000	0.000	0.000	0.000	0.000	0.000	0.000
CO2	0.000	0.000	0.059	0.023	0.036	0.036	0.000	0.000	0.000	0.000	0.000	0.000
H2O	2.027	0.000	0.000	0.000	0.000	0.000	0.000	0.000	0.000	0.000	8.370	8.370
CH4	0.000	0.000	0.009	0.006	0.002	0.002	0.000	0.000	0.000	0.000	0.000	0.000
ACETACID	0.000	0.000	0.000	0.000	0.000	0.000	0.000	0.000	0.000	0.000	0.000	0.000
PHENOL	0.000	0.000	0.078	0.000	0.078	0.013	0.064	0.000	0.000	0.000	0.000	0.000
TOLUENE	0.000	0.000	0.076	0.000	0.076	0.076	0.000	0.000	0.000	0.000	0.000	0.000
FURFURAL	0.000	0.000	0.000	0.000	0.000	0.000	0.000	0.000	0.000	0.000	0.000	0.000

263

TETRA-01	0.000	0.000	0.014	0.000	0.014	0.014	0.000	0.000	0.000	0.000	0.000	0.000
N-HEP-01	0.000	0.000	0.000	0.000	0.000	0.000	0.000	0.000	0.000	0.000	0.000	0.000
2:4-X-01	0.000	0.000	0.000	0.000	0.000	0.000	0.000	0.000	0.000	0.000	0.000	0.000
O-ETH-01	0.000	0.000	0.000	0.000	0.000	0.000	0.000	0.000	0.000	0.000	0.000	0.000
INDAN-01	0.000	0.000	0.097	0.000	0.097	0.000	0.097	0.000	0.000	0.000	0.000	0.000
2:6-D-01	0.000	0.000	0.000	0.000	0.000	0.000	0.000	0.000	0.000	0.000	0.000	0.000
NAPHT-01	0.000	0.000	0.000	0.000	0.000	0.000	0.000	0.000	0.000	0.000	0.000	0.000
DIBEN-01	0.000	0.000	0.168	0.000	0.168	0.000	0.000	0.000	0.168	0.000	0.000	0.000
FLUOR-01	0.000	0.000	0.210	0.000	0.210	0.000	0.000	0.000	0.000	0.210	0.000	0.000
2:4-D-01	0.000	0.000	0.179	0.000	0.179	0.000	0.000	0.000	0.000	0.179	0.000	0.000
NAPHT-02	0.000	0.000	0.000	0.000	0.000	0.000	0.000	0.000	0.000	0.000	0.000	0.000
ETHYL-01	0.000	0.000	0.187	0.000	0.187	0.050	0.137	0.000	0.000	0.000	0.000	0.000
N-HEX-01	0.000	0.000	0.509	0.002	0.507	0.507	0.000	0.000	0.000	0.000	0.000	0.000
CYCLO-01	0.000	0.000	1.361	0.003	1.358	1.358	0.000	0.000	0.000	0.000	0.000	0.000
M-XYL-01	0.000	0.000	0.275	0.000	0.275	0.000	0.275	0.000	0.000	0.000	0.000	0.000
METHY-01	0.000	0.000	0.456	0.001	0.455	0.000	0.455	0.000	0.000	0.000	0.000	0.000
1:3-C-01	0.000	0.000	1.159	0.003	1.156	0.000	1.156	0.000	0.000	0.000	0.000	0.000
3-MET-01	0.000	0.000	2.342	0.001	2.341	0.000	2.341	0.000	0.000	0.000	0.000	0.000
P-CRE-01	0.000	0.000	0.068	0.000	0.068	0.000	0.000	0.068	0.000	0.000	0.000	0.000
N-PRO-02	0.000	0.000	0.344	0.000	0.344	0.000	0.000	0.344	0.000	0.000	0.000	0.000
1:2:3-01	0.000	0.000	0.151	0.000	0.151	0.000	0.000	0.151	0.000	0.000	0.000	0.000
CIS-D-01	0.000	0.000	0.839	0.000	0.839	0.000	0.000	0.839	0.000	0.000	0.000	0.000
1:2-D-01	0.000	0.000	0.331	0.000	0.331	0.000	0.000	0.000	0.331	0.000	0.000	0.000
CYCLO-02	0.000	0.000	0.422	0.000	0.422	0.000	0.000	0.000	0.422	0.000	0.000	0.000
N-TET-01	0.000	0.000	0.434	0.000	0.434	0.000	0.000	0.000	0.434	0.000	0.000	0.000
DINON-01	0.000	0.000	0.181	0.000	0.181	0.000	0.000	0.000	0.000	0.181	0.000	0.000
N-TET-02	0.000	0.000	0.183	0.000	0.183	0.000	0.000	0.000	0.000	0.183	0.000	0.000
FUMAR-01	0.713	0.000	0.000	0.000	0.000	0.000	0.000	0.000	0.000	0.000	0.000	0.000
1:2-B-01	0.009	0.000	0.000	0.000	0.000	0.000	0.000	0.000	0.000	0.000	0.000	0.000
ETHAN-01	0.722	0.000	0.000	0.000	0.000	0.000	0.000	0.000	0.000	0.000	0.000	0.000

FURACETA	1.593	0.000	0.000	0.000	0.000	0.000	0.000	0.000	0.000	0.000	0.000	0.000
BENZOATE	0.000	0.000	0.000	0.000	0.000	0.000	0.000	0.000	0.000	0.000	0.000	0.000
METHPHEN	0.000	0.000	0.000	0.000	0.000	0.000	0.000	0.000	0.000	0.000	0.000	0.000
ETHYLGUA	0.000	0.000	0.000	0.000	0.000	0.000	0.000	0.000	0.000	0.000	0.000	0.000
MESHEPTA	0.000	0.000	0.000	0.000	0.000	0.000	0.000	0.000	0.000	0.000	0.000	0.000
BENZOFUR	0.000	0.000	0.000	0.000	0.000	0.000	0.000	0.000	0.000	0.000	0.000	0.000
TRIMEBEN	0.000	0.000	0.000	0.000	0.000	0.000	0.000	0.000	0.000	0.000	0.000	0.000
4PROPGUA	0.000	0.000	0.000	0.000	0.000	0.000	0.000	0.000	0.000	0.000	0.000	0.000
HMBENZAC	0.000	0.000	0.000	0.000	0.000	0.000	0.000	0.000	0.000	0.000	0.000	0.000
CONIFALC	0.000	0.000	0.000	0.000	0.000	0.000	0.000	0.000	0.000	0.000	0.000	0.000
ISOEUGEN	0.000	0.000	0.000	0.000	0.000	0.000	0.000	0.000	0.000	0.000	0.000	0.000
XANTHENE	0.000	0.000	0.000	0.000	0.000	0.000	0.000	0.000	0.000	0.000	0.000	0.000
P-DECANO	0.000	0.000	0.000	0.000	0.000	0.000	0.000	0.000	0.000	0.000	0.000	0.000
DNONDBEN	0.000	0.000	0.000	0.000	0.000	0.000	0.000	0.000	0.000	0.000	0.000	0.000
ETMEPHEN	0.000	0.000	0.117	0.000	0.117	0.000	0.000	0.117	0.000	0.000	0.000	0.000
1HINDANE	0.000	0.000	1.886	0.000	1.886	0.000	0.000	1.886	0.000	0.000	0.000	0.000
HYDFLUOR	0.000	0.000	1.843	0.000	1.843	0.000	0.000	0.000	1.843	0.000	0.000	0.000
HYDNAPH	0.000	0.000	1.344	0.000	1.344	0.000	0.000	0.000	0.000	1.344	0.000	0.000
C18H28	0.000	0.006	0.000	0.000	0.000	0.000	0.000	0.000	0.000	0.000	0.000	0.000
C21H24O4	0.000	0.000	0.000	0.000	0.000	0.000	0.000	0.000	0.000	0.000	0.000	0.000
C22H20O	0.000	0.000	0.000	0.000	0.000	0.000	0.000	0.000	0.000	0.000	0.000	0.000
METHA-01	0.002	0.000	0.002	0.000	0.002	0.002	0.000	0.000	0.000	0.000	0.000	0.000
ETHAN-02	0.027	0.000	0.027	0.008	0.019	0.019	0.000	0.000	0.000	0.000	0.000	0.000
PROPA-01	0.040	0.000	0.040	0.004	0.037	0.037	0.000	0.000	0.000	0.000	0.000	0.000
ISOBU-01	0.016	0.000	0.016	0.001	0.015	0.015	0.000	0.000	0.000	0.000	0.000	0.000
COKE2	0.000	3.390	0.000	0.000	0.000	0.000	0.000	0.000	0.000	0.000	0.000	0.000

E.14 Unit B3000 – H₂ Production
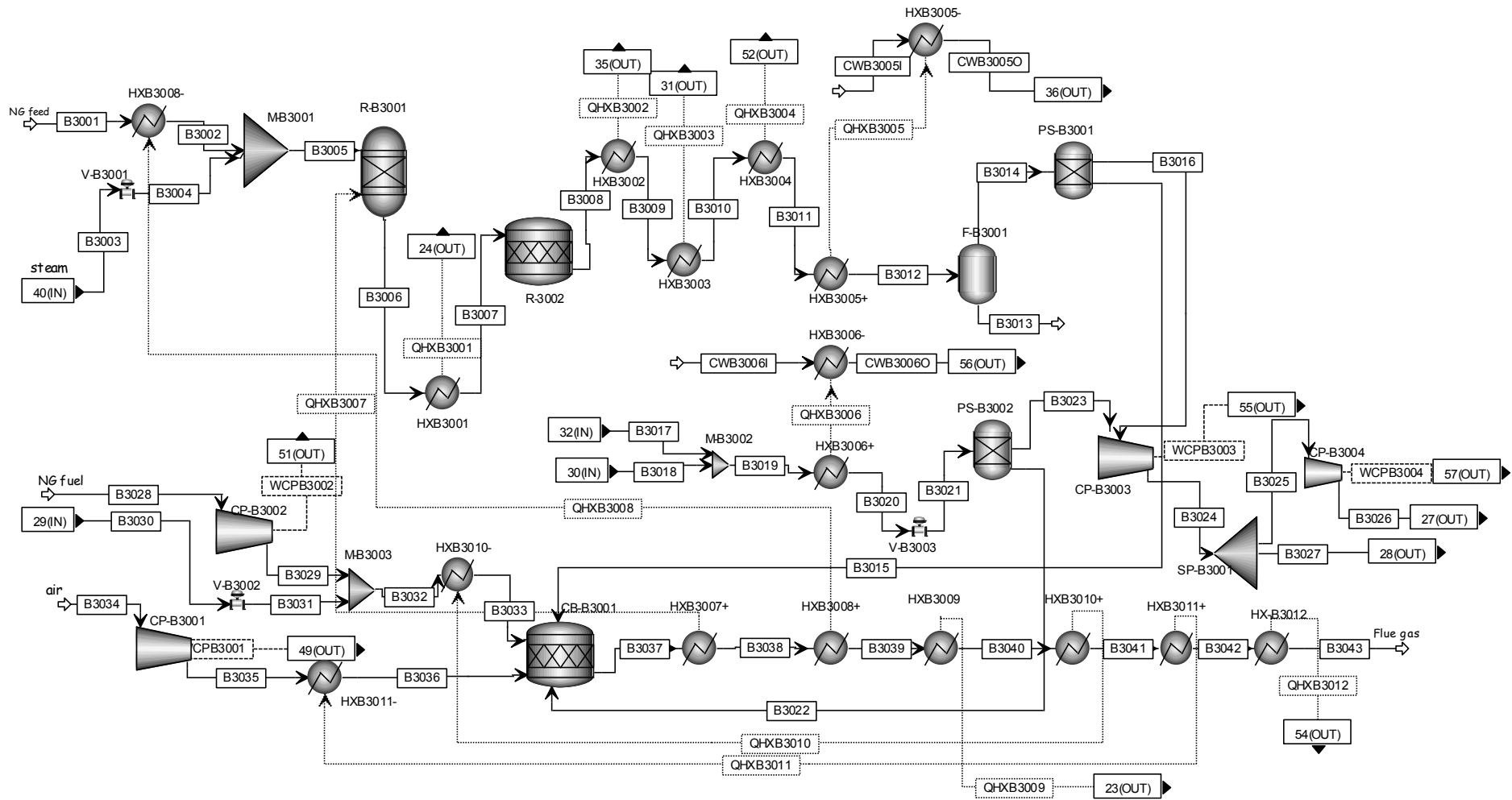
Figure 69 Process Flow Diagram for Unit B3000 – Hydrogen Production

Table 125 Mass Balances for Unit B3000 – Hydrogen Production, Part 1

	B3001	B3002	B3003	B3004	B3005	B3006	B3007	B3008	B3009	B3010
Mass Flow tons/h	9.170	9.170	45.787	45.787	54.958	54.958	54.958	54.958	54.958	54.958
Temperature C	25.000	371.000	399.700	399.700	392.500	857.000	350.000	390.200	369.700	157.000
Pressure bar	25.833	25.833	49.000	40.000	25.833	23.765	23.145	22.731	22.111	22.111
Vapor Frac	1.000	1.000	1.000	1.000	1.000	1.000	1.000	1.000	1.000	0.829
Enthalpy GJ/hr	-38.618	-30.556	-526.816	-526.816	-557.372	-403.999	-472.754	-472.754	-475.420	-526.255
MIXED										
Mass Flow tons/h										
N2	0.000	0.000	0.000	0.000	0.000	0.000	0.000	0.000	0.000	0.000
O2	0.000	0.000	0.000	0.000	0.000	0.000	0.000	0.000	0.000	0.000
H2	0.000	0.000	0.000	0.000	0.000	3.660	3.660	3.960	3.960	3.960
CO	0.000	0.000	0.000	0.000	0.000	5.559	5.559	1.390	1.390	1.390
CO2	0.000	0.000	0.000	0.000	0.000	13.656	13.656	20.206	20.206	20.206
H2O	0.000	0.000	45.787	45.787	45.787	31.033	31.033	28.352	28.352	28.352
CH4	9.170	9.170	0.000	0.000	9.170	1.050	1.050	1.050	1.050	1.050
AR	0.000	0.000	0.000	0.000	0.000	0.000	0.000	0.000	0.000	0.000
ACETACID	0.000	0.000	0.000	0.000	0.000	0.000	0.000	0.000	0.000	0.000
PHENOL	0.000	0.000	0.000	0.000	0.000	0.000	0.000	0.000	0.000	0.000
TOLUENE	0.000	0.000	0.000	0.000	0.000	0.000	0.000	0.000	0.000	0.000
TETRA-01	0.000	0.000	0.000	0.000	0.000	0.000	0.000	0.000	0.000	0.000
INDAN-01	0.000	0.000	0.000	0.000	0.000	0.000	0.000	0.000	0.000	0.000
ETHYL-01	0.000	0.000	0.000	0.000	0.000	0.000	0.000	0.000	0.000	0.000
N-HEX-01	0.000	0.000	0.000	0.000	0.000	0.000	0.000	0.000	0.000	0.000
CYCLO-01	0.000	0.000	0.000	0.000	0.000	0.000	0.000	0.000	0.000	0.000
M-XYL-01	0.000	0.000	0.000	0.000	0.000	0.000	0.000	0.000	0.000	0.000
METHY-01	0.000	0.000	0.000	0.000	0.000	0.000	0.000	0.000	0.000	0.000
1:3-C-01	0.000	0.000	0.000	0.000	0.000	0.000	0.000	0.000	0.000	0.000
3-MET-01	0.000	0.000	0.000	0.000	0.000	0.000	0.000	0.000	0.000	0.000

N-PRO-02	0.000	0.000	0.000	0.000	0.000	0.000	0.000	0.000	0.000	0.000
CIS-D-01	0.000	0.000	0.000	0.000	0.000	0.000	0.000	0.000	0.000	0.000
ETHAN-01	0.000	0.000	0.000	0.000	0.000	0.000	0.000	0.000	0.000	0.000
MESHEPTA	0.000	0.000	0.000	0.000	0.000	0.000	0.000	0.000	0.000	0.000
BENZOFUR	0.000	0.000	0.000	0.000	0.000	0.000	0.000	0.000	0.000	0.000
1HINDANE	0.000	0.000	0.000	0.000	0.000	0.000	0.000	0.000	0.000	0.000
METHA-01	0.000	0.000	0.000	0.000	0.000	0.000	0.000	0.000	0.000	0.000
ETHAN-02	0.000	0.000	0.000	0.000	0.000	0.000	0.000	0.000	0.000	0.000
PROPA-01	0.000	0.000	0.000	0.000	0.000	0.000	0.000	0.000	0.000	0.000
ISOBU-01	0.000	0.000	0.000	0.000	0.000	0.000	0.000	0.000	0.000	0.000

Table 126 Mass Balances for Unit B3000 – Hydrogen Production, Part 2

	B3011	B3012	B3013	B3014	B3015	B3016	B3017	B3018	B3019	B3020
Mass Flow tons/h	54.958	54.958	31.363	23.595	20.233	3.362	5.756	9.136	14.891	14.891
Temperature C	55.000	43.000	43.300	43.300	11.800	43.300	50.500	56.900	54.700	43.300
Pressure bar	22.111	22.111	26.045	26.045	1.379	26.045	100.000	104.000	100.000	67.153
Vapor Frac	0.609	0.604	0.000	1.000	1.000	1.000	1.000	1.000	1.000	1.000
Enthalpy Gcal/hr	-137.415	-137.988	-102.518	-35.470	-35.844	0.191	-1.818	-2.168	-3.985	-4.395
Enthalpy GJ/hr	-574.944	-577.342	-428.935	-148.406	-149.971	0.799	-7.607	-9.071	-16.673	-18.389
MIXED										
Mass Flow tons/h										
N2	0.000	0.000	0.000	0.000	0.000	0.000	0.000	0.000	0.000	0.000
O2	0.000	0.000	0.000	0.000	0.000	0.000	0.000	0.000	0.000	0.000
H2	3.960	3.960	0.005	3.955	0.593	3.362	3.843	7.377	11.220	11.220
CO	1.390	1.390	0.022	1.367	1.367	0.000	0.052	0.000	0.052	0.052
CO2	20.206	20.206	3.088	17.118	17.118	0.000	0.646	1.243	1.889	1.889
H2O	28.352	28.352	28.209	0.143	0.143	0.000	0.010	0.021	0.031	0.031
CH4	1.050	1.050	0.038	1.012	1.012	0.000	0.421	0.168	0.588	0.588
AR	0.000	0.000	0.000	0.000	0.000	0.000	0.000	0.000	0.000	0.000

ACETACID	0.000	0.000	0.000	0.000	0.000	0.000	0.000	0.010	0.010	0.010
PHENOL	0.000	0.000	0.000	0.000	0.000	0.000	0.000	0.000	0.000	0.000
TOLUENE	0.000	0.000	0.000	0.000	0.000	0.000	0.002	0.001	0.002	0.002
TETRA-01	0.000	0.000	0.000	0.000	0.000	0.000	0.001	0.000	0.002	0.002
INDAN-01	0.000	0.000	0.000	0.000	0.000	0.000	0.000	0.003	0.003	0.003
ETHYL-01	0.000	0.000	0.000	0.000	0.000	0.000	0.001	0.001	0.002	0.002
N-HEX-01	0.000	0.000	0.000	0.000	0.000	0.000	0.049	0.000	0.049	0.049
CYCLO-01	0.000	0.000	0.000	0.000	0.000	0.000	0.086	0.010	0.096	0.096
M-XYL-01	0.000	0.000	0.000	0.000	0.000	0.000	0.002	0.001	0.003	0.003
METHY-01	0.000	0.000	0.000	0.000	0.000	0.000	0.015	0.000	0.015	0.015
1:3-C-01	0.000	0.000	0.000	0.000	0.000	0.000	0.042	0.030	0.073	0.073
3-MET-01	0.000	0.000	0.000	0.000	0.000	0.000	0.021	0.027	0.048	0.048
N-PRO-02	0.000	0.000	0.000	0.000	0.000	0.000	0.001	0.000	0.001	0.001
CIS-D-01	0.000	0.000	0.000	0.000	0.000	0.000	0.000	0.000	0.001	0.001
ETHAN-01	0.000	0.000	0.000	0.000	0.000	0.000	0.032	0.214	0.246	0.246
MESHEPTA	0.000	0.000	0.000	0.000	0.000	0.000	0.000	0.001	0.001	0.001
BENZOFUR	0.000	0.000	0.000	0.000	0.000	0.000	0.000	0.001	0.001	0.001
1HINDANE	0.000	0.000	0.000	0.000	0.000	0.000	0.004	0.001	0.006	0.006
METHA-01	0.000	0.000	0.000	0.000	0.000	0.000	0.001	0.000	0.001	0.001
ETHAN-02	0.000	0.000	0.000	0.000	0.000	0.000	0.368	0.028	0.396	0.396
PROPA-01	0.000	0.000	0.000	0.000	0.000	0.000	0.138	0.000	0.138	0.138
ISOBU-01	0.000	0.000	0.000	0.000	0.000	0.000	0.022	0.000	0.022	0.022

Table 127 Mass Balances for Unit B3000 – Hydrogen Production, Part 3

	B3021	B3022	B3023	B3024	B3025	B3026	B3027	B3028	B3029	B3030
Mass Flow tons/h	14.891	5.355	9.537	12.898	8.255	8.255	4.644	2.372	2.372	2.131
Temperature C	43.300	30.700	43.300	237.400	237.400	289.900	237.400	25.000	25.900	50.300
Pressure bar	25.000	1.379	25.000	104.435	104.435	138.908	104.435	1.013	1.023	3.771
Vapor Frac	1.000	1.000	1.000	1.000	1.000	1.000	1.000	1.000	1.000	0.043
Enthalpy GJ/hr	-18.389	-20.983	2.264	35.932	22.995	28.706	12.937	-9.987	-9.983	-3.782

MIXED

Mass Flow   tons/h

N2	0.000	0.000	0.000	0.000	0.000	0.000	0.000	0.000	0.000	0.000
O2	0.000	0.000	0.000	0.000	0.000	0.000	0.000	0.000	0.000	0.000
H2	11.220	1.683	9.537	12.898	8.255	8.255	4.644	0.000	0.000	0.000
CO	0.052	0.052	0.000	0.000	0.000	0.000	0.000	0.000	0.000	0.000
CO2	1.889	1.889	0.000	0.000	0.000	0.000	0.000	0.000	0.000	0.036
H2O	0.031	0.031	0.000	0.000	0.000	0.000	0.000	0.000	0.000	0.000
CH4	0.588	0.588	0.000	0.000	0.000	0.000	0.000	2.372	2.372	0.002
AR	0.000	0.000	0.000	0.000	0.000	0.000	0.000	0.000	0.000	0.000
ACETACID	0.010	0.010	0.000	0.000	0.000	0.000	0.000	0.000	0.000	0.000
PHENOL	0.000	0.000	0.000	0.000	0.000	0.000	0.000	0.000	0.000	0.013
TOLUENE	0.002	0.002	0.000	0.000	0.000	0.000	0.000	0.000	0.000	0.076
TETRA-01	0.002	0.002	0.000	0.000	0.000	0.000	0.000	0.000	0.000	0.014
INDAN-01	0.003	0.003	0.000	0.000	0.000	0.000	0.000	0.000	0.000	0.000
ETHYL-01	0.002	0.002	0.000	0.000	0.000	0.000	0.000	0.000	0.000	0.050
N-HEX-01	0.049	0.049	0.000	0.000	0.000	0.000	0.000	0.000	0.000	0.507
CYCLO-01	0.096	0.096	0.000	0.000	0.000	0.000	0.000	0.000	0.000	1.358
M-XYL-01	0.003	0.003	0.000	0.000	0.000	0.000	0.000	0.000	0.000	0.000
METHY-01	0.015	0.015	0.000	0.000	0.000	0.000	0.000	0.000	0.000	0.000
1:3-C-01	0.073	0.073	0.000	0.000	0.000	0.000	0.000	0.000	0.000	0.000
3-MET-01	0.048	0.048	0.000	0.000	0.000	0.000	0.000	0.000	0.000	0.000
N-PRO-02	0.001	0.001	0.000	0.000	0.000	0.000	0.000	0.000	0.000	0.000
CIS-D-01	0.001	0.001	0.000	0.000	0.000	0.000	0.000	0.000	0.000	0.000
ETHAN-01	0.246	0.246	0.000	0.000	0.000	0.000	0.000	0.000	0.000	0.000
MESHEPTA	0.001	0.001	0.000	0.000	0.000	0.000	0.000	0.000	0.000	0.000
BENZOFUR	0.001	0.001	0.000	0.000	0.000	0.000	0.000	0.000	0.000	0.000
1HINDANE	0.006	0.006	0.000	0.000	0.000	0.000	0.000	0.000	0.000	0.000
METHA-01	0.001	0.001	0.000	0.000	0.000	0.000	0.000	0.000	0.000	0.002

	B3031	B3032	B3033	B3034	B3035	B3036	B3037	B3038	B3039	B3040
ETHAN-02	0.396	0.396	0.000	0.000	0.000	0.000	0.000	0.000	0.000	0.019
PROPA-01	0.138	0.138	0.000	0.000	0.000	0.000	0.000	0.000	0.000	0.037
ISOBU-01	0.022	0.022	0.000	0.000	0.000	0.000	0.000	0.000	0.000	0.015

Table 128 Mass Balances for Unit B3000 – Hydrogen Production, Part 4

	B3031	B3032	B3033	B3034	B3035	B3036	B3037	B3038	B3039	B3040
Mass Flow tons/h	2.131	4.502	4.502	278.231	278.231	278.231	308.322	308.322	308.322	308.322
Temperature C	43.200	5.400	250.900	25.000	26.200	250.000	1734.900	1354.300	1333.900	447.900
Pressure bar	1.020	1.020	1.020	1.013	1.023	1.023	1.020	1.020	1.020	1.020
Vapor Frac	0.115	0.913	1.000	1.000	1.000	1.000	1.000	1.000	1.000	1.000
Enthalpy GJ/hr	-3.782	-13.765	-11.075	-23.472	-23.179	34.543	-147.490	-300.863	-308.926	-637.608
MIXED										
Mass Flow tons/h										
N2	0.000	0.000	0.000	208.757	208.757	208.757	208.757	208.757	208.757	208.757
O2	0.000	0.000	0.000	63.965	63.965	63.965	18.485	18.485	18.485	18.485
H2	0.000	0.000	0.000	0.000	0.000	0.000	0.000	0.000	0.000	0.000
CO	0.000	0.000	0.000	0.000	0.000	0.000	0.000	0.000	0.000	0.000
CO2	0.036	0.036	0.036	0.139	0.139	0.139	41.907	41.907	41.907	41.907
H2O	0.000	0.000	0.000	1.836	1.836	1.836	35.639	35.639	35.639	35.639
CH4	0.002	2.374	2.374	0.000	0.000	0.000	0.000	0.000	0.000	0.000
AR	0.000	0.000	0.000	3.534	3.534	3.534	3.534	3.534	3.534	3.534
ACETACID	0.000	0.000	0.000	0.000	0.000	0.000	0.000	0.000	0.000	0.000
PHENOL	0.013	0.013	0.013	0.000	0.000	0.000	0.000	0.000	0.000	0.000
TOLUENE	0.076	0.076	0.076	0.000	0.000	0.000	0.000	0.000	0.000	0.000
TETRA-01	0.014	0.014	0.014	0.000	0.000	0.000	0.000	0.000	0.000	0.000
INDAN-01	0.000	0.000	0.000	0.000	0.000	0.000	0.000	0.000	0.000	0.000
ETHYL-01	0.050	0.050	0.050	0.000	0.000	0.000	0.000	0.000	0.000	0.000
N-HEX-01	0.507	0.507	0.507	0.000	0.000	0.000	0.000	0.000	0.000	0.000

CYCLO-01	1.358	1.358	1.358	0.000	0.000	0.000	0.000	0.000	0.000	0.000
M-XYL-01	0.000	0.000	0.000	0.000	0.000	0.000	0.000	0.000	0.000	0.000
METHY-01	0.000	0.000	0.000	0.000	0.000	0.000	0.000	0.000	0.000	0.000
1:3-C-01	0.000	0.000	0.000	0.000	0.000	0.000	0.000	0.000	0.000	0.000
3-MET-01	0.000	0.000	0.000	0.000	0.000	0.000	0.000	0.000	0.000	0.000
N-PRO-02	0.000	0.000	0.000	0.000	0.000	0.000	0.000	0.000	0.000	0.000
CIS-D-01	0.000	0.000	0.000	0.000	0.000	0.000	0.000	0.000	0.000	0.000
ETHAN-01	0.000	0.000	0.000	0.000	0.000	0.000	0.000	0.000	0.000	0.000
MESHEPTA	0.000	0.000	0.000	0.000	0.000	0.000	0.000	0.000	0.000	0.000
BENZOFUR	0.000	0.000	0.000	0.000	0.000	0.000	0.000	0.000	0.000	0.000
1HINDANE	0.000	0.000	0.000	0.000	0.000	0.000	0.000	0.000	0.000	0.000
METHA-01	0.002	0.002	0.002	0.000	0.000	0.000	0.000	0.000	0.000	0.000
ETHAN-02	0.019	0.019	0.019	0.000	0.000	0.000	0.000	0.000	0.000	0.000
PROPA-01	0.037	0.037	0.037	0.000	0.000	0.000	0.000	0.000	0.000	0.000
ISOBU-01	0.015	0.015	0.015	0.000	0.000	0.000	0.000	0.000	0.000	0.000

Table 129 Mass Balances for Unit B3000 – Hydrogen Production, Part 5

	B3041	B3042	B3043	CWB3005I	CWB3005O	CWB3006I	CWB3006O
Mass Flow tons/h	308.322	308.322	308.322	37.363	37.363	27.162	27.162
Temperature C	440.000	265.100	90.000	27.000	45.000	27.000	44.700
Pressure bar	1.020	1.020	1.020	1.030	1.030	1.030	1.030
Vapor Frac	1.000	1.000	1.000	0.000	0.000	0.000	0.000
Enthalpy GJ/hr	-640.298	-698.017	-753.358	-536.887	-534.489	-390.296	-388.585
MIXED							
Mass Flow tons/h							
N2	208.757	208.757	208.757	0.000	0.000	0.000	0.000
O2	18.485	18.485	18.485	0.000	0.000	0.000	0.000
H2	0.000	0.000	0.000	0.000	0.000	0.000	0.000
CO	0.000	0.000	0.000	0.000	0.000	0.000	0.000

CO2	41.907	41.907	41.907	0.000	0.000	0.000	0.000
H2O	35.639	35.639	35.639	37.363	37.363	27.162	27.162
CH4	0.000	0.000	0.000	0.000	0.000	0.000	0.000
AR	3.534	3.534	3.534	0.000	0.000	0.000	0.000
ACETACID	0.000	0.000	0.000	0.000	0.000	0.000	0.000
PHENOL	0.000	0.000	0.000	0.000	0.000	0.000	0.000
TOLUENE	0.000	0.000	0.000	0.000	0.000	0.000	0.000
TETRA-01	0.000	0.000	0.000	0.000	0.000	0.000	0.000
INDAN-01	0.000	0.000	0.000	0.000	0.000	0.000	0.000
ETHYL-01	0.000	0.000	0.000	0.000	0.000	0.000	0.000
N-HEX-01	0.000	0.000	0.000	0.000	0.000	0.000	0.000
CYCLO-01	0.000	0.000	0.000	0.000	0.000	0.000	0.000
M-XYL-01	0.000	0.000	0.000	0.000	0.000	0.000	0.000
METHY-01	0.000	0.000	0.000	0.000	0.000	0.000	0.000
1:3-C-01	0.000	0.000	0.000	0.000	0.000	0.000	0.000
3-MET-01	0.000	0.000	0.000	0.000	0.000	0.000	0.000
N-PRO-02	0.000	0.000	0.000	0.000	0.000	0.000	0.000
CIS-D-01	0.000	0.000	0.000	0.000	0.000	0.000	0.000
ETHAN-01	0.000	0.000	0.000	0.000	0.000	0.000	0.000
MESHEPTA	0.000	0.000	0.000	0.000	0.000	0.000	0.000
BENZOFUR	0.000	0.000	0.000	0.000	0.000	0.000	0.000
1HINDANE	0.000	0.000	0.000	0.000	0.000	0.000	0.000
METHA-01	0.000	0.000	0.000	0.000	0.000	0.000	0.000
ETHAN-02	0.000	0.000	0.000	0.000	0.000	0.000	0.000
PROPA-01	0.000	0.000	0.000	0.000	0.000	0.000	0.000
ISOBU-01	0.000	0.000	0.000	0.000	0.000	0.000	0.000

Table 130 Duty/ heat Streams for Unit B3000

	B3000. QHXB3001	B3000. QHXB3002	B3000. QHXB3003	B3000. QHXB3004	B3000. QHXB3005	B3000. QHXB3006	B3000. QHXB3007	B3000. QHXB3008	B3000. QHXB3009	B3000. QHXB3010	B3000. QHXB3011	B3000. QHXB3012
QCALC MJ/hr	68805.74	2667.02	50867.82	48720.03	2398.95	1713.55	153476.09	8066.39	328906.84	2689.02	57757.82	55379.72
TBEGIN C	856.97	390.24	369.70	156.99	55.00	54.69	1734.95	1354.25	1333.90	447.95	440.00	265.11
TEND C	350.00	369.70	156.99	55.00	43.00	43.30	1354.25	1333.90	447.95	440.00	265.11	90.00

E.15 Unit B4000 – Electricity Generation
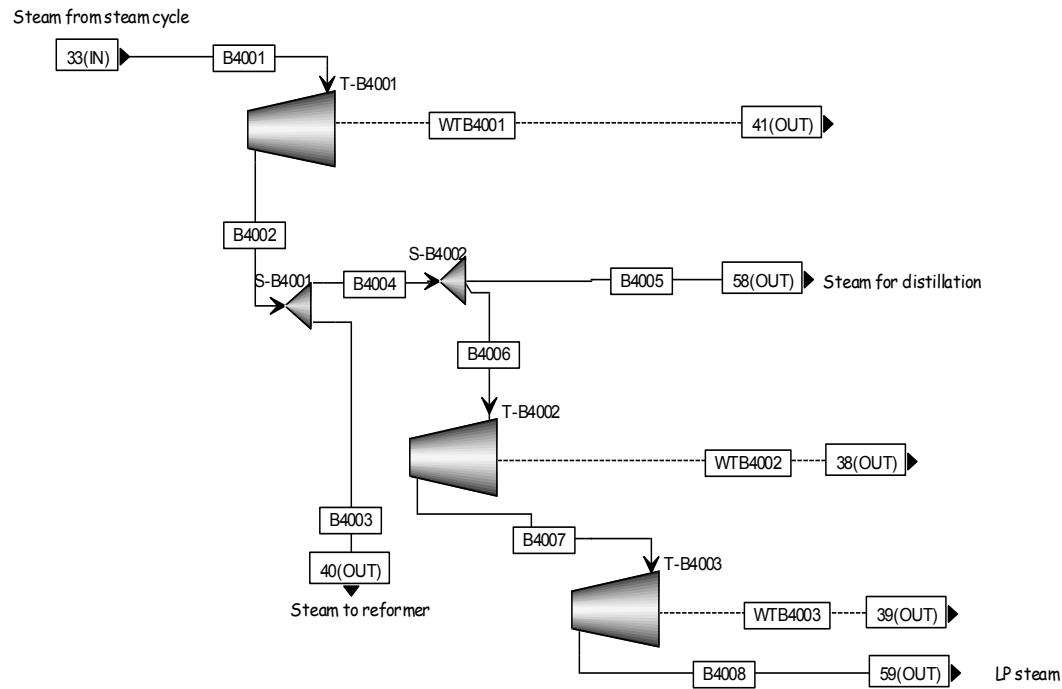
Figure 70 Process Flow Diagram for Unit B4000 – Electricty Generation

Table 131 Mass Balances for U4000 – Electricty Generation

	B4001	B4002	B4003	B4004	B4005	B4006	B4007	B4008
Mass Flow tons/h	382.168	382.168	45.787	336.380	5.821	330.559	330.559	330.559
Temperature C	500.000	399.700	399.700	399.700	399.700	399.700	224.600	120.300
Pressure bar	105.000	49.000	49.000	49.000	49.000	49.000	10.000	2.000
Vapor Frac	1.000	1.000	1.000	1.000	1.000	1.000	1.000	0.970
Enthalpy GJ/hr	-4324.2	-4397.08	-526.816	-3870.27	-66.9775	-3803.29	-3908.68	-3988.92
MIXED								
Mass Flow tons/h								
H2O	382.168	382.168	45.787	336.380	5.821	330.559	330.559	330.559

E.16 Process simulation input file

;Input Summary created by Aspen Plus Rel. 23.0 at 00:03:10 Mon Nov 23, 2015
;

DYNAMICS
    DYNAMICS RESULTS=ON

IN-UNITS SI ENTHALPY='J/kg' FLOW='tons/hr' MASS-FLOW='tons/hr' &
        MOLE-FLOW='kmol/hr' VOLUME-FLOW='cum/hr' &
        ENTHALPY-FLO='MJ/hr' POWER=MW PRESSURE=bar TEMPERATURE=C &
        DELTA-T=C ELEC-POWER=kW HEAT=MJ PDROP-PER-HT='mbar/m' &
        PDROP=bar

DEF-STREAMS MIXCISLD ALL

SIM-OPTIONS
    IN-UNITS MET VOLUME-FLOW='cum/hr' ENTHALPY-FLO='Gcal/hr' &
        HEAT-TRANS-C='kcal/hr-sqm-K' PRESSURE=bar TEMPERATURE=C &
        VOLUME=cum DELTA-T=C HEAD=meter MOLE-DENSITY='kmol/cum' &
        MASS-DENSITY='kg/cum' MOLE-ENTHALP='kcal/mol' &
        MASS-ENTHALP='kcal/kg' HEAT=Gcal MOLE-CONC='mol/l' &
        PDROP=bar
    SIM-OPTIONS FLASH-MAXIT=80 NPHASE=2 OLD-DATABANK=YES

DESCRIPTION "
    General Simulation with Metric Units :
    C, bar, kg/hr, kmol/hr, Gcal/hr, cum/hr.

    Property Method: None

    Flow basis for input: Mole

    Stream report composition: Mole flow

    "

DATABANKS PURE22 / AQUEOUS / SOLIDS / INORGANIC / &
    ASPENPCD / COMBUST / PURE93 / PURE856 / ETHYLENE &
    / AQU92

PROP-SOURCES PURE22 / AQUEOUS / SOLIDS / INORGANIC / &
    ASPENPCD / COMBUST / INHSPCD / PURE93 / PURE856 &
    / ETHYLENE / AQU92

IN-HOUSE-DATA PCD=YES

COMPONENTS
    N2 N2 /
    O2 O2 /
    H2 H2 /
    CO CO /
    NO2 NO2 /
    CO2 CO2 /
    H2O H2O /
    H3N H3N /
    CH4 CH4 /
    C2H4 C2H4 /
    C3H6-2 C3H6-2 /
    AR AR /
    ACETACID C2H4O2-1 /
    ACETOL C3H6O2-D1 /
    GUAIACOL C7H8O2-E1 /
    3:5-X-01 C8H10O-10 /
    FORMACID CH2O2 /
    N-PRO-01 C10H12O2 /
    PHENOL C6H6O /
    TOLUENE C7H8 /
    FURFURAL C5H4O2 /
    BENZENE C6H6 /
    CHAR C /
    ASH CAO /
    CELLULOS C6H10O5 /
    LIGNIN CXHXOX /

276

XYLAN C5H8O4 /
ARABINAN C5H8O4 /
MANNAN C6H10O5 /
GALACTAN C6H10O5 /
EXTRACT CXHXOXNXSX-1 /
TETRA-01 C4H8O-4 /
DILACID C6H10O5 /
N-HEP-01 C7H14O2-D3 /
2:4-X-01 C8H10O-6 /
O-ETH-01 C8H10O-1 /
INDAN-01 C9H10-E1 /
2:6-D-01 C15H24O-D1 /
NAPHT-01 C10H8 /
DIBEN-01 C12H8O /
FLUOR-01 C16H10-D1 /
2:4-D-01 C18H20 /
NAPHT-02 C18H12-D2 /
ETHYL-01 C8H10-4 /
N-HEX-01 C6H14-1 /
CYCLO-01 C6H12-1 /
M-XYL-01 C8H10-2 /
METHY-01 C7H14-6 /
1:3-C-01 C6H8-E1 /
3-MET-01 C8H18-3 /
P-CRE-01 C7H8O-5 /
N-PRO-02 C9H12-1 /
1:2:3-01 C10H12 /
CIS-D-01 C10H18-1 /
1:2-D-01 C14H14-D2 /
CYCLO-02 C12H16 /
N-TET-01 C14H30 /
DINON-01 C24H42O /
N-TET-02 C24H50 /
GLYCO-01 C2H4O3-D1 /
FUMAR-01 C4H4O4-D1 /
1:2-B-01 C6H6O2-E1 /
ETHAN-01 C2H6O-2 /
2,2PROPA C6H6O9 /
FURACETA C6H6O7 /
LEVOGLUC C6H10O5 /
4METGUA C8H10O2 /
ETHYLANI C9H12O /
BENZOATE C10H12O2 /
METHPHEN C9H10O2 /
ETHYLGUA C9H12O2 /
MESHEPTA C8H16O2 /
BENZOFUR C8H6O /
TRIMEBEN C9H12O3 /
4PROPGUA C10H14O2 /
HMBENZAC C8H8O4 /
METOCTAC C9H18O2 /
CONIFALC C10H12O3 /
ISOEUGEN C10H12O2 /
PHENKETO C14H12O3 /
XANTHENE C13H10O /
P-DECANO C16H32O2 /
DNONDBEN C24H42O2 /
PENTACOS C27H54O2 /
ETMEPHEN C9H12O /
1HINDANE C9H16 /
HYDFLUOR C16H26 /
HYDNAPH C18H30 /
C18H28 C18H28 /
C21H24O4 C21H24O4 /
C22H20O /
METHA-01 CH4O /
ETHAN-02 C2H6 /
PROPA-01 C3H8 /
ISOBU-01 C4H10-2 /
COKE1 /
COKE2 /
ACETY-01 C2H2 /
NAPHT-03 C10H8 /
AIR AIR

277

FORMULA 2,2PROPA C6H6O9 / FURACETA C6H6O7 / LEVOGLUC C6H10O5 / &
    4METGUA C8H10O2 / ETHYLANI C9H12O / BENZOATE C10H12O2 / &
    METHPHEN C9H10O2 / ETHYLGUA C9H12O2 / MESHEPTA C8H16O2 / &
    BENZOFUR C8H6O / TRIMEBEN C9H12O3 / 4PROPGUA C10H14O2 / &
    HMBENZAC C8H8O4 / METOCTAC C9H18O2 / CONIFALC C10H12O3 / &
    PHENKETO C14H12O3 / XANTHENE C13H10O / P-DECANO &
    C16H32O2 / DNONDBEN C24H42O2 / PENTACOS C27H54O2 / &
    1HINDANE C9H16 / HYDFLUOR C16H26 / HYDNAPH C18H30 / &
    C18H28 C18H28 / C21H24O4 C21H24O4

PC-USER
  PC-DEF ASPEN C22H20O NBP=475.424 LDEN=1143. MW=300.3928
  PC-DEF ASPEN COKE1 NBP=3929.85 LDEN=1615.06 MW=1572.10943
  PC-DEF ASPEN COKE2 NBP=3929.85 LDEN=1615.06 MW=1365.35209

ADA-SETUP
  ADA-SETUP PROCEDURE=REL9

FLOWSHEET
  HIERARCHY A1000
  CONNECT $C-24 IN=14 OUT=A1000.1002
  CONNECT $C-1 IN=A1000.1005 OUT=7
  HIERARCHY A2000
  CONNECT $C-2 IN=7 OUT=A2000.1005
  CONNECT $C-22 IN=13 OUT=A2000.6008
  CONNECT $C-20 IN=12 OUT=A2000.6006
  CONNECT $C-8 IN=2 OUT=A2000.5007
  CONNECT $C-3 IN=A2000.2004 OUT=8
  CONNECT $C-5 IN=A2000.2006 OUT=10
  HIERARCHY A3000
  CONNECT $C-4 IN=8 OUT=A3000.3001
  CONNECT $C-26 IN=15 OUT=A3000.3011
  CONNECT $C-23 IN=A3000.3010 OUT=14
  CONNECT $C-11 IN=A3000.3004 OUT=4
  CONNECT $C-15 IN=A3000.3007 OUT=6
  CONNECT $C-13 IN=A3000.3006 OUT=5
  CONNECT $C-29 IN=A3000.WCPA3001 OUT=1
  CONNECT $C-45 IN=A3000.3013 OUT=16
  HIERARCHY A4000
  CONNECT $C-6 IN=10 OUT=A4000.4001
  CONNECT $C-17 IN=A4000.QHX4001 OUT=11
  CONNECT $C-35 IN=A4000.WCPA4001 OUT=19
  CONNECT $C-37 IN=A4000.QHX4002 OUT=20
  CONNECT $C-39 IN=A4000.QHX4003 OUT=21
  CONNECT $C-41 IN=A4000.QHX4004 OUT=22
  HIERARCHY A5000
  CONNECT $C-14 IN=5 OUT=A5000.3021
  CONNECT $C-12 IN=4 OUT=A5000.3004
  CONNECT $C-28 IN=17 OUT=A5000.6003
  CONNECT $C-25 IN=A5000.5005 OUT=15
  CONNECT $C-31 IN=A5000.WPA5001 OUT=9
  CONNECT $C-49 IN=A5000.CWA5001O OUT=25
  CONNECT $C-7 IN=A5000.5007 OUT=2
  CONNECT $C-9 IN=A5000.5006 OUT=3
  HIERARCHY A6000
  CONNECT $C-16 IN=6 OUT=A6000.6001
  CONNECT $C-18 IN=11 OUT=A6000.QHX4001
  CONNECT $C-19 IN=A6000.6006 OUT=12
  CONNECT $C-21 IN=A6000.6008 OUT=13
  CONNECT $C-27 IN=A6000.6003 OUT=17
  CONNECT $C-33 IN=A6000.WCPA6001 OUT=18
  HIERARCHY A7000
  CONNECT $C-38 IN=20 OUT=A7000.QHX4002
  CONNECT $C-40 IN=21 OUT=A7000.QHX4003
  CONNECT $C-42 IN=22 OUT=A7000.QHX4004
  CONNECT $C-46 IN=16 OUT=A7000.3010
  CONNECT $C-44 IN=23 OUT=A7000.QHXB3009
  CONNECT $C-48 IN=24 OUT=A7000.QHXB3001
  CONNECT $C-66 IN=34 OUT=A7000.QHXB2002
  CONNECT $C-68 IN=35 OUT=A7000.QHXB3002
  CONNECT $C-82 IN=52 OUT=A7000.QHX3004
  CONNECT $C-80 IN=50 OUT=A7000.QHXB2004
  CONNECT $C-84 IN=53 OUT=A7000.QHXB1002

```
CONNECT $C-86 IN=54 OUT=A7000.QHXB3012
CONNECT $C-69 IN=A7000.7025 OUT=33
CONNECT $C-93 IN=A7000.WPA7001 OUT=42
CONNECT $C-103 IN=A7000.WPA7006 OUT=47
CONNECT $C-95 IN=A7000.WPA7002 OUT=43
CONNECT $C-97 IN=A7000.WPA7003 OUT=44
CONNECT $C-99 IN=A7000.WPA7004 OUT=45
CONNECT $C-101 IN=A7000.WPA7005 OUT=46
HIERARCHY A8000
CONNECT $C-30 IN=1 OUT=A8000.WCPA3001
CONNECT $C-32 IN=9 OUT=A8000.WPA5001
CONNECT $C-34 IN=18 OUT=A8000.WCPA6001
CONNECT $C-36 IN=19 OUT=A8000.WCPA4001
CONNECT $C-50 IN=25 OUT=A8000.CWA5001O
CONNECT $C-76 IN=39 OUT=A8000.WTB4003
CONNECT $C-74 IN=38 OUT=A8000.WTB4002
CONNECT $C-72 IN=41 OUT=A8000.WTB4001
CONNECT $C-88 IN=56 OUT=A8000.CWB3006O
CONNECT $C-90 IN=36 OUT=A8000.CWB3005O
CONNECT $C-92 IN=37 OUT=A8000.CWB2005O
CONNECT $C-94 IN=42 OUT=A8000.WPA7001
CONNECT $C-96 IN=43 OUT=A8000.WPA7002
CONNECT $C-98 IN=44 OUT=A8000.WPA7003
CONNECT $C-100 IN=45 OUT=A8000.WPA7004
CONNECT $C-102 IN=46 OUT=A8000.WPA7005
CONNECT $C-104 IN=47 OUT=A8000.WPA7006
CONNECT $C-106 IN=48 OUT=A8000.WPB1001
CONNECT $C-108 IN=49 OUT=A8000.WCPB3001
CONNECT $C-110 IN=51 OUT=A8000.WCPB3002
CONNECT $C-112 IN=55 OUT=A8000.WCPB3003
CONNECT $C-114 IN=57 OUT=A8000.WCPB3004
CONNECT $C-116 IN=58 OUT=A8000.STMDIST
CONNECT $C-118 IN=59 OUT=A8000.B4008
HIERARCHY B1000
CONNECT $C-10 IN=3 OUT=B1000.B1001
CONNECT $C-53 IN=27 OUT=B1000.B1005
CONNECT $C-64 IN=31 OUT=B1000.QHXB3003
CONNECT $C-51 IN=B1000.B1011 OUT=26
CONNECT $C-59 IN=B1000.B1007 OUT=30
CONNECT $C-83 IN=B1000.QHXB1002 OUT=53
CONNECT $C-105 IN=B1000.WPB1001 OUT=48
HIERARCHY B2000
CONNECT $C-52 IN=26 OUT=B2000.B2001
CONNECT $C-55 IN=28 OUT=B2000.B2003
CONNECT $C-57 IN=B2000.B2009 OUT=32
CONNECT $C-61 IN=B2000.B2017 OUT=29
CONNECT $C-65 IN=B2000.QHXB2002 OUT=34
CONNECT $C-79 IN=B2000.QHXB2004 OUT=50
CONNECT $C-91 IN=B2000.CWB2005O OUT=37
HIERARCHY B3000
CONNECT $C-58 IN=32 OUT=B3000.B3017
CONNECT $C-60 IN=30 OUT=B3000.B3018
CONNECT $C-62 IN=29 OUT=B3000.B3030
CONNECT $C-78 IN=40 OUT=B3000.B3003
CONNECT $C-54 IN=B3000.B3026 OUT=27
CONNECT $C-56 IN=B3000.B3027 OUT=28
CONNECT $C-47 IN=B3000.QHXB3001 OUT=24
CONNECT $C-43 IN=B3000.QHXB3009 OUT=23
CONNECT $C-63 IN=B3000.QHXB3003 OUT=31
CONNECT $C-67 IN=B3000.QHXB3002 OUT=35
CONNECT $C-85 IN=B3000.QHXB3012 OUT=54
CONNECT $C-81 IN=B3000.QHXB3004 OUT=52
CONNECT $C-87 IN=B3000.CWB3006O OUT=56
CONNECT $C-89 IN=B3000.CWB3005O OUT=36
CONNECT $C-109 IN=B3000.WCPB3002 OUT=51
CONNECT $C-107 IN=B3000.WCPB3001 OUT=49
CONNECT $C-111 IN=B3000.WCPB3003 OUT=55
CONNECT $C-113 IN=B3000.WCPB3004 OUT=57
HIERARCHY B4000
CONNECT $C-70 IN=33 OUT=B4000.B4001
CONNECT $C-75 IN=B4000.WTB4003 OUT=39
CONNECT $C-71 IN=B4000.WTB4001 OUT=41
CONNECT $C-73 IN=B4000.WTB4002 OUT=38
CONNECT $C-77 IN=B4000.B4003 OUT=40
```

279

```
    CONNECT $C-115 IN=B4000.B4005 OUT=58
    CONNECT $C-117 IN=B4000.B4008 OUT=59

PROPERTIES NRTL
    PROPERTIES PENG-ROB / SRK

STRUCTURES
    STRUCTURES 1HINDANE C1 C2 S / C1 C3 S / C1 C4 S /  &
        C2 C5 S / C2 C6 S / C3 C7 S / C4 C8 S / C5  &
        C7 S / C6 C9 S / C8 C9 S

PROP-DATA
    PROP-LIST ATOMNO / NOATOM
    PVAL 1HINDANE 6 1 / 9. 16.

STRUCTURES
    STRUCTURES 2,2PROPA C1 O2 S / O2 C3 S / C3 C4 S /  &
        C4 O5 S / C1 C6 S / C6 O7 S / C6 O8 D / C4  &
        O9 D / C1 C10 S / C3 C11 S / C11 O12 S / C11  &
        O13 D / C10 O14 S / C10 O15 D

PROP-DATA
    PROP-LIST ATOMNO / NOATOM
    PVAL 2,2PROPA 8 6 1 / 9. 6. 6.

STRUCTURES
    STRUCTURES 4METGUA C1 C2 D / C1 C3 S / C1 O4 S / C2  &
        C5 S / C2 O6 S / C3 C7 D / O4 C8 S / C5 C9  &
        D / C7 C10 S / C7 C9 S

PROP-DATA
    PROP-LIST ATOMNO / NOATOM
    PVAL 4METGUA 6 8 1 / 8. 2. 10.

STRUCTURES
    STRUCTURES 4PROPGUA C1 C2 S / C1 C3 D / C1 O4 S /  &
        C2 C5 D / C3 C6 S / C3 O7 S / O4 C8 S / C5  &
        C9 S / C5 C10 S / C6 C9 D / C10 C11 S / C11  &
        C12 S

PROP-DATA
    PROP-LIST ATOMNO / NOATOM
    PVAL 4PROPGUA 8 6 1 / 2. 10. 14.

STRUCTURES
    STRUCTURES BENZOATE C1 C2 D / C2 C3 S / C3 C4 D /  &
        C4 C5 S / C5 C6 D / C6 C1 S / C1 C7 S / C4  &
        C8 S / C6 C9 S / C9 O10 S / O10 C11 S / C9  &
        O12 D

PROP-DATA
    PROP-LIST ATOMNO / NOATOM
    PVAL BENZOATE 8 6 1 / 2. 10. 12.

STRUCTURES
    STRUCTURES BENZOFUR C1 C2 D / C1 C3 S / C1 C4 S /  &
        C2 O5 S / C2 C6 S / C3 C7 D / C4 C8 D / O5  &
        C7 S / C6 C9 D / C8 C9 S

PROP-DATA
    PROP-LIST ATOMNO / NOATOM
    PVAL BENZOFUR 8 6 1 / 1. 8. 6.

STRUCTURES
    STRUCTURES C18H28 C1 C2 S / C2 C3 S / C3 C4 S / C4  &
        C5 S / C5 C6 S / C6 C1 S / C7 C8 D / C8 C9  &
        S / C9 C10 S / C10 C11 S / C11 C12 D / C12 C7  &
        S / C5 C11 S / C13 C14 S / C14 C15 S / C15 C16  &
        S / C16 C17 S / C17 C18 S / C18 C13 S / C8 C17  &
        S

PROP-DATA
    PROP-LIST ATOMNO / NOATOM
    PVAL C18H28 6 1 / 18. 28.
```

STRUCTURES
  STRUCTURES C21H24O4 C1 C2 D / C2 C3 S / C3 C4 D / &
    C4 C5 S / C5 C11 D / C11 C1 S / C6 O7 S / O7 &
    C8 S / C8 C9 D / C9 C10 S / C10 C6 S / C6 C11 &
    S / C3 O12 S / C2 O13 S / O13 C14 S / C10 C15 &
    S / C9 C16 S / C16 C17 D / C17 C18 S / C18 C19 &
    D / C19 C8 S / C19 O20 S / O20 C21 S / C17 C22 &
    S / C22 C23 S / C23 C24 D / C24 C25 S

PROP-DATA
  PROP-LIST ATOMNO / NOATOM
  PVAL C21H24O4 6 8 1 / 21. 4. 24.

STRUCTURES
  STRUCTURES CONIFALC C1 C2 S / C2 C3 D / C3 C4 S / &
    C4 C5 S / C5 C6 D / C6 O7 S / O7 C8 S / C6 &
    C9 S / C9 O10 S / C9 C11 D / C11 C12 S / C4 &
    C12 D / C1 O13 S

PROP-DATA
  PROP-LIST ATOMNO / NOATOM
  PVAL CONIFALC 8 6 1 / 3. 10. 12.

STRUCTURES
  STRUCTURES DNONDBEN C1 C2 S / C2 C3 D / C3 C4 S / &
    C4 C5 D / C5 C6 S / C1 C6 D / C1 O7 S / C8 &
    C9 S / C9 C10 S / C10 C11 S / C11 C12 S / C12 &
    C13 S / C13 C14 S / C14 C15 S / C15 C16 S / C2 &
    C8 S / C17 C18 S / C18 C19 S / C19 C20 S / C20 &
    C21 S / C21 C22 S / C22 C23 S / C23 C24 S / &
    C24 C25 S / C3 C17 S

PROP-DATA
  PROP-LIST ATOMNO / NOATOM
  PVAL DNONDBEN 8 6 1 / 1. 24. 42.

STRUCTURES
  STRUCTURES ETHYLANI C1 C2 S / C1 C3 D / C1 C4 S / &
    C2 C5 D / C3 C6 S / C4 C7 S / C5 C8 S / C6 &
    C8 D / C8 O9 S / O9 C10 S

PROP-DATA
  PROP-LIST ATOMNO / NOATOM
  PVAL ETHYLANI 6 8 1 / 9. 1. 12.

STRUCTURES
  STRUCTURES ETHYLGUA C1 C2 S / C1 C3 D / C1 O4 S / &
    C2 C5 D / C3 C6 S / C3 O7 S / O4 C8 S / C5 &
    C9 S / C5 C10 S / C6 C9 D / C10 C11 S

PROP-DATA
  PROP-LIST ATOMNO / NOATOM
  PVAL ETHYLGUA 6 8 1 / 9. 2. 12.

STRUCTURES
  STRUCTURES ETMEPHEN C1 C2 S / C2 C3 D / C3 C4 S / &
    C4 C5 D / C5 C6 S / C1 C6 D / C4 C7 S / C8 &
    C9 S / C2 C8 S / C1 O10 S

PROP-DATA
  PROP-LIST ATOMNO / NOATOM
  PVAL ETMEPHEN 8 6 1 / 1. 9. 12.

STRUCTURES
  STRUCTURES FURACETA O1 C2 S / C3 O1 S / C2 C4 S / &
    C2 O5 D / C6 C3 S / C4 C6 D / C4 O7 S / C6 &
    O8 S / C3 C9 S / C9 C10 S / C9 O11 S / C10 &
    O12 S / C10 O13 D

PROP-DATA
  PROP-LIST ATOMNO / NOATOM
  PVAL FURACETA 8 6 1 / 7. 6. 6.

STRUCTURES
  STRUCTURES HMBENZAC C1 C2 S / C1 C3 D / C1 O4 S / &
    C2 C5 D / C3 C6 S / C3 O7 S / O4 C8 S / C5 &
    C9 S / C5 C10 S / C6 C9 D / C10 O11 S / C10 &
    O12 D

PROP-DATA
  PROP-LIST ATOMNO / NOATOM
  PVAL HMBENZAC 8 6 1 / 4. 8. 8.

STRUCTURES
  STRUCTURES HYDFLUOR C1 C2 S / C2 C3 S / C3 C4 S / &
    C4 C5 S / C5 C6 S / C6 C7 S / C7 C8 S / C8 &
    C9 S / C9 C10 S / C10 C11 S / C11 C12 S / C12 &
    C13 S / C13 C14 S / C9 C14 S / C14 C15 S / C1 &
    C15 S / C15 C16 S / C4 C16 S / C8 C16 S

PROP-DATA
  PROP-LIST ATOMNO / NOATOM
  PVAL HYDFLUOR 6 1 / 16. 26.

STRUCTURES
  STRUCTURES HYDNAPH C1 C2 S / C2 C3 S / C3 C4 S / C4 &
    C7 S / C6 C1 S / C5 C6 S / C6 C7 S / C7 C8 &
    S / C8 C11 S / C10 C5 S / C9 C10 S / C10 C11 &
    S / C11 C12 S / C12 C15 S / C14 C9 S / C13 C14 &
    S / C14 C15 S / C15 C16 S / C16 C17 S / C17 &
    C18 S / C18 C13 S

PROP-DATA
  PROP-LIST ATOMNO / NOATOM
  PVAL HYDNAPH 6 1 / 18. 30.

STRUCTURES
  STRUCTURES ISOEUGEN C1 C2 S / C1 C3 D / C1 O4 S / &
    C2 C5 D / C3 C6 S / C3 O7 S / O4 C8 S / C5 &
    C9 S / C5 C10 S / C6 C9 D / C10 C11 D / C11 &
    C12 S

PROP-DATA
  PROP-LIST ATOMNO / NOATOM
  PVAL ISOEUGEN 8 6 1 / 2. 10. 12.

STRUCTURES
  STRUCTURES LEVOGLUC C1 O2 S / C1 C3 S / C1 C4 S / &
    O2 C5 S / C3 C6 S / C3 O7 S / C4 O8 S / C5 &
    C9 S / C5 O8 S / C6 O10 S / C6 C9 S / C9 O11 &
    S

PROP-DATA
  PROP-LIST ATOMNO / NOATOM
  PVAL LEVOGLUC 8 6 1 / 5. 6. 10.

STRUCTURES
  STRUCTURES MESHEPTA C1 C2 S / C1 O3 S / C1 O4 D / &
    C2 C5 S / O3 C6 S / C5 C7 S / C7 C8 S / C8 &
    C9 S / C9 C10 S

PROP-DATA
  PROP-LIST ATOMNO / NOATOM
  PVAL MESHEPTA 6 8 1 / 8. 2. 16.

STRUCTURES
  STRUCTURES METHPHEN C1 C2 S / C1 C3 D / C1 O4 S / &
    C2 C5 D / C3 C6 S / O4 C7 S / C5 C8 S / C5 &
    C9 S / C6 O10 S / C6 C8 D / C8 C11 S

PROP-DATA
  PROP-LIST ATOMNO / NOATOM
  PVAL METHPHEN 8 6 1 / 2. 9. 12.

STRUCTURES
  STRUCTURES METOCTAC C1 C2 S / C1 C3 S / C1 C4 S / &
    C2 C5 S / C3 C6 S / C5 C7 S / C6 C8 S / C7 &

```
    O9 S / C7 O10 D / C8 C11 S

PROP-DATA
    PROP-LIST ATOMNO / NOATOM
    PVAL METOCTAC 8 6 1 / 2. 9. 18.

STRUCTURES
    STRUCTURES P-DECANO C1 C2 S / C1 C3 S / C2 C4 S /  &
        C3 C5 S / C4 C6 S / C5 C7 S / C6 C8 S / C7  &
        O9 S / C7 O10 D / C8 C11 S / O9 C12 S / C11  &
        C13 S / C13 C14 S / C14 C15 S / C15 C16 S /  &
        C16 C17 S / C17 C18 S

PROP-DATA
    PROP-LIST ATOMNO / NOATOM
    PVAL P-DECANO 8 6 1 / 2. 16. 32.

STRUCTURES
    STRUCTURES PENTACOS C1 C2 S / C2 C3 S / C3 C4 S /  &
        C4 C5 S / C5 C6 S / C6 C7 S / C7 C8 S / C8  &
        C9 S / C9 C10 S / C10 C11 S / C11 C12 S / C12  &
        C13 S / C13 C14 S / C14 C15 S / C15 C16 S /  &
        C16 C17 S / C17 C18 S / C18 C19 S / C19 C20 S /  &
        C20 C21 S / C21 C22 S / C22 C23 S / C23 C24 S /  &
        C24 C25 S / C1 O26 D / C1 O27 S / C28 C29 S /  &
        O27 C28 S

PROP-DATA
    PROP-LIST ATOMNO / NOATOM
    PVAL PENTACOS 6 8 1 / 27. 2. 54.

STRUCTURES
    STRUCTURES PHENKETO C1 C2 D / C2 C3 S / C3 C15 D /  &
        C15 C4 S / C4 C5 D / C5 C1 S / C6 C7 D / C7  &
        C8 S / C8 C9 D / C9 C10 S / C10 C11 D / C11  &
        C6 S / C11 O12 S / C10 C13 S / C13 C14 S / C14  &
        C15 S / C13 O16 D / C7 O17 S

PROP-DATA
    PROP-LIST ATOMNO / NOATOM
    PVAL PHENKETO 8 6 1 / 3. 14. 12.

STRUCTURES
    STRUCTURES TRIMEBEN C1 C2 S / C2 C3 D / C3 C4 S /  &
        C4 C5 D / C5 C6 S / C1 C6 D / O7 C8 S / C1  &
        O7 S / O9 C10 S / C2 O9 S / O11 C12 S / C3  &
        O11 S

PROP-DATA
    PROP-LIST ATOMNO / NOATOM
    PVAL TRIMEBEN 8 6 1 / 3. 9. 12.

STRUCTURES
    STRUCTURES XANTHENE C1 C2 D / C1 C3 S / C1 C4 S /  &
        C2 O5 S / C2 C6 S / C3 C7 S / C4 C8 D / O5  &
        C9 S / C6 C10 D / C7 C11 D / C7 C9 S / C8 C10  &
        S / C9 C12 D / C11 C13 S / C12 C14 S / C13 C14  &
        D

PROP-DATA
    PROP-LIST ATOMNO / NOATOM
    PVAL XANTHENE 6 8 1 / 13. 1. 10.

ESTIMATE ALL

PROP-DATA PCES-1
    IN-UNITS SI ENTHALPY='J/kg' FLOW='tons/hr'  &
        MASS-FLOW='tons/hr' MOLE-FLOW='kmol/hr'  &
        VOLUME-FLOW='cum/hr' ENTHALPY-FLO='MJ/hr' POWER=MW  &
        PRESSURE=bar TEMPERATURE=C DELTA-T=C ELEC-POWER=kW  &
        HEAT=MJ PDROP-PER-HT='mbar/m' PDROP=bar
    PROP-LIST ZC / VB / VLSTD
    PVAL EXTRACT .3071746180 / .0323255230 / .0164499564
    PROP-LIST VB / DHFORM / DGFORM / DHVLB / VLSTD /  &
```

283

```
  RKTZRA
  PVAL 2,2PROPA .0915533666 / -1.7110300E+9 / -1.4858800E+9 /  &
     8.96231837E+7 / .0576789407 / .1495306270
  PVAL FURACETA .0576425495 / -1.1890500E+9 / -9.9609000E+8 /  &
     1.32042764E+8 / .0353030428 / .1470389040
  PVAL BENZOFUR .1237619490 / 3.55300000E+7 / 1.31560000E+8 /  &
     4.28075664E+7 / .1048008390 / .2595839110
  PVAL TRIMEBEN .2272310370 / -3.7580000E+8 / -1.9695000E+8 /  &
     4.13432720E+7 / .1886998840 / .2710361420
  PVAL HMBENZAC .1021421300 / -6.2310900E+8 / -4.8427000E+8 /  &
     7.31657429E+7 / .0737191205 / .1971280420
  PVAL CONIFALC .1270386530 / -3.5872000E+8 / -1.8012000E+8 /  &
     7.46218293E+7 / .0901510069 / .1974733140
  PVAL PHENKETO .0955094804 / -3.2071900E+8 / -1.4634000E+8 /  &
     1.17201103E+8 / .0556444582 / .1382767170
  PVAL DNONDBEN .6297058550 / -4.7419000E+8 / 9.93600000E+7 /  &
     6.47097597E+7 / .4191853450 / .2186401840
  PVAL PENTACOS .8379447890 / -9.0595100E+8 / -1.3391000E+8 /  &
     5.19098250E+7 / .5655978390 / .2279350700
  PVAL 1HINDANE .1645984650 / -1.2903000E+8 / 1.10100000E+8 /  &
     3.66185342E+7 / .1414586370 / .2645742230
  PVAL C18H28 .3641926250 / -1.0978000E+8 / 2.22400000E+8 /  &
     6.00611363E+7 / .2696795750 / .2433488240
  PVAL C21H24O4 .3283337430 / -4.5911000E+8 / -5.2400000E+6 /  &
     1.07469599E+8 / .1950148880 / .1719800480
  PROP-LIST VB / DHVLB / VLSTD / RKTZRA
  PVAL LEVOGLUC .1824900000 / 5.59235000E+7 / .1608520000 /  &
     .1134317240
  PVAL MESHEPTA .1837530000 / 6.69570000E+7 / .1428460000 /  &
     .2396733620
  PROP-LIST VB / DHVLB / VLSTD
  PVAL 4METGUA .1630460000 / 6.03882000E+7 / .1290160000
  PVAL ETHYLGUA .1738910000 / 6.99000000E+7 / .1458920000
  PROP-LIST VB / DHVLB
  PVAL ETHYLANI .1688400000 / 4.16735000E+7
  PVAL BENZOATE .1991390000 / 4.65399000E+7
  PVAL METHPHEN .1764100000 / 4.50928000E+7
  PVAL 4PROPGUA .1963910000 / 6.11152000E+7
  PVAL METOCTAC .2281260000 / 5.66138000E+7
  PVAL ISOEUGEN .1991390000 / 4.65399000E+7
  PVAL XANTHENE .2085030000 / 5.42911000E+7
  PVAL P-DECANO .4095880000 / 6.44405000E+7
  PVAL ETMEPHEN .1688400000 / 4.16735000E+7
  PVAL HYDFLUOR .3428670000 / 5.15966000E+7
  PVAL HYDNAPH .4005870000 / 5.53087000E+7
  PROP-LIST VLSTD
  PVAL CHAR 7.45545000E-3
  PVAL DIBEN-01 .1522490000
  PVAL AIR .0329147000
  PROP-LIST VLSTD / RKTZRA
  PVAL ASH .8669275910 / .2917660970
  PVAL CELLULOS .1608520000 / .2060436120
  PVAL MANNAN .1608520000 / .2060436120
  PVAL GALACTAN .1608520000 / .2060436120
  PVAL DILACID .1608520000 / .2060436120
  PVAL NAPHT-02 .2079220000 / .2379844120
  PVAL DINON-01 .3070900000 / .1849207650
  PVAL FUMAR-01 .1084730000 / .1986360350

PROP-DATA TDE-1
  IN-UNITS SI ENTHALPY='J/kg' FLOW='tons/hr'  &
     MASS-FLOW='tons/hr' MOLE-FLOW='kmol/hr'  &
     VOLUME-FLOW='cum/hr' ENTHALPY-FLO='MJ/hr' POWER=MW  &
     DELTA-T=C ELEC-POWER=kW HEAT=MJ PDROP-PER-HT='mbar/m'  &
     PDROP=bar
  PROP-LIST OMEGA / ZC / VC / PC / TC / MW / TB
  PVAL 2,2PROPA 1.519 / 0.1968 / 0.408 / 3325377.1 / 829 /  &
     222.11 / 653.5
  PVAL FURACETA 1.5528 / 0.261 / 0.3661 / 6841437.9 /  &
     1155 / 190.11 / 877.5
  PVAL LEVOGLUC 1.9239 / 0.293 / 0.3662 / 5695977.1 / 857 /  &
     162.14 / 675.1
  PVAL 4METGUA 0.38799 / 0.252 / 0.414 / 3857875.8 / 764 /  &
     138.16 / 514
```

PVAL ETHYLANI 0.36741 / 0.216 / 0.45 / 2816352.3 / 705 / &
    136.19 / 485.4
PVAL BENZOATE 0.47828 / 0.203 / 0.488 / 2520816.7 / 728 / &
    164.2 / 517.7
PVAL METHPHEN 0.46102 / 0.246 / 0.47 / 3376278.4 / 774 / &
    152.19 / 535.5
PVAL ETHYLGUA 0.41259 / 0.251 / 0.47 / 3435911.3 / 773 / &
    152.19 / 528.8
PVAL MESHEPTA 0.54762 / 0.2574 / 0.514 / 2548185.5 / &
    612 / 144.21 / 440.7
PVAL BENZOFUR 0.3387 / 0.2658 / 0.3427 / 4565376.2 / &
    708 / 118.13 / 463.9
PVAL TRIMEBEN 0.21754 / 0.2262 / 0.495 / 2979538.9 / &
    784 / 168.19 / 517.5
PVAL 4PROPGUA 0.43769 / 0.2291 / 0.5282 / 2819517.2 / &
    782 / 166.22 / 546.7
PVAL HMBENZAC 1.0039 / 0.2598 / 0.4072 / 4322565.4 / &
    815 / 168.15 / 601.8
PVAL METOCTAC 0.73784 / 0.2284 / 0.5259 / 2537926.1 / &
    703 / 158.24 / 521.5
PVAL CONIFALC 0.99875 / 0.285 / 0.5478 / 3637734 / 842 / &
    180.2 / 628.7
PVAL ISOEUGEN 0.45588 / 0.2496 / 0.5091 / 3265306.1 / &
    801 / 164.2 / 554.9
PVAL PHENKETO 1.6435 / 0.265 / 0.6475 / 3530463.8 / &
    1036 / 228.24 / 821.3
PVAL XANTHENE 0.50039 / 0.2703 / 0.5345 / 3439942.9 / &
    818 / 182.22 / 569.5
PVAL P-DECANO 0.85566 / 0.215 / 0.9793 / 1323276.3 / &
    725 / 256.42 / 573.1
PVAL DNONDBEN 0.76428 / 0.1691 / 1.2708 / 1021383.6 / &
    923 / 346.59 / 739.1
PVAL PENTACOS 0.66485 / 0.1688 / 1.5472 / 744850.8 / &
    821 / 410.72 / 668.9
PVAL ETMEPHEN 0.39644 / 0.2403 / 0.4535 / 3251158.1 / &
    738 / 136.19 / 504.8
PVAL 1HINDANE 0.28573 / 0.2625 / 0.4316 / 3276530.3 / &
    648 / 124.22 / 431.6
PVAL HYDFLUOR 0.45684 / 0.2174 / 0.728 / 2066115.7 / &
    832 / 218.38 / 600.2
PVAL HYDNAPH 0.48671 / 0.2017 / 0.8215 / 1823166 / 893 / &
    246.43 / 654.5
PVAL C18H28 0.50803 / 0.2063 / 0.8155 / 1964815.6 / 934 / &
    244.41 / 682.8
PVAL C21H24O4 1.267 / 0.176 / 1.008 / 1667333.3 / 1150 / &
    340.41 / 928.3

PROP-DATA USRDEF
  IN-UNITS SI ENTHALPY='J/kg' FLOW='tons/hr' &
    MASS-FLOW='tons/hr' MOLE-FLOW='kmol/hr' &
    VOLUME-FLOW='cum/hr' ENTHALPY-FLO='MJ/hr' POWER=MW &
    PRESSURE=bar TEMPERATURE=C DELTA-T=C ELEC-POWER=kW &
    HEAT=MJ PDROP-PER-HT='mbar/m' PDROP=bar
  PROP-LIST MW
  PVAL 2,2PROPA 222.1062
  PVAL FURACETA 190.1074
  PVAL LEVOGLUC 162.1402
  PVAL 4METGUA 138.1634
  PVAL ETHYLANI 136.1905
  PVAL BENZOATE 164.2006
  PVAL METHPHEN 150.1741
  PVAL ETHYLGUA 152.1899
  PVAL MESHEPTA 144.2108
  PVAL BENZOFUR 118.1324
  PVAL TRIMEBEN 168.1893
  PVAL 4PROPGUA 166.2164
  PVAL HMBENZAC 168.1464
  PVAL METOCTAC 158.2373
  PVAL CONIFALC 180.2
  PVAL ISOEUGEN 164.2006
  PVAL PHENKETO 228.2428
  PVAL XANTHENE 182.2175
  PVAL P-DECANO 256.4228
  PVAL DNONDBEN 362.5874

285

```
    PVAL PENTACOS 410.7143
    PVAL ETMEPHEN 136.1905
    PVAL 1HINDANE 124.2227
    PVAL HYDFLUOR 218.3766
    PVAL HYDNAPH 246.4296
    PVAL C18H28 244.4138
    PVAL C21H24O4 340.4119


;TDE Aly-Lee ideal gas Cp
;  "Heat capacity (Ideal gas )"


PROP-DATA CPIALE-1
    IN-UNITS SI ENTHALPY='J/kg' FLOW='tons/hr'  &
        MASS-FLOW='tons/hr' MOLE-FLOW='kmol/hr'  &
        VOLUME-FLOW='cum/hr' ENTHALPY-FLO='MJ/hr' POWER=MW  &
        PRESSURE=bar DELTA-T=C ELEC-POWER=kW HEAT=MJ  &
        PDROP-PER-HT='mbar/m' PDROP=bar
    PROP-LIST CPIALEE
    PVAL 2,2PROPA 137698.1 218621.5 -544.1935 169902.5  &
        1501.607 0 8.31447 200 980
    PVAL FURACETA 115575.8 332367.1 -1071.789 158128 469.2106  &
        0 8.31447 200 980
    PVAL LEVOGLUC 78091.61 390113.5 -1091.194 203807.7  &
        483.9263 0 8.31447 200 980
    PVAL 4METGUA 106668.5 183816.5 582.2055 233911.4 1601.986  &
        0 8.31447 200 980
    PVAL ETHYLANI 103820.7 211199.9 -579.3748 256405.2  &
        1613.109 0 8.31447 200 980
    PVAL BENZOATE 109240.6 442645.3 -1206.206 222387.8  &
        531.3527 0 8.31447 200 980
    PVAL METHPHEN 119005.5 416647.3 -1259.579 201536.5  &
        551.1287 0 8.31447 200 980
    PVAL ETHYLGUA 114405.5 413017.9 -1234.497 205393.8  &
        542.0799 0 8.31447 200 980
    PVAL MESHEPTA 124368.6 236227.8 -573.7299 268540.8  &
        1601.317 0 8.31447 200 980
    PVAL BENZOFUR 46632.57 182580.1 535.8457 136293 1502.345  &
        0 8.31447 200 980
    PVAL TRIMEBEN 143384.5 425594.4 -1297.92 185405.4 565.0798  &
        0 8.31447 200 980
    PVAL 4PROPGUA 165397.3 360332.2 -846.646 21637.34  &
        -0.000000715800 0 8.31447 200 980
    PVAL HMBENZAC 117770.7 189350.5 -570.6729 217673.2 1566.56  &
        0 8.31447 200 980
    PVAL METOCTAC 122786.7 504214.8 -1222.761 286387.9  &
        540.3215 0 8.31447 200 980
    PVAL CONIFALC 141420.9 455488.7 -596.9693 -284733.5  &
        663.2716 0 8.31447 200 980
    PVAL ISOEUGEN 130022.5 451489 -1291.186 203652.4 562.5015  &
        0 8.31447 200 980
    PVAL PHENKETO 131247 533439.8 -1087.171 276223.9 484.9875  &
        0 8.31447 200 980
    PVAL XANTHENE 71817.49 470607.3 -1110.971 275660.8  &
        500.0295 0 8.31447 200 980
    PVAL P-DECANO 217794.8 857859.5 -573.9929 -470131.1  &
        -650.0583 0 8.31447 200 980
    PVAL DNONDBEN 278973 1187680 1210.835 651069.4 -535.2941  &
        0 8.31447 200 980
    PVAL PENTACOS 371376.5 801163.7 567.679 834156.3 -1599.763  &
        0 8.31447 200 980
    PVAL ETMEPHEN 94262.85 405125.6 -1217.575 212822.3  &
        536.8179 0 8.31447 200 980
    PVAL 1HINDANE 59203.35 529403.1 594.9684 -302355.3  &
        678.1469 0 8.31447 200 980
    PVAL HYDFLUOR 90475.47 892137.7 -1231.118 488780.8  &
        539.8448 0 8.31447 200 980
    PVAL HYDNAPH 123263.4 1025614 -587.5583 -585584.3  &
        -664.9991 0 8.31447 200 980
    PVAL C18H28 531883 594114.3 -1317.093 -794690.9 -192.0775  &
        0 8.31447 200 980
    PVAL C21H24O4 257866.4 471160.4 -581.701 597186 -1601.02  &
        0 8.31447 200 980
```

```
PROP-DATA CPIG-1
  IN-UNITS SI ENTHALPY='J/kg' FLOW='tons/hr'  &
    MASS-FLOW='tons/hr' MOLE-FLOW='kmol/hr'  &
    VOLUME-FLOW='cum/hr' ENTHALPY-FLO='MJ/hr' POWER=MW  &
    PRESSURE=bar TEMPERATURE=C DELTA-T=C ELEC-POWER=kW  &
    HEAT=MJ PDROP-PER-HT='mbar/m' PDROP=bar
  PROP-LIST CPIG
  PVAL 2,2PROPA 2.02099894E+5 484.8412141 -.3930160200  &
    1.16400000E-4 0.0 0.0 6.850000000 826.8500000  &
    36029.20000 36.14999940 1.500000000
  PVAL FURACETA 1.75162505E+5 434.0888657 -.3552285350  &
    1.13700000E-4 0.0 0.0 6.850000000 826.8500000  &
    36029.20000 30.32683060 1.500000000
  PVAL BENZOFUR 1.05732347E+5 449.0814805 -.4544221800  &
    2.07600000E-4 0.0 0.0 6.850000000 826.8500000  &
    36029.20000 4.908866340 1.704385280
  PVAL TRIMEBEN 2.02961688E+5 666.8379964 -.7063580576  &
    3.30477068E-4 0.0 0.0 6.850000000 826.8500000  &
    36029.20000 36.59689510 1.500000000
  PVAL HMBENZAC 1.58372758E+5 535.5955077 -.4917393044  &
    1.87022860E-4 0.0 0.0 6.850000000 826.8500000  &
    36029.20000 26.89037560 1.500000000
  PVAL CONIFALC 2.07873595E+5 665.4883069 -.6680130821  &
    2.96411366E-4 0.0 0.0 6.850000000 826.8500000  &
    36029.20000 37.64366930 1.500000000
  PVAL PHENKETO 2.36634840E+5 830.8266717 -.8113957362  &
    3.38394501E-4 0.0 0.0 6.850000000 826.8500000  &
    36029.20000 44.02258310 1.500000000
  PVAL DNONDBEN 4.79660380E+5 1658.348866 -1.255967309  &
    3.94417379E-4 0.0 0.0 6.850000000 826.8500000  &
    36029.20000 97.09782480 1.500000000
  PVAL PENTACOS 5.85246943E+5 1918.205462 -1.195785215  &
    2.25695619E-4 0.0 0.0 6.850000000 826.8500000  &
    36029.20000 120.0140600 1.500000000
  PVAL 1HINDANE 1.24498218E+5 759.9262881 -.5005890137  &
    1.00432765E-4 0.0 0.0 6.850000000 826.8500000  &
    36029.20000 .2894243010 2.251582290
  PVAL C18H28 2.94949116E+5 1335.544176 -.9456487627  &
    2.33060940E-4 0.0 0.0 6.850000000 826.8500000  &
    36029.20000 57.20536920 1.500000000
  PVAL C21H24O4 4.01255857E+5 1395.592489 -1.420384063  &
    6.35669384E-4 0.0 0.0 6.850000000 826.8500000  &
    36029.20000 79.97787350 1.500000000

;TDE equation for liquid Cp
;  "Heat capacity (Liquid vs. Gas )"


PROP-DATA CPLTDE-1
  IN-UNITS SI ENTHALPY='J/kg' FLOW='tons/hr'  &
    MASS-FLOW='tons/hr' MOLE-FLOW='kmol/hr'  &
    VOLUME-FLOW='cum/hr' ENTHALPY-FLO='MJ/hr' POWER=MW  &
    PRESSURE=bar DELTA-T=C ELEC-POWER=kW HEAT=MJ  &
    PDROP-PER-HT='mbar/m' PDROP=bar
  PROP-LIST CPLTDECS
  PVAL ETHYLANI 177782.3 32.82786 0.7357385 -0.0006021932  &
    5269.055 705 4 250 690
  PVAL BENZOATE 227438 -59.01253 0.9554111 -0.0007413349  &
    5713.238 728 4 250 713.44
  PVAL MESHEPTA 247442.9 -170.193 1.306971 -0.001103748  &
    5904.563 612 4 250 599.76
  PVAL HMBENZAC 478885.9 -892.6725 1.945207 -0.001197195  &
    7865.212 815 4 250 798.7
  PVAL METOCTAC 308293 -176.4044 1.293204 -0.001027442  &
    6693.357 703 4 250 688.94
  PVAL P-DECANO 377158.6 195.7698 1.325854 -0.001143662  &
    7127.312 725 4 250 710
  PVAL DNONDBEN 357781.1 976.4599 0.4292013 -0.0005860542  &
    7128.322 923 4 250 904.54
  PVAL ETMEPHEN 181113 55.74555 0.6854389 -0.0005670554  &
    5407.139 738 4 250 723.24
  PVAL 1HINDANE 68277.67 379.2323 0.4260128 -0.0004965524  &
    4954.54 648 4 250 635.04
  PVAL HYDNAPH 248338.6 502.0749 0.8646289 -0.0007476392  &
```

287

```
        7015.405 893 4 250 875.14

;TDE Watson equation for heat of vaporization
;  "Enthalpy of vaporization or sublimation (Liquid vs. Gas )"


PROP-DATA DHVLTD-1
    IN-UNITS SI ENTHALPY='J/kg' FLOW='tons/hr'  &
        MASS-FLOW='tons/hr' MOLE-FLOW='kmol/hr'  &
        VOLUME-FLOW='cum/hr' ENTHALPY-FLO='MJ/hr' POWER=MW  &
        PRESSURE=bar DELTA-T=C ELEC-POWER=kW HEAT=MJ  &
        PDROP-PER-HT='mbar/m' PDROP=bar
    PROP-LIST DHVLTDEW
    PVAL 4METGUA 18.22517 0.7805989 -0.5350756 0.1849547 764  &
        4 255 764
    PVAL ETHYLANI 17.99378 0.2893352 0.1805757 -0.01336794 705  &
        4 255 705
    PVAL METHPHEN 18.42221 1.246724 -1.317909 0.5369594 774 4  &
        255 774
    PVAL ETHYLGUA 18.31086 0.9901106 -0.8889284 0.3514099 773  &
        4 255 773
    PVAL MESHEPTA 17.94117 -0.1444003 1.032577 -0.4999111 612  &
        4 255 612
    PVAL BENZOFUR 18.08832 0.8067804 -0.6358534 0.2456707 708  &
        4 255 708
    PVAL METOCTAC 18.39381 0.3657079 0.2924482 -0.1906876 703  &
        4 255 703
    PVAL ISOEUGEN 18.4582 1.276996 -1.37441 0.5644197 801 4  &
        255 801
    PVAL XANTHENE 18.54069 1.315794 -1.381448 0.5349857 818 4  &
        255 818
    PVAL P-DECANO 18.2923 -0.7950066 2.491153 -1.264942 725 4  &
        255 725
    PVAL PENTACOS 18.33069 -0.4774254 1.816581 -0.843234 821  &
        4 255 821
    PVAL ETMEPHEN 18.14396 0.536578 -0.1258857 0.01750625 738  &
        4 255 738
    PVAL 1HINDANE 17.91305 0.7622159 -0.6416303 0.2871541 648  &
        4 255 648
    PVAL HYDFLUOR 18.56138 1.612651 -2.025089 0.8929773 832 4  &
        255 832
    PVAL FURACETA 19.55678 0.5927808 0.4683948 -0.585868 1155  &
        4 255 1155
    PVAL TRIMEBEN 17.95408 0.4574411 -0.1344849 0.09978933 784  &
        4 255 784
    PVAL 4PROPGUA 18.42429 1.349653 -1.548551 0.6683224 782 4  &
        255 782
    PVAL HMBENZAC 18.82319 0.4490038 0.573104 -0.5822868 815  &
        4 255 815
    PVAL PHENKETO 19.37654 -0.08833373 1.885669 -1.39057 1036  &
        4 255 1036
    PVAL HYDNAPH 18.71492 1.85766 -2.453337 1.094502 893 4  &
        255 893
    PVAL C18H28 18.76675 1.768587 -2.262759 0.9893689 934 4  &
        255 934

PROP-DATA DHVLWT-1
    IN-UNITS SI ENTHALPY='J/kg' FLOW='tons/hr'  &
        MASS-FLOW='tons/hr' MOLE-FLOW='kmol/hr'  &
        VOLUME-FLOW='cum/hr' ENTHALPY-FLO='MJ/hr' POWER=MW  &
        PRESSURE=bar TEMPERATURE=C DELTA-T=C ELEC-POWER=kW  &
        HEAT=MJ PDROP-PER-HT='mbar/m' PDROP=bar
    PROP-LIST DHVLWT
    PVAL ASH 2.99349255E+8 3396.850000 .4439946020 -.1498359780  &
        3396.850000
    PVAL 2,2PROPA 8.96231837E+7 380.3500000 .3830999540  &
        -.9988059080 380.3500000
    PVAL FURACETA 1.32042764E+8 604.3500000 .3765749010  &
        -.8914217440 604.3500000
    PVAL BENZOFUR 4.28075664E+7 190.7500000 .4360162600  &
        -.1990379640 190.7500000
    PVAL TRIMEBEN 4.13432720E+7 244.3500000 .4415970230  &
        -.1708285790 244.3500000
    PVAL HMBENZAC 7.31657429E+7 328.6500000 .4030745930  &
```

288

```
      -.5907993560 328.6500000
   PVAL CONIFALC 7.46218293E+7 355.5500000 .4039364140  &
      -.6115250380 355.5500000
   PVAL PHENKETO 1.17201103E+8 548.1500000 .3781480280  &
      -1.074490540 548.1500000
   PVAL DNONDBEN 6.47097597E+7 465.9500000 .4213322850  &
      -.6500312490 465.9500000
   PVAL PENTACOS 5.19098250E+7 395.7500000 .4277789000  &
      -.6389589320 395.7500000
   PVAL 1HINDANE 3.66185342E+7 158.4500000 .4387399660  &
      -.1899371700 158.4500000
   PVAL C18H28 6.00611363E+7 409.6500000 .4292143960  &
      -.3458524550 409.6500000
   PVAL C21H24O4 1.07469599E+8 655.1500000 .3984421130  &
      -.9550844420 655.1500000

;TDE Rackett parameters for liquid mass density
;  "Density (Liquid vs. Gas )"


PROP-DATA DNLRAC-1
   IN-UNITS SI ENTHALPY='J/kg' FLOW='tons/hr'  &
      MASS-FLOW='tons/hr' MOLE-FLOW='kmol/hr'  &
      VOLUME-FLOW='cum/hr' ENTHALPY-FLO='MJ/hr' POWER=MW  &
      PRESSURE=bar DELTA-T=C ELEC-POWER=kW HEAT=MJ  &
      PDROP-PER-HT='mbar/m' PDROP=bar
   PROP-LIST DNLRACK
   PVAL LEVOGLUC 0.2490633 0.2857143 857 5695977 110 857
   PVAL 4METGUA 0.2538818 0.2857143 764 3857876 100 764
   PVAL ETHYLANI 0.234192 0.2857143 705 2816352 100 705
   PVAL METHPHEN 0.2480427 0.2857143 774 3376278 100 774
   PVAL ETHYLGUA 0.2524382 0.2857143 773 3435911 100 773
   PVAL MESHEPTA 0.2426968 0.2857143 612 2548186 110 612
   PVAL BENZOFUR 0.2632219 0.2857143 708 4565376 100 708
   PVAL METOCTAC 0.2327796 0.2857143 703 2537926 110 703
   PVAL ISOEUGEN 0.2494821 0.2857143 801 3265306 100 801
   PVAL XANTHENE 0.2573441 0.2857143 818 3439943 110 818
   PVAL P-DECANO 0.2107584 0.2857143 725 1323276 110 725
   PVAL DNONDBEN 0.2056481 0.2857143 923 1021384 739.1079  &
      923
   PVAL PENTACOS 0.1943733 0.2857143 821 744850.8 100 821
   PVAL ETMEPHEN 0.2461575 0.2857143 738 3251158 100 738
   PVAL 1HINDANE 0.2631359 0.2857143 648 3276530 100 648
   PVAL HYDFLUOR 0.2312098 0.2857143 832 2066116 100 832
   PVAL 2,2PROPA 0.203972 0.2857143 829 3325377 110 829
   PVAL FURACETA 0.2405901 0.2857143 1155 6841438 110 1155
   PVAL TRIMEBEN 0.2438564 0.2857143 784 2979539 100 784
   PVAL 4PROPGUA 0.2383079 0.2857143 782 2819517 100 782
   PVAL HMBENZAC 0.2465032 0.2857143 815 4322565 110 815
   PVAL PHENKETO 0.2372971 0.2857143 1036 3530464 110 1036
   PVAL HYDNAPH 0.2215056 0.2857143 893 1823166 100 893
   PVAL C18H28 0.2240741 0.2857143 934 1964816 110 934
   PVAL C21H24O4 0.2059641 0.2857143 1150 1667333 928.34  &
      1150

PROP-DATA KLDIP-1
   IN-UNITS SI ENTHALPY='J/kg' FLOW='tons/hr'  &
      MASS-FLOW='tons/hr' MOLE-FLOW='kmol/hr'  &
      VOLUME-FLOW='cum/hr' ENTHALPY-FLO='MJ/hr' POWER=MW  &
      PRESSURE=bar TEMPERATURE=C DELTA-T=C ELEC-POWER=kW  &
      HEAT=MJ PDROP-PER-HT='mbar/m' PDROP=bar
   PROP-LIST KLDIP
   PVAL ASH -.7231763262 9.05163118E-4 -3.3466196E-7  &
      5.3064504E-11 -3.172466E-15 3396.850000 5686.650000
   PVAL 2,2PROPA -1.148009436 .0116487890 -4.0578678E-5  &
      6.19166737E-8 -3.559808E-11 380.3500000 547.5600000
   PVAL FURACETA -1.399365564 8.84034873E-3 -1.9340941E-5  &
      1.85507624E-8 -6.700659E-12 604.3500000 870.3000000
   PVAL BENZOFUR .0458530981 1.22518328E-3 -7.8925307E-6  &
      1.90945977E-8 -1.759409E-11 190.7500000 427.7700000
   PVAL TRIMEBEN -2.3466286E-3 1.37848027E-3 -6.9047407E-6  &
      1.36849067E-8 -1.029900E-11 244.3500000 503.0100000
   PVAL HMBENZAC -.3981090922 5.28705423E-3 -2.0542769E-5  &
      3.42663335E-8 -2.158608E-11 328.6500000 533.7000000
```

```
    PVAL CONIFALC -.5214343024 6.10109238E-3 -2.2090805E-5 &
        3.45534117E-8 -2.039733E-11 355.5500000 560.4300000
    PVAL PHENKETO -2.078323620 .0143182863 -3.5134755E-5 &
        3.79738429E-8 -1.544720E-11 548.1500000 752.4900000
    PVAL DNONDBEN -1.551645952 .0126116910 -3.6408226E-5 &
        4.62780458E-8 -2.214355E-11 465.9500000 640.6200000
    PVAL PENTACOS -1.517138710 .0145422451 -4.9607836E-5 &
        7.45463247E-8 -4.217237E-11 395.7500000 539.6400000
    PVAL 1HINDANE .0593087543 1.12295569E-3 -8.7903593E-6 &
        2.50763755E-8 -2.729863E-11 158.4500000 368.3700000
    PVAL C18H28 -.4300658451 4.38087570E-3 -1.3717278E-5 &
        1.85350504E-8 -9.450934E-12 409.6500000 651.5100000
    PVAL C21H24O4 -2.784213728 .0159693689 -3.3231015E-5 &
        3.05537204E-8 -1.056615E-11 655.1500000 865.3500000


;ThermoML polynomials for liquid thermal conductivity
;  "Thermal conductivity (Liquid vs. Gas )"


PROP-DATA KLTMLP-1
    IN-UNITS SI ENTHALPY='J/kg' FLOW='tons/hr'  &
        MASS-FLOW='tons/hr' MOLE-FLOW='kmol/hr'  &
        VOLUME-FLOW='cum/hr' ENTHALPY-FLO='MJ/hr' POWER=MW  &
        PRESSURE=bar DELTA-T=C ELEC-POWER=kW HEAT=MJ  &
        PDROP-PER-HT='mbar/m' PDROP=bar
    PROP-LIST KLTMLPO
    PVAL LEVOGLUC 0.3596188 -0.0005070721 0.000000349315  &
        -8.851801E-11 4 200 770
    PVAL 4METGUA 0.1837219 -0.0001702441 0.0000000786038 0 4  &
        200 680
    PVAL ETHYLANI 0.1713116 -0.00004189719 -0.000000161692 0 4  &
        200 630
    PVAL BENZOATE 0.1580841 -0.00004147571 -0.000000136416 0 4  &
        200 650
    PVAL METHPHEN 0.1748623 -0.0001701696 0.0000000792732 0 4  &
        200 690
    PVAL ETHYLGUA 0.1872094 -0.0001777998 0.0000000821860 0 4  &
        200 690
    PVAL MESHEPTA 0.17481 -0.00003586302 -0.000000244228 0 4  &
        200 550
    PVAL BENZOFUR 0.2099223 -0.00005051182 -0.000000193434 0 4  &
        200 630
    PVAL TRIMEBEN 0.1812111 -0.00004417639 -0.000000130921 0 4  &
        200 700
    PVAL 4PROPGUA 0.1930989 -0.0001906821 0.0000000887184 0 4  &
        200 700
    PVAL HMBENZAC 0.2433344 -0.0002823153 0.000000167939  &
        -3.096414E-11 4 200 730
    PVAL METOCTAC 0.1816364 -0.0000484879 -0.000000172905 0 4  &
        200 630
    PVAL CONIFALC 0.2635977 -0.0003082088 0.0000001844644  &
        -3.631424E-11 4 200 750
    PVAL ISOEUGEN 0.2000758 -0.0001945417 0.0000000995691  &
        -1.046157E-11 4 200 720
    PVAL PHENKETO 0.3552677 -0.0004289123 0.0000002539359  &
        -5.689867E-11 4 200 930
    PVAL XANTHENE 0.1923009 -0.000178608 0.0000001838991  &
        -2.053421E-10 4 200 730
    PVAL P-DECANO 0.1938491 -0.00005894714 -0.000000168249 0 4  &
        200 650
    PVAL DNONDBEN 0.2468004 -0.0003481122 0.0000002366787  &
        -6.080724E-11 4 200 830
    PVAL PENTACOS 0.2106489 -0.0002022289 0.0000001881003  &
        -2.104826E-10 4 200 730
    PVAL ETMEPHEN 0.1710547 -0.0001700213 0.0000000822211 0 4  &
        200 660
    PVAL 1HINDANE 0.14572 -0.00003044837 -0.000000173117 0 4  &
        200 580
    PVAL HYDFLUOR 0.1494931 -0.00013519 0.0000001315982  &
        -1.468795E-10 4 200 740
    PVAL HYDNAPH 0.1493113 -0.0001254363 0.0000001131146  &
        -1.187503E-10 4 200 800
    PVAL C18H28 0.1576565 -0.0001258627 0.0000001085015  &
        -1.096786E-10 4 200 840
```

290

```
  PVAL C21H24O4 0.294846 -0.0003494466 0.0000001998584 &
    -4.426214E-11 4 200 1030
  PVAL 2,2PROPA 0.305455 -0.0002887919 0.0000002761471 &
    -0.000000000304 4 200 740
  PVAL FURACETA 0.3416759 -0.0003131665 0.0000001476676 &
    -2.520539E-11 4 200 1030
```

;ThermoML polynomials for vapor thermal conductivity
; "Thermal conductivity (Gas)"


```
PROP-DATA KVTMLP-1
  IN-UNITS SI ENTHALPY='J/kg' FLOW='tons/hr'  &
    MASS-FLOW='tons/hr' MOLE-FLOW='kmol/hr'  &
    VOLUME-FLOW='cum/hr' ENTHALPY-FLO='MJ/hr' POWER=MW  &
    PRESSURE=bar DELTA-T=C ELEC-POWER=kW HEAT=MJ  &
    PDROP-PER-HT='mbar/m' PDROP=bar
  PROP-LIST KVTMLPO
  PVAL LEVOGLUC 0.0005938022 -0.000002045764 0.0000000265607 &
    -1.11499E-11 4 680 1280
  PVAL 4METGUA 0.004121693 -0.00001765223 0.0000001415443 &
    -5.846255E-11 4 520 1140
  PVAL ETHYLANI 0.002307927 -0.00001087078 0.0000001301311 &
    -5.375605E-11 4 490 1050
  PVAL METHPHEN 0.004438849 -0.00001797089 0.000000134317 &
    -5.469159E-11 4 540 1160
  PVAL ETHYLGUA 0.003057483 -0.00001233924 0.0000001321243 &
    -5.437276E-11 4 530 1150
  PVAL MESHEPTA -0.01383466 0.00006877538 0.0000000180988 0 &
    4 450 910
  PVAL BENZOFUR -0.007123394 0.0000287473 0.0000000841968 &
    -3.71125E-11 4 470 1060
  PVAL TRIMEBEN 0.008700291 -0.00003592121 0.0000001535446 &
    -6.27738E-11 4 520 1170
  PVAL 4PROPGUA 0.001940316 -0.000006923775 0.0000001154304 &
    -4.730223E-11 4 550 1170
  PVAL HMBENZAC 0.0008147167 -0.000000933616 0.0000000585278 &
    -2.431255E-11 4 610 1220
  PVAL METOCTAC -0.00308434 0.00001686703 0.0000000677869 &
    -2.729796E-11 4 530 1050
  PVAL CONIFALC 0.005502489 -0.00002085678 0.0000000847277 &
    -3.434256E-11 4 630 1260
  PVAL ISOEUGEN 0.008625234 -0.00003652334 0.0000001545196 &
    -6.241316E-11 4 560 1200
  PVAL XANTHENE -0.01080283 0.00004381742 0.0000000458225 &
    -1.916649E-11 4 570 1220
  PVAL P-DECANO -0.01285285 0.0000529393 -1.380344E-10 0 4 &
    580 1080
  PVAL DNONDBEN -0.006123024 0.00002448935 0.0000000261178 &
    -1.058156E-11 4 740 1380
  PVAL PENTACOS -0.003980825 0.00001892401 0.0000000413680 &
    -1.661394E-11 4 670 1230
  PVAL ETMEPHEN 0.00009690978 -0.000001188253 0.0000001215958 &
    -5.008658E-11 4 510 1100
  PVAL 1HINDANE 0.000450265 -0.00001747779 0.0000001937659 &
    -7.868177E-11 4 440 970
  PVAL HYDFLUOR -0.003707446 0.000007438802 0.0000001037873 &
    -4.016023E-11 4 610 1240
  PVAL 2,2PROPA -0.002707634 0.00001381225 0.0000000050713 &
    -2.246371E-12 4 660 1240
  PVAL FURACETA 0.006540863 0.00000835154 0 0 4 880 1730
  PVAL BENZOATE 0.00250521 -0.0000111376 0.0000001153016 &
    -4.868136E-11 4 520 1090
  PVAL PHENKETO -0.006285345 0.00002062107 2.817302E-11 &
    -1.556088E-12 4 830 1550
  PVAL HYDNAPH -0.00428024 0.000008878278 0.0000000922069 &
    -3.538065E-11 4 660 1330
  PVAL C18H28 -0.0056991 0.00001209087 0.0000000858701 &
    -3.31964E-11 4 690 1400
  PVAL C21H24O4 0.002819617 0.0000125033 0 0 4 930 1720

PROP-DATA MULAND-1
  IN-UNITS SI ENTHALPY='J/kg' FLOW='tons/hr'  &
    MASS-FLOW='tons/hr' MOLE-FLOW='kmol/hr'  &
```

```
        VOLUME-FLOW='cum/hr' ENTHALPY-FLO='MJ/hr' POWER=MW  &
        PRESSURE=bar TEMPERATURE=C DELTA-T=C ELEC-POWER=kW  &
        HEAT=MJ PDROP-PER-HT='mbar/m' PDROP=bar
      PROP-LIST MULAND
      PVAL CHAR 113.2909210 -50044.15760 -12.98075030 3929.850000  &
        6468.750000
      PVAL ASH 67.56957070 -27259.04230 -8.432322050 3396.850000  &
        5686.650000
      PVAL DIBEN-01 109.5031220 -8189.135310 -16.27699180  &
        285.1600000 542.6100000
      PVAL 2,2PROPA -11.51029580 3693.000010 1.07177615E-8  &
        380.3500000 485.6500000
      PVAL FURACETA -18.32913660 6602.999990 -1.1120789E-8  &
        604.3500000 770.8500000
      PVAL 4METGUA -14.00747530 2888.000040 7.39423526E-8  &
        240.8500000 299.8500000
      PVAL ETHYLGUA -14.29410600 2986.999920 -1.4437421E-7  &
        255.6500000 306.6000000
      PVAL BENZOFUR -10.68973170 1169.000010 1.52871108E-8  &
        190.7500000 257.8500000
      PVAL TRIMEBEN -12.07067440 1771.999970 -5.8249181E-8  &
        244.3500000 314.8500000
      PVAL HMBENZAC -13.74181240 3559.000000 0.0 328.6500000  &
        338.1000000
      PVAL CONIFALC -16.19379500 4587.485160 -.0135135135  &
        355.5500000 358.3500000
      PVAL PHENKETO -16.32898380 5213.000010 1.21079093E-8  &
        548.1500000 676.9700000
      PVAL DNONDBEN -16.34227560 4436.999970 -3.1710131E-8  &
        465.9500000 576.2900000
      PVAL PENTACOS -14.62296590 3269.000000 0.0 395.7500000  &
        487.0100000
      PVAL 1HINDANE -11.70959520 1518.000010 2.53530620E-8  &
        158.4500000 212.8500000
      PVAL C18H28 -13.40977030 2697.000000 0.0 409.6500000  &
        427.3500000
      PVAL C21H24O4 -15.78291020 4449.000010 8.17138330E-9  &
        655.1500000 788.1700000

;TDE equation for liquid viscosity
;  "Viscosity (Liquid vs. Gas )"


PROP-DATA MULNVE-1
    IN-UNITS SI ENTHALPY='J/kg' FLOW='tons/hr'  &
        MASS-FLOW='tons/hr' MOLE-FLOW='kmol/hr'  &
        VOLUME-FLOW='cum/hr' ENTHALPY-FLO='MJ/hr' POWER=MW  &
        PRESSURE=bar DELTA-T=C ELEC-POWER=kW HEAT=MJ  &
        PDROP-PER-HT='mbar/m' PDROP=bar
      PROP-LIST MULNVE
      PVAL ETHYLANI -11.11388 785.7908 279477.6 -23909350 270  &
        700
      PVAL ETHYLGUA -12.50654 1778.306 330827.8 -27387560 296  &
        770
      PVAL MESHEPTA -15.2437 5424.683 -1411657 160198900 270  &
        610
      PVAL TRIMEBEN -10.63146 226.0935 647099.6 -66589460 296.25  &
        780
      PVAL 4PROPGUA -12.30112 1578.23 460199 -43942410 296.25  &
        780
      PVAL PENTACOS -12.20113 3103.449 -442236.1 64879160 297.25  &
        820
      PVAL 1HINDANE -10.95791 849.9327 144884.1 -6113018 270  &
        640
      PVAL HYDFLUOR -11.04944 834.3223 504525.2 -55943680 297.5  &
        830
      PVAL C18H28 -10.59475 1350.544 650303.8 -76976670 300 930

;PPDS9 equation for liquid viscosity
;  "Viscosity (Liquid vs. Gas )"


PROP-DATA MULPPD-1
    IN-UNITS SI ENTHALPY='J/kg' FLOW='tons/hr'  &
```

```
        MASS-FLOW='tons/hr' MOLE-FLOW='kmol/hr'  &
        VOLUME-FLOW='cum/hr' ENTHALPY-FLO='MJ/hr' POWER=MW  &
        PRESSURE=bar DELTA-T=C ELEC-POWER=kW HEAT=MJ  &
        PDROP-PER-HT='mbar/m' PDROP=bar
    PROP-LIST MULPPDS9
    PVAL 4METGUA 0.00003236762 1.199874 2.793305 813.6119  &
        -44.46721 295.75 760
    PVAL BENZOATE 0.000004722919 3.305603 -0.03511997 999.012  &
        212.1278 294.75 720
    PVAL METHPHEN 0.000006469081 1.423727 1.052454 1472.569  &
        -18.52627 296 770
    PVAL BENZOFUR 0.00006653043 0.8956007 1.544681 779.0914  &
        -26.07742 270 700
    PVAL HMBENZAC 0.000001201718 5.347522 2.016434 989.6698  &
        16.87051 297 783
    PVAL METOCTAC 0.00002562171 1.943092 1.49981 863.3182  &
        -9.946922 294.25 700
    PVAL ISOEUGEN 0.00003312395 1.222142 2.999606 854.5664  &
        -53.43762 296.75 800
    PVAL XANTHENE 0.00006061779 1.188181 2.355939 889.3205  &
        -49.46251 297 783
    PVAL P-DECANO 0.00002721162 2.543035 0.6953508 802.7461  &
        55.57628 294.75 720
    PVAL DNONDBEN 0.00006987433 1.104093 3.375708 1020.607  &
        -83.16462 359.25 920
    PVAL ETMEPHEN 0.000057634 0.9696675 2.717398 769.8351  &
        -48.90768 295 730
    PVAL HYDNAPH 0.0001258932 -1.473876 0.3437652 4440.738  &
        -79.78578 299 890
    PVAL C18H28 0.00007076935 1.548173 2.084441 1052.064  &
        -47.80882 300 900
    PVAL C21H24O4 0.00004930419 2.169842 3.012604 1215.115  &
        -62.83628 516.75 1140

PROP-DATA MUVDIP-1
    IN-UNITS SI ENTHALPY='J/kg' FLOW='tons/hr'  &
        MASS-FLOW='tons/hr' MOLE-FLOW='kmol/hr'  &
        VOLUME-FLOW='cum/hr' ENTHALPY-FLO='MJ/hr' POWER=MW  &
        PRESSURE=bar TEMPERATURE=C DELTA-T=C ELEC-POWER=kW  &
        HEAT=MJ PDROP-PER-HT='mbar/m' PDROP=bar
    PROP-LIST MUVDIP
    PVAL 2,2PROPA 2.12392389E-8 .9734476780 0.0 0.0 0.0  &
        6.850000000 826.8500000
    PVAL FURACETA 2.15504795E-8 .9947970940 0.0 0.0 0.0  &
        6.850000000 826.8500000
    PVAL TRIMEBEN 2.40011256E-8 .9682210750 0.0 0.0 0.0  &
        6.850000000 826.8500000
    PVAL HMBENZAC 2.30082984E-8 .9719082650 0.0 0.0 0.0  &
        6.850000000 826.8500000
    PVAL CONIFALC 2.12612376E-8 .9748120660 0.0 0.0 0.0  &
        6.850000000 826.8500000
    PVAL PHENKETO 1.70200214E-8 .9894423320 0.0 0.0 0.0  &
        6.850000000 826.8500000
    PVAL DNONDBEN 1.36205549E-8 .9820779480 0.0 0.0 0.0  &
        6.850000000 826.8500000
    PVAL PENTACOS 1.29844071E-8 .9725771500 0.0 0.0 0.0  &
        6.850000000 826.8500000
    PVAL 1HINDANE 3.07458937E-8 .9462800490 0.0 0.0 0.0  &
        6.850000000 826.8500000
    PVAL C18H28 1.68708077E-8 .9829206990 0.0 0.0 0.0  &
        6.850000000 826.8500000

;ThermoML polynomials for vapor viscosity
;  "Viscosity (Gas )"


PROP-DATA MUVTML-1
    IN-UNITS SI ENTHALPY='J/kg' FLOW='tons/hr'  &
        MASS-FLOW='tons/hr' MOLE-FLOW='kmol/hr'  &
        VOLUME-FLOW='cum/hr' ENTHALPY-FLO='MJ/hr' POWER=MW  &
        PRESSURE=bar DELTA-T=C ELEC-POWER=kW HEAT=MJ  &
        PDROP-PER-HT='mbar/m' PDROP=bar
    PROP-LIST MUVTMLPO
    PVAL LEVOGLUC -0.000001281815 0.0000000282794 -2.450495E-12  &
```

```
          -3.14303E-16 4 680 1280
   PVAL 4METGUA -0.000000617518 0.0000000219059 -9.409513E-13 &
          -8.152437E-16 4 520 1140
   PVAL ETHYLANI -0.000000535558 0.0000000194918 -1.061825E-12 &
          -7.796186E-16 4 490 1050
   PVAL METHPHEN -0.000000647835 0.0000000209245 -1.124165E-12 &
          -6.55604E-16 4 540 1160
   PVAL ETHYLGUA -0.000000608468 0.0000000210266 -9.272177E-13 &
          -7.506187E-16 4 530 1150
   PVAL MESHEPTA -0.000000861825 0.0000000236917 -3.762639E-12 &
          0 4 450 910
   PVAL BENZOFUR -0.000000598375 0.0000000245764 -9.060915E-13 &
          -1.172964E-15 4 470 1060
   PVAL TRIMEBEN -0.000000522294 0.0000000195652 -6.204097E-13 &
          -7.761144E-16 4 520 1170
   PVAL 4PROPGUA -0.000000611479 0.0000000192026 -1.065696E-12 &
          -5.710999E-16 4 550 1170
   PVAL HMBENZAC -0.000000962315 0.0000000249739 -1.854182E-12 &
          -4.730474E-16 4 610 1220
   PVAL METOCTAC -0.000000678705 0.0000000202139 -1.772433E-12 &
          -5.000561E-16 4 530 1050
   PVAL CONIFALC -0.000000882145 0.0000000221818 -1.590212E-12 &
          -3.952398E-16 4 630 1260
   PVAL ISOEUGEN -0.000000658129 0.0000000204349 -1.07413E-12 &
          -5.925121E-16 4 560 1200
   PVAL XANTHENE -0.000000700203 0.0000000216936 -1.054864E-12 &
          -6.295311E-16 4 570 1220
   PVAL P-DECANO -0.000000758345 0.0000000168379 -2.297458E-12 &
          0 4 580 1080
   PVAL DNONDBEN -0.000000602855 0.0000000120981 -1.008313E-12 &
          -1.037565E-16 4 740 1380
   PVAL PENTACOS -0.000000563254 0.0000000122998 -1.217404E-12 &
          -1.079172E-16 4 670 1230
   PVAL ETMEPHEN -0.000000576001 0.0000000203017 -1.01791E-12 &
          -7.581625E-16 4 510 1100
   PVAL 1HINDANE -0.000000538714 0.0000000225731 -1.146618E-12 &
          -1.163751E-15 4 440 970
   PVAL HYDFLUOR -0.000000628059 0.0000000168521 -1.091443E-12 &
          -3.597294E-16 4 610 1240
   PVAL 2,2PROPA -0.00000106374 0.0000000240661 -2.187789E-12 &
          -2.731808E-16 4 660 1240
   PVAL FURACETA -0.00000137394 0.0000000241569 -1.368102E-12 &
          -1.991401E-16 4 880 1730
   PVAL BENZOATE -0.000000597418 0.0000000193565 -1.274066E-12 &
          -6.095518E-16 4 520 1090
   PVAL PHENKETO -0.000001097557 0.0000000196163 -1.457712E-12 &
          -1.331572E-16 4 830 1550
   PVAL HYDNAPH -0.000000618957 0.0000000152018 -9.516386E-13 &
          -2.692522E-16 4 660 1330
   PVAL C18H28 -0.000000651651 0.0000000151294 -9.329136E-13 &
          -2.345406E-16 4 690 1400
   PVAL C21H24O4 -0.000000814159 0.0000000128969 -8.867024E-13 &
          -6.462189E-17 4 930 1720

PROP-DATA PLXANT-1
   IN-UNITS SI ENTHALPY='J/kg' FLOW='tons/hr'  &
      MASS-FLOW='tons/hr' MOLE-FLOW='kmol/hr'  &
      VOLUME-FLOW='cum/hr' ENTHALPY-FLO='MJ/hr' POWER=MW  &
      PRESSURE=bar TEMPERATURE=C DELTA-T=C ELEC-POWER=kW  &
      HEAT=MJ PDROP-PER-HT='mbar/m' PDROP=bar
   PROP-LIST PLXANT
   PVAL ASH 37.53999674 -48457.53140 0.0 0.0 -2.964795110 &
      4.6976791E-24 6.000000000 3396.850000 5746.850000
   PVAL 2,2PROPA 166.1930585 -23661.04430 0.0 0.0  &
      -20.07970600 2.4425851E-18 6.000000000 380.3500000  &
      555.8500000
   PVAL FURACETA 177.5699875 -33638.30490 0.0 0.0  &
      -20.56612350 3.4076714E-19 6.000000000 604.3500000  &
      881.8500000
   PVAL BENZOFUR 51.24455684 -7908.790860 0.0 0.0  &
      -5.571576150 2.4636260E-18 6.000000000 190.7500000  &
      434.8500000
   PVAL TRIMEBEN 39.84986774 -7374.474320 0.0 0.0  &
      -4.097974860 1.1251648E-18 6.000000000 244.3500000  &
```

```
                510.8500000
        PVAL HMBENZAC 116.7785765 -17142.15940 0.0 0.0  &
            -13.80881390 1.9936998E-18 6.000000000 328.6500000  &
            541.8500000
        PVAL CONIFALC 116.8183735 -17679.71570 0.0 0.0  &
            -13.77871590 1.6367718E-18 6.000000000 355.5500000  &
            568.8500000
        PVAL PHENKETO 182.7500715 -31408.49050 0.0 0.0  &
            -21.56250650 6.8112415E-19 6.000000000 548.1500000  &
            762.8500000
        PVAL DNONDBEN 94.34301754 -16273.11690 0.0 0.0  &
            -10.96696000 7.9205682E-19 6.000000000 465.9500000  &
            649.8500000
        PVAL PENTACOS 82.89965204 -13246.01320 0.0 0.0  &
            -9.716948270 1.4634591E-18 6.000000000 395.7500000  &
            547.8500000
        PVAL 1HINDANE 45.53490434 -6742.376610 0.0 0.0  &
            -4.932066140 3.9037812E-18 6.000000000 158.4500000  &
            374.8500000
        PVAL C18H28 69.34049944 -12863.96800 0.0 0.0 -7.745053920  &
            5.7629429E-19 6.000000000 409.6500000 660.8500000
        PVAL C21H24O4 147.3217935 -28672.30790 0.0 0.0  &
            -17.06531610 2.9941618E-19 6.000000000 655.1500000  &
            876.8500000


    PROP-DATA SIGDIP-1
        IN-UNITS SI ENTHALPY='J/kg' FLOW='tons/hr'  &
            MASS-FLOW='tons/hr' MOLE-FLOW='kmol/hr'  &
            VOLUME-FLOW='cum/hr' ENTHALPY-FLO='MJ/hr' POWER=MW  &
            PRESSURE=bar TEMPERATURE=C DELTA-T=C ELEC-POWER=kW  &
            HEAT=MJ PDROP-PER-HT='mbar/m' PDROP=bar
        PROP-LIST SIGDIP
        PVAL CHAR 4.248235070 1.222222220 7.7118801E-11  &
            -8.538668E-11 3.4454565E-11 3929.850000 6400.650000
        PVAL ASH .1392135830 1.222222220 -2.171954E-10  &
            2.3955375E-10 -9.673330E-11 3396.850000 5626.450000
        PVAL EXTRACT .3160042810 1.222222220 2.15197241E-9  &
            -2.4008884E-9 9.1537117E-10 552.2500000 717.7280000
        PVAL 2,2PROPA .1343608000 1.222222220 -1.9838468E-9  &
            2.22489955E-9 -8.595950E-10 380.3500000 539.2700000
        PVAL FURACETA .2494272240 1.222222220 0.0 0.0 0.0  &
            604.3500000 858.7500000
        PVAL BENZOFUR .0796883433 1.222222220 1.58964006E-9  &
            -1.7713879E-9 7.1141489E-10 190.7500000 420.6900000
        PVAL TRIMEBEN .0549800102 1.222222220 -3.987499E-10  &
            4.4529629E-10 -1.786867E-10 244.3500000 495.1700000
        PVAL HMBENZAC .1263239970 1.222222220 -2.3345373E-9  &
            2.62588090E-9 -1.0336454E-9 328.6500000 525.5500000
        PVAL CONIFALC .1133397240 1.222222220 -3.6145812E-9  &
            4.06595486E-9 -1.5960377E-9 355.5500000 552.0100000
        PVAL PHENKETO .1581536370 1.222222220 3.11712788E-9  &
            -3.4930338E-9 1.34629625E-9 548.1500000 742.1300000
        PVAL DNONDBEN .0432187953 1.222222220 3.92353130E-9  &
            -4.3910011E-9 1.68633371E-9 465.9500000 631.3900000
        PVAL PENTACOS .0315011639 1.222222220 4.18324981E-9  &
            -4.6680969E-9 1.78100164E-9 395.7500000 531.4300000
        PVAL 1HINDANE .0588306955 1.222222220 -8.629043E-10  &
            9.6345221E-10 -3.862485E-10 158.4500000 361.8900000
        PVAL C18H28 .0567558932 1.222222220 7.5739453E-10  &
            -8.519710E-10 3.3610975E-10 409.6500000 642.1700000
        PVAL C21H24O4 .0842596923 1.222222220 3.58878886E-9  &
            -4.0114327E-9 1.53618130E-9 655.1500000 853.8500000
        PVAL AIR .0269191085 1.222222220 4.4937381E-10  &
            -4.940123E-10 1.9962172E-10 -194.4800000 -143.3490000


    ;TDE Wagner 25 liquid vapor pressure
    ;  "Vapor pressure (Liquid vs. Gas )"


    PROP-DATA WAGN25-1
        IN-UNITS SI ENTHALPY='J/kg' FLOW='tons/hr'  &
            MASS-FLOW='tons/hr' MOLE-FLOW='kmol/hr'  &
            VOLUME-FLOW='cum/hr' ENTHALPY-FLO='MJ/hr' POWER=MW  &
            DELTA-T=C ELEC-POWER=kW HEAT=MJ PDROP-PER-HT='mbar/m'  &
```

```
    PDROP=bar
  PROP-LIST WAGNER25
  PVAL LEVOGLUC -18.05759 12.38396 -26.81988 -3.393838  &
    15.55527 857 200 857
  PVAL 4METGUA -8.026671 2.094973 -3.346568 -3.475621  &
    15.16563 764 200 764
  PVAL ETHYLANI -7.912998 2.034469 -3.16879 -3.37252  &
    14.85095 705 200 705
  PVAL BENZOATE -8.531791 2.384554 -4.169148 -3.895326  &
    14.74009 728 200 728
  PVAL METHPHEN -8.434461 2.32618 -4.006597 -3.81923  &
    15.03228 774 200 774
  PVAL ETHYLGUA -8.163257 2.169973 -3.563801 -3.595235  &
    15.04979 773 200 773
  PVAL MESHEPTA -8.926947 2.633722 -4.848244 -4.181696  &
    14.75089 612 200 612
  PVAL BENZOFUR -7.755367 1.953499 -2.926872 -3.224116  &
    15.33401 708 200 708
  PVAL TRIMEBEN -7.101823 1.655609 -1.983353 -2.53869  &
    14.90728 784 200 784
  PVAL 4PROPGUA -8.303397 2.249494 -3.790727 -3.713199  &
    14.85208 782 200 782
  PVAL HMBENZAC -11.68248 4.852659 -10.34097 -5.285839  &
    15.27936 815 200 815
  PVAL METOCTAC -10.04282 3.436436 -6.921789 -4.806601  &
    14.74686 703 200 703
  PVAL CONIFALC -11.6496 4.821741 -10.26844 -5.280892  &
    15.10687 842 200 842
  PVAL ISOEUGEN -8.405504 2.309047 -3.958603 -3.796157  &
    14.99886 801 200 801
  PVAL PHENKETO -15.99872 9.655813 -21.03258 -4.55359  &
    15.07694 1036 200 1036
  PVAL XANTHENE -8.657151 2.461504 -4.381288 -3.990062  &
    15.05097 818 200 818
  PVAL P-DECANO -10.75749 4.021291 -8.361084 -5.075614  &
    14.09562 725 200 725
  PVAL DNONDBEN -10.20163 3.561843 -7.234455 -4.874826  &
    13.83667 923 200 923
  PVAL PENTACOS -9.609069 3.107732 -6.089545 -4.594629  &
    13.52094 821 200 821
  PVAL ETMEPHEN -8.073476 2.120393 -3.420568 -3.517131  &
    14.99452 738 200 738
  PVAL 1HINDANE -7.467311 1.814542 -2.49896 -2.936209  &
    15.0023 648 200 648
  PVAL HYDFLUOR -8.410897 2.31223 -3.967529 -3.800469  &
    14.54118 832 200 832
  PVAL HYDNAPH -8.579532 2.413626 -4.249571 -3.931836  &
    14.41609 893 200 893
  PVAL C18H28 -8.700573 2.488616 -4.45549 -4.022027 14.49091  &
    934 200 934
  PVAL 2,2PROPA -15.11691 8.565838 -18.67732 -4.904744  &
    15.01709 829 200 829
  PVAL FURACETA -15.35414 8.854122 -19.30317 -4.819452  &
    15.73851 1155 200 1155
  PVAL C21H24O4 -13.39351 6.588861 -14.3153 -5.306845  &
    14.32674 1150 200 1150

PROP-DATA NRTL-1
  IN-UNITS MET VOLUME-FLOW='cum/hr' ENTHALPY-FLO='Gcal/hr'  &
    HEAT-TRANS-C='kcal/hr-sqm-K' PRESSURE=bar TEMPERATURE=C  &
    VOLUME=cum DELTA-T=C HEAD=meter MOLE-DENSITY='kmol/cum'  &
    MASS-DENSITY='kg/cum' MOLE-ENTHALP='kcal/mol'  &
    MASS-ENTHALP='kcal/kg' HEAT=Gcal MOLE-CONC='mol/l'  &
    PDROP=bar
  PROP-LIST NRTL
  BPVAL H2O H3N -6.268400000 1525.454300 .3000000000 0.0 0.0  &
    0.0 10.00000000 91.50000000
  BPVAL H3N H2O 9.612100000 -3232.815900 .3000000000 0.0 0.0  &
    0.0 10.00000000 91.50000000
  BPVAL H2O PHENOL -.5363000000 1412.731600 .3000000000 0.0  &
    0.0 0.0 44.40000000 182.0000000
  BPVAL PHENOL H2O 2.301500000 -879.7008000 .3000000000 0.0  &
    0.0 0.0 44.40000000 182.0000000
  BPVAL H2O FURFURAL 7.107900000 -1265.836700 .3000000000 0.0  &
```

```
         0.0 0.0 58.20000000 161.7000000
BPVAL FURFURAL H2O -5.873200000 2335.049300 .3000000000 0.0  &
         0.0 0.0 58.20000000 161.7000000
BPVAL H2O BENZENE 140.0874000 -5954.307100 .2000000000 0.0  &
         -20.02540000 0.0 .8000000000 77.00000000
BPVAL BENZENE H2O 45.19050000 591.3676000 .2000000000 0.0  &
         -7.562900000 0.0 .8000000000 77.00000000
BPVAL C3H6-2 BENZENE 0.0 -3.794700000 .3000000000 0.0 0.0  &
         0.0 25.00000000 25.00000000
BPVAL BENZENE C3H6-2 0.0 151.4452000 .3000000000 0.0 0.0  &
         0.0 25.00000000 25.00000000
BPVAL 3:5-X-01 PHENOL 0.0 -380.7766000 .3000000000 0.0 0.0  &
         0.0 123.0000000 140.0000000
BPVAL PHENOL 3:5-X-01 0.0 654.1366000 .3000000000 0.0 0.0  &
         0.0 123.0000000 140.0000000
BPVAL FORMACID BENZENE 213.3302000 -9059.469700 .2000000000  &
         0.0 -31.93520000 0.0 3.800000000 73.00000000
BPVAL BENZENE FORMACID -54.59300000 3064.323500 .2000000000  &
         0.0 8.155000000 0.0 3.800000000 73.00000000
BPVAL PHENOL BENZENE 0.0 -15.05350000 .3000000000 0.0 0.0  &
         0.0 70.00000000 80.00000000
BPVAL BENZENE PHENOL 0.0 389.2036000 .3000000000 0.0 0.0  &
         0.0 70.00000000 80.00000000
BPVAL FURFURAL BENZENE -6.040500000 1990.515500 .3000000000  &
         0.0 0.0 0.0 80.10000000 161.5000000
BPVAL BENZENE FURFURAL 16.54180000 -5512.639200 .3000000000  &
         0.0 0.0 0.0 80.10000000 161.5000000
BPVAL H2O TOLUENE 627.0528000 -27269.35550 .2000000000 0.0  &
         -92.71820000 0.0 -9.000000000 93.00000000
BPVAL TOLUENE H2O -247.8792000 14759.75980 .2000000000 0.0  &
         35.58200000 0.0 -9.000000000 93.00000000
BPVAL FORMACID TOLUENE 0.0 874.3675000 .2000000000 0.0 0.0  &
         0.0 25.00000000 25.00000000
BPVAL TOLUENE FORMACID 0.0 176.7350000 .2000000000 0.0 0.0  &
         0.0 25.00000000 25.00000000
BPVAL PHENOL TOLUENE 14.73710000 -4747.815900 .3000000000  &
         0.0 0.0 0.0 110.5000000 172.7000000
BPVAL TOLUENE PHENOL -13.24850000 5101.815900 .3000000000  &
         0.0 0.0 0.0 110.5000000 172.7000000
BPVAL TOLUENE FURFURAL 0.0 333.4178000 .3000000000 0.0 0.0  &
         0.0 69.50000000 161.5000000
BPVAL FURFURAL TOLUENE 0.0 11.59840000 .3000000000 0.0 0.0  &
         0.0 69.50000000 161.5000000
BPVAL TOLUENE BENZENE 2.191100000 -863.7308000 .3000000000  &
         0.0 0.0 0.0 40.00000000 110.7500000
BPVAL BENZENE TOLUENE -2.885200000 1123.950100 .3000000000  &
         0.0 0.0 0.0 40.00000000 110.7500000
BPVAL H2O TETRA-01 4.760148000 -733.4016000 .4725526000 0.0  &
         0.0 0.0 63.41000000 100.0000000
BPVAL TETRA-01 H2O 1.214162000 157.7809000 .4725526000 0.0  &
         0.0 0.0 63.41000000 100.0000000
BPVAL TOLUENE TETRA-01 -.4930000000 348.1137000 .3000000000  &
         0.0 0.0 0.0 28.80000000 110.7000000
BPVAL TETRA-01 TOLUENE 1.221700000 -622.9771000 .3000000000  &
         0.0 0.0 0.0 28.80000000 110.7000000
BPVAL BENZENE TETRA-01 0.0 -280.7693000 .3000000000 0.0  &
         0.0 0.0 25.00000000 60.00000000
BPVAL TETRA-01 BENZENE 0.0 308.1593000 .3000000000 0.0 0.0  &
         0.0 25.00000000 60.00000000
BPVAL H2O N-HEP-01 3.015800000 918.8201000 .2000000000 0.0  &
         0.0 0.0 20.00000000 90.00000000
BPVAL N-HEP-01 H2O 2.982500000 929.6527000 .2000000000 0.0  &
         0.0 0.0 20.00000000 90.00000000
BPVAL H2O INDAN-01 0.0 2854.337400 .2000000000 0.0 0.0  &
         0.0 25.00000000 25.00000000
BPVAL INDAN-01 H2O 0.0 2854.337400 .2000000000 0.0 0.0  &
         0.0 25.00000000 25.00000000
BPVAL H2O ETHYL-01 1.005837000 2260.014000 .2000000000 0.0  &
         0.0 0.0 0.0 49.50000000
BPVAL ETHYL-01 H2O -10.50497000 4458.591000 .2000000000 0.0  &
         0.0 0.0 0.0 49.50000000
BPVAL PHENOL ETHYL-01 0.0 -85.00850000 .3000000000 0.0 0.0  &
         0.0 120.0000000 130.0000000
BPVAL ETHYL-01 PHENOL 0.0 499.0577000 .3000000000 0.0 0.0  &
```

297

```
     0.0 120.0000000 130.0000000
BPVAL TOLUENE ETHYL-01 0.0 -369.4589000 .3000000000 0.0  &
     0.0 0.0 100.0000000 134.0000000
BPVAL ETHYL-01 TOLUENE 0.0 549.2948000 .3000000000 0.0 0.0  &
     0.0 100.0000000 134.0000000
BPVAL FURFURAL ETHYL-01 0.0 158.9428000 .3000000000 0.0  &
     0.0 0.0 132.3000000 154.5000000
BPVAL ETHYL-01 FURFURAL 0.0 282.6479000 .3000000000 0.0  &
     0.0 0.0 132.3000000 154.5000000
BPVAL BENZENE ETHYL-01 -1.470100000 642.1115000 .3000000000  &
     0.0 0.0 0.0 80.08000000 136.1800000
BPVAL ETHYL-01 BENZENE 1.101700000 -515.4272000 .3000000000  &
     0.0 0.0 0.0 80.08000000 136.1800000
BPVAL TETRA-01 ETHYL-01 0.0 -211.7187000 .3000000000 0.0  &
     0.0 0.0 25.00000000 50.00000000
BPVAL ETHYL-01 TETRA-01 0.0 217.0624000 .3000000000 0.0  &
     0.0 0.0 25.00000000 50.00000000
BPVAL H2O N-HEX-01 0.0 3040.000000 .2000000000 0.0 0.0  &
     0.0 0.0 55.00000000
BPVAL N-HEX-01 H2O 0.0 1512.000000 .2000000000 0.0 0.0  &
     0.0 0.0 55.00000000
BPVAL PHENOL N-HEX-01 -2.700600000 1145.762300 .2000000000  &
     0.0 0.0 0.0 34.10000000 52.10000000
BPVAL N-HEX-01 PHENOL -5.283500000 2205.188700 .2000000000  &
     0.0 0.0 0.0 34.10000000 52.10000000
BPVAL TOLUENE N-HEX-01 -2.948300000 1259.245800 .3000000000  &
     0.0 0.0 0.0 24.80000000 110.6500000
BPVAL N-HEX-01 TOLUENE 1.518200000 -595.6702000 .3000000000  &
     0.0 0.0 0.0 24.80000000 110.6500000
BPVAL FURFURAL N-HEX-01 0.0 552.0042000 .3000000000 0.0  &
     0.0 0.0 69.40000000 125.0000000
BPVAL N-HEX-01 FURFURAL 0.0 538.6083000 .3000000000 0.0  &
     0.0 0.0 69.40000000 125.0000000
BPVAL BENZENE N-HEX-01 -1.554000000 797.5720000 .3000000000  &
     0.0 0.0 0.0 25.00000000 79.60000000
BPVAL N-HEX-01 BENZENE .4066000000 -213.7349000 .3000000000  &
     0.0 0.0 0.0 25.00000000 79.60000000
BPVAL TETRA-01 N-HEX-01 0.0 233.6258000 .3000000000 0.0  &
     0.0 0.0 30.00000000 68.69000000
BPVAL N-HEX-01 TETRA-01 0.0 -15.09590000 .3000000000 0.0  &
     0.0 0.0 30.00000000 68.69000000
BPVAL H2O CYCLO-01 13.14280000 -1066.976400 .2000000000 0.0  &
     0.0 0.0 10.00000000 53.00000000
BPVAL CYCLO-01 H2O -10.45850000 4954.897000 .2000000000 0.0  &
     0.0 0.0 10.00000000 53.00000000
BPVAL ACETACID CYCLO-01 10.61500000 -2362.794400 .2000000000  &
     0.0 0.0 0.0 -2.800000000 3.200000000
BPVAL CYCLO-01 ACETACID -16.13240000 4554.722200 .2000000000  &
     0.0 0.0 0.0 -2.800000000 3.200000000
BPVAL TOLUENE CYCLO-01 -.3062000000 171.9452000 .3000000000  &
     0.0 0.0 0.0 20.00000000 110.5600000
BPVAL CYCLO-01 TOLUENE -.1776000000 102.2200000 .3000000000  &
     0.0 0.0 0.0 20.00000000 110.5600000
BPVAL FURFURAL CYCLO-01 0.0 395.9760000 .3000000000 0.0  &
     0.0 0.0 81.80000000 147.9000000
BPVAL CYCLO-01 FURFURAL 0.0 499.1212000 .3000000000 0.0  &
     0.0 0.0 81.80000000 147.9000000
BPVAL BENZENE CYCLO-01 0.0 182.7545000 .3000000000 0.0 0.0  &
     0.0 77.40000000 80.75000000
BPVAL CYCLO-01 BENZENE 0.0 -43.34060000 .3000000000 0.0  &
     0.0 0.0 77.40000000 80.75000000
BPVAL TETRA-01 CYCLO-01 0.0 153.3146000 .3000000000 0.0  &
     0.0 0.0 25.00000000 60.00000000
BPVAL CYCLO-01 TETRA-01 0.0 31.13460000 .3000000000 0.0  &
     0.0 0.0 25.00000000 60.00000000
BPVAL ETHYL-01 CYCLO-01 0.0 -137.8274000 .3000000000 0.0  &
     0.0 0.0 30.00000000 50.00000000
BPVAL CYCLO-01 ETHYL-01 0.0 282.2470000 .3000000000 0.0  &
     0.0 0.0 30.00000000 50.00000000
BPVAL N-HEX-01 CYCLO-01 -.9898000000 167.9446000 .3000000000  &
     0.0 0.0 0.0 20.00000000 80.80000000
BPVAL CYCLO-01 N-HEX-01 1.263700000 -202.3037000 .3000000000  &
     0.0 0.0 0.0 20.00000000 80.80000000
BPVAL H2O M-XYL-01 140.0831000 -5322.935100 .2000000000 0.0  &
```

298

```
    -19.95500000 0.0 0.0 270.6000000
BPVAL M-XYL-01 H2O -50.08980000 5018.975100 .2000000000 0.0  &
    6.612300000 0.0 0.0 270.6000000
BPVAL TOLUENE M-XYL-01 0.0 -196.4410000 .3000000000 0.0  &
    0.0 0.0 110.5800000 139.1400000
BPVAL M-XYL-01 TOLUENE 0.0 376.4365000 .3000000000 0.0 0.0  &
    0.0 110.5800000 139.1400000
BPVAL BENZENE M-XYL-01 0.0 -115.5390000 .3000000000 0.0  &
    0.0 0.0 25.00000000 139.1400000
BPVAL M-XYL-01 BENZENE 0.0 140.4452000 .3000000000 0.0 0.0  &
    0.0 25.00000000 139.1400000
BPVAL CYCLO-01 M-XYL-01 0.0 166.5652000 .3000000000 0.0  &
    0.0 0.0 25.00000000 50.00000000
BPVAL M-XYL-01 CYCLO-01 0.0 -36.31910000 .3000000000 0.0  &
    0.0 0.0 25.00000000 50.00000000
BPVAL H2O METHY-01 9.764800000 340.6273000 .2000000000 0.0  &
    0.0 0.0 10.00000000 30.00000000
BPVAL METHY-01 H2O -9.473000000 4601.103000 .2000000000 0.0  &
    0.0 0.0 10.00000000 30.00000000
BPVAL PHENOL METHY-01 0.0 53.54940000 .3000000000 0.0 0.0  &
    0.0 101.1000000 150.0000000
BPVAL METHY-01 PHENOL 0.0 368.0504000 .3000000000 0.0 0.0  &
    0.0 101.1000000 150.0000000
BPVAL TOLUENE METHY-01 0.0 134.0625000 .3000000000 0.0 0.0  &
    0.0 100.8500000 110.6200000
BPVAL METHY-01 TOLUENE 0.0 -43.24040000 .3000000000 0.0  &
    0.0 0.0 100.8500000 110.6200000
BPVAL FURFURAL METHY-01 0.0 391.6801000 .3000000000 0.0  &
    0.0 0.0 101.1000000 120.3000000
BPVAL METHY-01 FURFURAL 0.0 505.9407000 .3000000000 0.0  &
    0.0 0.0 101.1000000 120.3000000
BPVAL BENZENE METHY-01 0.0 377.8787000 .3000000000 0.0 0.0  &
    0.0 75.00000000 100.9500000
BPVAL METHY-01 BENZENE 0.0 -197.2841000 .3000000000 0.0  &
    0.0 0.0 75.00000000 100.9500000
BPVAL TETRA-01 METHY-01 0.0 416.3870000 .3000000000 0.0  &
    0.0 0.0 30.00000000 50.00000000
BPVAL METHY-01 TETRA-01 0.0 -183.6248000 .3000000000 0.0  &
    0.0 0.0 30.00000000 50.00000000
BPVAL ETHYL-01 METHY-01 -1.888800000 539.4158000 .3000000000  &
    0.0 0.0 0.0 30.00000000 100.0000000
BPVAL METHY-01 ETHYL-01 1.694200000 -370.6175000 .3000000000  &
    0.0 0.0 0.0 30.00000000 100.0000000
BPVAL N-HEX-01 METHY-01 0.0 -202.3830000 .3000000000 0.0  &
    0.0 0.0 68.80000000 100.9500000
BPVAL METHY-01 N-HEX-01 0.0 269.5072000 .3000000000 0.0  &
    0.0 0.0 68.80000000 100.9500000
BPVAL CYCLO-01 METHY-01 0.0 63.86480000 .3000000000 0.0  &
    0.0 0.0 35.00000000 98.30000000
BPVAL METHY-01 CYCLO-01 0.0 -64.23720000 .3000000000 0.0  &
    0.0 0.0 35.00000000 98.30000000
BPVAL M-XYL-01 METHY-01 0.0 80.34570000 .3000000000 0.0  &
    0.0 0.0 75.00000000 75.00000000
BPVAL METHY-01 M-XYL-01 0.0 -8.869100000 .3000000000 0.0  &
    0.0 0.0 75.00000000 75.00000000
BPVAL H2O P-CRE-01 89.30080000 -4080.093000 .2000000000 0.0  &
    -12.07390000 0.0 17.20000000 139.4000000
BPVAL P-CRE-01 H2O 91.40280000 -3693.418500 .2000000000 0.0  &
    -14.10930000 0.0 17.20000000 139.4000000
BPVAL TOLUENE P-CRE-01 0.0 573.2656000 .3000000000 0.0 0.0  &
    0.0 110.7000000 202.2000000
BPVAL P-CRE-01 TOLUENE 0.0 -194.6938000 .3000000000 0.0  &
    0.0 0.0 110.7000000 202.2000000
BPVAL H2O N-PRO-02 0.0 2970.264400 .2000000000 0.0 0.0  &
    0.0 15.00000000 15.00000000
BPVAL N-PRO-02 H2O 0.0 2970.264400 .2000000000 0.0 0.0  &
    0.0 15.00000000 15.00000000
BPVAL PHENOL N-PRO-02 0.0 29.53720000 .3000000000 0.0 0.0  &
    0.0 120.0000000 130.0000000
BPVAL N-PRO-02 PHENOL 0.0 417.6902000 .3000000000 0.0 0.0  &
    0.0 120.0000000 130.0000000
BPVAL BENZENE N-PRO-02 0.0 30.50730000 .3000000000 0.0 0.0  &
    0.0 80.08000000 159.2400000
BPVAL N-PRO-02 BENZENE 0.0 -81.40820000 .3000000000 0.0  &
```

```
     0.0 0.0 80.08000000 159.2400000
BPVAL ETHYL-01 N-PRO-02 0.0 33.64000000 .3000000000 0.0  &
     0.0 0.0 100.0000000 100.0000000
BPVAL N-PRO-02 ETHYL-01 0.0 -34.10940000 .3000000000 0.0  &
     0.0 0.0 100.0000000 100.0000000
BPVAL METHY-01 N-PRO-02 0.0 64.89160000 .3000000000 0.0  &
     0.0 0.0 40.00000000 40.00000000
BPVAL N-PRO-02 METHY-01 0.0 17.95360000 .3000000000 0.0  &
     0.0 0.0 40.00000000 40.00000000
BPVAL FURFURAL 1:2:3-01 0.0 -381.2461000 .3000000000 0.0  &
     0.0 0.0 71.10000000 94.00000000
BPVAL 1:2:3-01 FURFURAL 0.0 623.6666000 .3000000000 0.0  &
     0.0 0.0 71.10000000 94.00000000
BPVAL N-HEX-01 1:2:3-01 0.0 85.13850000 .3000000000 0.0  &
     0.0 0.0 10.00000000 10.00000000
BPVAL 1:2:3-01 N-HEX-01 0.0 177.5102000 .3000000000 0.0  &
     0.0 0.0 10.00000000 10.00000000
BPVAL CYCLO-01 1:2:3-01 0.0 101.2840000 .3000000000 0.0  &
     0.0 0.0 10.00000000 10.00000000
BPVAL 1:2:3-01 CYCLO-01 0.0 61.58070000 .3000000000 0.0  &
     0.0 0.0 10.00000000 10.00000000
BPVAL P-CRE-01 1:2:3-01 0.0 118.4693000 .3000000000 0.0  &
     0.0 0.0 198.7000000 207.6000000
BPVAL 1:2:3-01 P-CRE-01 0.0 190.3468000 .3000000000 0.0  &
     0.0 0.0 198.7000000 207.6000000
BPVAL CYCLO-01 CIS-D-01 0.0 -322.0725000 .3000000000 0.0  &
     0.0 0.0 25.00000000 25.00000000
BPVAL CIS-D-01 CYCLO-01 0.0 911.5766000 .3000000000 0.0  &
     0.0 0.0 25.00000000 25.00000000
BPVAL PHENOL CYCLO-02 0.0 536.2388000 .3000000000 0.0 0.0  &
     0.0 109.7000000 138.7000000
BPVAL CYCLO-02 PHENOL 0.0 44.63110000 .3000000000 0.0 0.0  &
     0.0 109.7000000 138.7000000
BPVAL H2O N-TET-01 26.14467000 -3376.979000 .2000000000 0.0  &
     0.0 0.0 40.00000000 40.00000000
BPVAL N-TET-01 H2O -5.920609000 3739.217000 .2000000000 0.0  &
     0.0 0.0 40.00000000 40.00000000
BPVAL BENZENE N-TET-01 -2.093700000 1151.022500 .3000000000  &
     0.0 0.0 0.0 25.00000000 80.00000000
BPVAL N-TET-01 BENZENE -1.151900000 75.04250000 .3000000000  &
     0.0 0.0 0.0 25.00000000 80.00000000
BPVAL NAPHT-01 N-TET-01 0.0 315.0379000 .3000000000 0.0  &
     0.0 0.0 193.9000000 249.4000000
BPVAL N-TET-01 NAPHT-01 0.0 -191.4964000 .3000000000 0.0  &
     0.0 0.0 193.9000000 249.4000000
BPVAL CYCLO-01 N-TET-01 0.0 206.5706000 .3000000000 0.0  &
     0.0 0.0 35.00000000 35.00000000
BPVAL N-TET-01 CYCLO-01 0.0 -230.2448000 .3000000000 0.0  &
     0.0 0.0 35.00000000 35.00000000
BPVAL H2O ETHAN-01 3.457800000 -586.0809000 .3000000000 0.0  &
     0.0 0.0 24.99000000 100.0000000
BPVAL ETHAN-01 H2O -.8009000000 246.1800000 .3000000000 0.0  &
     0.0 0.0 24.99000000 100.0000000
BPVAL PHENOL ETHAN-01 .6637000000 173.8362000 .3000000000  &
     0.0 0.0 0.0 78.82000000 177.8000000
BPVAL ETHAN-01 PHENOL .1360000000 -604.4089000 .3000000000  &
     0.0 0.0 0.0 78.82000000 177.8000000
BPVAL TOLUENE ETHAN-01 -1.722100000 992.7367000 .3000000000  &
     0.0 0.0 0.0 26.80000000 110.6000000
BPVAL ETHAN-01 TOLUENE 1.145900000 -113.4658000 .3000000000  &
     0.0 0.0 0.0 26.80000000 110.6000000
BPVAL FURFURAL ETHAN-01 0.0 397.0705000 .3000000000 0.0  &
     0.0 0.0 50.00000000 134.0000000
BPVAL ETHAN-01 FURFURAL 0.0 68.27070000 .3000000000 0.0  &
     0.0 0.0 50.00000000 134.0000000
BPVAL BENZENE ETHAN-01 -.9155000000 882.0288000 .3000000000  &
     0.0 0.0 0.0 20.00000000 80.10000000
BPVAL ETHAN-01 BENZENE .5686000000 -54.80440000 .3000000000  &
     0.0 0.0 0.0 20.00000000 80.10000000
BPVAL TETRA-01 ETHAN-01 2.322500000 -524.9086000 .3000000000  &
     0.0 0.0 0.0 28.40000000 78.40000000
BPVAL ETHAN-01 TETRA-01 -2.777000000 905.7390000 .3000000000  &
     0.0 0.0 0.0 28.40000000 78.40000000
BPVAL ETHYL-01 ETHAN-01 17.04150000 -5731.194800 .3000000000  &
```

```
      0.0 0.0 0.0 78.30000000 136.2000000
BPVAL ETHAN-01 ETHYL-01 -17.84930000 6715.725100 .3000000000  &
      0.0 0.0 0.0 78.30000000 136.2000000
BPVAL N-HEX-01 ETHAN-01 0.0 738.6402000 .4700000000 0.0  &
      0.0 0.0 40.00000000 78.30000000
BPVAL ETHAN-01 N-HEX-01 0.0 497.8083000 .4700000000 0.0  &
      0.0 0.0 40.00000000 78.30000000
BPVAL CYCLO-01 ETHAN-01 1.627100000 214.0758000 .4500000000  &
      0.0 0.0 0.0 0.0 77.15000000
BPVAL ETHAN-01 CYCLO-01 -.1560000000 459.8772000 .4500000000  &
      0.0 0.0 0.0 0.0 77.15000000
BPVAL METHY-01 ETHAN-01 0.0 713.6257000 .4700000000 0.0  &
      0.0 0.0 20.00000000 55.00000000
BPVAL ETHAN-01 METHY-01 0.0 505.2368000 .4700000000 0.0  &
      0.0 0.0 20.00000000 55.00000000
BPVAL H2O METHPHEN 0.0 2210.180400 .2000000000 0.0 0.0  &
      0.0 25.00000000 25.00000000
BPVAL METHPHEN H2O 0.0 488.3325000 .2000000000 0.0 0.0  &
      0.0 25.00000000 25.00000000
BPVAL FURFURAL METOCTAC 0.0 138.0003000 .3000000000 0.0  &
      0.0 0.0 101.9000000 115.5000000
BPVAL METOCTAC FURFURAL 0.0 324.0849000 .3000000000 0.0  &
      0.0 0.0 101.9000000 115.5000000
BPVAL H2O METHA-01 2.732200000 -617.2687000 .3000000000 0.0  &
      0.0 0.0 24.99000000 100.0000000
BPVAL METHA-01 H2O -.6930000000 172.9871000 .3000000000 0.0  &
      0.0 0.0 24.99000000 100.0000000
BPVAL C3H6-2 METHA-01 0.0 660.5184000 .3000000000 0.0 0.0  &
      0.0 25.00000000 25.00000000
BPVAL METHA-01 C3H6-2 0.0 207.6027000 .3000000000 0.0 0.0  &
      0.0 25.00000000 25.00000000
BPVAL ACETACID METHA-01 0.0 197.9778000 .3000000000 0.0  &
      0.0 0.0 45.00000000 45.00000000
BPVAL METHA-01 ACETACID 0.0 -336.8086000 .3000000000 0.0  &
      0.0 0.0 45.00000000 45.00000000
BPVAL GUAIACOL METHA-01 1.066500000 -258.4877000 .3000000000  &
      0.0 0.0 0.0 64.70000000 205.0000000
BPVAL METHA-01 GUAIACOL -9.307000000 3586.999300 .3000000000  &
      0.0 0.0 0.0 64.70000000 205.0000000
BPVAL PHENOL METHA-01 0.0 -68.30160000 .3000000000 0.0 0.0  &
      0.0 64.70000000 181.6000000
BPVAL METHA-01 PHENOL 0.0 -159.7583000 .3000000000 0.0 0.0  &
      0.0 64.70000000 181.6000000
BPVAL TOLUENE METHA-01 0.0 446.8746000 .3000000000 0.0 0.0  &
      0.0 63.50000000 110.6000000
BPVAL METHA-01 TOLUENE 0.0 371.0837000 .3000000000 0.0 0.0  &
      0.0 63.50000000 110.6000000
BPVAL BENZENE METHA-01 11.58010000 -3282.554000 .4000000000  &
      0.0 0.0 0.0 55.00000000 80.10000000
BPVAL METHA-01 BENZENE -1.708600000 892.2404000 .4000000000  &
      0.0 0.0 0.0 55.00000000 80.10000000
BPVAL TETRA-01 METHA-01 0.0 224.1507000 .3000000000 0.0  &
      0.0 0.0 30.85000000 62.60000000
BPVAL METHA-01 TETRA-01 0.0 63.10510000 .3000000000 0.0  &
      0.0 0.0 30.85000000 62.60000000
BPVAL ETHYL-01 METHA-01 9.253900000 -2552.981200 .4700000000  &
      0.0 0.0 0.0 64.70000000 136.1500000
BPVAL METHA-01 ETHYL-01 -19.28690000 7068.902300 .4700000000  &
      0.0 0.0 0.0 64.70000000 136.1500000
BPVAL N-HEX-01 METHA-01 -3.651100000 1507.154500 .2000000000  &
      0.0 0.0 0.0 -17.80000000 42.85000000
BPVAL METHA-01 N-HEX-01 -1.154400000 734.5144000 .2000000000  &
      0.0 0.0 0.0 -17.80000000 42.85000000
BPVAL CYCLO-01 METHA-01 -4.675300000 2277.794200 .4300000000  &
      0.0 0.0 0.0 25.00000000 80.70000000
BPVAL METHA-01 CYCLO-01 1.386900000 224.7601000 .4300000000  &
      0.0 0.0 0.0 25.00000000 80.70000000
BPVAL M-XYL-01 METHA-01 0.0 417.3804000 .3000000000 0.0  &
      0.0 0.0 64.65000000 139.0000000
BPVAL METHA-01 M-XYL-01 0.0 443.7810000 .3000000000 0.0  &
      0.0 0.0 64.65000000 139.0000000
BPVAL METHY-01 METHA-01 0.0 919.6349000 .4700000000 0.0  &
      0.0 0.0 59.60000000 100.8000000
BPVAL METHA-01 METHY-01 0.0 814.5206000 .4700000000 0.0  &
```

301

```
     0.0 0.0 59.60000000 100.8000000
  BPVAL 3-MET-01 METHA-01 -2.170900000 1162.547900 .2000000000 &
     0.0 0.0 0.0 5.000000000 40.00000000
  BPVAL METHA-01 3-MET-01 -1.388500000 932.7700000 .2000000000 &
     0.0 0.0 0.0 5.000000000 40.00000000
  BPVAL N-TET-01 METHA-01 0.0 385.3467000 .2000000000 0.0 &
     0.0 0.0 25.00000000 25.00000000
  BPVAL METHA-01 N-TET-01 0.0 1258.972900 .2000000000 0.0 &
     0.0 0.0 25.00000000 25.00000000
  BPVAL ETHAN-01 METHA-01 -2.312700000 483.8436000 .3000000000 &
     0.0 0.0 0.0 20.00000000 78.40000000
  BPVAL METHA-01 ETHAN-01 4.711900000 -1162.294900 .3000000000 &
     0.0 0.0 0.0 20.00000000 78.40000000
  BPVAL N-TET-01 NAPHT-03 0.0 -191.4964000 .3000000000 0.0 &
     0.0 0.0 193.9000000 249.4000000
  BPVAL NAPHT-03 N-TET-01 0.0 315.0379000 .3000000000 0.0 &
     0.0 0.0 193.9000000 249.4000000

PROP-DATA PRKBV-1
  IN-UNITS SI ENTHALPY='J/kg' FLOW='tons/hr'  &
     MASS-FLOW='tons/hr' MOLE-FLOW='kmol/hr'  &
     VOLUME-FLOW='cum/hr' ENTHALPY-FLO='MJ/hr' POWER=MW  &
     PRESSURE=bar TEMPERATURE=C DELTA-T=C ELEC-POWER=kW  &
     HEAT=MJ PDROP-PER-HT='mbar/m' PDROP=bar
  PROP-LIST PRKBV
  BPVAL N2 O2 -.0119000000 0.0 0.0 -273.1500000 726.8500000
  BPVAL O2 N2 -.0119000000 0.0 0.0 -273.1500000 726.8500000
  BPVAL N2 H2 .1030000000 0.0 0.0 -273.1500000 726.8500000
  BPVAL H2 N2 .1030000000 0.0 0.0 -273.1500000 726.8500000
  BPVAL N2 CO .0307000000 0.0 0.0 -273.1500000 726.8500000
  BPVAL CO N2 .0307000000 0.0 0.0 -273.1500000 726.8500000
  BPVAL N2 CO2 -.0170000000 0.0 0.0 -273.1500000 726.8500000
  BPVAL CO2 N2 -.0170000000 0.0 0.0 -273.1500000 726.8500000
  BPVAL N2 H3N .2193000000 0.0 0.0 -273.1500000 726.8500000
  BPVAL H3N N2 .2193000000 0.0 0.0 -273.1500000 726.8500000
  BPVAL N2 CH4 .0311000000 0.0 0.0 -273.1500000 726.8500000
  BPVAL CH4 N2 .0311000000 0.0 0.0 -273.1500000 726.8500000
  BPVAL N2 C2H4 .0856000000 0.0 0.0 -273.1500000 726.8500000
  BPVAL C2H4 N2 .0856000000 0.0 0.0 -273.1500000 726.8500000
  BPVAL N2 C3H6-2 .0900000000 0.0 0.0 -273.1500000 &
     726.8500000
  BPVAL C3H6-2 N2 .0900000000 0.0 0.0 -273.1500000 &
     726.8500000
  BPVAL N2 AR -2.6000000E-3 0.0 0.0 -273.1500000 726.8500000
  BPVAL AR N2 -2.6000000E-3 0.0 0.0 -273.1500000 726.8500000
  BPVAL N2 BENZENE .1641000000 0.0 0.0 -273.1500000 &
     726.8500000
  BPVAL BENZENE N2 .1641000000 0.0 0.0 -273.1500000 &
     726.8500000
  BPVAL N2 N-HEX-01 .1496000000 0.0 0.0 -273.1500000 &
     726.8500000
  BPVAL N-HEX-01 N2 .1496000000 0.0 0.0 -273.1500000 &
     726.8500000
  BPVAL N2 METHA-01 -.2141000000 0.0 0.0 -273.1500000 &
     726.8500000
  BPVAL METHA-01 N2 -.2141000000 0.0 0.0 -273.1500000 &
     726.8500000
  BPVAL N2 ETHAN-02 .0515000000 0.0 0.0 -273.1500000 &
     726.8500000
  BPVAL ETHAN-02 N2 .0515000000 0.0 0.0 -273.1500000 &
     726.8500000
  BPVAL N2 PROPA-01 .0852000000 0.0 0.0 -273.1500000 &
     726.8500000
  BPVAL PROPA-01 N2 .0852000000 0.0 0.0 -273.1500000 &
     726.8500000
  BPVAL N2 ISOBU-01 .1033000000 0.0 0.0 -273.1500000 &
     726.8500000
  BPVAL ISOBU-01 N2 .1033000000 0.0 0.0 -273.1500000 &
     726.8500000
  BPVAL O2 AR .0104000000 0.0 0.0 -273.1500000 726.8500000
  BPVAL AR O2 .0104000000 0.0 0.0 -273.1500000 726.8500000
  BPVAL H2 CO .0919000000 0.0 0.0 -273.1500000 726.8500000
  BPVAL CO H2 .0919000000 0.0 0.0 -273.1500000 726.8500000
  BPVAL H2 CO2 -.1622000000 0.0 0.0 -273.1500000 726.8500000
```

302

```
BPVAL CO2 H2 -.1622000000 0.0 0.0 -273.1500000 726.8500000
BPVAL H2 CH4 .0156000000 0.0 0.0 -273.1500000 726.8500000
BPVAL CH4 H2 .0156000000 0.0 0.0 -273.1500000 726.8500000
BPVAL H2 C2H4 7.40000000E-3 0.0 0.0 -273.1500000  &
   726.8500000
BPVAL C2H4 H2 7.40000000E-3 0.0 0.0 -273.1500000  &
   726.8500000
BPVAL H2 C3H6-2 -.1037000000 0.0 0.0 -273.1500000  &
   726.8500000
BPVAL C3H6-2 H2 -.1037000000 0.0 0.0 -273.1500000  &
   726.8500000
BPVAL H2 TOLUENE -.5100000000 0.0 0.0 -273.1500000  &
   726.8500000
BPVAL TOLUENE H2 -.5100000000 0.0 0.0 -273.1500000  &
   726.8500000
BPVAL H2 N-HEX-01 -.0300000000 0.0 0.0 -273.1500000  &
   726.8500000
BPVAL N-HEX-01 H2 -.0300000000 0.0 0.0 -273.1500000  &
   726.8500000
BPVAL H2 1:2:3-01 -.3856000000 0.0 0.0 -273.1500000  &
   726.8500000
BPVAL 1:2:3-01 H2 -.3856000000 0.0 0.0 -273.1500000  &
   726.8500000
BPVAL H2 ETHAN-02 -.0667000000 0.0 0.0 -273.1500000  &
   726.8500000
BPVAL ETHAN-02 H2 -.0667000000 0.0 0.0 -273.1500000  &
   726.8500000
BPVAL H2 PROPA-01 -.0833000000 0.0 0.0 -273.1500000  &
   726.8500000
BPVAL PROPA-01 H2 -.0833000000 0.0 0.0 -273.1500000  &
   726.8500000
BPVAL CO CH4 .0300000000 0.0 0.0 -273.1500000 726.8500000
BPVAL CH4 CO .0300000000 0.0 0.0 -273.1500000 726.8500000
BPVAL CO ETHAN-02 -.0226000000 0.0 0.0 -273.1500000  &
   726.8500000
BPVAL ETHAN-02 CO -.0226000000 0.0 0.0 -273.1500000  &
   726.8500000
BPVAL CO PROPA-01 .0259000000 0.0 0.0 -273.1500000  &
   726.8500000
BPVAL PROPA-01 CO .0259000000 0.0 0.0 -273.1500000  &
   726.8500000
BPVAL CO2 H2O .1200000000 0.0 0.0 -273.1500000 726.8500000
BPVAL H2O CO2 .1200000000 0.0 0.0 -273.1500000 726.8500000
BPVAL CO2 CH4 .0919000000 0.0 0.0 -273.1500000 726.8500000
BPVAL CH4 CO2 .0919000000 0.0 0.0 -273.1500000 726.8500000
BPVAL CO2 C2H4 .0552000000 0.0 0.0 -273.1500000  &
   726.8500000
BPVAL C2H4 CO2 .0552000000 0.0 0.0 -273.1500000  &
   726.8500000
BPVAL CO2 C3H6-2 .0933000000 0.0 0.0 -273.1500000  &
   726.8500000
BPVAL C3H6-2 CO2 .0933000000 0.0 0.0 -273.1500000  &
   726.8500000
BPVAL CO2 TOLUENE .1056000000 0.0 0.0 -273.1500000  &
   726.8500000
BPVAL TOLUENE CO2 .1056000000 0.0 0.0 -273.1500000  &
   726.8500000
BPVAL CO2 BENZENE .0774000000 0.0 0.0 -273.1500000  &
   726.8500000
BPVAL BENZENE CO2 .0774000000 0.0 0.0 -273.1500000  &
   726.8500000
BPVAL CO2 N-HEX-01 .1100000000 0.0 0.0 -273.1500000  &
   726.8500000
BPVAL N-HEX-01 CO2 .1100000000 0.0 0.0 -273.1500000  &
   726.8500000
BPVAL CO2 CYCLO-01 .1052000000 0.0 0.0 -273.1500000  &
   726.8500000
BPVAL CYCLO-01 CO2 .1052000000 0.0 0.0 -273.1500000  &
   726.8500000
BPVAL CO2 METHA-01 .0230000000 0.0 0.0 -273.1500000  &
   726.8500000
BPVAL METHA-01 CO2 .0230000000 0.0 0.0 -273.1500000  &
   726.8500000
BPVAL CO2 ETHAN-02 .1322000000 0.0 0.0 -273.1500000  &
```

```
    726.8500000
BPVAL ETHAN-02 CO2 .1322000000 0.0 0.0 -273.1500000  &
    726.8500000
BPVAL CO2 PROPA-01 .1241000000 0.0 0.0 -273.1500000  &
    726.8500000
BPVAL PROPA-01 CO2 .1241000000 0.0 0.0 -273.1500000  &
    726.8500000
BPVAL CO2 ISOBU-01 .1200000000 0.0 0.0 -273.1500000  &
    726.8500000
BPVAL ISOBU-01 CO2 .1200000000 0.0 0.0 -273.1500000  &
    726.8500000
BPVAL H2O H3N -.2589000000 0.0 0.0 -273.1500000  &
    726.8500000
BPVAL H3N H2O -.2589000000 0.0 0.0 -273.1500000  &
    726.8500000
BPVAL H2O METHA-01 -.0778000000 0.0 0.0 -273.1500000  &
    726.8500000
BPVAL METHA-01 H2O -.0778000000 0.0 0.0 -273.1500000  &
    726.8500000
BPVAL H3N AR -.1800000000 0.0 0.0 -273.1500000 726.8500000
BPVAL AR H3N -.1800000000 0.0 0.0 -273.1500000 726.8500000
BPVAL CH4 C2H4 .0215000000 0.0 0.0 -273.1500000  &
    726.8500000
BPVAL C2H4 CH4 .0215000000 0.0 0.0 -273.1500000  &
    726.8500000
BPVAL CH4 C3H6-2 .0330000000 0.0 0.0 -273.1500000  &
    726.8500000
BPVAL C3H6-2 CH4 .0330000000 0.0 0.0 -273.1500000  &
    726.8500000
BPVAL CH4 AR .0230000000 0.0 0.0 -273.1500000 726.8500000
BPVAL AR CH4 .0230000000 0.0 0.0 -273.1500000 726.8500000
BPVAL CH4 TOLUENE .0970000000 0.0 0.0 -273.1500000  &
    726.8500000
BPVAL TOLUENE CH4 .0970000000 0.0 0.0 -273.1500000  &
    726.8500000
BPVAL CH4 BENZENE .0363000000 0.0 0.0 -273.1500000  &
    726.8500000
BPVAL BENZENE CH4 .0363000000 0.0 0.0 -273.1500000  &
    726.8500000
BPVAL CH4 N-HEX-01 .0422000000 0.0 0.0 -273.1500000  &
    726.8500000
BPVAL N-HEX-01 CH4 .0422000000 0.0 0.0 -273.1500000  &
    726.8500000
BPVAL CH4 CYCLO-01 .0389000000 0.0 0.0 -273.1500000  &
    726.8500000
BPVAL CYCLO-01 CH4 .0389000000 0.0 0.0 -273.1500000  &
    726.8500000
BPVAL CH4 M-XYL-01 .0844000000 0.0 0.0 -273.1500000  &
    726.8500000
BPVAL M-XYL-01 CH4 .0844000000 0.0 0.0 -273.1500000  &
    726.8500000
BPVAL CH4 1:2:3-01 .1452000000 0.0 0.0 -273.1500000  &
    726.8500000
BPVAL 1:2:3-01 CH4 .1452000000 0.0 0.0 -273.1500000  &
    726.8500000
BPVAL CH4 ETHAN-02 -2.6000000E-3 0.0 0.0 -273.1500000  &
    726.8500000
BPVAL ETHAN-02 CH4 -2.6000000E-3 0.0 0.0 -273.1500000  &
    726.8500000
BPVAL CH4 PROPA-01 .0140000000 0.0 0.0 -273.1500000  &
    726.8500000
BPVAL PROPA-01 CH4 .0140000000 0.0 0.0 -273.1500000  &
    726.8500000
BPVAL CH4 ISOBU-01 .0256000000 0.0 0.0 -273.1500000  &
    726.8500000
BPVAL ISOBU-01 CH4 .0256000000 0.0 0.0 -273.1500000  &
    726.8500000
BPVAL C2H4 BENZENE .0311000000 0.0 0.0 -273.1500000  &
    726.8500000
BPVAL BENZENE C2H4 .0311000000 0.0 0.0 -273.1500000  &
    726.8500000
BPVAL C2H4 ETHAN-02 8.90000000E-3 0.0 0.0 -273.1500000  &
    726.8500000
BPVAL ETHAN-02 C2H4 8.90000000E-3 0.0 0.0 -273.1500000  &
```

```
      726.8500000
    BPVAL C2H4 ACETY-01 .0652000000 0.0 0.0 -273.1500000  &
      726.8500000
    BPVAL ACETY-01 C2H4 .0652000000 0.0 0.0 -273.1500000  &
      726.8500000
    BPVAL C3H6-2 ETHAN-02 8.90000000E-3 0.0 0.0 -273.1500000  &
      726.8500000
    BPVAL ETHAN-02 C3H6-2 8.90000000E-3 0.0 0.0 -273.1500000  &
      726.8500000
    BPVAL C3H6-2 PROPA-01 7.40000000E-3 0.0 0.0 -273.1500000  &
      726.8500000
    BPVAL PROPA-01 C3H6-2 7.40000000E-3 0.0 0.0 -273.1500000  &
      726.8500000
    BPVAL C3H6-2 ISOBU-01 -.0144000000 0.0 0.0 -273.1500000  &
      726.8500000
    BPVAL ISOBU-01 C3H6-2 -.0144000000 0.0 0.0 -273.1500000  &
      726.8500000
    BPVAL BENZENE N-HEX-01 9.30000000E-3 0.0 0.0 -273.1500000  &
      726.8500000
    BPVAL N-HEX-01 BENZENE 9.30000000E-3 0.0 0.0 -273.1500000  &
      726.8500000
    BPVAL BENZENE ETHAN-02 .0322000000 0.0 0.0 -273.1500000  &
      726.8500000
    BPVAL ETHAN-02 BENZENE .0322000000 0.0 0.0 -273.1500000  &
      726.8500000
    BPVAL BENZENE PROPA-01 .0233000000 0.0 0.0 -273.1500000  &
      726.8500000
    BPVAL PROPA-01 BENZENE .0233000000 0.0 0.0 -273.1500000  &
      726.8500000
    BPVAL N-HEX-01 CYCLO-01 -3.0000000E-3 0.0 0.0 -273.1500000  &
      726.8500000
    BPVAL CYCLO-01 N-HEX-01 -3.0000000E-3 0.0 0.0 -273.1500000  &
      726.8500000
    BPVAL N-HEX-01 ETHAN-02 -.0100000000 0.0 0.0 -273.1500000  &
      726.8500000
    BPVAL ETHAN-02 N-HEX-01 -.0100000000 0.0 0.0 -273.1500000  &
      726.8500000
    BPVAL N-HEX-01 PROPA-01 7.00000000E-4 0.0 0.0 -273.1500000  &
      726.8500000
    BPVAL PROPA-01 N-HEX-01 7.00000000E-4 0.0 0.0 -273.1500000  &
      726.8500000
    BPVAL CYCLO-01 ETHAN-02 .0178000000 0.0 0.0 -273.1500000  &
      726.8500000
    BPVAL ETHAN-02 CYCLO-01 .0178000000 0.0 0.0 -273.1500000  &
      726.8500000
    BPVAL ETHAN-01 PROPA-01 .0315000000 0.0 0.0 -273.1500000  &
      726.8500000
    BPVAL PROPA-01 ETHAN-01 .0315000000 0.0 0.0 -273.1500000  &
      726.8500000
    BPVAL METHA-01 ETHAN-02 .0270000000 0.0 0.0 -273.1500000  &
      726.8500000
    BPVAL ETHAN-02 METHA-01 .0270000000 0.0 0.0 -273.1500000  &
      726.8500000
    BPVAL ETHAN-02 PROPA-01 1.10000000E-3 0.0 0.0 -273.1500000  &
      726.8500000
    BPVAL PROPA-01 ETHAN-02 1.10000000E-3 0.0 0.0 -273.1500000  &
      726.8500000
    BPVAL ETHAN-02 ISOBU-01 -6.7000000E-3 0.0 0.0 -273.1500000  &
      726.8500000
    BPVAL ISOBU-01 ETHAN-02 -6.7000000E-3 0.0 0.0 -273.1500000  &
      726.8500000
    BPVAL PROPA-01 ISOBU-01 -7.8000000E-3 0.0 0.0 -273.1500000  &
      726.8500000
    BPVAL ISOBU-01 PROPA-01 -7.8000000E-3 0.0 0.0 -273.1500000  &
      726.8500000

PROP-DATA SRKKIJ-1
  IN-UNITS SI ENTHALPY='J/kg' FLOW='tons/hr'  &
    MASS-FLOW='tons/hr' MOLE-FLOW='kmol/hr'  &
    VOLUME-FLOW='cum/hr' ENTHALPY-FLO='MJ/hr' POWER=MW  &
    PRESSURE=bar TEMPERATURE=C DELTA-T=C ELEC-POWER=kW  &
    HEAT=MJ PDROP-PER-HT='mbar/m' PDROP=bar
  PROP-LIST SRKKIJ
  BPVAL N2 C3H6-2 .1082000000 0.0 0.0 -273.1500000  &
```

```
   726.8500000
BPVAL C3H6-2 N2 .1082000000 0.0 0.0 -273.1500000 &
   726.8500000
BPVAL N2 TOLUENE .1996000000 0.0 0.0 -273.1500000 &
   726.8500000
BPVAL TOLUENE N2 .1996000000 0.0 0.0 -273.1500000 &
   726.8500000
BPVAL N2 M-XYL-01 .3000000000 0.0 0.0 -273.1500000 &
   726.8500000
BPVAL M-XYL-01 N2 .3000000000 0.0 0.0 -273.1500000 &
   726.8500000
BPVAL H2 CH4 -.0244851000 0.0 0.0 -273.1500000 726.8500000
BPVAL CH4 H2 -.0244851000 0.0 0.0 -273.1500000 726.8500000
BPVAL H2 C2H4 .0806016000 0.0 0.0 -273.1500000 726.8500000
BPVAL C2H4 H2 .0806016000 0.0 0.0 -273.1500000 726.8500000
BPVAL H2 C3H6-2 .1067960000 0.0 0.0 -273.1500000 &
   726.8500000
BPVAL C3H6-2 H2 .1067960000 0.0 0.0 -273.1500000 &
   726.8500000
BPVAL H2 N-HEX-01 .0819068000 0.0 0.0 -273.1500000 &
   726.8500000
BPVAL N-HEX-01 H2 .0819068000 0.0 0.0 -273.1500000 &
   726.8500000
BPVAL H2 ETHAN-02 .0163828000 0.0 0.0 -273.1500000 &
   726.8500000
BPVAL ETHAN-02 H2 .0163828000 0.0 0.0 -273.1500000 &
   726.8500000
BPVAL H2 PROPA-01 .1014650000 0.0 0.0 -273.1500000 &
   726.8500000
BPVAL PROPA-01 H2 .1014650000 0.0 0.0 -273.1500000 &
   726.8500000
BPVAL CO CO2 -.0154400000 0.0 0.0 -273.1500000 726.8500000
BPVAL CO2 CO -.0154400000 0.0 0.0 -273.1500000 726.8500000
BPVAL CO2 C3H6-2 .0831100000 0.0 0.0 -273.1500000 &
   726.8500000
BPVAL C3H6-2 CO2 .0831100000 0.0 0.0 -273.1500000 &
   726.8500000
BPVAL CO2 BENZENE .0880600000 0.0 0.0 -273.1500000 &
   726.8500000
BPVAL BENZENE CO2 .0880600000 0.0 0.0 -273.1500000 &
   726.8500000
BPVAL CO2 M-XYL-01 .1010000000 0.0 0.0 -273.1500000 &
   726.8500000
BPVAL M-XYL-01 CO2 .1010000000 0.0 0.0 -273.1500000 &
   726.8500000
BPVAL H3N BENZENE .1279000000 0.0 0.0 -273.1500000 &
   726.8500000
BPVAL BENZENE H3N .1279000000 0.0 0.0 -273.1500000 &
   726.8500000
BPVAL H3N PROPA-01 .1612000000 0.0 0.0 -273.1500000 &
   726.8500000
BPVAL PROPA-01 H3N .1612000000 0.0 0.0 -273.1500000 &
   726.8500000
BPVAL CH4 C2H4 .0174052000 0.0 0.0 -273.1500000 &
   726.8500000
BPVAL C2H4 CH4 .0174052000 0.0 0.0 -273.1500000 &
   726.8500000
BPVAL CH4 TOLUENE .0818031000 0.0 0.0 -273.1500000 &
   726.8500000
BPVAL TOLUENE CH4 .0818031000 0.0 0.0 -273.1500000 &
   726.8500000
BPVAL CH4 BENZENE .0313391000 0.0 0.0 -273.1500000 &
   726.8500000
BPVAL BENZENE CH4 .0313391000 0.0 0.0 -273.1500000 &
   726.8500000
BPVAL CH4 N-HEX-01 .0220731000 0.0 0.0 -273.1500000 &
   726.8500000
BPVAL N-HEX-01 CH4 .0220731000 0.0 0.0 -273.1500000 &
   726.8500000
BPVAL CH4 ETHAN-02 4.21992000E-4 0.0 0.0 -273.1500000 &
   726.8500000
BPVAL ETHAN-02 CH4 4.21992000E-4 0.0 0.0 -273.1500000 &
   726.8500000
BPVAL CH4 PROPA-01 .0241509000 0.0 0.0 -273.1500000 &
```

306

```
    726.8500000
BPVAL PROPA-01 CH4 .0241509000 0.0 0.0 -273.1500000  &
    726.8500000
BPVAL CH4 ISOBU-01 .0460715000 0.0 0.0 -273.1500000  &
    726.8500000
BPVAL ISOBU-01 CH4 .0460715000 0.0 0.0 -273.1500000  &
    726.8500000
BPVAL C2H4 BENZENE .0283552000 0.0 0.0 -273.1500000  &
    726.8500000
BPVAL BENZENE C2H4 .0283552000 0.0 0.0 -273.1500000  &
    726.8500000
BPVAL C2H4 ETHAN-02 3.21082000E-3 0.0 0.0 -273.1500000  &
    726.8500000
BPVAL ETHAN-02 C2H4 3.21082000E-3 0.0 0.0 -273.1500000  &
    726.8500000
BPVAL C2H4 ACETY-01 .0662315000 0.0 0.0 -273.1500000  &
    726.8500000
BPVAL ACETY-01 C2H4 .0662315000 0.0 0.0 -273.1500000  &
    726.8500000
BPVAL C3H6-2 ETHAN-02 .0117991000 0.0 0.0 -273.1500000  &
    726.8500000
BPVAL ETHAN-02 C3H6-2 .0117991000 0.0 0.0 -273.1500000  &
    726.8500000
BPVAL C3H6-2 PROPA-01 3.00000000E-3 0.0 0.0 -273.1500000  &
    726.8500000
BPVAL PROPA-01 C3H6-2 3.00000000E-3 0.0 0.0 -273.1500000  &
    726.8500000
BPVAL C3H6-2 ISOBU-01 -.0212580000 0.0 0.0 -273.1500000  &
    726.8500000
BPVAL ISOBU-01 C3H6-2 -.0212580000 0.0 0.0 -273.1500000  &
    726.8500000
BPVAL C3H6-2 ACETY-01 -.0205181000 0.0 0.0 -273.1500000  &
    726.8500000
BPVAL ACETY-01 C3H6-2 -.0205181000 0.0 0.0 -273.1500000  &
    726.8500000
BPVAL TOLUENE BENZENE .0200000000 0.0 0.0 -273.1500000  &
    726.8500000
BPVAL BENZENE TOLUENE .0200000000 0.0 0.0 -273.1500000  &
    726.8500000
BPVAL TOLUENE ETHAN-02 .0226260000 0.0 0.0 -273.1500000  &
    726.8500000
BPVAL ETHAN-02 TOLUENE .0226260000 0.0 0.0 -273.1500000  &
    726.8500000
BPVAL TOLUENE PROPA-01 .0330300000 0.0 0.0 -273.1500000  &
    726.8500000
BPVAL PROPA-01 TOLUENE .0330300000 0.0 0.0 -273.1500000  &
    726.8500000
BPVAL BENZENE N-HEX-01 .0145923000 0.0 0.0 -273.1500000  &
    726.8500000
BPVAL N-HEX-01 BENZENE .0145923000 0.0 0.0 -273.1500000  &
    726.8500000
BPVAL BENZENE ETHAN-02 .0362230000 0.0 0.0 -273.1500000  &
    726.8500000
BPVAL ETHAN-02 BENZENE .0362230000 0.0 0.0 -273.1500000  &
    726.8500000
BPVAL BENZENE PROPA-01 .0195580000 0.0 0.0 -273.1500000  &
    726.8500000
BPVAL PROPA-01 BENZENE .0195580000 0.0 0.0 -273.1500000  &
    726.8500000
BPVAL N-HEX-01 ETHAN-02 -.0433561000 0.0 0.0 -273.1500000  &
    726.8500000
BPVAL ETHAN-02 N-HEX-01 -.0433561000 0.0 0.0 -273.1500000  &
    726.8500000
BPVAL N-HEX-01 PROPA-01 3.05152000E-3 0.0 0.0 -273.1500000  &
    726.8500000
BPVAL PROPA-01 N-HEX-01 3.05152000E-3 0.0 0.0 -273.1500000  &
    726.8500000
BPVAL ETHAN-02 PROPA-01 1.69511000E-3 0.0 0.0 -273.1500000  &
    726.8500000
BPVAL PROPA-01 ETHAN-02 1.69511000E-3 0.0 0.0 -273.1500000  &
    726.8500000
BPVAL ETHAN-02 ISOBU-01 5.51229000E-3 0.0 0.0 -273.1500000  &
    726.8500000
BPVAL ISOBU-01 ETHAN-02 5.51229000E-3 0.0 0.0 -273.1500000  &
```

307

        726.8500000
    BPVAL PROPA-01 ISOBU-01 -2.9093200E-3 0.0 0.0 -273.1500000 &
        726.8500000
    BPVAL ISOBU-01 PROPA-01 -2.9093200E-3 0.0 0.0 -273.1500000 &
        726.8500000

DEF-STREAMS HEAT 11

DEF-STREAMS HEAT 20

DEF-STREAMS HEAT 21

DEF-STREAMS HEAT 22

DEF-STREAMS HEAT 23

DEF-STREAMS HEAT 24

DEF-STREAMS HEAT 31

DEF-STREAMS HEAT 34

DEF-STREAMS HEAT 35

DEF-STREAMS HEAT 50

DEF-STREAMS HEAT 52

DEF-STREAMS HEAT 53

DEF-STREAMS HEAT 54

DEF-STREAMS WORK 1

DEF-STREAMS WORK 9

DEF-STREAMS WORK 18

DEF-STREAMS WORK 19

DEF-STREAMS WORK 38

DEF-STREAMS WORK 39

DEF-STREAMS WORK 41

DEF-STREAMS WORK 42

DEF-STREAMS WORK 43

DEF-STREAMS WORK 44

DEF-STREAMS WORK 45

DEF-STREAMS WORK 46

DEF-STREAMS WORK 47

DEF-STREAMS WORK 48

DEF-STREAMS WORK 49

DEF-STREAMS WORK 51

DEF-STREAMS WORK 55

DEF-STREAMS WORK 57

HIERARCHY A1000

DEF-STREAMS MIXCISLD ALL

SOLVE

```
    PARAM METHOD=SM
    RUN-MODE MODE=SIM

FLOWSHEET
    BLOCK DR1001FL IN=1003 QDR1001 OUT=1004 1005
    BLOCK DR-1001 IN=1002 1001B OUT=1003 QDR1001
    BLOCK MULT1001 IN=1001A OUT=1001B

PROPERTIES NRTL FREE-WATER=STEAM-TA SOLU-WATER=3 TRUE-COMPS=YES
    PROPERTIES PENG-ROB / SRK

STREAM 1001A
    IN-UNITS MET VOLUME-FLOW='cum/hr' ENTHALPY-FLO='Gcal/hr' &
        HEAT-TRANS-C='kcal/hr-sqm-K' PRESSURE=bar TEMPERATURE=C &
        VOLUME=cum DELTA-T=C HEAD=meter MOLE-DENSITY='kmol/cum' &
        MASS-DENSITY='kg/cum' MOLE-ENTHALP='kcal/mol' &
        MASS-ENTHALP='kcal/kg' HEAT=Gcal MOLE-CONC='mol/l' &
        PDROP=bar
    SUBSTREAM MIXED TEMP=25. PRES=20. <psia>
    MASS-FLOW H2O 44.93151 <tons/hr> / EXTRACT 4.43151 <tons/hr>
    SUBSTREAM CISOLID TEMP=25. PRES=20. <psia> &
        MASS-FLOW=40.5 <tons/hr>
    MASS-FRAC CHAR 0. / ASH 0.011 / CELLULOS 0.457561 / &
        LIGNIN 0.3019504 / XYLAN 0.0998334 / ARABINAN &
        0.0094965 / MANNAN 0.1201587 / GALACTAN 0.

STREAM 1002
    IN-UNITS MET VOLUME-FLOW='cum/hr' ENTHALPY-FLO='Gcal/hr' &
        HEAT-TRANS-C='kcal/hr-sqm-K' PRESSURE=bar TEMPERATURE=C &
        VOLUME=cum DELTA-T=C HEAD=meter MOLE-DENSITY='kmol/cum' &
        MASS-DENSITY='kg/cum' MOLE-ENTHALP='kcal/mol' &
        MASS-ENTHALP='kcal/kg' HEAT=Gcal MOLE-CONC='mol/l' &
        PDROP=bar
    SUBSTREAM MIXED TEMP=200. PRES=20. <psia>
    MASS-FLOW N2 267209. / O2 81135.4

DEF-STREAMS HEAT QDR1001

BLOCK DR-1001 HEATER
    IN-UNITS MET VOLUME-FLOW='cum/hr' ENTHALPY-FLO='Gcal/hr' &
        HEAT-TRANS-C='kcal/hr-sqm-K' PRESSURE=bar TEMPERATURE=C &
        VOLUME=cum DELTA-T=C HEAD=meter MOLE-DENSITY='kmol/cum' &
        MASS-DENSITY='kg/cum' MOLE-ENTHALP='kcal/mol' &
        MASS-ENTHALP='kcal/kg' HEAT=Gcal MOLE-CONC='mol/l' &
        PDROP=bar
    PARAM TEMP=110. PRES=20. <psia>

BLOCK DR1001FL FLASH2
    IN-UNITS MET VOLUME-FLOW='cum/hr' ENTHALPY-FLO='Gcal/hr' &
        HEAT-TRANS-C='kcal/hr-sqm-K' PRESSURE=bar TEMPERATURE=C &
        VOLUME=cum DELTA-T=C HEAD=meter MOLE-DENSITY='kmol/cum' &
        MASS-DENSITY='kg/cum' MOLE-ENTHALP='kcal/mol' &
        MASS-ENTHALP='kcal/kg' HEAT=Gcal MOLE-CONC='mol/l' &
        PDROP=bar
    PARAM PRES=20. <psia>

BLOCK MULT1001 MULT
    PARAM FACTOR=2.0475608

ENDHIERARCHY A1000

HIERARCHY A2000


DEF-STREAMS MIXCISLD ALL

SOLVE
    PARAM METHOD=SM
    RUN-MODE MODE=SIM

FLOWSHEET
    BLOCK PY-2001 IN=6008 1005 OUT=2003
    BLOCK CY-2001 IN=2003 OUT=2005 2004
    BLOCK MX-2001 IN=6006 5007 2005 OUT=2006
```

```
PROPERTIES NRTL FREE-WATER=STEAM-TA SOLU-WATER=3 TRUE-COMPS=YES
    PROPERTIES PENG-ROB / SRK

STREAM 6006
    IN-UNITS MET VOLUME-FLOW='cum/hr' ENTHALPY-FLO='Gcal/hr'  &
        HEAT-TRANS-C='kcal/hr-sqm-K' PRESSURE=bar TEMPERATURE=C  &
        VOLUME=cum DELTA-T=C HEAD=meter MOLE-DENSITY='kmol/cum'  &
        MASS-DENSITY='kg/cum' MOLE-ENTHALP='kcal/mol'  &
        MASS-ENTHALP='kcal/kg' HEAT=Gcal MOLE-CONC='mol/l'  &
        PDROP=bar
    SUBSTREAM MIXED TEMP=105. PRES=45. <psia>
    MASS-FLOW H2 123.1 / CO 1362.2 / CO2 1128.3 / H2O 0.2 / &
        H3N 42.9 / CH4 7.3 / C2H4 29.6

STREAM 6008
    IN-UNITS MET VOLUME-FLOW='cum/hr' ENTHALPY-FLO='Gcal/hr'  &
        HEAT-TRANS-C='kcal/hr-sqm-K' PRESSURE=bar TEMPERATURE=C  &
        VOLUME=cum DELTA-T=C HEAD=meter MOLE-DENSITY='kmol/cum'  &
        MASS-DENSITY='kg/cum' MOLE-ENTHALP='kcal/mol'  &
        MASS-ENTHALP='kcal/kg' HEAT=Gcal MOLE-CONC='mol/l'  &
        PDROP=bar
    SUBSTREAM MIXED TEMP=650. PRES=45. <psia>
    MASS-FLOW H2 2614. / CO 28919.3 / CO2 23953.2 / H2O  &
        4.3 / H3N 911.6 / CH4 154.1 / C2H4 628.6 / &
        ACETACID 0.3 / ACETOL 0.3 / FORMACID 0.2 / TOLUENE  &
        0.1 / FURFURAL 0.9

BLOCK MX-2001 MIXER
    IN-UNITS MET VOLUME-FLOW='cum/hr' ENTHALPY-FLO='Gcal/hr'  &
        HEAT-TRANS-C='kcal/hr-sqm-K' PRESSURE=bar TEMPERATURE=C  &
        VOLUME=cum DELTA-T=C HEAD=meter MOLE-DENSITY='kmol/cum'  &
        MASS-DENSITY='kg/cum' MOLE-ENTHALP='kcal/mol'  &
        MASS-ENTHALP='kcal/kg' HEAT=Gcal MOLE-CONC='mol/l'  &
        PDROP=bar
    PARAM PRES=20. <psia>

BLOCK CY-2001 SEP
    IN-UNITS MET VOLUME-FLOW='cum/hr' ENTHALPY-FLO='Gcal/hr'  &
        HEAT-TRANS-C='kcal/hr-sqm-K' PRESSURE=bar TEMPERATURE=C  &
        VOLUME=cum DELTA-T=C HEAD=meter MOLE-DENSITY='kmol/cum'  &
        MASS-DENSITY='kg/cum' MOLE-ENTHALP='kcal/mol'  &
        MASS-ENTHALP='kcal/kg' HEAT=Gcal MOLE-CONC='mol/l'  &
        PDROP=bar
    PARAM MAXIT=30 TOL=0.0001
    FRAC STREAM=2005 SUBSTREAM=MIXED COMPS=N2 FRACS=0.
    FRAC STREAM=2005 SUBSTREAM=CISOLID COMPS=CHAR ASH FRACS=  &
        1. 1.

BLOCK PY-2001 RYIELD
    IN-UNITS MET VOLUME-FLOW='cum/hr' ENTHALPY-FLO='Gcal/hr'  &
        HEAT-TRANS-C='kcal/hr-sqm-K' PRESSURE=bar TEMPERATURE=C  &
        VOLUME=cum DELTA-T=C HEAD=meter MOLE-DENSITY='kmol/cum'  &
        MASS-DENSITY='kg/cum' MOLE-ENTHALP='kcal/mol'  &
        MASS-ENTHALP='kcal/kg' HEAT=Gcal MOLE-CONC='mol/l'  &
        PDROP=bar
    PARAM PRES=20. <psia> DUTY=0. MAXIT=100 TOL=0.01
    MASS-YIELD MIXED H2 0. / CO 0.3115 / CO2 0.4205 / H2O  &
        0.04787 / H3N 0. / CH4 0.02516046 / C3H6-2 0. / &
        ACETACID 0.00363 / N-PRO-01 0. / PHENOL 0.00059136 /  &
        TOLUENE 0. / FURFURAL 7.72E-005 / BENZENE 0. /  &
        TETRA-01 0. / DILACID 0. / CISOLID CHAR 0.038904 /  &
        MIXED N-HEP-01 0.00088469 / 2:4-X-01 0.00116841 /  &
        O-ETH-01 0.00032595 / INDAN-01 0.00694656 / 2:6-D-01  &
        0.00037409 / NAPHT-01 0.00338485 / DIBEN-01 0.00061256 /  &
        FLUOR-01 0.0070103 / 2:4-D-01 0.0006547 / NAPHT-02  &
        0.00455146 / GLYCO-01 0.03081705 / FUMAR-01 0.00279308 / &
        1:2-B-01 3.858E-005 / ETHAN-01 0. / 2,2PROPA  &
        0.02361469 / FURACETA 0.00825382 / LEVOGLUC 0.00018299 /  &
        4METGUA 0.00033198 / ETHYLANI 0.00274007 / BENZOATE  &
        0.00038429 / METHPHEN 0.00011808 / ETHYLGUA 0.00058644 /  &
        MESHEPTA 0.00243386 / BENZOFUR 0.00624624 / TRIMEBEN  &
        0.00121092 / 4PROPGUA 0.00301276 / HMBENZAC 0.00944927 /  &
        METOCTAC 0.01210387 / CONIFALC 0.00056743 / ISOEUGEN  &
```

```
        0.00172427 / PHENKETO 0.00151614 / XANTHENE 0.00175485 / &
        P-DECANO 0.00205281 / DNONDBEN 0.00069102 / PENTACOS &
        0.00080937 / ETMEPHEN 0. / C22H20O 0.0008551 / C18H28 &
        0.01117426 / C21H24O4 0.00039017
    INERTS ASH

ENDHIERARCHY A2000

HIERARCHY A3000


DEF-STREAMS MIXCISLD ALL

SOLVE
    PARAM METHOD=SM
    RUN-MODE MODE=SIM

FLOWSHEET
    BLOCK HX-3001- IN=30012B QHX3001 OUT=3013
    BLOCK HX-3001+ IN=3001 OUT=3002 QHX3001
    BLOCK HX-3002+ IN=3002 OUT=3003 QHX3002
    BLOCK CP-3001 IN=3008 OUT=3009 WCPA3001
    BLOCK HX-3002- IN=3009 QHX3002 OUT=3010
    BLOCK SC-3001 IN=3003 3011 OUT=3005 3004
    BLOCK ES-3001 IN=3005 OUT=3007 3006
    BLOCK MULT3009 IN=30012A OUT=30012B

PROPERTIES NRTL FREE-WATER=STEAM-TA SOLU-WATER=3 TRUE-COMPS=YES
    PROPERTIES PENG-ROB / SRK

STREAM 3008
    IN-UNITS MET VOLUME-FLOW='cum/hr' ENTHALPY-FLO='Gcal/hr'  &
        HEAT-TRANS-C='kcal/hr-sqm-K' PRESSURE=bar TEMPERATURE=C  &
        VOLUME=cum DELTA-T=C HEAD=meter MOLE-DENSITY='kmol/cum'  &
        MASS-DENSITY='kg/cum' MOLE-ENTHALP='kcal/mol'  &
        MASS-ENTHALP='kcal/kg' HEAT=Gcal MOLE-CONC='mol/l'  &
        PDROP=bar
    SUBSTREAM MIXED TEMP=25. PRES=14.7 <psia>  &
        MASS-FLOW=728.689285 <tons/hr>
    MASS-FRAC N2 0.7504 / O2 0.2299 / CO2 0.0004 / H2O  &
        0.0066 / AR 0.0127

STREAM 3011
    IN-UNITS MET VOLUME-FLOW='cum/hr' ENTHALPY-FLO='Gcal/hr'  &
        HEAT-TRANS-C='kcal/hr-sqm-K' PRESSURE=bar TEMPERATURE=C  &
        VOLUME=cum DELTA-T=C HEAD=meter MOLE-DENSITY='kmol/cum'  &
        MASS-DENSITY='kg/cum' MOLE-ENTHALP='kcal/mol'  &
        MASS-ENTHALP='kcal/kg' HEAT=Gcal MOLE-CONC='mol/l'  &
        PDROP=bar
    SUBSTREAM MIXED TEMP=-6.4 PRES=40. <psia>
    MASS-FLOW H2O 673.1 / C3H6-2 5.6 / ACETACID 217.5 /  &
        ACETOL 268.3 / GUAIACOL 22.5 / 3:5-X-01 139.6 /  &
        FORMACID 125. / N-PRO-01 600. / PHENOL 17.1 /  &
        TOLUENE 83.4 / FURFURAL 695.9 / BENZENE 28.3

STREAM 30012A
    IN-UNITS MET VOLUME-FLOW='cum/hr' ENTHALPY-FLO='Gcal/hr'  &
        HEAT-TRANS-C='kcal/hr-sqm-K' PRESSURE=bar TEMPERATURE=C  &
        VOLUME=cum DELTA-T=C HEAD=meter MOLE-DENSITY='kmol/cum'  &
        MASS-DENSITY='kg/cum' MOLE-ENTHALP='kcal/mol'  &
        MASS-ENTHALP='kcal/kg' HEAT=Gcal MOLE-CONC='mol/l'  &
        PDROP=bar
    SUBSTREAM MIXED TEMP=80. PRES=20. <psia>  &
        MASS-FLOW=2.9 <tons/hr>
    MASS-FRAC H2O 1.

DEF-STREAMS HEAT QHX3001

DEF-STREAMS HEAT QHX3002

DEF-STREAMS WORK WCPA3001

BLOCK ES-3001 SEP
    IN-UNITS MET VOLUME-FLOW='cum/hr' ENTHALPY-FLO='Gcal/hr'  &
```

311

```
        HEAT-TRANS-C='kcal/hr-sqm-K' PRESSURE=bar TEMPERATURE=C &
        VOLUME=cum DELTA-T=C HEAD=meter MOLE-DENSITY='kmol/cum' &
        MASS-DENSITY='kg/cum' MOLE-ENTHALP='kcal/mol' &
        MASS-ENTHALP='kcal/kg' HEAT=Gcal MOLE-CONC='mol/l' &
        PDROP=bar
    FRAC STREAM=3007 SUBSTREAM=MIXED COMPS=H2 CO CO2 H2O &
        H3N CH4 C2H4 C3H6-2 AR ACETACID ACETOL GUAIACOL &
        3:5-X-01 FORMACID N-PRO-01 PHENOL TOLUENE FURFURAL &
        BENZENE CHAR ASH CELLULOS LIGNIN XYLAN ARABINAN MANNAN &
        GALACTAN EXTRACT TETRA-01 DILACID N-HEP-01 2:4-X-01 &
        O-ETH-01 INDAN-01 2:6-D-01 NAPHT-01 DIBEN-01 FLUOR-01 &
        2:4-D-01 NAPHT-02 ETHYL-01 N-HEX-01 CYCLO-01 M-XYL-01 &
        METHY-01 1:3-C-01 3-MET-01 P-CRE-01 N-PRO-02 1:2:3-01 &
        CIS-D-01 1:2-D-01 CYCLO-02 N-TET-01 DINON-01 N-TET-02 &
        GLYCO-01 FUMAR-01 1:2-B-01 ETHAN-01 2,2PROPA FURACETA &
        LEVOGLUC 4METGUA ETHYLANI BENZOATE METHPHEN ETHYLGUA &
        MESHEPTA BENZOFUR TRIMEBEN 4PROPGUA HMBENZAC METOCTAC &
        CONIFALC ISOEUGEN PHENKETO XANTHENE P-DECANO DNONDBEN &
        PENTACOS ETMEPHEN 1HINDANE HYDFLUOR HYDNAPH C18H28 &
        C21H24O4 FRACS=1. 1. 1. 0.001 1. 1. 1. 0. 0. 0.001 &
        0.001 0. 0.001 0.001 0.001 0. 0.001 0.001 0. 0. 0. &
        0. 0. 0. 0. 0. 0. 0. 0.001 0.001 0.001 0.001 0.001 &
        0.001 0.001 0.001 0.001 0.001 0.001 0.001 0.001 0.001 &
        0.001 0.001 0.001 0.001 0.001 0.001 0.001 0.001 0.001 &
        0.001 0.001 0.001 0.001 0.001 0.001 0.001 0.001 0.001 &
        0.001 0.001 0.001 0.001 0.001 0.001 0.001 0.001 0.001 &
        0.001 0.001 0.001 0.001 0.001 0.001 0.001 0.001 0.001 &
        0.001 0.001 0.001 0.001 0.001 0.001 0.001 0.001 0.001
    FRAC STREAM=3007 SUBSTREAM=CISOLID COMPS=CHAR FRACS=0.

BLOCK SC-3001 SEP
    IN-UNITS MET VOLUME-FLOW='cum/hr' ENTHALPY-FLO='Gcal/hr' &
        HEAT-TRANS-C='kcal/hr-sqm-K' PRESSURE=bar TEMPERATURE=C &
        VOLUME=cum DELTA-T=C HEAD=meter MOLE-DENSITY='kmol/cum' &
        MASS-DENSITY='kg/cum' MOLE-ENTHALP='kcal/mol' &
        MASS-ENTHALP='kcal/kg' HEAT=Gcal MOLE-CONC='mol/l' &
        PDROP=bar
    PARAM
    FRAC STREAM=3005 SUBSTREAM=MIXED COMPS=H2 CO CO2 H2O &
        H3N CH4 C2H4 C3H6-2 AR ACETACID ACETOL GUAIACOL &
        3:5-X-01 FORMACID N-PRO-01 PHENOL TOLUENE FURFURAL &
        BENZENE CHAR ASH CELLULOS LIGNIN XYLAN ARABINAN MANNAN &
        GALACTAN EXTRACT TETRA-01 DILACID N-HEP-01 2:4-X-01 &
        O-ETH-01 INDAN-01 2:6-D-01 NAPHT-01 DIBEN-01 FLUOR-01 &
        2:4-D-01 NAPHT-02 ETHYL-01 N-HEX-01 CYCLO-01 M-XYL-01 &
        METHY-01 1:3-C-01 3-MET-01 P-CRE-01 N-PRO-02 1:2:3-01 &
        CIS-D-01 1:2-D-01 CYCLO-02 N-TET-01 DINON-01 N-TET-02 &
        GLYCO-01 FUMAR-01 1:2-B-01 ETHAN-01 2,2PROPA FURACETA &
        LEVOGLUC 4METGUA ETHYLANI BENZOATE METHPHEN ETHYLGUA &
        MESHEPTA BENZOFUR TRIMEBEN 4PROPGUA HMBENZAC METOCTAC &
        CONIFALC ISOEUGEN PHENKETO XANTHENE P-DECANO DNONDBEN &
        PENTACOS ETMEPHEN 1HINDANE HYDFLUOR HYDNAPH C18H28 &
        C21H24O4 FRACS=1. 1. 1. 1. 1. 1. 0.2 0. 0.2 &
        0.2 0.2 0.2 0.2 0.2 0.2 0.2 0.2 0. 0. 0. 0. &
        0. 0. 0. 0. 0. 0. 0. 0.2 0.2 0.2 0.2 0.2 0.2 0.2 &
        0.2 0.2 0.2 0.2 0.2 0.2 0.2 0.2 0.2 0.2 0.2 0.2 &
        0.2 0.2 0.2 0.2 0.2 0.2 0.2 0.2 0.2 0.2 0.2 0.2 &
        0.2 0.2 0.2 0.2 0.2 0.2 0.2 0.2 0.2 0.2 0.2 0.2 &
        0.2 0.2 0.2 0.2 0.2 0.2 0.2 0.2 0.2 0.2 0.2 0.2 &
        0.2 0.2
    FRAC STREAM=3005 SUBSTREAM=CISOLID COMPS=CHAR FRACS=0.

BLOCK HX-3001+ HEATER
    IN-UNITS MET VOLUME-FLOW='cum/hr' ENTHALPY-FLO='Gcal/hr' &
        HEAT-TRANS-C='kcal/hr-sqm-K' PRESSURE=bar TEMPERATURE=C &
        VOLUME=cum DELTA-T=C HEAD=meter MOLE-DENSITY='kmol/cum' &
        MASS-DENSITY='kg/cum' MOLE-ENTHALP='kcal/mol' &
        MASS-ENTHALP='kcal/kg' HEAT=Gcal MOLE-CONC='mol/l' &
        PDROP=bar
    PARAM TEMP=465. PRES=20. <psia>

BLOCK HX-3001- HEATER
    IN-UNITS MET VOLUME-FLOW='cum/hr' ENTHALPY-FLO='Gcal/hr' &
        HEAT-TRANS-C='kcal/hr-sqm-K' PRESSURE=bar TEMPERATURE=C &
```

```
            VOLUME=cum DELTA-T=C HEAD=meter MOLE-DENSITY='kmol/cum'  &
            MASS-DENSITY='kg/cum' MOLE-ENTHALP='kcal/mol'  &
            MASS-ENTHALP='kcal/kg' HEAT=Gcal MOLE-CONC='mol/l'  &
            PDROP=bar
        PARAM PRES=40. MAXIT=30 TOL=0.0001

    BLOCK HX-3002+ HEATER
        IN-UNITS MET VOLUME-FLOW='cum/hr' ENTHALPY-FLO='Gcal/hr'  &
            HEAT-TRANS-C='kcal/hr-sqm-K' PRESSURE=bar TEMPERATURE=C  &
            VOLUME=cum DELTA-T=C HEAD=meter MOLE-DENSITY='kmol/cum'  &
            MASS-DENSITY='kg/cum' MOLE-ENTHALP='kcal/mol'  &
            MASS-ENTHALP='kcal/kg' HEAT=Gcal MOLE-CONC='mol/l'  &
            PDROP=bar
        PARAM TEMP=28. PRES=20. <psia>

    BLOCK HX-3002- HEATER
        IN-UNITS MET VOLUME-FLOW='cum/hr' ENTHALPY-FLO='Gcal/hr'  &
            HEAT-TRANS-C='kcal/hr-sqm-K' PRESSURE=bar TEMPERATURE=C  &
            VOLUME=cum DELTA-T=C HEAD=meter MOLE-DENSITY='kmol/cum'  &
            MASS-DENSITY='kg/cum' MOLE-ENTHALP='kcal/mol'  &
            MASS-ENTHALP='kcal/kg' HEAT=Gcal MOLE-CONC='mol/l'  &
            PDROP=bar
        PARAM PRES=14.8 <psia>

    BLOCK CP-3001 COMPR
        IN-UNITS MET VOLUME-FLOW='cum/hr' ENTHALPY-FLO='Gcal/hr'  &
            HEAT-TRANS-C='kcal/hr-sqm-K' PRESSURE=bar TEMPERATURE=C  &
            VOLUME=cum DELTA-T=C HEAD=meter MOLE-DENSITY='kmol/cum'  &
            MASS-DENSITY='kg/cum' MOLE-ENTHALP='kcal/mol'  &
            MASS-ENTHALP='kcal/kg' HEAT=Gcal MOLE-CONC='mol/l'  &
            PDROP=bar
        PARAM TYPE=ISENTROPIC PRES=14.8 <psia>

    BLOCK MULT3009 MULT
        PARAM FACTOR=10.

    ENDHIERARCHY A3000

    HIERARCHY A4000


    DEF-STREAMS MIXCISLD ALL

    SOLVE
        PARAM METHOD=SM
        RUN-MODE MODE=SIM

    FLOWSHEET
        BLOCK CP-4001 IN=4002B OUT=4003 WCPA4001
        BLOCK MX-4001 IN=4001 4003 OUT=4004
        BLOCK CB-4001 IN=4004 OUT=4005 QCB-4001
        BLOCK MX-4002 IN=4012 4011 OUT=4013
        BLOCK HX4001+ IN=4005 OUT=4006 QHX4001
        BLOCK HX4002+ IN=4006 OUT=4007 QHX4002
        BLOCK HX4003+ IN=4007 OUT=4008 QHX4003
        BLOCK HX4004+ IN=4008 OUT=4009 QHX4004
        BLOCK CY-4001 IN=4009 OUT=4011 4010
        BLOCK RF-4001 IN=4013 OUT=4014 4015
        BLOCK MULT4002 IN=4002A OUT=4002B

    PROPERTIES NRTL FREE-WATER=STEAM-TA SOLU-WATER=3 TRUE-COMPS=YES
        PROPERTIES PENG-ROB / SRK

    STREAM 4002A
        IN-UNITS MET VOLUME-FLOW='cum/hr' ENTHALPY-FLO='Gcal/hr'  &
            HEAT-TRANS-C='kcal/hr-sqm-K' PRESSURE=bar TEMPERATURE=C  &
            VOLUME=cum DELTA-T=C HEAD=meter MOLE-DENSITY='kmol/cum'  &
            MASS-DENSITY='kg/cum' MOLE-ENTHALP='kcal/mol'  &
            MASS-ENTHALP='kcal/kg' HEAT=Gcal MOLE-CONC='mol/l'  &
            PDROP=bar
        SUBSTREAM MIXED TEMP=150. PRES=14.7 <psia>  &
            MASS-FLOW=150. <tons/hr>
        MASS-FLOW N2 0.7503 / O2 0.2299 / CO2 0.0005 / H2O  &
            0.0066 / AR 0.0127
```

313

STREAM 4012
  IN-UNITS MET VOLUME-FLOW='cum/hr' ENTHALPY-FLO='Gcal/hr' &
     HEAT-TRANS-C='kcal/hr-sqm-K' PRESSURE=bar TEMPERATURE=C &
     VOLUME=cum DELTA-T=C HEAD=meter MOLE-DENSITY='kmol/cum' &
     MASS-DENSITY='kg/cum' MOLE-ENTHALP='kcal/mol' &
     MASS-ENTHALP='kcal/kg' HEAT=Gcal MOLE-CONC='mol/l' &
     PDROP=bar
  SUBSTREAM MIXED TEMP=25. PRES=20. <psia>
  MASS-FLOW H2O 100.

DEF-STREAMS HEAT QCB-4001

STREAM QCB-4001
  IN-UNITS MET VOLUME-FLOW='cum/hr' ENTHALPY-FLO='Gcal/hr' &
     HEAT-TRANS-C='kcal/hr-sqm-K' PRESSURE=bar TEMPERATURE=C &
     VOLUME=cum DELTA-T=C HEAD=meter MOLE-DENSITY='kmol/cum' &
     MASS-DENSITY='kg/cum' MOLE-ENTHALP='kcal/mol' &
     MASS-ENTHALP='kcal/kg' HEAT=Gcal MOLE-CONC='mol/l' &
     PDROP=bar
  INFO HEAT DUTY=0.

DEF-STREAMS HEAT QHX4001

DEF-STREAMS HEAT QHX4002

DEF-STREAMS HEAT QHX4003

DEF-STREAMS HEAT QHX4004

DEF-STREAMS WORK WCPA4001

BLOCK MX-4001 MIXER
  IN-UNITS MET VOLUME-FLOW='cum/hr' ENTHALPY-FLO='Gcal/hr' &
     HEAT-TRANS-C='kcal/hr-sqm-K' PRESSURE=bar TEMPERATURE=C &
     VOLUME=cum DELTA-T=C HEAD=meter MOLE-DENSITY='kmol/cum' &
     MASS-DENSITY='kg/cum' MOLE-ENTHALP='kcal/mol' &
     MASS-ENTHALP='kcal/kg' HEAT=Gcal MOLE-CONC='mol/l' &
     PDROP=bar
  PARAM PRES=14.8

BLOCK MX-4002 MIXER
  IN-UNITS MET VOLUME-FLOW='cum/hr' ENTHALPY-FLO='Gcal/hr' &
     HEAT-TRANS-C='kcal/hr-sqm-K' PRESSURE=bar TEMPERATURE=C &
     VOLUME=cum DELTA-T=C HEAD=meter MOLE-DENSITY='kmol/cum' &
     MASS-DENSITY='kg/cum' MOLE-ENTHALP='kcal/mol' &
     MASS-ENTHALP='kcal/kg' HEAT=Gcal MOLE-CONC='mol/l' &
     PDROP=bar
  PARAM PRES=14.8 <psia>

BLOCK CY-4001 SEP
  PARAM
  FRAC STREAM=4011 SUBSTREAM=MIXED COMPS=N2 FRACS=0.
  FRAC STREAM=4011 SUBSTREAM=CISOLID COMPS=ASH FRACS=1.

BLOCK HX4001+ HEATER
  IN-UNITS MET VOLUME-FLOW='cum/hr' ENTHALPY-FLO='Gcal/hr' &
     HEAT-TRANS-C='kcal/hr-sqm-K' PRESSURE=bar TEMPERATURE=C &
     VOLUME=cum DELTA-T=C HEAD=meter MOLE-DENSITY='kmol/cum' &
     MASS-DENSITY='kg/cum' MOLE-ENTHALP='kcal/mol' &
     MASS-ENTHALP='kcal/kg' HEAT=Gcal MOLE-CONC='mol/l' &
     PDROP=bar
  PARAM TEMP=1141. PRES=14.8 <psia>

BLOCK HX4002+ HEATER
  IN-UNITS MET VOLUME-FLOW='cum/hr' ENTHALPY-FLO='Gcal/hr' &
     HEAT-TRANS-C='kcal/hr-sqm-K' PRESSURE=bar TEMPERATURE=C &
     VOLUME=cum DELTA-T=C HEAD=meter MOLE-DENSITY='kmol/cum' &
     MASS-DENSITY='kg/cum' MOLE-ENTHALP='kcal/mol' &
     MASS-ENTHALP='kcal/kg' HEAT=Gcal MOLE-CONC='mol/l' &
     PDROP=bar
  PARAM TEMP=700. PRES=14.8 <psia>

BLOCK HX4003+ HEATER

314

```
    IN-UNITS MET VOLUME-FLOW='cum/hr' ENTHALPY-FLO='Gcal/hr'  &
        HEAT-TRANS-C='kcal/hr-sqm-K' PRESSURE=bar TEMPERATURE=C  &
        VOLUME=cum DELTA-T=C HEAD=meter MOLE-DENSITY='kmol/cum'  &
        MASS-DENSITY='kg/cum' MOLE-ENTHALP='kcal/mol'  &
        MASS-ENTHALP='kcal/kg' HEAT=Gcal MOLE-CONC='mol/l'  &
        PDROP=bar
    PARAM TEMP=500. PRES=14.8 <psia>

BLOCK HX4004+ HEATER
    IN-UNITS MET VOLUME-FLOW='cum/hr' ENTHALPY-FLO='Gcal/hr'  &
        HEAT-TRANS-C='kcal/hr-sqm-K' PRESSURE=bar TEMPERATURE=C  &
        VOLUME=cum DELTA-T=C HEAD=meter MOLE-DENSITY='kmol/cum'  &
        MASS-DENSITY='kg/cum' MOLE-ENTHALP='kcal/mol'  &
        MASS-ENTHALP='kcal/kg' HEAT=Gcal MOLE-CONC='mol/l'  &
        PDROP=bar
    PARAM TEMP=120. PRES=14.8 <psia>

BLOCK CB-4001 RSTOIC
    IN-UNITS MET VOLUME-FLOW='cum/hr' ENTHALPY-FLO='Gcal/hr'  &
        HEAT-TRANS-C='kcal/hr-sqm-K' PRESSURE=bar TEMPERATURE=C  &
        VOLUME=cum DELTA-T=C HEAD=meter MOLE-DENSITY='kmol/cum'  &
        MASS-DENSITY='kg/cum' MOLE-ENTHALP='kcal/mol'  &
        MASS-ENTHALP='kcal/kg' HEAT=Gcal MOLE-CONC='mol/l'  &
        PDROP=bar
    PARAM PRES=14.8 <psia> DUTY=0. COMBUSTION=YES PROD-NOX=NO2

BLOCK CP-4001 COMPR
    IN-UNITS MET VOLUME-FLOW='cum/hr' ENTHALPY-FLO='Gcal/hr'  &
        HEAT-TRANS-C='kcal/hr-sqm-K' PRESSURE=bar TEMPERATURE=C  &
        VOLUME=cum DELTA-T=C HEAD=meter MOLE-DENSITY='kmol/cum'  &
        MASS-DENSITY='kg/cum' MOLE-ENTHALP='kcal/mol'  &
        MASS-ENTHALP='kcal/kg' HEAT=Gcal MOLE-CONC='mol/l'  &
        PDROP=bar
    PARAM TYPE=ISENTROPIC PRES=14.8 <psia>

BLOCK MULT4002 MULT
    PARAM FACTOR=2.2716

BLOCK RF-4001 SSPLIT
    FRAC CISOLID 4014 1.
    FRAC MIXED 4015 1.

ENDHIERARCHY A4000

HIERARCHY A5000


DEF-STREAMS MIXCISLD ALL

SOLVE
    PARAM METHOD=SM
    RUN-MODE MODE=SIM

FLOWSHEET
    BLOCK T-5001 IN=3021 3004 6003 OUT=5001
    BLOCK P-5001 IN=5001 OUT=5002 WPA5001
    BLOCK HX-5001+ IN=5002 OUT=5003 QHX5001
    BLOCK HX-5001- IN=CWA5001I QHX5001 OUT=CWA5001O
    BLOCK SP-5001 IN=5003 OUT=5005 5004
    BLOCK S-5001 IN=5004 OUT=5006 5007

PROPERTIES NRTL FREE-WATER=STEAM-TA SOLU-WATER=3 TRUE-COMPS=YES
    PROPERTIES PENG-ROB / SRK

STREAM CWA5001I
    IN-UNITS MET VOLUME-FLOW='cum/hr' ENTHALPY-FLO='Gcal/hr'  &
        HEAT-TRANS-C='kcal/hr-sqm-K' PRESSURE=bar TEMPERATURE=C  &
        VOLUME=cum DELTA-T=C HEAD=meter MOLE-DENSITY='kmol/cum'  &
        MASS-DENSITY='kg/cum' MOLE-ENTHALP='kcal/mol'  &
        MASS-ENTHALP='kcal/kg' HEAT=Gcal MOLE-CONC='mol/l'  &
        PDROP=bar
    SUBSTREAM MIXED TEMP=21.1 PRES=15. <psia>
    MASS-FLOW H2O 14804.8
```

DEF-STREAMS HEAT QHX5001

DEF-STREAMS WORK WPA5001

BLOCK T-5001 MIXER
    IN-UNITS MET VOLUME-FLOW='cum/hr' ENTHALPY-FLO='Gcal/hr' &
        HEAT-TRANS-C='kcal/hr-sqm-K' PRESSURE=bar TEMPERATURE=C &
        VOLUME=cum DELTA-T=C HEAD=meter MOLE-DENSITY='kmol/cum' &
        MASS-DENSITY='kg/cum' MOLE-ENTHALP='kcal/mol' &
        MASS-ENTHALP='kcal/kg' HEAT=Gcal MOLE-CONC='mol/l' &
        PDROP=bar
    PARAM PRES=26. <psia>

BLOCK S-5001 FSPLIT
    FRAC 5007 0.35

BLOCK SP-5001 SEP
    IN-UNITS MET VOLUME-FLOW='cum/hr' ENTHALPY-FLO='Gcal/hr' &
        HEAT-TRANS-C='kcal/hr-sqm-K' PRESSURE=bar TEMPERATURE=C &
        VOLUME=cum DELTA-T=C HEAD=meter MOLE-DENSITY='kmol/cum' &
        MASS-DENSITY='kg/cum' MOLE-ENTHALP='kcal/mol' &
        MASS-ENTHALP='kcal/kg' HEAT=Gcal MOLE-CONC='mol/l' &
        PDROP=bar
    FRAC STREAM=5005 SUBSTREAM=MIXED COMPS=N2 O2 H2 CO CO2 &
        H2O H3N CH4 C2H4 C3H6-2 AR ACETACID ACETOL GUAIACOL &
        3:5-X-01 FORMACID N-PRO-01 PHENOL TOLUENE FURFURAL &
        BENZENE CHAR ASH CELLULOS LIGNIN XYLAN ARABINAN MANNAN &
        GALACTAN EXTRACT TETRA-01 DILACID N-HEP-01 2:4-X-01 &
        O-ETH-01 INDAN-01 2:6-D-01 NAPHT-01 DIBEN-01 FLUOR-01 &
        2:4-D-01 NAPHT-02 ETHYL-01 N-HEX-01 CYCLO-01 M-XYL-01 &
        METHY-01 1:3-C-01 3-MET-01 P-CRE-01 N-PRO-02 1:2:3-01 &
        CIS-D-01 1:2-D-01 CYCLO-02 N-TET-01 DINON-01 N-TET-02 &
        GLYCO-01 FUMAR-01 1:2-B-01 ETHAN-01 2,2PROPA FURACETA &
        LEVOGLUC 4METGUA ETHYLANI BENZOATE METHPHEN ETHYLGUA &
        MESHEPTA BENZOFUR TRIMEBEN 4PROPGUA HMBENZAC METOCTAC &
        CONIFALC ISOEUGEN PHENKETO XANTHENE P-DECANO DNONDBEN &
        PENTACOS ETMEPHEN 1HINDANE HYDFLUOR HYDNAPH C18H28 &
        C21H24O4 FRACS=0.15 0.15 0.15 0.15 0.15 0.15 0.15 &
        0.15 0.15 0.15 0.15 0.15 0.15 0.15 0.15 0.15 0.15 &
        0.15 0.15 0.15 0.15 0.15 0.15 0.15 0.15 0.15 0.15 &
        0.15 0.15 0.15 0.15 0.15 0.15 0.15 0.15 0.15 0.15 &
        0.15 0.15 0.15 0.15 0.15 0.15 0.15 0.15 0.15 0.15 &
        0.15 0.15 0.15 0.15 0.15 0.15 0.15 0.15 0.15 0.15 &
        0.15 0.15 0.15 0.15 0.15 0.15 0.15 0.15 0.15 0.15 &
        0.15 0.15 0.15 0.15 0.15 0.15 0.15 0.15 0.15 0.15 &
        0.15 0.15 0.15 0.15 0.15 0.15 0.15 0.15 0.15 0.15 &
        0.15 0.15
    FRAC STREAM=5005 SUBSTREAM=CISOLID COMPS=CHAR FRACS=0.
    FLASH-SPECS 5005 TEMP=25. PRES=40. <psia>
    FLASH-SPECS 5004 TEMP=25. PRES=40. <psia>

BLOCK HX-5001+ HEATER
    IN-UNITS MET VOLUME-FLOW='cum/hr' ENTHALPY-FLO='Gcal/hr' &
        HEAT-TRANS-C='kcal/hr-sqm-K' PRESSURE=bar TEMPERATURE=C &
        VOLUME=cum DELTA-T=C HEAD=meter MOLE-DENSITY='kmol/cum' &
        MASS-DENSITY='kg/cum' MOLE-ENTHALP='kcal/mol' &
        MASS-ENTHALP='kcal/kg' HEAT=Gcal MOLE-CONC='mol/l' &
        PDROP=bar
    PARAM TEMP=25. PRES=40. <psia>

BLOCK HX-5001- HEATER
    IN-UNITS MET VOLUME-FLOW='cum/hr' ENTHALPY-FLO='Gcal/hr' &
        HEAT-TRANS-C='kcal/hr-sqm-K' PRESSURE=bar TEMPERATURE=C &
        VOLUME=cum DELTA-T=C HEAD=meter MOLE-DENSITY='kmol/cum' &
        MASS-DENSITY='kg/cum' MOLE-ENTHALP='kcal/mol' &
        MASS-ENTHALP='kcal/kg' HEAT=Gcal MOLE-CONC='mol/l' &
        PDROP=bar
    PARAM PRES=15. <psia>

BLOCK P-5001 PUMP
    IN-UNITS MET VOLUME-FLOW='cum/hr' ENTHALPY-FLO='Gcal/hr' &
        HEAT-TRANS-C='kcal/hr-sqm-K' PRESSURE=bar TEMPERATURE=C &
        VOLUME=cum DELTA-T=C HEAD=meter MOLE-DENSITY='kmol/cum' &
        MASS-DENSITY='kg/cum' MOLE-ENTHALP='kcal/mol' &

```
        MASS-ENTHALP='kcal/kg' HEAT=Gcal MOLE-CONC='mol/l'  &
        PDROP=bar
    PARAM PRES=40. <psia>

ENDHIERARCHY A5000

HIERARCHY A6000


DEF-STREAMS MIXCISLD ALL

SOLVE
    PARAM METHOD=SM
    RUN-MODE MODE=SIM

FLOWSHEET
    BLOCK HX-6001+ IN=6001 OUT=6002 QHX6001
    BLOCK FL-6001 IN=6002 OUT=6004 6003
    BLOCK CP-6001 IN=6004 OUT=6005 WCPA6001
    BLOCK HX-4001- IN=6007 QHX4001 OUT=6008
    BLOCK FSPLIT IN=6005 OUT=6007 6006
    BLOCK HX-6001- IN=CHW6001I QHX6001 OUT=CHW6001O

PROPERTIES NRTL FREE-WATER=STEAM-TA SOLU-WATER=3 TRUE-COMPS=YES
    PROPERTIES PENG-ROB / SRK

STREAM CHW6001I
    SUBSTREAM MIXED TEMP=4. PRES=15. <psia> MASS-FLOW=179.677
    MASS-FRAC H2O 1.

DEF-STREAMS HEAT QHX4001

DEF-STREAMS HEAT QHX6001

DEF-STREAMS WORK WCPA6001

BLOCK FSPLIT FSPLIT
    IN-UNITS MET VOLUME-FLOW='cum/hr' ENTHALPY-FLO='Gcal/hr'  &
        HEAT-TRANS-C='kcal/hr-sqm-K' PRESSURE=bar TEMPERATURE=C  &
        VOLUME=cum DELTA-T=C HEAD=meter MOLE-DENSITY='kmol/cum'  &
        MASS-DENSITY='kg/cum' MOLE-ENTHALP='kcal/mol'  &
        MASS-ENTHALP='kcal/kg' HEAT=Gcal MOLE-CONC='mol/l'  &
        PDROP=bar
    PARAM PRES=45. <psia>
    FRAC 6007 0.955

BLOCK HX-4001- HEATER
    IN-UNITS MET VOLUME-FLOW='cum/hr' ENTHALPY-FLO='Gcal/hr'  &
        HEAT-TRANS-C='kcal/hr-sqm-K' PRESSURE=bar TEMPERATURE=C  &
        VOLUME=cum DELTA-T=C HEAD=meter MOLE-DENSITY='kmol/cum'  &
        MASS-DENSITY='kg/cum' MOLE-ENTHALP='kcal/mol'  &
        MASS-ENTHALP='kcal/kg' HEAT=Gcal MOLE-CONC='mol/l'  &
        PDROP=bar
    PARAM PRES=45. <psia>

BLOCK HX-6001+ HEATER
    IN-UNITS MET VOLUME-FLOW='cum/hr' ENTHALPY-FLO='Gcal/hr'  &
        HEAT-TRANS-C='kcal/hr-sqm-K' PRESSURE=bar TEMPERATURE=C  &
        VOLUME=cum DELTA-T=C HEAD=meter MOLE-DENSITY='kmol/cum'  &
        MASS-DENSITY='kg/cum' MOLE-ENTHALP='kcal/mol'  &
        MASS-ENTHALP='kcal/kg' HEAT=Gcal MOLE-CONC='mol/l'  &
        PDROP=bar
    PARAM TEMP=7. PRES=20. <psia>

BLOCK HX-6001- HEATER
    PARAM PRES=15. <psia>

BLOCK FL-6001 FLASH2
    IN-UNITS MET VOLUME-FLOW='cum/hr' ENTHALPY-FLO='Gcal/hr'  &
        HEAT-TRANS-C='kcal/hr-sqm-K' PRESSURE=bar TEMPERATURE=C  &
        VOLUME=cum DELTA-T=C HEAD=meter MOLE-DENSITY='kmol/cum'  &
        MASS-DENSITY='kg/cum' MOLE-ENTHALP='kcal/mol'  &
        MASS-ENTHALP='kcal/kg' HEAT=Gcal MOLE-CONC='mol/l'  &
        PDROP=bar
```

```
    PARAM TEMP=7. PRES=20. <psia>

BLOCK CP-6001 COMPR
   IN-UNITS MET VOLUME-FLOW='cum/hr' ENTHALPY-FLO='Gcal/hr'  &
      HEAT-TRANS-C='kcal/hr-sqm-K' PRESSURE=bar TEMPERATURE=C  &
      VOLUME=cum DELTA-T=C HEAD=meter MOLE-DENSITY='kmol/cum'  &
      MASS-DENSITY='kg/cum' MOLE-ENTHALP='kcal/mol'  &
      MASS-ENTHALP='kcal/kg' HEAT=Gcal MOLE-CONC='mol/l'  &
      PDROP=bar
   PARAM TYPE=ISENTROPIC PRES=45. <psia>

ENDHIERARCHY A6000

HIERARCHY A7000


DEF-STREAMS MIXCISLD ALL

SOLVE
   PARAM METHOD=SM
   RUN-MODE MODE=SIM

FLOWSHEET
   BLOCK P-7001 IN=7001 OUT=7002 WPA7001
   BLOCK HX4004- IN=7016 QHX4004 OUT=7017
   BLOCK HXB3002- IN=7019 QHXB3002 OUT=7020
   BLOCK HXB2002- IN=7020 QHXB2002 OUT=7021
   BLOCK HXB3001- IN=7021 QHXB3001 OUT=7022
   BLOCK HXB3009- IN=7022 QHXB3009 OUT=7023
   BLOCK HX4003- IN=7023 QHX4003 OUT=7024
   BLOCK HX4002- IN=7024 QHX4002 OUT=7025
   BLOCK P-7006 IN=3010 OUT=7018 WPA7006
   BLOCK MX-7003 IN=7017 7018 OUT=7019
   BLOCK HXB3004- IN=7004 QHX3004 OUT=7005
   BLOCK HXB2004- IN=7007 QHXB2004 OUT=7008
   BLOCK HXB1002- IN=7010 QHXB1002 OUT=7011
   BLOCK HXB3012- IN=7013 QHXB3012 OUT=7014
   BLOCK MX-7001 IN=7005 7008 7011 7014 OUT=7015
   BLOCK MX-7002 IN=7015 7002 OUT=7016
   BLOCK P-7002 IN=7003 OUT=7004 WPA7002
   BLOCK P-7003 IN=7006 OUT=7007 WPA7003
   BLOCK P-7004 IN=7009 OUT=7010 WPA7004
   BLOCK P-7005 IN=7012 OUT=7013 WPA7005

PROPERTIES NRTL FREE-WATER=STEAM-TA SOLU-WATER=3 TRUE-COMPS=YES
   PROPERTIES PENG-ROB / SRK

STREAM 7001
   SUBSTREAM MIXED TEMP=25. PRES=1. <atm> MASS-FLOW=83.15
   MASS-FRAC H2O 1.

STREAM 7003
   SUBSTREAM MIXED TEMP=25. PRES=1. <atm> MASS-FLOW=117.
   MASS-FRAC H2O 1.

STREAM 7006
   SUBSTREAM MIXED TEMP=25. PRES=1. <atm> MASS-FLOW=26.
   MASS-FRAC H2O 1.

STREAM 7009
   SUBSTREAM MIXED TEMP=25. PRES=1. <atm> MASS-FLOW=65.
   MASS-FRAC H2O 1.

STREAM 7012
   SUBSTREAM MIXED TEMP=25. PRES=1. <atm> MASS-FLOW=60.
   MASS-FRAC H2O 1.

DEF-STREAMS HEAT QHX3004

DEF-STREAMS HEAT QHX4002

DEF-STREAMS HEAT QHX4003

DEF-STREAMS HEAT QHX4004
```

DEF-STREAMS HEAT QHXB1002

DEF-STREAMS HEAT QHXB2002

DEF-STREAMS HEAT QHXB2004

DEF-STREAMS HEAT QHXB3001

DEF-STREAMS HEAT QHXB3002

DEF-STREAMS HEAT QHXB3009

DEF-STREAMS HEAT QHXB3012

DEF-STREAMS WORK WPA7001

DEF-STREAMS WORK WPA7002

DEF-STREAMS WORK WPA7003

DEF-STREAMS WORK WPA7004

DEF-STREAMS WORK WPA7005

DEF-STREAMS WORK WPA7006

BLOCK MX-7001 MIXER

BLOCK MX-7002 MIXER

BLOCK MX-7003 MIXER

BLOCK HX4002- HEATER
   PARAM PRES=-0.

BLOCK HX4003- HEATER
   PARAM PRES=-0.

BLOCK HX4004- HEATER
   PARAM PRES=-0.

BLOCK HXB1002- HEATER
   PARAM PRES=-0.

BLOCK HXB2002- HEATER
   PARAM PRES=-0.

BLOCK HXB2004- HEATER
   PARAM PRES=-0.

BLOCK HXB3001- HEATER
   PARAM PRES=-0.

BLOCK HXB3002- HEATER
   PARAM PRES=-0.

BLOCK HXB3004- HEATER
   PARAM PRES=-0.

BLOCK HXB3009- HEATER
   PARAM PRES=-0.

BLOCK HXB3012- HEATER
   PARAM PRES=-0.

BLOCK P-7001 PUMP
   PARAM PRES=105.

BLOCK P-7002 PUMP
   PARAM PRES=105.

BLOCK P-7003 PUMP
   PARAM PRES=105.

```
BLOCK P-7004 PUMP
    PARAM PRES=105.

BLOCK P-7005 PUMP
    PARAM PRES=105.

BLOCK P-7006 PUMP
    PARAM PRES=105.

ENDHIERARCHY A7000

HIERARCHY A8000


DEF-STREAMS MIXCISLD ALL

SOLVE
    PARAM METHOD=SM
    RUN-MODE MODE=SIM

FLOWSHEET
    BLOCK MX-8001 IN=WPA5001 WCPA3001 WCPA6001 WCPA4001  &
        WTB4003 WTB4002 WTB4001 WPA7001 WPA7002 WPA7003 WPA7004  &
        WPA7005 WPA7006 WPB1001 WCPB3001 WCPB3002 WCPB3003  &
        WCPB3004 WGRIND WCW WDISTIL WESP WCHW OUT=WEXCESS
    BLOCK MX-8002 IN=CWA5001O CWB3006O CWB3005O CWB2005O  &
        CWDIST OUT=HOTCW
    BLOCK MX-8006M IN=FUELH2PR FUELDIST OUT=FUELTOT
    BLOCK MX-8005M IN=STMDIST2 OUT=PRSTMTOT
    BLOCK MX-8004 IN=DH2ODIST OUT=DH2OTOT
    BLOCK HX-8001 IN=STMDIST OUT=STMDIST2 QSTMDISC
    BLOCK MX-8005Q IN=QSTMDISA OUT=QSTMDISB
    BLOCK CB-8001 IN=FUELDIS AIRDIS OUT=PRODDIS QFLDISC
    BLOCK MX-8006Q IN=QFLDISA OUT=QFLDISB
    BLOCK S-8002 IN=B4008 OUT=LPTOT STMPSA
    BLOCK HX-8002 IN=STMPSA OUT=WPSA QPSAC
    BLOCK MX-8007 IN=QPSAA OUT=QPSAB
    BLOCK CWT-8001 IN=CWCIRC OUT=EVAPLOSS COOLEDCW QEVAP
    BLOCK S-8001 IN=COOLEDCW OUT=DRIFLOSS CWUTIL BLOWDOWN
    BLOCK MX-8003 IN=MAKEUPCW HOTCW OUT=CWCIRC
    BLOCK HX-8003 IN=CHW OUT=CHWTOT QCHW
    BLOCK MX-8006 IN=CHWTOT OUT=CHWUTIL CHWLOSS

PROPERTIES NRTL FREE-WATER=STEAM-TA SOLU-WATER=3 TRUE-COMPS=YES
    PROPERTIES PENG-ROB / SRK

STREAM AIRDIS
    SUBSTREAM MIXED TEMP=25. PRES=1. <atm> MASS-FLOW=7.
    MASS-FRAC N2 0.7503 / O2 0.2299 / CO2 0.0005 / H2O  &
        0.0066 / AR 0.0127

STREAM CHW
    SUBSTREAM MIXED TEMP=12. PRES=15. <psia> MASS-FLOW=191.18706
    MASS-FRAC H2O 1.

STREAM CWDIST
    SUBSTREAM MIXED TEMP=49. PRES=1.03 MASS-FLOW=21.51
    MASS-FRAC H2O 1.

STREAM DH2ODIST
    SUBSTREAM MIXED TEMP=49. PRES=1.03 MASS-FLOW=1.357
    MASS-FRAC H2O 1.

STREAM FUELDIS
    SUBSTREAM MIXED TEMP=25. PRES=1. <atm> MASS-FLOW=0.272648
    MASS-FRAC CH4 1.

STREAM FUELDIST
    SUBSTREAM MIXED TEMP=25. PRES=1. <atm> MASS-FLOW=0.27265354
    MASS-FRAC CH4 1.

STREAM FUELH2PR
    SUBSTREAM MIXED TEMP=25. PRES=1. <atm> MASS-FLOW=2.36975253
```

320

```
    MASS-FRAC CH4 1.

STREAM MAKEUPCW
    SUBSTREAM MIXED TEMP=43.9 PRES=1.03 MASS-FLOW=3.00662898
    MASS-FRAC H2O 1.

DEF-STREAMS HEAT QCHW

DEF-STREAMS HEAT QEVAP

DEF-STREAMS HEAT QFLDISA

STREAM QFLDISA
    INFO HEAT DUTY=9737.95

DEF-STREAMS HEAT QFLDISB

DEF-STREAMS HEAT QFLDISC

DEF-STREAMS HEAT QPSAA

STREAM QPSAA
    INFO HEAT DUTY=341.

DEF-STREAMS HEAT QPSAB

DEF-STREAMS HEAT QPSAC

DEF-STREAMS HEAT QSTMDISA

STREAM QSTMDISA
    INFO HEAT DUTY=1458.5

DEF-STREAMS HEAT QSTMDISB

DEF-STREAMS HEAT QSTMDISC

DEF-STREAMS WORK WCHW

STREAM WCHW
    INFO WORK POWER=0.3

DEF-STREAMS WORK WCPA3001

DEF-STREAMS WORK WCPA4001

DEF-STREAMS WORK WCPA6001

DEF-STREAMS WORK WCPB3001

DEF-STREAMS WORK WCPB3002

DEF-STREAMS WORK WCPB3003

DEF-STREAMS WORK WCPB3004

DEF-STREAMS WORK WCW

STREAM WCW
    INFO WORK POWER=0.

DEF-STREAMS WORK WDISTIL

STREAM WDISTIL
    INFO WORK POWER=0.13

DEF-STREAMS WORK WESP

STREAM WESP
    INFO WORK POWER=146. <MJ/hr>

DEF-STREAMS WORK WEXCESS

DEF-STREAMS WORK WGRIND
```

321

```
STREAM WGRIND
   INFO WORK POWER=4.96

DEF-STREAMS WORK WPA5001

DEF-STREAMS WORK WPA7001

DEF-STREAMS WORK WPA7002

DEF-STREAMS WORK WPA7003

DEF-STREAMS WORK WPA7004

DEF-STREAMS WORK WPA7005

DEF-STREAMS WORK WPA7006

DEF-STREAMS WORK WPB1001

DEF-STREAMS WORK WTB4001

DEF-STREAMS WORK WTB4002

DEF-STREAMS WORK WTB4003

BLOCK MX-8001 MIXER
   IN-UNITS MET VOLUME-FLOW='cum/hr' ENTHALPY-FLO='Gcal/hr'  &
      HEAT-TRANS-C='kcal/hr-sqm-K' PRESSURE=bar TEMPERATURE=C  &
      VOLUME=cum DELTA-T=C HEAD=meter MOLE-DENSITY='kmol/cum'  &
      MASS-DENSITY='kg/cum' MOLE-ENTHALP='kcal/mol'  &
      MASS-ENTHALP='kcal/kg' HEAT=Gcal MOLE-CONC='mol/l'  &
      PDROP=bar

BLOCK MX-8002 MIXER
   IN-UNITS MET VOLUME-FLOW='cum/hr' ENTHALPY-FLO='Gcal/hr'  &
      HEAT-TRANS-C='kcal/hr-sqm-K' PRESSURE=bar TEMPERATURE=C  &
      VOLUME=cum DELTA-T=C HEAD=meter MOLE-DENSITY='kmol/cum'  &
      MASS-DENSITY='kg/cum' MOLE-ENTHALP='kcal/mol'  &
      MASS-ENTHALP='kcal/kg' HEAT=Gcal MOLE-CONC='mol/l'  &
      PDROP=bar

BLOCK MX-8003 MIXER

BLOCK MX-8004 MIXER

BLOCK MX-8005M MIXER

BLOCK MX-8005Q MIXER

BLOCK MX-8006M MIXER

BLOCK MX-8006Q MIXER

BLOCK MX-8007 MIXER

BLOCK MX-8006 FSPLIT
   MASS-FLOW CHWUTIL 179.6776

BLOCK S-8001 FSPLIT
   FRAC DRIFLOSS 0.0030799 / BLOWDOWN 0.0307979

BLOCK S-8002 FSPLIT
   FRAC LPTOT 0.999509

BLOCK HX-8001 HEATER
   PARAM TEMP=263. PRES=-0.

BLOCK HX-8002 HEATER
   PARAM TEMP=115. PRES=-0.

BLOCK HX-8003 HEATER
   PARAM TEMP=7. PRES=-0.
```

322

```
BLOCK CWT-8001 FLASH2
    PARAM TEMP=27. VFRAC=0.025857

BLOCK CB-8001 RSTOIC
    PARAM TEMP=406. PRES=1. <atm> COMBUSTION=YES

ENDHIERARCHY A8000

HIERARCHY B1000


DEF-STREAMS MIXCISLD ALL

SOLVE
    PARAM METHOD=SM
    RUN-MODE MODE=SIM

FLOWSHEET
    BLOCK R-B1001 IN=B1003 B1005 OUT=B1004
    BLOCK F-B1001 IN=B1006 OUT=B1007 B1008
    BLOCK HXB1002+ IN=B1004 OUT=B1006 QHXB1002
    BLOCK S-B1001 IN=B1008 OUT=B1010 B1009
    BLOCK HXB1001 IN=B1002 QHXB3003 OUT=B1003
    BLOCK P-B1001 IN=B1001 OUT=B1002 WPB1001
    BLOCK S-B1002 IN=B1010 OUT=B1012 B1011

PROPERTIES NRTL FREE-WATER=STEAM-TA SOLU-WATER=3 TRUE-COMPS=YES
    PROPERTIES PENG-ROB / SRK

STREAM B1005
    SUBSTREAM MIXED TEMP=25. PRES=2000. <psig> MASS-FLOW=1.8
    MASS-FRAC H2 1.

DEF-STREAMS HEAT QHXB1002

DEF-STREAMS HEAT QHXB3003

DEF-STREAMS WORK WPB1001

BLOCK S-B1001 SEP
    PARAM
    FRAC STREAM=B1010 SUBSTREAM=MIXED COMPS=N2 O2 H2 CO NO2  &
        CO2 H2O H3N CH4 C2H4 C3H6-2 AR ACETACID ACETOL  &
        GUAIACOL 3:5-X-01 FORMACID N-PRO-01 PHENOL TOLUENE  &
        FURFURAL BENZENE CHAR ASH CELLULOS LIGNIN XYLAN  &
        ARABINAN MANNAN GALACTAN EXTRACT TETRA-01 DILACID  &
        N-HEP-01 2:4-X-01 O-ETH-01 INDAN-01 2:6-D-01 NAPHT-01  &
        DIBEN-01 FLUOR-01 2:4-D-01 NAPHT-02 ETHYL-01 N-HEX-01  &
        CYCLO-01 M-XYL-01 METHY-01 1:3-C-01 3-MET-01 P-CRE-01  &
        N-PRO-02 1:2:3-01 CIS-D-01 1:2-D-01 CYCLO-02 N-TET-01  &
        DINON-01 N-TET-02 GLYCO-01 FUMAR-01 1:2-B-01 ETHAN-01  &
        2,2PROPA FURACETA LEVOGLUC 4METGUA ETHYLANI BENZOATE  &
        METHPHEN ETHYLGUA MESHEPTA BENZOFUR TRIMEBEN 4PROPGUA  &
        HMBENZAC METOCTAC CONIFALC ISOEUGEN PHENKETO XANTHENE  &
        P-DECANO DNONDBEN PENTACOS ETMEPHEN 1HINDANE HYDFLUOR  &
        HYDNAPH C18H28 C21H24O4 C22H20O METHA-01 ETHAN-02  &
        PROPA-01 ISOBU-01 COKE1 FRACS=1. 1. 1. 1. 1. 1.  &
        1. 1. 1. 1. 1. 1. 1. 1. 1. 1. 1. 1. 1. 1.  &
        1. 1. 1. 1. 1. 1. 1. 1. 1. 1. 1. 1. 1. 1.  &
        1. 1. 1. 1. 1. 1. 1. 1. 1. 1. 1. 1. 1. 1.  &
        1. 1. 1. 1. 1. 1. 1. 1. 0.933594 0.822421 0. 0.  &
        0.705875 1. 1. 1. 1. 1. 1. 1. 1. 1. 1. 1. 1.  &
        1. 1. 1. 1. 1. 1. 1. 1. 1. 1. 1. 1. 0. 1.  &
        1. 1. 1.
    FRAC STREAM=B1010 SUBSTREAM=CISOLID COMPS=CHAR FRACS=0.

BLOCK S-B1002 SEP
    PARAM
    FRAC STREAM=B1012 SUBSTREAM=MIXED COMPS=N2 O2 H2 CO NO2  &
        CO2 H2O H3N CH4 C2H4 C3H6-2 AR ACETACID ACETOL  &
        GUAIACOL 3:5-X-01 FORMACID N-PRO-01 PHENOL TOLUENE  &
        FURFURAL BENZENE CHAR ASH CELLULOS LIGNIN XYLAN  &
        ARABINAN MANNAN GALACTAN EXTRACT TETRA-01 DILACID  &
        N-HEP-01 2:4-X-01 O-ETH-01 INDAN-01 2:6-D-01 NAPHT-01  &
```

323

```
        DIBEN-01 FLUOR-01 2:4-D-01 NAPHT-02 ETHYL-01 N-HEX-01  &
        CYCLO-01 M-XYL-01 METHY-01 1:3-C-01 3-MET-01 P-CRE-01  &
        N-PRO-02 1:2:3-01 CIS-D-01 1:2-D-01 CYCLO-02 N-TET-01  &
        DINON-01 N-TET-02 GLYCO-01 FUMAR-01 1:2-B-01 ETHAN-01  &
        2,2PROPA FURACETA LEVOGLUC 4METGUA ETHYLANI BENZOATE  &
        METHPHEN ETHYLGUA MESHEPTA BENZOFUR TRIMEBEN 4PROPGUA  &
        HMBENZAC METOCTAC CONIFALC ISOEUGEN PHENKETO XANTHENE  &
        P-DECANO DNONDBEN PENTACOS ETMEPHEN 1HINDANE HYDFLUOR  &
        HYDNAPH C18H28 C21H24O4 C22H20O METHA-01 ETHAN-02  &
        PROPA-01 ISOBU-01 COKE1 FRACS=0. 0. 0. 0. 0. 0. 0.  &
        0. 0. 0. 0. 0. 0. 0. 0. 0. 0. 0. 0. 0. 0. 0. 0. 0.  &
        0. 0. 0. 0. 0. 0. 0. 0. 0. 0. 0. 0. 0. 0. 0. 0. 0.  &
        0. 0. 0. 0. 0. 0. 0. 0. 0. 0. 0. 0. 0. 0. 0. 0. 0.  &
        0. 0. 0. 0. 0. 0. 0. 0. 0. 0. 0. 0. 0. 0. 0. 0. 1.  &
        1. 0. 0. 0. 0. 0. 0. 0. 0. 0. 0. 0. 0. 0. 0. 0. 0.  &
        0. 0. 0. 0. 0. 0. 0. 0. 0. 0. 0. 0. 0. 0. 0. 0. 1.
    FRAC STREAM=B1011 SUBSTREAM=CISOLID COMPS=CHAR FRACS=0.

BLOCK HXB1001 HEATER
    PARAM PRES=-0.

BLOCK HXB1002+ HEATER
    PARAM TEMP=57. PRES=-0.62 NPHASE=2
    BLOCK-OPTION FREE-WATER=YES

BLOCK F-B1001 FLASH2
    PARAM PRES=104. DUTY=0. NPHASE=2
    BLOCK-OPTION FREE-WATER=YES

BLOCK R-B1001 RSTOIC
    PARAM PRES=2000. <psig> DUTY=0. HEAT-OF-REAC=NO
    STOIC 1 MIXED ACETACID -1. / H2 -2. / ETHAN-01 1. /  &
        H2O 1.
    STOIC 2 MIXED GLYCO-01 -1. / H2 -3. / ETHAN-01 1. /  &
        H2O 2.
    STOIC 3 MIXED FURFURAL -1. / H2 -4. / TETRA-01 1. /  &
        METHA-01 1.
    STOIC 4 MIXED BENZOATE -1. / H2 -2. / TOLUENE 1. /  &
        CH4 2. / CO2 1.
    STOIC 5 MIXED METHPHEN -1. / H2 -5. / TOLUENE 1. /  &
        CH4 2. / H2O 2.
    STOIC 6 MIXED ETHYLGUA -1. / H2 -3. / ETHYL-01 1. /  &
        CH4 1. / H2O 2.
    STOIC 7 MIXED N-HEP-01 -1. / H2 -1. / N-HEX-01 1. /  &
        H2O 1. / CO 1.
    STOIC 8 MIXED MESHEPTA -1. / H2 -1. / N-HEX-01 1. /  &
        CH4 1. / CO2 1.
    STOIC 9 MIXED BENZOFUR -1. / H2 -7. / CYCLO-01 1. /  &
        H2O 1. / ETHAN-02 1.
    STOIC 10 MIXED TRIMEBEN -1. / H2 -9. / CYCLO-01 1. /  &
        CH4 3. / H2O 3.
    STOIC 11 MIXED PHENOL -1. / H2 -4. / CYCLO-01 1. /  &
        H2O 1.
    STOIC 12 MIXED TRIMEBEN -1. / H2 -5. / PHENOL 1. /  &
        CH4 3. / H2O 2.
    STOIC 13 MIXED 2:4-X-01 -1. / H2 -1. / M-XYL-01 1. /  &
        H2O 1.
    STOIC 14 MIXED O-ETH-01 -1. / H2 -1. / ETHYL-01 1. /  &
        H2O 1.
    STOIC 15 MIXED ETHYLGUA -1. / H2 -3. / ETHYL-01 1. /  &
        H2O 2. / CH4 1.
    STOIC 16 MIXED 4PROPGUA -1. / H2 -6. / METHY-01 1. /  &
        PROPA-01 1. / H2O 2.
    STOIC 17 MIXED HMBENZAC -1. / H2 -4. / 1:3-C-01 1. /  &
        CH4 1. / CO2 1. / H2O 2.
    STOIC 18 MIXED METOCTAC -1. / 3-MET-01 1. / CO2 1.
    STOIC 19 MIXED 2:6-D-01 -1. / H2 -2. / P-CRE-01 1. /  &
        ISOBU-01 2.
    STOIC 20 MIXED 4PROPGUA -1. / H2 -2. / P-CRE-01 1. /  &
        PROPA-01 1. / H2O 1.
    STOIC 21 MIXED CONIFALC -1. / H2 -4. / ETMEPHEN 1. /  &
        CH4 1. / H2O 2.
    STOIC 22 MIXED ISOEUGEN -1. / H2 -4. / N-PRO-02 1. /  &
        CH4 1. / H2O 2.
```

324

```
    STOIC 23 MIXED NAPHT-01 -1. / H2 -2. / 1:2:3-01 1.
    STOIC 24 MIXED NAPHT-01 -1. / H2 -5. / CIS-D-01 1.
    STOIC 25 MIXED INDAN-01 -1. / H2 -3. / 1HINDANE 1.
    STOIC 26 MIXED PHENKETO -1. / H2 -4. / 1:2-D-01 1. / &
        H2O 3.
    STOIC 27 MIXED XANTHENE -1. / H2 -6. / CYCLO-02 1. / &
        CH4 1. / H2O 1.
    STOIC 28 MIXED P-DECANO -1. / H2 -1. / N-TET-01 1. / &
        CO2 1. / CH4 1.
    STOIC 29 MIXED FLUOR-01 -1. / H2 -8. / HYDFLUOR 1.
    STOIC 30 MIXED DNONDBEN -1. / H2 -1. / DINON-01 1. / &
        H2O 1.
    STOIC 31 MIXED NAPHT-02 -1. / H2 -9. / HYDNAPH 1.
    STOIC 32 MIXED PENTACOS -1. / H2 -1. / N-TET-02 1. / &
        CO2 1. / ETHAN-02 1.
    STOIC 33 MIXED LEVOGLUC -0.545886 / 4METGUA -1.161296 / &
        ETHYLANI -9.715441 / COKE1 1.
    CONV 1 MIXED ACETACID 0.000292
    CONV 2 MIXED GLYCO-01 1.
    CONV 3 MIXED FURFURAL 0.248429
    CONV 4 MIXED BENZOATE 0.174409
    CONV 5 MIXED METHPHEN 0.219105
    CONV 6 MIXED ETHYLGUA 0.10208
    CONV 7 MIXED N-HEP-01 0.
    CONV 8 MIXED MESHEPTA 2.11E-005
    CONV 9 MIXED BENZOFUR 0.036142
    CONV 10 MIXED TRIMEBEN 0.02123
    CONV 11 MIXED PHENOL 0.307631
    CONV 12 MIXED TRIMEBEN 0.02807
    CONV 13 MIXED 2:4-X-01 0.32901
    CONV 14 MIXED O-ETH-01 0.271077
    CONV 15 MIXED ETHYLGUA 0.12027
    CONV 16 MIXED 4PROPGUA 0.
    CONV 17 MIXED HMBENZAC 0.587761
    CONV 18 MIXED METOCTAC 1.
    CONV 19 MIXED 2:6-D-01 0.
    CONV 20 MIXED 4PROPGUA 0.
    CONV 21 MIXED CONIFALC 0.296892
    CONV 22 MIXED ISOEUGEN 0.091514
    CONV 23 MIXED NAPHT-01 0.03983
    CONV 24 MIXED NAPHT-01 0.20583
    CONV 25 MIXED INDAN-01 0.222397
    CONV 26 MIXED PHENKETO 1.
    CONV 27 MIXED XANTHENE 0.084447
    CONV 28 MIXED P-DECANO 0.016815
    CONV 29 MIXED FLUOR-01 0.183652
    CONV 30 MIXED DNONDBEN 0.311366
    CONV 31 MIXED NAPHT-02 0.2299772
    CONV 32 MIXED PENTACOS 1.
    CONV 33 MIXED LEVOGLUC 1.

BLOCK P-B1001 PUMP
    PARAM PRES=2000. <psig>

ENDHIERARCHY B1000

HIERARCHY B2000


DEF-STREAMS MIXCISLD ALL

SOLVE
    PARAM METHOD=SM
    RUN-MODE MODE=SIM

FLOWSHEET
    BLOCK R-B2001 IN=B2003 B2002 OUT=B2004
    BLOCK HXB2001 IN=B2001 QHXB2003 OUT=B2002
    BLOCK F-B2001 IN=B2008 OUT=B2009 B2010
    BLOCK HXB2002+ IN=B2004 OUT=B2005 QHXB2002
    BLOCK S-B2001 IN=B2010 OUT=B2012 B2011
    BLOCK S-B2002 IN=B2011 OUT=B2014 B2013
    BLOCK F-B2002 IN=B2014 OUT=B2015 B2016
    BLOCK D-B2001 IN=B2016 OUT=B2017 B2018 B2019 B2020 B2021
```

325

```
    BLOCK HXB2004+ IN=B2006 OUT=B2007 QHXB2004
    BLOCK HXB2003 IN=B2005 OUT=B2006 QHXB2003
    BLOCK HXB2005+ IN=B2007 OUT=B2008 QHXB2005
    BLOCK HXB2005- IN=CWB2005I QHXB2005 OUT=CWB2005O


PROPERTIES NRTL FREE-WATER=STEAM-TA SOLU-WATER=3 TRUE-COMPS=YES
    PROPERTIES PENG-ROB / SRK


STREAM B2003
    SUBSTREAM MIXED TEMP=25. PRES=1500. <psig> MASS-FLOW=3.
    MASS-FRAC H2 1.


STREAM CWB2005I
    SUBSTREAM MIXED TEMP=27. PRES=1.03 MASS-FLOW=6.78
    MASS-FRAC H2O 1.


DEF-STREAMS HEAT QHXB2002


DEF-STREAMS HEAT QHXB2003


DEF-STREAMS HEAT QHXB2004


DEF-STREAMS HEAT QHXB2005


BLOCK D-B2001 SEP
    FRAC STREAM=B2017 SUBSTREAM=MIXED COMPS=N2 O2 H2 CO NO2  &
        CO2 H2O H3N CH4 C2H4 C3H6-2 AR ACETACID PHENOL  &
        TOLUENE TETRA-01 ETHYL-01 N-HEX-01 CYCLO-01 METHA-01  &
        ETHAN-02 PROPA-01 ISOBU-01 FRACS=1. 1. 1. 1. 1.  &
        1. 1. 1. 1. 1. 1. 1. 0.170708 1. 1. 0.267023 1.  &
        1. 1. 1. 1. 1.
    FRAC STREAM=B2017 SUBSTREAM=CISOLID COMPS=CHAR FRACS=0.
    FRAC STREAM=B2018 SUBSTREAM=MIXED COMPS=PHENOL BENZENE  &
        INDAN-01 ETHYL-01 M-XYL-01 METHY-01 1:3-C-01 3-MET-01  &
        FRACS=0.829292 1. 1. 0.732977 1. 1. 1. 1.
    FRAC STREAM=B2018 SUBSTREAM=CISOLID COMPS=CHAR FRACS=0.
    FRAC STREAM=B2019 SUBSTREAM=MIXED COMPS=P-CRE-01 N-PRO-02  &
        1:2:3-01 CIS-D-01 ETMEPHEN 1HINDANE FRACS=1. 1. 1. 1.  &
        1. 1.
    FRAC STREAM=B2019 SUBSTREAM=CISOLID COMPS=CHAR FRACS=0.
    FRAC STREAM=B2020 SUBSTREAM=MIXED COMPS=DIBEN-01 1:2-D-01  &
        CYCLO-02 N-TET-01 HYDFLUOR FRACS=1. 1. 1. 1. 1.
    FRAC STREAM=B2020 SUBSTREAM=CISOLID COMPS=CHAR FRACS=0.


BLOCK S-B2001 SEP
    PARAM
    FRAC STREAM=B2011 SUBSTREAM=MIXED COMPS=N2 O2 H2 CO NO2  &
        CO2 H2O H3N CH4 C2H4 C3H6-2 AR ACETACID ACETOL  &
        GUAIACOL 3:5-X-01 FORMACID N-PRO-01 PHENOL TOLUENE  &
        FURFURAL BENZENE CHAR ASH CELLULOS LIGNIN XYLAN  &
        ARABINAN MANNAN GALACTAN EXTRACT TETRA-01 DILACID  &
        N-HEP-01 2:4-X-01 O-ETH-01 INDAN-01 2:6-D-01 NAPHT-01  &
        DIBEN-01 FLUOR-01 2:4-D-01 NAPHT-02 ETHYL-01 N-HEX-01  &
        CYCLO-01 M-XYL-01 METHY-01 1:3-C-01 3-MET-01 P-CRE-01  &
        N-PRO-02 1:2:3-01 CIS-D-01 1:2-D-01 CYCLO-02 N-TET-01  &
        DINON-01 N-TET-02 GLYCO-01 FUMAR-01 1:2-B-01 ETHAN-01  &
        2,2PROPA FURACETA LEVOGLUC 4METGUA ETHYLANI BENZOATE  &
        METHPHEN ETHYLGUA MESHEPTA BENZOFUR TRIMEBEN 4PROPGUA  &
        HMBENZAC METOCTAC CONIFALC ISOEUGEN PHENKETO XANTHENE  &
        P-DECANO DNONDBEN PENTACOS ETMEPHEN 1HINDANE HYDFLUOR  &
        HYDNAPH C18H28 C21H24O4 C22H20O METHA-01 ETHAN-02  &
        PROPA-01 ISOBU-01 FRACS=1. 1. 1. 1. 1. 0. 1. 1.  &
        1. 1. 1. 1. 1. 1. 1. 1. 1. 1. 1. 1. 1. 1.  &
        1. 1. 1. 1. 1. 1. 1. 1. 1. 1. 1. 1. 1. 1.  &
        1. 1. 1. 1. 1. 1. 1. 1. 1. 1. 1. 1. 1. 1.  &
        1. 1. 1. 1. 1. 1. 0. 0. 0. 0. 0. 1. 1. 1. 1.  &
        1. 1. 1. 1. 1. 1. 1. 1. 1. 1. 1. 1. 1. 1.  &
        1. 1. 1. 1. 1. 1. 0.5 0.5 0.5 0.5
    FRAC STREAM=B2011 SUBSTREAM=CISOLID COMPS=CHAR FRACS=0.


BLOCK S-B2002 SEP
    PARAM
    FRAC STREAM=B2013 SUBSTREAM=MIXED COMPS=N2 O2 H2 CO NO2  &
        CO2 H2O H3N CH4 C2H4 C3H6-2 AR ACETACID ACETOL  &
```

```
    GUAIACOL 3:5-X-01 FORMACID N-PRO-01 PHENOL TOLUENE  &
    FURFURAL BENZENE CHAR ASH CELLULOS LIGNIN XYLAN  &
    ARABINAN MANNAN GALACTAN EXTRACT TETRA-01 DILACID  &
    N-HEP-01 2:4-X-01 O-ETH-01 INDAN-01 2:6-D-01 NAPHT-01  &
    DIBEN-01 FLUOR-01 2:4-D-01 NAPHT-02 ETHYL-01 N-HEX-01  &
    CYCLO-01 M-XYL-01 METHY-01 1:3-C-01 3-MET-01 P-CRE-01  &
    N-PRO-02 1:2:3-01 CIS-D-01 1:2-D-01 CYCLO-02 N-TET-01  &
    DINON-01 N-TET-02 GLYCO-01 FUMAR-01 1:2-B-01 ETHAN-01  &
    2,2PROPA FURACETA LEVOGLUC 4METGUA ETHYLANI BENZOATE  &
    METHPHEN ETHYLGUA MESHEPTA BENZOFUR TRIMEBEN 4PROPGUA  &
    HMBENZAC METOCTAC CONIFALC ISOEUGEN PHENKETO XANTHENE  &
    P-DECANO DNONDBEN PENTACOS ETMEPHEN 1HINDANE HYDFLUOR  &
    HYDNAPH C18H28 C21H24O4 C22H20O METHA-01 ETHAN-02  &
    PROPA-01 ISOBU-01 COKE1 COKE2 FRACS=0. 0. 0. 0. 0.  &
    0. 0. 0. 0. 0. 0. 0. 0. 0. 0. 0. 0. 0. 0. 0. 0.  &
    0. 0. 0. 0. 0. 0. 0. 0. 0. 0. 0. 0. 0. 0. 0. 0.  &
    0. 0. 0. 0. 0. 0. 0. 0. 0. 0. 0. 0. 0. 0. 0. 0.  &
    0. 0. 0. 0. 0. 0. 0. 0. 0. 0. 0. 0. 0. 0. 0. 0.  &
    0. 0. 0. 0. 0. 0. 0. 0. 0. 0. 0. 0. 0. 0. 0. 0.  &
    0. 0. 0. 0. 0. 0. 0. 0. 1. 0. 1. 0. 0. 0. 0.  &
    0. 1.
    FRAC STREAM=B2013 SUBSTREAM=CISOLID COMPS=CHAR FRACS=0.

BLOCK HXB2001 HEATER
    PARAM PRES=-0.

BLOCK HXB2002+ HEATER
    PARAM TEMP=369.7 PRES=-0.62

BLOCK HXB2003 HEATER
    PARAM TEMP=352.82805 PRES=-0.

BLOCK HXB2004+ HEATER
    PARAM TEMP=55. PRES=-0.

BLOCK HXB2005+ HEATER
    PARAM TEMP=50. PRES=-0.

BLOCK HXB2005- HEATER
    PARAM PRES=-0.

BLOCK F-B2001 FLASH2
    PARAM PRES=100. DUTY=0. NPHASE=2
    BLOCK-OPTION FREE-WATER=YES

BLOCK F-B2002 FLASH2
    PARAM PRES=40. <psig> DUTY=0.

BLOCK R-B2001 RSTOIC
    PARAM PRES=1500. <psig> DUTY=0. HEAT-OF-REAC=NO
    STOIC 1 MIXED ACETACID -1. / H2 -2. / ETHAN-01 1. /  &
      H2O 1.
    STOIC 2 MIXED GLYCO-01 -1. / H2 -3. / ETHAN-01 1. /  &
      H2O 2.
    STOIC 3 MIXED FURFURAL -1. / H2 -4. / TETRA-01 1. /  &
      METHA-01 1.
    STOIC 4 MIXED BENZOATE -1. / H2 -2. / TOLUENE 1. /  &
      CH4 2. / CO2 1.
    STOIC 5 MIXED METHPHEN -1. / H2 -5. / TOLUENE 1. /  &
      CH4 2. / H2O 2.
    STOIC 6 MIXED ETHYLGUA -1. / H2 -3. / ETHYL-01 1. /  &
      CH4 1. / H2O 2.
    STOIC 7 MIXED N-HEP-01 -1. / H2 -1. / N-HEX-01 1. /  &
      H2O 1. / CO 1.
    STOIC 8 MIXED MESHEPTA -1. / H2 -1. / N-HEX-01 1. /  &
      CH4 1. / CO2 1.
    STOIC 9 MIXED BENZOFUR -1. / H2 -7. / CYCLO-01 1. /  &
      H2O 1. / ETHAN-02 1.
    STOIC 10 MIXED TRIMEBEN -1. / H2 -9. / CYCLO-01 1. /  &
      CH4 3. / H2O 3.
    STOIC 11 MIXED PHENOL -1. / H2 -4. / CYCLO-01 1. /  &
      H2O 1.
    STOIC 12 MIXED TRIMEBEN -1. / H2 -5. / PHENOL 1. /  &
      CH4 3. / H2O 2.
```

327

```
    STOIC 13 MIXED 2:4-X-01 -1. / H2 -1. / M-XYL-01 1. /  &
        H2O 1.
    STOIC 14 MIXED O-ETH-01 -1. / H2 -1. / ETHYL-01 1. /  &
        H2O 1.
    STOIC 15 MIXED ETHYLGUA -1. / H2 -3. / ETHYL-01 1. /  &
        H2O 2. / CH4 1.
    STOIC 16 MIXED 4PROPGUA -1. / H2 -6. / METHY-01 1. /  &
        PROPA-01 1. / H2O 2.
    STOIC 17 MIXED HMBENZAC -1. / H2 -4. / 1:3-C-01 1. /  &
        CH4 1. / CO2 1. / H2O 2.
    STOIC 18 MIXED METOCTAC -1. / 3-MET-01 1. / CO2 1.
    STOIC 19 MIXED 2:6-D-01 -1. / H2 -2. / P-CRE-01 1. /  &
        ISOBU-01 2.
    STOIC 20 MIXED 4PROPGUA -1. / H2 -2. / P-CRE-01 1. /  &
        PROPA-01 1. / H2O 1.
    STOIC 21 MIXED CONIFALC -1. / H2 -4. / ETMEPHEN 1. /  &
        CH4 1. / H2O 2.
    STOIC 22 MIXED ISOEUGEN -1. / H2 -4. / N-PRO-02 1. /  &
        CH4 1. / H2O 2.
    STOIC 23 MIXED NAPHT-01 -1. / H2 -2. / 1:2:3-01 1.
    STOIC 24 MIXED NAPHT-01 -1. / H2 -5. / CIS-D-01 1.
    STOIC 25 MIXED INDAN-01 -1. / H2 -3. / 1HINDANE 1.
    STOIC 26 MIXED PHENKETO -1. / H2 -4. / 1:2-D-01 1. /  &
        H2O 3.
    STOIC 27 MIXED XANTHENE -1. / H2 -6. / CYCLO-02 1. /  &
        CH4 1. / H2O 1.
    STOIC 28 MIXED P-DECANO -1. / H2 -1. / N-TET-01 1. /  &
        CO2 1. / CH4 1.
    STOIC 29 MIXED FLUOR-01 -1. / H2 -8. / HYDFLUOR 1.
    STOIC 30 MIXED DNONDBEN -1. / H2 -1. / DINON-01 1. /  &
        H2O 1.
    STOIC 31 MIXED NAPHT-02 -1. / H2 -9. / HYDNAPH 1.
    STOIC 32 MIXED PENTACOS -1. / H2 -1. / N-TET-02 1. /  &
        CO2 1. / ETHAN-02 1.
    STOIC 33 MIXED C22H20O -0.3131404 / C21H24O4 -0.1262399 /  &
        C18H28 -5.0255485 / COKE2 1.
    CONV 1 MIXED ACETACID 1.
    CONV 2 MIXED GLYCO-01 1.
    CONV 3 MIXED FURFURAL 1.
    CONV 4 MIXED BENZOATE 1.
    CONV 5 MIXED METHPHEN 1.
    CONV 6 MIXED ETHYLGUA 0.45
    CONV 7 MIXED N-HEP-01 1.
    CONV 8 MIXED MESHEPTA 1.
    CONV 9 MIXED BENZOFUR 1.
    CONV 10 MIXED TRIMEBEN 0.5595
    CONV 11 MIXED PHENOL 1.
    CONV 12 MIXED TRIMEBEN 0.4405
    CONV 13 MIXED 2:4-X-01 1.
    CONV 14 MIXED O-ETH-01 1.
    CONV 15 MIXED ETHYLGUA 0.55
    CONV 16 MIXED 4PROPGUA 0.9661
    CONV 17 MIXED HMBENZAC 1.
    CONV 18 MIXED METOCTAC 1.
    CONV 19 MIXED 2:6-D-01 1.
    CONV 20 MIXED 4PROPGUA 0.0339
    CONV 21 MIXED CONIFALC 1.
    CONV 22 MIXED ISOEUGEN 1.
    CONV 23 MIXED NAPHT-01 0.1574
    CONV 24 MIXED NAPHT-01 0.8426
    CONV 25 MIXED INDAN-01 0.93425
    CONV 26 MIXED PHENKETO 1.
    CONV 27 MIXED XANTHENE 1.
    CONV 28 MIXED P-DECANO 1.
    CONV 29 MIXED FLUOR-01 0.86581491
    CONV 30 MIXED DNONDBEN 1.
    CONV 31 MIXED NAPHT-02 1.
    CONV 32 MIXED PENTACOS 1.
    CONV 33 MIXED C21H24O4 1.

EO-CONV-OPTI

ENDHIERARCHY B2000
```

HIERARCHY B3000

DEF-STREAMS MIXCISLD ALL

SOLVE
  PARAM METHOD=SM
  RUN-MODE MODE=SIM

FLOWSHEET
  BLOCK R-B3001 IN=B3005 QHXB3007 OUT=B3006
  BLOCK SP-B3001 IN=B3024 OUT=B3027 B3025
  BLOCK PS-B3002 IN=B3021 OUT=B3023 B3022
  BLOCK CP-B3003 IN=B3023 B3016 OUT=B3024 WCPB3003
  BLOCK CP-B3004 IN=B3025 OUT=B3026 WCPB3004
  BLOCK HXB3006+ IN=B3019 OUT=B3020 QHXB3006
  BLOCK V-B3003 IN=B3020 OUT=B3021
  BLOCK PS-B3001 IN=B3014 OUT=B3015 B3016
  BLOCK HXB3001 IN=B3006 OUT=B3007 QHXB3001
  BLOCK F-B3001 IN=B3012 OUT=B3014 B3013
  BLOCK CB-B3001 IN=B3022 B3015 B3036 B3033 OUT=B3037
  BLOCK CP-B3001 IN=B3034 OUT=B3035 WCPB3001
  BLOCK R-3002 IN=B3007 OUT=B3008
  BLOCK HXB3002 IN=B3008 OUT=B3009 QHXB3002
  BLOCK CP-B3002 IN=B3028 OUT=B3029 WCPB3002
  BLOCK HXB3007+ IN=B3037 OUT=B3038 QHXB3007
  BLOCK M-B3001 IN=B3002 B3004 OUT=B3005
  BLOCK HXB3008+ IN=B3038 OUT=B3039 QHXB3008
  BLOCK HXB3008- IN=B3001 QHXB3008 OUT=B3002
  BLOCK HXB3009 IN=B3039 OUT=B3040 QHXB3009
  BLOCK HXB3011- IN=B3035 QHXB3011 OUT=B3036
  BLOCK HXB3011+ IN=B3041 OUT=B3042 QHXB3011
  BLOCK M-B3002 IN=B3018 B3017 OUT=B3019
  BLOCK M-B3003 IN=B3029 B3031 OUT=B3032
  BLOCK HXB3010- IN=B3032 QHXB3010 OUT=B3033
  BLOCK HXB3010+ IN=B3040 OUT=B3041 QHXB3010
  BLOCK V-B3002 IN=B3030 OUT=B3031
  BLOCK HX-B3012 IN=B3042 OUT=B3043 QHXB3012
  BLOCK HXB3003 IN=B3009 OUT=B3010 QHXB3003
  BLOCK HXB3004 IN=B3010 OUT=B3011 QHXB3004
  BLOCK HXB3006- IN=CWB3006I QHXB3006 OUT=CWB3006O
  BLOCK HXB3005+ IN=B3011 OUT=B3012 QHXB3005
  BLOCK HXB3005- IN=CWB3005I QHXB3005 OUT=CWB3005O
  BLOCK V-B3001 IN=B3003 OUT=B3004

PROPERTIES NRTL FREE-WATER=STEAM-TA SOLU-WATER=3 TRUE-COMPS=YES
  PROPERTIES PENG-ROB / SRK

STREAM B3001
  SUBSTREAM MIXED TEMP=25. PRES=24.82 <barg> &
    MASS-FLOW=9.17040611
  MOLE-FRAC CH4 1.

STREAM B3017
  SUBSTREAM MIXED TEMP=25. PRES=1. <atm> MASS-FLOW=4.8
  MASS-FRAC H2 1.

STREAM B3023
  SUBSTREAM MIXED TEMP=25. PRES=1. <atm> MASS-FLOW=9.426
  MASS-FRAC H2 1.

STREAM B3026
  SUBSTREAM MIXED TEMP=25. PRES=2000. <psig> MASS-FLOW=1.8
  MASS-FRAC H2 1.

STREAM B3027
  SUBSTREAM MIXED TEMP=25. PRES=1500. <psig> MASS-FLOW=3.
  MASS-FRAC H2 1.

STREAM B3028
  SUBSTREAM MIXED TEMP=25. PRES=1. <atm> MASS-FLOW=2.5
  MASS-FRAC CH4 1.

STREAM B3034

```
    SUBSTREAM MIXED TEMP=25. PRES=1. <atm> MASS-FLOW=278.
    MASS-FRAC N2 0.7503 / O2 0.2299 / CO2 0.0005 / H2O &
      0.0066 / AR 0.0127

STREAM CWB3005I
    SUBSTREAM MIXED TEMP=27. PRES=1.03 MASS-FLOW=30.5
    MASS-FRAC H2O 1.

STREAM CWB3006I
    SUBSTREAM MIXED TEMP=27. PRES=1.03 MASS-FLOW=27.5
    MASS-FRAC H2O 1.

DEF-STREAMS HEAT QHXB3001

DEF-STREAMS HEAT QHXB3002

DEF-STREAMS HEAT QHXB3003

DEF-STREAMS HEAT QHXB3004

DEF-STREAMS HEAT QHXB3005

DEF-STREAMS HEAT QHXB3006

DEF-STREAMS HEAT QHXB3007

DEF-STREAMS HEAT QHXB3008

DEF-STREAMS HEAT QHXB3009

DEF-STREAMS HEAT QHXB3010

DEF-STREAMS HEAT QHXB3011

DEF-STREAMS HEAT QHXB3012

DEF-STREAMS WORK WCPB3001

DEF-STREAMS WORK WCPB3002

DEF-STREAMS WORK WCPB3003

DEF-STREAMS WORK WCPB3004

BLOCK M-B3001 MIXER
    PARAM PRES=-0.

BLOCK M-B3002 MIXER
    PARAM PRES=-0.

BLOCK M-B3003 MIXER
    PARAM PRES=-0.
    PROPERTIES NRTL FREE-WATER=STEAM-TA SOLU-WATER=3 &
      TRUE-COMPS=YES

BLOCK SP-B3001 FSPLIT
    FRAC B3027 0.36002109

BLOCK PS-B3001 SEP
    PARAM PRES=-0.
    FRAC STREAM=B3016 SUBSTREAM=MIXED COMPS=N2 O2 H2 CO NO2 &
      CO2 H2O H3N CH4 C2H4 C3H6-2 AR ACETACID ACETOL &
      GUAIACOL 3:5-X-01 FORMACID N-PRO-01 PHENOL TOLUENE &
      FURFURAL BENZENE CHAR ASH LIGNIN XYLAN ARABINAN MANNAN &
      GALACTAN EXTRACT TETRA-01 DILACID N-HEP-01 2:4-X-01 &
      O-ETH-01 INDAN-01 2:6-D-01 NAPHT-01 DIBEN-01 FLUOR-01 &
      2:4-D-01 NAPHT-02 ETHYL-01 N-HEX-01 CYCLO-01 M-XYL-01 &
      METHY-01 1:3-C-01 3-MET-01 P-CRE-01 N-PRO-02 1:2:3-01 &
      CIS-D-01 1:2-D-01 CYCLO-02 N-TET-01 DINON-01 N-TET-02 &
      GLYCO-01 FUMAR-01 1:2-B-01 ETHAN-01 2,2PROPA FURACETA &
      LEVOGLUC 4METGUA ETHYLANI BENZOATE METHPHEN ETHYLGUA &
      MESHEPTA BENZOFUR TRIMEBEN 4PROPGUA HMBENZAC METOCTAC &
      CONIFALC ISOEUGEN PHENKETO XANTHENE P-DECANO DNONDBEN &
      PENTACOS ETMEPHEN 1HINDANE HYDFLUOR HYDNAPH C18H28 &
```

330

```
      C21H24O4 C22H20O METHA-01 ETHAN-02 PROPA-01 ISOBU-01  &
      COKE1 COKE2 ACETY-01 NAPHT-03 FRACS=0. 0. 0.85 0. 0.  &
      0. 0. 0. 0. 0. 0. 0. 0. 0. 0. 0. 0. 0. 0. 0. 0. 0.  &
      0. 0. 0. 0. 0. 0. 0. 0. 0. 0. 0. 0. 0. 0. 0. 0. 0.  &
      0. 0. 0. 0. 0. 0. 0. 0. 0. 0. 0. 0. 0. 0. 0. 0. 0.  &
      0. 0. 0. 0. 0. 0. 0. 0. 0. 0. 0. 0. 0. 0. 0. 0. 0.  &
      0. 0. 0. 0. 0. 0. 0. 0. 0. 0. 0. 0. 0. 0. 0. 0. 0.  &
      0. 0. 0. 0. 0. 0. 0. 0. 0. 0. 0. 0. 0. 0. 0. 0. 0.  &
      0. 0. 0.
    FRAC STREAM=B3016 SUBSTREAM=CISOLID COMPS=CHAR FRACS=0.
    FLASH-SPECS B3015 PRES=20. <psia> VFRAC=1.

BLOCK PS-B3002 SEP
    PARAM PRES=-0.
    FRAC STREAM=B3023 SUBSTREAM=MIXED COMPS=N2 O2 H2 CO NO2  &
      CO2 H2O H3N CH4 C2H4 C3H6-2 AR ACETACID ACETOL  &
      GUAIACOL 3:5-X-01 FORMACID N-PRO-01 PHENOL TOLUENE  &
      FURFURAL BENZENE CHAR ASH CELLULOS LIGNIN XYLAN  &
      ARABINAN MANNAN GALACTAN EXTRACT TETRA-01 DILACID  &
      N-HEP-01 2:4-X-01 O-ETH-01 INDAN-01 2:6-D-01 NAPHT-01  &
      DIBEN-01 FLUOR-01 2:4-D-01 NAPHT-02 ETHYL-01 N-HEX-01  &
      CYCLO-01 M-XYL-01 METHY-01 1:3-C-01 3-MET-01 P-CRE-01  &
      N-PRO-02 1:2:3-01 CIS-D-01 1:2-D-01 CYCLO-02 N-TET-01  &
      DINON-01 N-TET-02 GLYCO-01 FUMAR-01 1:2-B-01 ETHAN-01  &
      2,2PROPA FURACETA LEVOGLUC 4METGUA ETHYLANI BENZOATE  &
      METHPHEN ETHYLGUA MESHEPTA BENZOFUR TRIMEBEN 4PROPGUA  &
      HMBENZAC METOCTAC CONIFALC ISOEUGEN PHENKETO XANTHENE  &
      P-DECANO DNONDBEN PENTACOS ETMEPHEN 1HINDANE HYDFLUOR  &
      HYDNAPH C18H28 C21H24O4 C22H20O METHA-01 ETHAN-02  &
      PROPA-01 ISOBU-01 COKE1 COKE2 ACETY-01 NAPHT-03 FRACS= &
      0. 0. 0.85 0. 0. 0. 0. 0. 0. 0. 0. 0. 0. 0. 0. 0.  &
      0. 0. 0. 0. 0. 0. 0. 0. 0. 0. 0. 0. 0. 0. 0. 0. 0.  &
      0. 0. 0. 0. 0. 0. 0. 0. 0. 0. 0. 0. 0. 0. 0. 0. 0.  &
      0. 0. 0. 0. 0. 0. 0. 0. 0. 0. 0. 0. 0. 0. 0. 0. 0.  &
      0. 0. 0. 0. 0. 0. 0. 0. 0. 0. 0. 0. 0. 0. 0. 0. 0.  &
      0. 0. 0. 0. 0. 0. 0. 0. 0. 0. 0. 0. 0. 0. 0. 0. 0.  &
      0. 0. 0. 0. 0. 0. 0. 0. 0.
    FRAC STREAM=B3023 SUBSTREAM=CISOLID COMPS=CHAR FRACS=0.
    FLASH-SPECS B3022 PRES=20. <psia> VFRAC=1.

BLOCK HX-B3012 HEATER
    PARAM TEMP=90. PRES=-0.

BLOCK HXB3001 HEATER
    PARAM TEMP=350. PRES=-0.62

BLOCK HXB3002 HEATER
    PARAM TEMP=369.7 PRES=-0.62

BLOCK HXB3003 HEATER
    PARAM TEMP=156.99311 PRES=-0.

BLOCK HXB3004 HEATER
    PARAM TEMP=55. PRES=-0.

BLOCK HXB3005+ HEATER
    PARAM TEMP=43. PRES=-0.

BLOCK HXB3005- HEATER
    PARAM PRES=-0.

BLOCK HXB3006+ HEATER
    PARAM TEMP=43.3 VFRAC=1.

BLOCK HXB3006- HEATER
    PARAM PRES=-0.

BLOCK HXB3007+ HEATER
    PARAM TEMP=1354.25 PRES=-0.

BLOCK HXB3008+ HEATER
    PARAM TEMP=1333.9 PRES=-0.

BLOCK HXB3008- HEATER
```

```
      PARAM PRES=-0.

BLOCK HXB3009 HEATER
      PARAM TEMP=447.95 PRES=-0.

BLOCK HXB3010+ HEATER
      PARAM TEMP=440. PRES=-0.

BLOCK HXB3010- HEATER
      PARAM PRES=-0.

BLOCK HXB3011+ HEATER
      PARAM TEMP=265.108 PRES=-0.

BLOCK HXB3011- HEATER
      PARAM PRES=-0.

BLOCK F-B3001 FLASH2
      PARAM TEMP=43.3 DUTY=0.

BLOCK CB-B3001 RSTOIC
      PARAM PRES=-0. DUTY=0. COMBUSTION=YES

BLOCK R-3002 RSTOIC
      PARAM PRES=-0.414 DUTY=0.
      STOIC 1 MIXED CO -1. / H2O -1. / CO2 1. / H2 1.
      CONV 1 MIXED CO 0.75

BLOCK R-B3001 RYIELD
      PARAM PRES=-2.068
      MASS-YIELD MIXED CH4 0.01910836 / H2 0.06659096 / H2O  &
          0.56467704 / CO 0.1011446 / CO2 0.24847904

BLOCK CP-B3001 COMPR
      PARAM TYPE=ISENTROPIC DELP=0.01

BLOCK CP-B3002 COMPR
      PARAM TYPE=ISENTROPIC DELP=0.01

BLOCK CP-B3003 COMPR
      PARAM TYPE=ISENTROPIC PRES=1500. <psig> SEFF=0.82

BLOCK CP-B3004 COMPR
      PARAM TYPE=ISENTROPIC PRES=2000. <psig> SEFF=0.82

BLOCK V-B3001 VALVE
      PARAM P-OUT=40.

BLOCK V-B3002 VALVE
      PARAM P-OUT=1.02

BLOCK V-B3003 VALVE
      PARAM P-OUT=25.

ENDHIERARCHY B3000

HIERARCHY B4000


DEF-STREAMS MIXCISLD ALL

SOLVE
      PARAM METHOD=SM
      RUN-MODE MODE=SIM

FLOWSHEET
      BLOCK T-B4001 IN=B4001 OUT=B4002 WTB4001
      BLOCK T-B4002 IN=B4006 OUT=B4007 WTB4002
      BLOCK T-B4003 IN=B4007 OUT=B4008 WTB4003
      BLOCK S-B4001 IN=B4002 OUT=B4003 B4004
      BLOCK S-B4002 IN=B4004 OUT=B4006 B4005

PROPERTIES NRTL FREE-WATER=STEAM-TA SOLU-WATER=3 TRUE-COMPS=YES
      PROPERTIES PENG-ROB / SRK
```

332

```
DEF-STREAMS WORK WTB4001

DEF-STREAMS WORK WTB4002

DEF-STREAMS WORK WTB4003

BLOCK S-B4001 FSPLIT
   MASS-FLOW B4003 45.787479

BLOCK S-B4002 FSPLIT
   FRAC B4006 0.98265

BLOCK T-B4001 COMPR
   PARAM TYPE=ISENTROPIC PRES=49. SEFF=0.84 MEFF=0.98  &
      MODEL-TYPE=TURBINE

BLOCK T-B4002 COMPR
   PARAM TYPE=ISENTROPIC PRES=10. SEFF=0.85 MEFF=0.98  &
      MODEL-TYPE=TURBINE

BLOCK T-B4003 COMPR
   PARAM TYPE=ISENTROPIC PRES=2. SEFF=0.85 MEFF=0.98  &
      MODEL-TYPE=TURBINE

ENDHIERARCHY B4000

DESIGN-SPEC AIRCOM-H
   DEFINE O2EXIT MASS-FLOW STREAM="B3000.B3037" SUBSTREAM=MIXED  &
      COMPONENT=O2
   DEFINE COMBPR STREAM-VAR STREAM="B3000.B3037"  &
      SUBSTREAM=MIXED VARIABLE=MASS-FLOW
   SPEC "O2EXIT/COMBPR" TO "0.06"
   TOL-SPEC "0.0001"
   VARY STREAM-VAR STREAM="B3000.B3034" SUBSTREAM=MIXED  &
      VARIABLE=MASS-FLOW
   LIMITS "260" "290" STEP-SIZE=0.01

DESIGN-SPEC AIRCOM-P
   DEFINE AIRCOM MASS-FRAC STREAM="A4000.4005" SUBSTREAM=MIXED  &
      COMPONENT=O2
   SPEC "AIRCOM" TO ".071"
   TOL-SPEC ".001"
   VARY STREAM-VAR STREAM="A4000.4002A" SUBSTREAM=MIXED  &
      VARIABLE=MASS-FLOW
   LIMITS "20" "500"

DESIGN-SPEC ASHQUENC
   DEFINE ASHQUE STREAM-VAR STREAM="A4000.4013" SUBSTREAM=MIXED  &
      VARIABLE=TEMP
   SPEC "ASHQUE" TO "40"
   TOL-SPEC ".001"
   VARY STREAM-VAR STREAM="A4000.4012" SUBSTREAM=MIXED  &
      VARIABLE=MASS-FLOW
   LIMITS "0.09" "2"

DESIGN-SPEC BFWATER
   DEFINE TSTEAM STREAM-VAR STREAM="A7000.7025" SUBSTREAM=MIXED  &
      VARIABLE=TEMP
   SPEC "TSTEAM" TO "500"
   TOL-SPEC "0.01"
   VARY STREAM-VAR STREAM="A7000.7001" SUBSTREAM=MIXED  &
      VARIABLE=MASS-FLOW
   LIMITS "83" "86" STEP-SIZE=0.01

DESIGN-SPEC CW2005
   DEFINE THIN STREAM-VAR STREAM="B2000.B2007" SUBSTREAM=MIXED  &
      VARIABLE=TEMP
   DEFINE TCOUT STREAM-VAR STREAM="B2000.CWB2005O"  &
      SUBSTREAM=MIXED VARIABLE=TEMP
   SPEC "TCOUT" TO "THIN-10"
   TOL-SPEC "0.01"
   VARY STREAM-VAR STREAM="B2000.CWB2005I" SUBSTREAM=MIXED  &
      VARIABLE=MASS-FLOW
```

333

```
     LIMITS "5" "10"

DESIGN-SPEC CW3005
   DEFINE TCOUT STREAM-VAR STREAM="B3000.CWB3005O" &
      SUBSTREAM=MIXED VARIABLE=TEMP
   DEFINE THIN STREAM-VAR STREAM="B3000.B3011" SUBSTREAM=MIXED &
      VARIABLE=TEMP
   SPEC "TCOUT" TO "THIN-10"
   TOL-SPEC "0.01"
   VARY STREAM-VAR STREAM="B3000.CWB3005I" SUBSTREAM=MIXED &
      VARIABLE=MASS-FLOW
   LIMITS "25" "50"

DESIGN-SPEC CW3006
   DEFINE THIN STREAM-VAR STREAM="B3000.B3019" SUBSTREAM=MIXED &
      VARIABLE=TEMP
   DEFINE TCOUT STREAM-VAR STREAM="B3000.CWB3006O" &
      SUBSTREAM=MIXED VARIABLE=TEMP
   SPEC "TCOUT" TO "THIN-10"
   TOL-SPEC "0.01"
   VARY STREAM-VAR STREAM="B3000.CWB3006I" SUBSTREAM=MIXED &
      VARIABLE=MASS-FLOW
   LIMITS "25" "50"

DESIGN-SPEC DRYERAIR
   DEFINE DRYAIR STREAM-VAR STREAM="A1000.1005" SUBSTREAM=MIXED &
      VARIABLE=MASS-FLOW
   SPEC "DRYAIR" TO "7.0102"
   TOL-SPEC ".0001"
   VARY STREAM-VAR STREAM="A3000.3008" SUBSTREAM=MIXED &
      VARIABLE=MASS-FLOW
   LIMITS "250" "1500"

DESIGN-SPEC DS-1
   DEFINE WFLOW BLOCK-VAR BLOCK="A3000.HX-3001-" VARIABLE=TEMP &
      SENTENCE=PARAM
   SPEC "WFLOW" TO "250"
   TOL-SPEC ".001"
   VARY STREAM-VAR STREAM="A3000.30012A" SUBSTREAM=MIXED &
      VARIABLE=MASS-FLOW
   LIMITS "1" "10"

DESIGN-SPEC FAIRTEMP
   DEFINE FAIRTE BLOCK-VAR BLOCK="A2000.PY-2001" VARIABLE=TEMP &
      SENTENCE=PARAM
   SPEC "FAIRTE" TO "500"
   TOL-SPEC ".001"
   VARY BLOCK-VAR BLOCK="A4000.HX4001+" VARIABLE=TEMP &
      SENTENCE=PARAM
   LIMITS "600" "1500"

DESIGN-SPEC NGFUEL
   DEFINE NGFUEL STREAM-VAR STREAM="B3000.B3028" &
      SUBSTREAM=MIXED VARIABLE=MASS-FLOW
   DEFINE LIGHTS STREAM-VAR STREAM="B3000.B3030" &
      SUBSTREAM=MIXED VARIABLE=MASS-FLOW
   DEFINE PSAOFR STREAM-VAR STREAM="B3000.B3022" &
      SUBSTREAM=MIXED VARIABLE=MASS-FLOW
   DEFINE PSAOFG STREAM-VAR STREAM="B3000.B3015" &
      SUBSTREAM=MIXED VARIABLE=MASS-FLOW
   SPEC "(LIGHTS+NGFUEL)/(PSAOFG+PSAOFR+LIGHTS+NGFUEL)" TO &
      "0.15"
   TOL-SPEC "0.001"
   VARY MASS-FLOW STREAM="B3000.B3028" SUBSTREAM=MIXED &
      COMPONENT=CH4
   LIMITS "1" "3" STEP-SIZE=0.25

DESIGN-SPEC PY2001T
   DEFINE T2001 STREAM-VAR STREAM="A2000.2003" SUBSTREAM=MIXED &
      VARIABLE=TEMP
   SPEC "T2001" TO "500"
   TOL-SPEC "0.1"
   VARY BLOCK-VAR BLOCK="A5000.S-5001" SENTENCE=FRAC &
      VARIABLE=FRAC ID1=5007
```

334

```
    LIMITS "0" "0.4" STEP-SIZE=0.02

DESIGN-SPEC QFLDIST
    DEFINE QFLM INFO-VAR INFO=HEAT VARIABLE=DUTY  &
        STREAM="A8000.QFLDISC"
    DEFINE QFLD INFO-VAR INFO=HEAT VARIABLE=DUTY  &
        STREAM="A8000.QFLDISB"
    SPEC "QFLM" TO "QFLD"
    TOL-SPEC "0.1"
    VARY STREAM-VAR STREAM="A8000.FUELDIS" SUBSTREAM=MIXED  &
        VARIABLE=MASS-FLOW
    LIMITS "0.25" "0.29"

DESIGN-SPEC QPSA
    DEFINE QPSAC INFO-VAR INFO=HEAT VARIABLE=DUTY  &
        STREAM="A8000.QPSAC"
    DEFINE QPSAB INFO-VAR INFO=HEAT VARIABLE=DUTY  &
        STREAM="A8000.QPSAB"
    SPEC "QPSAC" TO "QPSAB"
    TOL-SPEC "0.001"
    VARY BLOCK-VAR BLOCK="A8000.S-8002" SENTENCE=FRAC  &
        VARIABLE=FRAC ID1=LPTOT
    LIMITS "0.90" "0.99955"

DESIGN-SPEC QSTMDIST
    DEFINE QSTMM INFO-VAR INFO=HEAT VARIABLE=DUTY  &
        STREAM="A8000.QSTMDISC"
    DEFINE QSTMD INFO-VAR INFO=HEAT VARIABLE=DUTY  &
        STREAM="A8000.QSTMDISB"
    SPEC "QSTMM" TO "QSTMD"
    TOL-SPEC "0.01"
    VARY BLOCK-VAR BLOCK="B4000.S-B4002" SENTENCE=FRAC  &
        VARIABLE=FRAC ID1=B4006
    LIMITS "0.9825" "0.9828"

DESIGN-SPEC SHYD1H2O
    DEFINE WFRAC MASS-FRAC STREAM="B1000.B1010" SUBSTREAM=MIXED  &
        COMPONENT=H2O
    SPEC "WFRAC" TO "0.026999"
    TOL-SPEC "0.0001"
    VARY BLOCK-VAR BLOCK="B1000.S-B1001" SENTENCE=FRAC  &
        VARIABLE=FRACS ID1=MIXED ID2=B1010 ELEMENT=7
    LIMITS "0" "0.2" STEP-SIZE=0.025

DESIGN-SPEC TAIRCOM
    DEFINE TAIR STREAM-VAR STREAM="B3000.B3036" SUBSTREAM=MIXED  &
        VARIABLE=TEMP
    SPEC "TAIR" TO "250"
    TOL-SPEC "0.01"
    VARY BLOCK-VAR BLOCK="B3000.HXB3010+" VARIABLE=TEMP  &
        SENTENCE=PARAM
    LIMITS "438" "442" STEP-SIZE=0.001

DESIGN-SPEC TNGEXIT
    DEFINE TNGEX STREAM-VAR STREAM="B3000.B3002" SUBSTREAM=MIXED  &
        VARIABLE=TEMP
    SPEC "TNGEX" TO "371"
    TOL-SPEC "0.1"
    VARY BLOCK-VAR BLOCK="B3000.HXB3008+" VARIABLE=TEMP  &
        SENTENCE=PARAM
    LIMITS "1330" "1334" STEP-SIZE=0.01

DESIGN-SPEC TREFEXIT
    DEFINE TREFEX STREAM-VAR STREAM="B3000.B3006"  &
        SUBSTREAM=MIXED VARIABLE=TEMP
    SPEC "TREFEX" TO "857"
    TOL-SPEC "0.2"
    VARY BLOCK-VAR BLOCK="B3000.HXB3007+" VARIABLE=TEMP  &
        SENTENCE=PARAM
    LIMITS "1353.5" "1354.5" STEP-SIZE=0.01

EO-CONV-OPTI

CALCULATOR DISTIL
```

335

```
    DEFINE WDIST INFO-VAR INFO=WORK VARIABLE=POWER  &
      STREAM="A8000.WDISTIL"
    DEFINE FEED STREAM-VAR STREAM="B2000.B2016" SUBSTREAM=MIXED  &
      VARIABLE=MASS-FLOW
    DEFINE CWDIST STREAM-VAR STREAM="A8000.CWDIST"  &
      SUBSTREAM=MIXED VARIABLE=MASS-FLOW
    DEFINE DWDIST STREAM-VAR STREAM="A8000.DH2ODIST"  &
      SUBSTREAM=MIXED VARIABLE=MASS-FLOW
    DEFINE QSDIST INFO-VAR INFO=HEAT VARIABLE=DUTY  &
      STREAM="A8000.QSTMDISA"
    DEFINE AIRCOM STREAM-VAR STREAM="A8000.AIRDIS"  &
      SUBSTREAM=MIXED VARIABLE=MASS-FLOW
    DEFINE FDIST STREAM-VAR STREAM="A8000.FUELDIS"  &
      SUBSTREAM=MIXED VARIABLE=MASS-FLOW
    DEFINE QFDIST INFO-VAR INFO=HEAT VARIABLE=DUTY  &
      STREAM="A8000.QFLDISA"
    DEFINE FH2UT STREAM-VAR STREAM="A8000.FUELH2PR"  &
      SUBSTREAM=MIXED VARIABLE=MASS-FLOW
    DEFINE FH2PR STREAM-VAR STREAM="B3000.B3028" SUBSTREAM=MIXED  &
      VARIABLE=MASS-FLOW
    DEFINE FDISUT STREAM-VAR STREAM="A8000.FUELDIST"  &
      SUBSTREAM=MIXED VARIABLE=MASS-FLOW
F        WDIST=FEED*0.0087
F        CWDIST=FEED*1.409289*0.992025664
F        DWDIST=FEED*0.09092184*0.970495384
F        QSDIST=FEED*94.955034
F        AIRCOM=FDIST/0.04195902
F        QFDIST=FEED*633.0335
F        FH2UT=FH2PR
F        FDISUT=FDIST
    READ-VARS FEED FDIST FH2PR
    WRITE-VARS WDIST CWDIST DWDIST QSDIST AIRCOM QFDIST FH2UT  &
      FDISUT


CALCULATOR PSA
    DEFINE QPSA INFO-VAR INFO=HEAT VARIABLE=DUTY  &
      STREAM="A8000.QPSAA"
    DEFINE FEED01 STREAM-VAR STREAM="B3000.B3014"  &
      SUBSTREAM=MIXED VARIABLE=MASS-FLOW
    DEFINE FEED02 STREAM-VAR STREAM="B3000.B3021"  &
      SUBSTREAM=MIXED VARIABLE=MASS-FLOW
F        QPSA=(FEED01+FEED02)*8.913307983
    READ-VARS FEED01 FEED02


CALCULATOR W-CHW
    DEFINE WCHW INFO-VAR INFO=WORK VARIABLE=POWER  &
      STREAM="A8000.WCHW"
    DEFINE QCHW INFO-VAR INFO=HEAT VARIABLE=DUTY  &
      STREAM="A8000.QCHW"
F        WCHW=(QCHW/3600)/3
    READ-VARS QCHW
    WRITE-VARS WCHW


CALCULATOR W-CW
    DEFINE WCW INFO-VAR INFO=WORK VARIABLE=POWER  &
      STREAM="A8000.WCW"
    DEFINE QCW INFO-VAR INFO=HEAT VARIABLE=DUTY  &
      STREAM="A8000.QEVAP"
    DEFINE M STREAM-VAR STREAM="A8000.MAKEUPCW" SUBSTREAM=MIXED  &
      VARIABLE=MASS-FLOW
    DEFINE HOTCW STREAM-VAR STREAM="A8000.HOTCW" SUBSTREAM=MIXED  &
      VARIABLE=MASS-FLOW
    DEFINE TIN STREAM-VAR STREAM="A8000.HOTCW" SUBSTREAM=MIXED  &
      VARIABLE=TEMP
    DEFINE VAPFRA BLOCK-VAR BLOCK="A8000.CWT-8001"  &
      VARIABLE=VFRAC SENTENCE=PARAM
F      M=(0.00153*(TIN-27)+0.033)*HOTCW/(1-(0.00153*(TIN-27)+0.033))
F      VAPFRA=0.00085*1.8*(TIN-27)
F      WCW=(QCW/7)/3600
    READ-VARS QCW HOTCW TIN
    WRITE-VARS WCW M VAPFRA


CALCULATOR W-ESP
    DEFINE STDCON STREAM-VAR STREAM="A3000.3005" SUBSTREAM=MIXED  &
```

336

```
          VARIABLE=STDVOL-FLOW
     DEFINE WESP INFO-VAR INFO=WORK VARIABLE=POWER  &
        STREAM="A8000.WESP"
F        WESP=(1.0954608*133285.094)/3600000
     READ-VARS STDCON
     WRITE-VARS WESP


CALCULATOR W-GRIND
     DEFINE WGRIND INFO-VAR INFO=WORK VARIABLE=POWER  &
        STREAM="A8000.WGRIND"
     DEFINE DRIEDS STREAM-VAR STREAM="A1000.1005"  &
        SUBSTREAM=CISOLID VARIABLE=MASS-FLOW
     DEFINE DRIEDM STREAM-VAR STREAM="A1000.1005" SUBSTREAM=MIXED  &
        VARIABLE=MASS-FLOW
F        WGRIND=(DRIEDM+DRIEDS)*0.05
     READ-VARS DRIEDS DRIEDM
     WRITE-VARS WGRIND


SENSITIVITY FRACLIQR
     DEFINE SPLIT BLOCK-VAR BLOCK="A5000.S-5001" SENTENCE=FRAC  &
        VARIABLE=FRAC ID1=5007
     DEFINE PYTEMP STREAM-VAR STREAM="A2000.2003" SUBSTREAM=MIXED  &
        VARIABLE=TEMP
     TABULATE 1 "SPLIT"
     TABULATE 2 "PYTEMP"
     VARY BLOCK-VAR BLOCK="A5000.S-5001" SENTENCE=FRAC  &
        VARIABLE=FRAC ID1=5007
     RANGE LOWER="0.3" UPPER="0.5" INCR="0.02"


SENSITIVITY HEATDUTY
     DEFINE HDUTY BLOCK-VAR BLOCK="A2000.PY-2001" VARIABLE=QCALC  &
        SENTENCE=PARAM
     TABULATE 1 "HDUTY"
     VARY BLOCK-VAR BLOCK="A5000.S-5001" SENTENCE=FRAC  &
        VARIABLE=FRAC ID1=5007 LABEL="FRACTION"
     RANGE LOWER=".46" UPPER=".47" INCR=".001"


SENSITIVITY P-F1HYD1
     DEFINE HEXB07 MASS-FLOW STREAM="B1000.B1007" SUBSTREAM=MIXED  &
        COMPONENT=N-HEX-01
     DEFINE HEXB04 MASS-FLOW STREAM="B1000.B1004" SUBSTREAM=MIXED  &
        COMPONENT=N-HEX-01
     DEFINE CYCBO7 MASS-FLOW STREAM="B1000.B1007" SUBSTREAM=MIXED  &
        COMPONENT=CYCLO-01
     DEFINE CYCBO4 MASS-FLOW STREAM="B1000.B1004" SUBSTREAM=MIXED  &
        COMPONENT=CYCLO-01
     DEFINE TFHYD1 STREAM-VAR STREAM="B1000.B1007"  &
        SUBSTREAM=MIXED VARIABLE=TEMP
     DEFINE THXHYD BLOCK-VAR BLOCK="B1000.HXB1002+" VARIABLE=TEMP  &
        SENTENCE=PARAM
     DEFINE TETB07 MASS-FLOW STREAM="B1000.B1007" SUBSTREAM=MIXED  &
        COMPONENT=TETRA-01
     DEFINE TETB04 MASS-FLOW STREAM="B1000.B1004" SUBSTREAM=MIXED  &
        COMPONENT=TETRA-01
     TABULATE 1 "HEXB07/HEXB04"
     TABULATE 2 "CYCBO7/CYCBO4"
     TABULATE 3 "TETB07/TETB04"
     TABULATE 4 "TFHYD1"
     TABULATE 5 "THXHYD"
     VARY BLOCK-VAR BLOCK="B1000.F-B1001" VARIABLE=PRES  &
        SENTENCE=PARAM
     RANGE LOWER="104" UPPER="104" INCR="0"
     VARY BLOCK-VAR BLOCK="B1000.HXB1002+" VARIABLE=TEMP  &
        SENTENCE=PARAM
     RANGE LOWER="40" UPPER="75" INCR="5"


SENSITIVITY P-F1HYD2
     DEFINE HEX206 MASS-FLOW STREAM="B2000.B2009" SUBSTREAM=MIXED  &
        COMPONENT=N-HEX-01
     DEFINE HEX204 MASS-FLOW STREAM="B2000.B2004" SUBSTREAM=MIXED  &
        COMPONENT=N-HEX-01
     DEFINE BEN206 MASS-FLOW STREAM="B2000.B2009" SUBSTREAM=MIXED  &
        COMPONENT=BENZENE
     DEFINE BEN204 MASS-FLOW STREAM="B2000.B2004" SUBSTREAM=MIXED  &
```

337

```
            COMPONENT=BENZENE
      DEFINE TET206 MASS-FLOW STREAM="B2000.B2009" SUBSTREAM=MIXED  &
            COMPONENT=TETRA-01
      DEFINE TET204 MASS-FLOW STREAM="B2000.B2004" SUBSTREAM=MIXED  &
            COMPONENT=TETRA-01
      DEFINE CYC206 MASS-FLOW STREAM="B2000.B2009" SUBSTREAM=MIXED  &
            COMPONENT=CYCLO-01
      DEFINE CYC204 MASS-FLOW STREAM="B2000.B2004" SUBSTREAM=MIXED  &
            COMPONENT=CYCLO-01
      TABULATE 1 "BEN206/BEN204"
      TABULATE 2 "HEX206/HEX204"
      TABULATE 3 "TET206/TET204"
      TABULATE 4 "CYC206/CYC204"
      VARY BLOCK-VAR BLOCK="B2000.F-B2001" VARIABLE=PRES  &
            SENTENCE=PARAM
      RANGE LOWER="10" UPPER="100" INCR="10"
      VARY BLOCK-VAR BLOCK="B2000.HXB2002+" VARIABLE=TEMP  &
            SENTENCE=PARAM
      RANGE LOWER="25" UPPER="75" INCR="5"

SENSITIVITY QHX3003B
      DEFINE Q3003B INFO-VAR INFO=HEAT VARIABLE=DUTY  &
            STREAM="B3000.QHXB3003"
      TABULATE 1 "Q3003B"
      VARY BLOCK-VAR BLOCK="B3000.HXB3003" VARIABLE=TEMP  &
            SENTENCE=PARAM
      RANGE LOWER="156.99310" UPPER="156.9933" INCR="0.00001"

STREAM-REPOR MOLEFLOW MASSFLOW

PROPERTY-REP PCES NOPARAM-PLUS

DISABLE
      SENSITIVITY FRACLIQR HEATDUTY P-F1HYD1 P-F1HYD2 QHX3003B
      DESIGN-SPEC DRYERAIR DS-1 FAIRTEMP
```

338